8. iconst

"Science for Sustainable Technology"

2025

8. International Conferences On
Science And Technology

28-30 May / Budapest,HUNGARY

Abstract & Fulltext
E-BOOK

Engineering Science and Technology

2025

iconst.org

2025

Engineering Science and Technology

iconst.org

ICONST EST 2025

International Conferences on Science and Technology
Engineering Science and Technology
May 28-30, 2025 in Budapest - HUNGARY

Editors
Assoc. Prof. Dr. Mustafa Karaboyacı
Assoc. Prof. Dr. Abdullah Beram
Assoc. Prof. Dr. Hamza Kandemir
Assoc. Prof. Dr. Serkan Özdemir

Technical Editors
Asst. Prof. Dr. Tunahan Çınar
Asst. Prof. Dr. Ahmet Acarer
Dr. Ayşegül Tekeş Düdükçü
MSc. Oğuzhan Erfidan
MSc. Murat Görgöz

Cover design & Layout
MSc. Şerafettin Atmaca

Published by
Association of Kutbilge Academicians, Isparta, Turkiye
E-Mail: iconst.iconsr.conferences@gmail.com

Publication Date: 11/08/2025
ISBN: 978-625-98911-9-4

ICONST EST 2025

International Conferences on Science and Technology

Engineering Science and Technology

May 28-30, 2025 in Budapest - HUNGARY

Scientific Honorary Committee

Prof. Dr. Levente Kovács, Óbuda University, Hungary
Prof. Dr. Yılmaz Çatal, Isparta University of Applied Sciences, Türkiye
Prof. Dr. İlker Hüseyin Çarıkçı, Member of Council of Higher Education, Türkiye
Prof. Dr. Mehmet Saltan, Suleyman Demirel University, Türkiye
Prof. Dr. Bahri Şahin, İstanbul Gelisim University, Türkiye
Prof. Dr. Edmond Hajrizi, University of Business and Technology, Kosovo
Prof. Dr. Mentor Alishani, University of Prizren, Kosovo
Prof. Dr. Naime Brajshori,Kolegji Heimerer, Kosovo
Prof. Dr. Arian Idrizaj, University of Medical Sciences Rezonanca, Kosovo
Prof. Dr. Nermina Hadžigrahić, University of Tuzla, Bosnia and Herzegovina
Prof. Dr. Shkëlqim Fortuzi, Durres "Aleksandër Moisiu" University, Albania
Prof. Dr. Rade Ratkovic, FBT-Budva University, Montenegro
Prof. Dr. Vujadin Vešović, FSKL-Budva, Montenegro

Organizing Committee

Assoc.Prof.Dr. Mustafa Karaboyacı, Suleyman Demirel University, Türkiye
Assoc.Prof.Dr. Hamza Kandemir, Isparta University of Applied Sciences, Türkiye
Assoc. Prof. Dr. Abdullah Beram, Pamukkale University, Türkiye
Assoc. Prof. Dr. Serkan Özdemir, KU Leuven, Belgium

Local Chairman of the Conference

Prof. Dr. János Varga, Óbuda University, Hungary

Local Organizing Committee

Prof. Dr. Ágnes Csiszárik-Kocsir, Óbuda University, Hungary
Dr. János Varga, Óbuda University, Hungary
Prof. Dr. Mónika Garai-Fodor, Óbuda University, Hungary
Attila Balogh, Óbuda University, Hungary
Dr. Ádám Béla Horváth, Óbuda University, Hungary
Pál Fehér Polgár, Óbuda University, Hungary
Oszkár Dobos, Óbuda University, Hungary
Dr. Győző Szilágyi, Óbuda University, Hungary
Dr. Alfonz Antoni, Óbuda University, Hungary
Prof. Dr. Zoltán Rajnai, Óbuda University, Hungary
Dr. Richárd Horváth , Óbuda University, Hungary
Dr. Tibor Farkas, Óbuda University, Hungary
Dr. Ferenc Kiss , Óbuda University, Hungary
Dr. Tibor Wührl, Óbuda University, Hungary
Asst. Prof. Dr. Yunus Şahinler, Istanbul Gelisim University, Türkiye
Assoc. Prof. Dr. Mustafa Can Koç, Istanbul Gelisim University, Türkiye
Asst. Prof. Dr. Mahmut Ulukan, Istanbul Gelisim University, Türkiye
Prof Dr. Indrit Bimi, Durres University, Albania
Prof. Dr. Izabela Zimoch, Silesian University of Technology, Poland
Dr. Iwona Klosok-Bazan, Opole University of Technology, Poland
Prof. Dr. Joanna Machnik-Slomka, Silesian University of Technology, Poland
Prof. Dr. Elzbieta Pawlowska, Silesian University of Technology, Poland

ICONST EST 2025

International Conferences on Science and Technology

Engineering Science and Technology

May 28-30, 2025 in Budapest - HUNGARY

ICONST EST 2025

International Conferences on Science and Technology

Engineering Science and Technology

May 28-30, 2025 in Budapest - HUNGARY

ICONST EST 2025

International Conferences on Science and Technology
Engineering Science and Technology
May 28-30, 2025 in Budapest - HUNGARY

Dear Readers;

The 8th of ICONST organizations was held in Budapest-HUNGARY between May 28-30, 2025 with the theme of 'science for sustainable technology' again. In recent years, weather changes due to climate change have reached a perceptible level for everyone and have become a major concern. For this reason, scientific studies that transform technological progress into a sustainable one is seen as the only solution for humanity's salvation. Here we ask ourselves "which branch of science is responsible for sustainability?". Sustainability science is an interdisciplinary field of study that covers all basic sciences with social, economic, ecological dimensions. If we consider technology as the practical application of scientific knowledge, the task of scientists under these conditions is to design products that consume less energy, require less raw materials, and last longer.

ICONST organizations organize congresses on sustainability issues of three main fields of study at the same time in order to present different perspectives to scientists. This year, 215 papers from 20 different countries presented by scientists in ICONST Organizations.

98 papers from 8 countries (Albania, Bosnia and Herzegovina, Crotia, Czech Republic, Greece, Hungary, India, Iran, Italy, Kosovo, Montengro, Morocco, Pakistan, Poland, Türkiye) presented in our International Conference on Engineering Science and Technology organized under ICONST organizations. Turkey is the country with the highest participation with 48%, followed by Poland and Kosovo with 14.2%, Albania with %8, Hungary with 5.1%, Iran and Czech Republic with 2%, the other countries with 1%. Outside of Türkiye participant rate is totally 52%.

As ICONST organizations, we will continue to organize organizations with the value you deserve in order to exchange ideas against the greatest threat facing humanity, to inspire each other and to contribute to science. See you at your future events.

ICONST Organizing Committee

Use of Design Thinking metod in MedTech innovation projects

MARTA PENKALA*[1], JOANNA MACHNIK-SŁOMKA[2] , ELŻBIETA PAWŁOWSKA[3]

Abstract: The dynamic development of modern medical technologies and the changing needs of patients and medical staff present the MedTech industry with new challenges in designing innovative solutions. The aim of this article is to evaluate the application of the Design Thinking method in the medical technology sector as an approach to support the innovation creation process. The method is user-centered and based on empathy, interdisciplinary collaboration and problem solving. Furthermore, its tenets are gaining increasing importance in innovation projects in many sectors such as information technology, education, finance, the public sector or industry. This confirms its versatility and flexibility in application in different areas.
The research was conducted using the literature review method and the case study method. The research analyzed selected examples of the application of the Design Thinking method in MedTech innovation projects worldwide. It presents the key stages of the design process - empathy, problem definition, idea generation, prototyping and testing - and identifies the value creation and benefits of their implementation.
The conclusions of the analysis confirm that the Design Thinking method can be a valuable tool to support the development of innovative products and services in the medical industry. The use of this approach fosters the creation of solutions better tailored to the real needs of users and increases the chances of successful implementation of an innovative solution. The article can be helpful for both practitioners and researchers in the healthcare field interested in using the Design Thinking method in the context of creating modern, user-centered innovative products or services.

Keywords: Design Thinking, innovation, innovation project, MedTech, health.

[1]**Address:** Silesian University of Technology, Faculty of Organization and Management, Poland
[2]**Address:** Silesian University of Technology, Faculty of Organization and Management, Poland
[3]**Address:** Silesian University of Technology, Faculty of Organization and Management, Poland

***Corresponding author**: marta.penkala@polsl.pl

Corrosion Performance of WC-Co Die Inserts Borided at Different Temperatures for Cold Forming

KÜBRA ÖZTÜRK GÜLER*[1,2,3], BAHADIR UYULGAN[1,2]

Abstract: WC-Co cemented carbides are composite materials produced by binding hard WC particles within a metallic Co matrix via liquid phase sintering. Due to their excellent wear resistance and toughness, they are widely utilized in cold forming dies; however, the cobalt matrix exhibits low corrosion resistance in aggressive environments. enhance surface properties, boriding treatments are employed, forming a hard and chemically stable boride layer that improves both wear and corrosion resistance. Process parameters such as boriding temperature and duration significantly affect the structural integrity of this layer, thus effecting corrosion performance. In this study, WC-Co material containing 19% Co was subjected to pack boriding at 900 °C, 950 °C, and 1000 °C for 4 hours to evaluate the effect of boriding temperature on corrosion behavior. Corrosion resistance was assessed using potentiodynamic polarization tests in a 1 M 3.5% NaCl solution, and corrosion rates (mm/year) were determined via Tafel extrapolation. XRD analysis confirmed the formation of CoB, Co_2B, and W_2CoB_2 phases in the borided layers. The results demonstrated that boriding temperature critically impacts corrosion resistance by altering the microstructure and stability of the boride layer. The sample borided at 1000 °C exhibited the best corrosion resistance, with the lowest corrosion rate of 9.09×10^{-2} mm/year, while the untreated sample showed the highest rate at 3.783×10^{-1} mm/year. This significant improvement suggests that boriding at elevated temperatures facilitates the formation of a more compact and chemically stable boride layer, thereby substantially increasing the material's resistance to corrosive attack.

Keywords: WC-Co, boriding, corrosion, tafel extrapolation, cold forming

[1]**Address:** Department of Metallurgical and Materials Engineering, Dokuz Eylul University, İzmir, Turkey
[2]**Address:** [2]The Graduate School of Natural and Applied Sciences, Department of Metallurgical and Materials Engineering, Dokuz Eylul 35390 Izmir, Turkey
[3] **Address**: R&D Center, Norm İzmir Cıvata San. ve Tic. A.Ş., AOSB, İzmir, Turkey

***Corresponding author**: kubra.ozturk@normfasteners.com

The Rise of Cyber Threats in Albania: Challenges and Security Measures

REXHION-QAFA*[1], AUTHOR EZMOLDA-BAROLLI*[2]

Abstract: In recent years, Albania has undergone a profound digital transformation, characterized by the rapid adoption of e-governance platforms, digital financial systems, and online public services. While these advancements have improved administrative efficiency and public accessibility, they have concurrently introduced new cybersecurity vulnerabilities and significantly expanded the national attack surface. This paper critically examines the evolving landscape of cyber threats confronting Albania, with a particular focus on attack typologies such as ransomware, data breaches, state-sponsored cyber operations, and disruptions targeting critical infrastructure. Employing a multidisciplinary methodology that integrates case study analysis, cybersecurity policy evaluation, and comparative frameworks grounded in European Union and NATO standards, the study investigates both technological deficiencies and institutional vulnerabilities that impede the development of robust cyber resilience. Findings indicate structural weaknesses, including the inadequacy of the existing legal framework, limited inter-institutional coordination, underinvestment in cybersecurity infrastructure, and a shortage of specialized human capital in the cybersecurity sector. Furthermore, the research assesses the current national strategic response, analyzing the effectiveness of Albania's cybersecurity strategy, incident response frameworks, and initiatives aimed at fostering public-private collaboration. The paper concludes with a set of targeted policy recommendations, advocating for comprehensive legislative reforms, enhanced institutional coordination, increased financial commitment to cybersecurity, and systematic alignment with international cybersecurity norms and best practices. Strengthening these areas is critical to safeguarding Albania's digital sovereignty, ensuring the resilience of critical infrastructures, and promoting a sustainable, secure digital environment in an increasingly contested and volatile cyber domain.

Keywords: Albania, cybersecurity, digital infrastructure, cyber-threats, cybersecurity-frameworks, cyber-resilience
[1]**Address:** University of Tirana, Faculty of Economics, Tirana/Albania
[2]**Address:** University of Tirana, Faculty of Economics, Tirana/Albania

***Corresponding author**: rexhion_qafa.festudentdr@unitir.edu.al , ezmolda.barolli@unitir.edu.al

Tailoring Materials and Transducer Architectures for SAW-Based Devices in Environmental Sensing

ONUR ALEV*[1,2]

Abstract: The increasing release of hazardous and toxic gases—such as volatile organic compounds (VOCs), NO_2, CO_2, NH_3, and H_2S—due to industrial activities poses serious risks to both environmental and public health. Effective and real-time monitoring of these pollutants is essential. Surface Acoustic Wave (SAW)-based sensors offer a promising solution, combining high sensitivity, wireless operation, and low power consumption. These devices detect changes in surface conditions—such as mass loading or conductivity—through variations in acoustic wave propagation, making them highly effective for gas sensing applications. This work focuses on tailoring advanced sensing materials and optimizing transducer architectures for SAW-based devices, specifically targeting environmental sensing technologies. Functional materials—including conductive polymers, semiconductors, and composites—are explored for their ability to enhance sensor performance in terms of selectivity, sensitivity, and long-term stability. These materials are engineered to respond selectively to specific target gases, enabling precise detection even in complex environments. Furthermore, the integration of SAW devices with wireless sensor networks (WSNs) and the Internet of Things (IoT) is discussed, highlighting their potential for scalable, remote environmental monitoring. This combined approach to material design and transducer engineering paves the way for next-generation smart, efficient, and application-specific environmental sensors.

Keywords: Surface acoustic wave, Gas sensor, Environmental monitoring, Sensing material.

[1]**Address:** Norwegian University of Science and Technology, Faculty of Engineering, Gjøvik/Norway
[2]**Address:** Gebze Technical University, Faculty of Science, Kocaeli/Turkiye

***Corresponding author**: onur.alev@ntnu.no

Analysis of G-Forces Acting on a Light Aircraft Pilot at Various Stages of Training, Including Glider Towing Operations

MICHAŁ SUJKOWSKI*[1]

Abstract: This article presents an analysis of G-Forces (accelerations) acting on a light aircraft pilot at various stages of training toward the Commercial Pilot License (CPL(A)), including glider towing operations. The theoretical section outlines the structure of flight training leading to the commercial license, with particular emphasis on supplemental training – especially glider towing – as a part of flight time building and gaining additional operational experience.Data collection was conducted using a custom-designed measurement device developed by the author, based on the MPU9250 sensor and Arduino Mega 2560 microcontroller, allowing for tri-axial acceleration recording. Additional data sources included a GPS-based flight data logger and video recordings of the instrument panel. Measurements were gathered during instructional training flights on Aero AT-3 and Cessna C150 aircraft, as well as during glider towing operations using the Yakovlev Yak-12M within the scope of dedicated training for the "glider towing" qualification.The study analyzed accelerations occurring in various phases of flight, including non-standard tasks such as simulated emergency scenarios. For glider towing flights, the analysis also considered atmospheric conditions and the specific nature of thermal-lift-oriented operations. The results indicate significant differences in acceleration profiles and increased pilot workload during towing missions. These findings may support the assessment of pilot suitability for subsequent training stages and contribute to the optimization of flight training programs.

Keywords: pilot training, in-flight accelerations, glider towing, light aircraft, flight dynamics

[1]**Address:** Silesian University of Technology, Faculty of Transport and Aviation Engineering, Department of Air Transport

***Corresponding author**: mail@mail.com

Drop of Life: A Centralized Mobile and Web Platform for Humanitarian and Blood Donations

TARIK BULJUBAŠIĆ, ALI JUSIĆ, ADEM SINANOVIĆ, ZEYNEP SAĞIR

Abstract: Effective and timely humanitarian aid and blood donations are essential to saving lives in crisis situations, yet current practices remain fragmented and vulnerable to fraud. Donation appeals are often scattered across social media, local networks, and isolated organizational channels, resulting in delayed information dissemination, limited visibility of urgent needs, and an estimated 10–15% of campaigns containing fraudulent elements. In Bosnia and Herzegovina, where 70% of blood supplies rely on family donations and no centralized system exists, these challenges are even more pronounced.

In order to address these issues, Drop of Life was developed,as a unified platform, featuring a cross-platform mobile-web system built with modern full-stack technologies, supported by a secure backend and centralized database.Donors can browse both humanitarian and blood donation campaigns, filter by urgency or blood type, and contribute funds or pledge blood in real time. Key features include a multi-step campaign verification process, real-time push notifications, instant fund transfers to organization accounts, and personalized alerts based on user profiles.

The project is currently in the advanced stages of development with a minimum viable product (MVP) nearing completion. Future performance will be evaluated using key indicators such as platform engagement, donation efficiency, system reliability, adoption by NGOs, and user satisfaction through surveys and retention metrics.

By consolidating donation workflows and enforcing strict verification, Drop of Life enhances transparency, accelerates interventions, and builds public trust. The platform directly supports the United Nations Sustainable Development Goals by promoting efficient resource mobilization and multi-stakeholder collaboration.

Keywords: donation platform; humanitarian aid; blood donation; real-time notifications; secure payments; data analytics

[1]**Address:** International University of Sarajevo, Faculty of Engineering and Natural Sciences, Sarajevo/Bosnia and Herzegovina

***Corresponding author**: btarik47@gmail.com

Assessment of the Impact of Temperature on the Performance of Photovoltaic Cells for Sustainable Energy Solutions

VEHEBI SOFIU, BESA VESELI, SAMI GASHI, NEXHAT BALAJ, MUHAXHERIN SOFIU

Abstract: Photovoltaic cells represent a key source of renewable energy; however, their performance is significantly affected by ambient and operating temperature. This study provides a detailed assessment of the impact of temperature on the efficiency of photovoltaic (PV) cells by combining experimental analyses—conducted in both controlled laboratory conditions and open environments—with a theoretical review of current literature. As temperature increases, the open-circuit voltage of solar cells drops due to higher charge carrier recombination, leading to reduced power output. The relationship between operating temperature and energy production has been found to be linear, with the PV material playing a crucial role in temperature sensitivity. The study evaluates temperature coefficients for monocrystalline modules and examines various mathematical models used to predict cell temperature in different PV system configurations, including free-standing panels and building-integrated systems. Furthermore, the geographic distribution of photovoltaic energy potential is explored, with consideration of how altitude and climate affect system performance. High-altitude regions—such as the Himalayas and Antarctica—typically offer better performance ratios due to lower operating temperatures, favoring more temperature-sensitive modules. The findings of this work contribute to the optimal selection of photovoltaic technology based on climate conditions and support the development of sustainable energy production solutions.

Keywords: Photovoltaic cells, operating temperature, electrical efficiency, temperature coefficient, energy performance, monocrystalline modules.

Address: UBT- University for Business and Technology, Faculty of Energy, Kalabria, 61, Prishtin, 10000, Kosovë

***Corresponding author**: besa.veseli@ubt-uni.net

Different Methods of Speed Control of Switched Reluctance Motors Drives: An Overview

BLERTA GËRMËNJI*[1], AIDA SPAHIU[2]

Abstract: Electric Drives with Switched Reluctance Motor (SRM) are driving innovation across industries and they are used in different applications such as: general purpose industrial drives; domestic drives: washing machines, vacuum cleaners; electric vehicle; aircraft applications; compressors, fans, pumps, centrifuges etc. Usage in important applications and the advantages of SRM motor like robust construction, easy maintenance and low cost, flexible controls, and the ability to operate in harsh environments such as high temperatures and high pressure made the SRM an alternative to both alternative and direct current machines used in adjustable electric drives. The SRM also comes with a few disadvantages among which torque ripple and acoustic noise are the most critical. The double saliency construction and the discrete nature of torque production by the independent phases lead to higher torque ripple compared with other machines. The aim of this paper is to present a literature review on the electric drives with SRM knowing that these electric drives are more efficient, reliable, and sustainable drives. In particular, the focus will be on the different methods of speed control of the electric drives with SRM. Based on the reviewed literature will be discussed the advantages, disadvantages and the performance of various types of speed control methods in terms of their efficiency, reliability and robust work for the different applications. The key contribution of the paper is to provide a valuable basis for detailed analyses of the electric drives with SRM focus on, advanced control, sensing technologies and sustainability.

Keywords: Switched Reluctance Motor, control method, applications, reviewed literature

[1]**Address:** Aleksandër Moisiu Durrës University, Faculty of Professional Studies, Durrës/Albania
[2]**Address:** Polytechnic University of Tirana, Faculty of Electrical Engineering, Tirana/Albania

***Blerta Gërmënji**: blertagermenji@uamd.edu.al

Techno-economic assessment of PHA production scenarios by utilizing extremophilic microorganisms

ABDULLAH BİLAL ÖZTÜRK[1,2], XENIE KOURILOVA[2], IVA BUCHTIKOVA[2], STANISLAV OBRUCA[2]

Abstract: This study investigates the techno-economic viability of varied polyhydroxyalkanoates (PHA) production scenarios from lignocellulosic biomass by utilizing extremophilic microorganisms. Microbial platforms characterized by halophilic and thermophilic properties, specifically *Halomonas halophila* and *Caldimonas thermodepolymerans*, were employed to eliminate issues related to sterility demands, process efficiency, and sustainability. Scenarios incorporating rice straw and discarded softwood, which are low-cost lignocellulosic feedstocks that do not interfere with the human food supply, were modeled as resources for PHA production. Additionally, a comparison was conducted between traditional chloroform extraction methods and environmentally friendly hypotonic lysis to recover PHA from extremophilic microbial cultures prone to this treatment. Economic indicators such as net present value (NPV), internal rate of return (IRR), and payback period (PB), were estimated to evaluate the financial viability of the proposed scenarios. Results clarify that incorporating extremophilic microorganisms alongside waste valorization techniques could make PHA production economically feasible, thereby decreasing dependence on fossil-derived plastics while simultaneously addressing environmental issues. This initial research demonstrates the necessity for subsequent scale-up investigations to authenticate the proposed methodology, which shows potential for the sustainable production of PHA.

Keywords: polyhydroxyalkanoates, process simulation, techno-economic assessment, Halomonas halophila, Caldimonas thermodepolymerans

[1]**Address:** Department of Chemical Engineering, Faculty of Chemical and Metallurgical Engineering, Yildiz Technical University, İstanbul/Türkiye
[2]**Address:** [2]Department of Food Chemistry and Biotechnology, Faculty of Chemistry, Brno University of Technology, Purkynova 118, 612 00 Brno, Czech Republic
***Corresponding author**:

Bridging Humans and Machines: Determinants of Collaborative Robot Acceptance

MURAT TAHİR ÇALDAĞ*[1]

Abstract: The emergence of collaborative robots (Cobots) is a modern concept based on human-machine interaction in a shared workspace. However, the antecedents of the idea behind robots assisting humans can be seen in the mythology and history of ancient Greece, Egypt, and China. The industrial revolutions and disruptive technological advancements presented new ways of production, logistics, and development. Cobots are one of the trending technologies providing ease of use and productivity gains with high-volume tasks. With the widespread of robotics, investments in Cobot technologies are predicted to rise to 7 billion $ in 2030. Even though the main adopter of Cobot technologies can be seen as manufacturing, other industries such as tourism, healthcare, logistics, education, and energy are providing innovative solutions with Cobot integrations. Cobots present opportunities such as increased productivity, enhanced worker safety, eco-friendly production, and ergonomic designs. However, there can be some drawbacks of Cobots as societal problems concerning worker unemployment, anxiety, social exclusions in the workplace, and mental health issues of workers. Also, investment and training costs can create significant burdens for small businesses. The aim of this study is to identify the determinants of Cobot acceptance and provide insights for further analysis. A systematic literature review (SLR) is conducted to identify the determinants influencing Cobot acceptance. The findings of the SLR presented the significant factors assisting the adoption decision of Cobots in various industries. Ease of use, product quality, mobility, flexibility, perceived safety, performance expectancy, decreased error rates, and innovativeness are some of the significant enablers of Cobot acceptance in businesses. Even though the benefits can provide increased customer satisfaction and competitiveness compatibility issues, infrastructural constraints, perceived anxiety, over-dependence, social exclusion, trust, financial costs, and fear of unemployment are some of the identified barriers to the acceptance of Cobots. Also, SLR results indicate the majority of the research in Cobot acceptance is conducted from individual perspectives. There is a research gap in organizational and national perspectives. This study provides significant insights and a comprehensive analysis of the literature for Cobot acceptance. The results of this study can be used as a foundation in various industries for individuals and businesses for Cobot acceptance decisions.

Keywords: Collaborative Robot, Technology Acceptance, Industry 4.0, Human-Machine Interaction

[1]**Address:** Başkent University, Department of Technology and Knowledge Management, Ankara/Türkiye

***Corresponding author**: mtcaldag@baskent.edu.tr

Analysis of the Eutrophication Process Progress in the Dal Lake, India

IRFAN ALI*[1], ELENA NEVEROVA-DZIOPAK[2], ZBIGNIEW KOWALEWSKI[3]

Abstract: Dal Lake, an iconic freshwater body is in the Himalayan region of Jammu and Kashmir in India, has been experiencing a significant ecological change due to the elevated level of eutrophication. The main cause of eutrophication are different human activities in the lake catchment area, intensive lake resources exploitation, and the lack of integrated water management strategy. Such stress factors bring to adverse negative changes in the lake ecosystem functioning, which in turn contributes to problems with drinking water supply, fishing, tourism sector development and general deterioration of residents' living conditions. The study presents the results of analysis of eutrophication process development in the Dal Lake and its separate basins for the period 2019 – 2023. The methodology used for trophic status assessment was based on the Index of Tropic State (ITS); the data bank for analysis consisted of five-year lake monitoring data. The results revealed the steady significant growth of the tropic level in separate basins and lake as a whole during the period considered. The results highlight a very disturbing trend of ecosystem degradation due to anthropogenic activities, additionally intensified by climate change. The actual Dal Lake ecosystem status emphasizes the necessity for elaboration of basin-specific management solutions to alleviate eutrophication and maintain the unique ecosystem of the Dal Lake. The spatio-temporal approach and applied assessment methodology offers significant insights for policymakers and environmentalists seeking to repair and maintain the integrity of this essential freshwater resource.

Keywords: Dal lake, Eutrophication, Tropic state assessment, Management strategy

[1]**Address:** AGH University of Krakow, Faculty of Geo-Data Science, Geodesy and Environmental Engineering
[2]**Address:** AGH University of Krakow, Faculty of Geo-Data Science, Geodesy and Environmental Engineering
[3]**Address:** AGH University of Krakow, Faculty of Geo-Data Science, Geodesy and Environmental Engineering

***Corresponding author**: aliirafn@agh.edu.pl

Cultural eutrophication treatment with innovative clay-based materials

IEROTHEOS ZACHARIAS[1*], BILIANI IRENE[1]

Abstract: Anthropogenic activities in aquatic ecosystems deteriorate water bodies' quality status through sewage discharge, deposition of suspended or heavy materials, fertilizers run-offs, and many others, emphasizing the urgent need for restoration applications. Today, scientists have concluded that marine and inland water bodies' cultural eutrophication treatment can be achieved by applying innovative natural clay-based materials. Zeolite, Bentonite, Perlite, and Calcite have been proven to absorb nutrients from aquatic environments for ecosystem restoration applications. The BLUE-GREENWAY Project tests some of the above materials because they present many advantages: ecologically friendly materials, low cost, and easily accessible. Their applications for freshwaters restoration consist of both natural and modified. The primary purpose of this work is to present natural and modified clay materials that have been successfully applied to laboratories and aquatic environments. This study compares the adsorbance efficiency of nitrogen and phosphorus loads found within the water column under different environments. The results indicate that successful application is highly linked with the aquatic environment's initial conditions. Treatment with clay-based materials can be performed in a time-effective process provided that the sources of eutrophication are also treated.

Keywords:

[1]Address: [1]Laboratory of Environmental Engineering, Department of Civil Engineering, University of Patras, University Campus, 26500, Patras, Greece

***Corresponding author**: izachari@upatras.gr

Electrochemical Immunosensor for HE-4 Detection: A Practical and Cost-Effective Approach

BURÇAK DEMİRBAKAN *[1]

Abstract: Human Epididymis Protein 4 (HE-4) is widely utilized in gynecologic oncology and cancer diagnostics, particularly for the detection and monitoring of ovarian and endometrial cancers. Due to its high specificity, HE-4 serves as a valuable biomarker for early diagnosis and disease monitoring. The objective of this research is to develop an immunosensor for the detection of the HE-4 antigen. For this purpose, an indium tin oxide-polyethylene terephthalate (ITO-PET) working electrode—selected for its practicality, affordability, and high sensitivity—was modified using Carboxyethylsilanetriol (CESE) 1-Ethyl-3-(3-dimethylaminopropyl)carbodiimide (EDC), and N-Hydroxysuccinimide (NHS). All parameters, which are concentrations and incubation times of the proposed immunosensor, were optimized. Electrochemical impedance spectroscopy and cyclic voltammetry techniques were employed to monitor the immobilization process and to perform the analytical characterization of the designed immunosensor system. The analytical characterization studies, including repeatability, reproducibility, and the linear detection range (0.01 fg/mL - 25 fg/mL), demonstrated that the designed biosensor possesses an ultra-wide detection range and exhibits practicality, stability, and high sensitivity. Additionally, the applicability of the biosensor system was tested in commercial human serum samples, yielding promising results that support its potential use in clinical applications.This study highlights the significance of developing advanced biosensing platforms for cancer biomarker detection, contributing to the ongoing efforts to improve early diagnosis and personalized medicine approaches.

Keywords: Ovarian cancer, indium tin oxide-polyethylene terephthalate, immunosensor, Human Epididymis Protein 4

[1]**Address:** Çanakkale Onsekiz Mart University, Faculty of Engineering, Çanakkale/ Türkiye

***Corresponding author**: burcakdemirbakan@comu.edu.tr

Electrochemical Biosensor Platform for CA125 Detection: A Promising Tool for Ovarian Cancer

BURCU EROĞLU*[1]

Abstract: Ovarian cancer is the leading cause of mortality associated with gynecological cancers. Ovarian cancer is a malignancy that originates in the ovary and cellular proliferation that occurs in the ovaries. Although ovarian cancer is not one of the most common gynecological cancers in women, it has the highest mortality rate. The main reason for this is that the disease is usually silent and does not cause any obvious symptoms in its early stages. Therefore, early diagnosis is of critical importance for this cancer. For the diagnosis of ovarian cancer, Cancer Antigen 125 (CA125) protein has recently gained acceptance as biomarkers owing to their excellent specificity. The goal of this research is to create an immunosensor that can detect CA125 antigen. For this purpose, the indium tin oxide-polyethylene terephthalate (ITO-PET) working electrode, which is preferred due to its practicality, cheapness and high sensitivity, was modified with 3-mercaptopropyldimethoxysilane (3-MPDS) agent and N-Hydroxysuccinimide (NHS). Electrochemical impedance spectroscopy and Cyclic voltammetry techniques were used to follow the immobilization steps and determine analytical characterization of the designed immunosensor system. To obtain a linear and stable immunosensor system all effective parameters were optimized. The results obtained from analytical characterization studies such as repeatability, reproducibility and linear range (0.5 fg/mL- 500 fg/mL) prove that the designed biosensor has an ultra-wide detection range, is practical, stable and sensitive. The applicability of the designed biosensor system to the commercial human serum was also tested and obtained promising results.

Keywords: Ovarian cancer, indium tin oxide-polyethylene terephthalate, biosensor, Cancer Antigen 125

[1]**Address:** Çanakkale Onsekiz Mart University, Faculty of Engineering, Çanakkale/ Türkiye

***Corresponding author**: burcuozcan@comu.edu.tr

Hydrothermal Carbonization of Cow Manure: A Sustainable Pathway for Waste Valorization

MEHBOOB IQBAL[1*], ROBERT JUNGA[2], MAŁGORZATA WZOREK[1]

Abstract: This study investigates and explores the feasibility of hydrothermal carbonization as a sustainable approach for the valorization of cow manure. Experiments were conducted in a 2-liter batch Parr reactor under varying conditions, including reaction times of 60 to 120 minutes, solid-to-liquid ratios ranging from 1:5 to 1:9, and a constant reaction temperature of 200 °C. The results demonstrated an increase in carbon content from 44.60% to 51.35%, along with enhanced energy densification of the produced char. The higher heating value of the produced chars ranged from 19.11 to 20.50 MJ/kg. The maximum energy yield of 58.46% was achieved at a solid-to-liquid ratio of 1:5 and a 60-minute reaction time, suggesting that shorter processing times may be more efficient for char production.

Keywords: hydrothermal carbonization, cow manure, char and waste valorization.

[1]**Address:** Department of Process and Environmental Engineering, Opole University of Technology, 5 Mikołajczyka St, 45-271, Opole, Poland
[2]**Address:** Department of Thermal Engineering and Industrial Facilities, Opole University of Technology, 5 Mikołajczyka St, 45-271, Opole, Poland

***Corresponding author**: m.iqbal@student.po.edu.pl

Comparative Assessment and Use Cases of Hyperledger Blockchain Frameworks

ZEKİYE CEREN ULUDOĞAN[1], SADETTİN MELENLİ[1], ALİ HAKAN IŞIK*[1]

Abstract: Blockchain technology is increasingly used in various sectors such as finance, healthcare, supply chain and public administration by providing secure, transparent and decentralized data management. In terms of enterprise solutions, open source projects are of great importance, and Hyperledger is one of the most comprehensive initiatives in this field. The Hyperledger project, supported by the Linux Foundation, consists of a series of frameworks and tools developed for enterprise blockchain applications. In this study, the most widely used frameworks in the Hyperledger ecosystem, Fabric, Sawtooth, Indy, Iroha and Besu, are discussed. The architectural structure, consensus mechanisms, security features and usage areas of each framework are examined in detail and the main differences between them are compared. For example, Hyperledger Fabric offers scalable solutions thanks to its modular structure, while Sawtooth draws attention with its innovative PoET (Proof of Elapsed Time) consensus algorithm. While Indy is optimized for identity management applications, Iroha focuses on integration with mobile devices. Besu addresses financial and enterprise use cases thanks to its Ethereum compatibility. Hyperledger's permissioned blockchain structures provide great advantages in terms of data security and privacy, and are also evaluated in terms of scalability and flexibility. In addition, use cases of Hyperledger technology in areas such as supply chain management, health records, financial services and identity verification are discussed. The study discusses the future potential of the Hyperledger ecosystem, current challenges in this area and its impact on academic research. This study provides a comprehensive resource for researchers and industry professionals who want to evaluate blockchain technology from an institutional perspective.

Keywords: Blockchain, Hyperledger, Fabric, Sawtooth, Indy, Iroha, Besu, Consensus Mechanisms

[1]**Address:** Burdur Mehmet Akif Ersoy University, Institute of science, Burdur/Türkiye

***Corresponding author**: ahakan@mehmetakif.edu.tr

BioPrint Life for Space Exploration

JULIA GODZWON*[1], JOANNA SZCZEPAŃSKA [1], OLIWIA PAJĄK [1]

Abstract: 3D bioprinting represents an innovative additive manufacturing technique with proven potential in tissue engineering and regenerative medicine. As this technology advances, it could enable the development of functional organs in space, allowing astronauts to print tissues for medical treatments, including organ transplants and wound healing.

The BioPrintLife project addresses key limitations of current bioprinting technology, specifically high costs and limited bioink availability. We develop eco-friendly bioinks composed of hydrogels containing live bacterial cultures that maintain functional properties while reducing costs.

We have successfully optimized alginate and gelatine-based hydrogels, enhancing their rapid crosslinking capabilities, injectability, and viscosity control to ensure structural integrity and cell viability following extrusion. Initial experiments with E. coli and S. aureus bacteria cultures demonstrate the bioinks' capacity to maintain cell viability. Responses to relevant stressors have been tested, including UV exposure, methacrylate, photoinitiator, and antibiotics. Subsequent research will incorporate more complex cellular systems and evaluate performance under microgravity conditions.

Bioprinting technology holds immense potential for long-term space missions, enabling on-demand production of biomaterials, pharmaceuticals, and tissues for medical treatments. This work paves the way for sustainable and independent crew healthcare during extended space travel and extraterrestrial colonization, by reducing reliance on Earth-based supplies.

Keywords: bacteria, bioprinting, hydrogels, tissue engineering

[1]**Address:** AGH University of Krakow, Faculty of Materials Science and Ceramics, Cracow/Poland

***Corresponding author**: juliagodzwon@student.agh.edu.pl

Surface Defect Detection in Steel Manufacturing Industry Using Deep Learning

PORCHELVI N, NAVEENKUMAR S, MELWIN DANIEL R, NEEREJ S

Abstract: Steel surface defect detection is important in maintaining product quality and maximizing production processes. Being based on human vision or outdated computer vision algorithms, traditional inspection methods are inefficient, prone to errors, and not scalable. For precise steel surface fault detection and categorization, this project proposes a mechanized deep learning technique from ResNet-18. The NEU Surface Defects Database of six defects—scratches, pitted surfaces, rolled-in scale, patches, inclusions, and crazing—is used to train and validate the models. Flipping, rotation, and contrast data augmentation methods are utilized to boost model generalisation. Grad-CAM has also been utilized for visualising defect positions to enhance interpretability. The proposed ResNet-18 model in this work is more robust than common CNN architectures regarding the accuracy of locating defects as well as being cost-effective. ResNet-18 is a specific and high-resource steel quality check platform for efficient smart manufacturing without defects against the traditional methods.

Keywords:

[1]**Address:** Ponamalle, Chennai, India

***Corresponding author**: naveenkumarsbtech@gmail.com

Investigation of the Thermal Performance and Flow Characteristics of a Tall Building with Facades Positioned at Various Angles

MOHAMMAD SAMI[1], MOHAMMAD KHATTAB[1], MAHDI TABATABAEI MALAZI[1]

Abstract: This study examined the impact of facades on the flow behavior surrounding a standard tall building model having facades. The objective of the study is to decrease wind loads while enhancing energy savings and natural ventilation. The aerodynamics and thermal performance of buildings with facades were analyzed under different wind speeds, façade orientations, and ambient temperatures. The drag force, velocity, pressure, and temperature distribution around the building were calculated using computational fluid dynamics (CFD) approaches. The realizable k-ε turbulence model was used to simulate turbulent flow around the building with facades. Research findings indicate that wind velocity and facade positioning significantly affect drag force and temperature distributions. The building faces a significant increase in pressure when wind speed increases from 1 to 5 m/s. The building undergoes a notable reduction in temperature when wind velocity rises from 1 to 5 m/s. The information provided aims to improve wind management by passive flow control techniques, minimize building weathering, reduce wind load, enhance natural ventilation, save energy, and offer building designers a comprehensive selection of computational simulations.

Keywords: Computational Fluid Dynamics (CFD), Facade design, Wind load reduction, Natural ventilation

[1]**Address:** Department of Mechanical Engineering, Faculty of Engineering Istanbul Aydin University, Istanbul, 34295, Turkey
***Corresponding author**: mohammadkhattab@stu.aydin.edu.tr

Metal(loid) immobilization in severely contaminated soils under various environmental conditions: efficiency of commercial, synthesized, and waste-derived (in)organic amendments

SZIMONA ZARZSEVSZKIJ[1], MARTINA VÍTKOVÁ[1], ANNA KARLOVA[1], BARBORA BÖSERLE HUDCOVÁ[1]

Abstract: Chemical immobilization is a cost-efficient, sustainable, and environmentally friendly alternative to traditional soil remediation techniques especially at large and severely polluted areas. It utilizes soil amendments to capture and/or transform pollutants to reduce/prevent their leachability, mobility, availability, and toxicity. However, the immobilization efficiency is influenced by a complexity of factors, requiring a comprehensive assessment of amendments prior to their full-scale application. Therefore, we tested various (in)organic amendments under varying environmental and geochemical conditions to elucidate on their suitability for soil remediation. The effects of soil moisture, soil properties, and contamination type and level on metal(loid) immobilization were assessed by laboratory soil incubation experiments. For sustainability and circularity, waste materials (iron-chips, iron-mud, sludge-char, compost) were tested along with commercial/synthesized products (nanoscale zerovalent iron (nZVI), biochar (BC), and BC composites (nZVI-BC and Fe/FeS-BC)). Moreover, a field experiment involving composted sewage sludge application to a degraded brownfield soil was conducted to assess its overall effects on soil quality. Metal(loid) mobility and availability were assessed by traditional single and sequential soil extractions/leaching tests and the diffusive gradients in thin films (DGT) technique. Metal(loid) sorption in the solid phase was analyzed by scanning electron microscopy (SEM), and geochemical modeling was used to predict solid/liquid speciation and solubility controlling phases of the metal(loid)s. The overall results showed that soil properties including moisture content, redox potential, pH, organic and mineral contents; metal(loid) type and concentration; and amendment characteristics have significant effects on amendment efficiency. Generally, iron-based amendments exhibited close to 100% immobilization efficiency, while organic amendments increased metal(loid) availability in most cases, which, however, was overcome by combining them with iron-based amendments. SEM confirmed metal(loid) associations with iron phases, many of which were predicted as solubility-controlling phases. Metal(loid) mobility in the field experiment showed a seasonal trend over 2.5 years, driven by the interactions between metal(loid)s and organic matter and influenced by (a)biotic factors. In conclusion, metal(loid) immobilization in severely polluted soils is feasible, but a complex and challenging task calling for further research, especially in multiple-elements contaminated soils and under real and long-term conditions.

Keywords: adsorption, stabilization, sorbents, PHREEQC, Visual MINTEQ, risk elements

[1]**Address:** Department of Environmental Geosciences, Faculty of Environmental Sciences, Czech University of Life Sciences Prague, Kamýcká 129, 165 00, Praha – Suchdol, Czech Republic

***Corresponding author**: zarzsevszkij@fzp.czu.cz

Analysis Of The Components Constituting Drill Bit Geometry In Drilling Ti6Al4V Titanium Alloy By Finite Elements Method

TUNCER DEMİREL*[1], ABDULLAH KURT[2]

Abstract: In this study, the effects of the components constituting the drill bit geometry in the drilling operations performed under the coolant of Ti6Al4V Titanium alloy were investigated by means of finite element assisted simulations. Different combinations of notch angle, web thickness and splitting angle were used as determinants of drill bit geometry, while tool models with other geometric properties kept constant were analyzed with outputs such as thrust force, torque and temperature. The data analyses and simulations obtained as a result of drilling were performed using ThirdWave Advantedge software. In the simulations performed, split-tip, two-flute, helical and solid carbide drills with a diameter of 6.8 mm were preferred using different parameters such as notch angle (30°,45°,60°), web thickness (0.5;1.0;1.5 mm) and splitting angle (120°,135°,150°). As a result; while high thrust forces were observed as a result of simulations performed with tool designs with a notch angle of 30° and 60°, web thickness of 0.5 and 1.5 mm, and splitting angles of 120° and 150°, which are the components constituting the drill bit geometry, lower thrust forces were determined as a result of simulations performed with tool designs with a notch angle of 45°, web thickness of 1.0 mm and splitting angle of 135°. When torque values were analyzed; similar results were obtained with thrust forces. When the temperature values are analyzed, high temperature values are observed as a result of simulations performed with tool designs with notch angles of 30° and 60° and splitting angles of 120° and 150°, while lower temperature values are obtained as a result of simulations performed with tool designs with a notch angle of 45° and splitting angle of 135°. However, an increase in temperature values was observed as the web thickness increased.

Keywords: Drilling, Drill Bit Geometry, Ti6Al4V, Notch Angle, Web Thickness, Splitting Anle

[1]**Address:** Baskent University, Kahramankazan Vocational School, Ankara/Türkiye
[2]**Address:** Gazi University, Faculty of Technology, Department of Manufacturing Engineering, Ankara/Türkiye

***Corresponding author**: tuncerdemirel@baskent.edu.tr

Rocket Design Optimization

SÜREYYA SEVİNÇ VAROL*[1], BİLGE ALBAYRAK ÇEPER[2]

Abstract: Studies on rockets are accelerating with the development of new technologies. At the forefront of these developments are optimization studies that emphasize time saving. By using various optimization methods, rockets with high performance are produced at low cost. Wings, which are an important component of rockets, are exposed to high stresses during flight. High stresses cause damage to the wing structure and adversely affect the flight performance. This study focuses on the optimization of a conical arrow-shaped wing. In the study, a CAD structure was created in accordance with the wing dimensions. With ANSYS software, the amount of stress on the model was determined and the regions subjected to maximum stress were determined. With the optimization study, improvements were made on the regions exposed to maximum stress and a new wing model was created. The maximum stresses of the original wing structure and the optimized wing structure are given graphically. The outputs of both models are compared and the amount of improvement on the model is emphasized. The optimization study was carried out with ANSYS Topology Optimization and nTop programs. It is aimed to prove the accuracy of the results by utilizing two software programs that use different algorithms and approaches.

Keywords: Conical Arrow-Shaped Wing, Maximum Stress, Rocket, Topology Optimization

[1]**Address:** Erciyes University, Faculty of Aeronautics and Astronautics, Kayseri/Turkiye

***Corresponding author**: sureyyavarol@erciyes.edu.tr

Electron Transfer In A Periodic Electronic System Containing Two Defects With High Performance

ABDELOUAHID EZZARFI[1,3*], YASSINE BOUCHAFR[1], FATIMA ZAHRA ELAMRI[1], YOUSSEF BEN-ALI[1,2], DRISS BRIA[1]

Abstract: This article presents a theoretical analysis of the impact of defect layers on electronic states in CdTe/CdMnTe multi-quantum wells (MQWs). The approach employed is based on transfer matrices. The incorporation of one or two defect layers into periodic structures comprising quantum wells (CdTe) and barriers (CdMnTe) is demonstrated to alter the band structure, resulting in the formation of localized states within the band gaps. The influence of defect thickness and concentration on the formation of localized states within the band gaps is also demonstrated. The results revealed that thicker defects tend to shift the energies of localized states towards lower values, while increased concentrations of defects have the effect of raising these energies. It is evidenced that configurations comprising identical defect types are capable of producing highly transmissive localized states under specific conditions of thickness and concentration. Furthermore, structures incorporating different defect types are shown to yield distinctive patterns of localized states, particularly when the parameters of the defects are optimized. This study highlights the potential for MQWs to be utilized in applications such as frequency-selective filters, waveguides, and photonic devices, emphasizing the significance of defect engineering in tailoring electronic properties for advanced technologies.

Keywords: Multi Quantum Wells; Defect thickness; Localized states; Transmission coefficient

[1]**Address:** Laboratory of Materials, Waves, Energy and Environment, Team of Acoustics, Photonics and Materials, Faculty of Science, Mohamed First University, Oujda, Morocco
[2]**Address:** Engineering Sciences Laboratory (LSI), Multidisciplinary, Faculty of Taza, Sidi Mohamed Ben Abdellah University, Morocco
[3]**Address:** Higher Institute of Nursing and Health Technology Professions, Rabat, Morocco

***Corresponding author**: a.ezzarfi@yahoo.fr

The Impact of Artificial Intelligence on High School Students' Education and Career Choices

METEHAN KARTAL[1], ASLIHAN ARSLAN KARTAL[2], NESLİHAN BOZDAĞ ÇİMEN*[1]

Abstract: Artificial intelligence is the ability of a computer or computer-controlled robot to perform tasks typically associated with intelligent beings, and it is a technological model where certain features developed by humans are taught and then enhanced according to their areas of application to be presented to people. Artificial intelligence (AI) enables certain tasks that a human can perform to be done more quickly with more data, and it can facilitate individuals' lives with applications such as updatable and customizable voice assistants, language translations, recommendation systems, navigation, social security, healthcare, e-commerce, and assistive robots [1-3]. It is believed that artificial intelligence can enhance both learning and teaching, and help develop the best programs for students and teachers in the field of education. However, it is also stated that artificial intelligence is controversial in some aspects such as the role of teachers in education, data privacy, and ethics [2]. This study is a research that evaluates the adoption, use, emotional effects, and potential impacts on future career choices of artificial intelligence in education by students. The research was conducted with 10th grade students of Denizli Hasan Tekin Ada Anatolian High School during the 2024-2025 academic year. A total of 15 questions were administered in the form of a survey, with three being open-ended and twelve multiple-choice, and 157 students participated on a voluntary basis. The students' perspectives on artificial intelligence, its contributions and drawbacks to education, emotional effects such as fear, happiness, anxiety, and its impact on career choices have been evaluated and compiled based on the responses given. Students describe artificial intelligence as a sea of information and a useful technology that makes life easier, while also expressing it as an emotionless, conscious, dependency-increasing, thought-reducing, and concerning companion. The students' perspectives on artificial intelligence, its contributions and drawbacks to education, emotional effects such as fear, happiness, and anxiety, and its impact on career choices have been evaluated and compiled based on the responses given. While students describe artificial intelligence as a sea of information and a useful technology that makes life easier, they also express it as an emotionless, conscious, addiction-increasing, thought-reducing, and concerning companion. Out of the 157 students who participated in the survey, 145 use an AI-supported application in education. The usage rates are 33% every day, 47% a few times a week, 18% once a month, and 2% never. 15% of the students think that artificial intelligence could negatively affect education, while 49% are undecided. 54% of students think that artificial intelligence could replace professions, and 60% say it would affect their own career choices. Teachers are expected to use AI-supported applications while teaching, but the replacement of teachers by AI technologies is not desired. Students who participated in the survey do not want to give up on their teachers and the teaching profession, who care about their moods and feelings, equip them with original ideas, and prepare them for life, no matter how advanced artificial intelligence and technology become.

Keywords: Artificial intelligence, high school student, education, future

[1]**Address:** Hasan Tekin Ada Anadolu Lisesi, Yunus Emre Mah. 6461 Sk. No 2/A Denizli/Türkiye
[2]**Address:** PamukkaleUniversity, Science Faculty, Denizli/Türkiye

***Corresponding author**: Neslihan.Bozdağ@hotmail.com

Health Effects of Elevated Fluoride in Municipal Drinking Water: A Risk-Based Approach to Water Safety Management

IWONA KLOSOK-BAZAN*[1], IZABELA ZIMOCH[2]

Abstract: This study evaluates the health impact of elevated fluoride concentrations in municipal drinking water using a risk-based approach. The research focuses on hazard identification, exposure assessment, and risk characterization to determine the potential adverse effects of prolonged fluoride consumption. A review of literature and historical water quality data analysis was conducted to assess fluoride levels and their health implications, considering geological and anthropogenic sources. Findings indicate that fluoride concentrations in the studied water supply fluctuate significantly, with some samples exceeding recommended limits. While moderate fluoride levels (below 2 mg/L) provide dental health benefits, higher concentrations pose risks, particularly for vulnerable populations such as children. Prolonged exposure to fluoride levels above regulatory thresholds increases the likelihood of dental and skeletal fluorosis, with the severity of effects dependent on age, exposure duration, and cumulative intake from other sources like food and dental products. A quantitative risk assessment was conducted using the hazard quotient (HQ) method, evaluating daily fluoride intake across different age groups. The analysis revealed that while the general population faces minimal health risks, young children are more susceptible to mild to moderate dental fluorosis when consuming water with fluoride levels exceeding 2 mg/L. Risk mitigation strategies include implementing water treatment technologies to reduce fluoride levels, public awareness campaigns on dietary fluoride intake, and promoting alternative drinking water sources for high-risk groups. The study emphasizes the need for continuous water quality monitoring and regulatory compliance to ensure public health protection. Recommendations highlight a multi-faceted approach, integrating technological interventions and public health policies to manage fluoride exposure effectively. These findings provide valuable insights for policymakers and water management authorities in developing strategies for safe drinking water supply while minimizing potential fluoride-related health risks.

Keywords: fluoride, drinking water, risk assessment, health effects

[1]**Address:** Opole University of Technology, Faculty of Mechanical Engineering, Department of Thermal Engineering and Industrial Facilities, Mikolajczyka 5, Opole 45-271, Poland
[2]**Address:** Silesian University of Technology; Faculty of Energy and Environmental Engineering; Institute of Water and Wastewater Engineering, Konarskiego 18, Gliwice 44-100, Poland

***Corresponding author**: i.klosok-bazan@po.edu.pl

Legionella Bacteria in Drinking Water – A Contemporary Public Health Threat

IZABELA ZIMOCH*[1], EWA ŁOBOS-MOYSA[1]

Abstract: This paper presents an analysis of public health risks associated with the presence of Legionella bacteria in drinking water systems. Particular attention is given to the issue of colonization within internal water installations and the lack of effective procedures for managing microbiological risks. Legionella is a widely distributed waterborne bacterium that finds favorable conditions for growth in water distribution systems, especially in domestic hot water installations. The study discusses current national and European legal frameworks, including the requirements of Directive 2020/2184 on the quality of water intended for human consumption, which obligates EU Member States to implement risk assessment and management systems across the entire water supply chain, including internal building plumbing. The analysis highlights the insufficient use of epidemiological data in Poland and the lack of detailed guidelines on prevention, monitoring, and response to contamination by Legionella spp. The article also presents data from selected countries (including the USA and Germany), where comprehensive monitoring of Legionnaires' disease has been conducted for years. It shows that the actual number of cases may be significantly underestimated due to limited diagnostic practices and the absence of systematic disease reporting procedures. The need to establish a nationwide support system for water quality management and databases enabling microbiological risk assessment is strongly emphasized. The article concludes with a call for urgent inclusion of Legionella-related issues in national public health strategies, as well as in technical, environmental, and health education.

Keywords: Legionella, water quality, public health, risk management, water supply systems, Directive 2020/2184, Legionnaires' disease, drinking water

[1]**Address:** Silesian University of Technology; Faculty of Energy and Environmental Engineering; Institute of Water and Wastewater Engineering, Konarskiego 18, Gliwice 44-100, Poland

***Corresponding author**: izabela.zimoch@polsl.pl

Electrolysis Unit Design to Improve The Combustion Process in a Diesel Engine

TALİP AKBIYIK*[1], NAFİZ KAHRAMAN[2], TARIK TANER[1], AHMET BÖĞREK[3]

Abstract: In recent years, the climate change problem that our world has faced and the measures that are being developed against this problem have attracted the attention of researchers. The most important factor affecting climate change is the pollutant emissions resulting from combustion. Natural gas is largely used to reduce pollutant emissions resulting from home heating, and gasoline and diesel used in internal combustion engines are also classified as hydrocarbon fuels. The carbon atoms found in these fuels react with oxygen and release CO2 gas as a result of complete combustion. This emerges as the most important cause of the problem called the greenhouse gas effect. Theoretically, just like the CO2 gas resulting from complete combustion, CO gas is also released as a result of incomplete combustion. This gas also has a negative effect on the environment. In the studies conducted, there are many studies, especially on engine technologies, in the field of low-emission combustion. Due to the high flame temperatures that occur in these studies, the amount of NOX gas from pollutant emissions increases. The study conducted aims to reduce emission values and increase performance by improving the combustion process in diesel engines. In order to improve the combustion processes in a diesel engine, an electrolysis unit was designed and the distance between the plates was changed as (2, 4, 6, ...) and KOH and NaCl were added to the electrolyte liquid as catalysts at different rates per liter (5, 10, 15, 20, 25, 30, 35 and 40) in the experiments. Constant voltage (3, 6, 9, ... 27, 30 V) and constant current (5, 10, 15, 20, ... 45, 50 A) were applied from the variable power source. The amount of HHO produced was measured with a gas flow meter and the data was recorded. The ideal rates were determined.

Keywords: Diesel engine, HHO, Emission, Alternative Fuels, Combustion Efficiency.

[1]**Address:** Aksaray University, Vocational School of Technical Sciences, Aksaray/Türkiye
[2]**Address:** Erciyes University, Faculty of Aeronautics and Astronautics, Kayseri/Türkiye
[3]**Address:** Ondokuz Mayıs University, Vocational School of Information Technologies, Samsun/Türkiye

***Corresponding author**: talipakbiyik@aksaray.edu.tr

Investigation of a Rocket with Different Nose Cone-Wing Configurations

SÜREYYA SEVİNÇ VAROL*[1], BİLGE ALBAYRAK ÇEPER[1]

Abstract: It is well known that the nose cone and wings significantly affect the flight performance of rockets. For this reason, when designing a rocket, these parts must be selected according to the rocket's intended use. Changes in the nose cone and control surfaces cause changes in the center of gravity and center of pressure. These changes lead to an increase or decrease in the static margin. This causes changes in the stability of the rocket. To ensure stable flight, the appropriate combination must be determined. Various studies have been conducted on the effect of nose cone (conical, ogive, elliptical, etc.) and wing (rectangular, trapezoidal, arrow-shaped, etc.) structures on rocket performance. In this study, a rocket model was created using the OpenRocket program. Four different configurations were created using two nose cones and two wing structures on the model. Separate flight simulations were performed for each configuration using the OpenRocket program. The simulation results (velocity off rod, agogee, velocity at deployment, optimum delay, maximum velocity, maximum acceleration time to apogee, and flight time) are presented in a table. The Stability vs. Time graphs obtained from the program were analyzed, and the stabilities of the configurations were compared. As a result of the comparison, the optimal configuration was determined.

Keywords: Rocket, Nose-cone, Wings, OpenRocket, Stability

[1]**Address:** Erciyes University, Faculty of Aeronautics and Astronautics, Kayseri/Türkiye

***Corresponding author**: sureyyavarol@erciyes.edu.tr

Essential oil properties of Thymbra spicata var. spicata plant and usage areas of some taxa

ZEKİ SEVEROĞLU[1*], ÖMER KILIÇ[2], TALİP ŞAHİN[3], BAHAR ILKINER[4], ASLI GÜL ACAR[5], KADYRBAİ CHEKİROV[6]

Abstract: In this study, the essential oil composition of Thymbra spicata var. spicata, a species belonging to the Lamiaceae family, was investigated. In addition, the biological activities and usage areas of certain taxa belonging to the genus Thymbra L. were explored. The plant material was collected from the Çelikhan district (Adıyaman, Turkey), and essential oil was obtained via hydrodistillation. The composition of the oil was analyzed using the GC-MS (Gas Chromatography-Mass Spectrometry) method. From 100 g of plant material, 0.4 ml of essential oil was obtained, indicating that the plant is rich in essential oils. A total of twenty-two components were identified in the essential oil, with the main constituents being carvacrol (29.59%), terpinene (18.60%), and p-cymene (9.61%). The findings are consistent with those of Ünlü et al., particularly regarding the high concentration of carvacrol. While both studies share carvacrol and p-cymene as common major components, differences were observed in the presence of trans-caryophyllene and γ-terpinene as major constituents in our study. The composition and amount of essential oils can vary depending on the species, the plant part used, the production method, climatic conditions, and the geographical characteristics of the growing area. The studied Thymbra spicata plant was found to be rich in both the quantity and chemical diversity of essential oil components, suggesting its high economic value.

Keywords: Thymbra spicata var. spicata, Lamiaceae, Essential oil, Hydrodistillation, GC-MS analysis

[1]**Address:** Marmara University, Faculty of arts and sciences, Department of Biology / Manas University, Faculty of arts and sciences, Department of Biology, Istanbul/Türkiye
[2]**Address:** Adiyaman University, Faculty of Pharmacy, Department of Pharmaceutical Botanic, Adiyaman/Türkiye
[3]**Address:** Adiyaman University, Faculty of arts and sciences, Department of Biology, Adiyaman/Türkiye
[4]**Address:** Adiyaman University, Faculty of arts and sciences, Department of Biology, Adiyaman/Türkiye
[5]**Address:** Uludag University, Gemlik Asim Kocabiyik Vocational School, Bursa/Türkiye
[6]**Address:** Kadyrbai Chekirov, Kyrgyz-Turkish Manas University, Bishkek, Kyrgyz Republic

***Corresponding author**: zseveroglu@marmara.edu.tr

Why fundamental methodologies of sustainability should resemble those of military logistics

ZOLTÁN BODROG*[1], CSILLA MILE[2], ANDREA TICK[3]

Abstract: Sustainability, especially climate sustainability is the largest-ever and the most complex management task for humanity. Moreover, the survival of our society as we know it now is at stake, and according to the scientific consensus, the task is extremely urgent. The most stringent quality of this urgent task is that it comes with well-defined deadlines with respect to the global trajectory. This all should give more than enough motivation to take this huge task seriously, but the most important obstacle on the way is consumerism, that means the society itself we live in and we want to conserve. The deadlines mentioned above are near, but humanity is so slow to react, that it is not far from the truth to say that we are in a paralyzed state. What can be the most relevant and efficient answer to this situation at the strategic level? The overall deadlines must be broken down into subprocesses in all the aspects of sustainability, e.g. to trajectories of industries, other activities, regions, countries, etc., down to everyday projects, developments and functioning of our economy and society, regardless of how hard the resulting requirements seem. Ultimately, these subtrajectories have to be planned in detail, monitored, regularly evaluated, and tightly controlled. The above-outlined deep and sophisticated control of these processes in every industrial and societal level resembles logistical requirements of military supply, especially in wartime. All the subsystems of military logistics build upon the idea that products of them contain fulfillment of deadlines as a definitive property: a product (or a service) in military logistics is flawed, and therefore uncompleted as a task, if it is not fully finished on time. Fulfillment beyond deadline is not fulfillment. As a consequence, we have to build the fundamentals of military logistics into every aspect of everyday sustainability management as principles, in order to be able to include sustainability goals. In our paper, we give a quick overview about how this fundamental inclusion can be accomplished as for the very basic methodology of military logistics.

Keywords: sustainability, strategic management, military logistics, climate trajectories

[1]**Address:** Óbuda University, Keleti Károly Faculty of Business and Management, Budapest, Hungary
[2]**Address:** Óbuda University, Keleti Károly Faculty of Business and Management, Budapest, Hungary
[3]**Address:** Óbuda University, Keleti Károly Faculty of Business and Management, Budapest, Hungary

***Corresponding author**: bodrog.zoltan@uni-obuda.hu

Bartın Basin Rainfall Sensor IoT Data and Integration into Hydrological Model in Flood Early Warning System

MEHMET SAFA AYDIN[1], FURKAN AYAZ[2], MUHAMMED ZAKİR KESKİN[3], ERSİN ALAYBEYOĞLU*[4], EVRİM GÜLER[5], ERCAN GEMİCİ[6]

Abstract: In major natural disasters such as floods, early warning systems increase life and property safety as much as possible. Undoubtedly, measuring the amount of rainfall instantly in floods and evaluating it in the light of meteorological data has an important role in any flood disaster that may occur in any basin. The amount of rainfall that occurs predominantly in the entire basin directly affects the amount of water that will flow towards the settlement or agricultural area that needs to be protected. In this study, the contribution of 16 rainfall sensors installed in the flood early warning system developed for use in Bartın Center and its surroundings in Bartın Basin, Turkey, to the hydrological model used is presented. The rainfall sensor is a hydrological, meteorological instrument used to measure the amount of rainfall and converts the rainfall into a pulse signal output. The unprocessed data obtained with the used rainfall sensor was used to measure the rainfall intensity and duration in a unique way within the scope of the study. The unprocessed data from the rainfall sensor was obtained using Raspberry Pi via RS485 communication protocol and transferred to the data center located in Bartın University Kutlubey Campus as IoT data. Energy harvesting was performed using solar panels at the sensor ends and the data obtained was obtained dynamically at 5-minute intervals.

Keywords: IoT, climate change, level sensor, early flood warning system

[1]**Address:** Bartın University, Faculty of Engineering, Architecture and Design, Department of Electrical and Electronics Engineering, Bartın//Türkiye
[2]**Address:** Bartın University, Faculty of Engineering, Architecture and Design, Department of Computer Engineering, Bartın /Türkiye
[3]**Address:** Bartın University, Faculty of Engineering, Architecture and Design, Department of Civil Engineering, Bartın/Türkiye
[4]**Address:** Bartın University, Faculty of Engineering, Architecture and Design, Department of Electrical and Electronics Engineering,Bartın/Turkiye
[5]**Address:** Bartın University, Faculty of Engineering, Architecture and Design, Department of Computer Engineering, Bartın/Türkiye
[6]**Address:** Bartın University, Faculty of Engineering, Architecture and Design, Department of Civil Engineering, Bartın/Türkiye

***Corresponding author**: ealaybeyoglu@bartin.edu.tr

Radar Range Sensor IoT Data and Using It in Calculating Stream Flow and Bartın Basin Flood Early Warning System Application

MEHMET SAFA AYDIN[1], FURKAN AYAZ[2], MUHAMMED ZAKİR KESKIN[3], ERSIN ALAYBEYOĞLU*[4], EVRİM GÜLER[5], ERCAN GEMİCİ[6]

Abstract: In flood disasters, which are among the large-scale natural disasters, the activation of early warning systems is of critical importance in terms of protecting human life, minimizing loss of life and reducing material damage. The fact that such systems enable the necessary precautions to be taken before the disaster allows the effects of the disaster to become more manageable. A certain amount of the precipitation that occurs predominantly in the entire basin is absorbed by the soil and a certain part of it moves towards the river bed and therefore towards the settlement or agricultural area that needs to be protected. Especially in sudden and destructive natural events such as floods, the real-time measurement of the flow rate of water in the rivers and the interpretation of this data with meteorological analyzes make it possible to predict and intervene in advance the possible floods that may occur in any river basin or settlement area. In this study, the contribution of 8 radar sensor IoT data installed in the flood early warning system developed for use in Bartın Center and its surroundings in Bartın Basin, Turkey, to the hydrological model used is presented. The radar sensor was placed on bridges over streams and used to calculate the stream flow at its current location. The radar sensors were used to perform measurements up to 20m, especially on high bridges. The flow calculation was obtained by performing different measurements at the water height at the locations where the radar sensor was located within the framework of the measurements obtained via Acoustic Doppler Current Profiler (ADCP). The unprocessed data obtained with the radar sensor used was used to calculate the stream flow in a unique way within the scope of the study. The unprocessed data from the radar sensor was obtained using Raspberry Pi via RS485 communication protocol and transferred to the data center located in Kutlubey Campus of Bartın University as IoT data. Energy harvesting was performed by using solar panels at the sensor ends and the data obtained in this way was obtained dynamically at 5-minute intervals.

Keywords: IoT, climate change, level sensor, early flood warning system.

[1]**Address:** Bartın University, Faculty of Engineering, Architecture and Design, Department of Electrical and Electronics Engineering, Bartın/Türkiye
[2]**Address:** Bartın University, Faculty of Engineering, Architecture and Design, Department of Computer Engineering, Bartın/Türkiye
[3]**Address:** Bartın University, Faculty of Engineering, Architecture and Design, Department of Civil Engineering, Bartın/Türkiye
[4]**Address:** Bartın University, Faculty of Engineering, Architecture and Design, Department of Electrical and Electronics Engineering, Bartın/Türkiye
[5]**Address:** Bartın University, Faculty of Engineering, Architecture and Design, Department of Computer Engineering, Bartın/Türkiye
[6]**Address:** Bartın University, Faculty of Engineering, Architecture and Design, Department of Civil Engineering, Bartın/Türkiye

***Corresponding author**: ealaybeyoglu@bartin.edu.tr

Enhancing Discharge Measurements in Mid-Sized Rivers Using ADCP: A Case Study from the Bartın River Basin

MUHAMMED ZAKİR KESKİN[1], FURKAN AYAZ[2], MEHMET SAFA AYDIN[3], ERCAN GEMICI*[1], ERSİN ALAYBEYOĞLU[3], EVRİM GÜLER[2]

Abstract: Accurate measurement of river discharge is a crucial step for hydrological modeling, water resources management, and flood forecasting. In this study, high-resolution flow and velocity measurements were conducted in the Bartın River Basin, located in northern Türkiye, using a StreamPro model Acoustic Doppler Current Profiler (ADCP) by Teledyne RD Instruments. The basin is characterized by diverse channel geometries and non-wadable sections, posing technical challenges for conventional gauging methods. ADCP technology offers a non-contact, rapid, and safer alternative, providing spatially distributed flow data across the cross-section. The aim of this research is to evaluate the performance of the StreamPro ADCP under typical hydraulic and geomorphological conditions of mid-sized Turkish rivers and to assess its suitability for long term hydrometric monitoring. Multiple reciprocal transects were measured at representative sites along the Bartın River under varying flow regimes. Data were processed in accordance with USGS protocols, and uncertainties were analyzed considering both random and systematic sources of error. In line with recent literature, this study also observed that ensemble averaging and bidirectional transects significantly reduce measurement uncertainty in shallow and low velocity flows. Moreover, comparisons with existing rating curves and historical records indicated that the ADCP measurements fall within a ±5% error margin, confirming their reliability. The study highlights the critical influence of measurement protocols particularly transect duration, bed mobility, and cross-sectional geometry on data accuracy. Practical recommendations are provided for field implementation, including minimum transect duration, number of passes, and signal quality thresholds. The findings support the scientific integration of ADCP based measurements into operational hydrometric networks. Future research will focus on incorporating ADCP data into AI-assisted rating curve development and early warning systems. This study represents a significant step toward more resilient and adaptive river monitoring systems in the face of climate induced hydrological variability.

Keywords: Acoustic Doppler Current Profiler (ADCP), Discharge Measurement, Bartın River Basin, Rating Curve, Hydrometric Monitoring, Smart and Sustainable Environment

[1]**Address:** Bartın University, Faculty of Engineering, Architecture and Design, Department of Civil Engineering, Bartın/Türkiye
[2]**Address:** Bartın University, Faculty of Engineering, Architecture and Design, Department of Computer Engineering, Bartın/Türkiye
[3]**Address:** Bartın University, Faculty of Engineering, Architecture and Design, Department of Electrical and Electronics Engineering, Bartın/Türkiye

***Corresponding author**: egemici@bartin.edu.tr

Coupling Soil Moisture Sensing and Guelph Permeametry for Infiltration Characterization in Climate Adaptive Flood Monitoring

MUHAMMED ZAKIR KESKIN[1], FURKAN AYAZ[2], MEHMET SAFA AYDIN[3], ERCAN GEMICI[1], ERSIN ALAYBEYOĞLU[3], EVRIM GÜLER*[2]

Abstract: The increasing flood risk driven by climate change and the growing need for groundwater management necessitate the accurate characterization of soil–water interactions in basins with varying subsurface properties. This study investigates the relationship between subsurface soil moisture distribution, saturation levels, and saturated hydraulic conductivity (Kfs) in the Bartın River Basin, located in the Black Sea region of Türkiye, with the aim of improving the hydraulic components of a flood early warning system. High-resolution soil moisture data were collected at depths of 20, 40, and 80 cm using in situ sensors, concurrently with Kfs measurements obtained via the Guelph permeameter. The Guelph permeameter determines Kfs by analyzing three-dimensional water flow, comprising both vertical and lateral components, through a saturated soil column under controlled field conditions. This makes it particularly advantageous for measurements in sloped and heterogeneous terrains where traditional methods are impractical. In this study, the Guelph method was implemented using two constant-head pressure levels and analyzed based on the formulations developed by Reynolds and Elrick in 1985. The resulting conductivity values were evaluated in relation to soil texture, porosity, seasonal moisture fluctuations, and local groundwater dynamics. The findings indicate a strong correlation between soil moisture and hydraulic conductivity. Notably, conductivity increased during spring and summer, coinciding with heightened evapotranspiration and root activity. In contrast, clay-rich soils with low permeability yielded relatively lower Kfs values, a result attributed to both microstructural pore constraints and air entrapment within the field matrix. Seasonal variability and depth-specific analysis were shown to enhance the accuracy of soil infiltration dynamics in hydrological models. In this context, the combined use of soil moisture sensors and Guelph permeameter measurements offers a reliable field-based methodology for permeability assessment and provides critical input data for improving the performance of infiltration modules in flood early warning systems. The study emphasizes the importance of site-specific determination of regional hydraulic parameters for effective flood risk management.

Keywords: Saturated Hydraulic Conductivity, Guelph Permeameter, Infiltration Modeling, Soil–Water Interaction, Smart and Sustainable Environment.

[1]**Address:** Bartın University, Faculty of Engineering, Architecture and Design, Department of Civil Engineering, Bartın/Türkiye
[2]**Address:** Bartın University, Faculty of Engineering, Architecture and Design, Department of Computer Engineering, Bartın/Türkiye
[3]**Address:** Bartın University, Faculty of Engineering, Architecture and Design, Department of Electrical and Electronics Engineering, Bartın/Türkiye

***Corresponding author**: evrimguler@bartin.edu.tr

CO_2 Emissions of 3D-Printed Geopolymer Composites and Their Sustainable Use in Climate-Resilient Cities

BURAK BODUR[*1], MUHAMMED ZAKİR KESKİN[2], FURKAN AYAZ[3], MEHMET SAFA AYDIN[4], ERCAN GEMİCİ[2], ERSİN ALAYBEYOĞLU[4], EVRİM GÜLER[3]

Abstract: In the face of intensifying global climate change, radical transformations are increasingly required across various domains, particularly in urbanization policies. Rising temperatures, extreme weather events, and resource scarcity necessitate the development of more resilient, sustainable, and low-carbon construction solutions in urban areas. The construction sector, due to its high carbon emissions and intensive consumption of natural resources, stands out as one of the most critical domains for such transformation. In this context, 3D-printed geopolymer-based construction materials have emerged as a promising alternative for the development of climate-resilient cities, owing to their environmentally friendly characteristics and technical advantages. Geopolymers are eco-friendly materials synthesized through the activation of industrial wastes (e.g., fly ash, slag, alumina residues) and offer significantly lower carbon emissions compared to conventional cement-based binders. The application of these materials via 3D printing technology, which eliminates the need for formwork and generates minimal waste, not only reduces environmental impacts during the production phase but also facilitates faster, more flexible, and resource-efficient construction processes. Moreover, the use of waste materials as secondary raw inputs aligns with circular economy principles and contributes to the overall sustainability of the construction industry. Studies indicate that the incorporation of waste-based materials (especially industrial by-products and recycled aggregates) into geopolymer composites plays a key role in reducing environmental impacts and lowering costs. Such additions not only limit carbon emissions but also enhance mechanical performance. Furthermore, the controlled use of micro-reinforcements and specialty additives improves the shape stability, extrudability, and workability of geopolymer mixtures, thereby enabling the development of composites more suitable for 3D printing. This demonstrates that geopolymer-based composites can support sustainable construction objectives not only from an environmental perspective but also from a technical standpoint. In conclusion, geopolymer composites produced via 3D printing technology possess the potential to serve as a fundamental building block in the development of climate-resilient cities, owing to their low carbon emissions, reuse of waste materials, and production efficiency. The widespread adoption of this technology will contribute to reducing the environmental footprint of the construction sector and fostering a more sustainable urban future in the context of climate change adaptation.

Keywords: Climate-Resilient Cities, Carbon Emissions, Geopolymer Composites, 3D printing

[1]**Address:** Bartın University, Project and Technology Office, Bartın/Türkiye
[2]**Address:** Bartın University, Faculty of Engineering, Architecture and Design, Department of Civil Engineering, Bartın/Türkiye
[3]**Address:** Bartın University, Faculty of Engineering, Architecture and Design, Department of Computer Engineering, Bartın /Türkiye
[4]**Address:** Bartın University, Faculty of Engineering, Architecture and Design, Department of Electrical and Electronics Engineering, Bartın/Türkiye

***Corresponding author**: bbodur@bartin.edu.tr

Prioritization in Traffic of Electric Vehicles for Sustainable Mobility in Durrës, Albania

LUIZA LLURI*[1], ELI VYSHKA[2], FALDI LLURI[3]

Abstract: This study explores how giving electric vehicles (EVs) priority in Durrës traffic system can support sustainable urban mobility solutions. As Durrës grows as Albania's second largest city with its major seaport status, it struggles to handle transportation demands which surge from urbanization and tourism growth while remaining dependent on ICE vehicles. These patterns create significant problems of air pollution, noise and traffic jams which endanger public health alongside environmental quality. The study investigates if Durrës can achieve a more sustainable transport system by prioritizing electric vehicles through dedicated traffic management policies and infrastructure investments as global cities move towards greener mobility solutions. The research combines multiple methods by analyzing traffic flow data alongside air quality reports and public survey results as well as conducting stakeholder interviews with city planners, EV users, and transport authorities. Although the adoption rate of EVs remains low, public support for environmentally friendly transportation options continues to grow among younger citizens and those with environmental concerns. The study recommends creating dedicated lanes for electric vehicles as well as traffic light systems that prioritize EVs and introduce financial benefits like reduced toll fees and complimentary parking spaces. The research report highlights the critical necessity for extensive growth in EV charging infrastructure which requires combined efforts from government bodies and private sector investment. Studies indicate that Durrës can lead sustainable mobility in the Western Balkans using an electric vehicle strategy implemented in stages and effectively shared with the public despite high costs and public awareness challenges.

Keywords: Electric Vehicles (EVs), sustainable mobility, traffic prioritization, smart traffic management, environmental

[1]**Address:** Aleksandër Moisiu University, Faculty of Professional Studies, Durrës, Albania
[2]**Address:** Aleksandër Moisiu University, Faculty of Professional Studies, Durrës, Albania
[3]**Address:** Aleksandër Moisiu University, Faculty of Information Technology, Durrës, Albania

***Corresponding author**: luizalluri@uamd.edu.al

Plastic Recycling and Sustainable Waste Management in Albania

LUIZA LLURI*[1], FALDI LLURI[2], DRITA HIMA[3]

Abstract: Albania's plastic waste management system faces several challenges because of insufficient recycling infrastructure and weak public understanding of recycling processes together with inadequate policy implementation. Albania faces unique challenges in combating plastic pollution because of underdeveloped waste infrastructure and feeble regulatory systems along with lackluster public engagement. The study examines plastic recycling methods in Albania using circular economy principles to improve waste management systems and decrease plastic consumption which will help build a sustainable economic model. This research utilizes a mixed-methods approach that includes stakeholder interviews and literature reviews together with waste management data analysis to reveal important barriers including fragmented collection systems and missing Extended Producer Responsibility schemes. The combination of systematic approaches in legal frameworks with public-private partnerships and community participation holds the potential to significantly enhance plastic recycling efficiency in Albania. The research advocates for strengthening recycling infrastructure through regulatory reforms while promoting public educational programs and developing markets for recycled plastics. Albania intends to increase its recycling rates while decreasing environmental pollution through context-specific integrated solutions which will also support sustainable economic development within EU environmental standards.

Keywords: waste management, circular economy, sustainable development, public awareness, recycling challenges

[1]**Address:** Aleksandër Moisiu University, Faculty of Professional Studies, Durrës, Albania
[2]**Address:** Aleksandër Moisiu University, Faculty of Information Technology, Durrës, Albania
[3]**Address:** Aleksandër Moisiu University, Faculty of Professional Studies, Durrës, Albania

***Corresponding author**: luizalluri@uamd.edu.al

AHP-Based Spatial Suitability Model for Solar Power Plant Installation with Sentinel-2 Derived NDVI, Albedo, and Solar Radiation Data: A Case Study of Çorum Province

FAZLI ENGİN TOMBUŞ*[1]

Abstract: It is well known that renewable energy sources present a significant opportunity for today's world in terms of avoiding the use of fossil fuels and ensuring the sustainability of energy resources. Especially, solar energy stands as one of the most important options contributing greatly to clean and sustainable energy production worldwide and is becoming increasingly widespread. Considering that the installation processes of Solar Power Plants (SPP) are quite challenging, it is evident that the selection of suitable locations is often the most critical issue. The problem of determining suitable locations is typically solved using Geographic Information Systems (GIS) along with various decision support systems. The Analytic Hierarchy Process (AHP) method is one of the prominent methods within these decision support systems. In this study, Sentinel-2 satellite data, integrated with an AHP-based decision support system, has been used to analyze areas suitable for SPP installation. The solar radiation, albedo, and NDVI (Normalized Difference Vegetation Index) parameters derived from Sentinel-2 satellite data have been considered the most important criteria for suitability analysis. Solar radiation data represent the radiation levels directly affecting the efficiency of the plant, while the NDVI value is used to determine the vegetation density of the area and consequently, potential shading effects. Albedo, on the other hand, shows the surface's ability to reflect light, which has a significant impact on panel efficiency. The study was conducted using data from 2023 and 2024 for four different days in July, the month with the highest solar exposure and lowest cloud cover, focusing on four districts (Bayat, Uğurludağ, Sungurlu, and Alaca) in the Çorum Province, located in the Central Anatolia Region. As a result of the suitability analysis, areas characterized by high solar radiation and low albedo values were identified as the most suitable regions for SPP investment. Additionally, areas with high NDVI values were excluded to protect agricultural activities and ecosystem integrity.

Keywords: Solar Power Plant (SPP), Analytic Hierarchy Process (AHP), Geographic Information Systems (GIS), Remote Sensing, Suitability Analysis

[1]**Address:** Hitit University, Vocational School of Technical Sciences, Dept. of Architecture and Urban Planning, Çorum/Türkiye

***Corresponding author**: fengintombus@hitit.edu.tr

Automated Design of Heuristics for the Electric Vehicle Routing Problem by Genetic Programming

MARKO ĐURASEVIĆ*[1]

Abstract: The vehicle routing problem (VRP) is an important combinatorial optimisation problem found in various logistic processes in the real world. The goal in this problem is to determine routes for a number of vehicles in order to visit all the given customers by optimising various criteria, such as the total travel time, total travel distance, lateness, etc. VRP is found in various logistics processes in the real world, which resulted in a significant amount of research being carried out in designing new methods to efficiently solve the problem. large However, in recent years, environmental concers have become increasingly pronounced and there is a rising need to reduce human impact on the environment. Since logistics are one of the largest polluters, there is also a growing need to reduce their effect on the environment, usually in the form of using vehicles running on alternative fuels, usually electric energy. This gave rise to the electric VRP (EVRP) variant, in which the fleet consists of electric vehicles. This problem variant introduces additional challenges, such as limited range of the vehicles and the need to reful the vehicles at a limited number of charging stations. Since VRP, and by extension EVRP, have proven to be NP-hard, it is impossible to solve larger problems exactly, meaning that it is required to fall back to using heuristics. Although metahueristtics are commonly used to solve EVRP, they have a limited applicability in dynamic scenarios or for larger problems. Therefore, routing rules (RRs) represent an alternative to solve EVRP in a short amount of time, but also with the possibility to adapt to changing situations in the problem. RRs are simple constructive heuristics that construct the solution to the problem incrementally, meaning that each time a decision needs to be made, i.e., a customer needs to be assigned to a vehicle, the RR determines the most suitable decision. Although quite simple, designing RRs is complex and requires good domain knowledge. Therefore, in recent years, genetic programming (GP) has commonly been used to automatically desing new RRs efficiently. Such an approach of automatically designing new heuristics is usually called a hyper-heuristic. In this way, not only is the user is relieved of the tedious task of having to design new RRs by hand, but it is also possible to design RRs which achieve a better performance in comparison to many of the manually designed RRs. The way in which GP is utilised to automatically design RRs is by constructing a mathematical expression that is used to rank all the decisions in each decision moment, and then simply select the best ranking one. Such an approach allows us to design an arbitrary number of heuristics for problems with various optimisation criteria. And although the automated desing or RRs brings many advantages, there are still certain issues that need to be addressed in future research, such as further improving the performance of generated heuristics, improving their interpretability, and adapting them for a wider range of problems encountered in the real world.

Keywords: Genetic programming, Electric Vehicle Routing Problem, Routing Rules, Hyper-Heuristics, Metaheuristics

[1]**Address:** University of Zagreb Faculty of Electrical Engineering and Computing, Unska 3, 10 000 Zagreb/Croatia
***Corresponding author**: marko.durasevic@fer.hr

ICT Innovation at the Hungarian SMEs and its economical effects

ÁDÁM BÉLA HORVÁTH[1]

Abstract: The aim of this research is to examine the state of Information and Communication Technology (ICT) infrastructure and the adoption of cloud-based services among small and medium-sized enterprises (SMEs) in Hungary. Based on a questionnaire survey, the study received 498 responses from various SMEs. It investigates the current condition of traditional on-premise ICT infrastructure and the extent of cloud service utilization. Additionally, the research explores the impact of Industry 4.0 on the adoption of these technologies, examining how this technological shift influences infrastructure choices and service usage. Moreover, the study includes a statistical analysis to assess the contribution of independent technological solutions—those not directly interconnected—to the competitiveness of SMEs. It also investigates the relationship between these technology adoptions and the information security risks associated with them. By analyzing the connection between technological innovation, competitiveness, and security exposure, the research aims to provide insights into the digital transformation challenges faced by Hungarian SMEs. The findings emphasize the importance of strategic technology investments in enhancing business performance while addressing potential security vulnerabilities in an increasingly digital environment.

Keywords: ICT, Industry 4.0, Innovation, Cloud, IoT, Security

[1]**Address:** Óbuda University, Keleti Károly Faculty of Business and Management, Budapest / Hungary

***Corresponding author**: horvath.adam@kgk.uni-obuda.hu

Water Resources and Climate Change in the Context of Water Balance in a Polish Municipality

JADWIGA DZIEDZIC*[1], MAREK KOPACZ[1]

Abstract: Climatic water balance (CWB) describes the relationship between precipitation and evaporation in a region. It is an important hydrological and meteorological indicator that allows for the assessment of water availability in the natural environment (mainly for crops) and the impact of changing climatic conditions on water resources. Therefore, the Climate Water Balance during the growing season plays a key role in shaping the conditions for vegetation development, especially in regions with a large share of agriculture.
The aim of this work was to analyze the Climatic Water Balance in the Radymno commune based on multi-year data recorded within the Agricultural Drought Monitoring System. This system has been implemented for years by the Institute of Cultivation, Fertilization and Soil Science - State Research Institute (IUNG).
The analysis included average monthly historical data from 2007 to 2023. To obtain annual values, monthly data were aggregated at the annual level, which allowed for the extraction of average water balance values in the longer term, as well as the assessment of the impact of climate change on the level of water deficit or excess.
The research results indicate the systematic occurrence of water deficits during the growing season, especially in the summer months, which negatively affects the potential of plant production. This applies primarily to crops with high water requirements. These changes significantly limit the availability of water in key stages of plant development. Data analysis confirmed that the period under study was characterized mainly by negative CWB values. Positive CWB was recorded twice, in 2010 (165,31 mm) and 2014 (30,12 mm), while the largest water deficit was recorded in 2015 (-296,46 mm).
The conclusions of the research emphasize the need to implement adaptive measures, such as the development of retention systems, improved irrigation and the selection of plant species resistant to water stress. The results can form the basis for planning a water resources management strategy in the commune and supporting the sustainable development of agriculture in the conditions of ongoing climate change.

Keywords: CWB, evapotranspiration variability, water resources, climate change, growing season

[1]**Address:** Faculty of Mining Surveying and Environmental Engineering, AGH University of Science and Technology in Krakow

***Corresponding author**: jdziedz@agh.edu.pl

Impact of Variability of Socio-Structural Factors on Surface Water Quality in Non-Urbanized Areas

KRZYSZTOF GOŁBA[*1]

Abstract: The state of the environment, especially surface water quality, is a key indicator of the condition of ecosystems, including natural resources used by local communities. The main goal of the research is to identify factors affecting the environment, such as the intensification of agricultural activities, demographic changes, land ownership and use structure, and environmental protection strategies in the Małopolska Voivodeship. Each of these elements affects different multi-criterial aspects of water quality, including nutrient content, chemical contamination and sedimentation, mainly organic compounds. The study will discuss the results of the research and recommendations for more effective prevention and management of water resources. Based on the analysis, the state of the water environment in the province was determined and the need for corrective and preventive measures was assessed. A positive aspect of the research is the observed changes in the amount of mineral fertilizers applied and the effect of these measures on yields, where crop productivity is increasing. This is due to the more rational and conscious use of fertilizers by food producers, as well as the development of technology and improved production of agricultural produce. This phenomenon is particularly beneficial from the point of view of environmental protection, especially water resources. The obtained results constitute an extension of the analysis and study of the impact of socio-structural changes on the environment in the Małopolska Voivodeship. Changes in aspects of human existence, as well as the structure of agricultural production, livestock and crops will allow us to determine among others NPK balance or the occurrence and concentration of biogenic compounds, and then estimation of the impact of these factors on eutrophication processes. Research conducted in this area and the results and conclusions obtained may be particularly helpful for decision-makers and communities participating in the development of non-urbanized areas.

Keywords: environment, NPK, surface water quality, land use, agriculture, sustainable development, environmental protection

[1]**Address:** AGH University of Science and Technology, Faculty of Mining Surveying and Environmental Engineering, Cracow, Poland

***Corresponding author**: kgolba@agh.edu.pl

A Novel High-Entropy Alloy with Dual Functionality: Optimized Soft Magnetic and Radiation Shielding Properties

TELEM ŞIMŞEK[*1], TUNCAY ŞIMŞEK[2], ESRA UYAR[3,4], MUHARREM PUL[5], GÜL ATALI[1], GÖKÇEN ASLAN AYDEMIR[6]

Abstract: This study explores the structural, magnetic, and radiation shielding characteristics of $(FeCoCr)_{94}Al_6$ high-entropy alloys (HEAs) synthesized through mechanical milling. X-ray diffraction (XRD) and scanning electron microscopy (SEM) confirmed a single-phase bcc solid solution formation after 20 hours of milling, with energy-dispersive X-ray spectroscopy (EDS) validating the alloy's composition and purity. The HEAs displayed soft ferromagnetic behavior, with the 7-hour milled sample achieving optimal performance—151 emu/g saturation magnetization and 37 Oe coercivity—making it suitable for soft magnetic applications. Additionally, a high Curie temperature (~800 K) highlights the alloy's potential in high-temperature environments. Radiation shielding capabilities against gamma and X-rays demonstrated efficiency, with 93% attenuation for low-energy gamma rays and 91% for X-rays, suggesting its suitability for nuclear and medical applications. The findings underscore the versatility of $(FeCoCr)_{94}Al_6$ HEAs in industrial settings that demand combined magnetic and radiation shielding properties.

Keywords: High-entropy alloys, mechanical milling, magnetic materials, radiation shielding, gamma rays, X-ray attenuation.

[1]**Address:** Hacettepe University, Institute of Science, Nanotechnology and Nanomedicine Division, Ankara 06800, Turkey
[2]**Address:** Department of Mechanical and Metal Technologies, Kırıkkale University, 71450, Kırıkkale, Turkey
[3]**Address:** Gazi University, Faculty of Sciences, Department of Physics, 06500, Ankara, Turkiye
[4]**Address:**Gazi University, Basic and Engineering Sciences Central Laboratory Application and Research Center (GUTMAM), 06500, Ankara, Turkiye
[5]**Address:** Department of Electricity and Energy, Kırıkkale Vocational School, 71450, Kırıkkale, Turkey
[6]**Address:** Gazi University, Graduate school of Natural and Applied Sciences, Department of Advanced Technologies, Ankara, Turkey

***Corresponding author**: telem@hacettepe.edu.tr

Trust and Security Issues- Cognitive-based and Emotional Trust

MIZSER CSILLA ILONA*[1]

Abstract: The basis of all communication is security and trust. This study aims to be a secondary research summarizing scientific articles and research investigating effective organizational communication. Effective organizational communication is important, among other relevant factors, in terms of the quality of life of the employees in the organization, in terms of the organization's partner relationships, and in the issue of adapting to continuous changes. Effective organizational communication enables people to interpret reality together, summarizing individual interpretations.

Keywords: Effective Organizational Communication; Trust and Security; Employee Quality of Life; Organizational Adaptation

[1]**Address:** Keleti Károly Faculty of Business and Management, Department: Institute of Economics, Finance and Accounting, Budapest, Hungary

***Corresponding author**: mizser.csilla@kgk.uni-obuda.hu

Artificial Intelligence-Driven Dynamic Pricing Optimization for the Albanian Electronics Market

ANNA MARIA-KOSOVA*[1], MARSIDA KRASNIQI[2]

Abstract: The pricing options that can be employed in any given situation are of great importance for businesses seeking competitive advantage and value capture, particularly in the context of Albania's electronics market, which is characterized by its rapid development. Most retailers, however, operate on a static pricing model that does not respond to competitor price changes or market developments. Price optimization strategies for dynamic pricing systems are the main focus of the research in this paper. Data scraping techniques will be used for the purposes of gathering pricing data from top Electronics shops in Albania. Such systems will be able to suggest best price changes based on Machine learning methods like reinforcement learning (Q-learning, Deep Q-Networks) and time series analysis (ARIMA, Prophet). This is done to make price information possible to be turned into valuable insights and decision-making by businesses automatically. A prototype in the form of a Telegram bot or web interface will be developed. Initial outcomes should illustrate how price enabled by AI allows businesses to react more strongly towards competitive pricing and increase profit with market competitiveness. The study will highlight the impact real-time information has on strategic decision making and show how traditional pricing models can be disrupted. Ultimately, this is what the study seeks to do: leave Albanian companies with a working prototype of an AI optimized price control tool.

Keywords: Dynamic pricing optimization, machine learning, real-time pricing, predictive analytics, predictive analytics, competitive pricing.

[1]**Address:** Polis University, Faculty of Research and Development, Tirana/Albania
[2]**Address:** University "Aleksandër Moisiu" Durrës, Faculty of Professional Studies, Durrës/Albania

***Corresponding author**: annamariakosova98@gmail.com

Use Of Mineral Waste for Production of Lightweight Artificial Aggregates

ADAM MASŁOŃ*[1], MAKSYMİLİAN CEİŚLA[1], RENATA GRUCA-ROKOSZ[1], LESŁAW BİCHAJŁO[1], ANDRZEJ NOWOTNİK[1], MACIEJ PYTEL[1], MAŁGORZATA FRANUS[2], KATARZYNA KALİNOWSKA-WİCHROWSKA[3]

Abstract: The studies investigate the production of lightweight artificial aggregates from mineral waste, specifically bottom sediment from water reservoir, concrete dust and fly ash generated from municipal waste incineration.
The technology for creating this new type of lightweight aggregate involves thermal and pressure synthesis, effectively neutralizing hazardous substances, including heavy metal compounds present in the raw materials. This process permanently and irreversibly integrates these substances into the crystal structure of the aggregates, resulting in a fully ecological building material. The aggregates are inert in natural environments and do not release harmful chemical substances.
Laboratory tests on the lightweight artificial aggregates focused on evaluating their physical, mechanical, and chemical properties. From a waste processing perspective, the chemical composition of the produced aggregates is crucial, as it can influence interactions with cement and other building materials, which is vital for achieving the desired quality of concrete. These properties also determine the potential applications of lightweight artificial aggregates, as well as their efficiency and durability in construction.
Research has demonstrated the feasibility of processing bottom sediments in conjunction with other mineral waste to produce synthetic aggregates suitable not only for construction but also for horticulture and agriculture, including hydroponics, green roofs, and rain gardens.
The research leading to these results has received funding from the commissioned task entitled „VIA CARPATIA Universities of Technology Network named after the President of the Republic of Poland Lech Kaczyński” contract no. MEiN/2022/DPI/2575 dated 20.10.2022 action entitled „ISKRA – building inter-university research teams.

Keywords: Lightweight aggregates, bottom sediment, fly ash, concrete dust

[1]**Address:** Rzeszow University of Technology, Rzeszów/Poland
[2]**Address:** Lublin University of Technology, Lublin/Poland
[3]**Address:** Bialystok University of Technology, Bialystok/, Poland

***Corresponding author**: amaslon@prz.edu.pl

The Effect of Environmental Factors on the Design of Heat Exchangers Used in Aircraft

Rahime İNYURT[1], Talip AKBIYIK*[2], Nafiz KAHRAMAN[3]

Abstract: This study investigates the performance optimization of an air-to-air two-pass cross-flow heat exchanger using bleed air data extracted from the engine for use in an aircraft's Environmental Control System (ECS). The performance and efficiency of the heat exchanger were analyzed by considering different flight cases (ground operation, climb) using ECS data. These data, including mass flow rate (kg/s), temperature (K), and absolute pressure (bar), were integrated into a CFD analysis to simulate the performance at different altitudes and evaluate the system's behavior under defined conditions. Additionally, heat exchanger sizing calculations were performed to estimate the required dimensions for optimal heat transfer and system performance. The following data were used in the study: Ground and cruise conditions were modeled using temperature and pressure conditions specific to each case. Mass Flow Rate (kg/s): Various values such as 0,208 and0,322 kg/s were considered to simulate bleed air flow under different altitude conditions. Temperature (K): Values ranging from 540,75 K to 702,2 K and 373,75 K to 298.86 K were used to simulate environmental conditions during cruise flight at 30000ft altitude. Pressure (bar): Absolute pressures ranging from 3.2 bar to 1 bar were considered to assess the performance of the ECS at higher altitudes. The heat exchanger's efficiency was evaluated through temperature distribution, heat transfer, and pressure drop analyses. In addition to CFD analysis, sizing calculations were performed using standard heat exchanger design equations to determine the required dimensions, surface area, and configuration for efficient heat transfer between the bleed air and the environmental control system. The CFD simulation results, combined with the manual calculations, provide insights into the necessary design improvements and operational parameters to optimize the heat exchanger's performance at different flight phases (ground and climb). In conclusion, the analysis of different flight phases (ground and climb) reveals the need for design optimizations and operational parameter adjustments to ensure the heat exchanger functions efficiently. This study aims to contribute to the enhancement of heat exchanger technologies used in aircraft environmental control systems, improving overall performance and efficiency.

Keywords: Keywords: environmental control system, bleed air, climb, ground position, air-to-air heat exchanger, CFD, performance analysis, efficiency optimization

[1]**Address:** Erciyes University, Faculty of Engineering,Mechanical Engineering , Kayseri/Türkiye
[2]**Address:** Aksaray University, Vocational School of Technical Sciences, Aksaray/Türkiye
[3]**Address:** Erciyes University, Faculty of Aeronautics and Astronautics, Kayseri/Türkiye

***Corresponding author**: r.rahimeyildiz@gmail.com

Production and Characterization of 1-Tetradecanol/Gelatin-Gum Arabic/ZnO Microcapsules with Thermal Energy Storage and Photothermal Properties by Environmentally Friendly Pickering Emulsion-Complex Coacervation Method

CEMİL ALKAN[1], MÜYESSER SELDA TÖZÜM[2,3], SENA DEMİRBAĞ GENÇ[*2,4]

Abstract: In the study, the production of photothermal and thermal energy-storing microcapsules with gelatin-gum arabic shells was carried out via ZnO nanoparticles stabilized Pickering emulsion complex coacervation method, and the resulting microcapsules were coated with ZnO nanoparticles for energy harvesting by photothermal effect. In Pickering emulsion, stabilization is achieved through solid particles adsorbed at the boundary between the two phases. Using Pickering stabilizers instead of surfactants, which are detrimental to the environment and hard to eliminate from the final product, the complex coacervation method becomes more environmentally friendly in the microcapsule production. In this study, ZnO nanoparticles functioned as the stabilizer in the Pickering emulsion and as a coating material for the gelatin-gum arabic shell structure. 1-tetradecanol was used as the phase change material (PCM). The microcapsules were produced using 0.1% Pickering stabilizer (ZnO) and were subsequently coated with ZnO nanoparticles at a concentration of 4%. According to scanning electron microscope (SEM) and particle size analysis results, the produced microcapsules exhibited a spherical morphology with an average particle size of 64.13 μm. Fourier transform infrared spectroscopy–attenuated total reflectance (FTIR-ATR) spectroscopy was used to characterize the chemical structure of the microcapsules. Microcapsules demonstrated effective photothermal performance, in addition to a high thermal storage capacity of 97.7 J/g.

Keywords: Microcapsule, Pickering emulsion, complex coacervation, thermal energy, photothermal effect, energy harvesting

[1]**Address:** Tokat Gaziosmanpaşa University, Faculty of Arts and Sciences, Tokat/Türkiye
[2]**Address:** Uşak University, Faculty of Engineering and Natural Sciences, Uşak/Türkiye
[3]**Address:** Uşak University, Scientific Analysis Technological Application and Research Center, Uşak/Türkiye
[4]**Address:** Uşak University, Leather Textile and Seramics Design Application and Research Center, Uşak/Türkiye

***Corresponding author**: sena.demirbag@usak.edu.tr

INTRODUCTION

In recent years, the environmental damage caused by fossil fuels and the risk of their depletion have significantly increased interest in renewable and sustainable energy alternatives (Fan et al., 2022; Zhao et al., 2022). There are many energy sources available in nature, among which solar energy stands out due to its abundance, universality, and environmentally friendly nature. With these characteristics, solar energy is considered one of the most promising renewable and sustainable energy sources (Chen et al., 2020; Chen et al., 2021). Therefore, the development of materials and technologies that enable more efficient utilization of solar energy has become a highly attractive research area for scientists. In this context, studies on photothermal conversion technology have increased significantly in recent years, as this technology-capable of directly converting solar radiation into thermal energy- has drawn considerable attention from researchers due to its potential to enhance the efficiency of solar energy utilization (Zhang et al., 2019a; Xue et al., 2021).

Conventional phase change materials (PCMs), which are used as energy storage materials, cannot effectively utilize solar radiation because they are unable to adequately absorb and convert solar energy into heat. In contrast, the integration of photothermal materials with PCMs enables more efficient utilization of solar energy (Chai et al., 2024; Li et al., 2024). Unlike traditional PCMs, PCMs with photothermal conversion capabilities can directly absorb sunlight, convert it into thermal energy, and store this energy, thereby offering significantly higher efficiency. However, PCMs have some drawbacks, such as low thermal conductivity and leakage during the solid-liquid phase transition (Sun et al., 2024). To overcome these disadvantages and combine photothermal materials, which convert solar energy into thermal energy, with phase change materials, microencapsulation technology provides an effective solution (Maithya et al., 2021; Liu et al., 2022). In the production of photothermal microcapsules, methods such as in-situ polymerization (Wang et al., 2018; Huang et al., 2020; Wang et al., 2021), sol-gel method (Hou et al., 2022; Li et al., 2022), polycondensation method (Ma et al., 2018), and emulsion-templated in-situ precipitation technology (Liu et al., 2021a) have been used. On the other hand, much of the work on the production of photothermal microcapsules has focused on the use of Pickering emulsion stabilizers, with methods such as Pickering emulsion in-situ polymerization, surface polymerization, suspension polymerization, and templated precipitation. These studies have shown that photothermal materials are used as Pickering

stabilizers in these processes (Zhao et al., 2019a; Zhao et al., 2019b; Maithya et al., 2020; Zhao et al., 2020a; Liu et al., 2021b; Sun et al., 2021; Maithya et al., 2021; Du et al., 2022; Tian et al., 2022; Xu et al., 2023; Chen et al., 2024).

Pickering emulsion is a surfactant-free emulsion stabilized by solid particles with partial wettability with both the oil and water phases (Bordes et al. 2021). Compared to conventional emulsions stabilized with surfactants, Pickering emulsions offer several advantages, including enhanced stability, lower toxicity, greater sustainability, and improved biocompatibility (de Carvalho-Guimaraes et al., 2022 Alkan et al., 2023). In this study, unlike existing studies, the Pickering emulsion system was integrated into the complex coacervation method, which is known for utilizing natural, biocompatible, and biodegradable polymeric materials as wall materials, resulting in the development of an environmentally friendly microencapsulation technique. In this way, a highly sustainable production process was achieved without the need for environmentally harmful and difficult-to-remove surfactants during the emulsion formation stage.

In this study, the preparation and characterization of microcapsules with photothermal properties using a newly developed environmentally friendly method were aimed. For this purpose, microcapsules were synthesized via the Pickering emulsion complex coacervation method, and their surfaces were subsequently coated with ZnO (zinc oxide) nanoparticles to impart photothermal functionality. The morphology, chemical structure, and particle size distribution of the prepared microcapsules were thoroughly investigated. Additionally, their photothermal conversion performance was evaluated and analyzed in terms of potential application areas.

2. MATERIAL AND METHOD

2.1. Material /Materyal

In the production of microcapsules, a gelatin (Type A, Sigma Aldrich)–gum Arabic (Sigma Aldrich) polymer pair was used as the wall material, while 1-tetradecanol was selected as the core substance. Zinc oxide nanoparticles (Sigma Aldrich,ZnO) were incorporated into the capsule wall structure both to act as a Pickering stabilizer and to impart photothermal properties to the capsules. For the stabilization of the microcapsules, glutaraldehyde (25%, Sigma Aldrich) was used as a cross-linking agent. During the production process, pH adjustments were performed using acetic acid and sodium hydroxide solutions.

2.2. Preparation of 1-tetradecanol/gelatin-gum arabic/ZnO microcapsules /1-tetradekanol/jelatin-arap zamkı/ ZnO mikrokapsüllerinin hazırlanması

In this study, the preparation of 1-tetradecanol/gelatin–gum arabic/ZnO (TD@G/GA/ZnO) microcapsules was carried out in two stages. First, TD@G/GA/ZnO microcapsules were produced using the Pickering emulsion complex coacervation method. In the second stage, ZnO nanoparticles were deposited onto the capsule wall structure.

In the first stage of microcapsule production, 2.5 g of 1-tetradecanol, used as the core material, was emulsified in a gelatin–water polymer solution in the presence of ZnO nanoparticles (0.1 wt % of core material) (serving as the Pickering stabilizer). Subsequently, a polyanionic gum arabic–water polymer solution was added dropwise into the emulsion. The pH of the mixture was adjusted to 4 using acetic acid to initiate complex coacervation. After one hour, the complex formation was halted by adjusting the pH to 9 using sodium hydroxide. The reaction medium was then cooled to 5 °C, and 0.8 g of glutaraldehyde was added to stabilize the microcapsules. In the final step, the microcapsules were treated with a 5% tannic acid solution for 10 hours, then filtered and washed. A core/wall ratio of 1:1 was used in the production process.

In order to impart photothermal properties to the microcapsules, their wall structures were coated with zinc oxide (ZnO) nanoparticles at a concentration of 4% by weight. In this step, the microcapsules—washed and filtered after production—and the ZnO nanoparticles (4%) were separately mixed using a mechanical stirrer at 750 rpm for 30 minutes. At the end of the pre-mixing stage, the ZnO nanoparticle solution was added dropwise into the microcapsule suspension, and the pH of the mixture was adjusted to 4. The resulting suspension was then subjected to stirring at 750 rpm and a temperature of 70 °C for 4 hours to allow for reaction. After stirring, the samples were left to stand at room temperature overnight. Finally, the ZnO nanoparticle-coated microcapsules were subjected to a filtration process to obtain the final product.

2.3. Characterization of Microcapsule/Mikrokapsül karakterizasyonu

The morphology of TD@G/GA/ZnO microcapsules was examined using Scanning Electron Microscopy (SEM). The particle size of the capsules was determined using Perkin-Elmer Malvern MS2000E model particle size analyzer. The chemical structure of the capsules was investigated by Fourier Transform Infrared Spectroscopy with Attenuated Total Reflectance (FTIR-ATR) analysis, and the measurements were performed in the wavenumber range of 4000–400 cm^{-1}. The phase change temperatures and thermal storage/release enthalpies of the microcapsules containing 1-tetradecanol as the core material were determined by differential scanning calorimetry (DSC). The DSC measurements were conducted

under a nitrogen atmosphere in the temperature range of -20 °C to 50 °C with a heating rate of 5 °C/min. The photothermal performance of the capsules was evaluated using a setup consisting of a thermal camera, a polyurethane box, a UV lamp, and a computer system. Prior to the test, 4 g of microcapsule sample was compacted into a polyurethane-based insulated box with dimensions of 3 × 3 cm and cooled in a refrigerator to temperatures below the melting point of the capsules. The conditioned sample was then irradiated under a UV lamp (25 W power, 0.17 W/cm² intensity) for 10 minutes at a distance of 12 cm. After irradiation, the light source was turned off, and the sample was allowed to cool naturally at room temperature. During the test, the surface temperature of the microcapsule sample was recorded every 15 seconds using a thermal camera. The data were transferred to a computer and temperature versus time graphs were plotted. Additionally, the photothermal conversion efficiency of the capsule sample was calculated using the equation given in Equation 1. (In the equation, m represents the mass of the microcapsule, ΔH is the melting enthalpy obtained from the DSC analysis of the composite material, P is the light irradiation intensity, S is the surface area exposed during the measurement, t_{mo} is the end time of the phase transition, t_{me} is the onset time of the phase transition, and Δt is the duration of the phase change process.

$$\eta = \frac{m \cdot \Delta H}{P \cdot S \cdot (t_{me} - t_{mo})} = \frac{m \cdot \Delta H}{P \cdot S \cdot \Delta t_l}$$

Equation 1

3. RESULTS

3.1. Morphological characterization and particle size distribution of microcapsules/Mikrokapsüllerin morfolojik karakterizasyonu ve parçacık boyut dağılımı

SEM images of microcapsules are presented in Figure 1a. The SEM images revealed that the microcapsules exhibited a spherical morphology with smooth surfaces. Additionally, the microcapsules were smaller than 200 nm and exhibited a nearly homogeneous size distribution. The PSD curves of microcapsules are given in Figure 1b. It was seen that microcapsules exhibited a single peak distribution. The mean particle size of the microcapsules was 64.13 µm, with a particle size distribution ranging from 16.63 to 100.68 µm. When comparing the results from SEM and PSD analyses, the microcapsules were smaller in size according to the SEM analysis than those measured by PSD. This observation is consistent with literature, which suggests that it resulted from the clustering of nano-sized particles, causing them to be measured as a single particle by the particle size analyzer (Alay-Aksoy et al., 2017).

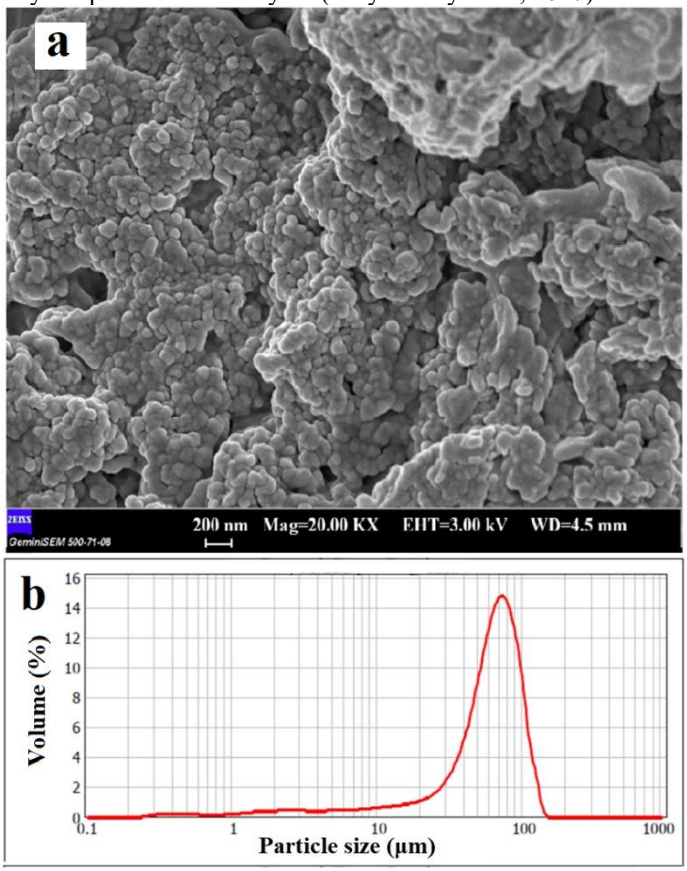

Figure 1. SEM images a) and particle size distribution b) of microcapsules

3.2. Chemical characterization of microcapsules by FTIR-ATR analysis/ FTIR-ATR analizi ile mikrokapsüllerin kimyasal karakterizasyonu

Figure 2 presents the IR spectra of the microcapsules, 1-tetradecanol, gelatin, gum arabic and ZnO nanoparticles. The broad peak around 3300 cm^{-1} in the spectrum of microcapsules was the combination of the -OH stretching vibration of the gum arabic polymer and the N-H stretching vibration of the gelatin polymer. In the spectrum of microcapsules, the sharp peaks observed at 2918 and 2850 cm^{-1} were C–H stretching vibrations of 1-tetradecanol. The C–N stretching peak observed at 1084 cm^{-1} in the IR spectrum of gelatin polymer appeared at around 1060 cm^{-1} in the IR spectrum of the microcapsules. The characteristic Zn-O band observed in the spectra of ZnO between 720 and 575 cm^{-1}, appeared as a small, broad peak at approximately 680 cm^{-1} in the IR spectra of the microcapsules.

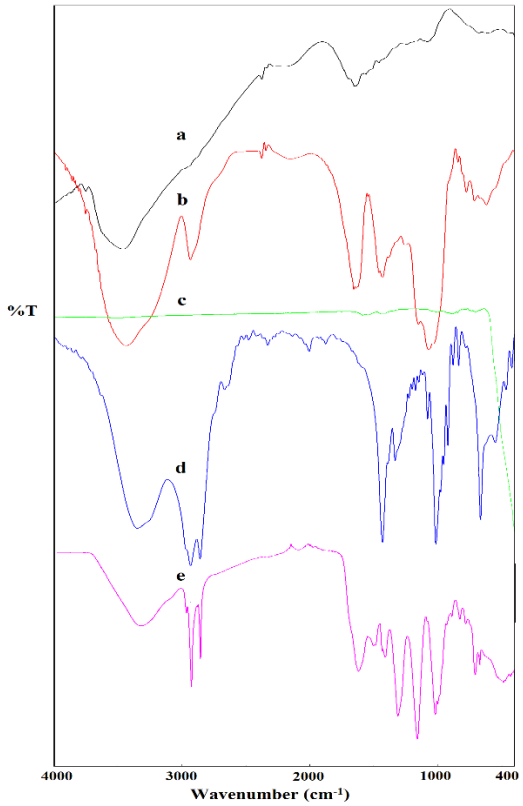

Figure 2. FTIR spectra of gelatin (a), gum arabic (b), ZnO (c), n-tetradecanol (d), TD@G/GA/ZnO microcapsules (e)

3.3. Thermal characterization of microcapsules by DSC analysis/ DSC analizi ile mikrokapsüllerin termal karakterizasyonu

The phase change temperatures and latent heat storage capacities of microcapsules were determined by DSC. The DSC graph of the microcapsules is displayed in Figure 3. According to DSC graph, the microcapsules stored latent heat of 97.7 J/g at a melting temperature of 35.8 °C. The microcapsules had a solidification temperature of 35.8°C, with a heat release capacity of -81.6 J/g during the solidification process. An examination of the literature indicated that the latent heat storage capacities of gelatin/ gum arabic -walled microcapsules containing paraffin ranged from 79 to 115 J/g (Demirbağ and Alay Aksoy, 2016; Malekipirbazari et al.,2014; Bayés-García et al., 2010). Compared to the results of the present study, these findings demonstrated that the high heat storage capacity of the microcapsules, along with their melting point compatible with body temperature, made them suitable candidates for a wide range of applications, including thermal energy storage systems and energy-conserving materials.

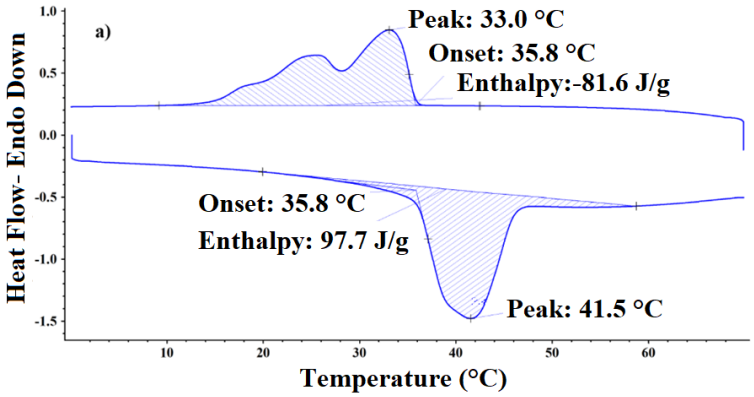

Figure 3. DSC graph of microcapsules

3.4. Evaluation of photothermal performance of microcapsules/ Mikrokapsüllerin fototermal performansının değerlendirilmesi

The photothermal conversion performance of microcapsules was evaluated by monitoring the temperature change on the surface of microcapsules during UV light exposure. The surface temperatures of the microcapsules were monitored with a thermal camera while exposed to a UV lamp acting as a solar simulator, and temperature-time curves were obtained at the end of the measurement, as shown in Figure 4. According to Figure 4, ZnO metal oxide nanoparticles coated on the microcapsules walls efficiently absorbed solar radiation and converted it into thermal energy through molecular vibrations, leading to a rapid increase in microcapsule surface temperature. In the temperature range of approximately 35–36 °C, the rate of surface temperature increase of the microcapsules decreased due to the onset of the solid–liquid phase transition of 1-tetradecanol, which constitutes the core material. TD@G/GA/ZnO microcapsules completed the phase transition in 270 seconds and reached a maximum temperature of 47.4°C. The photothermal conversion efficiency was calculated to be 94.60%. These findings demonstrate that microcapsule samples are capable of effectively absorbing UV light and converting it into thermal energy.

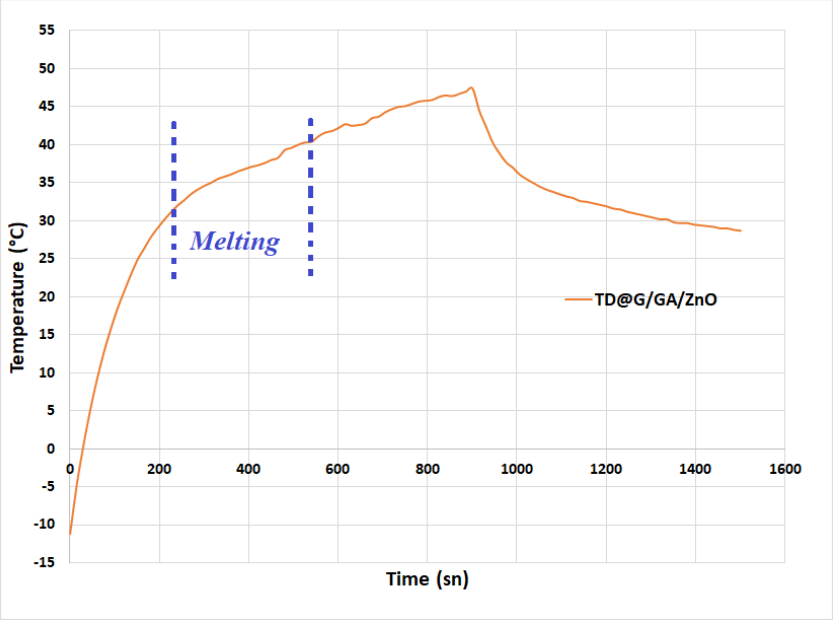

Figure 4. Temperature changes observed on the microcapsules surface during UV light exposure

4. DISCUSSION AND CONCLUSIONS

This study focused on the production and characterization of photothermal microcapsules using an environmentally friendly method. Microcapsules with an 1-tetradecanol core and gelatin/gum arabic shell were fabricated via the Pickering emulsion complex coacervation method using a ZnO Pickering stabilizer, and then coated with ZnO nanoparticles to impart photothermal functionality. FTIR analysis confirmed the successful formation of the microcapsules. The spherical microcapsules were found to store 97.7 J/g of thermal energy at 35.8 °C. In addition, the capsules demonstrated effective

photothermal conversion performance with a photothermal conversion efficiency of 94.60%. These results suggest that the developed microcapsules have strong potential for use in energy storage and photothermal applications.

Acknowledgements / Teşekkür

This work was financially supported by The Scientific and Technological Research Council of Türkiye (TÜBİTAK). (Project No. 123M172).

Ethics Committee Approval / Etik Kurul Onayı
N/A

Peer-review / Akran Değerlendirmesi
Externally peer-reviewed.

Author Contributions / Yazar Katkıları
Conceptualization: C.A., M.S.T., S.D.G.; Investigation: C.A., M.S.T., S.D.G.; Material and Methodology: C.A., M.S.T., S.D.G.; Supervision: C.A., M.S.T., S.D.G.; Visualization: C.A., M.S.T., S.D.G.; Writing-Original Draft: C.A., M.S.T., S.D.G.; Writing-review & Editing: C.A., M.S.T., S.D.G.; Other: All authors have read and agreed to the published version of manuscript.

Conflict of Interest / Çıkar Çatışması
The authors have no conflicts of interest to declare.

Funding / Finansal Destek

This work was financially supported by The Scientific and Technological Research Council of Türkiye (TÜBİTAK). (Project No. 123M172).

REFERENCES

Alay Aksoy, S., Alkan, C., Tözüm, M. S., Demirbağ, S., Altun Anayurt, R., & Ulcay, Y. (2017). Preparation and textile application of poly (methyl methacrylate-co-methacrylic acid)/n-octadecane and n-eicosane microcapsules. The Journal of the Textile Institute, 108(1), 30-41. https://doi.org/10.1080/00405000.2015.1133128

Alkan, C., Alakara, E. H., Aksoy, S. A., & Demir, İ. (2023). Cement mortar composites including 1-tetradecanol@ PMMA Pickering emulsion particles for thermal energy management of buildings. Chemical Engineering Journal, 476, 146843. https://doi.org/10.1016/j.cej.2023.146843

Bayés-García, L., Ventolà, L., Cordobilla, R., Benages, R., Calvet, T., & Cuevas-Diarte, M. A. (2010). Phase Change Materials (PCM) microcapsules with different shell compositions: Preparation, characterization and thermal stability. Solar Energy Materials and Solar Cells, 94(7), 1235-1240. https://doi.org/10.1016/j.solmat.2010.03.014

Bordes, C., Bolzinger, M. A., El Achak, M., Pirot, F., Arquier, D., Agusti, G., & Chevalier, Y. (2021). Formulation of Pickering emulsions for the development of surfactant-free sunscreen creams. International Journal of Cosmetic Science, 43(4), 432-445.

Chai, Z., Fang, M., & Min, X. (2024). Composite phase-change materials for photo-thermal conversion and energy storage: A review. Nano Energy, 109437. https://doi.org/10.1016/j.nanoen.2024.109437

Chen, X., Tang, Z., Gao, H., Chen, S., & Wang, G. (2020). Phase change materials for electro-thermal conversion and storage: from fundamental understanding to engineering design. Iscience, 23(6):101208. http://creativecommons.org/licenses/by-nc-nd/4.0/

Chen, J., Zhang, Y., Wu, F., Guan, B., Du, X., & Wang, H. (2021). Cellulose nanofiber/melanin hybrid aerogel supported phase change materials with improved photothermal conversion efficiency and superior energy storage density. Cellulose, 28(15), 9739-9750. https://doi.org/10.1007/s10570-021-03857-z

Chen, K., Chen, J., Xu, C., Zhu, H., Hu, J., & Yu, K. (2025). Design and Synthesis of Multi-compartment Microcapsules via Pickering Emulsion Polymerization for Infrared Stealth and Adaptive Camouflage Applications. Small, 21(5), 2405543. https://doi.org/10.1002/smll.202405543.

Demirbağ, S., Alay Aksoy, S., (2016) Encapsulation of phase change materials by complex coacervation to improve thermal performances and flame-retardant properties of the cotton fabrics. Fiber and Polymer, 17:408-417. DOI 10.1007/s12221-016-5113-z

de Carvalho-Guimarães, F. B., Correa, K. L., de Souza, T. P., Rodriguez Amado, J. R., Ribeiro-Costa, R. M., & Silva-Júnior, J. O. C. (2022). A review of Pickering emulsions: perspectives and applications. Pharmaceuticals, 15(11), 1413. doi:10.3390/ph15111413

Du, M., Yu, X., Zhang, Z., Shao, M., Zhou, L., Zhu, G., ... & Zhang, G. (2022). CuS nanoparticle-based microcapsules for solar-induced phase-change energy storage. ACS Applied Nano Materials, 5(9), 13009-13017. https://doi.org/10.1021/acsanm.2c02804

Fan, R., Zheng, N., & Sun, Z. (2022). A modified method to quantify the photo-thermal conversion efficiency of shape-stable phase change materials. Solar Energy Materials and Solar Cells, 237, 111572. https://doi.org/10.1016/j.solmat.2021.111572.

Huang, C., Li, Q., Yang, Y., Wei, S., Ji, R., Zhang, Q., ... & Xia, Y. (2020). A novel bifunctional microencapsulated phase change material loaded with ZnO for thermal energy storage and light–thermal energy conversion. Sustainable Energy & Fuels, 4(10), 5203-5214. https://doi.org/10.1039/D0SE00718H.

Hou, M., Jiang, Z., Chu, F., Zhang, X., & Lai, N. C. (2022). N-eicosane@ TiO2/TiN composite phase change microcapsules: Efficient visible light-driven reversible solid-liquid phase transition. Colloids and Surfaces A: Physicochemical and Engineering Aspects, 651, 129674. https://doi.org/10.1016/j.colsurfa.2022.129674

Li, S., Ji, W., Zou, L., Li, L., Li, Y., & Cheng, X. (2022). Crystalline TiO2 shell microcapsules modified by Co3O4/GO nanocomposites for thermal energy storage and photocatalysis. Materials Today Sustainability, 19, 100197. https://doi.org/10.1016/j.mtsust.2022.100197

Li, J., Long, Y., Cao, X., Sun, H., Jiao, R., Zhu, Z., Liang, W & Li, A. (2024). Recent advances and perspectives in solar photothermal conversion and storage systems: A review. Advances in Colloid and Interface Science, 103118. https://doi.org/10.1016/j.cis.2024.103118

Liu, H., Tian, X., Ouyang, M., Wang, X., Wu, D., & Wang, X. (2021a). Microencapsulating n-docosane phase change material into CaCO3/Fe3O4 composites for high-efficient utilization of solar photothermal energy. Renewable Energy, 179, 47-64. https://doi.org/10.1016/j.renene.2021.07.024
Liu, H., Qian, Z., Liao, G., & Wang, X. (2021). Integration of magnetic phase-change microcapsules with black phosphorus nanosheets for efficient harvest of solar photothermal energy. ACS Applied Energy Materials, 4(11), 13248-13262. https://doi.org/10.1021/acsaem.1c02835

Liu, H., Shen, H., Zhang, H., & Wang, X. (2022). Development of photoluminescence phase-change microcapsules for comfort thermal regulation and fluorescent recognition applications in advanced textiles. Journal of Energy Storage, 49, 104158. https://doi.org/10.1016/j.est.2022.104158

Ma, X., Liu, Y., Liu, H., Zhang, L., Xu, B., & Xiao, F. (2018). Fabrication of novel slurry containing graphene oxide-modified microencapsulated phase change material for direct absorption solar collector. Solar energy materials and solar cells, 188, 73-80. https://doi.org/10.1016/j.solmat.2018.08.021

Malekipirbazari, M., Sadrameli, S. M., Dorkoosh, F., & Sharifi, H. (2014). Synthetic and physical characterization of phase change materials microencapsulated by complex coacervation for thermal energy storage applications. International journal of energy research, 38(11), 1492-1500. https://doi.org/10.1002/er.3153

Maithya, O. M., Zhu, X., Li, X., Korir, S. J., Feng, X., Sui, X., & Wang, B. (2021). High-energy storage graphene oxide modified phase change microcapsules from regenerated chitin Pickering Emulsion for photothermal conversion. Solar Energy Materials and Solar Cells, 222, 110924. https://doi.org/10.1016/j.solmat.2020.110924

Maithya, O. M., Li, X., Feng, X., Sui, X., & Wang, B. (2020). Microencapsulated phase change material via Pickering emulsion stabilized by graphene oxide for photothermal conversion. Journal of materials science, 55, 7731-7742. https://doi.org/10.1007/s10853-020-04499-5

Sun, W., Zhang, Z., Zhang, Z., He, N., Wei, Q., Feng, L., Wang, Z., Wu, J., Liu, C., Fu, S., Hou, Y., Sebe G., & Zhou, G. (2024). Photothermal phase change material microcapsules via cellulose nanocrystal and graphene oxide co-stabilized Pickering emulsion for solar and thermal energy storage. Science China Materials, 67(10), 3225-3235.

Sun, W., Hou, Y., & Zhang, X. (2021). Bi-functional paraffin@ polyaniline/TiO2/PCN-222 (Fe) microcapsules for solar thermal energy storage and CO2 photoreduction. Nanomaterials, 12(1), 2. https://doi.org/10.3390/nano12010002

Tian, D., Shi, T., Wang, X., Liu, H., & Wang, X. (2022). Magnetic field-assisted acceleration of energy storage based on microencapsulation of phase change material with CaCO3/Fe3O4 composite shell. Journal of Energy Storage, 47, 103574. https://doi.org/10.1016/j.est.2021.103574

Wang, X., Li, C., & Zhao, T. (2018). Fabrication and characterization of poly (melamine-formaldehyde)/silicon carbide hybrid microencapsulated phase change materials with enhanced thermal conductivity and light-heat performance. Solar Energy Materials and Solar Cells, 183, 82-91. https://doi.org/10.1016/j.solmat.2018.03.019

Wang, X., Zhang, C., Wang, K., Huang, Y., & Chen, Z. (2021). Highly efficient photothermal conversion capric acid phase change microcapsule: Silicon carbide modified melamine urea formaldehyde. Journal of Colloid and Interface Science, 582, 30-40. https://doi.org/10.1016/j.jcis.2020.08.014

Xu, S., Du, M., Yu, X., Zhang, Z., Zhou, L., Zhu, G., Militky, J., Kremenakova, D., & Zhang, G. (2023). Preparation of photothermal conversion and energy storage microcapsules based on Pickering emulsions with poly (p-phenylenediamine) as stabilizer and photothermal materials. Journal of Energy Storage, 59, 106564. https://doi.org/10.1016/j.est.2022.106564

Xue, C. H., Du, M. M., Guo, X. J., Liu, B. Y., Wei, R. X., Li, H.G., Huang, MC, Deng FQ, & Jia, S. T. (2021). Fabrication of superhydrophobic photothermal conversion fabric via layer-by-layer assembly of carbon nanotubes. Cellulose, 28, 5107-5121. https://doi.org/10.1007/s10570-021-03857-z

Zhao, Q., He, F., Zhang, Q., Fan, J., He, R., Zhang, K., Yan H, & Yang, W. (2019a). Microencapsulated phase change materials based on graphene Pickering emulsion for light-to-thermal energy conversion and management. Solar Energy Materials and Solar Cells, 203, 110204. https://doi.org/10.1016/j.solmat.2019.110204

Zhao, Q., Yang, W., Zhang, H., He, F., Yan, H., He, R., Zhang, K. & Fan, J. (2019b). Graphene oxide Pickering phase change material emulsions with high thermal conductivity and photo-thermal performance for thermal energy management. Colloids and Surfaces A: Physicochemical and Engineering Aspects, 575, 42-49. https://doi.org/10.1016/j.colsurfa.2019.05.007

Zhao, Q., Yang, W., Li, Y., He, Z., Li, Y., Zhou, Y., Wang, R., Fan, J., & Zhang, K. (2020a). Multifunctional phase change microcapsules based on graphene oxide Pickering emulsion for photothermal energy conversion and superhydrophobicity. International Journal of Energy Research, 44(6), 4464-4474. https://doi.org/10.1002/er.5224

Zhao, K., Wang, J., Xie, H., & Guo, Z. (2022). Enhanced photothermal conversion and thermal conductivity of phase change n-Octadecane microcapsules shelled with nano-SiC doped crosslinked polystyrene. Energy Storage and Saving, 1(4), 284-292. https://doi.org/10.1016/j.enss.2022.09.003

Experimental examination of the effect of using fusel oil as a fuel additive in diesel engines on performance and emissions

DERVIŞ EROL*[1], HALIL ERDI GÜLCAN[2]

Abstract: In this study, the effects of using fusel oil as a fuel additive on the performance and emissions of a single-cylinder, four-stroke, water-cooled diesel engine were experimentally investigated. Fusel oil was blended with diesel fuel at volumetric ratios of 10% and 20%, and the results were compared with those obtained using 100% diesel fuel as the reference. The experiments were conducted at five different engine torque levels (10 Nm, 20 Nm, 30 Nm, 40 Nm, and 50 Nm) at a constant engine speed of 1500 rpm. The results showed that the addition of 10% and 20% fusel oil increased the brake specific fuel consumption (BSFC) by approximately 1% and 3.1%, respectively. The lower heating value (LHV) of fusel oil reduces the overall LHV of the blend, requiring more fuel injection to deliver the same power output. Furthermore, due to the oxygen content in fusel oil, carbon monoxide (CO) emissions were reduced by an average of 32% with the 10% fusel oil addition and by 6.5% with the 20% fusel oil addition. On the other hand, nitrogen oxides (NOx) emissions increased by approximately 25% and 39% for the 10% and 20% fusel oil blends, respectively. Considering that the 10% fusel oil blend provides performance results close to those of pure diesel fuel, it is regarded as a suitable alternative fuel for diesel engines.

Keywords: Emissions, engine performance, fusel oil, alternative fuel

[1]**Address:** Kırıkkale University, Kırıkkale Vocational School, Department of Automotive Technology, Kırıkkale/Türkiye
[2]**Address:** Selçuk University, Faculty of Technology, Department of Mechanical Engineering, Konya/Türkiye

***Corresponding author**: derol40@gmail.com

1. INTRODUCTION

The constant fluctuations in oil prices and the fear that reserves will be depleted in the coming years have increased the interest in biofuels in diesel engines (Demirbaş, 2001). In addition, the direct use of petroleum-based fuels results in the spread of harmful pollutants into the environment. This poses a significant threat to both living beings and the environment (Al-Rubaye et. al., 2023; Speight, 2020). For this reason, researchers and scientists have started to search for bio-based fuels instead of petroleum-based fuels.

The amount of oxygen in the chemical structure of bio-based fuels has significant effects on combustion characteristics and pollutant formation (Emiroğlu and Şen, 2018; Abu-Qudais et. al., 2000; Ağbulut et. al., 2019). They are generally known for reducing carbon emissions due to their low carbon content and improving combustion characteristics, especially at high-speed conditions (Ma et. al., 2017).

Today, studies on the use of alcohol or waste oil in traditional fuels continue. For instance, Ağbulut et al. added 10%, 15% and 20% isoamyl alcohol to diesel fuel. They reported that CO and NO_X emissions decreased significantly in experiments carried out under different load conditions, but HC emissions gave the opposite result (Ağbulut et. al., 2020). Another study, Awad et al. investigated the use of fusel oil in diesel engine operating at different speeds. It was reported that BSFC increased slightly in the mixture containing 20% fusel oil (F20) by volume, while F20 increased the ignition delay (Awad et. al., 2017). Similarly, Yılmaz tested diesel-fusel oil mixtures in a diesel engine operating under different loads. Here, the fusel content in the test fuels is 5% to 10%. When the results were examined, it was observed that as the amount of fusel oil increased, CO increased, but NO_X and soot pollutants decreased. Additionally, some increase in BSFC has also been reported Yılmaz, 2019). Also, Akçay and Özer published their study in 2019 reporting that NO_X and smoke pollutants were reduced by adding fusel oil to diesel fuel. In this study conducted at different loads, it was also stated that the use of fusel oil reduced combustion pressure (Akcay and Özer, 2024). In another study, Solmaz investigated the use of fusel oil in an SI engine. While fusel oil was used at rates of 50% to 100% in the study, it was reported that BTE decreased by 3.3% and 8.6%, respectively. Additionally, it has been reported that combustion pressure decreases with increasing fusel ratio (Solmaz, 2015). Hassan Pour et al. conducted a study on the ternary blend (diesel-biodiesel-fuel oil). The author emphasized that the presence of fusel oil in the blend reduced NO_X emissions but significantly increased CO and HC emissions (Hassan Pour et. al., 2018). Ardebili et al. conducted a study on the effect of nano-biochar additive on a diesel-fueled engine. The results showed that 10% fusel additive and also 100 ppm nanoadditive provided optimum performance and emission results (Ardebili et. al., 2020).

In this study, the effects of 100% diesel, 10% fusel oil and 20% fusel oil added fuels on the performance and emissions of a single cylinder water-cooled diesel engine under different loads are investigated.

2. MATERIAL AND METHOD

2.1 The preparation of test fuel blends

The fusel oil used in the experimental studies was obtained from the Alcohol Production Department of the Eskişehir Sugar Factory, while the diesel fuel was supplied from the Kırıkkale branch of a corporate fuel company operating in Turkey. The fuel blends were prepared as 100% diesel (D100), 10% fusel oil and 90% diesel (F10), and 20% fusel oil and 80% diesel (F20).

2.2 Experimental setup and test engine

The experimental studies were conducted on a test setup involving a single-cylinder, water-cooled, four-stroke, direct-injection diesel engine, as shown in Figure 1. The technical specifications of the diesel engine used in the experimental studies are given in Table 1.

Figure 1. Experimental setup

Table 1. The technical specifications of test engine

Parameters	**Specification**	**Parameters**	**Specification**
Engine supplier	Erin Engine Corporation Inc.	Ignition	Compression-ignition
Brand	Erin Engine	Cooling system	Water-cooled
Model	1.16L Diesel	Idle speed	600 rpm
Cylinder number	1	Swept volume	1160 cm^3
Engine cycle	4	Cylinder bore	108 mm
Maximum engine power	18 kW @ 2400 rpm	Stroke	127 mm
Maximum engine torque	80 Nm @ 1800 rpm	Compression ratio	14.6:1
Type of fuel injection	Direct injection	Injector nozzle number	6

3. EXPERIMENTAL RESULTS

3.1. Engine performance

Figure 2 presents the variations in BSFC curves under different load conditions for the F0, F10, and F20 fuels. As seen, the highest BSFC values for all three fuels are measured at 10 Nm. As the load increases from 10 Nm to 40 Nm, BSFC shows a decreasing trend. The main reason for this is that combustion temperatures are relatively lower at low loads, which negatively affects combustion stability and thus reduces engine performance. With increasing load, combustion temperatures rise, and unburned fuel particles are burned (increasing combustion efficiency), leading to improved combustion stability. As a result, BSFC tends to decrease. At 50 Nm, however, a slight increase in BSFC is observed for all three fuels. This is likely due to excessive enrichment of the mixture caused by higher fuel injection into the combustion chamber, leading to insufficient oxygen for complete combustion. This situation decreases combustion efficiency and increases fuel consumption. Overall, the lowest fuel consumption is recorded with F0, while the addition of 10% and 20% fusel oil increases BSFC. The lower heating value (LHV) of fusel oil reduces the overall LHV of the blend, requiring more fuel injection to deliver the same power output. Consequently, fuel consumption increases. Within the given load range, the BSFC values of F10 and F20 show an increasing trend of approximately 1.9% and 4.3%, respectively, compared to F0.

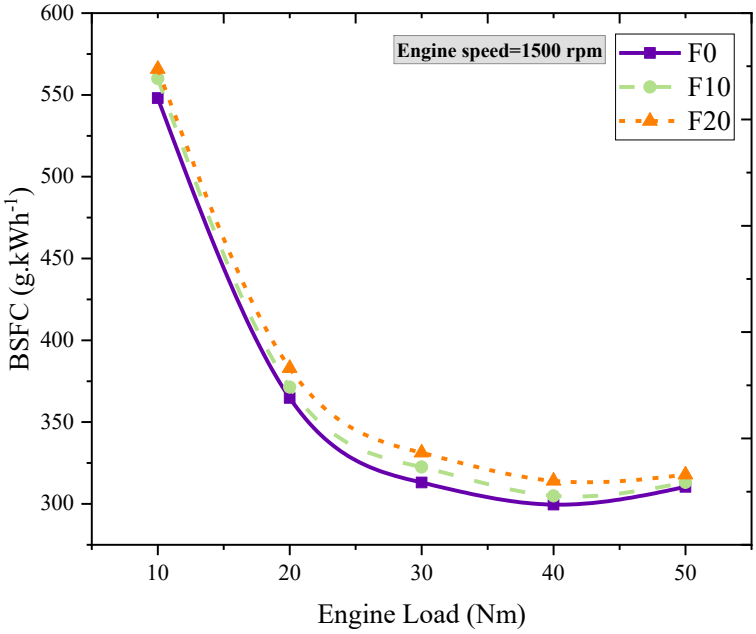

Figure 2. Variation of BSFC curves of F0, F10, and F20 fuels versus engine load

Figure 3 presents the variations in exhaust gas temperature (EGT) curves under different load conditions for the F0, F10, and F20 fuels. As seen, the EGT values of the three fuels are quite similar at 10 and 20 Nm; however, with an increase in engine load from 20 Nm to 50 Nm, notable differences in the results begin to appear. This can be attributed to the prolonged combustion duration due to increased fuel injection. The lower LHV and cetane number of the fusel oil blends cause delayed ignition, which shifts the main combustion phase toward the expansion period, resulting in higher EGT. Overall, the highest EGT values are measured with F0. The main reason for this is that F0 has a higher LHV compared to the others. For the specified load conditions, F10 and F20 reduce EGT by an average of approximately 2.7% and 3.1%, respectively, compared to F0.

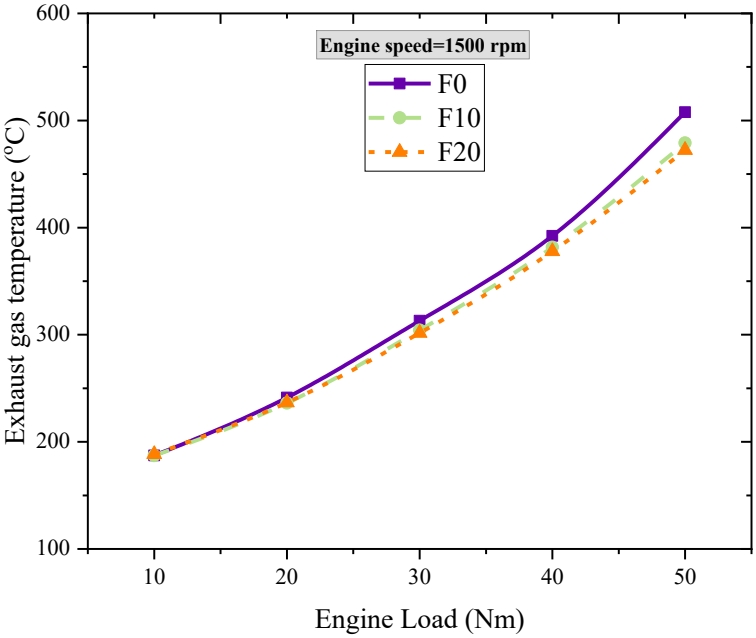

Figure 3. Variation of EGT curves of F0, F10, and F20 fuels versus engine load

3.2. Engine emissions

CO emissions occur in rich mixture regions where oxygen is insufficient, causing carbon to be released as CO instead of being fully oxidized to CO_2 (Pulkrabek, 2004; Heywood, 2018). Figure 4 presents the variations in CO emission curves under different load conditions for the F0, F10, and F20 fuels. It is observed that CO emissions remain below 0.2% between 10 Nm and 40 Nm but increase significantly as the engine load rises from 40 Nm to 50 Nm. This is due to the substantial increase in fuel injection into the combustion chamber at higher loads. Consequently, the air–fuel ratio decreases, leading to more rich mixture regions and a reduction in available O_2. As a result, carbon is released as CO instead of being converted into CO_2. Additionally, due to the overly rich mixture, combustion efficiency drops, resulting in unburned fuel particles. The oxygen content of fusel oil helps support combustion in these excessively rich regions, partially reducing CO emissions. Compared to F0, the F10 and F20 fuels reduce CO emissions by approximately 31% and 6.1%, respectively, within the specified load range.

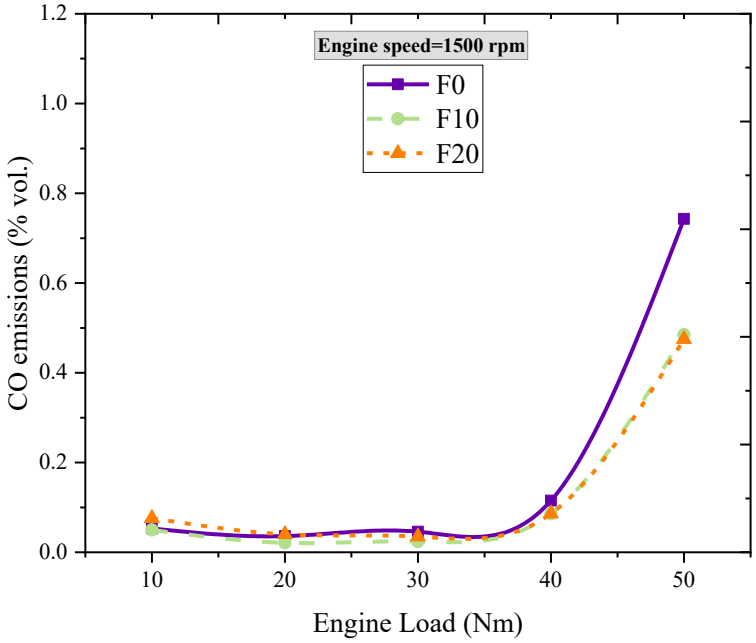

Figure 4. Variation of CO emission curves of F0, F10, and F20 fuels versus engine load

Figure 5 presents the variations in carbon dioxide (CO_2) emission curves under different load conditions for the F0, F10, and F20 fuels. With increasing engine load, CO_2 emissions tend to rise for all three fuels. As the load increases, greater fuel injection leads to higher combustion temperatures, which in turn enhances complete combustion, resulting in increased CO_2 emissions. The use of fusel oil in diesel fuel reduces CO_2 emissions at all load levels. The main reason fusel oil reduces both CO and CO_2 emissions compared to diesel fuel is its significantly lower carbon content and higher oxygen content in its chemical structure. Within the specified load range, CO_2 emissions of F10 and F20 are reduced by an average of 4.8% and 6.9%, respectively, compared to F0.

Figure 6 presents the variations in hydrocarbon (HC) emission curves under different load conditions for the F0, F10, and F20 fuels. The use of fusel oil as a fuel additive in diesel engines significantly increases HC emissions at low loads. This is probably due to the lower combustion temperatures at low loads. Lower combustion temperatures reduce combustion efficiency, leading to an increase in unburned HC. In addition, the rich mixture regions increase due to the increased BSFC resulting from the use of fusel oil at low loads. This causes unburned HC to spread to the environment during the exhaust stroke. In addition, due to the physicochemical properties of the fusel oil (low cetane, high viscosity), the combustion efficiency of the fuel decreases. Additionally, the lower LHV of F10 and F20 compared to F0 requires more fuel injection to produce the same power, leading to higher HC emissions. Increasing combustion temperatures with increasing load contribute to more efficient combustion of fusel mixtures with O2 content. The O2 content of the fusel contributes to the reduction of HC emissions by accelerating the oxidation process under high temperatures. In general, the highest HC emissions are observed with the F0 fuel at 50 Nm, reaching 47 ppm. Under low-load conditions, lower combustion temperatures increase combustion instability and reduce combustion efficiency. The lowest HC emissions for fusel-blended fuels are measured at 29 ppm with F20 fuel under 50 Nm load.

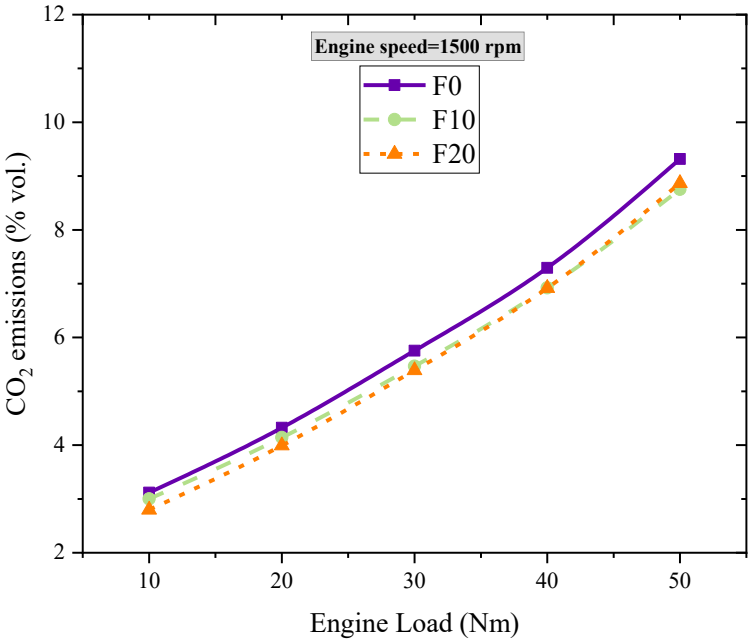

Figure 5. Variation of CO_2 emission curves of F0, F10, and F20 fuels versus engine load

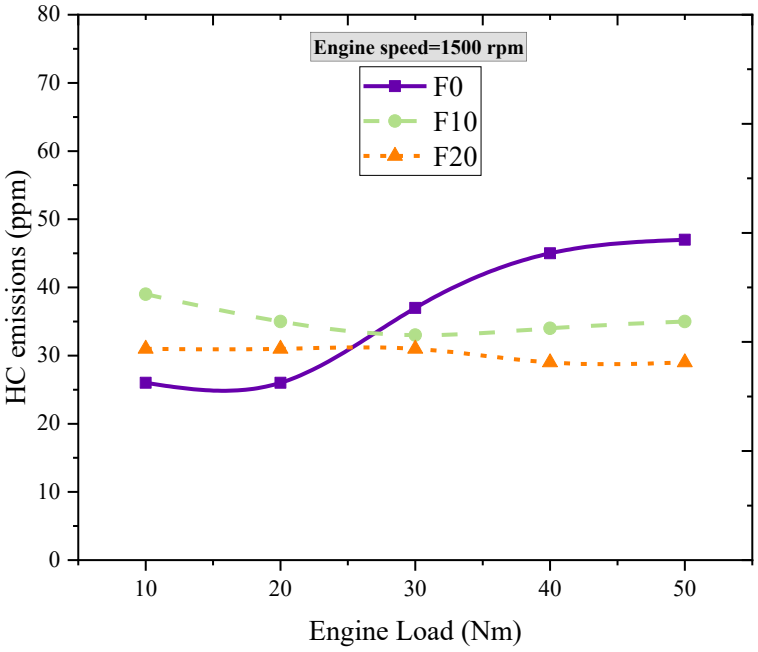

Figure 6. Variation of HC emission curves of F0, F10, and F20 fuels versus engine load

Figure 7 presents the variations in NO_X emission curves under different load conditions for the F0, F10, and F20 fuels. The addition of fusel oil significantly affects NO_X emissions, likely due to the high oxygen content in its chemical structure. NO_X emissions increase considerably at high temperatures and elevated O_2 concentrations through thermal formation mechanisms. The highest NO_X emissions are recorded at 30 Nm, with the NO_X levels of F0, F10, and F20 fuels being 599 ppm, 564 ppm, and 662 ppm, respectively. The lowest NO_X emissions are observed at 10 Nm, with values of 340 ppm, 295 ppm, and 278 ppm for F0, F10, and F20, respectively. This is attributed to the lower combustion temperatures under low-load conditions. Under full load, combustion deteriorates due to an excessively rich mixture, which results in reduced NO_X emissions. Overall, within the specified load range, NO_X emissions for F20 increase by approximately 0.8%, but for F10 decrease by approximately 8.7% compared to F0.

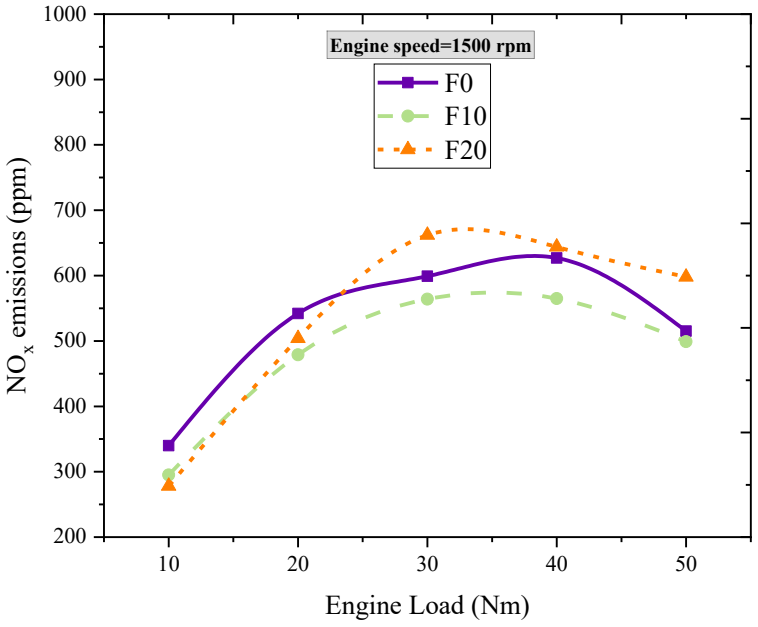

Figure 7. Variation of NO_X emission curves of F0, F10, and F20 fuels versus engine load

4. DISCUSSION AND CONCLUSIONS

In this study, the performance and emission changes of 10% and 20% volumetric fusel oil addition to diesel fuel under five different load and constant speed conditions were observed. The main findings of this experimental study are summarized below:

- The use of 10% and 20% volumetric fusel oil in diesel fuel increases fuel consumption. This is due to the lower LHV of fusel oil compared to diesel. In full load conditions, it was determined that the BSFC values increased due to the excessively rich mixture created by the fuel injected into the combustion chamber. In addition, although F10 showed a higher BSFC value compared to F0 on average, this value remained below 2%.

- The lowest EGT throughout the study was obtained in mixtures with fusel oil addition. The highest decrease in EGT was recorded as 7% at 50 Nm with F20.

- The O_2 content of fusel oil causes a decrease in CO and CO_2 emissions. The best reduction rate in CO emissions is shown by F10 fuel with an average of 31%, while the best reduction rate in CO_2 emissions is shown by F20 fuel with an average of 6.1%.

- Adding 10% fusel oil to diesel fuel by volume increases it by an average of 5.5%, while providing a 26% reduction under all load conditions. Adding 20% fusel oil to diesel fuel by volume reduces HC emissions by an average of 10%. The increase in O_2 density with the increase in fusel oil contributes significantly to the reduction of HC emissions.

- NO_X emissions decrease with the addition of F10, while there is a general increase in F20 fuel. F10 reduces NO_X emissions by an average of 8.7% compared to F0, while F20 fuel increases it by an average of 1%.

- As a result, the use of fusel oil in diesel fuel increases fuel consumption while increasing HC emissions. However, F10 fuel seems more interesting because it reduces both CO and CO_2 emissions. In addition, the performance results of F10 fuel are quite close to diesel performance results. In future studies, the economic and environmental cost of using F10 fuel can be calculated.

Acknowledgment
This study was supported by the Scientific Research Projects Coordination Unit of Kırıkkale University (Project No: 2023/080), and their financial support is gratefully acknowledged.

Ethics Committee Approval
N/A

Author Contributions / Yazar Katkıları
Conceptualization: D.E., H.E.G.; Investigation: D.E., H.E.G.; Material and Methodology: D.E., H.E.G.; Supervision: D.E., H.E.G.; Visualization: D.E., H.E.G.; Writing-Original Draft: D.E., H.E.G.; Writing-review & Editing: D.E., H.E.G.; Other: All authors have read and agreed to the published version of manuscript.

Conflict of Interest
The authors have no conflicts of interest to declare.

Funding
This study was financial supported by the Scientific Research Projects Coordination Unit of Kırıkkale University.

REFERENCES

Abu-Qudais, M., Haddad, O., Qudaisat, M. (2000). The effect of alcohol fumigation on diesel engine performance and emissions. Energy Conversion and Management, 41(4), 389-399. https://doi.org/10.1016/S0196-8904(99)00099-0

Ağbulut, Ü., Sarıdemir, S., Albayrak, S. (2019). Experimental investigation of combustion, performance and emission characteristics of a diesel engine fuelled with diesel–biodiesel–alcohol blends. Journal of the Brazilian Society of Mechanical Sciences and Engineering, 41(9), 389. https://doi.org/10.1007/s40430-019-1891-8

Ağbulut, Ü., Sarıdemir, S., Karagöz, M. (2020). Experimental investigation of fusel oil (isoamyl alcohol) and diesel blends in a CI engine. Fuel, 267, 117042. https://doi.org/10.1016/j.fuel.2020.117042

Akcay, M., Ozer, S. (2024). Experimental investigation on performance and emission characteristics of a CI diesel engine fueled with fusel oil/diesel fuel blends. Energy Sources, Part A: Recovery, Utilization, and Environmental Effects, 46(1), 2600-2615. https://doi.org/10.1080/15567036.2019.1689317

Al-Rubaye, A. H., Jasim, D. J., Ameen, H. F. M., Al-Robai, H. A., Al-Assal, J. R. (2023, April). The Impacts of Petroleum on Environment. In IOP Conference Series: Earth and Environmental Science 1158(3), 032014. https://doi.org/10.1088/1755-1315/1158/3/032014

Ardebili, S. M. S., Taghipoor, A., Solmaz, H., Mostafaei, M. (2020). The effect of nano-biochar on the performance and emissions of a diesel engine fueled with fusel oil-diesel fuel. Fuel, 268, 117356. https://doi.org/10.1016/j.fuel.2020.117356

Awad, O. I., Mamat, R., Ali, O. M., Yusri, I. M., Abdullah, A. A., Yusop, A. F., Noor, M. M. (2017). The effect of adding fusel oil to diesel on the performance and the emissions characteristics in a single cylinder CI engine. Journal of the Energy Institute, 90(3), 382-396. https://doi.org/10.1016/j.joei.2016.04.004

Demirbaş, A. (2001). Energy balance, energy sources, energy policy, future developments and energy investments in Turkey. Energy Conversion and Management, 42(10), 1239-1258. https://doi.org/10.1016/S0196-8904(00)00109-6

Emiroğlu, A. O., Şen, M. (2018). Combustion, performance and emission characteristics of various alcohol blends in a single cylinder diesel engine. Fuel, 212, 34-40. https://doi.org/10.1016/j.fuel.2017.10.016

Hassan Pour, A., Safieddin Ardebili, S. M., Sheikhdavoodi, M. J. (2018). Multi-objective optimization of diesel engine performance and emissions fueled with diesel-biodiesel-fusel oil blends using response surface method. Environmental science and pollution research, 25, 35429-35439. https://doi.org/10.1007/s11356-018-3459-z

Heywood, J. B. (2018). Internal combustion engine Fundamentals. 2nd edition, Published by McGraw-Hill Education, ISBN: 978-1-26-011611-3

Ma, Y., Huang, S., Huang, R., Zhang, Y., Xu, S. (2017). Ignition and combustion characteristics of n-pentanol–diesel blends in a constant volume chamber. Applied Energy, 185, 519-530. https://doi.org/10.1016/j.apenergy.2016.11.002

Pulkrabek, W. W. (2004). Engineering fundamentals of the internal combustion engine. 2nd edition, Published by Pearson, ISBN: 978-0-13-140570-7

Solmaz, H. (2015). Combustion, performance and emission characteristics of fusel oil in a spark ignition engine. Fuel Processing Technology, 133, 20-28. https://doi.org/10.1016/j.fuproc.2015.01.010

Speight, J. G. Petroleum refining and environmental control and environmental effects. In Fossil Energy (pp. 101-131). Springer, New York, 2020. https://doi.org/10.1007/978-1-4939-9763-3_70

Yılmaz, E. (2019). Investigation of the effects of diesel-fusel oil fuel blends on combustion, engine performance and exhaust emissions in a single cylinder compression ignition engine. Fuel, 255, 115741. https://doi.org/10.1016/j.fuel.2019.115741

Taxonomic and Functional Diversity of Coastal Wetland Vegetation Zones in Minakaleh Peninsula

MOHAMMAD KARIMI[1], MEHDI ABEDI*[1], ARDALAN DARYAEİ[2]

Abstract: The Miankaleh Peninsula is an important international wetland located in the southern part of the Caspian Sea. However, the wetland vegetation in Miankaleh has been rarely investigated. To address this, we evaluated the taxonomic diversity of three wetland zones, each dominated by a dominant species: Salicornia, Juncus, and Tamarix. These zones were selected due to their proximity to the wetland and their distinct dominant vegetation types. We sampled five macroplots in each zone and calculated several commonly used indices of biodiversity and evenness, including the Shannon, Simpson, and Margalef diversity indices, as well as the McIntosh and Smith-Wilson evenness indices. Functional diversity was also assessed using multiple indices, including functional richness, evenness, divergence, dispersion, and Rao's quadratic entropy to complement the taxonomic analysis. The data revealed significant ecological differences between these zones, with the Juncus zone exhibiting the highest species richness, while the Salicornia zone had the lowest. NMDS results also showed differences in vegetation composition. The diversity and evenness indices, as well as the functional diversity indices, were highest in the Juncus and Tamarix zones and lowest in the Salicornia zone. These findings suggest that dominant vegetation types can significantly influence species composition and patterns of community-level diversity even within a geographically limited area. These results highlight that, similar to taxonomic patterns, functional trait diversity is strongly influenced by the dominant species in each zone, resulting in distinct ecological structures even in closely situated wetland habitats.

Keywords: diversity, evenness, Caspian Sea, vegetation ecology

[1]**Address:** Department of Range Management, Faculty of Natural Resources and Marine Sciences, Tarbiat Modares University, Noor, Mazandaran Province, Iran
[2]**Address:** University of Natural Resources and Life Sciences, Vienna (BOKU), Institute of Geomatics, Peter-Jordan-Straße 82, A-1190, Vienna, Austria

***Corresponding author**: mehdi.abedi@modares.ac.ir

1. INTRODUCTION

Wetlands are critical ecosystems that provide a multitude of essential environmental services. They play a significant role in flood control, climate regulation, carbon storage, and aquifer recharge, making them indispensable for maintaining ecological balance (Costa, Silva, & Evans, 2013; Whigham, 2018). Wetlands are highly diverse, serving as breeding grounds and habitats for numerous species of plants, invertebrates, fish, and wildlife, thus contributing significantly to global biodiversity (Costa, Silva & Evans, 2013; Gaiser & Rühland, 2010). Despite the recognized ecological importance of wetland vegetation, many wetlands, like Miankaleh, remain poorly investigated in terms of diversity patterns (Shokri, Safaian, Ahmadi, & Amiri, 2004; Sharifnia, Asri, & Gholami-Te, 2007; Amirnezhad, Rafiei, & Atghaei, 2010).

To address this gap, the present study examines the taxonomic and functional diversity of wetland vegetation across three ecologically distinct zones within the Miankaleh Peninsula, each characterized by a different dominant plant genus: Salicornia, Juncus, and Tamarix. These zones were selected for their proximity to the wetland and their contrasting dominant vegetation, which are hypothesized to influence species composition and ecological functioning. This study seeks to quantify and compare community-level diversity and trait composition across zones by employing a variety of commonly used taxonomic diversity indices (such as Shannon, Simpson, Margalef) and evenness metrics (like McIntosh, Smith-Wilson) (Spellerberg & Fedor, 2003), as well as functional diversity indices (including FRic, FEve, FDiv, FDis, and RaoQ) (Mendes, Evangelista, Thomaz, Agostinho, & Gomes, 2008; Villéger, Mason, & Mouillot, 2008).

2. MATERIAL AND METHOD

Study Area

Miankaleh is a peninsula located in Mazandaran Province, Iran, covering an area of 68,800 hectares. This peninsula, located in the southeastern part of the Caspian Sea, is renowned for its unique flora, fauna, and high conservation value (Fig. 1). It is one of Iran's thirteen biosphere reserves under the Man and the Biosphere (MAB) Programme. It is considered a suitable habitat for terrestrial and aquatic plants, animals, and migratory birds (Ejtehadi et al., 2003). The region receives an average annual precipitation of 675 mm and has a mean annual temperature of 17.6°C. The area's climate is classified as semi-humid (Ghahroudi Tali et al., 2012).

Miankaleh hosts over 261 plant species from 60 families and 177 genera. The most represented families include Asteraceae, Poaceae, Papilionaceae, Cyperaceae, and Brassicaceae. The most frequent life forms in Miankaleh are therophytes (annual plants) and hemicryptophytes (perennial plants), accounting for 52.5% and 29% of the species, respectively (Sharifnia, Asri, & Gholami-Te, 2007).

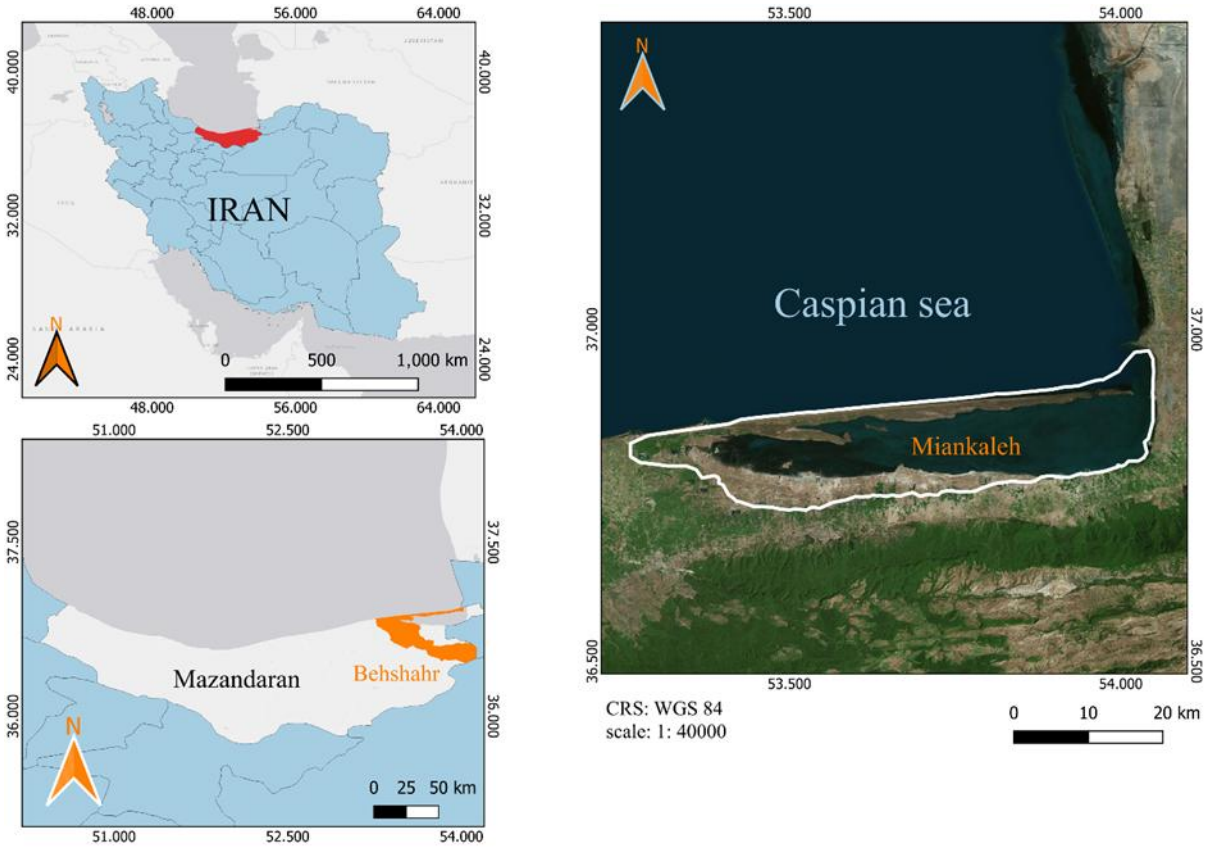

Fig 1. Study area location

Sampling Method

Three vegetation zones, including Tamarix, Salicornia, and Juncus, were selected (Fig. 2). Vegetation sampling was conducted during the appropriate growing season for these plants in late spring 2023. Fifteen 30 m × 30m plots were established near the Miankaleh wetland, with five plots located in each vegetation zone. Within each plot, the percentage cover of the dominant species (excluding annuals), ground cover, and the geographical coordinates of the plot were recorded (Arzani & Abedi, 2015). To assess taxonomic diversity indices, the *adiv* package and for functional indices FD package in R software were used (Pavoine, 2020; Laliberté & Legendre, 2010; Laliberté, Legendre, & Shipley, 2014). Various indices were calculated to analyze biodiversity, species richness, and evenness. GLMM for comparisons, PCA for diversity indices, and NMDS for vegetation compositions were applied for statistical analysis.

Traits

To assess plant functional diversity across the study zones, a set of key functional traits was measured for the dominant species in each plot. The selected traits included: chlorophyll content, fresh leaf mass (g), dry leaf mass (g), leaf thickness (cm), leaf area (cm^2), specific leaf area (SLA, cm^2/g), leaf dry matter content (LDMC), plant height (m), and leaf length (cm).

Fresh leaves were collected from representative individuals and processed according to standard protocols for functional traits (Cornelissen et al., 2003). Chlorophyll content was measured using a portable SPAD 504. Fresh mass was recorded immediately after collection. Leaves were then scanned to determine leaf area, measured for thickness using a digital caliper, and dried at 60°C for 48 hours to obtain dry mass. SLA was calculated as the ratio of leaf area to dry mass, while LDMC was calculated as the ratio of dry mass to fresh mass. Plant height was measured from the base to the apex of each individual, and leaf length was taken as the longest dimension of the leaf blade. These traits were used to calculate taxonomic and functional diversity indices to compare vegetation zones.

Fig 2. Landscape of study wetland zones

3. RESULTS

According to Table 1, only Margalef diversity and species richness were statistically significant among all taxonomic indices. The Juncus zone (4) showed higher values compared to both the Tamarix (3) and Salicornia (2.8) zones, with significant differences observed. In terms of Margalef diversity, the Juncus zone again exhibited the highest value (0.71), compared to the Tamarix (0.52) and Salicornia (0.49) zones. none of the functional diversity indices showed any significant differences among the three vegetation zones.

Indices	Salicornia	Tamarix	Juncus	F Value	P Value
Richness	2.80 ± 0.20b	3.00 ± 0.32b	4.00 ± 0.00a	8.86	0.00
Simpson diversity	1.64 ± 0.21	1.93 ± 0.18	1.85 ± 0.23	0.50	0.62
Shannon diversity	0.61 ± 0.11	0.76 ± 0.10	0.74 ± 0.16	0.42	0.67
Margalef diversity	0.49 ± 0.06b	0.52 ± 0.06b	0.71 ± 0.02a	6.31	0.01
McIntosh evenness	0.49 ± 0.11	0.63 ± 0.07	0.48 ± 0.12	0.72	0.51
SmithWilson evenness	0.43 ± 0.07	0.47 ± 0.08	0.30 ± 0.08	1.22	0.33
FRic	4.78 ± 0.60	3.57 ± 1.46	1.98 ± 0.42	2.65	0.12
FEve	0.60 ± 0.13	0.61 ± 0.14	0.65 ± 0.12	0.04	0.96
FDiv	0.74 ± 0.08	0.86 ± 0.05	0.87 ± 0.05	1.40	0.29
FDis	1.57 ± 0.35	2.24 ± 0.30	1.61 ± 0.44	1.04	0.38
RaoQ	4.08 ± 1.02	6.35 ± 0.92	4.39 ± 1.32	1.25	0.32

Table 1. Analysis of variance (ANOVA) of Taxonomic indices across vegetation zones

The NMDS (Non-metric Multidimensional Scaling) plot (Fig. 3) illustrates the variation in plant community composition across the Juncus, Salicornia, and Tamarix zones (Stress=0.1). All three zones showed differences in plant compositions (F=4.45; P< 0.01 according to PERMANOVA results).

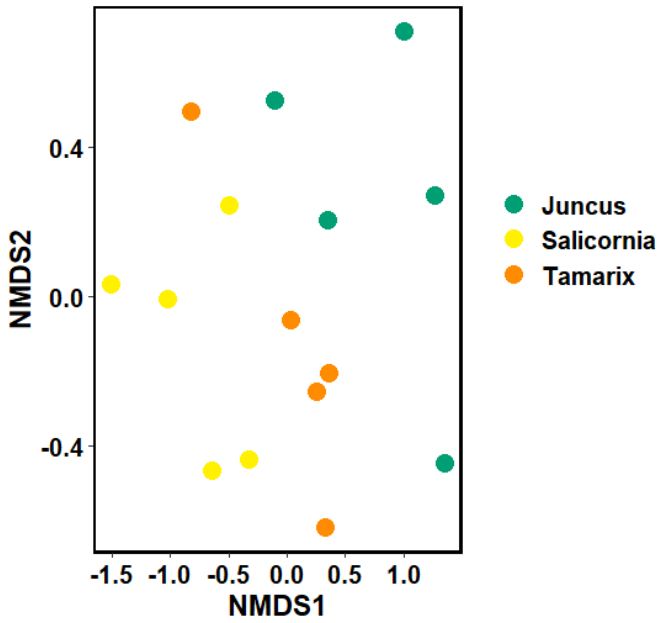

Fig 3. Compositional differentiation of shrub communities based on NMDS analysis

In the principal component analysis (PCA), the indices FRic, FEve, FDiv, Margalef diversity, and Richness clustered together on the positive side of the first dimension (Dim1) and on the negative side of the second dimension (Dim2), which is associated with the Juncus zone. The indices Smith-Wilson evenness, McIntosh evenness, Functional Dispersion (FDis), Rao's Quadratic Entropy (RaoQ), Shannon diversity, and Simpson diversity were positioned on the positive side of both the first dimension (Dim1) and the second dimension (Dim2) in the PCA, associated with the Tamariz zone. The Salicornia zone is also mainly located in the negative part of Axis 1, which is negatively associated with most taxonomic and functional indices. The first axis explains 53.6% of the variation, while the second axis accounts for 22.8% of the variation. Results of heatmaps also confirm the PCA patterns(Fig.4).

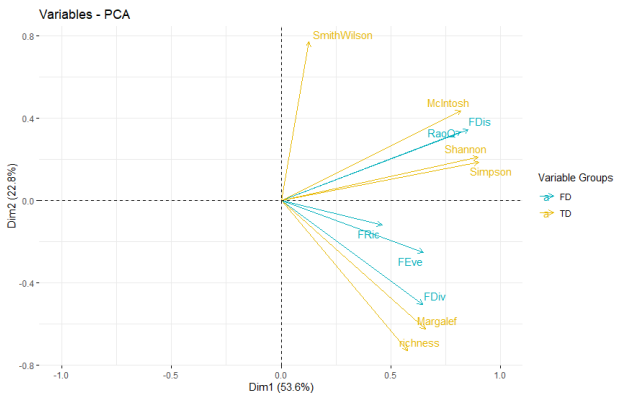

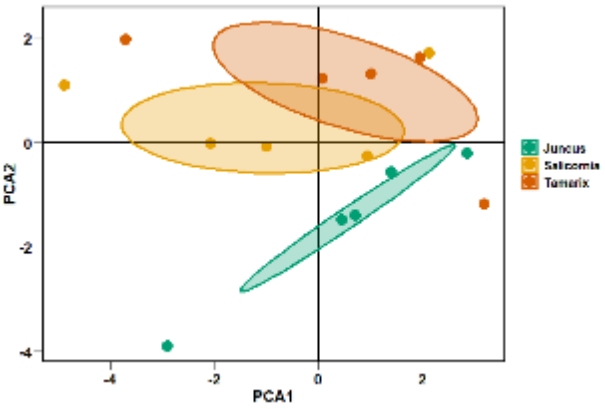

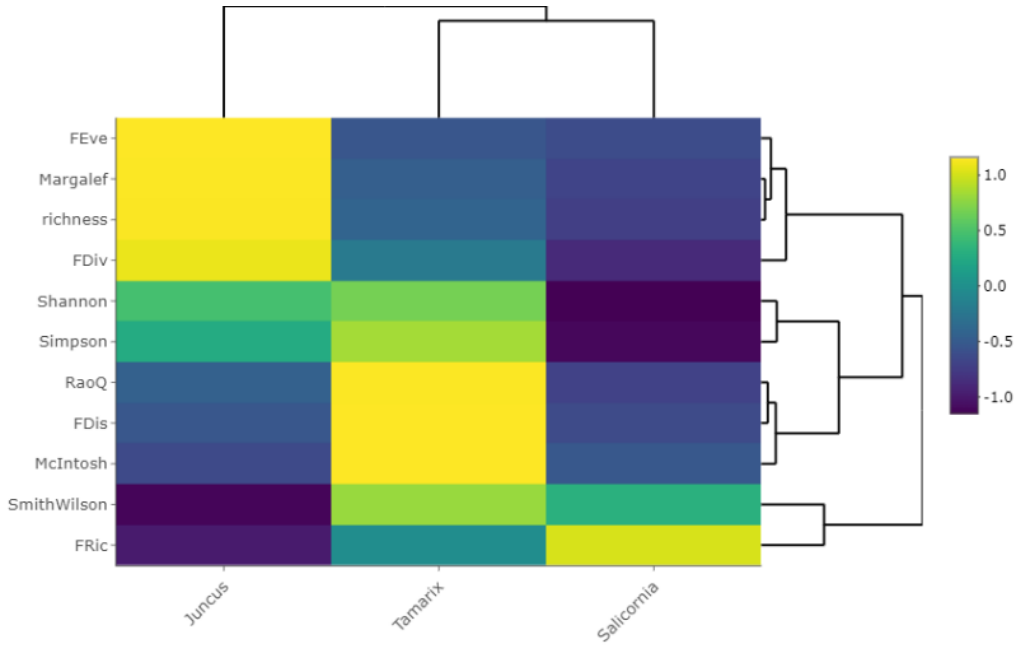

Fig4. PCA analysis and Heatmap on taxonomic and functional indices in 3 zones

4. DISCUSSION AND CONCLUSIONS

This study revealed distinct taxonomic and functional diversity patterns among the three wetland zones. The Juncus and Tamarix zones generally exhibited greater diversity and functional complexity, while the Salicornia zone consistently showed the lowest values, likely due to stronger environmental filters such as salinity and waterlogging (Dembicz et al., 2020; Matthews & Endress, 2010).

The Salicornia zone showed the lowest levels of both taxonomic and functional diversity, indicating a limited and simplified community composition. This pattern arises from extreme salinity, anoxia, and high abiotic stress, leading to the dominance of one or a few highly stress-tolerant species. Such dominance results in strong environmental filtering, as the species possess similar traits, such as succulence and salt tolerance, ultimately reflecting minimal ecological multifunctionality and low niche differentiation (Nathan, Osem, Shachak, & Meron, 2016). This phenomenon may be attributed to convergence in functional traits due to similar adaptive strategies across all zones or to limitations in trait variability at the community level (Pakeman, 2011; Ricotta, 2005; Maire et al., 2012). The Tamarix zone, on the other hand, was associated with several indices such as Shannon, Simpson, RaoQ, FDis, and both evenness indices, indicating a balanced community structure and trait distribution in a moderately stressful environment. The consistent abundance along with moderate richness suggests a balance between filtering processes and the coexistence of stress-tolerant strategies. High functional dispersion indices (FDis) and RaoQ reveal the presence of functionally dissimilar species that thrive despite taxonomic constraints. This indicates functional divergence in response to stress rather than simply an increase in species richness. The Juncus zone is characterized by various indices, including Richness, Margalef, Functional Richness (FRic), Evenness (FEve), and Functional Diversity (FDiv), suggesting a highly functional and niche-structured community. The high levels of taxonomic and functional richness indicate niche complementarity and minimal environmental filtering. Elevated FRic and FDiv demonstrate a broad range of traits and their divergence, facilitating efficient resource use and coexistence among species. As a result, these zones contribute to enhanced multifunctionality, resilience. The low functional redundancy in Salicornia suggests reduced ecological stability and productivity (da Silva Camilo et al., 2018), while higher functional diversity in Juncus and Tamarix zones points to more resilient ecosystems.

Despite the lack of statistically significant differences in univariate functional diversity indices among the three vegetation zones, multivariate analyses (PCA and NMDS) revealed clear patterns in trait and species composition (Legendre & Legendre, 2012). This highlights the value of ordination techniques in uncovering subtle ecological gradients and community-level functional structure that may not be evident through univariate statistics alone.
Overall, our findings suggest that wetland ecosystems are vulnerable due to their limited support for a small number of species, which are threatened by declining water levels in the Caspian Sea. Therefore, enhanced conservation plans are crucial for protecting these habitats.

Acknowledgements
We acknowledge TMU for its support of this study.

Ethics Committee Approval
N/A

Peer-review
Externally peer-reviewed.

Author Contributions
Conceptualization: M.A.; Investigation: M.A.; Material and Methodology: M.A., A.D; Supervision: M.A., A.D; Visualization: M.K., A.D; Writing-Original Draft: M.K.; Writing-review & Editing: M.A.; Other: All authors have read and agreed to the published version of the manuscript.

Conflict of Interest
The authors declare no conflicts of interest.

Funding
The authors declared that this study has received no financial support.

REFERENCES

1. Amirnezhad, H., Rafiei, H., & Atghaei, M. (2010). Estimating the preservation value of environmental resources (Case study: Miankaleh International Wetland).

2. Arzani, H., & Abedi, M. (2015). *Rangeland assessment: Survey and monitoring*. https://www.researchgate.net/publication/277813219

3. Cornelissen, J. H. C., Lavorel, S., Garnier, E., Díaz, S., Buchmann, N., Gurvich, D. E., Reich, P. B., ter Steege, H., Morgan, H. D., van der Heijden, M. G. A., Pausas, J. G., & Poorter, H. (2003). A handbook of protocols for standardised and easy measurement of plant functional traits worldwide. *Australian Journal of Botany, 51*(4), 335–380. https://doi.org/10.1071/BT02124

4. Costa, M. P. F., Silva, T. S., & Evans, T. L. (2013). Wetland classification. In *Remote sensing of natural resources* (pp. 461–490).

5. Da Silva Camilo, G., de Freitas Terra, B., & Araújo, F. G. (2018). Using the relationship between taxonomic and functional diversity to assess functional redundancy in streams of an altered tropical watershed. *Environmental Biology of Fishes, 101*(9), 1395–1405. https://doi.org/10.1007/s10641-018-0786-3

6. Death, R. (2008). Margalef's Index. In *Encyclopedia of Ecology* (pp. 2209–2210). Elsevier. https://doi.org/10.1016/B978-008045405-4.00117-8

7. Dembicz, I., Velev, N., Boch, S., Janišová, M., Palpurina, S., Pedashenko, H., Vassilev, K., & Dengler, J. (2020). Drivers of plant diversity in Bulgarian dry grasslands vary across spatial scales and functional-taxonomic groups. *Journal of Vegetation Science, 32*(1), e12935. https://doi.org/10.1111/jvs.12935

8. Gaiser, E., & Rühland, K. (2010). Diatoms as indicators of environmental change in wetlands and peatlands. In J. P. Smol & E. F. Stoermer (Eds.), *The Diatoms: Applications for the environmental and earth sciences* (2nd ed., pp. 473–496). Cambridge University Press. https://doi.org/10.1017/CBO9780511763175.026

9. Ghahroudi Tali, M., Sadough, S. H., Nezammahalleh, M. A., & Nezammahalleh, S. K. (2012). Multi-criteria evaluation to select sites for ecotourism facilities: A case study Miankaleh Peninsula. *Anatolia, 23*(3), 373–394. https://doi.org/10.1080/13032917.2012.712872

10. Laliberté, E., & Legendre, P. (2010). A distance-based framework for measuring functional diversity from multiple traits. *Ecology, 91*(1), 299–305. https://doi.org/10.1890/08-2244.1

11. Laliberté, E., Legendre, P., & Shipley, B. (2014). *FD: Measuring functional diversity from multiple traits, and other tools for functional ecology* (R package version 1.0-12.3). https://CRAN.R-project.org/package=FD

12. Legendre, P., & Legendre, L. (2012). *Numerical ecology* (Vol. 24). Elsevier.

13. Maire, V., Gross, N., Börger, L., Proulx, R., Wirth, C., da Silveira Pontes, L., Soussana, J., & Louault, F. (2012). Habitat filtering and niche differentiation jointly explain species relative abundance within grassland communities along fertility and disturbance gradients. *New Phytologist, 196*(2), 497–509. https://doi.org/10.1111/j.1469-8137.2012.04287.x

14. Matthews, J. W., & Endress, A. G. (2010). Rate of succession in restored wetlands and the role of site context. *Applied Vegetation Science, 13*(3), 346–355. https://doi.org/10.1111/j.1654-109X.2010.01076.x

15. Mendes, R. S., Evangelista, L. R., Thomaz, S. M., Agostinho, A. A., & Gomes, L. C. (2008). A unified index to measure ecological diversity and species rarity. *Ecography, 31*(4), 450–456. https://doi.org/10.1111/j.0906-7590.2008.05469.x

16. Nathan, J., Osem, Y., Shachak, M., & Meron, E. (2016). Linking functional diversity to resource availability and disturbance: A mechanistic approach for water-limited plant communities. *Journal of Ecology, 104*(2), 419–429. https://doi.org/10.1111/1365-2745.12525

17. Pakeman, R. J. (2011). Functional diversity indices reveal the impacts of land use intensification on plant community assembly. *Journal of Ecology, 99*(5), 1143–1151. https://doi.org/10.1111/j.1365-2745.2011.01853.x

18. Pavoine, S. (2020). *adiv: An R package to analyse biodiversity in ecology*. *Methods in Ecology and Evolution, 11*(9), 1106–1112. https://doi.org/10.1111/2041-210X.13430

19. Ricotta, C. (2005). A note on functional diversity measures. *Basic and Applied Ecology, 6*(5), 479–486. https://doi.org/10.1016/j.baae.2005.02.008

20. Sharifnia, F., Asri, Y., & Gholami-Te, T. (2007). Plant diversity in Miankaleh Biosphere Reserve (Mazandaran Province) in North of Iran. *Pakistan Journal of Biological Sciences, 10*(10), 1723–1727. https://doi.org/10.3923/pjbs.2007.1723.1727

21. Shokri, M., Safaian, N., Ahmadi, M. Z. T., & Amiri, B. J. (2004). A second look on biogeographical province of Miankaleh biosphere reserve. *Applied Ecology and Environmental Research, 2*(1), 105–117.

22. Simpson, E. H. (1949). Measurement of diversity. *Nature, 163*(4148), 688. https://doi.org/10.1038/163688a0

23. Smith, B., & Wilson, J. B. (1996). A consumer's guide to evenness indices. *Oikos, 76*(1), 70–82. https://doi.org/10.2307/3545749

24. Spellerberg, I. F., & Fedor, P. J. (2003). A tribute to Claude Shannon (1916–2001) and a plea for more rigorous use of species richness, species diversity and the 'Shannon–Wiener' Index. *Global Ecology and Biogeography, 12*(3), 177–179. https://doi.org/10.1046/j.1466-822X.2003.00015.x

25. Villéger, S., Mason, N. W. H., & Mouillot, D. (2008). New multidimensional functional diversity indices for a multifaceted framework in functional ecology. *Ecology, 89*(8), 2290–2301. https://doi.org/10.1890/07-1206.1

26. Wang, G., & Weng, Q. (Eds.). (2013). *Remote sensing of natural resources*. CRC Press. https://doi.org/10.1201/b15159

27. Whigham, D. (2018). Ecosystem processes. In C. M. Finlayson, G. R. Milton, R. C. Prentice, & N. C. Davidson (Eds.), *The Wetland Book* (pp. 285–296). Springer. https://doi.org/10.1007/978-90-481-9659-3_68

28. Yachi, S., & Loreau, M. (1999). Biodiversity and ecosystem productivity in a fluctuating environment: The insurance hypothesis. *Proceedings of the National Academy of Sciences, 96*(4), 1463–1468. https://doi.org/10.1073/pnas.96.4.1463

Total phenolic content and antioxidant capacity of *Verbascum thapsus* L. variations along the altitude gradient

RAHELEH-BORHANIAN[1], GHASEM ALI-DIANATI TILAKI*[1], MEHDI ABEDI[1]

Abstract: This study aimed to investigate the effects of altitude on the biochemical parameters of *Verbascum thapsus* L. leaves in the rangelands of Chahardangeh, Sari. Specifically, we measured the total phenolic content and antioxidant capacity using DPPH in leaf samples collected from three distinct elevation zones (1300-1400, 1400-1500, 1500-1600). The results indicated that as altitude increased, the mean total phenolic content rose from 6,801.1 mg GAE/Kg FW at an altitude of 1,300–1,400 meters to 11759.8 mg GAE/Kg FW at 1,500–1,600 meters. Similarly, the mean DPPH radical scavenging activity increased from 72.9% at 1,300–1,400 meters to 87.9% at 1,500–1,600 meters. Understanding how altitude affects the production of secondary metabolites in medicinal plants is crucial, both scientifically and practically, in the context of climate change scenarios. This research provides valuable insights into the relationship between altitude and secondary metabolite accumulation in *V. thapsus*, highlighting the plant's biochemical response to this crucial ecological factor.

Keywords: Phytochemistry, Mountain grasslands, Bioactive compounds

[1]Address: Department of Range Management, Faculty of Natural Resources and Marine Sciences, Tarbiat Modares University, Noor, Mazandaran Province, Iran

***Corresponding author**: dianatig@modares.ac.ir

1. INTRODUCTION

Iran's varied climate and geography support a rich array of flora, featuring numerous plant species known for their notable medicinal properties. Recent scientific advancements have sparked increased interest in substituting synthetic components in pharmaceuticals with natural, plant-based alternatives. In various nations, these natural compounds have become vital to contemporary healthcare and therapeutic practices, indicating a worldwide transition towards more sustainable and biocompatible treatment methods (Ji et al., 2009). Iran boasts a variety of ecological conditions that support the growth of more than 2,500 species of medicinal plants. Numerous studies have shown that many of these plants harbor valuable bioactive compounds, offering potential uses in the pharmaceutical, food, and cosmetic sectors. By enhancing research infrastructure and combining traditional knowledge with modern scientific methods, we can discover and commercialize new compounds that hold significant value (Azarnivand & Zare Chahooki, 2010). Multiple factors can affect both the quantity and quality of secondary metabolites in medicinal plants. These factors include the specific plant part utilized, the species of the plant, ecological conditions, phenological stages, biotic stresses like grazing, harvesting time, post-harvest management, and the method of extracting active compounds (Feduraev et al., 2019). *Verbascum thapsus L.,* a biennial member of the Scrophulariaceae family, can reach heights exceeding 2 meters. Its small yellow flowers are closely grouped along a tall flowering stem that emerges from a substantial rosette of basal leaves. This plant thrives in diverse habitats but favors sunny locations. It can germinate from long-lived seeds, which remain viable in the soil for many years. As a herbaceous species, *V. thapsus* disperses quickly by producing a large number of seeds (Badad et al., 2023). From a phytochemical standpoint, *V. thapsus* yields various secondary metabolites, such as phenylethanoid glycosides, iridoid glycosides, tetraglycosidic triterpenes, saponins, terpenes, flavonoids, carotenoids, and carbohydrates (Jan et al., 2022). This plant is known for a multitude of biological activities, including antiviral, antioxidant, analgesic, sedative, anti-inflammatory, hypnotic, antibacterial, antifungal, and anticancer effects (Gupta et al., 2022). Considering this species is found in mountainous habitats, we aimed to study the variations in phenolic compounds and antioxidants along an altitude gradient.

2. MATERIAL AND METHOD

Mazandaran Province, with an area of approximately 23,756 square kilometers, is bordered by Golestan Province to the east, Gilan Province to the west, and Semnan, Tehran, Alborz, and Qazvin to the south. This study was conducted in the rangelands of the Chahardangeh region, Sari County, Mazandaran Province, located at a longitude of 53°43′36″E and a latitude of 36°26′55″N. The average annual precipitation in this area is approximately 300 mm, with a yearly mean temperature of 11°C. Field surveys were carried out to identify the distribution of *Verbascum thapsus* across different elevation ranges (1300–1400 m, 1400–1500 m, and 1500–1600 m above sea level). To investigate the effect of elevation on the antioxidant activity of the studied species, 12 individual plants were randomly selected from their growing areas within each elevation range. Sufficient leaf samples were collected from each plant in triplicate during the full flowering stage. Notably, after harvesting the leaves from the 12 plants, the samples were mixed in three sets of four replicates each, resulting in 3 samples per elevation range and 9 samples across all three elevation ranges. The collected samples were then transported to the laboratory under appropriate conditions. **Total phenolic content was determined using the Folin-**

Ciocalteu colorimetric method with gallic acid as the standard(Singleton et al., 1999**), and antioxidant activity was assessed via the DPPH radical scavenging assay(**Brand-Williams et al., 1995**). Principal Component Analysis (PCA) was employed to examine the relationship between the total phenolic content, antioxidant capacity of the target plant's leaves, and the specified altitudes. A heatmap was also generated to visualize this relationship better.**

3. RESULTS

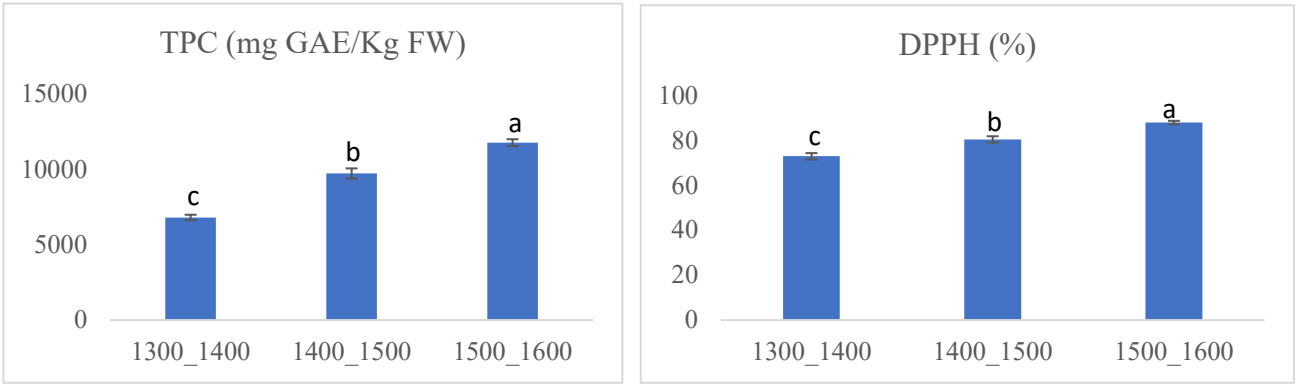

Figure1. Mean±SE (n=3) of TPC and DPPH in three altitudes.

In the analysis of variance for the evaluated parameters (Table 1), the lowest F-value was observed for DPPH, while the highest belonged to TPC. It is noteworthy that both TPC and DPPH parameters were statistically significant. According to the mean comparison chart (Figure 1), the values of the parameters increased with elevation; therefore, the highest levels of TPC and DPPH were recorded at the 1500–1600 m elevation range.

Table 1. Analysis of variance (ANOVA) results for TPC and DPPH parameters

Factor	Df	F-value	Significance level
TPC (mg GAE/Kg FW)	**3**	**93.33**	**P < 0.001**
DPPH (%)	**3**	**30.35**	**P < 0.001**

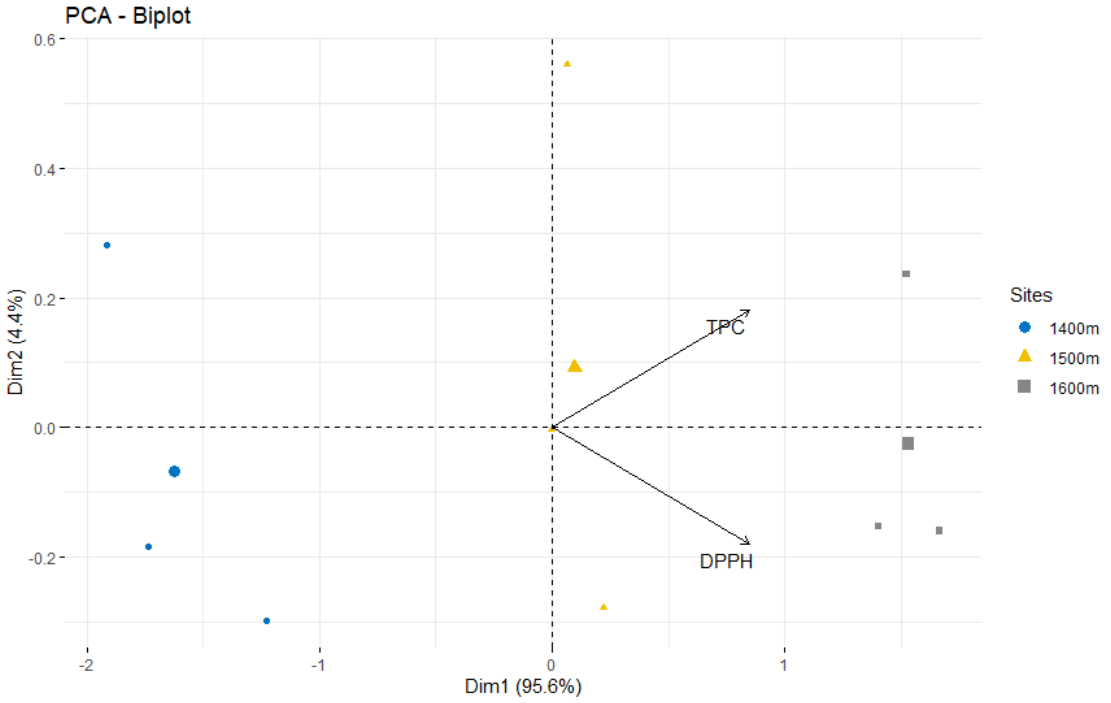

Figure2. Biplot of Principal Component Analysis (PCA) based on total phenolic content (TPC) and antioxidant capacity (DPPH) in samples from different altitudes (1400, 1500, and 1600 m).

Principal Component Analysis (PCA) in Figure 2, showed that the first component (Dim1), accounting for 95.6% of the variance, provided the most significant separation among the samples based on altitude. Samples from the 1600 m

elevation exhibited the highest total phenolic content (TPC) and antioxidant capacity (DPPH) levels. Higher altitude is at the positive end of PCA1, while 1400m is at the negative end of PCA1.

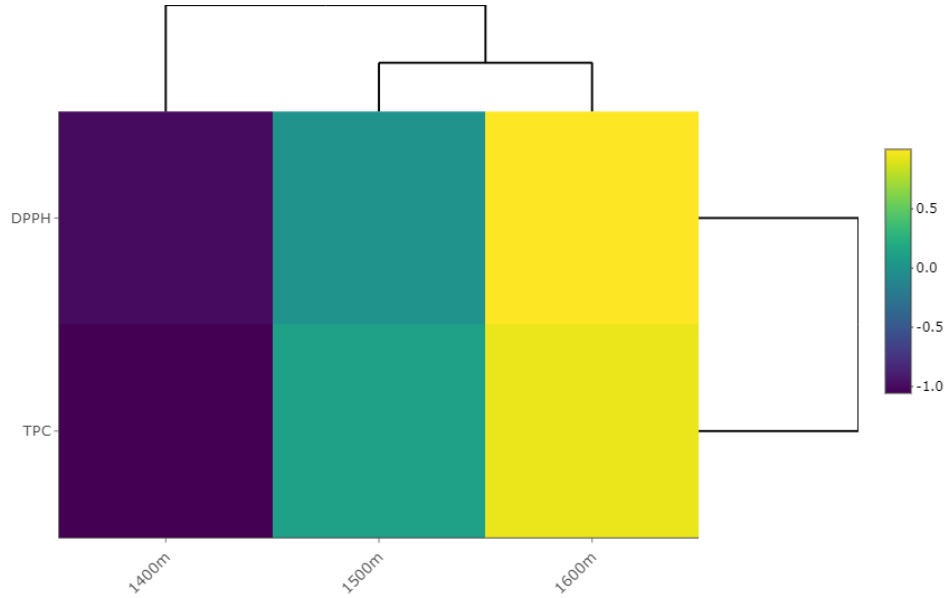

Figure3. The heat map shows TPC and DPPH values at different altitudes.

The heatmap clustering(Figure 3) indicates that both TPC and DPPH levels are substantially higher at 1600 m than at lower altitudes. Also, parameters at 1400 m are located in separate clusters.

4. DISCUSSION AND CONCLUSIONS

Research indicates that temperature, relative humidity, wind speed, and light intensity variations at higher altitudes can change how plants respond physiologically, influencing their secondary metabolite composition (Hashim et al., 2020). In this study, the measured parameters were found to increase with elevation, reaching the highest total phenolic content (TPC) and DPPH levels at an altitude of 1500–1600 m. Likewise, a study of Tartary buckwheat seeds and hulls reported a notable rise in total phenol content and antioxidant potential with increasing altitude (Kishore et al., 2010). A similar increase in total phenol content and DPPH antioxidant activity with altitude was observed in Paeonia emodi, an important plant found in the Himalayas (Joshi et al., 2022). This trend was also noted in Taxus wallichiana (Adhikari et al., 2022). The elevation-related rise in TPC and DPPH is thought to result from enhanced biosynthetic pathways for phenolic compounds in Verbascum thapsus, leading to greater total phenol content and antioxidant activity (Rana et al., 2020). Higher altitudes correlate with increased oxidative stress due to reduced oxygen pressure and heightened UV radiation. This stress drives plants to bolster their antioxidant defenses, resulting in increased production of phenolic compounds and antioxidant enzymes (Cui et al., 2016). Additionally, plants at higher elevations face more extreme temperatures and elevated UV radiation, which can harm cellular components. To counteract this damage, they produce more phenolic compounds that serve as UV shields and antioxidants (Agrawal et al., 2024). Furthermore, at elevated altitudes, plants often increase the synthesis of secondary metabolites like phenols, flavonoids, and tannins. These compounds exhibit potent antioxidant properties and are crucial for safeguarding the plant from environmental stresses. While further research is necessary to fully comprehend how altitude affects the total phenol content and antioxidant capacity of Verbascum thapsus, existing evidence highlights altitude's vital role in regulating secondary metabolite production in this species. More in-depth studies could provide deeper insights into this phenomenon, aiding in the enhancement of yield and quality in medicinal plants. Thus, altitude significantly influences both the composition and concentration of secondary metabolites in plants.

Acknowledgements / Teşekkür
We acknowledge Tarbiat Modares University for its support.

Ethics Committee Approval / Etik Kurul Onayı
N/A

Peer-review / Akran Değerlendirmesi
Externally peer-reviewed.

Author Contributions / Yazar Katkıları

Conceptualization: H.S.; Investigation: R.B.; Material and Methodology: M.A., GA.DT.; Supervision: M.A., GA.DT; Visualization: R.B; Writing-Original Draft: R.B.; Writing-review & Editing: M.A., GA.DT.; Other: All authors have read and agreed to the published version of the manuscript.

Conflict of Interest / Çıkar Çatışması
The authors have no conflicts of interest to declare.

Funding / Finansal Destek
The authors declared that this study has received no financial support.

REFERENCES

Adhikari, P., Joshi, K., Singh, M., & Pandey, A. (2020). Influence of altitude on secondary metabolites, antioxidants, and antimicrobial activities of Himalayan yew (*Taxus wallichiana*). *Plant Biosystems - An International Journal Dealing with All Aspects of Plant Biology*, *156*(1), 187–195. https://doi.org/10.1080/11263504.2020.1845845

Agrawal, S., & Saklani, P. (2023). Physiological responses of the leaves of a high-altitude plant Picrorhiza kurroa to cold stress. *Plant Science Today*. https://doi.org/10.14719/pst.2861

Azarneivand, H., & Zare Chahouki, M. (2010). *Rangeland improvement [Eslah-e marate']*. University of Tehran Press. [in Persian]

Badad, O., Pirro, S., Lahlimi, Q., & Ghazal, H. (2023). The Complete Genome Sequence of *Verbascum thapsus* (Scrophulariaceae, Lamiales), the Common Mullein. *Biodiversity genomes*, *2023*, 10.56179/001c.73050. https://doi.org/10.56179/001c.73050

Brand-Williams, W., Cuvelier, M.-E., & Berset, C. (1995). Use of a free radical method to evaluate antioxidant activity. *LWT-Food Science and Technology*, *28*(1), 25–30. https://doi.org/10.1016/S0023-6438(95)80008-5

Cui, G., Wei, X., Degen, A. A., Wei, X., Zhou, J., Ding, L., … Long, R. (2016). Trolox-equivalent antioxidant capacity and composition of five alpine plant species growing at different elevations on the Qinghai–Tibetan Plateau. *Plant Ecology & Diversity*, *9*(4), 387–396. https://doi.org/10.1080/17550874.2016.1261952

Feduraev, P., Chupakhina, G., Maslennikov, P., Tacenko, N., & Skrypnik, L. (2019). Variation in Phenolic Compounds Content and Antioxidant Activity of Different Plant Organs from *Rumex crispus* L. and *Rumex obtusifolius* L. at Different Growth Stages. *Antioxidants (Basel, Switzerland)*, *8*(7), 237. https://doi.org/10.3390/antiox8070237

Gupta, A., Atkinson, A. N., Pandey, A. K., & Bishayee, A. (2022). Health-promoting and disease-mitigating potential of Verbascum thapsus L. (common mullein): A review. *Phytotherapy research : PTR*, *36*(4), 1507–1522. https://doi.org/10.1002/ptr.7393

Hashim, A. M., Alharbi, B. M., Abdulmajeed, A. M., Elkelish, A., Hozzein, W. N., & Hassan, H. M. (2020). Oxidative Stress Responses of Some Endemic Plants to High Altitudes by Intensifying Antioxidants and Secondary Metabolites Content. *Plants (Basel, Switzerland)*, *9*(7), 869. https://doi.org/10.3390/plants9070869

Jan, F., Jan, B., Akbar Dar, M., Sofi, F. A., Alsuwayni, B. M., Afzal, S., & Fawzi Mahomoodally, M. (2022). A Review on Traditional Uses, Phytochemistry, and Pharmacological Activities of *Verbascum thapsus*. In *Edible Plants in Health and Diseases: Volume II: Phytochemical and Pharmacological Properties* (Vol. 2).https://doi.org/10.22146/farmaseutik.v21i1.99621

Ji, H. F., Li, X. J., & Zhang, H. Y. (2009). Natural products and drug discovery. Can thousands of years of ancient medical knowledge lead us to new and powerful drug combinations in the fight against cancer and dementia?. *EMBO reports*, *10*(3), 194–200. https://doi.org/10.1038/embor.2009.12

Joshi, K., Adhikari, P., Bhatt, I. D., & Pande, V. (2022). Source dependent variation in phenolics, antioxidant and antimicrobial activity of *Paeonia emodi* in west Himalaya, India. *Physiology and molecular biology of plants : an international journal of functional plant biology*, *28*(9), 1785–1798. https://doi.org/10.1007/s12298-022-01242-z

Kishore, G., Ranjan, S., Pandey, A., & Gupta, S. (2010). Influence of Altitudinal Variation on the Antioxidant Potential of Tartar Buckwheat of Western Himalaya. *Food Science and Biotechnology*, *19*, 1355–1363. https://doi.org/10.1007/s10068-010-0193-9

Rana, P. S., Saklani, P., & Chandel, C. (2020). Research article influence of altitude on secondary metabolites and antioxidant activity of Coleus forskohlii root extracts. *Res. J. Med. Plants*, *14*(43-52), 2020. https://scialert.net/abstract/?doi=rjmp.2020.43.52

Singleton, V. L., Orthofer, R., & Lamuela-Raventós, R. M. (1999). [14] Analysis of total phenols and other oxidation substrates and antioxidants by means of folin-ciocalteu reagent. In *Methods in enzymology* (Vol. 299, pp. 152–178). Elsevier. https://doi.org/10.1016/S0076-6879(99)99017-1

A Bibliometric Review on Compressed Air Energy Storage System

HAMZA GEREKAN*[1,3], ASIM SINAN KARAKURT[2], IBRAHIM OZSARI[3]

Abstract: While the demand for energy is increasing day by day, the environmental impacts of fossil fuels are increasing. For this reason, the trend towards renewable energy sources has gained momentum. Compressed air energy storage (CAES) systems have attracted attention as one of the renewable energy source alternatives. In this study, 1592 articles obtained from Web of Science in BibTeX format in 2000-2024 were analyzed using the Biblioshiny interface in Bibliometrix in R Studio. "Word Cloud", 'Annual Scientific Production', 'Most Relevant Sources', 'Most Relevant Authors', 'Most Relevant Affiliations', 'Co-occurance Network', 'Co-citation Network' and 'Collaboration Network' graphical and network outputs were obtained. As a result of these analyzes, it was determined that the annual number of publications varied between 0-8 in the years 2000-2010; gradually increased between 27-77 in 2012-2017; increased between 102-209 in 2018-2023; and reached a peak in 2024 and 262 articles were published. The journals that published the most articles are Journal of Energy with 241 articles, Energy journal with 185 articles and Applied Energy journal with 125 articles. Chen H. published 96 articles and Xu Y. published 69 articles on CAES. As institutions; Instute of Engineering Thermophysics and Xi'an Jiaotong University were found to be very active in this subject by publishing 212 and 205 articles, respectively. In the institutional distribution analysis, it is understood that CAES-related studies are carried out in Chinese-dominated institutions. In the "Co-occurance network" analysis, it was found that the terms "Optimization", "Performance", "System", "Simulation", "Design" and "Thermodynamic Analysis" were used together. In the "Co-citation Network" map, Budt M. (2016), Luo X. (2015) and Alirahimi SM. (2021) studies formed the main clusters, and in the "Collaboration Network" analysis, it was seen that collaborations among Chinese authors were intense and there were many co-authorship organizations. As a result, it is predicted that the number of publications related to CAES has increased steadily over the last 25 years; the main focuses are performance optimization and simulation-based designs, and international collaborations will increase thematic diversity in the future.

Keywords: Compressed air energy storage, energy storage, bibliometric analysis, research trends

[1]**Address:** Yildiz Technical University, Graduate School of Science and Engineering, Istanbul/Turkiye
[2]**Address:** Yildiz Technical University, Faculty of Naval Architecture and Maritime, Istanbul/Turkiye
[3]**Address:** Bursa Technical University, Faculty of Maritime, Bursa/Turkiye

***Corresponding author**: hamza.gerekan@btu.edu.tr

1. INTRODUCTION

The rapid increase in the world's energy use has bolstered economic expansion while intensifying its effects on the environment. Energy consumption has grown by 2.2% a year due to expansion in industry, transportation, and services; this has an impact on energy prices and causes adjustments to cost and export balances (Mujtaba et al., 2022). Consequently, the usage of fossil fuels in energy production has caused CO_2 emissions, accounting for almost 75% of all CO_2 emissions. Measures to lessen the carbon footprint have to be put in place because of the rise in emissions (Friedlingstein et al., 2022). Because renewable energy sources are intermittent, energy storage has become essential in response to the growing demand for them (Domínguez et al., 2025). To address this demand, a variety of storage systems—including thermal, mechanical, chemical, electrochemical, electromagnetic, and hybrid—have been create (Chen et al., 2009). While Pumped Storage Hydroelectric Power Plants (PDHES) and Compressed Air Energy Storage (CAES) systems are notable for mechanical storage, Phase Change Materials (PCM) and Thermal Energy Storages (TES) are utilized for thermal storage (Budt et al., 2016). Batteries and battery technology are employed for electrochemical storage, although synthetic fuels are favored for chemical storage (Ratz et al., 2020). Although electromagnetic storage uses supercapacitors and superconducting magnetic materials, hybrid storage combines these technologies. Compressed air energy storage (CAES) systems employ a compressor to pressurize and store air, which is then later used by a turbine to produce electricity (Shanmugam et al., 2024; Xie et al., 2020). Power grids, wind and solar power plants, ships, industrial buildings, and undersea constructions may all include these technologies(Grönman et al., 2025a; Narasimalu & Chelliah, 2018). Diabatic (D-CAES), adiabatic (A-CAES), isothermal (I-CAES), and liquefied air energy storage (LAES) are the four categories of CAES technology; in D-CAES, the heat generated during compression is released into the environment (Zohbi, 2019). This heat is recycled during discharge in A-CAES (Fan et al., 2025). The pressurization and discharge procedures in I-CAES are conducted at a temperature that is constant or almost constant (Zhao et al., 2024). Cryogenic tanks are used in LAES to store liquid air (Fang & Zhang, 2022). The quantitative features of scientific publications are revealed by bibliometric analysis, which makes it possible to examine current research trends, citation networks, and partnerships (Donthu et al., 2021). Tools like VOSviewer and Biblioshiny may be used to visualize conceptual maps of research, keyword clusters, and country/author performances (Secinaro et al., 2020; van Eck & Waltman, 2010). Karakurt et al., 2022 reviewed steam turbine studies from 2000 to 2020, whereas Ozsari, 2023a, the

bibliometric analysis approach was used to examine the literature produced in the field of exercise between 1992 and 2021, and scientific impact criteria were used to assess the leading nations, authors, journals, and institutions, also Ozsari, 2023b evaluated hydrogen energy research from 1992 to 2021. In the study Karadağ et al., 2024, almost 19,000 papers in the Scopus database between 2000 and 2023 were examined using the bibliometric analysis approach to assess research trends, notable authors, institutions, and primary research themes on thermal energy storage (TES) systems. Bibliometric mapping on pumped hydroelectric energy storage by, Odoi-Yorke et al., 2024 bibliometric mapping on energy storage technologies from 2013–2022 by Grönman et al., 2025, and Borri et al., 2022 A bibliometric analysis of 350 CAES articles demonstrates how the discipline has evolved. Only the Biblioshiny interface and the Python programming language were utilized, and this study has more datasets (1592 papers published between 2000 and 2024) than the research of Borri et al., 2022 (Aria & Cuccurullo, 2017).

2. MATERIAL AND METHOD

All data used in this study were accessed through Web of Science. Data between 2000 and 2024 were used and only articles that contain the phrase “Compressed Air Energy Storage” in the title, record or keywords and only articles in the article type were included in the research. As a result of the aforementioned research, 1592 articles were found. The articles found were exported in BibTeX format. Exporting was done by selecting “Full Record and Cited References”. As a result, a full-text output of the articles was obtained, including bibliographic information and citations in the bibliography. Then, using the Biblioshiny interface in the Bibliometrix package running in R Studio, the exported documents were uploaded to the system for the necessary analysis. A “World Cloud” was created through the “Documents” section in Biblioshiny and a map diagram of the most used keywords was obtained. With the “Annual Scientific Production” in the “Overview” section, a graph of how many studies were conducted year by year in 2000-2024 was obtained. Afterwards, with the help of “Most Relevent Sources” in the “Sources” section, a graph was obtained about how many publications were made in which journals on the subject. With the “Most Relevant Authors” in the “Authors” section, a graph was prepared to show which authors conducted the most studies on the subject and how many of them. Through “Most Relevant Affiliations”, a graph showing the information about the institutions working on the subject and how many studies they have conducted was prepared. “Co-occurance Network” was selected by selecting ‘Conceptual Structure’ from the menu. Here, the connections of terms with each other are shown as clusters. By selecting “Co-Citation Network” from the “Intellectual Structure” menu, a network map was created to show which sources are cited more by those who work on the subject together. Finally, by selecting “Collaboration Network” from the “Social Structure” section, their joint publications and collaboration links with other researchers were shown as a network map. The obtained graphics and network maps were created in PNG format and made ready to be displayed in the “Results” section by making them dominant with appropriate scale, label size and color codes.

3. RESULTS AND DISCUSSION

The major ideas that are prevalent in the research are shown by the word cloud shown in Figure 1. The phrases "optimization" and "performance" are used most frequently, which suggests that energy systems analysis and improvement procedures are centered on efficiency. Thermodynamic-based modeling and simulation studies are also at the forefront, particularly for the design and integration of compressed air energy storage (CAES) systems, as indicated by terminology like "system," "simulation," and "thermodynamic analysis."

Figure 1. Shows the proportionate distribution of the most popular terms in CAES research papers from 2000 to 2024

The yearly production of scientific articles from 2000 to 2024 is depicted in Figure 2. The number of publications fell from two to zero between 2000 and 2003, showing a near total halt in research production. The annual number of publications remained low between 2004 and 2010, ranging from 2 to 8. The notable upward trend, which began with 17 publications in 2011, proceeded with 38 publications in 2012, 63 publications in 2014, 102 publications in 2018, 190 publications in 2021, and then peaked in 2024 with 262 publications. This consistent rise indicates that the field's study agenda is broadening and that scholarly interest is rising quickly.

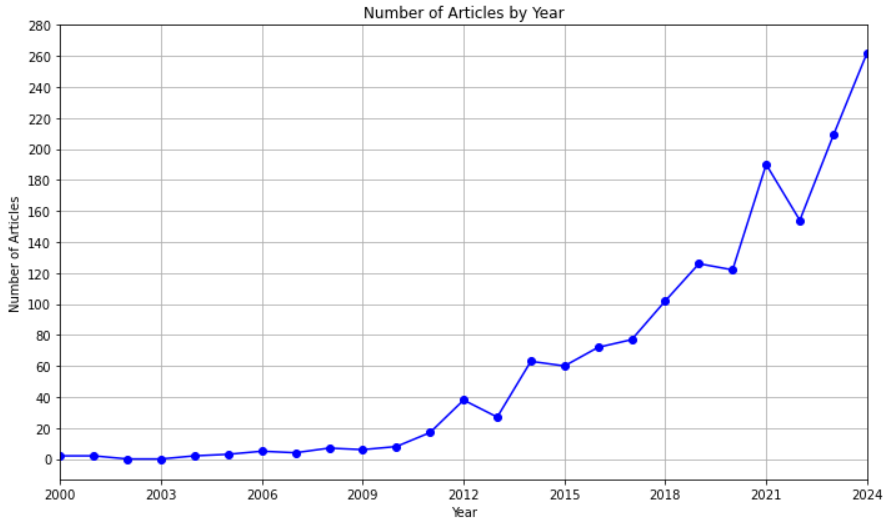

Figure 2. Shows the publication and citation timeline for CAES from 2000 to 2024

With 241 articles, the Journal of Energy Storage ranks first in the field's top publishing sources, followed by Energy (185), Applied Energy (125) and Energy Conversion and Management (120), according to the graph in Figure 3. The International Journal of Energy Research (28), Journal of Cleaner Production (22) and International Journal of Electrical Power & Energy Systems (18) have less publications than Energies (79), Renewable Energy (53) and Applied Thermal Engineering (52), which have moderate contributions. This distribution shows how scholarly activity is concentrated in a small number of high-impact journals and how important these journals are to the subject.

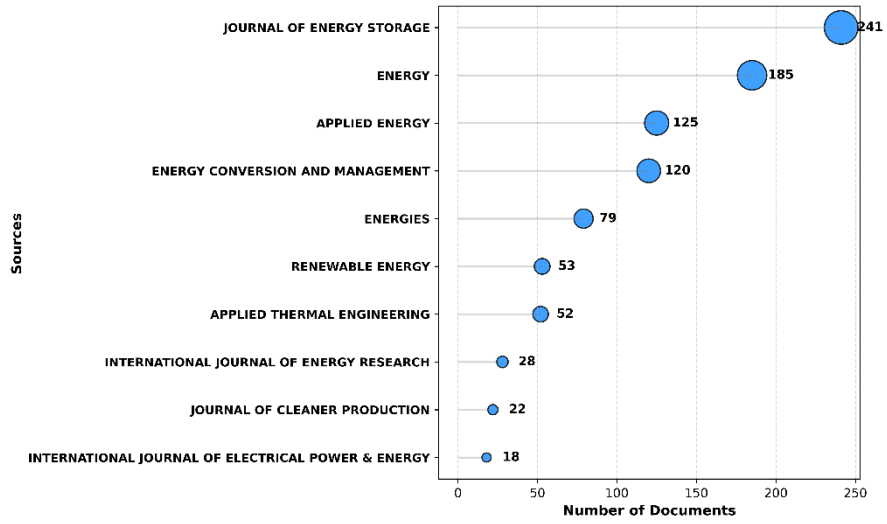

Figure 3. The scientific sources that published the most on CAES between 2000 and 2024

CHEN H is by far the most prolific researcher with 96 documents, followed by XU Y with 69 documents and LI Y with 64 documents, according to the comparative distribution of the number of papers published by the 10 researchers with the greatest document output shown in Figure 4. With 38 documents, WANG Y contributed the least to the lower section, suggesting that CHEN H performs noticeably better than other writers in terms of productivity.

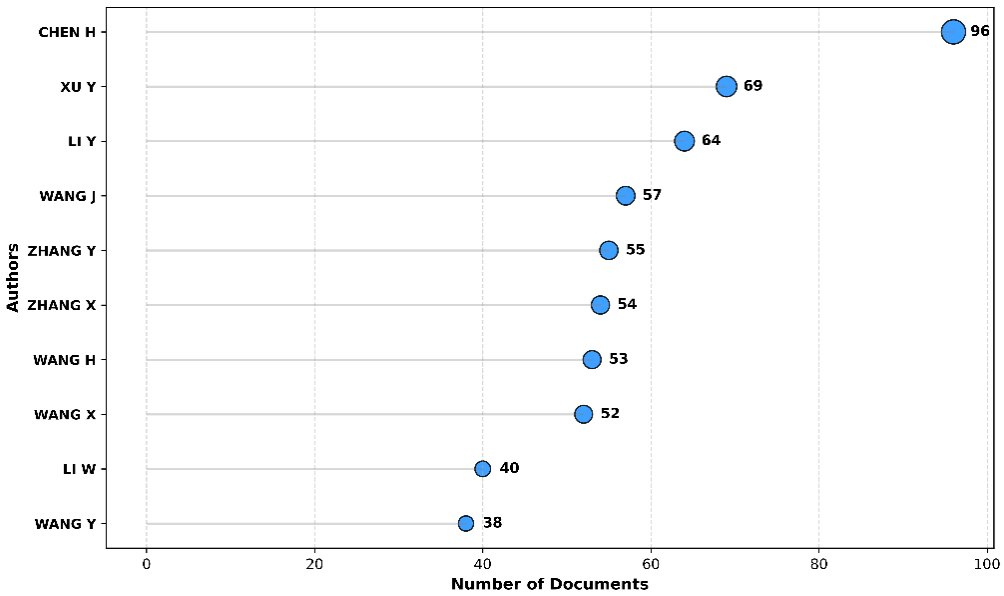

Figure 4. From 2000 to 2024, the authors that contributed the most scientifically to CAES

The comparative distribution of the top ten universities for article creation is displayed in Figure 5. North China Electric Power University (129), University of Waterloo (102) and Tsinghua University (95) comprise the middle segment, while the three top-ranked institutions are the Institute of Engineering Thermophysics (212 papers), Xi'an Jiaotong University (205) and the University of Chinese Academy of Sciences (170). With 55 publications, Islamic Azad University is at the bottom of the list.

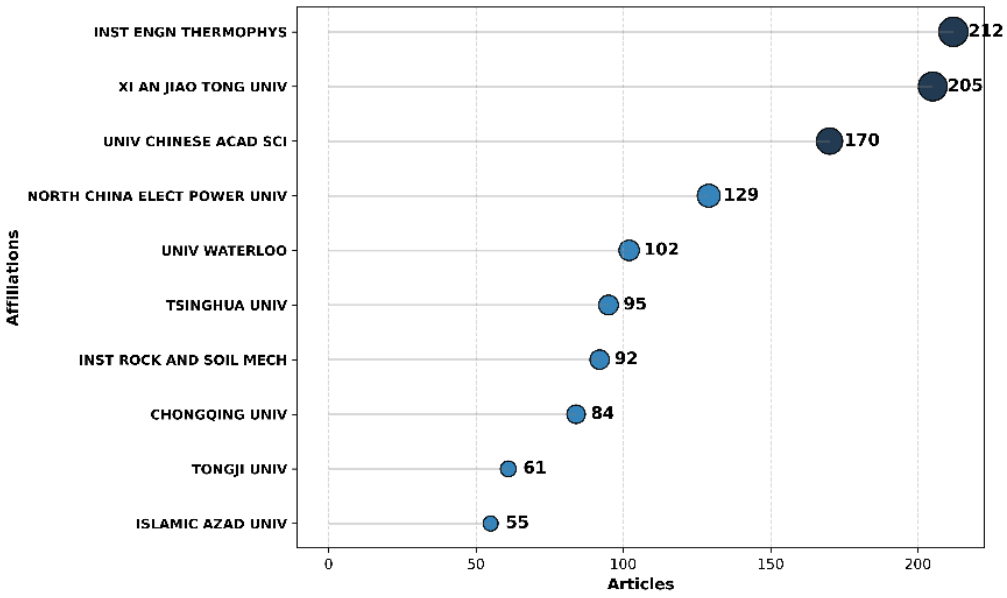

Figure 5. Organizations and institutions that published the most in CAES between 2000 and 2024

Three separate topic clusters in CAES research are depicted in the keyword co-occurrence network in Figure 6. While the second cluster (green) points to thermodynamic design and efficiency concerns with the keys "thermodynamic analysis," "design," and "exergy analysis," the first cluster (red) is focused on "optimization," "system performance," and "CAES," with an emphasis on enhancing system performance. With terms like "temperature," "pressure variations," and "caverns," the smaller third cluster (blue) stands for experimental and field-oriented parametric research.

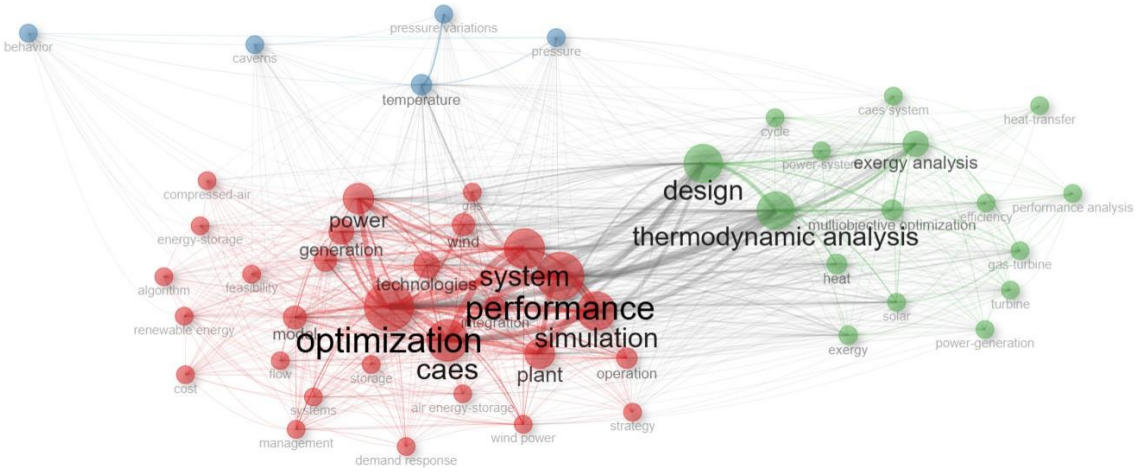

Figure 6. Analysis of co-occurrence networks demonstrating concurrent phrase transitions

The author of the co-citation network study Budt m 2016 is situated in the core of the network with high betweenness and PageRank values, marking a methodological milestone, according to the network graph in Figure 7. The graph's blue-coded studies concentrate on a methodological approach, whilst the red-coded studies highlight thematic variations in practice. The second category is well-represented by the writers of Razmi a 2019 and Alirahmi sm 2021, highlighting the literature's topic richness and the rigor of scholarly exchange.

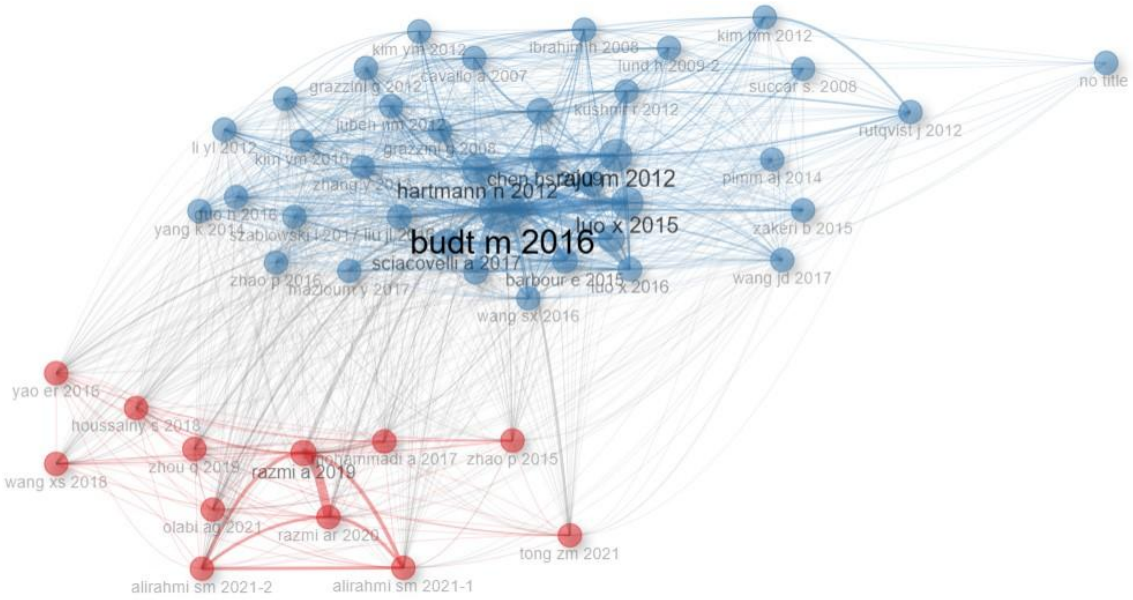

Figure 7. Co-citation network analysis illustrating the connections among authors who have been co-cited in the literature

The structure and clustering patterns of academic relationships between authors are displayed in the Collaboration Network shown in Figure 8. According to the graph, authors like Chen H., Yang Y., Wang H., Wang J., and Chen X. serve as links between various study groups and are positioned in the network's core with high betweenness centrality values. This demonstrates how crucial these writers are to preserving scientific engagement and fostering multidisciplinary partnerships.

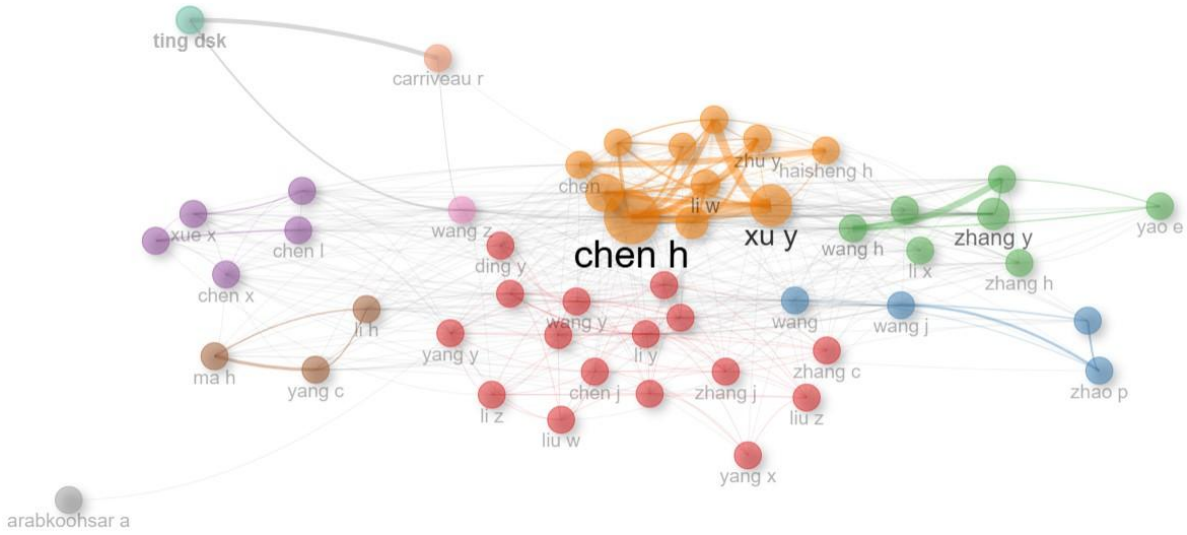

Figure 8. Visualization of the collaboration network among writers working on collaborative projects in the literature

4. CONCLUSIONS

In this study, 1592 articles with the keyword "Compressed Air Energy Storage" between 2000 and 2024 were analyzed by bibliometric analysis through Web of Science. Necessary analyses were created with the biblioshiny interface of bibliometrix in the R Studio program. The graphs and network maps obtained as a result of the analyzes allowed a deeper examination of research trends related to CAES. According to the "Annual Scientific Production" graph, it was observed that between 27-72 articles related to CAES were published between 2012-2016, with a significant increase after 2016. 102 articles were published in 2018, 190 in 2021 and 262 in 2024. With this increase, it is inferred that the interest in renewable energy systems and the need for energy storage systems have increased worldwide. With the "Most Relevant Sources" graph, the journals that published the most articles in the field of CAES were obtained. The most prominent journals here are: Journal of Energy Storage (241), Energy (185) and Applied Energy (125). These journals are the leading publications in the fields of energy technologies and engineering. When the "Most Relevant Authors" graph is analyzed, it is seen that Chen H. published 96 articles, Xu Y. 69 articles and Lı Y. 64 articles on CAES and it is determined that they are the authors who published the most articles on this subject. Looking at the "Most Relevant Affiliations" graph, it was seen that Insitute of Engineering Thermophysics (212 articles) and Xi'an Jiatong University (205 articles) were the institutions that published the most studies on CAES. As a result, it was found that the majority of the studies on the subject originated from China. Therefore, it is understood that there are intensive academic and industrial studies on CAES in China. With the "Co-occurance Network" network map, the frequency of co-occurrence of the most commonly used key concepts in the literature was analyzed. Here, it was noticed that the terms "performance", "optimization", "system", "simulation", "design" and "thermodynamic analysis" were frequently used together and dense clusters were formed. It was then realized that CAES-related work is also linked to system efficiency, performance evaluation and engineering-based modeling processes. Using the "Co-citation Network" network map, it was concluded that studies such as Budt M. (2016), Raju M. (2012) and Luo X. (2015) are among the main references related to CAES and cited by the authors. These studies provided important findings for thermodynamic analysis, system design and economic evaluation of CAES systems. The "Collaboration Network" network map shows that international collaborations are increasing day by day and there are clusters around 5 main researcher teams (Chen H., Yang Y., Wang H., Wang J. and Chen X.). As a result, it is observed that most of the CAES-related studies are conducted in universities and research institutions in China. It is foreseen that in the future, research on "optimization", "integrated system analysis", "renewable energy integration", "economic assessment" and "sustainability" will increase in the literature. Bibliometric analyses in this direction will be very helpful to follow the development process of the field and to find new areas of study.

Acknowledgements
I would like to thank my esteemed professors Asim Sinan Karakurt and Ibrahim Ozsari for their support.

Ethics Committee Approval
N/A

Peer-review
Externally peer-reviewed.

Author Contributions
Conceptualization: H.G., A.S.K., I.O.; Investigation: H.G.; Material and Methodology: H.G.; Supervision: H.G; Visualization: H.G.; Writing-Original Draft: H.G.; Writing-review & Editing: H.G. A.S.K., I.O.; Other: All authors have read and agreed to the published version of manuscript.

Conflict of Interest
The authors have no conflicts of interest to declare.

Funding
The authors declared that this study has received no financial support.

REFERENCES

Aria, M., & Cuccurullo, C. (2017). *bibliometrix*: An R-tool for comprehensive science mapping analysis. *Journal of Informetrics*, *11*(4), 959–975. https://doi.org/10.1016/j.joi.2017.08.007

Borri, E., Tafone, A., Comodi, G., Romagnoli, A., & Cabeza, L. F. (2022). Compressed Air Energy Storage—An Overview of Research Trends and Gaps through a Bibliometric Analysis. *Energies*, *15*(20), 7692. https://doi.org/10.3390/en15207692

Budt, M., Wolf, D., Span, R., & Yan, J. (2016). A review on compressed air energy storage: Basic principles, past milestones and recent developments. *Applied Energy*, *170*, 250–268. https://doi.org/10.1016/j.apenergy.2016.02.108

Chen, H., Cong, T. N., Yang, W., Tan, C., Li, Y., & Ding, Y. (2009). Progress in electrical energy storage system: A critical review. *Progress in Natural Science*, *19*(3), 291–312. https://doi.org/10.1016/j.pnsc.2008.07.014

Domínguez, M., Fernández-Cardador, A., Fernández-Rodríguez, A., Cucala, A. P., Pecharromán, R. R., Urosa Sánchez, P., & Vadillo Cortázar, I. (2025). Review on the use of energy storage systems in railway applications. *Renewable and Sustainable Energy Reviews*, *207*, 114904. https://doi.org/10.1016/j.rser.2024.114904

Donthu, N., Kumar, S., Mukherjee, D., Pandey, N., & Lim, W. M. (2021). How to conduct a bibliometric analysis: An overview and guidelines. *Journal of Business Research*, *133*, 285–296. https://doi.org/10.1016/j.jbusres.2021.04.070

Fan, C.-H., Li, M.-J., Li, M.-J., Chen, L.-J., & Liu, Z.-B. (2025). Performance analysis and optimization of an adiabatic compressed air energy storage system coupled with the packed-bed thermal energy storage device. *Energy*, *324*(C). https://ideas.repec.org//a/eee/energy/v324y2025ics0360544225015816.html

Fang, R., & Zhang, R. (2022). Preface to the special issue on advances in Hybrid Energy Storage Systems and smart energy grid applications. *Journal of Energy Storage*, *55*, 105781. https://doi.org/10.1016/j.est.2022.105781

Friedlingstein, P., O'Sullivan, M., Jones, M. W., Andrew, R. M., Gregor, L., Hauck, J., Le Quéré, C., Luijkx, I. T., Olsen, A., Peters, G. P., Peters, W., Pongratz, J., Schwingshackl, C., Sitch, S., Canadell, J. G., Ciais, P., Jackson, R. B., Alin, S. R., Alkama, R., … Zheng, B. (2022). Global Carbon Budget 2022. *Earth System Science Data*, *14*(11), 4811–4900. https://doi.org/10.5194/essd-14-4811-2022

Grönman, A., Sihvonen, V., & Honkapuro, S. (2025a). Emerging and maturing grid-scale energy storage technologies: A bibliometric review. *Journal of Energy Storage*, *107*, 114996. https://doi.org/10.1016/j.est.2024.114996

Grönman, A., Sihvonen, V., & Honkapuro, S. (2025b). Emerging and maturing grid-scale energy storage technologies: A bibliometric review. *Journal of Energy Storage*, *107*, 114996. https://doi.org/10.1016/j.est.2024.114996

Karadağ, M., Akçay, İ. T., & Karakurt, A. S. (2024). Trends and Emerging Themes in Thermal Energy Storage: A Bibliometric Study. *Journal of Marine and Engineering Technology*, *4*(2), 44–53. https://doi.org/10.58771/joinmet.1584084

Karakurt, A. S., Özsari, İ., Başhan, V., & Güneş, Ü. (2022). Evolution of steam turbines: A bibliometric approach. *Journal of Thermal Engineering*, *8*(5), 681–690. https://doi.org/10.18186/thermal.1187839

Mujtaba, A., Jena, P. K., Bekun, F. V., & Sahu, P. K. (2022). Symmetric and asymmetric impact of economic growth, capital formation, renewable and non-renewable energy consumption on environment in OECD countries. *Renewable and Sustainable Energy Reviews*, *160*, 112300. https://doi.org/10.1016/j.rser.2022.112300

Narasimalu, S., & Chelliah, B. (2018). Integration of Energy Storage System with Renewable Energy Source. *2018 Asian Conference on Energy, Power and Transportation Electrification (ACEPT)*, 1–7. https://doi.org/10.1109/ACEPT.2018.8610661

Odoi-Yorke, F., Abbey, A. A., Frimpong, T. A., Asante, E., Amewornu, E. M., Davis, J. E., Agyekum, E. B., & Atepor, L. (2024). A bird's eye view of pumped hydro energy storage: A bibliometric analysis of global research trends and future directions. *Journal of Energy Storage*, *103*, 114339. https://doi.org/10.1016/j.est.2024.114339

Ozsari, I. (2023a). Historical research trends and overview about exergy: A comprehensive analysis. *ResearchGate*. https://doi.org/10.1504/IJEX.2023.128522

Ozsari, I. (2023b). Trend analysis and evaluation of hydrogen energy and hydrogen storage research. *ResearchGate*. https://doi.org/10.1002/est2.471

Ratz, H., Robichaud, R., Bird, L., & Hutchinson, N. (2020). The Role of Long-Duration Energy Storage in Deep Decarbonization: Policy Considerations. *World Resources Institute*. https://doi.org/10.46830/WRIIB.19.00134

Secinaro, S., Brescia, V., Calandra, D., & Biancone, P. (2020). Employing bibliometric analysis to identify suitable business models for electric cars. *Journal of Cleaner Production*, *264*, 121503. https://doi.org/10.1016/j.jclepro.2020.121503

Shanmugam, C., Nattuthurai, S., & Muthusamy, S. (2024). Optimized control of hybrid energy storage systems for electric vehicles using BWPOA-MFPIDNN approach. *Journal of Energy Storage*, *104*, 114317. https://doi.org/10.1016/j.est.2024.114317

van Eck, N. J., & Waltman, L. (2010). Software survey: VOSviewer, a computer program for bibliometric mapping. *Scientometrics*, *84*(2), 523–538. https://doi.org/10.1007/s11192-009-0146-3

Xie, H., Liu, X., Wu, R., Liu, J., Wu, J., & Li, L. (2020). High-Performance Supercapacitor with Faster Energy Storage and Long Cyclic Life Based on CuO@MnO2 Nano-Core–Shell Array on Carbon Fiber Surface. *ACS Applied Energy Materials*, *3*(8), 7325–7334. https://doi.org/10.1021/acsaem.0c00590

Zhao, C., Liu, M., Ni, G., & Yan, J. (2024). Proposal design and thermodynamic optimization of an afterburning-type isothermal compressed air energy storage system integrated with molten salt thermal storage. *Journal of Energy Storage*, *102*, 114163. https://doi.org/10.1016/j.est.2024.114163

Zohbi, G. (2019). *Thermodynamic Analysis of Diabatic and Adiabatic Compressed Air Energy Storage Systems*. https://www.academia.edu/93839574/Thermodynamic_Analysis_of_Diabatic_and_Adiabatic_Compressed_Air_Energy_Storage_Systems

Different Methods of Speed Control of Switched Reluctance Motors Drives: An Overview*

BLERTA GËRMËNJI*[1], AIDA SPAHIU[2]

Abstract: Electric Drives with Switched Reluctance Motor (SRM) are driving innovation across industries and they are used in different applications such as: general purpose industrial drives; domestic drives: washing machines, vacuum cleaners; electric vehicle; aircraft applications; compressors, fans, pumps, centrifuges etc. Usage in important applications and the advantages of SRM motor like robust construction, easy maintenance and low cost, flexible controls, and the ability to operate in harsh environments such as high temperatures and high pressure made the SRM an alternative to both alternative and direct current machines used in adjustable electric drives. The SRM also comes with a few disadvantages among which torque ripple and acoustic noise are the most critical. The double saliency construction and the discrete nature of torque production by the independent phases lead to higher torque ripple compared with other machines. The aim of this paper is to present a literature review on the electric drives with SRM knowing that these electric drives are more efficient, reliable, and sustainable drives. In particular, the focus will be on the different methods of speed control of the electric drives with SRM. Based on the reviewed literature will be discussed the advantages, disadvantages and the performance of various types of speed control methods in terms of their efficiency, reliability and robust work for the different applications. The key contribution of the paper is to provide a valuable basis for detailed analyses of the electric drives with SRM focus on, advanced control, sensing technologies and sustainability.

Keywords: Switched Reluctance Motor, control method, applications, reviewed literature.

[1]**Address:** Aleksandër Moisiu Durrës University, Faculty of Professional Studies, Durrës/Albania
[2]**Address:** Polytechnic University of Tirana, Faculty of Electrical Engineering, Tirana/Albania

***Blerta Gërmënji**: blertagermenji@uamd.edu.al

1. INTRODUCTION

Switched Reluctance Motors (SRMs) are gaining popularity and have emerged as promising candidates for industrial, automotive, and renewable energy applications due to their fault tolerance, rugged construction, and high-speed capabilities. However, their highly nonlinear and complex dynamics make speed control challenging. Various control strategies have been developed to regulate SRM speed effectively. This review discusses the key speed control methods, their advantages, and limitations, such as double-salient structure, magnetic saturation, and torque ripple, which pose significant challenges for speed regulation. This section reviews the evolution of SRM speed control strategies, emphasizing conventional, advanced, and hybrid methods, as well as recent trends in artificial intelligence (AI)-based approaches.

2. DIFFERENT METHODS OF SPEED CONTROL OF SWITCHED RELUCTANCE MOTORS DRIVES

In this section, are presented some different methods of speed control of Switched Reluctance Motors Drives. They are classified in three categories: in Conventional Control Methods, Advanced Control Strategies and Hybrid Control Techniques. Below we will see how it is classified each of them.

2.1. Conventional Control Methods

Conventional Control Methods include three subcategories: **(a) Hysteresis (Bang-Bang) Control**, **(b) Proportional-Integral (PI) Control** and **(c) Proportional-Integral-Derivative (PID) Control.** Each of them has its principle, advantages and disadvantages.

(a) Hysteresis (Bang-Bang) Control: Hysteresis control, one of the earliest methods, regulates phase currents within predefined bands to track speed references. While simple, its high torque ripple and acoustic noise due to variable switching frequencies were critical drawbacks. Husain & Ehsani (1996) demonstrated its viability for low-cost applications but highlighted the need for supplementary ripple mitigation techniques. The motor speed is controlled by switching the phase currents between upper and lower hysteresis bands. The controller compares the actual speed with a reference speed and switches the motor phases ON/OFF when the speed error exceeds a predefined hysteresis band.

The phase current is regulated within upper and lower bounds. This method has a simple implementation and a fast dynamic response, but it has a high torque ripple and variable switching frequency which causes acoustic noise.

(b) Proportional-Integral (PI) Control: A PI controller adjusts the duty cycle of the converter to minimize speed error. This method has two major advantages: Well-established and easy to tune and good steady-state performance, but it has poor performance under dynamic load changes due to SRM nonlinearities and requires gain scheduling for wide speed ranges.
(c) Proportional-Integral-Derivative (PID) Control: Enhances PI control by adding a derivative term for better transient response. A Proportional-Integral (PI) or Proportional-Integral-Derivative (PID) controller adjusts the duty cycle of the converter to minimize speed error. The integral term eliminates steady-state error, while the derivative term improves transient response. Linear PI/PID controllers became popular for their steady-state accuracy and ease of tuning. However, their performance degrades under SRM nonlinearities and dynamic load changes. Lee et al. (2015) proposed gain-scheduling PID to adapt to varying operating points, but the method required extensive empirical tuning. Proportional-Integral-Derivative (PID) Control improves dynamic response compared to PI, but it is very sensitive to noise (derivative action) and still struggles with nonlinearities.

2.2. Advanced Control Strategies

To address nonlinearities, researchers shifted to model-based and intelligent control techniques.
Advanced Control Strategies include five subcategories: **(a) Sliding Mode Control (SMC)**, **(b) Fuzzy Logic Control (FLC), (c) Adaptive Control, (d) Model Predictive Control (MPC)** and **(e) Neural Network-Based Control.** Let's see their principle, advantages and disadvantages.
(a) Sliding Mode Control (SMC): It uses a discontinuous control law to drive the system toward a sliding surface, ensuring robustness. Forces the system trajectory to slide along a predefined surface (sliding surface) using a discontinuous control law. This control methods are it's robust against parameter variations and disturbances and good dynamic response, but it has a chattering effect (high- frequency switching) and a complex tuning.
SMC gained traction for its robustness against parameter variations. By forcing the system trajectory onto a sliding surface, SMC minimizes sensitivity to disturbances. Sahoo & Panda (2008) reduced torque ripple by 30% using SMC but noted chattering issues. Recent work by Zhang et al. (2020) integrated boundary layer techniques to suppress chattering while retaining robustness.
(b) Fuzzy Logic Control (FLC): Uses heuristic rules (IF-THEN) to adjust control inputs without requiring a precise mathematical model. It handles nonlinearities effectively and it has no need for exact system modeling. The disadvantages of this method it is that it is very computationally intensive. FLC eliminates dependency on precise mathematical models by using heuristic rules. Li & Shamsi (2014) achieved 15% lower torque ripple compared to PI in EV applications. However, designing optimal rule bases remains subjective, as noted by Lee & Ahn (2019).
(c) Adaptive Control: This control method continuously adjusts controller parameters based on real-time system behavior. Its advantages are self-tuning capability for varying operating conditions and improved performance over fixed-gain controllers. Despite the advantages, it has a complex implementation and requires accurate system identification.
(d) Model Predictive Control (MPC): Optimizes future control actions based on a predictive model of the SRM. It handles constraints (e.g., current/voltage limits) effectively and has a good dynamic performance, but this method requires an accurate motor model and has high computational burden. MPC optimizes future control actions using a predictive model. Vujičić & Kovačević (2019) demonstrated 5% torque ripple and fast settling times in SRMs but emphasized computational complexity. Recent advancements in explicit MPC (Torres et al., 2022) reduced online computation, making it feasible for real-time applications.
(e) Neural Network-Based Control: This control method uses AI to learn and adapt to SRM dynamics. It can model highly nonlinear systems and improves with training data, but it requires extensive training and it is very challenging to be implemented in Real-time. Neural networks (NNs) and reinforcement learning (RL) are emerging to handle SRM nonlinearities adaptively. Zhang et al. (2022) used deep RL to achieve near-optimal speed tracking without prior modeling. However, training data requirements and hardware limitations hinder industrial adoption.

2.3. Hybrid Control Techniques

These methods balance robustness and complexity but require careful integration to avoid instability. To overcome individual limitations, hybrid methods combine two or more strategies, such as:
Fuzzy-PI Control: Fuzzy logic adjusts PI gains dynamically.
SMC with PID: Sliding mode provides robustness while PID improves steady-state performance.
Adaptive Fuzzy-Neural Control: Combines learning capability of neural networks with fuzzy logic's rule-based approach.

Below we have presented a comparative analysis of the above-mentioned control methods in tabular form in terms of Robustness, Complexity, Torque Ripple, Dynamic Response and Implementation Ease and in terms of advantages, disadvantages and their applications.

Table 1. Comparative analysis

Control Method	Robustness	Complexity	Torque Ripple	Dynamic Response	Implementation Ease
Hysteresis (Bang-Bang)	Low	Low	High	Fast	Easy
PI/PID	Medium	Low-Medium	Medium	Moderate	Easy
Sliding Mode (SMC)	High	Medium	Low-Medium	Fast	Moderate
Fuzzy Logic (FLC)	High	Medium-High	Low	Good	Moderate
Model Predictive (MPC)	High	High	Very Low	Excellent	Complex
Neural Networks	Very High	Very High	Very Low	Excellent	Very Complex

Table 2. Comparative analysis focusing on advantages, disadvantages and type of application

Control Method	Advantages	Disadvantages	Applications
Hysteresis (Bang-Bang)	Simple and easy to implement. Fast dynamic response. No need for complex modeling.	High torque ripple due to abrupt switching. Variable switching frequency causes acoustic noise. Poor performance at very low/high speeds.	Low-cost applications where torque ripple is not critical. Basic industrial drives.
PI/PID	Well-established and easy to tune. Good steady-state accuracy. Works well for linear systems.	Poor performance under nonlinear loads (SRM has nonlinear inductance). Requires gain scheduling for wide speed ranges. Derivative noise amplification (in PID).	Industrial motor drives with moderate dynamic requirements. Systems where simplicity is preferred over high performance.
Sliding Mode (SMC)	Robust against load disturbances & parameter variations. Fast dynamic response. Works well for nonlinear systems.	Chattering problem (high-frequency switching). Requires careful tuning of sliding coefficients.	High-performance drives (e.g., electric vehicles). Systems requiring robustness against uncertainties.
Fuzzy Logic (FLC)	No need for precise mathematical modeling. Handles nonlinearities effectively. Good for uncertain systems.	Rule-base design is heuristic (requires expertise). Computationally heavier than PI.	Home appliances, HVAC systems. Industrial drives with varying loads.
Model Predictive (MPC)	Handles constraints (current, voltage limits). Excellent dynamic performance. Low torque ripple.	High computational load. Requires accurate SRM model.	High-performance servo drives. Aerospace & automotive applications.
Neural Networks	Self-learning capability. Can model highly nonlinear systems.	Requires large training data. Real-time implementation challenges.	Cutting-edge research (e.g., autonomous robots). Future smart motor drives.

Based on the advantages and disadvantages of each control method, the table below presents the relevant recommendations regarding the field of application of each method.

Table 3. Reccomended Control Method

Application	Recommended Control Method
Low-cost, simple drives	Hysteresis / PI Control
Industrial automation	Fuzzy-PI / Adaptive Control
High-performance EVs	MPC / Sliding Mode Control
Cutting-edge research	Neural Networks / Deep RL

3. RESULTS

Below we have presented a comparative analysis and research gaps. A synthesis of recent studies reveals the following trends:

Table 4. A synthesis of recent studies focusing on strengths,limitations and industrial adoption

Method	Strengths	Limitations	Industrial Adoption
Hysteresis/PI	Simplicity, low cost	High ripple, poor dynamics	Widely adopted
SMC/FLC	Robustness, adaptability	Heuristic design, chattering	Moderate
MPC	Optimal performance	Computational cost	Emerging
AI-Based	Self-learning, adaptability	Data/training requirements	Experimental

Research Gaps:
Real-Time Implementation: Most AI and MPC methods are simulation-proven but lack hardware validation.
Standardization: No universal framework for hybrid controller design.
Cost-Complexity Trade-off: High-performance methods (e.g., MPC) remain expensive for mass-market applications.

Recent Trends (2020–2024)
Edge AI for SRM Control: Deploying lightweight NNs on microcontrollers (TinyML).
Digital Twin-Assisted Control: Using real-time digital twins for predictive maintenance.
Wide Bandgap (WBG) Converters: SiC/GaN-based drives enabling high-frequency MPC.

4. DISCUSSION AND CONCLUSIONS

While conventional methods dominate industrial applications due to their simplicity, advanced strategies like MPC and AI-based control are reshaping high-performance domains. Future research should prioritize real-time implementation, hardware-in-loop validation, and cost reduction to bridge the gap between academia and industry. The SRM drive is a rapidly evolving technology with significant potential, but several challenges remain unresolved. The future of SRM drives hinges on solving torque ripple, noise, and control complexity while leveraging AI, WBG devices, and digital twins. If these challenges are addressed, SRMs could disrupt industries like EVs, aerospace, and industrial automation. Below are the key future research areas and open discussions in academia and industry:

1. Torque Ripple Mitigation
Current Challenge: SRMs inherently produce high torque ripple (10–25%), causing vibration and acoustic noise.
Future Research Directions:
Advanced Control Algorithms: Hybrid MPC + AI (e.g., reinforcement learning for real-time ripple optimization). Iterative learning control (ILC) for repetitive load cycles.
Machine Learning-Based Compensation: Neural networks to predict and cancel ripple dynamically.
Novel Motor Designs: Segmented rotor or dual-stator SRMs for smoother torque.

Open Questions: Can torque ripple be reduced to <5% without compromising efficiency? How to implement AI-based ripple control in real-time embedded systems?
2. Acoustic Noise Reduction
Current Challenge: High-frequency switching and radial magnetic forces generate noise (70–90 dB).

Future Research Directions:
Active Noise Cancellation (ANC): Using anti-phase current injection to cancel vibrations.
Soft Switching Techniques: Resonant converters (e.g., LLC) to reduce dv/dt-induced noise.
Material Science Solutions: Damping materials in motor housings.
Open Questions: Can SRMs achieve noise levels comparable to BLDC/PMSM motors? Is sensorless ANC feasible without increasing cost?

3. Sensorless Control Advancements
Current Challenge: Most SRM drives rely on encoders, increasing cost and reducing reliability.
Future Research Directions: High-Frequency Injection (HFI) Methods:
Pulsing high-frequency signals to estimate rotor position.
Flux/Current Observer Techniques: Sliding-mode observers, Kalman filters, and AI-based estimators.
Self-Sensing SRMs: Using saliency-tracking algorithms for position estimation.
Open Questions: Can sensorless SRMs achieve <1° position error at zero speed? How to handle magnetic saturation effects in sensorless schemes?

4. AI and Digital Twin Integration
Current Challenge: Traditional control struggles with SRM nonlinearities under varying loads.
Future Research Directions:
Deep Reinforcement Learning (DRL): Autonomous tuning of controllers under dynamic conditions.
Digital Twin-Assisted Control: Real-time motor emulation for predictive maintenance and fault detection.
Edge AI for SRMs:Deploying lightweight neural networks on microcontrollers (TinyML).
Open Questions:Can AI replace classical control entirely, or will hybrid approaches dominate? How to ensure real-time inference on low-cost hardware?

5. Wide Bandgap (WBG) Semiconductor Adoption
Current Challenge:Silicon (Si) IGBTs limit switching frequency, increasing losses.
Future Research Directions:SiC/GaN-Based SRM Drives:
Enabling 100+ kHz switching for higher efficiency.
Integrated Motor-Drives: Co-packaging WBG devices with motor controllers.
Open Questions: Can WBG devices make SRMs more efficient than PM motors?
How to mitigate EMI issues at ultra-high frequencies?

6. Sustainability and Recycling
Current Challenge: Rare-earth-free SRMs are eco-friendly, but end-of-life recycling is understudied.
Future Research Directions: Circular Economy Models:Designing SRMs for easy disassembly and material recovery.
Second-Life Applications: Repurposing SRMs for energy storage or wind turbines.
Open Questions: Can SRMs become the "greenest" motor option when considering full lifecycle impact?

7. Standardization and Commercialization
Current Challenge:Lack of universal standards limits mass adoption.
Future Research Directions: IEEE/IEC Standardization Efforts:
Defining SRM control protocols, testing procedures. Industry-Academia Collaboration: Moving from lab prototypes to commercial products (e.g., EVs, HVAC).
Open Questions: Will SRMs replace induction/PMSM motors in any major industry?
What are the cost benchmarks for SRMs to compete with BLDC motors?

Acknowledgements
I am extremely grateful to my research supervisor, Prof. Dr. Aida Spahiu, Professor, Polytechnic University of Tirana, Albania, for giving me the opportunity to do research and providing invaluable guidance throughout this research. Her vision, sincerity and motivation have deeply inspired me.

Ethics Committee Approval
N/A

Peer-review
Externally peer-reviewed.

Author Contributions
Writing-Original Draft: B.G.; Writing-review & Editing: B.G., A.S.; Other: All authors have read and agreed to the published version of manuscript.

Conflict of Interest
The authors have no conflicts of interest to declare.

Funding
The authors declared that this study has received no financial support.

REFERENCES

1. Husain, I., & Ehsani, M. (1996). "Torque ripple minimization in switched reluctance motor drives by PWM current control." IEEE Transactions on Power Electronics. Volume 11, issue 1, 83-88.
2. Sahoo, N. C., Xu, J. X., & Panda, S. K. (2001). "Low-ripple torque control of switched reluctance motors using iterative learning." IEEE Transactions on Energy Conversion.
3. Li, H., & Shamsi, P. (2014). "Fuzzy logic-based speed control of switched reluctance motors for electric vehicles." IEEE Transactions on Industrial Informatics.
4. Vujičić, V., & Kovačević, A. (2019). "Predictive torque control of switched reluctance motors with reduced torque ripple." IEEE Transactions on Industrial Electronics.
5. Zhang, X., et al. (2022). "Deep reinforcement learning for adaptive speed control of switched reluctance motors." IEEE Transactions on Neural Networks and Learning Systems.
6. Krishnan, R. (2001). Switched Reluctance Motor Drives: Modeling, Simulation, Analysis, Design, and Applications. CRC Press, Boca Raton London New York Washington, D.C.
7. Krishnan (2001) formalized PI control design for SRMs in Switched Reluctance Motor Drives.
8. Sahoo et al. (2005) highlighted PID limitations in handling magnetic saturation.
9. Miller, T. J. E. (1989), Brushless Permanent-Magnet and Reluctance Motor Drives. Clarendon Press, Oxford.
10. Singh, S., et al. (2020). "A comprehensive review of control strategies for switched reluctance motor drives." IEEE Transactions on Transportation Electrification.
11. Lee, D. H., & Ahn, J. W. (2021). "Advanced control techniques for torque ripple mitigation in SRMs." Energies Journal.
12. IEEE Standard 1783-2009: Guide for Switched Reluctance Motor Drives.
13. IEC 61800-9: Adjustable speed electrical power drive systems.
14. IEEE Transactions on Industrial Electronics, Special Issue on SRM Drives (2021).
15. IEEE Transactions on Power Electronics review on AI for motor control (2023).

Investigation of Quality Characteristics and Colour Fastness Values of Cotton Yarns Dyed with Bath Containing PCM Microcapsules

SAADET MIHÇI*[1], SENNUR ALAY AKSOY[2]

Abstract: This study investigates the yarn quality and colour fastness values of microcapsule-treated combed tricot yarns during the bobbin dyeing process. The study also investigated the effectiveness of bleaching and cationisation processes prior to microcapsule application. For this aim, a series of quality tests were carried out on yarns that had undergone pretreatment processes before dyeing and dyed yarns. The results of these tests indicated a decline in yarn strength and elongation values following the bleaching process. Conversely, the cationisation process resulted in enhanced yarn strength, though this varied with the process conditions. Similar results were obtained for elongation at break. The strength of the yarns also increased after dyeing and microcapsule application process. This increase is thought to be related to the fact that the microcapsules incorporated into the yarn structure adhere to the fibre surface and increase the fibre-fibre friction in the yarn cross-section. According to the yarn unevenness test, CVm values generally did not change after pre-treatment and dyeing processes. However, the number of thin places varied according to the processing conditions and generally decreased after dyeing. Although the number of thick places and neps (+200) varied according to the process conditions, it increased with the bleaching process, generally decreased after the cationisation process and increased after the dyeing process. The yarn hairiness did not show any significant change after the treatments. According to the colour fastness test results of the yarns, low fastness values were obtained in cotton staining at washing fastness, and wet rubbing fastness tests, except for two samples. However, the dry rubbing, acid and alkaline perspiration and water fastness test results of all the yarns showed acceptable fastness values.

Keywords: Cotton yarn, bobbin dyeing, yarn imperfection, evenness, hairiness, color fastness.

[1]**Address:** Başyazıcıoğlu Tekstil San. ve Tic. A.Ş, Kayseri, Türkiye
[2]**Address:** Süleyman Demirel University, Faculty of Engineering and Natural Sciences, Isparta/Turkiye

***Corresponding author**: sennuralay@sdu.edu.tr

1. INTRODUCTION

Nowadays, research on the production of garment systems which play a role in the active control of heat and moisture transfer processes in the body-clothing-environment by adapting to changes in environmental conditions and activity level has become remarkable (Koncar, 2016). One of the materials used to manufacture these textiles is phase change materials. Phase change materials (PCMs), also known as latent heat storage materials, are materials that can absorb and release latent heat energy during phase change processes. These materials melt and solidify at a certain constant temperature and store and release latent heat energy at high capacity (Giro-Paloma, 2016). When the ambient temperature reaches the melting temperature, the PCM starts to melt and absorbs latent heat from the environment until the melting is complete. When the temperature drops to the solidification temperature, the PCM gives back the heat energy stored until the solidification process is completed (Mondal, 2008). The PCMs offer thermoregulation (temperature regulation, supporting the temperature to remain constant within a certain range) function in cases of sudden temperature changes with the ability to store/dissipate latent energy during solid-liquid phase change.

When the studies on microcapsule applications to textile structures and industrial applications are examined, it is generally seen that microcapsule applications are carried out by methods such as impregnation, exhaustion and coating on the fabric material. When the commercially available microcapsules are examined, it is seen that various active substances such as pleasant odour, PCM, and antimicrobial agent are microencapsulated for application to textile materials. It is seen that manufacturers generally recommend the impregnation method and rarely the exhaustion method for textile application of these microcapsules. To produce yarn containing microcapsules, placing microcapsules on the fiber cross-section in the synthetic yarn production process is also a commercially used method. Microcapsule added yarns are limited to the synthetic yarns mentioned, and there is no commercial product example developed by applying microcapsules to staple yarns made of natural fibres in the national and international market. The most important reason for this situation is that most of the microcapsule structures developed do not have a wall structure that will allow them to be efficiently taken up by the fibre by the exhaustion method and the impregnation method is a more efficient method in terms of fabric application. However, the

application of microcapsules to the fabric by impregnation method also has serious disadvantages such as the significant weakening of fabric handle, permeability and strength properties due to the excessive amount of binder used and the inability to transfer all the excessive amount of microcapsule added to the liquor to the fabric. When all these issues are evaluated, the development of a process for the application of microcapsules to yarns made of staple natural or man-made fibres without requiring an additional process and without adversely affecting the yarn attitude will provide an important development in this regard. From this point of view, in this study, microcapsules with a wall structure (polymethyl methacrylate-co-glycidyl methacrylate), which have the potential to be applied to textiles by the exhaustion method, were produced and applied to tricot twisted cotton yarns by bobbin dyeing process was investigated. In this study, yarn quality parameters of these microcapsule-applied yarns were measured and the effect of dyeing process and microcapsule application on yarn properties were evaluated.

2. MATERIAL AND METHOD

2.1 MATERIAL

In this study, poly(methyl methacrylate-co-glycidyl methacrylate) (PMMA-co-GMA) walled microcapsules containing phase change agent (1-tetradecanol), which were produced and characterised in our previous study, were used (Mıhçı ve Alay Aksoy, 2023). 100% cotton using the following specifications of yarn were spinned: yarn counts 20/1, twisted 598 t/m. The yarns were used to knitt single jersey fabric in order to investigate dyeing properties. For pre-treatment, cationized agent (REWIN FSN, CHT) was used which was determined suitable conditions both acidic and base. For dyeing, reactive dyestaff was used (compatible inditex). Acrylic based binder was used in the bond (CHT).

2.2 METHOD

2.2.1. Yarn Test and Analysis

The yarns tested in this study were microcapsule applied and dyed simultaneously with the bobbin dyeing process in our previous study (Mıhçı ve Alay Aksoy, 2023). The process details of pre-dyeing pre-treatments (such as bleaching, cationisation) and dyeing process are given in the previous study (Tablo 1). In this study, unlike the previous study, the technical quality parameters of the yarns were measured and the effect of the pre-treatments (such as bleaching, cationisation) before dyeing, dyeing-microcapsule application method on the properties and quality of the yarns was investigated. Colour fastness tests of the fabrics knitted from the yarns were also carried out.

Table 1. Process information for yarns (Mıhçı ve Alay Aksoy, 2023)

Yarn sample	Cationization Conditions			Cationiciser concentration (%)
	Temperature(°C)	pH	Time (min.)	
CO-1	90	5,5	60'	20
CO-2	90	9,5	60'	20
CO-3	90	5,5	60'	30
CO-4	90	9,5	60'	30
CO-5	70	5,5	60'	20
CO-6	70	9,5	60'	20
CO-7	70	5,5	60'	30
CO-8	70	9,5	60'	30

In the study, tests were carried out to determine the properties of the produced yarns. Before the measurements were carried out, the prepared samples were conditioned for 24 hours under standard atmospheric conditions (20±2°C temperature and 65±2% humidity). The yarns were subjected to strength and irregularity tests. In addition, colour control after dyeing, colour fastness tests and colour measurements with spectrophotometer were performed.

2.2.1.1. Yarn Quality Tests

Yarn count measurements were performed according to the skein method specified in TS 244 EN ISO 260 standard using the yarn spinning wheel shown in Figure 3.10. In the tests, 100 metre skeins prepared with the Zweigle T600 MSH yarn spinning wheel were weighed on a precision balance and the count values were calculated as Ne from the values obtained. The twisting of the yarns was carried out with Zweigle D 314 twist tester using the opening

and closing method. The strength tests of the yarns were carried out with Uster Tensorapid 5 yarn strength tester. The speed of the measuring device was used as 5000 mm/min. For each yarn, 10 tests were carried out according to TS EN ISO 2062 test standard. As a result of the test, breaking strength (cN/tex) and elongation at break (%) values were obtained. The unevenness tests of the yarns were carried out on a Uster Tester 6 yarn unevenness tester. The test speed of the device was set to 800 m/min. For each yarn test, 3 tests were performed in accordance with ASTM 1425 test standards. As a result of the irregularity test, the results of irregularity (% CVm), thin spot (-40%), thick spot (+50%), neps (+200%) and hairiness (H) of the yarns were obtained. A light booth was used for colour comparisons of the yarns produced in the study. The samples were examined under D65 artificial daylight. For the colour evaluation, a stand was placed at an angle of 45°C and in the same colour as the cabinet and the image direction was perpendicular to the surface plane.

2.2.1.2. Fastness tests

Wash Fastness: was measured according to ISO 105 C01-C02-C03-C04-C05. 10*4 cm fabric was cut from each yarn skein about 50 gr. A multifiber adjacant fabric was used and same dimension of multifiber was cut and attached in one end of fabric by sewing at one of the shorter edges. The following recipe was followed 4g/L ECE DETERGENT, 1 g/L sodium perborate dissolved in 1L of distilled water was used for the liquor. The fabric was washed in liquor ratio of 1.5 at 60 C for 30 minutes. The fabric was washed in liquor ratio of 1:50 at 60c for 30 minutes with 10 steel balls in each container.After the washing the fabric it was rinsed three times An then it was dried etuv. The results of wash fastness were assessed in grey scala.

Perspiration Fastness: was measured **a**ccording to ISO 105 E04 standardına göre yapılmıştır. For experiment was prepared acidic and base solution. 10*4 cm was cut from each yarn about 50 gr three sample. A multifiber adjacant fabric was used and same dimension of multifiber was cut and attached in one end of fabric by sewing at one of the shorter edges. The sample was prepared both acidic (pH 5,5) and base (pH 8,5) and waited at room temperature for 4 hour and dried etuve 37c for 4 hour.The results of wash fastness were assessed in grey scala.

Water Fastness: was measured according to ISO 105-E01; 2013. 10*4 cm fabric was cut from each yarn skein about 50 gr. And a multifiber adjacent fabric was placed the sample and added weight on it for 4 hours. And then dried etuv at 60c. The results of wash fastness were assessed in grey scala.

Rubbing Fastness: was measured according to the (TS 717 EN ISO 105-X12) 2000, ISO 105-A03. 10*20 cm was cut from each fabric for four sample. As rubbing fabric was used friction cloth. The experiment was done the devices of crocmeter both wet and dry. The results of wash fastness were assessed in grey scala.

3. RESULTS

Table 2 shows the elongation at break and strength test results of raw and bleached combed cotton yarns, Table 2 shows the elongation at break and strength test results of cationised cotton yarns, Table 4 shows the elongation at break and strength test results of dyed and microcapsule treated cotton yarns. When the results were examined, after the bleaching process, the strength values of the yarns decreased. However, the strength values of the yarns increased after the cationisation process. During the cationisation process, the cellulose chains of cotton gain positive charges caused by ionic cross-links. In the cationisation stage, thanks to the wet process, it provides active groups by bonding with hydrogen bonds, thus significantly improving the breaking strength due to the positive changes in the cellulose structure of the cross-links.

Table 2. Strength test results of raw yarn and bleaching yarns

Yarn samples	B-Force, gF	Extension %	Strength (RKM)
Raw	434.6	5.33	14.73
Bleached	375.1	4,56	12.7

Table 3. Strength test results of cationised yarns

Yarn samples	B-Force(gF)	Extension (%)	Strength (RKM)
C-CO-1	468	6.35	15.86
C-CO-2	478	6.52	16.23
C-CO-3	450	6.12	15.25
C-CO-4	462	6.5	15.63
C-CO-5	456	6.22	15.47
C-CO-6	468	6.32	15.72
C-CO-7	472	6.36	16.21
C-CO-8	465	6.24	15.89

Table 4 shows the strength (RKM) values measured after PCM microcapsule application to the same yarns during dyeing. Figure 1 shows strength and Figure 2 shows the breaking strain test results of all yarns. The graph given in Figure 1 is the breaking strength values of ring yarns with the same yarn count and twist coefficient and it was determined that the strength of the yarns after dyeing increased by 11% compared to the raw yarn values. When compared with the raw yarn strength, a 14% decrease was observed in the strength values after bleaching process, but a 10% increase occurred after cationising process. According to the findings obtained in the study, while the strength loss in yarns was higher after conventional dyeing process, the strength loss was determined to be lower after microcapsule application and dyeing process application in the study. It is concluded that the lower level of strength loss is related to the strength increase during cationisation. In addition, it is thought that reducing the amount of salt (NaCl) and soda used during the dyeing process in which microcapsule application is performed is also effective in the lower strength loss.

Table 4. Strength test results of yarns after bobbin dyeing and FDM microcapsule application process

Yarn samples	B-Force(gF)	Extension (%)	Strength (RKM)
CO-1	496	5.19	17.81
CO-2	439	6.49	15.89
CO-3	457	6.61	16.51
CO-4	429	6.33	15.54
CO-5	462	5.05	16.67
CO-6	458	6.12	16.28
CO-7	456	6.22	17.12
CO-8	455	6.64	16.41

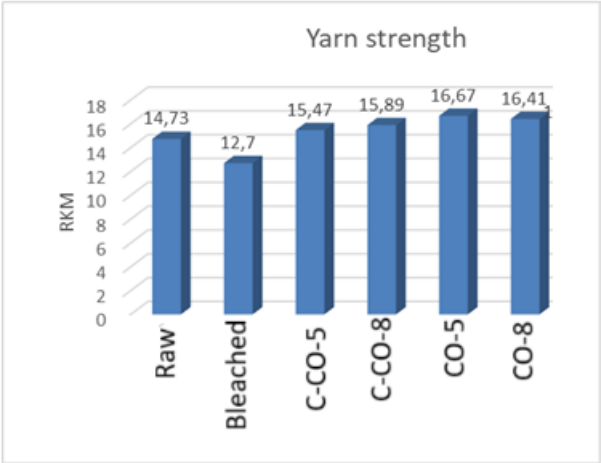

Figure 1. Strength values of cotton yarns

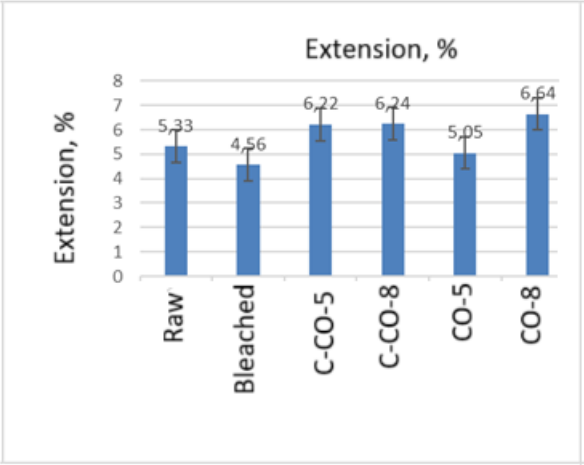

Figure 2. Extension values of cotton yarn

The imperfections are grouped as thin place, thick place and neps and they cause high unevenness in the yarn and adversely affect the overall quality of the yarn. Thin place fault is shown as -40 % and a thin place fault is considered to be 40 % or less of the average yarn cross-section. The thick place fault is shown as +50 % and 50 % and more of the average yarn cross-section is considered as thick place. Neps defect is shown as +200 % for ring yarns and 200 % (2 times) of the average yarn thickness will be considered as thick place defect. The values of unevenness, thin place, thick place, neps, hairiness of the raw yarn, cationised yarns and dyed and microcapsule treated-yarns are given in Table 5 and Table 6, respectively. The obtained values are given as graphs in Figure 3-Figure 6.

Table 5. Irregularity, imperfections and hairiness values of raw cotton and cationised cotton yarns

Yarn	% CVm	Thin place (-40)	Thick place (+50)	Neps +140	Neps +200	Hairiness
Raw	10,4	5	7.5	40	5	6.82
Bleached	10,73	7.5	12	10	10	6.84
C-CO-1	10,64	12.5	10	5	7.5	7.45
C-CO-2	10,79	2.5	5	15	5.8	7.01
C-CO-3	10,77	2.5	5	10	7.5	6.63
C-CO-4	10,84	5	2.5	20	5	6.70
C-CO-5	10,57	0	5	5	0	6.86
C-CO-6	10,47	10	10	16	2.3	6.93
C-CO-7	10,50	7.5	7.5	13	10	6.04
C-CO-8	10,55	5	2.5	10	5	7.92

Table 6. Irregularity, defect and hairiness values of cotton dyed and microcapsule treated-yarns

Yarn	% CVm	Thin place (-40)	Thick place (+50)	Neps +200	Hairiness
	Ort	Ort	Ort	Ort	Ort
CO-1	10,17	0	7.5	25	7.13
CO-2	10,58	7.5	12.5	32.5	6.61
CO-3	10,41	2.5	5	17.5	6.56
CO-4	10,60	0	10	15	6.78
CO-5	10,12	2.5	10	5	6.84
CO-6	10,76	0	10	12.5	6.87
CO-7	10,57	0	15	27.5	6.93
CO-8	10,16	0	10	25	6.88

When the CVm values of the yarns were analysed, it was determined that they were very close to each other and the pretreatment and dye-microcapsule application processes did not affect the yarn irregularity significantly.

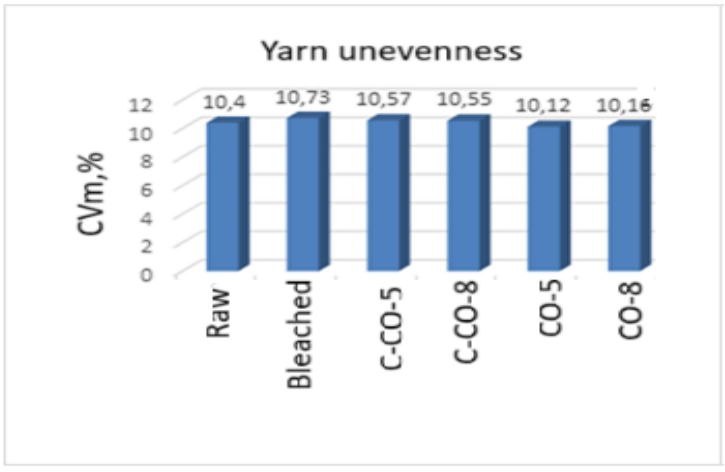

Figure 3. Unevenness measurement results of cotton yarns

When the thin place (-40) fault is examined, it is seen that the yarns show a positive decrease in the yarn groups after dyeing from raw yarn. It is predicted that the thin place value is low and smoother fabric appearances can be

obtained. It is seen that the thick place (+50) fault value is low at varying rates. However, according to the data obtained, it is predicted that there is a decrease between the values obtained from raw yarn to post-dyeing measurements in the thick place fault in cotton-B5 sample and these values are acceptable values. When the results were analysed, no significant yarn defect values were found in thin place (-40), thick place (+50) and neps (+200) defects. However, there is an increasing trend in the neps (+200) value in cotton B8 yarns.

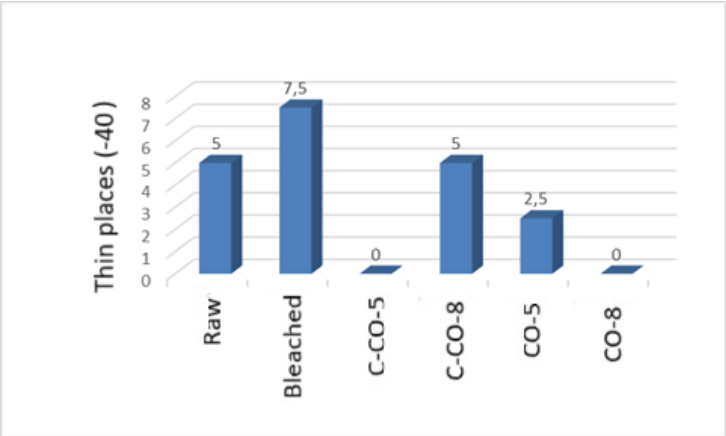

Figure 4. Thin places values of the yarns

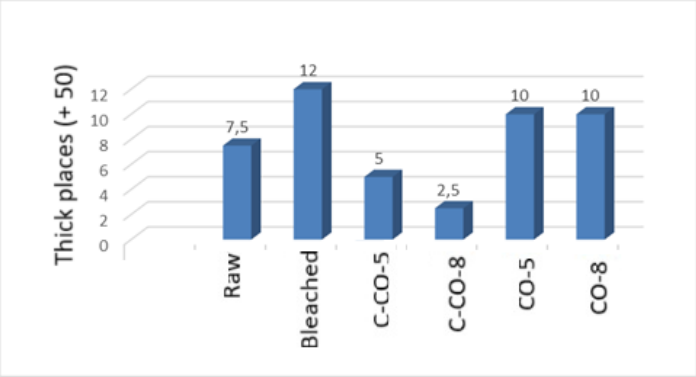

Figure 5. Thick places values of the yarns

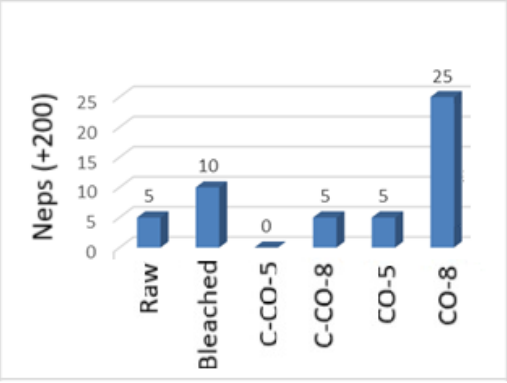

Figure 6. Neps values of the yarns

Figure 7 shows the hairiness values of the yarns. When the change in the Uster H hairiness values of the yarns belonging to the study was examined, it was preliminarily observed that there were no significant differences between the hairiness values of the yarns used in the study and the results obtained were acceptable values. However, it is clear that the yarn hairiness values in the cationised yarn B8 study are very high.

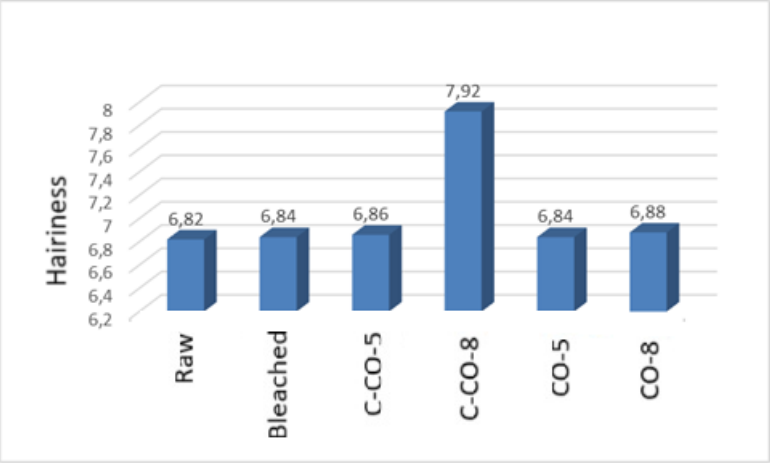

Figure 7. Hairiness values of the yarns

In this study, washing, perspiration and rubbing fastness tests were carried out to investigate the colour fastness properties of PCM microcapsule treated cotton yarns. As a result of the fastness tests of PCM microcapsules applied cotton yarns, colour change (fading) and bleaching (staining) after washing, both acidic and basic sweat fastness tests and water fastness tests were performed. The fastness results are given in Table 7. According to the washing fastness test results, it was determined that the fastness values were generally at an acceptable level and no staining and discolouration were observed. When the perspiration fastness results were evaluated, it was observed that the values obtained in cotton yarns treated with PCM-containing microcapsules were acceptable values. According to the staining and colour change results determined in the water fastness test, it was determined that the fastness values were at an acceptable level and no staining and colour change was observed.

Table 7. Washing, water and perspiration color fastness test results

Washing fastness test results								**Water fastness test results**							
		Staining								**Staining**					
Yarn	**Fading**	Acetate	Cotton	Nylon	Polyester	acrylic	wool	**Yarn**	**Fading**	Acetate	Cotton	Nylon	Polyester	acrylic	wool
CO-1	5	5	2	5	5	5	5	CO-1	5	5	5	5	5	5	5
CO-2	5	5	3	5	5	5	5	CO-2	5	5	5	5	5	5	5
CO-3	5	5	2/3	4/5	5	5	5	CO-3	5	5	2/3	5	5	5	5
CO-4	5	5	3/4	5	5	5	5	CO-4	5	5	5	5	5	5	5
CO-5	5	5	4/5	5	5	5	5	CO-5	5	5	5	5	5	5	5
CO-6	5	5	4	5	5	5	5	CO-6	5	5	5	5	5	5	5
CO-7	5	5	2	4	5	5	5	CO-7	5	5	5	4	5	5	5
CO-8	5	5	4/5	5	5	5	5	CO-8	5	5	5	5	5	5	5
Perspiration (acidic)								**Perspiration (basic)**							
		Staining								**Staining**					
Yarn	**Fading**	Acetate	Cotton	Nylon	Polyester	acrylic	wool	**Yarn**	**Fading**	Acetate	Cotton	Nylon	Polyester	acrylic	wool
CO-1	5	5	4/5	5	5	5	5	CO-1	5	5	4/3	5	5	5	5
CO-2	5	5	4/5	5	5	5	5	CO-2	5	5	4	5	5	5	5
CO-3	5	5	5	5	5	5	5	CO-3	5	5	4/5	5	5	5	5
CO-4	5	5	5	5	5	5	5	CO-4	5	5	5	5	5	5	5
CO-5	5	5	5	5	5	5	5	CO-5	5	5	5	5	5	5	5
CO-6	5	5	5	5	5	5	5	CO-6	5	5	5	5	5	5	5
CO-7	5	5	5	4	5	5	5	CO-7	5	5	5	4	5	5	5
CO-8	5	5	5	5	5	5	5	CO-8	5	5	5	5	5	5	5

In the study, the colour change (fading) and running (staining) values of the microcapsule treated yarns after wet and dry rubbing test are given in Table 2. It was determined that the rubbing fastness values were at acceptable level for C-5 and C-8 samples, but the wet fastness values were low for the other samples. It was concluded that these low colour fastness values were because the dye could not be completely absorbed during the dyeing of the yarns.

Table 8. Rubbing fastness test results

Yarn	Dry	Wet
CO-1	5/4	4/3
CO-2	5/4	3
CO-3	5	2
CO-4	5	1/2
CO-5	5	4
CO-6	5/4	1/2
CO-7	5/4	2
CO-8	5/4	4

4. DISCUSSION AND CONCLUSIONS

In this study, FDM microcapsules were applied to tricot twisted 100% cotton yarns by bobbin dyeing process. The produced microcapsules were exhausted together with the dye bath on cotton yarns cationised under different conditions. It was observed that the strength values of the cationised cotton yarns increased after cationisation. It was observed that the cationisation process increased the breaking strength of the cotton cellulose chains by loading the ionic cross-links with positive charges. An increase was observed in the breaking strength values of the yarns after dyeing/microcapsule application process. The salt used during normal dyeing enters between the cotton fibres and weakens the fibres and causes a decrease in strength. In this study, in addition to the strength increase caused by the cationisation process, it was evaluated that the lower amount of salt and soda used in the developed microcapsule application/dyeing process compared to normal dyeing was effective in increasing the strength of the final yarns. When the unevenness test results of cotton yarns were examined, it was determined that despite the effect of the cationisation process, no significant difference was observed in the quality values (thin place, thick place, neps and hairiness) of the final dyed/capsule-containing yarns and the values obtained were found to be acceptable values. When the colour fastness test results of the cotton yarns containing PCM microcapsules were examined, it was observed that the washing, water, perspiration and dry rubbing fastnesses were good, while the wet rubbing fastnesses were moderate but commercially acceptable. In conclusion, in this study, PCM-containing microcapsules were successfully produced by emulsion polymerisation method. In addition, it was seen that it is possible to apply microcapsules in textile applications at lower concentrations by the exhaustion method.

Acknowledgements
The authors would like to express their gratitude to Süleyman Demirel University Scientific Research Projects Coordination Unit (BAP) for supporting the study with the project titled “A Research on Developing Microencapsulation Processes in Yarn Dyeing Process” numbered FYL-2020-7974.

Ethics Committee Approval
N/A

Peer-review
Externally peer-reviewed.

Author Contributions
Conceptualization: S.A.A.; Investigation: S.M and S.A.A.; Material and Methodology: S.M and S.A.A; Supervision: S.A.A; Visualization: S.M.; Writing-Original Draft: S.M.; Writing-review & Editing: S.M and S.A.A.; Other: All authors have read and agreed to the published version of manuscript.

Conflict of Interest
The authors have no conflicts of interest to declare.

Funding
The authors declared that this study has received no financial support.

REFERENCES

Giro-Paloma, J., Martinez, M., Gabeza, L., Fernandez, A., I., 2016. Types, Methods,Techniques,and Applications for Microencapsulated Phase Changematerials (MPCM). Renewable and Sustainable Energy Reviews, 53, 1059-

Koncar, V., 2016. Introduction To Smart Textiles and Their Applications. In Koncar, V. (Ed.) Smart Textiles and Their Applications (1-8), Woodhead Publishing Association with The Textile Institute, 695p, Duxford.

Mıhçı, S., Alay Aksoy, S., (2023). Pamuk İplik Boyama Sürecinde FDM Mikrokapsül Aplikasyonu ve Isı Düzenleyen İplik Üretimi, Mühendislik Bilimleri ve Tasarım Dergisi, 11(2), 592-606

Mondal, S., 2008. Phase Change Materials for Smart Textiles-an Overview. Applied Thermal Engineering, 28, 1536-50.

Production of Polymethyl Methacrylate/Capric Acid Nanofibers With Latent Heat Storage Property

GIZEM ÖZMEN[1], SENNUR ALAY AKSOY *[1]

Abstract: In the present study, phase change material nanofibers (PCM nanofibers) with latent heat energy storage/dissipation properties were prepared using a unidirectional electrospinning system.The prepared nanofibres consist of capric acid (CA), a type of fatty acid, as PCM and poly(methyl methacrylate) (PMMA) polymer as support material. SEM analysis of the nanofibres showed that pure PMMA polymer produced uniform nanofibres with a homogeneous diameter. However, it was found that the addition of CA to the polymer caused bead formation in the nanofibre structure and increasing the CA ratio increased the bead formation. As shown by the DSC results, the incorporation of CA into the polymer solution at a concentration of 30% (w/w) and above resulted in an increase in the latent heat storage and release capacity in the nanofibres. The TGA results showed that all samples exhibited two-stage degradation. In general, the first stage of degradation was above 200 °C. The initial degradation of CA-containing nanofibres at 10% and 30% concentration resulted in mass loss of 35.8% and 51.9%, respectively. However, the mass loss of nanofibres containing 50% and 100% CA was found to be more than 75%. The leakage test results show that no leakage was detected in the samples containing 10% CA when exposed to oven temperatures of 60°C for half an hour; however, wetting of the absorber paper substrate on which the nanofibres were placed was observed in the sample containing 30% CA. However, in the nanofibres containing more than 50% CA, a high leakage rate was observed to wet the absorbent surface on which the nanofibres were placed. As a result, PCM nanofibres with 30% CA content were found to have acceptable thermal stability, in addition to their high heat storage and dissipation properties. However, in order to increase the thermal stability of these fibres, it was found that research could be carried out into post-spinning cross-linking or the production of nanofibres by emulsion electrospinning.

Keywords: Phase change material, nanofiber, electrospinning, PCM nanofibers.

[1]**Address:** Süleyman Demirel University, Faculty of Engineering and Natural Sciences, Isparta/Turkiye

***Corresponding author**: sennuralay@sdu.edu.tr

1. INTRODUCTION

Thermal energy storage is the process of temporarily storing heat energy for later use (Mondal, 2008). In the methods applied in heat storage, physical processes are divided into two as sensible heat and latent heat storage (Alevay Kılıç, 2018). Among thermal energy storage techniques, latent heat storage is among the most studied methods due to its high heat storage capacity (Mondal, 2008). Latent heat is defined as the heat stored or emitted during the phase change of the substance (Alay, 2010; Tözüm, 2013; Alevay Kılıç, 2018). Solid-liquid phase change materials are mostly used in the market because they allow the storage of high amounts of energy in a narrow and fixed temperature range (Süpüren, 2007). However, the fact that these substances flow away from the structure, especially in the liquid phase, creates problems in many end-use areas. The most widely used method to solve this problem is encapsulation. Encapsulation is based on confining the PCM within a wall or sheath structure, and the PCM performs the phase change cycle within this structure. Different methods are used for encapsulation, and the production of PCM structures in the form of nanofibers by electrospinning has an important place among these methods. Different approaches are used in PCM nanofiber production by electrospinning method. These are; production of nanofiber from polymer/PCM mixed solution with single nozzle system and production of core-sheath structured nanofiber with PCM in the center and polymer in the sheath structure with intertwined, coaxial spinneret system (Sun et al., 2015; Zdraveva et al., 2015; Dang et al., 2015; Noyan et al., 2018).

In the single-nozzle electrospinning method, phase change nanofibers can be obtained by directly spinning the PCM/polymer mixture from the solution (Chen et al., 2007; Chen et al., 2009a; Chen et al., 2009b; Cai et al., 2012; Golestaneh et al., 2018; Esmaeilzadeh et al., 2018; Darzi et al., 2019) or by spinning the PCM nanofibers from the emulsified polymer solution (Zdraveva et al., 2015; Chalco-Sandoval et al., 2016). In this study, the focus was on the production of PCM nanofibers from a polymer solution mixed with PCM by electrospinning. For this purpose, capric acid, a type of fatty acid, was used as a phase change substance and was mixed into the solution of polymethyl methacrylate polymer in certain proportions. The possibility of producing PCM nanofibers from the prepared mixtures was investigated. There are studies in the literature on composite nanofibers produced by the single-nozzle electrospinning method using fatty acids as FDM (Cai et al., 2012; Golestaneh et al., 2018). However, in this study, unlike literature, PMMA polymer was used as a supporting polymer matrix for the production of FDM/polymer composite nanofibers.

2. MATERIAL AND METHOD

2.1. Production of Nanofibers

Polymethyl methacrylate (Aldrich, molecular weight 350,000) polymer was used to form the sheath structure in the production of PCM nanofibers with latent heat storage. Capric acid (CA; $C_9H_{19}COOH$, decanoic acid, Alfa Aesar) with a purity of 98% and above was used as a phase change material with latent heat storage properties. The melting temperature of the fatty acid is in the temperature range of 29-33 °C and the enthalpies of melting and solidification are 156 and -154 j/g, respectively. Ethanol (Sigma Aldrich) and chloroform (Sigma Aldrich) were used as solvents to dissolve the PMMA polymer.

PMMA polymer, which will form the sheath structure in nanofiber production, was dissolved in a solvent mixture containing 40 ml ethanol and 60 ml chloroform and the concentration of the polymer solution was adjusted to 12% (w/v).CA was added to the prepared solution at ratios ranging from 10% to 100% of the polymer weight. Nanofiber production was carried out from the prepared CA/PMMA polymer solution in the electrospinning system (Inovenso Ne 100), the schematic representation and photograph of which are given in Figure 1. Table 1 shows the production conditions of the nanofibers produced in the study. Nanofibers were produced at room temperature and in an open air environment.

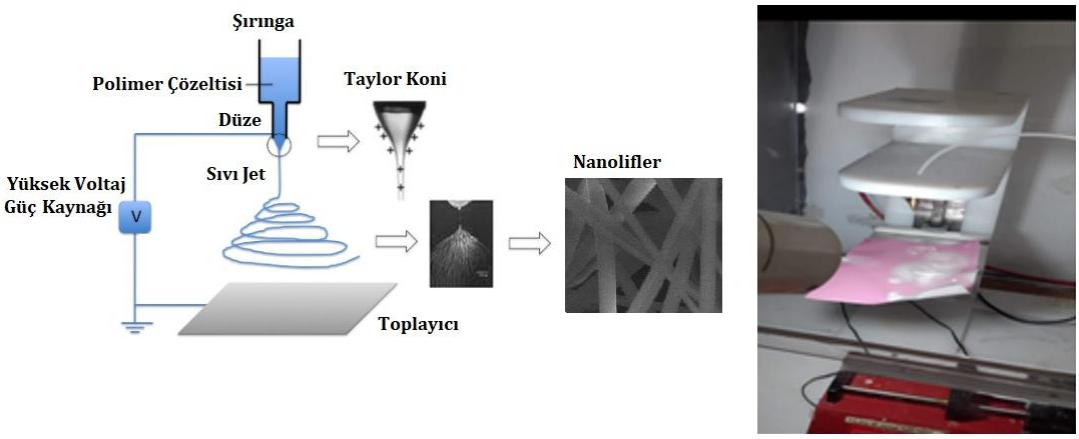

Figure 1. Schematic view of electrospinning system (Li et al., 2010) and photograph

Table 1. Nanofiber Production Conditions

Sample code	Contents	Distance between electrodes (cm)	Feed rate (ml/h)	Power (kW)
Pure PMMA	%12 PMMA	16	3.0	1.50
PMMA/CA-10	%12 PMMA + %10 CA	16	3.0	1.50
PMMA/CA-30	%12 PMMA + %30 CA	16	4.0	1.50
PMMA/CA-50	%12 PMMA + %50 CA	16	3.0	1.82
PMMA/CA-100	%12 PMMA + %100 CA	16	3.0	2.18

2.1. Characterization of Nanofibers

The morphology of the produced nanofibers was examined using scanning electron microscopy (SEM, Quanta FEG 250) images. Before SEM analysis, the surface of the nanofibers was coated with gold powder to obtain conductive surfaces. The FT-IR spectra of the samples were recorded by scanning the samples prepared by the KBr pellet technique in the mid infrared region of 4000-400 cm^{-1} in the range of 2 cm^{-1} on a Perkin Elmer Spectrum BX device. During the analysis, the number of scans was set to 16 and resolution to 4 cm^{-1}. The latent heat storage and release temperature and enthalpy (energy storage capacity) values of the nanofibers were measured by differential scanning calorimetry (DSC) analysis. The analyses were carried out in a nitrogen (N_2) atmosphere at a heating/cooling rate of 5 °C/d between 0 °C and +80 °C using a DSC Perkin Elmer Fronter DSC device. According to the results of DSC analysis, the encapsulation rate and encapsulation efficiency values of the nanofibers produced were calculated using Equation 1 and Equation 2, respectively.

Encapsulation rate (%)=$\frac{\Delta Hm-nanofibers}{\Delta Hm-PCM} x\ 100$ (Equation 1)

Encapsulation efficiency (%) = $\frac{\Delta Hm-nanofiber+\Delta Hc-nanofiber}{\Delta Hm-PCM+\Delta Hc-PCM}\ x\ 100$ (Equation 2)

In the equations

ΔHm- Nanofiber : Melting enthalpy value of nanofibers (j/g),
ΔHm- PCM : Melting enthalpy of CA fatty acid (j/g),
ΔHc- Nanofiber : Solidification enthalpy value of nanofibers (j/g),
ΔHc- PCM : Solidification enthalpy of CA fatty acid (j/g),

TGA (Thermal gravimetric analysis) was performed to determine the thermal stability of nanofibers. The analyses were carried out using a Perkin Elmer TGA7 device at a heating rate of 10 °C/d in an argon gas atmosphere in the temperature range of 25-500 °C.

To determine the leakage of PCM from the nanofibers, the nanofiber surfaces were placed on an absorbent surface and placed in an oven at 60 °C for half an hour. The leaching of the capric acid contained in the nanofibers was investigated by visually examining whether the nanofibers wet the absorbent surface.

3. RESULTS

3.1. SEM analysis

According to the SEM images (3000 X and 1000X) given in Figure 2.a., it is seen that PMMA nanofibers with uniform morphology and homogeneous diameter distribution were obtained from PMMA solution at 12% concentration. When SEM images of nanofibers produced by adding different amounts of CA to the PMMA polymer solution are examined, bead formation is remarkable (Figure 2.b-2.c). In particular, it is noteworthy that as the amount of capric acid added to the polymer solution increases (50% and above), fiber spinning becomes more difficult, fiber morphology deteriorates and dripping PCM structures are present (Figure 2.d-2.e). This is thought to be related to the inhibition of fiber formation due to the increase in the ratio of fatty acid added into the polymer solution to the amount of fiber-forming polymer.

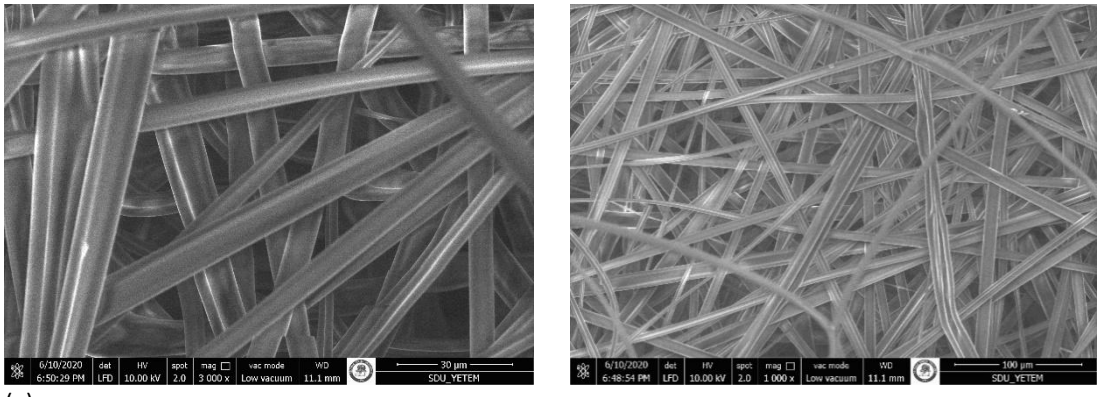

(a)

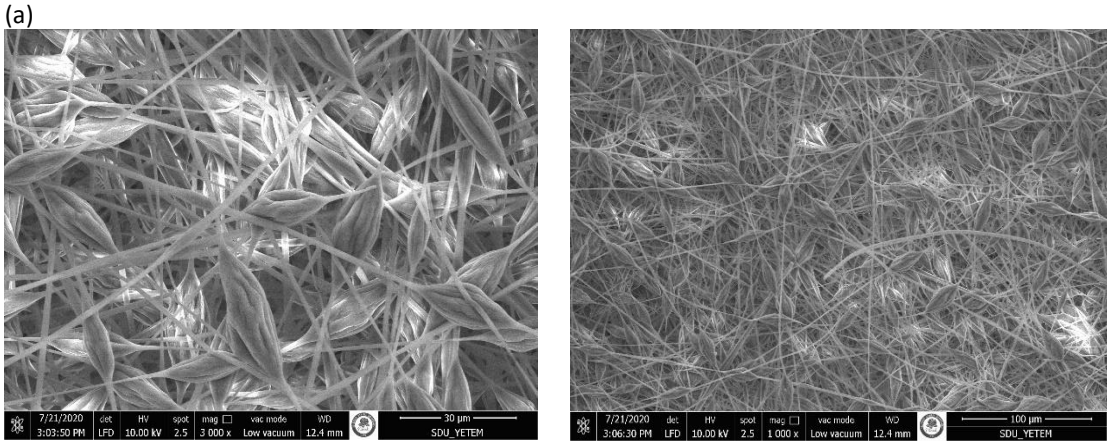

(b)

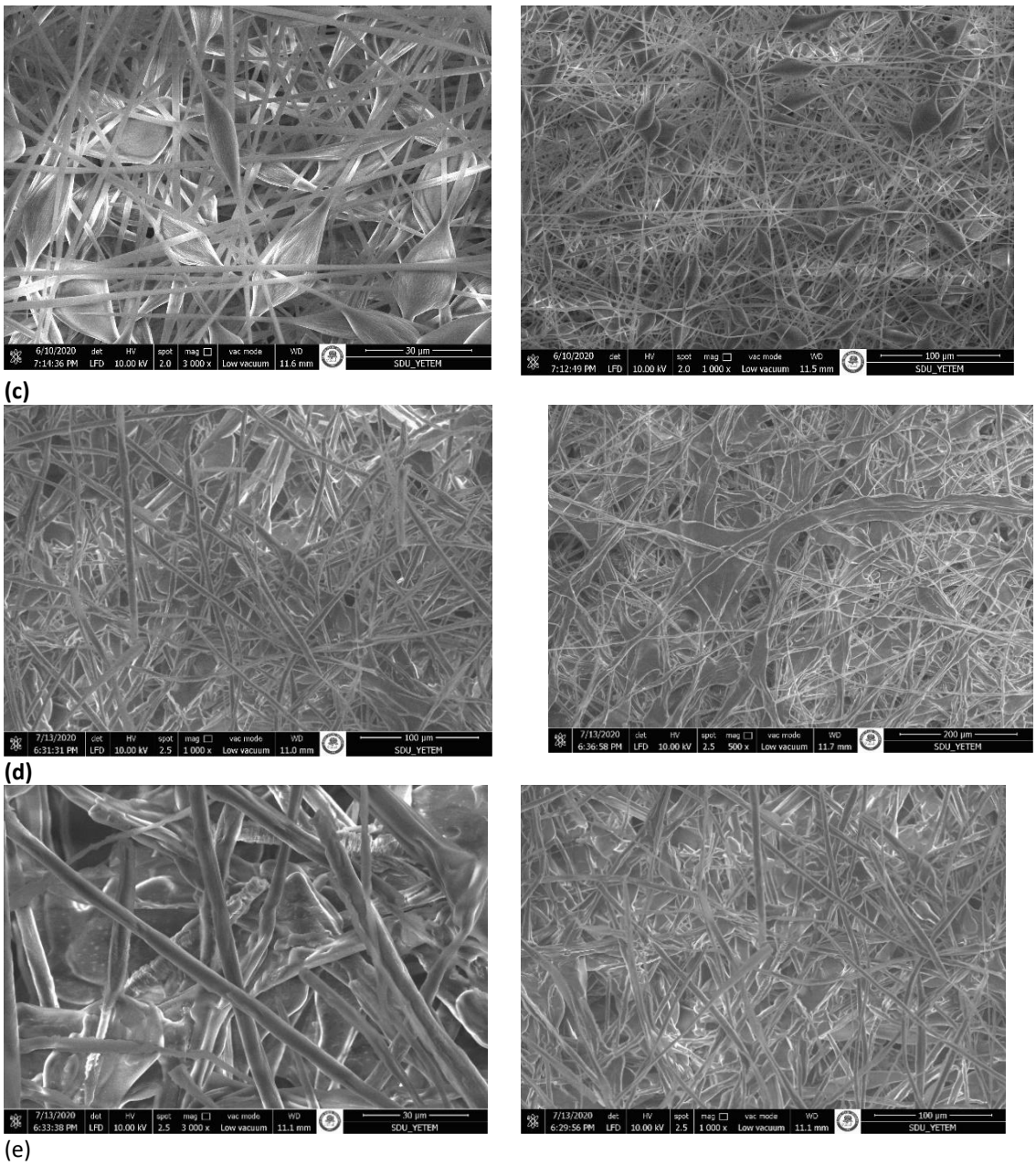

Figure 2. SEM Images of PMMA/CA Nanofibers (a: Pure PMMA Nanofibers; b: PMMA/CA-10 Nanofibers; c: PMMA/CA-30 Nanofibers; d: PMMA/CA-50 Nanofibers e: PMMA/CA-100 Nanofibers)

3.2. FT-IR spectroscopy analysis

In order to prove the presence of fatty acids in the structure of nanofibers obtained from PMMA/CA blend polymer solutions, chemical structure analysis was performed by FT-IR spectroscopy. analysis was performed. Figure 3 shows the FT-IR spectrum of pure PMMA nanofiber. In the FT-IR spectrum of nanofibers produced from pure PMMA polymer, the peaks in the wavelength range 3000-2954 cm^{-1} represent C-H stretching peaks in the CH_3 group. The sharp peak at a wavelength of approximately 1733 cm^{-1} is the stress peak of the carbonyl (C=O) group in the polymer structure. In addition, the peaks at wavelengths 1100-1300 cm^{-1} are the characteristic stress peaks of the C-O-C bond (Hong et al., 2006; Lee and Jan, 1996).

Figure 3 shows the FT-IR spectra of PMMA/CA nanofibres. In the spectrum of PMMA/CA-10 coded nanofibre, it was determined that the stretching peak belonging to the C=O group appeared at a wavelength of 1733 cm^{-1}. On the other hand, as the amount of fatty acid added to the polymer solution increases (PMMA/CA-30, PMMA/CA-50 and PMMA/CA-100), it is seen that the carbonyl peak of PMMA polymer appears around 1702 cm^{-1}-1712 cm^{-1}. This is due to the absorption of the interaction peaks of PMMA polymer by fatty acid peaks due to the presence of high amount of capric acid in the nanofibre structure (Alkan and Sarı, 2008). On the other hand, the reason for the emergence of the C=O group stretching peak at 1733 cm^{-1} in the PMMA/CA-10 coded nanofiber spectrum is the low mass fractions of fatty acids contained in the polymer structure. However, when compared with the spectrum of pure PMMA nanofibers, in addition

to the C-H stretching peaks at 3000 cm^{-1} and 2954 cm^{-1} wavelengths in the spectra of composite nanofibers, new C-H stretching peaks at 2928 cm^{-1} and 2856 cm^{-1} were revealed. These peaks are characteristic of fatty acids and the presence or absence of C-H stretching peaks indicates the presence of fatty acids in the structure.

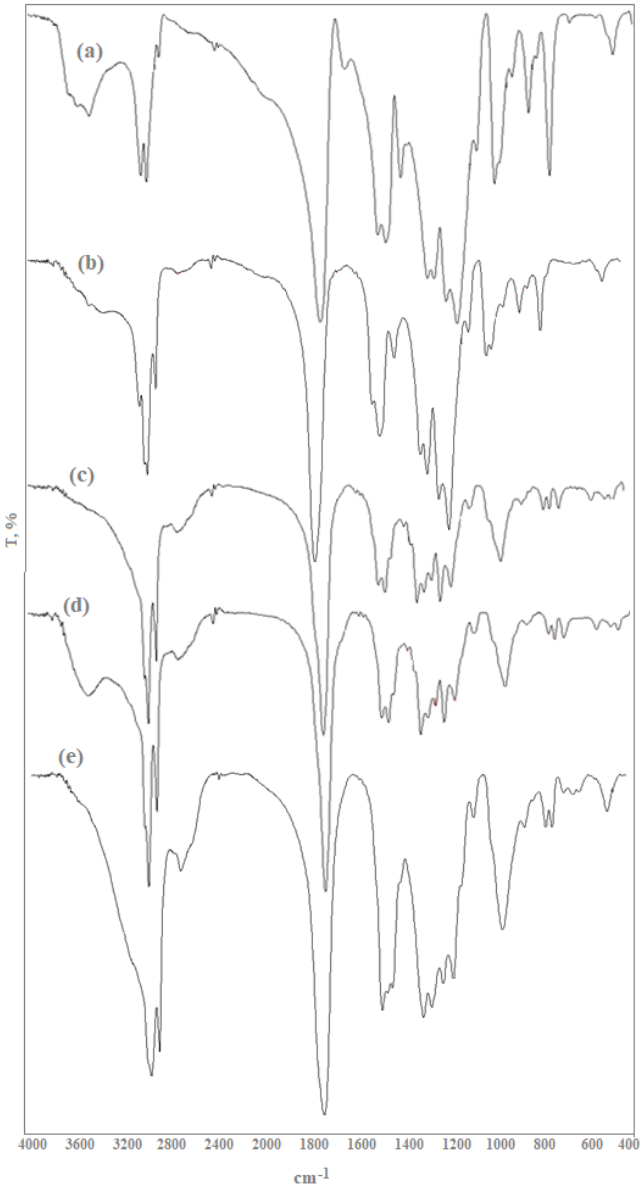

Figure 3. FT-IR spectra of PMMA/CA Nanofibers (a: Pure PMMA Nanofibers; b: PMMA/CA-10 Nanofibers; c: PMMA/CA-30 Nanofibers; d: PMMA/CA-50 Nanofibers e:PMMA/CA-100 Nanofibers)

3.3. DSC analysis

The latent heat energy storage and release capacities and temperatures of PMMA/capric acid nanofibers were determined by DSC analysis. The curves obtained from the DSC analysis are given in Figure 4 and the data obtained from these curves are given in Table 2. According to the results given in the table, PMMA/CA-10 nanofibers produced by adding 10% capric acid to the polymer solution have a heat storage capacity of 29.82 j/g and a heat release capacity of -32.16 j/g, and the heat storage and release temperatures are 29.4 °C and 27.4 °C, respectively. PMMA/CA-30 nanofibers produced by adding 30% capric acid to the polymer solution have a heat storage capacity of 91.11 j/g and a heat dissipation capacity of -93.11 j/g, and the heat storage and dissipation temperatures are 29.5 °C and 27.1 °C, respectively. PMMA/CA-50 nanofibers produced by adding 50% capric acid to the polymer solution have a heat storage capacity of 136.7 j/g and a heat dissipation capacity of -137.2 j/g, and the heat storage and dissipation temperatures are 29.8 °C and 30.3 °C, respectively. PMMA/CA-100 nanofibers produced by adding 100% capric acid into the polymer solution have a heat storage capacity of 150.7 j/g and a heat release capacity of -152.1 j/g, and the heat storage and release temperatures are 30.1 °C and 27.2 °C, respectively. When the measured thermal properties are evaluated, the latent heat storage/release capacity of the nanofibers increases as the amount of capric acid added to the polymer solution increases. In particular, it is thought that PMMA/CA-30 nanofiber structures, which can be produced without drops despite the formation of beads, can be used as thermal energy storage materials with their high latent heat storage capacities. When compared with the

findings of studies on the production of different types of PCM-containing nanofibers, it has been determined that the thermal energy storage capacities of the produced nanofibers are significantly high (McCann et al., 2006; Chen et al., 2013; Wan et al., 2016; Haghighat et al., 2018; Özmen and Alay Aksoy 2020; Kızıldağ, 2021). The encapsulation rate and encapsulation efficiency values of the nanofibers were calculated as 19.11% and 19.99% for PMMA/CA-10 nanofibers, 58.40% and 59.42% for PMMA/CA-30 nanofibers, 87.62% and 88.35% for PMMA/CA-50 nanofibers and 96.15% and 97.51% for PMMA/CA-100 nanofibers, respectively. Considering the encapsulation ratio and encapsulation efficiency values, it was concluded that the produced nanofibers have high thermal energy storage capacities.

Table 2. DSC analysis results of PMMA/capric acid composite nanofibers.

Nanolif	Melting temperature (°C)	Melting Enthalpy (j/g)	Solidification temperature (°C)	Solidification Enthalpy (j/g)	Encapsulation rate (%)	Encapsulation efficiency (%)
Pure PMMA	-	-	-	-	-	-
PMMA/CA-10	29.4	29.82	27.4	-32.16	19.11	19.99
PMMA/CA-30	29.5	91.11	27.1	-93.11	58.40	59.42
PMMA/CA-50	29.8	136.7	30.3	-137.2	87.62	88.35
PMMA/CA-100	30.1	150.7	27.2	-152.1	96.15	97.51

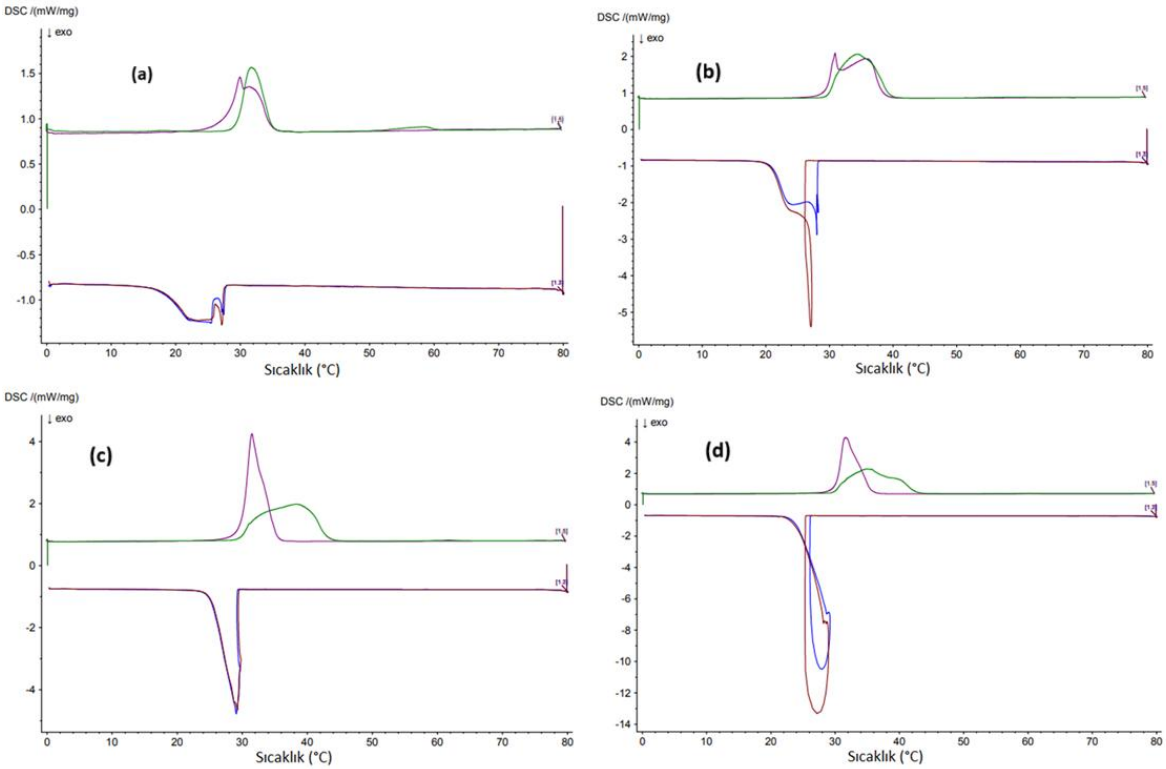

Figure 4. DSC curves of the nanofibers (a: PMMA/CA-10 Nanofibers; b: PMMA/CA-30 Nanofibers; c: PMMA/CA-50 Nanofibers d:PMMA/CA-100 Nanofibers)

3.4. TGA analysis

TG analysis was applied to determine the thermal stability properties of the produced nanofibers. The findings obtained from the TG analysis are given in Table 3. The TGA curves of the nanofibers are given in Figure 5. According to the available research in the literature, nanofibers produced from PMMA polymer exhibit single-stage thermal degradation occurring around 300 °C (Macossay et al., 2007; Carrizales et al., 2008; Pelfrey et al., 2010). The thermal degradation of pure capric acid occurs as a single-stage in the range of 110-240 °C. According to the TGA curves, all produced fibers exhibited two-stage thermal degradation behavior. According to the Table 3 and TGA curves, the nanofiber produced by

adding 10 g of CA coded PMMA/CA-10 started to degrade at 206.8 °C and lost 35.8% mass in the first degradation step. The second degradation for the nanofiber started at 355 °C and the total mass loss in this step was determined as 58.2%. The nanofiber produced by adding 30 g of CA coded PMMA/CA-30 started to degrade at 220.8 °C and lost 51.9% mass in the first degradation step. The second degradation for the nanofiber started at 361.2 °C and the total mass loss in this step was determined as 43.2%. The nanofiber produced by adding 50 g of CA coded PMMA/CA-50 started to degrade at 222.7 °C and lost 88.3% mass in the first degradation step. The second degradation for the nanofiber started at 363 °C and the total mass loss in this step was determined as 7.1%. The nanofiber produced by adding 100 g of CA coded PMMA/CA-100 started to degrade at 208.2 °C and lost 76.4% mass in the first degradation step. The second degradation for the nanofiber started at 363.6 °C and the total mass loss in this step was measured as 8.8%.

The first degradation step of PMMA/CA composite nanofibers belongs to the CA fatty acid component in the nanofiber structure. As the amount of capric acid added to the polymer solution used in nanofiber production increased, the first-stage degradation mass loss values of the fibers increased. The encapsulation of capric acid by the PMMA sheath increased the thermal resistance for all fibers produced. However, the mass loss rates in the first degradation steps of the fibers were generally found to be directly proportional to the amounts of capric acid they contained due to the enthalpy values measured in the DSC analysis. When the TGA curves were examined, it was seen that the first-stage degradation resulted in very high mass loss, especially in the TGA curves of the nanofibers to which capric acid was added as 50 g and 100 g. The second-stage degradation of the nanofibers belongs to the PMMA polymer forming the fiber structure.

Table 3. TG analysis results of PMMA/capric acid composite nanofibers

Nanolifler	1. Stage			2. Stage		
	Onset (°C)	End (°C)	Weight loss %	Onset (°C)	End (°C)	Weight loss %
PMMA/CA-10	206.8	281.2	35.8	355.0	380.3	58.2
PMMA/CA-30	220.8	272.8	51.9	361.2	412.6	43.7
PMMA/CA-50	222.7	255.5	88.3	363.0	414.9	7.1
PMMA/CA-100	208.2	243.2	76.4	363.6	407.9	8,8

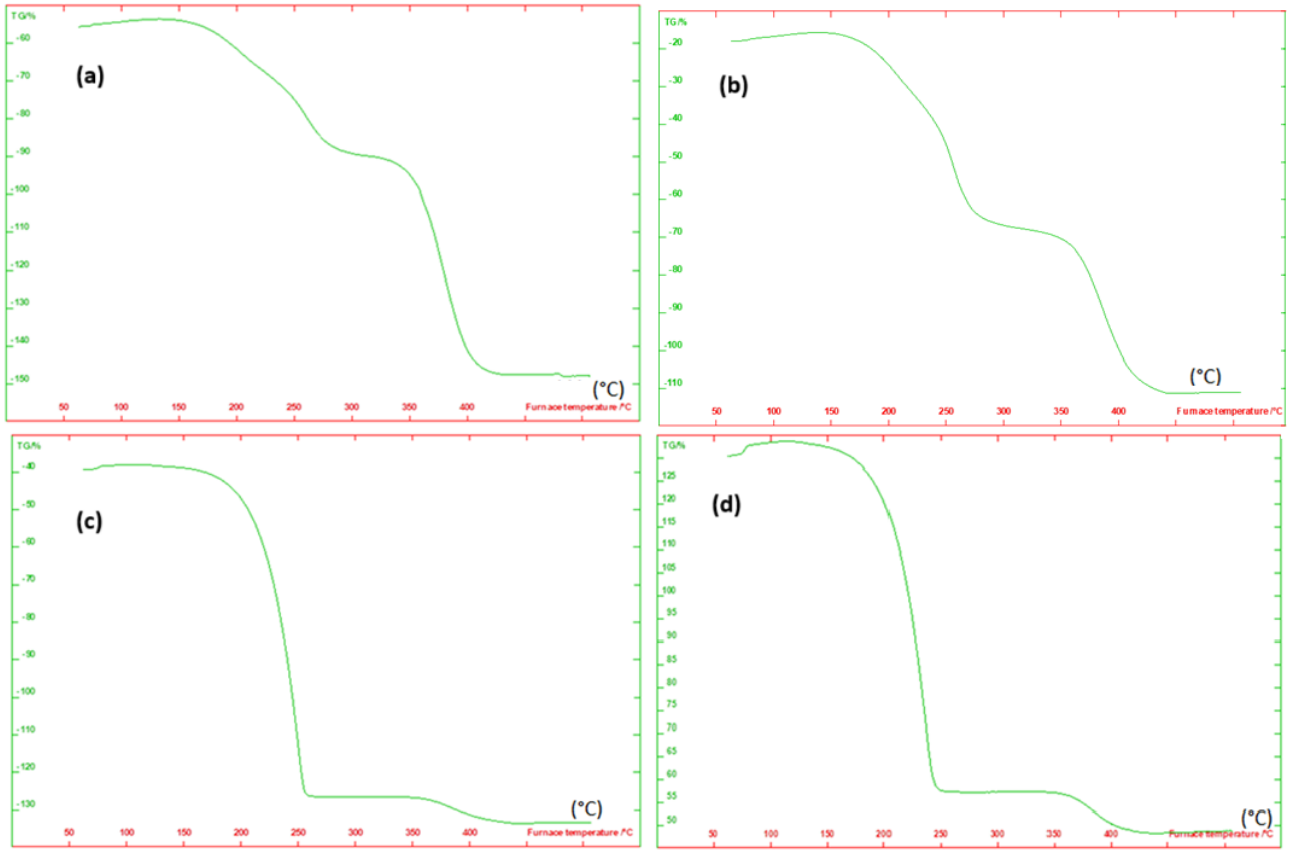

Figure 5. TGA curves of the nanofibers (a: PMMA/CA-10 Nanofibers; b: PMMA/CA-30 Nanofibers; c: PMMA/CA-50 Nanofibers d:PMMA/CA-100 Nanofibers)

3.5. Leakage test

In the study, the capric acid encapsulated in the structure of the produced PMMA/CA nanofibers is a type of PCM that performs latent heat exchange during the solid-liquid phase change process. A leakage test was performed to examine the leakage of the capric acid encapsulated in the nanofiber structure from the nanofiber wall structure when it transitions to the liquid phase. In this test, the nanofiber structures were placed on an absorbent paper and kept in an oven for half an hour at a temperature well above the melting temperature of CA. After the test, it was examined whether the absorbent paper got wet or not. Figure 6 shows images of the nanofibers subjected to testing. Figure 7 shows images of the absorbent papers on which the nanofibers were placed after the leakage test. As seen in the images, the absorbent paper surface on which the nanofibers containing 100% and 50% CA were placed was completely wet. A some wetting was also detected in the sample containing 30% CA. However, no wetting was observed in the sample containing 10% CA. It was determined that this sample did not leak CA.

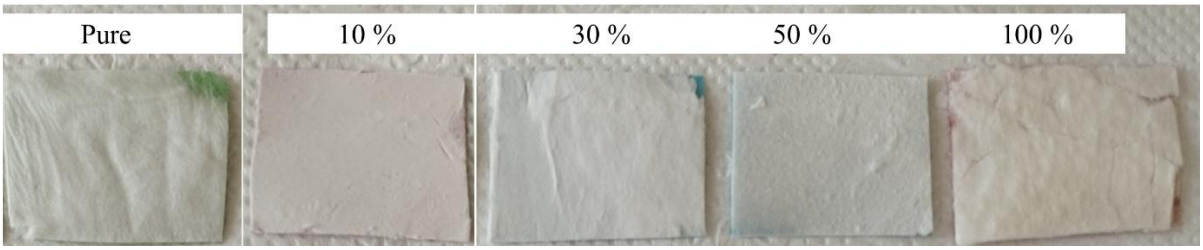

Figure 6. Images of nanofibers subjected to leakage test

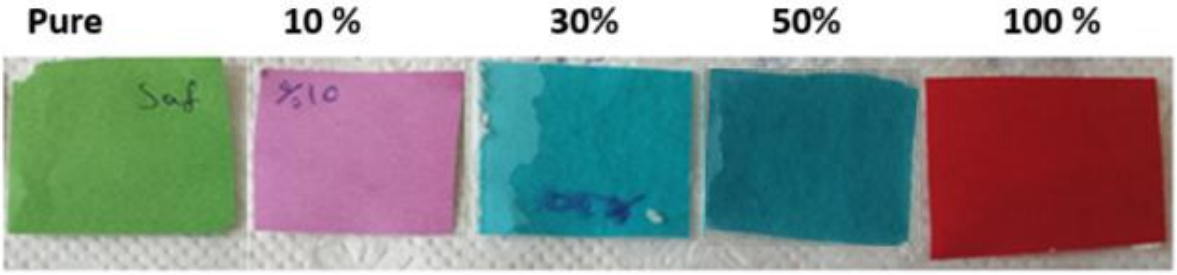

Figure 7. Images of nanofibers subjected to leakage test

4. DISCUSSION AND CONCLUSIONS

In this study, it is aimed to produce thermal energy storage nanofibers containing phase change material. For this purpose, composite nanofiber production was carried out by single needle electrospinning method by adding different amounts of capric acid to PMMA solution. In the study, nanofiber production trials with capric acid content of 10%, 30%, 50% and 100% were carried out. Electrospinning became more difficult as the amount of CA added to the polymer solution increased. Despite the formation of beads from the polymer solution containing 30% CA, nanofiber production can be easily carried out. However, at 50% and above, dripping of polymer liquid and non-spin polymer residues occur and fiber morphology deteriorates. Considering the leakage and thermal gravimetric analysis results as well as fiber morphology, it was evaluated that it was not possible to produce nanofibers suitable for the purpose from polymer solutions containing 50% and more CA. It was determined that nanofibers containing 30% CA exhibited acceptable thermal resistance and leakage properties as well as high thermal energy storage properties and offered suitable morphology. On the other hand, despite the relatively low but acceptable thermal energy storage properties, it was determined that the most suitable nanofibers in terms of both morphology, thermal stability and leakage properties were nanofibers with 10% CA content. As a continuation of this study, it is thought that research can be conducted on the production of nanofibers with CA content below 30% and higher thermal energy storage properties as well as sufficient thermal stability and sealing properties. As another suggestion, it is thought that the leakage and thermal stability properties of the nanofiber structure can be improved by inorganic nanomaterial reinforcement or crosslinking reactions.

Acknowledgements
It should be written as short as possible and expressing the contribution made without giving the number.

Ethics Committee Approval
N/A

Peer-review
Externally peer-reviewed.

Author Contributions
Conceptualization: S.A.A.; Investigation: G.Ö and S.A.A ; Material and Methodology: G.Ö.; Supervision: S.A.A.; Visualization: G.Ö.; Writing-Original Draft: G.Ö.; Writing-review & Editing: G.Ö and S.A.A ; Other: All authors have read and agreed to the published version of manuscript.

Conflict of Interest
The authors have no conflicts of interest to declare.

Funding
The authors declared that this study has received no financial support.

REFERENCES
Alay, S., 2010. Isıl Enerji Depolama Özellikli Mikrokapsüller İçeren Akıllı Tekstil Ürünlerinin Geliştirilmesi, Süleyman Demirel Üniversitesi, Fen Bilimleri Enstitüsü, Doktara Tezi, 202s, Isparta.

Alevay Kılıç G., 2018. Endüstriyel Soğutma Uygulamalarında Ötektik Soğutucuların Etüdü ve Parametrelerinin İncelenmesi. Balıkesir Üniversitesi, Fen Bilimleri Üniversitesi, Doktora Tezi, 111s, Balıkesir.

Alkan, C., Sarı, A., 2008. Fatty acid/poly (Methyl Methacrylate)(PMMA) Blends As Form-Stable Phase Change Materials For Latent Heat Thermal Energy Storage. Solar Energy, 82,2, 118-124.

Cai, Y., Ke, H., Lin, L., Fei, X., Wei, Q., Song, L., Hu, Y., Fong, H., 2012. Preparation, Morphology and Thermal Properties of Electrospun Fatty Acid Eutectics/Polyethylene Terephthalate Form-Stable Phase Change Ultrafine Composite Fibers for Thermal Energy Storage. Energy Conversion and Management, 64, 245-255.

Carrizales, C., Pelfrey, S., Rincon, R., Eubanks, T. M., Kuang, A., McClure, M. J., Bowlin, G. L., Macossay, J. 2008. Thermal and Mechanical Properties of Electrospun PMMA, PVC, Nylon 6, and Nylon 6, 6. Polymers for Advanced Technologies, 19(2), 124-130.

Chalco-Sandoval, W., Fabra, M. J., López-Rubio, A., Lagaron, J. M., 2016. Development of an Encapsulated Phase Change Material via Emulsion and Coaxial Electrospinning. Journal of Applied Polymer Science, 133(36), 1-9.

Chen, C.Z., L.G. Wang, Huang, Y., 2007. Electrospinning of Thermo-Regulating Ultrafine Fibers Based On Polyethylene Glycol/Cellulose Acetate Composite. Polymer, 48, 5202–5207.

Chen, C.Z., L.G.Wang, Huang Y., 2009a. Role of Mn of PEG in The Morphology and Properties of Electrospun PEG/CA Composite Fibers For Thermal Energy Storage. AIChE Journal, 55, 820–827.

Chen, C.Z., L.G. Wang, Huang, Y., 2009b. Crosslinking of the Electrospun Polyethylene Glycol/Cellulose Acetate Composite Fibers as Shape-Stabilized Phase Change Materials. Materials Letters, 63, 569–571.

Chen, C., Zhao, Y., Liu, W., 2013. Electrospun Polyethylene Glycol/Cellulose Acetate Phase Change Fibers with Core–Sheath Structure for Thermal Energy Storage. Renewable Energy, 60, 222-225.

Dang, T. T., Nguyen, T. T. T., Chung, O. H., Park, J. S., 2015. Fabrication of Form-Stable Poly (Ethylene Glycol)-Loaded Poly (Vinylidene Fluoride) Nanofibers via Single and Coaxial Electrospinning. Macromolecular Research, 23(9), 819-829.

Darzi, M. E., Golestaneh, S. I., Kamali, M., Karimi, G., 2019. Thermal and Electrical Performance Analysis of Co-Electrospun-Electrosprayed PCM Nanofiber Composites in The Presence of Graphene and Carbon Fiber Powder. Renewable Energy, 135, 719-728.

Esmaeilzadeh, Z., Rezaei, B., Mousavi Shoushtari, A., Mojtahedi, M. R. M., 2018. Enhancing the Thermal Characteristics of Shape-Stabilized Phase Change Nanocomposite Nanofibers by Incorporation of Multiwalled Carbon Nanotubes within the Nanofibrous Structure. Advances in Polymer Technology, 37(1), 185-193.

Golestaneh, S. I., Karimi, G., Babapoor, A., Torabi, F., 2018. Thermal Performance of Co-Electrospun Fatty Acid Nanofiber Composites in The Presence of Nanoparticles. Applied Energy, 212, 552-564.

Haghighat, F., Ravandi, S. A. H., Esfahany, M. N., & Valipouri, A. 2018. A Comprehensive Study on Optimizing and Thermoregulating Properties of Core–Shell Fibrous Structures Through Coaxial Electrospinning. Journal of materials science, 53(6), 4665-4682.

Hong, R. Y., Qian, J. Z., Cao, J. X., 2006. Synthesis and Characterization of PMMA Grafted ZnO Nanoparticles. Powder Technology, 163(3), 160-168.

Kızıldag, N. (2021). Smart composite nanofiber mats with thermal management functionality. Scientific Reports, 11(1), 4256.

Lee, D. C., Jang, L. W., 1996. Preparation and Characterization of PMMA–Clay Hybrid Composite by Emulsion Polymerization. Journal of Applied Polymer Science, 61(7), 1117-1122.

Li, F., Zhao, Y., Song, Y. 2010. Core-Shell Nanofibers: Nano Channel And Capsule By Coaxial Electrospinning. Nanofibers, 2, 418-438.

Macossay, J., Marruffo, A., Rincon, R., Eubanks, T., & Kuang, A. 2007. Effect of Needle Diameter on Nanofiber Diameter and Thermal Properties of Electrospun Poly (Methyl Methacrylate). Polymers for Advanced Technologies, 18(3), 180-183.

McCann, J.T., Marquez, M., Xia, Y.N., 2006. Melt Coaxial Electrospinning: A Versatile Method for The Encapsulation of Solid Materials and Fabrication of Phase Change Nanofibers. Nano Letters, 6, 2868–2872.

Mondal, S., 2008. Phase Change Materials for Smart Textiles-an Overview. Applied Thermal Engineering, 28, 1536-50.

Noyan, E. C., Onder, E., Sarier, N., Arat, R., 2018. Development of Heat Storing Poly(Acrylonitrile) Nanofibers by Coaxial Electrospinning. Thermochimica Acta, 662, 135-148

Özmen, G., Alay Aksoy, S., 2020, Eş Eksenli Elektro Lif Çekim Yöntemi Ile Termal Enerji Depolama Özellikli Kompozit Nanolif Üretimi Üzerine Bir Araştirma. Mühendislik Bilimleri ve Tasarım Dergisi, 8(4), 1248 – 1259.

Pelfrey, S., Cantu, T., Papantonakis, M. R., Simonson, D. L., McGill, R. A., & Macossay, J. 2010. Microscopic and Spectroscopic Studies of Thermally Enhanced Electrospun PMMA Micro-and Nanofibers. Polymer chemistry, 1(6), 866-869.

Sun, S-X., Xie, R., Wang, X-X., Wen, G-Q., Liu, Z., Wang, W., Ju, X-J., Chu, L-Y. 2015. Fabrication of Nanofibers with Phase-Change Core and Hydrophobic Shell, via Coaxial Electrospinning Using Nontoxic Solvent. Journal of materials science, 50(17), 5729-5738.

Tözüm, M.S,, 2013. Isı Depolama Özellikli Mikrokapsül Uygulanmış Kumaşların Isı Düzenleme ve Konfor Özelliklerinin Belirlenmesi. Süleyman Demirel Üniversitesi, Fen Bilimleri Enstitüsü, Yüksek Lisans Tezi, 124s, Isparta.

Wan, Y., Zhou, P., Liu, Y., & Chen, H., 2016. Novel Wearable Polyacrylonitrile/Phase-Change Material Sheath/Core Nano-Fibers Fabricated By Coaxial Electro-Spinning. RSC advances, 6(25), 21204-21209.

Zdraveva, E., Fang, J., Mijovic, B., Lin, T., 2015. Electrospun Poly(Vinyl Alcohol)/Phase Change Material Fibers: Morphology, Heat Properties, And Stability. Industrial & Engineering Chemistry Research, 54(35), 8706-8712.

Micro- and Nanostructured Composite Films for Passive Radiative Cooling in Indoor Environments

NAZIFE KORKMAZ MEMİŞ*[1], SIBEL KAPLAN[2]

Abstract: Global warming and energy crises have intensified attention in passive cooling technology materials having self-cooling effect with zero energy consumption and low carbon emission as a sustainable solution in recent years. In indoor environment scenarios without sun, developing spectrally selective material with tunable mid-infrared emissivity within atmospheric windows is crucial for passive radiative cooling performance. Hierarchical porous polymer films prepared by phase separation having pores with several micrometers size exhibit strong mid-infrared scattering hence emissivity. Porous structure, pore size, and also mid-infrared emissivity hence cooling performance of the polymer films could regulate by selecting suitable polymer type, adding micro/nanoparticles, adjusting the ratio of polymer/particles, and controlling phase separation method parameters. Here, micro-nano porous nanocomposite films with randomly distributed nanoparticles are fabricated through non-solvent induced phase separation method, employing polyvinylidene fluoride (PVDF) and zinc oxide (ZnO) nanoparticles (30 nm) at varying content (5-20% compared to polymer content). Porous structure and cooling performance of the nanocomposite films were evaluated by SEM and self-made hotplate system, respectively. To understand the role of material and nanoparticle content on infrared radiation emission and reflection, spectral reflectance and transmittance of the films in the atmospheric window wavelength ranges were characterized using an FT-IR spectrometer interfaced with integrating spheres in the diffuse reflectance mode. Nanoparticles embedded in the polymer matrix especially at higher content led to macro and nano-micro heterogeneous porous structure. The nanocomposite films having 20% nanoparticle content selectively average atmospheric window emissivity of 86%, enabling an average temperature drop of 1.97°C and 1.65°C hence passive cooling performance in indoor environment scenario respectively, compared with nonporous and porous PVDF film without ZnO particle. This cooling performance could result in cooling-energy-consumption savings about approximately 20% in indoor conditions, indicating high potential as a sustainable material in a wide range of fields, from personal thermal management textiles to energy-saving elements in a simple, cost-effective, and scalable manner.

Keywords: Passive radiative cooling, indoor cooling, nonsolvent-induced phase separation, ZnO, PVDF, composite film

[1]**Address:** Süleyman Demirel University, Faculty of Engineering and Natural Sciences, Textile Engineering Department, Isparta, Türkiye
[2]**Address:** Süleyman Demirel University, Faculty of Engineering and Natural Sciences, Textile Engineering Department, Isparta, Türkiye

***Corresponding author**: nazifekorkmaz@sdu.edu.tr

1. INTRODUCTION

Nowadays, with the continuously increasing awareness of energy conservation and the intensifying impacts of global warming, and population growth, development of energy-efficient and sustainable thermal management materials/technologies especially cooling ones is critical in the context of reduce energy costs, greenhouse gas emissions, and associated thermal issues (Chen et al., 2022; Aili et al., 2024; Guo et al., 2024). From cooling aspect, passive radiative cooling technology is the most promising strategy which facilitates heat dissipation from surfaces into the cold outer space through thermal radiation, requiring no external energy input without any greenhouse gas release (Liu et al., 2022). For indoor environment scenario without sun contrast to daytime ones, high mid-infrared emittance which radiates the heat to surrounding space, lead to energy-free cooling performance. Spectral selective emittance within atmospheric windows hence cooling performance of the materials for indoor environment scenario, can be regulate by intrinsic material properties and structural formations (Liu et al., 2025). Recently, many researchers have realized passive radiative cooling materials for indoor environment by selecting polymers such as PVDF (Song et al., 2020a,b), polyvinylidene fluoride-co-hexafluoropropylene (Mandal et al., 2018), polyethylene oxide (Li et al., 2021), etc. These polymers have many functional groups/bonds, such as C-F and C-O, overlap with the atmospheric longwave infrared radiation transmittance window, hence resulted high thermal mid-infrared emittance thereby passive cooling performance. Also, the thermal mid-infrared emittance in the atmospheric longwave infrared radiation transmittance window can be enhanced by inorganic particles such as zinc oxide, titanium dioxide, silicon dioxide etc., and porous structure in the material. In this manner, designing a composite/nanocomposite material by selecting suitable polymer and particles in the porous film structure may be an alternative for developing cooling material in indoor environment. These porous composite/nanocomposite materials especially in the film form could be produced by phase separation method especially

non-solvent induced phase separation (NIPS)by regulating porous structure, pore size, pore number through selecting polymer matrix, particle type and diameter, polymer content, non-solvent: solvent content with low-cost and large production scale (Korkmaz Memiş and Kaplan, 2024a, b). Although, until now many studies using PVDF polymer (Zhong et al., 2021; Shi et al., 2023; Huang et al., 2024; Yang et al., 2024a) were realized on porous materials having cooling performance, these studies have focused on the passive daytime cooling performance depend on solar reflection and emissivity for outdoor environments rather than indoor environment without sun effect. Also, the effect of adding inorganic particle in the manner of particle type, particle diameter and also content on the porous structure and thermal mid-infrared emittance hence cooling performance especially for indoor environment, has not been examined in detail. Therefore, the strategy determining the relationship between cooling performance and parameters such as porosity, particle amount, polymer type, is still need to develop energy-free cooling materials for indoor environment.

Herein, hierarchical micro-nano porous nanocomposite films were utilized by using PVDF polymer and ZnO nanoparticles at varying content through NIPS method. By combining molecular level design and controllable porous structure by NIPS method and varying nanoparticle content, PVDF-ZnO nanocomposite films have development potential for passive radiative cooling in indoor environment as a thermal management, building materials, and versatile.

2. MATERIAL AND METHOD

2.1. Materials

Polyvinylidene fluoride (PVDF, Kynar® 721, melting temperature: 168°C, glass transition temperature: -40°C) as matrix material, was kindly purchased from Arkema, France. ZnO nanoparticles having 30 nm diameter and sunlight reflectivity (Zhu and Feng, 2021), was provided by Nanografi, Türkiye. N, N dimethyl acetamide (Sigma Aldrich, DMAc), acetone (Acros Organics, ACE), and deionized water, were employed as binary solvent system (solvent, co-solvent) (DMAc, ACE) and non-solvent, respectively to produce nanocomposite films through NIPS method. Dispersion of ZnO nanoparticles in the polymer matrix was obtained with using non-ionic surfactant (sorbitan monostearate, Span60, Sigma Aldrich) in ultrasonic treatment.

2.2. Methods

Nanocomposite film production

Nanocomposite films having heterogeneous porous structure with randomly distributed ZnO particles were prepared by NIPS method using solvent, co-solvent and, non-solvent system. PVDF solutions were prepared by dissolving polymer chips at content of 10 wt. % in the binary solvent system consisting of DMAc and ACE (with a volume ratio of 1:1) at 50°C for 6 h using mechanical stirrer. Dispersions of ZnO nanoparticles in the PVDF solution were obtained by adding non-ionic surfactant (Span60, with a ZnO/Span60 weight ratio of 1:2) and mechanical stirring for another 1 h followed ultrasonic mixing for 2 h. The mass ratios of PVDF to ZnO nanoparticles were set at 5, 10, and 20%. To create more heterogeneous porous structure, water as non-solvent was added dropwise into the PVDF-ZnO dispersion by a syringe pump at a 0.2 mL/min feeding rate, with mass ratio of binary solvent system to water set to 13:1 (Korkmaz Memiş and Kaplan, 2024a;b). These mixtures were stirred mechanically for 3 h to form the casting solution. The prepared nanocomposite solutions were drop-cast to the petri-dishes at 400 μm thickness and dried at 20°C for 24 h. For comparison, porous and non-porous PVDF films were prepared without ZnO particles. The films produced are abbreviated as PVDF_nonporous which without water, PVDF_porous with water, PVDF-30ZnO5, PVDF-30ZnO10, PVDF-30ZnO20 which nanocomposite ones with varying ZnO nanoparticle.

Characterizations

A Fei Quanta FEG 250 scanning electron microscope (SEM) was used to investigate the surface morphology of the films. To determine chemical composition of the films, Fourier Transform Infrared (FT-IR) spectrum were acquired using an FT-IR spectrometer (JASCO FT/IR 4700) equipped with a diamond ATR (Attenuated total reflectance) in the 400-4000 cm^{-1} range, 2 cm^{-1} resolution, and 16 scan at room temperature.

For determining infrared radiation emission and reflection properties, the spectral reflectance ($\rho(\lambda)$) and transmittance ($\tau(\lambda)$) of the samples in the atmospheric window wavelength ranges (8-14 μm) were obtained using an FT-IR spectrometer (VERTEX 70v, Bruker) coupled with an MIR integrating sphere in the diffuse reflectance mode. According to Kirchhoff's Law, the spectral absorptivity ($\alpha(\lambda)$) = emissivity ($\varepsilon(\lambda)$) when an object in thermodynamic equilibrium; thus, $\alpha(\lambda)$ or $\varepsilon(\lambda)$ can be calculated as $\varepsilon(\lambda) = 1 - \rho(\lambda) - \tau(\lambda)$.

Radiative cooling performance measurement

Indoor cooling performance of the films based on IR reflection and emission without any solar heating/cooling effect, was tested using a self-made hotplate system simulating skin. This self-made system consists of heating sheet, 8 K-type sensors and a data acquisition system. The heating sheet was employed to simulate the metabolic heat generation (104 W/m^2) and acted as the human skin. The actual temperature of the films was measured at every 5 s for 1 min while

stabilizing and 10 min with environment temperature at 21-24°C and relative humidity at 56-59%. The maximum temperatures of the samples were recorded by at least three replications.

3. RESULTS

Passive radiative cooling performance of the materials can be tunable by selection polymer type having high mid-infrared emissivity based on molecular bonds vibrating, porous structure, and also incorporation of micro-nanoparticles. In the typical indoor scenarios without sun energy, the emissive materials ensure effective dissipation of the heat generated by the human body's normal metabolism into the surrounding environment via the atmospheric window (8-13 μm). Therefore, to design a radiative cooling material, it is crucial to precisely tune the optical properties especially emissivity of the material in the atmospheric window and pore size for Rayleigh scattering. Herein, hierarchical micro-nano porous nanocomposite films were developed by selecting suitable polymer, nanoparticle, and NIPS production method, enabling human body cooling in the indoor environment.

Porous structure of the produced films was determined by examining the SEM images of the surfaces, given in Figure 1. As seen in Figure 1, adding water as non-solvent into the binary solvent system resulted in porous structure by rapid evaporation of ACE enabling phase separation, slow exchanging of DMAc, and water evaporation (Korkmaz Memiş and Kaplan, 2024a, b). Also, macro and nano-micro heterogeneous pores were enriched (Ma et al., 2024) by adding ZnO particles into the PVDF matrix due to changing of continuity of the polymer-rich phase with penetration of nanoparticles into the polymer clusters. As amount of ZnO particles increases the number and distribution of macro and nano-micro heterogeneous pores formed on the film surface. ZnO particles at higher concentrations inevitably led to the formation of numerous uneven surfaces and more nano-sized pores. This resulted in a hierarchically porous structure through the slowing down of solvent evaporation and the delaying of the phase inversion process due to higher viscosity (Qi et al., 2022). In addition to micro-nano pores, macro voids were clearly formed in the nanocomposite films by surface-driven phase separation and crystallization induction (Cardoso et al., 2015). This structure especially having higher ZnO content is conducive to enhancing mid-infrared light absorption by PVDF and ZnO particles resulted in emissivity hence cooling performance.

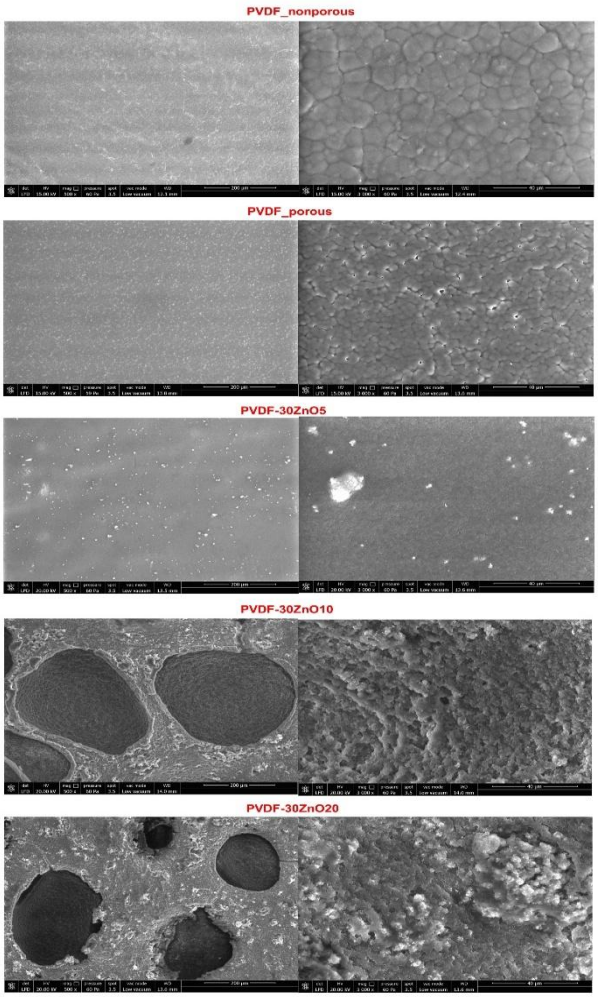

Figure 1. Surface SEM images of non-porous PVDF, porous PVDF, and nanocomposite films with varying ZnO particle content at 500x and 3000x magnification

According to Kirchhoff's Law, the materials with selective mid-infrared wavelength emission inside the atmospheric transparency window (8-13 μm) could enable efficient passive radiative cooling. In order to prove high emissivity of the selected material, absorbance spectrum measured by FT-IR spectrum overlaps the atmospheric transparency window (8-13 μm) corresponded exactly to the absorption at 1250-780 cm^{-1}. As shown in Figure 2, the characteristic peak of PVDF in the FT-IR spectrum of all films are located at 1167, 1074, and 870 cm^{-1}, arising from the stretching vibrations of C-F and C-H bonds. Also, the characteristic peaks at a wavelength of 831 cm^{-1} in all films are the vibrations of -CH_2- bonds and the deforming vibrations of -CF_2- bonds. These peaks in the PVDF molecule imply that PVDF has selective emissivity in the atmospheric window. In addition to the mentioned bonds, -OH and C-H tension vibrations of the water molecule were detected at wavelengths of 3508, 1634, and 2359 cm^{-1}, respectively in the porous PVDF films produced by adding water to the binary solvent system. The IIR spectrum of the nanocomposite films with varying ZnO particle content, exhibits the stretching vibration peaks of Zn-O at 400 and 667 cm^{-1}, becoming more evident with higher particle content. All films especially nanocomposite ones with higher nanoparticle content exhibit strong infrared absorption due to the mentioned molecular vibration peaks which significantly overlap the atmospheric transparency window and also triple phonon polariton resonance with ZnO, providing superior radiative cooling.

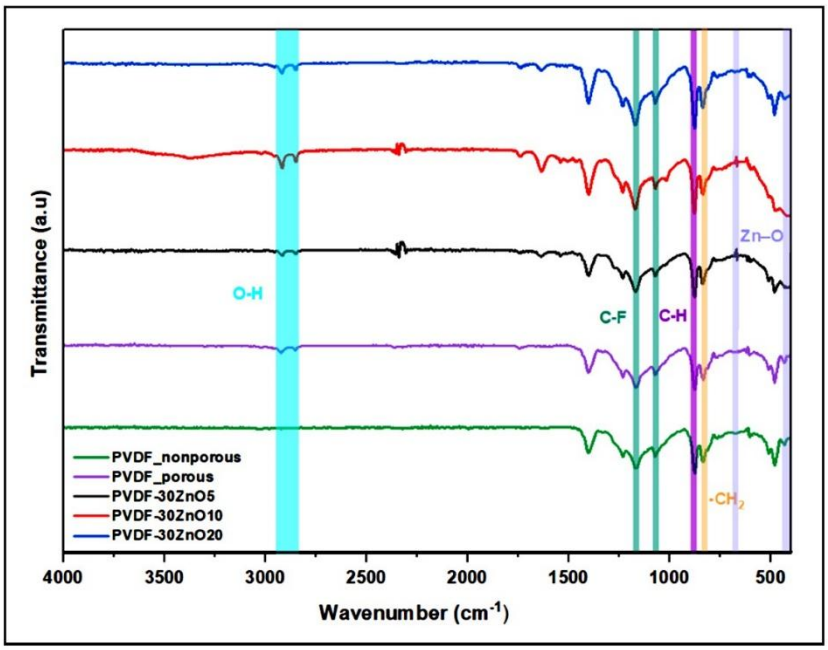

Figure 2. FT-IR spectra of non-porous PVDF, porous PVDF, and nanocomposite films with varying ZnO particle content

The corresponding spectral emissivity of the films in the atmospheric window is shown in Figure 3. Films prepared with addition of water as non-solvent (PVDF_porous) exhibit extremely low average atmospheric window emissivity, (around 10%) contrary to expectations. The mentioned lower emissivity values may be a result of pore volume increase and the polymer content decrease (Huang et al., 2024). Meanwhile, ZnO particle addition leads to significant increase in infrared emissivity, reaching a maximum value of 86% at a particle amount of 20%. Although ZnO particles provide a high increase in emissivity values, the average atmospheric window emissivity of radiative cooling films with 10% and 20% nanoparticles is the same (86%). Considering the effect of the ZnO particles on the average atmospheric window emissivity, it was determined that the emissivity values did not change significantly with ZnO concentration. As compared to nonporous and porous PVDF film, the macro and nano-micro heterogeneous pores and ZnO particles in the nanocomposite films (seen in SEM images) lead to a decrease in the refractive index, thereby a more gradual refractive index transition across the polymer-air interface, thus increasing the impedance compatibility between the film and air and thermal dissipation (emission) (Huang et al., 2024). Also, strong molecular vibration peaks overlapping the atmospheric transparency window (Figure 2) and triple phonon polariton resonance with ZnO particles (Huang et al., 2024) in the nanocomposite film structure enhanced the emissivity, thereby improving the radiative cooling performance.

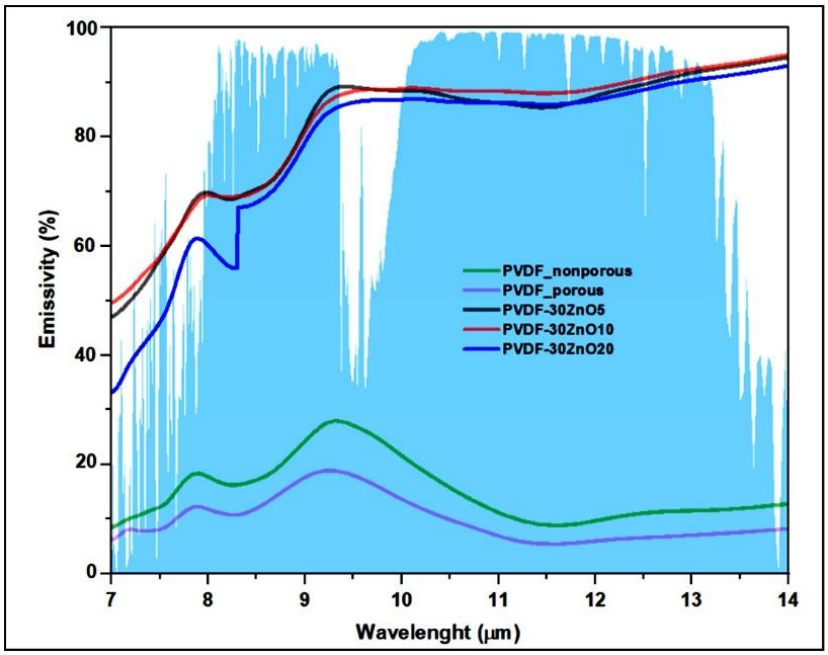

Figure 3. Spectral emissivity in the atmospheric window of non-porous PVDF, porous PVDF, and nanocomposite films with varying ZnO particle content

The corresponding spectral reflectivity of the films in the atmospheric window is shown in Figure 4. As expected, all films showed opposite trend to their emittance performance. As seen in Figure 4, the highest reflectance performance in the atmospheric window was detected in porous PVDF film while the reflectance performance of the nanocomposite films is lower than nonporous PVDF films without ZnO particles. However, no clear trend was detected regarding the ZnO concentration.

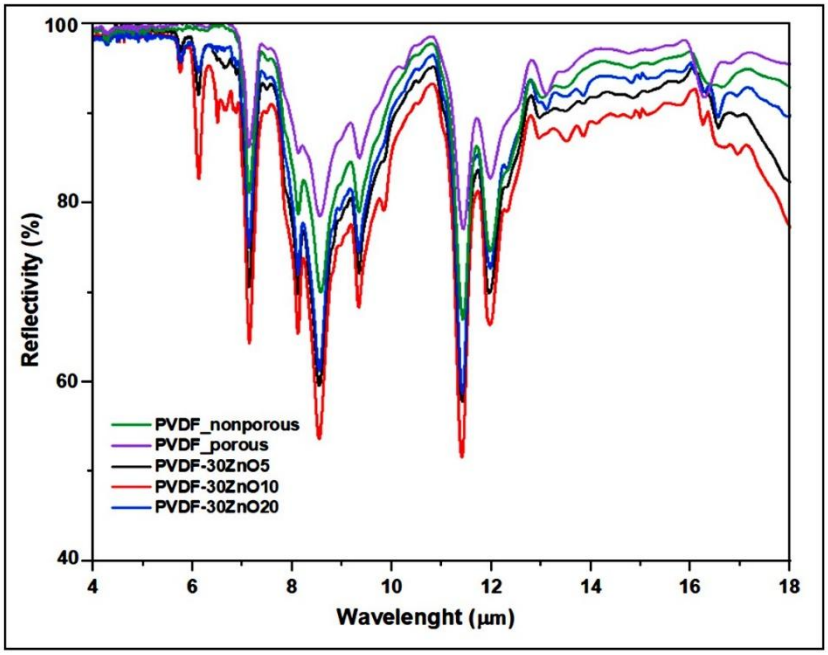

Figure 4. Spectral reflectivity in the atmospheric window of non-porous PVDF, porous PVDF, and nanocomposite films with varying ZnO particle content

Cooling performance of the films were measured by designed hotplate system for a period of 10 minutes under indoor condition. The real-time temperature curves and temperature differences relative to each other and the bare hotplate are given in Figure 5 and Table 1, respectively. The average temperature of the PVDF-30ZnO20 nanocomposite films including ZnO particles at 20% concentration was lower than non-porous and porous PVDF films. The cooling effects of both heterogeneous pore structure and ZnO nanoparticles were recorded that while a temperature drop of 0.37°C was detected as a result of pores, the temperature drop, hence the cooling effect increased to 1.65°C with ZnO nanoparticles

(Table 1). The mentioned cooling performance is consistent with the temperature difference of 1.97°C between non-porous film and PVDF30-ZnO20. Moreover, PVDF-30ZnO20 samples exhibited 0.32°C lower temperature as compared to the blank hotplate surface simulating the body without clothing. Under indoor conditions without sun light, hierarchically porous films especially nanocomposite ones allowed for mid-infrared radiation emission from human body as a result of higher mid-infrared emissivity (Qi et al., 2022), resulted in passive cooling performance (Yang et al., 2024b). According to literature (Hoyt et al., 2005) a 1-4°C of cooling performance can provide up to an energy savings of 7-45% in indoor conditions, which may be valid for clothing applications of the nanocomposite films produced in this study.

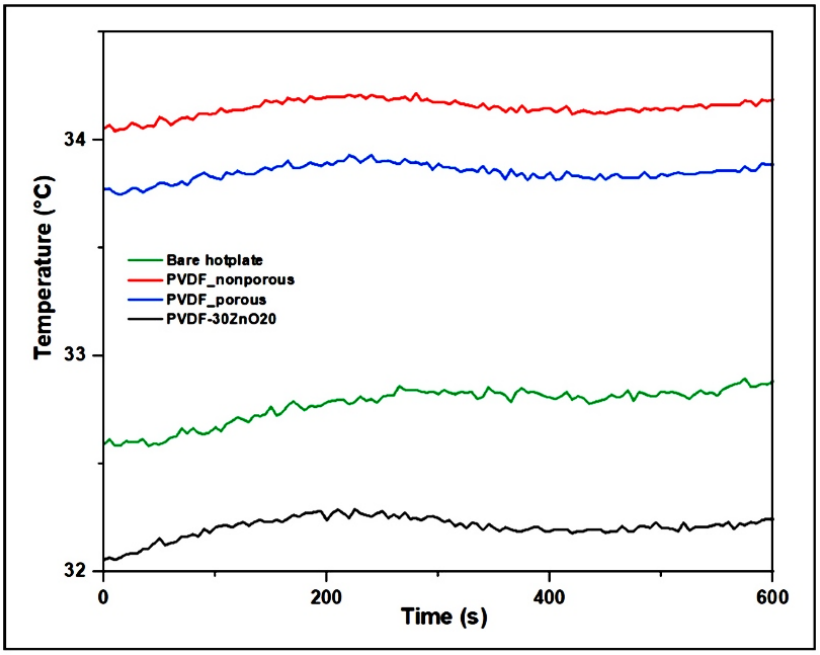

Figure 5. Real-time temperature curves of the films and bare hotplate

Table 1. Real-time temperature difference of the films

Sample	ΔT (°C)
PVDF_non-porous-PVDF porous	0.37
PVDF_porous-PVDF_30ZnO20	1.65
PVDF_nonporous-PVDF_30ZnO20	1.97
Bare hotplate-PVDF_nonporous	-1.18
Bare hotplate-PVDF_porous	-0.65
Bare hotplate-PVDF-30ZnO20	0.32

4. DISCUSSION AND CONCLUSIONS

In this study, hierarchical micro-nano porous PVDF nanocomposite films with ZnO nanoparticles at different concentrations were prepared using a simple non-solvent induced phase separation method for effective radiative cooling performance. The resulting nanocomposite films had macro and nano-micro heterogeneous pores and pores were enhanced by increasing ZnO concentration. The nanocomposite film including 20% ZnO nanoparticle exhibited average atmospheric window emissivity of 86% while demonstrating indoor cooling performance of around 2°C when compared to the nonporous film without ZnO. The mentioned cooling performance conducted with the enhanced emissivity of the nanocomposite structure without the sun light effect, is thought to be promising for further clothing applications of the developed nanocomposite solution.

Acknowledgements
This work was financially supported by the Scientific and Technological Research Council of Türkiye (TUBITAK) (grant agreement no: 123M553). Polymer supply from Arkema, France is gratefully acknowledged.

Ethics Committee Approval
N/A
Peer-review
Externally peer-reviewed.

Author Contributions
Conceptualization: N.K.M., S.K.; Investigation: N.K.M; Material and Methodology: N.K.M., S.K.; Supervision: S.K.; Visualization: N.K.M.; Writing-Original Draft: N.K.M., S.K.; Writing-review & Editing: N.K.M., S.K.; Other: All authors have read and agreed to the published version of manuscript.

Conflict of Interest
The authors have no conflicts of interest to declare.

Funding
This work was financially supported by the Scientific and Technological Research Council of Türkiye (TUBITAK) (grant agreement no: 123M553).

REFERENCES

Aili, A., Jiang, T., Chen, J., Wen, Y., Yang, R., Yin, X., Tan, G. (2024). Passive daytime radiative cooling: Moving beyond materials towards real-world applications. Next Energy, 3, 100121.

Cardoso, V.F., Lopes, A.C., Botelho, G., Lanceros-Mendez, S. (2015). Poly (vinylidene fluoride-trifluoroethylene) porous films: Tailoring microstructure and physical properties by solvent casting strategies, Soft Materials, 13(4), 243-253.

Chen, M., Pang, D., Chen, X., Yan, H., Yang, Y. (2022). Passive daytime radiative cooling: Fundamentals, material designs, and applications. EcoMat, 4(1), e12153.

Guo, H., Ma, B., Yu, J., Wang, X., Si, Y. (2024). Photonic metafabric with biomimetic triangular light track for passive radiative cooling. Advanced Fiber Materials, 1-11.

Hoyt, T., Lee, K.H., Zhang, H., Arens, E., Webster, T. (2005). Energy savings from extended air temperature setpoints and reductions in room air mixing.

Huang, L., Hu, Y., Yao, X., Chesman, A.S., Wang, H., Sagoe-Crentsil, K., Duan, W. (2024). Designing nanoporous polymer films for high-performance passive daytime radiative cooling. ACS Applied Materials & Interfaces, 16(40), 54401-54411.

Korkmaz Memiş, N., Kaplan, S., (2024a). Drying temperature optimization of PVDF-ZnO porous passive radiative cooling films. 14th International Conference Textile Science and Economy - TNP2024, 25th October, 2024, Zrenjanin, Serbia.

Korkmaz Memiş, N., Kaplan, S., (2024b). PVDF films with optimized porous structure using non-solvent induced phase separation for passive radiative cooling. 7th International Scientific Conference Contemporary Trends And Innovations in Textile Industry- CT&ITI 2024, 19-20th September, 2024, Belgrade, Serbia.

Li, D., Liu, X., Li, W., Lin, Z., Zhu, B., Li, Z., Li, B., Fan, S., Xie, J., Zhu, J. (2021). Scalable and hierarchically designed polymer film as a selective thermal emitter for high-performance all-day radiative cooling. Nature Nanotechnology, 16(2), 153-158.

Liu, J., Tang, H., Jiang, C., Wu, S., Ye, L., Zhao, D., Zhou, Z. (2022). Micro-nano porous structure for efficient daytime radiative sky cooling. Advanced Functional Materials, 32(44), 2206962.

Liu, R., Wang, S., Zhou, Z., Zhang, K., Wang, G., Chen, C., Long, Y. (2025). Materials in radiative cooling technologies. Advanced Materials, 37(2), 2401577.

Ma, C.Q., Xue, C. H., Guo, X.J., Shi, W., Wang, H.D., Huang, M.C., Cheng, J. (2024). Fabrication of passive cooling fabric as thermal management curtain for building energy-saving. Chemical Engineering Journal, 497, 154431.

Mandal, J., Fu, Y., Overvig, A.C., Jia, M., Sun, K., Shi, N.N., Zhou, N., Xia, X., Yu, N., Yang, Y. (2018). Hierarchically porous polymer coatings for highly efficient passive daytime radiative cooling. Science, 362(6412), 315-319.

Qi, M., Wang, Y., Chang, G., Li, R. (2022). Energy-saving cooling coated fabric with robust solar reflection and water repellent properties. Fibers and Polymers, 23(7), 1881-1887.

Shi, M., Song, Z., Ni, J., Du, X., Cao, Y., Yang, Y., Wang, W., Wang, J. (2023). Dual-mode porous polymeric films with coral-like hierarchical structure for all-day radiative cooling and heating. ACS Nano, 17(3), 2029-2038.
Song, Y. N., Lei, M. Q., Lei, J., Li, Z.M. (2020a). Spectrally selective polyvinylidene fluoride textile for passive human body cooling. Materials Today Energy, 18, 100504.

Song, Y. N., Li, Y., Yan, D. X., Lei, J., Li, Z.M. (2020b). Novel passive cooling composite textile for both outdoor and indoor personal thermal management. Composites Part A: Applied Science and Manufacturing, 130, 105738.

Yang, X., Yang, Y., Chen, L., Zhu, L., Yu, W., Zeng, Z. (2024a). A switchable dual-mode film with designed intercalated and hierarchical structures for highly efficient passive radiation cooling and solar heating. Chemical Engineering Journal, 152920.

Yang, C., Han, R., Guo, X., Zhang, S., Tang, B., Zhang, Y. (2024b). Efficient daytime radiative cooling films originating from controllable multi-scattering effect. Solar Energy Materials and Solar Cells, 272, 112917.

Zhong, H., Li, Y., Zhang, P., Gao, S., Liu, B., Wang, Y., Meng, T., Zhou, Y., Hou, H., Xue, C., Zhao, Y., Wang, Z. (2021). Hierarchically hollow microfibers as a scalable and effective thermal insulating cooler for buildings. ACS Nano, 15(6), 10076-10083.

Web Accessibility: Designin Inclusive And User-Friendly Websites

ELVIS MULAJ[1], FATON KABASHI[2], LAMIR SHKURTI[3], VEHEBI SOFIU[4] SAMI GASHI[5]

Abstract: Website accessibility is a key aspect of designing and developing web pages and applications. The primary goal is to ensure that all users, regardless of their abilities or differences, have an equal and easy experience in navigating and benefiting from online content. This study explores best practices and guidelines for designing and developing websites that are user-friendly for all users, including those with disabilities, the elderly, and those using assistive technologies. In examining this topic, I aim to identify the challenges and opportunities offered by a well-organized website, analyze best practices and existing studies, and provide recommendations for designers and developers to improve accessibility and user experience on the web. Additionally, the use of various technologies such as animations and voice technologies will be reviewed, and how they can be implemented on current websites will be discussed. In conclusion, this abstract provides an overview of the topic and the objectives set out in this thesis. Through the development of this project, the goal is to contribute to the advancement of knowledge and best practices in the field of Front-End development and to offer a high level of professionalism in this domain, ensuring that all users have an enhanced and suitable experience through the aid of advanced technologies.

Keywords: Website accessibility, design, development, Website accessibility, design, development, user friendly websites.

Address: UBT, Higher Education Institution, Kosova

***Corresponding author**: em46354@ubt-uni.net, faton.kabashi@ubt-uni.net, lamir.shkurti@ubt-uni.net, vehebi.sofiu@ubt-uni.net, sami.gashi@ubt-uni.net

INTRODUCTION

1. Literature review

The rapid advancement of technology has not yet allowed for clear studies and analyses on how individuals with disabilities access websites, nor has it provided accurate information on the factors that help or hinder their ability to browse the internet. In the book *Handbook of Communication and Aging Research* (2004) [3], there is a summary of studies conducted over three decades, highlighting the importance of web accessibility and its significant impact on marketing and business in the section *Marketing to Older Adults* [4].

At the 4th International Conference on Web Accessibility and Human-Computer Interaction, held in 2007 [5], more information on web accessibility was presented. Eye-tracking analysis by Thomas Tullis revealed differences between how young and elderly individuals view websites [6]. It was found that older adults take 42% longer to view website content than younger users. However, this analysis was insufficient to fully understand accessibility, as it only included reading and not visual effects like images, audio, and other web features.

Kress and Van Leeuwen, in their book *Reading Images: The Grammar of Visual Design*, discuss how tools are used to analyze images on the web [7]. Meanwhile, Mandeep Singh, in his publication *Standards and Techniques for Developing User-Friendly Websites*, emphasizes that website design always depends on the target audience [8]. He highlights the importance of security in social networks and e-commerce sites, including the placement of components such as the header, main menu, container, footer, and other elements to ensure accessibility for all users.

Shawn Lawton Henry [9], in his publication *Understanding the Impact of Web Accessibility*, explains that web accessibility means providing services to individuals with disabilities so they can understand, navigate, and interact with the web, taking into account limitations in vision, hearing, physical abilities, speech, and more. He also offers several suggestions for website design, including larger navigation options, distinctively colored links, and clear locations.

Another publication by Peter Williams and Christian Henning, titled *Optimizing Website Designs for People with Learning Disabilities*, analyzed the needs and requirements of individuals with disabilities. In this study, they recommend that main pages should have simple content and audio interpretations, as suggested by the W3C (World Wide Web Consortium) convention of 1999. The use of high-resolution images created longer pages, which limited content comprehension because some users did not realize they needed to scroll. Additionally, many participants preferred larger text sizes and styles according to British Standards (British Standards Institute, 2006).

According to Peter Williams and Christian Henning [10], one of the key aspects was the positioning of the menu on a website, as most pages were connected to it. The analysis showed that the horizontal option was preferred, as it allowed the entire menu to be visible, although this positioning was opposed by some accessibility experts such as Burzagli, Emiliani, and Gabbanin, who preferred the 'drop-down' or 'fly-out' options for easier access.

2. **Problem statement**

The future of many businesses lies in online platforms, focusing on well-maintained, accessible, and secure websites. Inclusive design is essential, particularly for the elderly and people with disabilities. Adhering to standards and tools provided by organizations such as the World Wide Web Consortium (W3C) is crucial to address these needs. Many developers encounter challenges due to a lack of deep knowledge about these specific requirements and the tools that support these communities.

Today, a user-friendly website is vital for its success, as it enhances user experience and impacts traffic, regardless of whether it is a news portal, e-commerce, or informational platform. However, designing and developing these platforms face numerous challenges, including user interface, overall design, colors, fonts, speed, and navigation.

2.1. Navigation

Navigation is one of the most critical aspects of website design. Creating a clear and easy-to-navigate structure is vital to ensure users do not get lost and leave the site. 'Breadcrumbs,' a type of secondary navigation, is a solution that helps users understand the site's hierarchy and move easily between its pages. This approach not only improves user experience but also enhances the website's retention and efficiency.

2.2. Optimization

With the increase in mobile device usage, it is essential for websites to be optimized for all types of devices. Failing to optimize for different devices can drive users away, significantly reducing the site's effectiveness. Utilizing techniques such as media queries to create responsive websites is an effective solution that enhances user experience and SEO by meeting key standards.

2.3. Content

The organization and presentation of content are critical for readability and usability. To ensure clear and readable content, it is important to use appropriate text sizes, clear separation between paragraphs and headings, and sufficient color contrasts. The use of numbered lists and images should be measured to support and illustrate content rather than overwhelm it.

2.4. Support

For websites offering more than just information, such as social networks or e-commerce, providing user support is essential. Various forms of support, such as direct contact, live chat, and a FAQ section, help manage user issues and improve their experience on the website.

2.5. Security

Security is a key aspect of any website. Using HTTPS and SSL certificates is essential to protect user data and increase their trust in the platform. Implementing security measures such as two-factor authentication and continuous monitoring for suspicious activities helps create a secure environment for all users.

2.6. Speed

Website speed directly impacts user experience. Using optimized images and videos, as well as implementing appropriate servers and code optimization techniques, are strategies that help improve website performance.

2.7. Accessibility

Accessibility is crucial to ensure a website is available to everyone, regardless of their physical abilities. Failing to adhere to WCAG guidelines and not providing proper support for users with disabilities can exclude a large portion of the audience. Tools such as "WebbIE" and "Stark" help improve accessibility and expand the website's audience.

The use of open standards and advanced technologies, along with regular accessibility testing and user feedback, can significantly improve user experience and ensure the website is accessible to all.

3. METHODOLOGY

The methodology in this study aims to provide research, structuring, and analysis of the aspects of accessibility and user-friendly design in websites. A review of the literature and scientific sources provides a solid foundation for understanding the knowledge and challenges associated with this topic. The primary goal is to identify best practices and standards that are acceptable to all users, including people with disabilities. This research is based on the exploration and analysis of existing sources, including scientific articles, books, technical reports, and international guidelines available on platforms such as EBSCO, Google Scholar, and ResearchGate. A review of key standards like the Web Content Accessibility Guidelines (WCAG) published by the W3C outlines the technical requirements and practical guidelines that should be followed in web development. Additionally, literature from various professionals, along with insights from community

forums such as StackOverflow and suggestions from the programming community on social networks like LinkedIn, has been included to support the research. The synthesis of research gathered from previous surveys and testing has helped in designing concrete steps that outline specific strategies and recommendations for website design. The inclusion of performance optimization and accessibility techniques is essential to ensure that websites are accessible and usable for everyone. Another important aspect is the use of advanced tools for testing accessibility, such as "WebbIE" for visually impaired users and Stark for designing graphics that are easily perceivable by people with color identification issues. Implementing these tools in the web development process can significantly enhance the user experience and increase accessibility.In conclusion, this research aims to provide a comprehensive guide for creating websites that are both accessible and user friendly, ensuring that all requirements and standards are successfully met.

4. RESULTS

Since the creation of the first website in 1991, there have been many changes in the requirements and services that a website provides. In addition to these changes, there were also anomalies that required different solutions. If we compare websites from the 90s, such as Amazon.com, and the same website in 2024, they look nothing alike (see Figure 1)

This shows the great changes that have taken place over the years. The first coding was done with the FORTRAN programming language, which did not offer many options. Then the PERL scripting language was used, and so on. Nowadays we have over 300 programming languages, which shows that we have different ways of programming, such as in the web, software, artificial intelligence and many other fields.

In the coding part of the design, HTML has never been replaced, but over time there has been an addition of elements within it. The part of adding interactive functions is supported by JavaScript, along with its frameworks like React.js and Vue.js. SQL, MySQL, etc. are used for data storage.

The design part is the most important part of a website, as it is the user's first interaction with the platform. Always be careful with the choice of colors, content, speed, and many other elements. The Human Interface Guidelines (HIG) are a set of design principles and guidelines provided by platforms such as Apple's iOS and Google's Android, to ensure a meaningful and usable experience in their ecosystems and needs.

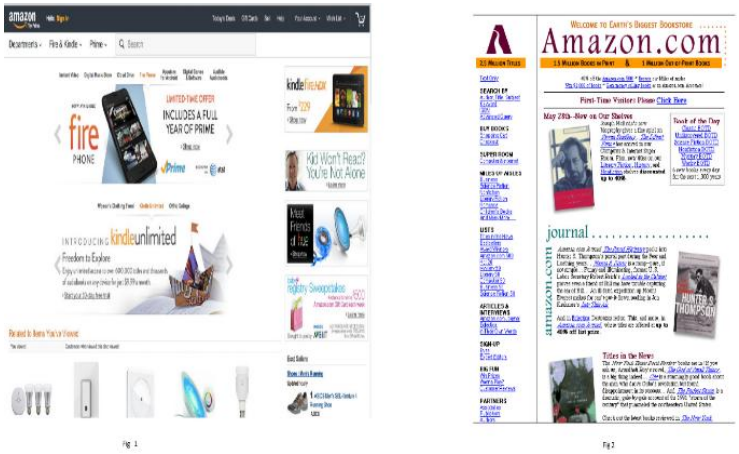

Figure 1. Amazon

These interface design patterns provide valuable solutions for designers and developers, allowing them to create more efficient and aesthetically pleasing digital products. By implementing these patterns, they can provide great user experiences and increase the quality of their front-end design projects. Also, the development of animated graphics and improved visualizations has helped improve the usability and aesthetics of web pages and applications. The use of technologies such as CSS animations, SVG and WebGL has allowed developers to create attractive animations and attractive visual effects, making content more engaging and interactive for users.

4.1. WCAG Guidelines

To ensure that accessibility is one of the key pillars in the design and development part of web pages, it is very necessary to follow the advice and guidelines of WCAG, which are divided into four main principles:

4.1.1. Perceptibility
The information and content of the site should be presented in a simple way for everyone to understand. This includes using alt text for pictures in case the picture is not displayed and captioning for parts that have video or audio content.

4.1.2. Comprehensibility
The information rendered in the browser must be understandable. Operations that receive information from users (filling in forms, registration, application, etc.) must be designed in such a way as not to cause confusion to users.

4.1.3. Operability
User interfaces and navigation (menu) should be clear. This ensures that the functionalities are more accessible and simpler for everyone to understand.

4.1.4. Durability
The site must be accessible through all the technologies and devices we use. Content must be readable and functional across all types of devices and browsers, to ensure a consistent and satisfying user experience.

4.2. Web design for people with disabilities

5.2.1 People with hearing problems
For the hearing impaired, developers should ensure that all video and audio materials have subtitles. Also, animations should be provided that visually show the meaning of the content.

5.2.2 People with learning difficulties
During various user experiences, we also come across people who have a hard time understanding and quickly learning the content we offer. In this case, we should develop the division of this content into smaller parts and focus on the visualization part, such as images and animations, that support and clarify the text. Using illustrations graphically can help people with this problem more easily understand the content being shown to them. This community also includes people who are identified with autism and those who have attention disorders, mainly people who have overloads with their senses. In these cases, it is always preferable that if we have any sliders or animations, the possibility of stopping (pause) is offered in order not to cause distraction to these people (see Figure 2).

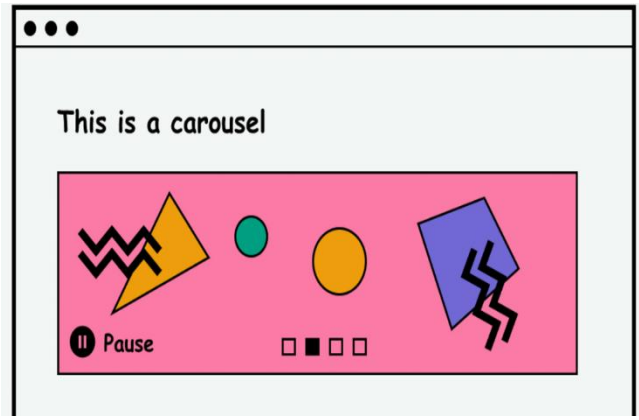

Figure 2. Interface visualization for people with learning disabilities

Although it does not seem like a big issue for people who do not have this problem, for this sensitive category it is very important. This issue is also referenced in WCAG standards [12], in the section on interactions with animations and setting options for pause, stop and hide.

5.2.3 People with Vision Problems
The part of designing as friendly as possible for users who get information only from the visual part should be taken very seriously by the developers. People with vision problems are the most sensitive and challenging group to treat. But with the development of technology, we can use screen readers to help these people. The condition for screen readers to be able to read the content is that our website is compatible with these technologies. For people with color problems, the right colors should be used, and the images and videos should have the right contrast using some plugins to design in the right way.

5.3 Best Practices for Web Design

5.3.1 Structuring
Page layout, which is done with HTML, is the main part of website organization. Through it we can divide, merge and structure the page in the way we want. Correct use of these properties is an essential part of ensuring that content is accessible to everyone, especially people who use assistive devices. Paragraphs, headings, lists and forms must be structured correctly so that the information reaches the user. The structuring of the information should be divided into

several smaller parts, because in this way it is easier to concentrate and the information is much easier to understand, especially for people who have problems with fast reading.

5.3.2 Color and Text Section

One of the most important parts of the web is the proper use of color. The use of colors that are heavier on the eye, such as red and blue, should not be used when building pages (except for buttons), but those that are known to be lighter should be preferred. In reality, we have to think about how a person who is colorblind sees that page. Do these colors provide enough contrast to understand the content? Contrast in content and colors are key points for these people. Although WCAG (Web Content Accessibility Guidelines) is always making changes to the rules of how a good website should be designed, they have had some failures. In Figure 3, we see some of the flaws that most platforms had, especially in color contrast, empty links, lack of alternative text, lack of buttons, etc.

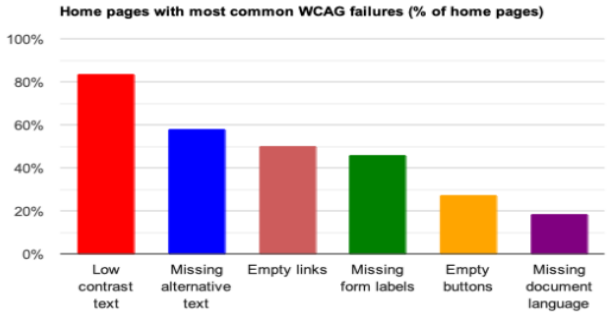

Figure 3. Mistakes

As a solution to the problem, we must consider the ratio between the colors and the contrast used in the text. According to WCAG 2.0 standards, level AA requires the ratio for normal text to be 4.5:1 and 3:1 for larger text. Figure 4 shows what a text with a background color should look like to be readable and meet the appropriate standards.

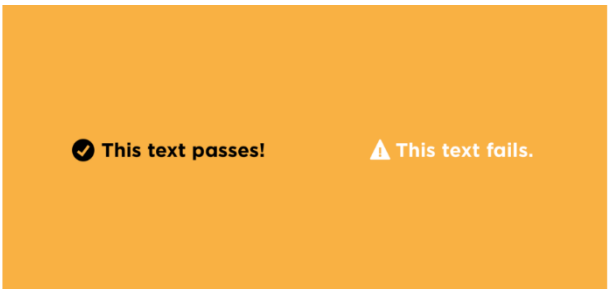

Figure 4. Color and text

Also, when presenting graphs, which we usually present with colors or percentages, it is preferable to have a graphic layer behind them, because this helps differentiate them from people with vision problems. It looks like this in Figure 5.

Figure 5. Color blind

5.3.4 Tools

One of the most useful tools are screen readers, which are already integrated into smartphones. For example, on iOS systems we have 'Apple iOS VoiceOver', while on Android systems we have 'Android TalkBack'. On computer systems there is Microsoft Narrator, JAWS, and many others.
Another useful tool used when designing is Stark, which simulates how people who are color blind see colors. This tool offers over eight levels of color blindness, helping to determine the right levels for our platform (Figure 6).

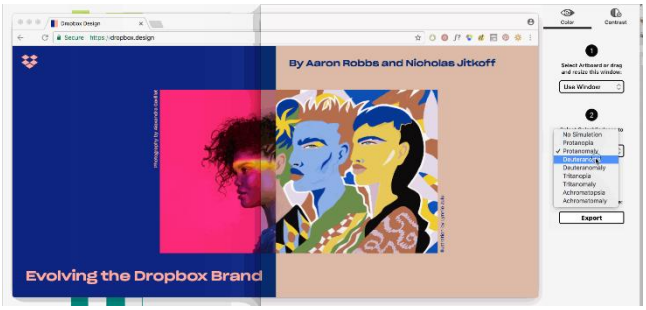

Figure 6. Stark Plugin

MouthStick is a device that facilitates web access for people with mobility disabilities, amputations, paralysis and other illnesses. The MouthStick is a device that is held in the mouth and through which one can surf the Internet, press buttons, type and interact with the website.

5.3.5 Buttons

Although earlier red color was preferred for buttons, now in modern designs buttons with a contrast ratio of 10.79:1 as in Figure 7 are preferred.

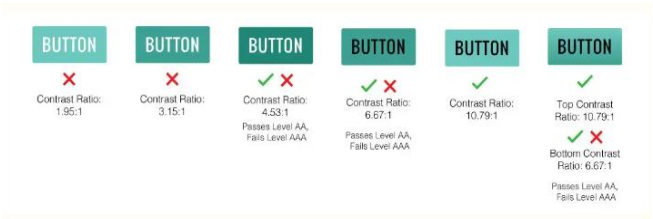

Figure 7. Buttons

One of the functions that is most preferred, but still not enough progress, is to create a visualization option similar to 'Dark Mode' and 'Light Mode'. This option would allow the visually impaired to apply a customized visualization, providing them with an easier and more convenient approach.

According to Accessibility Checker, a platform that checks websites for accessibility, there are some important design tips to improve user experience:

- Never place text over images that are in the background: This can cause reading difficulties, especially for users with poor vision.
- Users have the ability to change the text size: This increases flexibility and accessibility for those who need larger text for easier reading.
- Convey more information using icons rather than text: Icons are easier to understand and help improve website navigation and usability.
- Always have alt text on images in case they are not displayed: Alt text is critical for users using screen readers and for those who cannot see images for technical reasons.
- Links should be limited: This helps avoid confusion and information overload, making navigation simpler and clearer.
- Buttons and links always have a description of what they are for: This is essential to help users understand the function of each element on the web page, improving accessibility and user experience.
- Ads should be limited: Ads can be annoying and often hinder navigation. Limiting them increases focus on key content and improves the overall user experience.

In figure 8 below, we have some suggestions from 'Zera Creative' on how to make a user-friendly website, where eight main suggestions are mentioned [12].

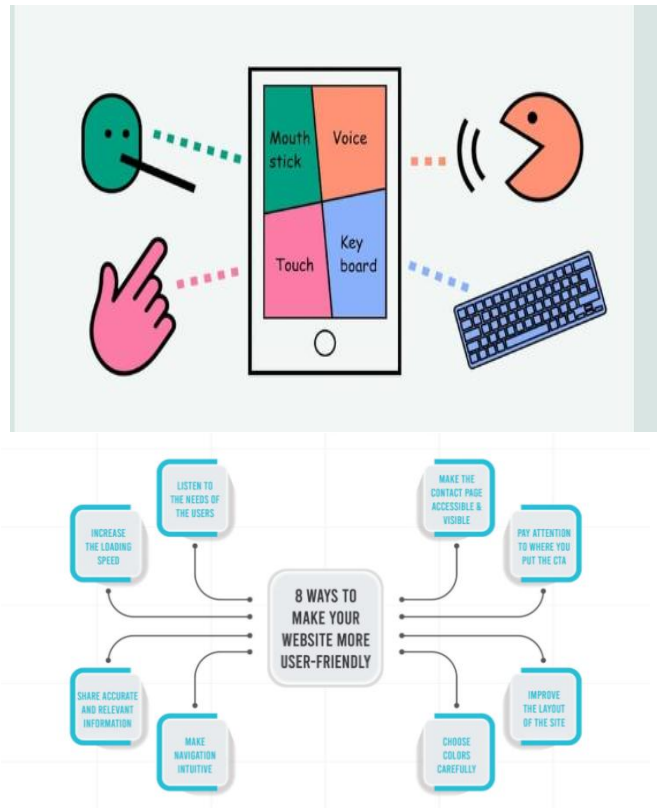

Figure 8. Zera Creative

5.4 New Website Technologies

The web development part has undergone major changes over time. New frameworks, artificial intelligence, the addition of various features and animations have made it much easier to create user-friendly designs. One of the biggest effects has been the animations and visual effects, which have improved the user experience and avoided the possibility of confusion or difficulties. However, animations and effects should be used with care, as frequent use can cause overload.

In the technology part, we also have the development of virtual assistants, which are part of artificial intelligence, but which have helped a lot in accessibility. Nor should we forget the ARIA (Accessible Rich Internet Applications) technology, which helps improve accessibility, mainly in applications that have dynamic content by providing attributes that are used for screen readers.
If we have a site related to people with special needs, it is necessary that on the first interaction with the site we get information about how we want to access the site, for example, as in Figure 9, and the user t is allowed to choose one of the ways offered.

Figure 9. Choice of approach.

However, the challenges of electronic commerce have increased with the expansion of the electronic market, requiring more advanced business strategies to attract customers and meet their needs. These challenges drive continuous research in the field of electronic commerce and user behaviors.

5. RESULTS

Easy accessibility and user-friendly web pages bring several advantages that help improve human-computer interaction.

6.1 Advantages

- Increasing Access: Increasing access means access for everyone, including people with disabilities. This is ensured by using screen readers, assistive devices and specific software to navigate the website. Designing for all existing devices also contributes to this increased access.
- Financial Benefits: Increasing the audience through a user-friendly site that ranks higher in search engines increases the potential for financial income, whether from e-commerce sales or advertising.
- Improvement and User Retention: User-friendly sites have users who stay longer and interact more, indicating a good experience with the site. Speed and easy navigation are key to creating loyal users.
- Performance: Clear and well-organized designs increase site performance and make it easier to maintain and update. This helps in adding new options and adapting to new technologies.
- SEO (Search Engine Optimization): Sites well optimized for accessibility rank higher in search engines, bringing better results and more visitors.

6.2 Disadvantages

- Time: Developing a site that meets accessibility requirements and standards takes a lot of time for planning, design, and constant updates with new laws and technologies.
- Limitations: Compliance with accessibility guidelines limits design and function choices, limiting aesthetic and creative options.
- Maintenance: Accessibility is not a one-time task; must be constantly updated to stay compliant with new standards and technologies, including continuous monitoring and testing.
- Testing: Testing the site with people who have disabilities is difficult and takes a lot of time and energy, but it is necessary to ensure full accessibility.
- Legal Issues: Many countries have strict laws and regulations on site accessibility. Failure to comply with these rules can lead to fines and lawsuits, as well as significant reputational damage.
- Ethical Issue: User-friendly and comprehensive design reflects the commitment to social responsibility and helps to create a good reputation. Failure to comply with this responsibility can damage personal and company reputation.
- Balancing Requirements: The different needs of different user groups create confusion, and it is difficult to balance between their different requirements, making it challenging to provide a one-size-fits-all solution.

Despite these challenges, websites should always be accessible to everyone. With good planning, all these problems can be overcome. Accessibility is an ethical and moral responsibility for developers, testers and all web professionals. We must ensure that no category of users is excluded and alleviate their problems with increased dedication and care.

6. CONCLUSIONS

This topic will hopefully help all developers in the field of web development, providing examples of how to keep in mind programming standards for all users, regardless of ability or limitation. While researching this topic, I came across aspects of programming and rules that I didn't know before. We have reviewed several details and various frameworks, tools and methodologies that form a part that is missing from most companies involved in the development of these technologies.
Exploring how to create a website that meets all the requirements is not easy at all and requires care in many aspects. To think for a moment that we have in front of a page developed by us and condition a person to interact with our work or not, is something we have not thought about before.
I hope that exploring new assistive technologies will help everyone in terms of accessibility and user-friendly design. We analyzed the techniques and gave suggestions for colors, optimization, contrast, buttons. We are familiar with tools and plugins that help a lot in terms of design. To go deeper, we have taken concrete cases of how solutions should be made for people with impaired vision, for people with hearing problems and many other cases.
The path to this degree topic has led us to research with new methodologies, with different approaches and keeping control of the scientific literature and internet research. As we look to the future, we anticipate further innovations and transformations in Internet technologies and are committed to staying on top of these advances.
This graduation theme is not only a culmination of our journey, but also a testament to the continued evolution of front-end site development. It serves as a valuable resource for developers, providing insights, best practices, and deep insight into the trends driving the digital landscape. In a world where user experience is key, continuous exploration and deep knowledge of new web technologies remain imperative.

REFERENCES

Web Accessibily Begins . https://pressbooks.library.torontomu.ca/pwaa/chapter/the-evolution-of-web-accessibility/
Word Website Statistic http://gg.gg/1acoh0

NUSSBAUM, J. & COUPLAND, J. (EDS): Handbook of communication and aging. London: Laërence Earlbaum Associates, 2004.

BALAZS, A.: Marketing to Older Adults. In: J. Nussbaum & J. Coupland (eds), Handbook of communication and aging, 329-351, London: Lawrence Earlbaum Associates, 2004.

STEPHANIDIS, C. (ED.): Universal access in human computer interaction. Coping ëith diversity. Reihe: Lecture Notes in Computer Science (LNCS), Neë York: Springer, 2007.

TULLIS, T. (2007): Older adults and the Web: Lessons learned from Eye-Tracking. In: C. Stephanidis (ed.), Universal access in human computer interaction. Coping ëith diversity. Reihe: Lecture Notes in Computer Science (LNCS), 1030-1039, Neë York: Springer, 2007.

KRESS, G. & LEEUwEN, T. VAN: The meaning of composition' of their book Reading images: The grammar of visual design. Neë York: Routledge, 2006.

https://books.google.com/books?id=dlJ94KZqëqcC&newbks=1&newbks_redir=0&printsec=frontcover&dq=web+accessibility&hl=en#v=onepage&q=web%20accessibility&f=false

https://www.researchgate.net/publication/259687891_Optimising_website_designs_for_people_with_learning_disabilities

https://www.w3.org/WAI/standards-guidelines/wcag/docs/#wcag-2-standard

]https://www.w3.org/WAI/WCAG21/Understanding/pause-stop-hide.html

https://www.accessibilitychecker.org/blog/website-accessible-for-the-blind-community/

https://www.zeracreative.com/blog/8-ways-to-make-your-website-more-user-friendly/

The Transformative Impact of Apple Vision Pro on Healthcare and Medical Practice

PRANVERA JASHARI[1], FATON KABASHI[2] VEHEBI SOFIU[3], LAMIR SHKURTI[4], SAMI GASHI[5]

Abstract: Apple Vision Pro is a device a headset that merges digital and real-world content, offering users an integrated and advanced experience. The high-level development technology in Apple Vision Pro has the potential to fully transform every aspect of life, especially in the field of healthcare, including health care, digital therapy, and the education of both medical staff and patients. Apple Vision Pro aims to provide healthcare professionals and staff with the ability to make safe and accurate decisions in treating patients. This advanced system, with its sophisticated algorithms, allows for the creation of complex models so that medical staff can identify potential risks and develop personalized treatment plans for their patients. Apple Vision Pro can process information to highlight possible diagnoses and treatment options, providing instant access to all the information medical staff need, thus easing their workload. It helps medical staff secure new medical information by enabling them to access the latest knowledge and recommendations. Some other benefits include faster and more accurate diagnosis, automation, and continuous patient monitoring through Apple Vision Pro throughout its use. It also positively impacts patients, leading to improved quality of life outcomes. Apple Vision Pro enhances patient engagement and education through its 3D camera, helping patients better understand how a disease functions in their body, how the therapy works, and the entire healing process through visuals that make it easier for them to grasp. In particular, it positively impacts patients' mental health, making their lives more dynamic and helping them avoid negative thoughts or real-life situations that they may wish to avoid experiencing.

Keywords: Apple Vision Pro, Digital health, Medical education, Patient care

Address: University for Business and Technology (UBT), Pristina, Kosovo.

***Corresponding author**: pj51936@ubt-uni.net, faton.kabashi@ubt-uni.net, vehebi.sofiu@ubt-uni.net, lamir.shkurti@ubt-uni.net, sami.gashi@ubt-uni.net

1. INTRODUCTION

Apple Vision Pro is a new device with highly advanced development technology, designed to push the limits of innovation and merge the real world with the digital. It comes in storage capacities of 256GB, 512GB, or 1TB. The display includes the highest level of advancement, with 23 million pixels, 3D views, a 7.5-micron pixel pitch, and more. It is also powered by two chips, the M2 and R1. The M2 consists of a central processing unit with 8 performance cores and 4 efficiency cores, designed for parallel processing with 10 cores, along with 16 cores from the neural engine, which is a specialized processor that enhances performance, and 16GB of unified memory. The R1 chip performs extensive image signal processing, with a memory bandwidth of 256GB/s. The main stereoscopic 3D system, used by the camera, creates an illusion of depth in images and videos. It also captures spatial photos and videos, enabling moments to be revisited in time. The sensors include two high-resolution main cameras, six tracking cameras, four units for gaze tracking, four inertial measurement units, a vibration sensor, and an ambient light sensor. Apple Vision Pro's security system uses Optic ID, encrypted and accessible only by the Secure Enclave processor, ensuring the protection of personal data within the application. The device includes Spatial Audio technology, creating an immersive audio experience with both audio and video playback. The battery provides approximately 2 hours of general use, up to 2.5 hours of video playback, and can be used while charging. Apple Vision Pro supports wireless and Bluetooth connectivity, with VisionOS as its operating system. The device weighs about 600-650g. [1]The use of Apple Vision Pro aids individuals with disabilities. It has the potential to impact the medical field, healthcare, and digital health by focusing on education and training for various medical procedures, such as assisting surgeons in surgical planning and mental health care. It also encompasses digital therapy, involving medical interventions for the prevention, management, and treatment of diseases or disorders, patient monitoring and care, as well as research and development through the analysis of medical data to develop new treatments and therapies. Its use enhances accuracy, efficiency, and access to medical care. Apple Vision Pro also has an ergonomic design, making it very comfortable to use.

2. LITERATURE REVIEW

The advanced technology of Apple Vision Pro promises enhanced ease and accuracy in the medical field. Its application in healthcare has started in the U.S., where its ability to blend the digital and physical worlds has improved the management and safety of various medical procedures. With advanced sensors, Apple Vision Pro opens up different possibilities for medical staff, patients, improvement of mental health therapies, surgical planning, and the transformation and education of healthcare.
The combination of artificial intelligence and imaging capabilities of Apple Vision Pro provides the best option for diagnosis and easier monitoring of diseases remotely, reducing the burden on healthcare institutions by saving patients' time and easing the management workload for staff. According to a study at Cedars-Sinai, in collaboration with artificial intelligence experts, an application was developed to improve patients' mental health by leveraging Apple Vision Pro's unique capabilities, serving Los Angeles and beyond. The application enables patients to engage in AI-powered talk therapy and experience relaxing, immersive environments that provide a real-life feeling of serenity. It offers users therapy sessions. [2] "Apple Vision Pro provides a gateway into Xaia's immersive, interactive behavioral health support – taking steps I can only describe as a quantum leap beyond previous technologies," said Brennan Spiegel, MD, MSHS, Professor of Medicine and Director of Health Services Research. A group of researchers is exploring how virtual reality could affect the treatment and healing of the body, as Apple Vision Pro's advanced mechanisms train the brain and body to reduce pain without medication. Studies have shown that users experience a more relaxed mental state and find it easier to reduce pain while using the device. Dr. Jeffrie is planning a study on how Apple Vision Pro's virtual reality mechanisms, when interacting with the immune system, can detect inflammation in joints, bones, and internal organs, subsequently reducing pain.

A pilot study by national surgeons like [3] M. Orione, G. Rubeqni, R. Tartaro, and G. M. Tosi explored the application of Apple Vision Pro in ophthalmic surgery, assessing results during its use. Apple Vision Pro was used by 10 surgeons during an eyelid surgical intervention, where the device was employed throughout the process. The results were positively evaluated by the surgeons, who expressed high regard for the freedom of movement and workflow integration provided. Surgeons assessed the improvement in visualization, enhanced accuracy, and easier communication between surgical teams during the process.

[4]Elsevier, a company supporting the work of healthcare researchers and professionals, offers students a first-time experience in learning about the heart through 3D images, models, and simulations with Apple Vision Pro. They created the HeartX application, which combines animations, 3D models, images, and videos, making heart education more engaging for students. Jan Herzoff, President of Elsevier, stated that this was a significant aid for students by offering a new learning experience, with real-time, accurate images of how cardiac health functions, the occurrence of heart diseases, and their prevention. The study focuses on an in-depth exploration of the heart and cardiovascular system and on cardiac conditions, providing students with a real experience of how they function. Apple Vision Pro is one of the most efficient devices for tumor detection.

"Three-dimensional visualization of medical images in an immersive space creates exciting opportunities for improving patient care. Technology that enables sophisticated eye and gesture controls for reviewing 2D and 3D medical images can potentially assist in effective tumor board reviews and create collaborative spaces in healthcare," said Dr. Paul Murphy, Clinical Associate Professor at UC San Diego School of Medicine and radiologist at UC San Diego Health [5]. The advanced artificial intelligence in Apple Vision Pro improves client experiences in its products and services, and based on studies, it is expected to become an essential device for performing medical services.

3. PROBLEM STATEMENT

Apple Vision Pro is a device that has impacted every industry. The purpose of this topic is to explore its influence and significance, particularly in the field of medicine. This topic will include research on what services Apple Vision Pro can provide and the improved outcomes resulting from its use in the relevant field. In general, I will address the advanced technology of this device.

The problems that have brought us to this topic are:

- The world's lack of knowledge about the importance of Apple Vision Pro
- Absence and improper treatment of patients
- Deterioration of results in the industry overall
- Concerns about the security and privacy of patient and medical staff data.
- Non-application of surgical trials before starting the procedure
- Absence of digital therapy.

4. METHODOLOGY

This research paper aims to evaluate the impact of Apple Vision Pro on healthcare practices, focusing on how this technology will diagnose and treat diseases. From this research, we will be able to understand all the advantages and challenges that the use of this technology will bring for the staff of healthcare centers as well as for patients. To accurately analyze this research, we have employed several methods, one of which is case studies on how Apple Vision Pro has been used in hospitals and clinics, where we have understood its effectiveness and benefits in everyday practice. Additionally, for this research, we have used statistical data from other studies that analyze and show the impact of similar technologies, which help us gain a clearer understanding of the impact of Apple Vision Pro in healthcare. To ensure we have all the theories and clear data, we have researched scientific literature from specialized books and articles, which allows us to gain a broad perspective on what Apple Vision Pro will offer us, what advantages it contains, and the criticisms and limitations we might face with this advanced technology.

5. THE IMPACT OF APPLE VISION PRO ON MEDICINE

Apple Vision Pro creates new opportunities for digital interaction by combining augmented reality and virtual reality. It is also focused on the healthcare context and medical education. Its technology is beneficial in specific areas of medicine, making the staff's work easier and providing higher security for patients. The capabilities of this device are advanced, allowing for its application in improving clinical procedures, surgical navigation, and patient care. Apple Vision Pro facilitates the reduction of procedural errors. Augmented reality and virtual reality enable the creation of medical simulations for staff, which aids in preparing them to develop complex medical procedures, enhancing their skills while reducing risks for patients and improving medical outcomes overall.

Apple Vision Pro is a device that helps improve the emotional or mental state of its users. This device assists in escaping reality and immersing the mind in an illusion where the user wishes to be, experiencing the feeling of reality. This can make it easier to cope with depression, anxiety, and other mental health conditions. Many patients with severe mental health conditions positively influence their well-being through the use of this device, such as reliving beautiful moments, like memories of a loved one who has passed away.Medical staff can examine patients in detail using Apple Vision Pro, offering accurate diagnoses. The greatest advantage of its use is among students in their training. With its use, students gain a better understanding of anatomy and medical processes, as Apple Vision Pro presents clearer and more detailed visualizations of the body.

5.1. Surgical Application

With the use of Apple Vision Pro headsets, surgeons can visualize and interact with 3D models of each part of the patient's body anatomy, assisting in the surgical planning process. The visualization of anatomy feels realistic, and the use of the headsets is comfortable, without causing eye strain. Apple Vision Pro provides security for the staff when initiating surgical procedures after virtually analyzing the anatomy. It reduces the time needed for surgical treatment and allows for the pre-preparation of surgical interventions without directly practicing on human patients. Apple Vision Pro enables high-resolution viewing of the patient's anatomy, patient examinations, and all 3D models in real time, facilitating more precise strategies for the operation. The use of Apple Vision Pro helps to minimize accidental injuries. [6]The device also allows for the identification of potential damages or accidents during surgical procedures, which overall enhances the accuracy of patient outcomes. Surgeons have begun to adopt this technology in many parts of the world, especially in India, for performing surgeries on various issues such as stomach cancer and fistulas. With its advanced technology, Apple Vision Pro is set to become an essential tool in these surgical procedures, as it increases efficiency and accuracy in patient outcomes.

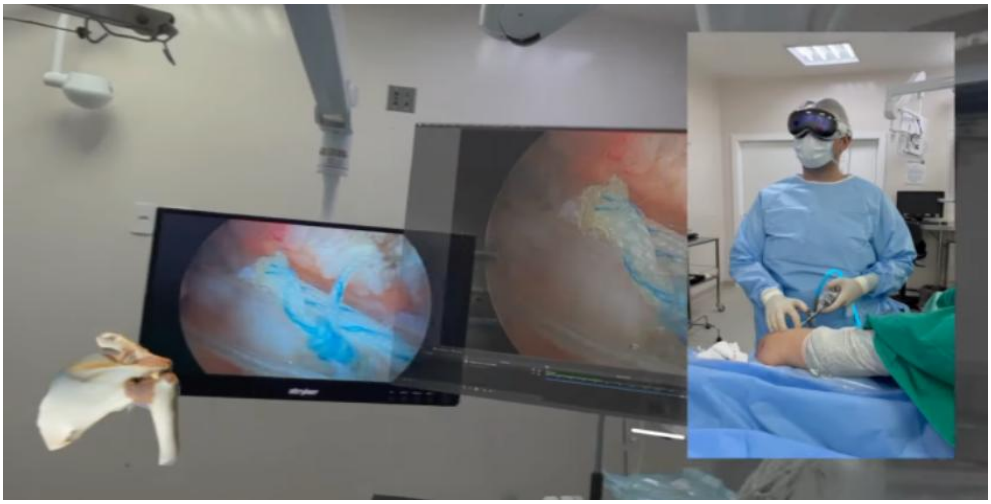

Figure 1. The Use of Apple Vision Pro in the Surgical Sector of Medicine

5.2. Improvement of pychological health

Apple Vision Pro plays a significant role in alleviating stress, offering new therapy options, and enhancing psychological well-being, positively impacting emotional states. With its virtual environments, Apple Vision Pro enables users to relax. This device allows for the simulation of various scenarios, facilitating an escape from reality and creating an illusion that provides treatment for phobias, anxiety disorders, and other mental health issues. By putting on the headset, users can transport themselves to a calming place, experiencing a sense of tranquility while lying on the couch. [7]Apple Vision Pro can be regarded as a type of at-home therapist that empowers users to take control of their mental health. The advanced device supports mental health applications such as meditation or those addressing specific disorders. Overall, Apple Vision Pro is a promising tool in the battle against mental health challenges through virtual technology and the possibility of time travel.

5.3. Education and medical treatment

Apple Vision Pro significantly impacts the education of both staff and patients. Through its use, medical personnel enhance their skills, enabling them to make more accurate diagnoses. Healthcare staff utilize 3D models combined with augmented reality to explain patients' conditions through visual representations, allowing patients to better understand their health status. These models enable patients to grasp how therapy affects them and how the healing process unfolds. Apple Vision Pro improves accuracy in patient care plans by providing alerts for medications, monitoring, and treatments. It facilitates the education of anatomy and anatomical practice, eliminating the need for cadavers. Additionally, Apple Vision Pro offers medical students valuable insights, helping them understand medical procedures more effectively.

5.4. Discovery of skin cancer

Apple Vision Pro captures high-resolution images of the skin, enabling analysis and diagnosis by dermatologists. [8]The 3D imagery allows dermatologists to enlarge and examine images in detail. Apple Vision Pro detects early signs of skin cancer, such as irregularities in texture, shape, appearance, and color. Early detection can prevent the progression of this disease, and successful outcomes are anticipated with the use of Apple Vision Pro in the treatment of skin conditions.

5.5. Application in dental health

Apple Vision Pro can be used for oral health by capturing images of teeth and gums. Dentists can identify dental health issues in detail, such as tooth diseases, cavities, and oral cancers. By using this technology, dentists can provide their patients with preventive measures, reduce the risk of complex procedures, and enhance their treatment plans. Patients using Apple Vision Pro can improve their overall oral health.

6. ADVANTAGES AND DISADVANTAGES

Apple Vision Pro is expected to become an essential device in healthcare due to its comprehensive functionality.

6.1. Advantages of using Apple Vision Pro in Healthcare

- Improvement of various procedures in a realistic environment, as well as the potential to enhance the skill acquisition of medical staff.
- Information is generated more quickly regarding diagnoses and possible treatment options.
- Accelerating the diagnostic process and increasing accuracy.
- Provides accurate analysis of medical data using artificial intelligence.
- Staff feel more confident in making decisions and improving treatment outcomes for their patients after using them.
- Facilitates the work of medical staff in identifying potential health risks and creating personalized patient plans.
- Eases the planning of surgical procedures through the visualization of 3D models.
- Medical trainees notice an increase in their knowledge through close examination of complex anatomies and medical procedures after using Apple Vision Pro.
- Medical staff reduces the time needed to access relevant clinical data, treatment guidelines, or patient interactions. So, it enables faster access to make accurate and up-to-date decisions in real-time.
- Easier remote collaboration among staff, staff-patient, or student-staff located in different destinations.
- Medical staff improves proactive skills and knowledge through the integration of various systems in Apple Vision Pro, which provide immediate feedback.

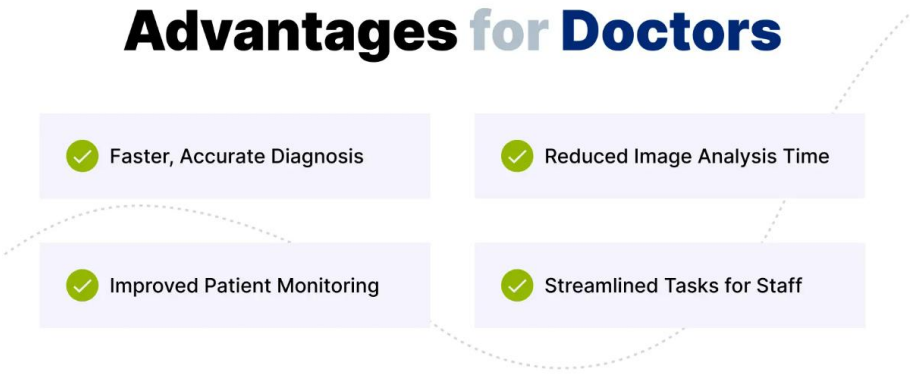

Figure 2. Advantages for Medical Staff Using Apple Vision Pro

- Improvement of patient's quality of life by reducing the likelihood of hospital stays.
- Increased patient engagement and education.
- Patients more easily understand their medical conditions, treatment procedures, and diagnoses.
- Patients can be more accurate with their treatment plans and medication schedules after using Apple Vision Pro.
- Patient safety is enhanced through advanced algorithms of Apple Vision Pro, which alert doctors and pharmacists to potential medication risks.

Figure 3. Advantages for Patients After Using Apple Vision Pro

6.2. Disadvantages of Using Apple Vision Pro in Healthcare

- The high price after purchasing Apple Vision Pro may be a financial burden for healthcare institutions.
- Medical professionals express difficulties in adapting to the virtual technology and augmented reality of Apple Vision Pro after its use.
- Staff may experience fatigue or discomfort after using Apple Vision Pro, which can negatively impact the successful performance of medical procedures.
- Patients feel less emotionally connected to the staff after using Apple Vision Pro.
- Patients may be negatively affected in their emotional state when they understand how the disease operates in their body.
- Excessive use of Apple Vision Pro may lead to addiction in patients and subsequently develop social isolation for them.
- Patients may develop a dependency on using Apple Vision Pro, making it a tool for managing their emotions rather than controlling and managing them on their own.

7. CONCLUSION

Apple Vision Pro offers advanced new technology to develop new opportunities in healthcare. Apple Vision Pro provides a series of applications that serve patient health care. Healthcare institutions find it easier to organize patients with its use. Medical staff can reduce waiting times through online consultations and more easily manage and systematize patients. Apple Vision Pro, with the most advanced technology in recent years, is used in every medical clinical field, such as abdominal, psychiatric, ear treatment or nose treatment, vascular, and others. Its advanced system is capable of alerting to patients' diseases, offering the possibility of treating them before they develop. Apple Vision Pro provides security for patient data. Its users can change their emotional state through virtual reality, where they can go back in time, meaning

reliving moments with loved ones who are no longer alive, experiencing these moments as if they were real. Medical staff using it achieve more efficient results as it offers complete security with the ability to view 3D images, providing every possible detail.
In addition to medical staff, its use is also widespread in pharmacies, as they receive quick and accurate information about whether a diagnosis may lead to side effects for patients. Patients using it can discover more about their illness, how it is treated, how therapy affects them, how the healing process works, and whether there are any side effects. Medical staff enhance their knowledge by viewing in detail everything they need in real time. This device provides patients with services such as security for their data, immediate treatment, disease prevention, accurate digital diagnoses, and many other services. This technology promises to become mandatory in healthcare institutions.

8. REFERENCES

A. Thompson, "Apple wants Vision Pro to be a medical hub," 21 3 2024. [Online]. Available: https://www.fastcompany.com/91055214/apple-vision-pro-medical-hub-health-organizations-already-using-it.

N. Charles, "Virtual Reality and the Brain-Body Connection," 05 04 2024. [Online]. Available: https://www.cedars-sinai.org.

E. J. Ophthalmol, "Utilization of apple vision pro in ophthalmic surgery: A pilot study," 14 08 2024. [Online]. Available: https://pubmed.ncbi.nlm.nih.gov.

C. West, "Elsevier launches Complete HeartX™, the world's first heart education experience in spatial computing," 05 04 2024. [Online]. Available: https://www.elsevier.com.

Visage, "Introducing the new Visage Ease VP for Apple Vision Pro," 07 02 2024. [Online]. Available: https://www.digitalhealthglobal.com.

C. Martin, "Apple Vision Pro is revolutionizing surgical procedures worldwide," 20 04 2024. [Online]. Available: https://appleinsider.com.

Dr.Charlotin, "Apple Vision Pro Therapy tool Mental Health," [Online]. Available: https://www.drcpsychologist.com/.
H. Castro, "Apple Vision Pro rebooting medical diagnosis," 19 02 2024. [Online]. Available: https://www.kevinmd.com.

Development of A Financial Web Application For Budget And Expense Management For Individual And Company

GENIT SOPA[1], FATON KABASHI[2], VEHEBİ SOFIU[3], LAMIR SHKURTI[4], SAMI GASHI[5]

Abstract: This project presents the development and implementation of a financial web application, dedicated to budget and expense management for individuals and companies. The project focuses on creating an innovative and comprehensive platform that addresses common challenges in financial management using modern technologies and advanced development methodologies. The application aims to provide a comprehensive solution for users including functionalities such as budget tracking, expense categorization, product management, profit estimation and generation of customized financial reports. The application is designed to be accessible from any device with a web browser, thus providing a smooth and easy user experience. One of the main objectives of this project is to ensure a high level of security and privacy for user data. For this purpose, advanced encryption technologies and protection mechanisms are used to guarantee the protection of sensitive financial information. This focus on security is essential to gain users' trust and ensure that their data is protected from unauthorized access. Another important aspect of this project is the use of data analytics to provide personalized insights and recommendations to users. These analyzes help users make more informed financial decisions and optimize the management of their financial resources. Analyzes include estimates on spending, consumption trends and recommendations for budget optimization. Furthermore, the application is designed to be scalable, enabling high performance even in cases of large user and transaction loads. This feature makes the platform suitable for a wide range of users, from individuals managing their personal budget to companies looking for an efficient tool for managing their corporate finances. In conclusion, this project represents an important step in the development of digital financial tools, providing a safe, efficient and easy solution for users to improve the management of their finances. The platform not only fulfills the current needs of users, but also has the potential to serve as a model for future developments in the field of financial technology.

Keywords: API - Application Programming Interface, BPM - Business Process Management, CRM - Customer Relationship Management, ERP - Enterprise Resource Planning, FinTech - Financial Technology, IoT - Internet of Things, KPI - Key Performance Indicator, SaaS - Software as a Service, SDLC - Software Development Life Cycle, UI/UX - User Interface/User Experience, UML - Unified Modeling Language

[1,2,3,4,5]**Address:** UBT, Higher Education Institution, Kosova

***Corresponding author**: faton.kabashi@ubt-uni.ne

1. INTRODUCTION

Financial management is an essential component of personal and business life, requiring advanced tools and strategies to ensure economic stability and success. In the digital age, technology has revolutionized the way we manage our finances, offering innovative and automated solutions to help individuals and businesses monitor and control their finances. One of these solutions is the development of financial web applications that facilitate budget and expense management.
Nowadays, individuals face numerous challenges in managing their personal finances. Unforeseen expenses, lack of budget planning and inability to track income and expenses in real time are some of the main problems that individuals face. Additionally, many people have difficulty understanding and analyzing their financial data, which makes informed financial decisions difficult. On the other hand, businesses, especially small and medium-sized ones, face various challenges in managing their finances. Managing inventory, tracking operational expenses, estimating profits, and generating accurate and detailed financial reports are some of the challenges these businesses face. Moreover, the lack of an integrated system for managing these aspects can lead to financial losses and wrong decisions. Security and privacy of financial data are also major concerns in the digital age. With the increase in cyber security incidents, the protection of personal and financial information has become critical. Individuals and businesses require tools that not

only provide advanced functionality for financial management, but also ensure that their data is protected from unauthorized access and cyber-attacks.
This project aims to develop a financial web application that will provide a comprehensive budget and expense management solution for individuals and businesses. The application will address the problems mentioned above by providing a user-friendly interface, advanced financial management tools, strong security measures and customized

reports. This platform will help individuals and businesses make informed decisions and achieve their financial goals effectively and safely.
The application will include multiple functionalities to meet the needs of different users. Users will be able to create and manage their own budgets for different categories of expenses, such as food, transportation, entertainment and business expenses. This process will be simplified with the help of an intuitive and easy-to-use interface that allows setting budget limits and monitoring expenses in real time. This will help users avoid budget overruns and have a clear overview of their finances.

2. LITERATURE REVIEW

The development of financial applications for budget and expense management has been an area of great interest to researchers and professionals. These apps are designed to help individuals and businesses organize their finances, track expenses and plan budgets more effectively.
A study by Fisher and Lay [1] evaluates the impact of mobile financial applications on improving personal finance management. The study found that using such apps helps users track their spending, identify spending patterns and make informed financial decisions.
Another study by Riquelme and Rios [2] examines the role of technology in business financial management. They evaluate the use of financial applications in small and medium-sized businesses and find that these applications help automate financial processes, generate financial reports and improve the tracking of operational expenses.
Another important aspect is the design and user interface of these applications. A study by Chen et al. [3] analyzes the impact of user interface design on the efficiency of financial applications. The study highlights the importance of a simple and intuitive design that facilitates use and improves the user experience.
Another research by Kapoor and Gunta [4] focuses on data security and privacy in financial applications. They emphasize the importance of using advanced encryption technologies and safeguards to ensure that users' financial data is protected from cyber-attacks and unauthorized access.
According to a study done by Brown and Black [5], financial applications can also be used to educate users about financial management. The study suggests that apps integrate educational features, such as financial advice and budget management courses, to help users improve their financial knowledge and make better financial choices.
A study by Suryadevara and Babu [6] focuses on using artificial intelligence and machine learning algorithms to personalize financial recommendations for users. Financial applications that use these technologies can analyze spending and income patterns to provide specific, personalized advice that helps users optimize the management of their finances.
A research by Kaczorowski et al. [7] studies the impact of financial applications on improving financial control and reducing finance-related stress. The results show that regular use of financial apps helps users have a better understanding of their financial situation and helps them feel more confident and less stressed about their finances.
Another study by Johansson and Olsson [8] examines the impact of financial applications on strategic business decision-making. The study shows that the use of financial applications helps business managers have a clear picture of the company's financial condition and make better strategic decisions that positively affect the growth and sustainability of the business.
The development of financial applications for budget and expense management has a positive impact on personal and business financial management. Financial apps provide powerful tools for tracking and analyzing expenses, budgeting, and securing data, helping users achieve their financial goals and improve their financial health. The integration of advanced technologies, intuitive design and strong security measures contribute to the effectiveness and popularity of these applications.

3. PROBLEM STATEMENT

The development of a financial web application for budget and expense management is the purpose of this research and the achievement of some results related to this technology. The impact and applications of financial technology in budget and expenditure management, problems, challenges and others. The result of this work predicts that it will be the gain of knowledge about the use of financial applications, namely the understanding of how and where this technology can influence in the future. The overall objective is to explain the development of financial technology and its use. The problems that have brought us to this research are:
• Lack of knowledge and appropriate tools for effective management of personal and business finances.
• Inability to track income and expenses in real time.

• Difficulty in analyzing and interpreting financial data to make informed decisions.
• Increasing cyber security threats and the need to protect financial data.
• The complexity of integrating different financial tools into a single, easy-to-use platform.

4. METHODOLOGY

The methodology in this thesis describes the methods and techniques that will be used to realize the goals and objectives of the project. It includes the steps to be followed, the materials to be used, and the sources from which these materials

will be obtained. The main goal is to provide a structured and sustainable approach to the development and implementation of the financial web application.

4.1 Research Approach

The project will use a mixed approach, combining qualitative and quantitative research methodologies:
• Secondary Research: Compilation of existing literature, academic articles, and industry reports to create a solid theoretical foundation and identify best practices in the development of financial applications and financial technology (FinTech) [9].
• Primary Research: Conducting interviews and surveys with potential users to understand their specific needs and requirements for a financial web application. This will help create an interface and functionalities that are convenient and usable.

4.2 Development Process

The web application development process will be followed in structured phases to ensure efficiency and quality:
1. Requirements Analysis:
o Summary of functional and non-functional requirements through interviews and surveys [10].
o Documenting the specifications of development requirements.
2. System Design:
o Designing the application architecture using UML (Unified Modeling Language) models to represent the structure and interactions of the various system components.
o Developing database schemas to ensure efficient data management.
3. Development and Implementation:
o Using development languages and frameworks such as Angular for the user interface and .NET for the server part [11] [12].
o Integration of external APIs for additional functionality such as payment and financial data processing.
4. Testing:
o Conduct functional and non-functional testing to ensure the application meets requirements and is stable.
o Security testing to identify and address potential security issues.
5. Implementation and Maintenance:
o Deploying the application to a production environment and providing user support.
o Monitoring performance and performing regular updates to improve functionality and security.

4.3 Materials and Resources

• Literature and Articles: Academic resources and scientific articles will be used to support development theory and practices [9].
• Development Tools: Tools and platforms such as Visual Studio Code, GitHub, and cloud environments for application testing and development.
• Databases: Relational databases such as MySQL for financial data management [13].
• Security Resources: Security protocols and tools to protect data and financial transactions from cyber threats.

5. PROJECT ANALYSIS AND PLANNING

5.1 Scope of the Project

Overview

A financial web application is an online platform that provides users (individuals and companies) with a variety of financial tools and services to help them manage their finances. The application will be accessible from any web browser and will have two different login interfaces for individuals and companies.

Individual users will have access to features such as budget tracking and expense tracking to help them manage their personal finances. In turn, companies can use the platform to manage and showcase their products. They can add information about their products, manage the quantity sold and remaining inventory, track expenses and estimate the profits they will make.
The platform will provide users with customized reports and analysis based on their financial activities, and they can generate financial statements for personal or business use. Additionally, the app will have built-in security features to ensure the safety and privacy of user data.

Objectives

The objectives of the financial web application are as follows:
• To develop a user-friendly interface for both individuals and companies that provides a seamless experience while managing their financial activities.
• Enable individuals to track their spending, set budgets and generate reports that help them understand their financial position and make informed decisions.

• Allow companies to add, manage and provide tools to track their inventory, expenses and profits.
• To guarantee the security and privacy of user data by implementing strong security measures and respecting the relevant data protection regulations.
• Provide users with valuable insights and analysis based on their financial data, enabling them to make informed decisions and take the necessary actions to achieve their financial goals.
• Provide prompt customer support and service to address user questions and concerns regarding platform functionality.
• Continuously improve and update platform features based on user feedback and market trends, providing a reliable and up-to-date financial management solution.

Application Features
The financial web application will include the following features:
1. Product Management: The platform will enable companies to add their products and manage their inventory, sales and profits in real time.
2. Profit estimation: Companies can estimate their profits based on their sales and expenses, allowing them to make informed decisions about pricing and inventory management.
3. Financial reports: The platform will generate customizable financial reports for individuals and companies, including balance sheets, income statements and cash flow statements.
4. Data Analytics: The Platform will use data analytics to provide users with insights and trends related to their financial activities, helping them make informed decisions about their finances.
5. Categorizing expenses: The platform will enable individuals to categorize their expenses automatically or manually, making it easy to identify areas where they can reduce spending.
6. Goal setting: The platform will allow individuals to set financial goals and track their progress towards achieving them, providing motivation and guidance towards financial success.
7. Secure Data Storage: The Platform will store user data securely, using encryption and other security measures to protect sensitive information from unauthorized access.
8. Customer Support: The platform will provide customer support through a variety of channels, including email, chat and phone, ensuring that users can quickly get help with any issues they encounter.

Restrictions
The following limitations will be considered during the development of the online financial application:
• Cross-Browser Compatibility: The application must be designed to be compatible with all major web browsers.
• Data Privacy: The application must comply with data privacy regulations and protect users' financial data from unauthorized access.
• Scalability: The application must be designed to handle large numbers of users and transactions as it scales.
• Performance: The application should be optimized for performance to ensure that it runs smoothly and efficiently.
Project products
The following products will be provided at the end of the project:
• Fully functional financial web application accessible from any web browser.
• User manuals and documentation.
• Source code and project documentation.
• Quality assurance and test reports.

5.2 Technical and Technological Analysis

Presentation
In today's fast-paced world, managing personal and business finances is becoming increasingly complex. An online financial application can provide users with an efficient and convenient way to manage their finances. The proposed financial web application aims to provide individuals and companies with a user-friendly platform to manage their finances, track expenses, generate reports and make informed decisions.
This analysis will discuss the technology, system architecture, external systems, tools, equipment, and software needed to develop an online financial application. We will also analyze the technical feasibility of the project and explore potential challenges and constraints that need to be considered. The purpose of this analysis is to provide a comprehensive overview of the proposed online financial application and lay the foundations for its successful development and implementation.

Technology Used
When developing a financial web application, it is essential to use technologies that ensure security and reliability. The programming languages that will be used in the development of this application are: Angular for frontend and .NET for backend. These programming languages are compatible and have strong community support, which will ensure that the application is developed and maintained effectively [11] [12].
In addition to programming languages, the database used in the application will also play a decisive role in its success. For this online financial application, MSSQL will be used as the database management system. MSSQL is known for its reliability and scalability, which are essential for a financial application [13]. With this stack of technology, the financial web application will be developed to provide a secure, reliable and efficient platform for users to manage their finances.

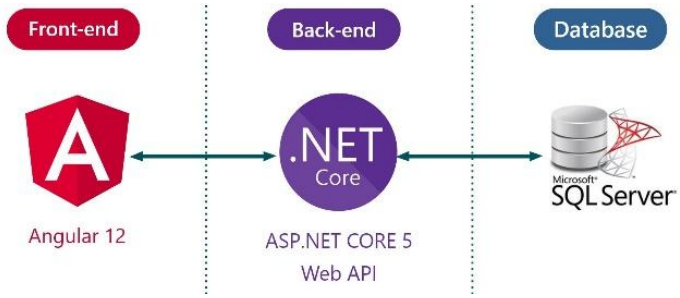

Figure 1. The technology used

User Interface (UI)
The user interface (UI) is the front end of the application that allows users to interact with the tool. It includes the design, layout and functionality of websites or mobile applications. Angular technology provides a powerful and flexible environment for creating dynamic and responsive interfaces that improve the user experience [11].

System Architecture
The system architecture of a web application defines how its components interact with each other. A well-designed architecture ensures that the web application is scalable, secure and reliable.
• Application Server: The application server is the back end of the application that handles the business logic and interacts with the database. It is responsible for processing user requests, managing user accounts and generating reports.
• Database Server: The database server stores and retrieves data from the application. It is responsible for storing project information, user data and other related information.
• Collaboration tools: Collaboration tools enable team members to work together and share project-related information. These tools include messaging systems, document sharing, and file storage.
• Task management: The task management component allows users to create and assign tasks, set deadlines and track progress. It includes features such as to-do lists, calendars and progress trackers.
• Reporting and analytics: The reporting and analytics component provides users with insights into project performance, team productivity, and other important metrics. It includes features such as dashboards, dashboards and custom reports.

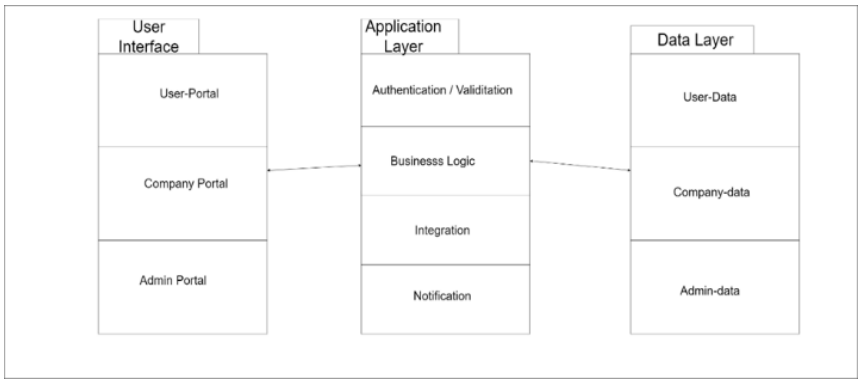

Figure 2. System architecture structure

Integrated Systems
Embedded systems are used to improve the functionality and performance of the web application. The following embedded systems can be used for an online financial application:
1. Authentication and authorization: For user authentication and authorization, external services such as Google API Login, Facebook Login or OAuth2 [15] can be used. These services allow users to authenticate with your web application using their existing social media accounts or email accounts.
2. Syncfusion: Syncfusion provides modern and user-friendly graphs and charts for real-time data visualization and reporting. Syncfusion's suite of more than 1,600 components and frameworks for .NET, JavaScript, Angular, React, Vue, and Xamarin development helps build these features quickly and easily, saving time and money [14].

Figura 3. System syncfusion

Technical Feasibility Analysis and Project Risk

Technical Feasibility

The project involves the development of a financial web application that requires the integration of several technologies, including web development frameworks, database systems, and third-party APIs. The technical feasibility of the project depends on several factors, including:

1. Availability of skilled resources: The development team must have access to skilled resources with expertise in the required technologies. If qualified resources are not available, the technical feasibility of the project may be at risk.
2. Compatibility of technologies: The technologies used in the project must be compatible with each other. Compatibility issues can arise during integration, leading to delays and technical issues.
3. Infrastructure: The project requires adequate infrastructure, such as servers, networking and storage, to host the application. The availability and cost of such infrastructure may affect the feasibility of the project.
4. Third Party API Availability: The project relies on third party APIs for functions such as email notifications and SMS reminders. The availability and reliability of these APIs can affect the feasibility of the project.

Technical Risks

Web application development for scheduling and booking carries several technical risks that must be managed to ensure its successful completion. Some of the main risks associated with the project include:

1. Security: The application includes sensitive user data and must be designed with strong security measures to prevent unauthorized access, data breaches and other security threats.
2. Scalability: The application should be able to handle a large number of users and transactions. Therefore, the architecture should be designed to scale horizontally or vertically as traffic increases.
3. Reliability: The application should be available 24/7 and should be able to handle failures gracefully. Therefore, the application should be designed with fault-tolerant architecture and backup systems.
4. Integration Challenges: Integrating the various technologies required for the project can be challenging and the development team must have the necessary expertise to manage this process.
5. User Experience: The success of the application depends on the user experience and the development team must ensure that the application is intuitive and easy to use.

In general, the technical feasibility and riskiness of the project depend on several factors, including the availability of qualified resources, the compatibility of technologies, the availability of infrastructure and the reliability of third-party APIs. The risks associated with the project must be managed to ensure its successful completion.

5.3 Definition of Product Backlog & User Stories

Table 1. Product Backlog Table for Cash Control System

Product Backlog Table for Cash Control System					
ID	LIKE A..	I WANT...	THAT...	**PRIORITETI**	**SPRINT**
		EPIC 1 - User Registration			
US01.	USERS	to register in the system	to have access to the system through the profile.	Must Have	1
US02.	USERS	login to the system	to have access to the system through the profile.	Must Have	1
US03.	USERS	a secure identification system	allows me to access the info. needed safely.	Must Have	1
US04.	USERS	change my credentials	(if) I forgot them.	Must Have	1
		EPIC 2 - Management by Administrator			
US05.	Administrator	delete a user's data	not be accessible if the user no longer uses the system.	Must Have	1
US06.	Administrator	change user data	manage user requests as desired.	Must Have	1
US07.	Administrator	to give access to the client	to be able to ensure proper access and control over the system.	Must Have	1
		EPIC 3 – Implementimi i Live Chat			
US08.	USERS	use a live chat service	to communicate with the customer support department.	Should Have	2
US09.	USERS	to have 24/7 access	to chat with customer service whenever necessary.	Should Have	2

		EPIC 4 - Cost Management			
US10.	USERS	track my expenses	to be able to monitor my spending habits and stay within my budget.	Must Have	1
US11.	USERS	to categorize my expenses	see where my money is going.	Must Have	1
US12.	USERS	create a savings plan and track my progress toward my savings goals	reach my financial goals.	Must Have	1
		EPIC 5 - Product Management			
US13.	Company Owner	be able to add info. about my products in the system	potential customers to see and buy them.	Must Have	1
US14.	Company Owner	be able to track the quantity sold and remaining inventory of products mine	to be able to effectively manage my stock levels	Must Have	1
US15.	Company Owner	estimate the profits I will make based on my sales and expenses	make informed business decisions.	Could Have	2
		EPIC 6 - Reporting and Analysis			
US16.	USERS	create personalized reports for my financial activity	better understand my financial situation.	Must Have	1

US17.	Company Owner	create financial statements for my business	be able to keep track of my finances for tax and reporting purposes.	Should Have	2
		EPIC 7 - Interface (UI)			
US18.	USERS	system to have an easy-to-use interface	to be able to easily navigate to the relevant parts.	Must Have	1
US19.	USERS	view recent transactions on the main page of the system	to check the financial situation quickly.	Must Have	1

5.4 3C Analysis

3C analysis focuses on three main components that help develop successful strategies: Company, Competition and Customers. Using this analysis, we can identify the strengths and weaknesses of our company, the opportunities and threats from the competition, as well as the needs and desires of our customers. [16]

Company
In this project, the company aims to provide a platform that allows users to manage passwords, request support through a live chat service, categorize and track expenses, and manage product and transaction data. The use of such a platform helps the company to improve its service offering and increase efficiency in the management of user data.

Competition
Our competitors also offer similar services, but by analyzing User Stories and our users' requests, we have the opportunity to differentiate ourselves by offering additional features such as password change confirmation emails, 24/7 live chat, and detailed expense reports. This allows us to create a competitive advantage by providing an improved user experience.

Customers
To meet the needs of consumers, our platform is built to address their specific requirements, identified through User Stories. This includes the ability to change passwords, request fast and efficient support, manage expenses and generate financial reports, as well as inventory tracking for vendors. This helps us ensure that our platform is tailored to the real needs of our users.

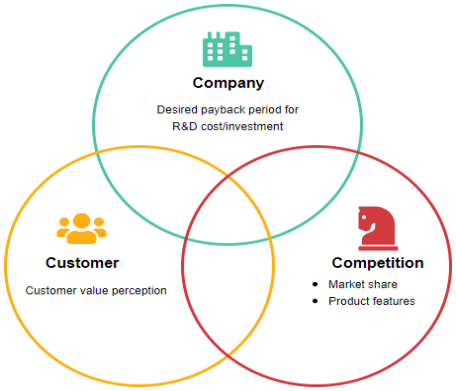

Figure 4. 3C Analysis

User Story
US04: Change Password
Card: I, as a user, want to change my password after registering.
Conversation:
• Q: Should we make it possible for you to accept confirmation when changing your password?
• A: Yes, I want to receive a confirmation email when changing my password.
• Q: Is it necessary to have a limit after changing the password?
• A: Yes, after changing the password the old password must not be set again and the new password must not be changed for 48 hours.
Confirmation: After registration, the user will have the possibility to change the password which will be confirmed by email, and will not be able to change it after a certain time. Also, he won't be able to use a password he's used before.

US05: Deletion of User Data
Card: As an administrator I want to be able to delete a user's data. Conversation:
• Q: What kind of data do you want to delete for a user?
• A: I want to be able to delete all data associated with a user account, such as their personal information, login credentials, purchase history, and any other data associated with their account.
• Q: Do you want to be able to delete data for all users or only specific users?
• A: I want to be able to delete data for specific users.
Confirmation: The administrative solution allows the administrator to delete all data associated with a specific user account, including personal information, login credentials, purchase history and any other data associated with his account.
US08 & US09: Support via Live Chat
Card: I, as a user, would like to request support, help or information from a business or organization via a live chat service platform. Conversation:
• Q: When would you like to have the live chat service available?

• A: I want it to be accessible 24/7.
• Q: What questions should be available to the customer?
• A: I want to include a list of basic questions and a list of frequently asked questions.
Confirmation: User requests support, help or information from a business or organization via live chat 24/7. The user may have questions, concerns, or issues they need help with, and the customer service representative provides real-time support to address their needs.

US12: Expense Tracking and Report Generation
Card: As an individual user, I want to track my expenses and generate reports to understand my financial position and make informed decisions.
Conversation:
• Q: How often do you want to track your expenses?
• A: I would like to track my expenses on a weekly basis.
• Q: What types of reports would be most useful to you?
• A: I would like to generate reports that show me my spending habits and trends over time.
Confirmation: The platform allows users to track their spending on a weekly basis and generates customizable reports that show spending habits and trends over time, helping users understand their financial position and make informed decisions.

US13: Categorization of Expenses
Card: As a user, I want to categorize my expenses to see where my money is going.
Conversation:
• Q: Which categories are most important to you?
• A: The most important are the food category, utilities (water, electricity, etc.), debts, entertainment and the health category.
• Q: How often do you review your expenses?
• A: I review them every month.
Confirmation: The user can categorize their expenses into different lists and view and analyze expenses by category, allowing them to see where their money is going. Also, the user can review their expenses on a monthly basis and access the expenses for the previous month.

US16: Product Information Management
Card: As a product manager, I want to be able to add information about my products to the system so I can keep track of their data and manage it efficiently.
Conversation:
• Q: What kind of information should you add about your products?
• A: I need to add the product name, description, SKU, price, weight and any other relevant details.
• Q: Do you need to add different variations of the same product?
• A: Yes, I need to add different variations, such as different sizes, colors and styles for each product.
Confirmation: The product management solution allows the product manager to add information about each product to the system, including the product name, description, SKU, price, weight and any other relevant details. The product manager can also add different variations of each product, such as different sizes, colors and styles.

US17: Track Sold Quantity and Inventory
Card: As a seller, I want to track the sold quantity and remaining inventory of my products so that I can manage my inventory and avoid overselling.
Conversation:
• Q: How do you currently track your inventory?
• A: I currently keep track of my inventory in a spreadsheet and manually update it when a product sells.
• Q: How often do you update your inventory data?
• A: I update my inventory data after every sale.
• Q: How do you know when to refill your products?
• A: I usually restock my products when the remaining inventory reaches a certain threshold.
Confirmation: The inventory tracking solution allows the seller to track the quantity sold and the remaining inventory of their products. The seller can easily update the sold quantity and remaining inventory of each product after each sale, allowing them to avoid overselling and replenish their products when necessary.

US19: Viewing Past Transactions
Card: As a user I want to be able to view past transactions.
Conversation:
• Q: What kind of previous transactions do you want to view?
• A: I want to view all transactions I've made in the past, including purchases, refunds, and cancellations.
• Q: How far back would you like to be able to view your past transactions?

• A: I want to be able to see all my past transactions, starting with the first one I made on the platform.
Confirmation: The platform will have a "Transaction History" section where users can view all their past transactions, including purchases, refunds and cancellations.

5.5 Functional and Non-functional Requirements

No	Functional Requirements	Non-Functional Requirements
1	Access from Multiple Devices	Identification Security
2	Custom Reports and Analytics	Compatibility with Multiple Devices
3	Generation of Financial Statements	Easy To Use Interface
4	Data Security	Compliance with Data Privacy Regulations
5	Compliance with Regulations	Handling a Large Number of Users
6	Informed Decisions	Availability 24/7
7	Customer Support and Service	Scalability
8	Addressing Questions and Concerns	Customizability
9	Reliable Financial Management	Flexibility
10	Friendly User Interface	User Tutorial
11	Paneli (Dashboard)	Ease of Maintenance and Updates
12	Categorization of Expenses	Fulfillment of Technical and Business Specific Requirements
13	Budget Management	High Performance
14	Revenue Tracking	Protection from Hacker Attacks
15	Investment Tracking	Customizable User Interface
16	Savings Tracking	Big Data Processing
17	Generation of Tax Reports	User Experience
18	Generating Reports for Lenders and Investors	Action History
19	Generation of Financial Reports	Interoperation with Other Applications
20	Search function	Technical Support
21	Importing Financial Data	Efficiency at Work
22	Export of Financial Data	Endurance
23	Password Recovery	
24	Two Factor Authentication	
25	Managing Roles and Permissions Users	
26	Account Management	
27	User Analytics	
28	User Profile Management	
29	Modification of Personal and Financial Information	
30	Deleting a User Account	
31	Customizing the Dashboard	
32	Tools for the Analysis of Financial Statements	
33	Customization of Product and Price Lists	
34	Insurance Recommendations	
35	Integration of Bank Accounts and Credit Cards	
36	Statement of Expenses and Income	
37	Setting Financial Goals	
38	Management of Payments and Invoices	

39	Categorization of Transactions	
40	Creation and Management of Personalized Financial Reports	
41	Budgeting for Different Categories of Expenses	
42	Creating and Pursuing Financial Goals	
43	Investment Performance Reports	
44	Signals for Financial Events	
45	Dashboard and Interface Customization	
46	Reminders for Financial Events	
47	General Registry of Transactions	
48	Tracking of Sources of Income	
49	Creating and Tracking Invoices	

Table 2. Functional and non-functional requirements

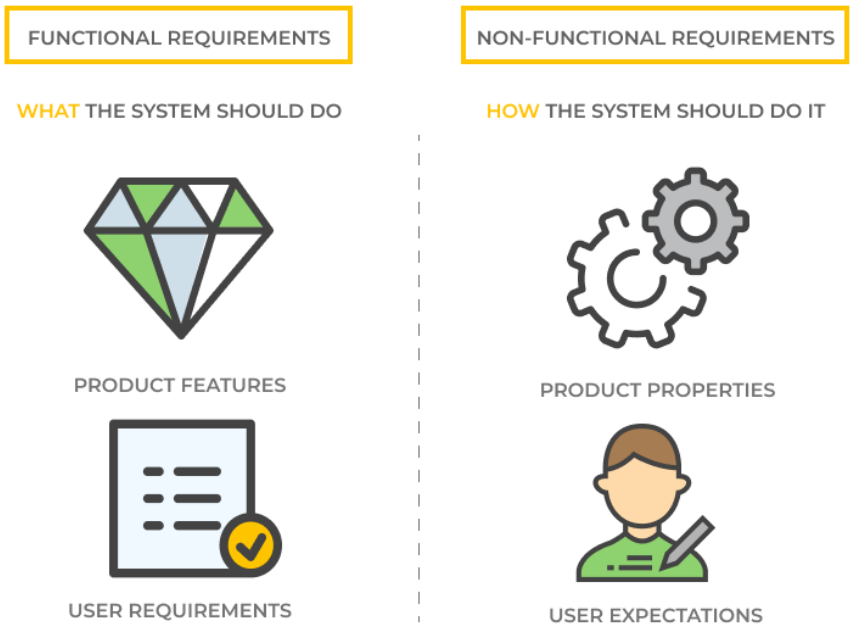

Figure 5. Difference between functional and non-functional requirements

6. SYSTEM DESIGN AND ARCHITECTURE

6.1 GUI designs

Defining user interface requirements

Defining user interface requirements is the initial step in the GUI design process and involves gathering and documenting the functional and non-functional requirements that the interface must meet. These requirements may include:

• Functional requirements: The functionalities that the interface should provide, such as buttons, menus, forms, and user interactions with the application.

• Non-functional requirements: Quality aspects of the interface, such as speed of response, aesthetic design, and consistency in use.

Interface sketching and prototyping

Sketching and prototyping are important stages to visualize and test the interface design before full implementation. [17]

• Sketching: Creating simple and quick drawings to present initial design ideas. Sketches can be created by hand or using digital tools.

• Prototyping: Creating more detailed and interactive interface models using tools like Figma, Adobe XD, or Sketch. Prototypes help test usability and identify potential problems before implementation.

User Interface Design Link: Figma Prototype

Usability and Accessibility Guidelines
Usability and accessibility guidelines ensure that the interface is easy to use by all users, including those with disabilities.
• Usability: Ensuring that the interface is intuitive, easy to learn and efficient to perform user tasks. Instructions include:
o Consistency in design and navigation
o Quick response of the interface to user actions
o Providing guidance and assistance to users at every step
• Accessibility: Ensuring that the interface is accessible to users with disabilities. Instructions include:
o Using high-contrast colors for text and visual elements
o Use of alternative texts for images and graphics
o Ensuring that the interface is navigable via keyboard and provides support for screen readers.

6.2 System Architecture Conceptual Design

Description of the Main System Components
The system architecture consists of several main components that cooperate to provide the necessary functionalities of a financial application. These components are:
1. Client-Side (UI): This component is responsible for handling the user interface, displaying data and interacting with the user. The technology used to develop this component is Angular. The main modules include:
o User Interface
o Product Management
o Financial Reports
o Dashboard visualization (using Syncfusion) [14]
2. Server-Side (Application Layer): This component handles data processing and business logic. It is developed using .NET technology and consists of modules such as:
o Product Management
o Categorization of Expenses
o Profit Estimation
o Data Analytics
3. Database (Database Layer): This component is responsible for storing and retrieving data, using MySQL for database management. The preceding tables include:
o User Information
o Product Data
o Financial Reports
o Categorization and Expenditure Data

Relationships between Components
The various components of the system interact in a synchronized manner to ensure the full functionality of the financial application. Below are some of the main links between them:
• Client-Side and Server-Side: The user interface (UI) on the client-side (client-side) communicates with the business logic and data processing on the server-side (server-side) through API calls.
• Server-Side and Database: The server-side interacts directly with the database to store and retrieve the necessary data.
• Database and Client-Side: The data obtained from the database (database) is displayed in the user interface (UI) through the server-side.

Architectural Patterns and Styles Used
For the development of this system, several architectural models and styles have been used to ensure a clear and manageable structure:
1. MVC (Model-View-Controller) pattern: This pattern helps to divide responsibilities between business logic, user interface and data processing.
2. RESTful API: For communication between the client side and the server, a RESTful API is used, which provides a standardized and efficient way to exchange data.
3. Microservices: Some system modules are developed as independent microservices to provide scalability and easier code maintenance.[12]

To illustrate the conceptual design of the system architecture, a table is attached below that describes the main components and the relationships between them.

Table 2. System Architecture Conceptual Design

Component	Responsibility	Tools/Frameworks	Modules/Tables
Client-Side	Handles user interface, displays data, and interacts with user	Angular	UI, Product Management, Financial Reports,
			Session Management, Product Management
Server-Side	Handles data processing and logic	.NET	Product Management, Expense Categorization, Profit Estimation, Data Analytics, User Authentication, Authorization,
			Product Inventory, Sales Tracking, Expense Categorization, Profit Estimation, Data Analytics
Database	Stores and retrieves data	MySQL	User Information, Product Information, Financial Reports, Expense Categorization Data
			Product Inventory, Generated Financial Reports, Expense Categorization Data

6.3 Designing Modules

Identification and Description of Main Modules

The main modules of this system include:

• User Management: Related to the Security module to ensure the privacy and security of user data. Uses encryption and other security measures to protect sensitive user data.

• Product Management: Related to User Management and Security for similar reasons, as well as to provide data encryption and access control policies.

• Expense Tracking: Linked to user management and revenue monitoring modules to categorize and track expenses. It relies on user and revenue data.

• Income Tracking: Linked to the Expense Tracking and User Management modules to categorize and track income. It relies on user and spending data.

Interaction between Modules

The modules cooperate in a synchronized manner to ensure the full functionality of the system. Below are some of the main links between them:

• User Management and Security: Uses encryption and other security measures to protect user data.

• Product Management and User Management: Related to ensure that product data is protected and controlled.

• Expense Tracking and Income Tracking: Linked to ensure that expense and income data are categorized and tracked accurately.

Implementation and Sharing of Responsibilities

Each module has clear and separate responsibilities to ensure the full functionality of the system. For example:

• User Management: Handles user management and authentication.

• Product Management: Handles product management and inventory tracking.

• Expense Tracking: Handles the categorization and tracking of expenses.

• Income Tracking: Handles income categorization and tracking.

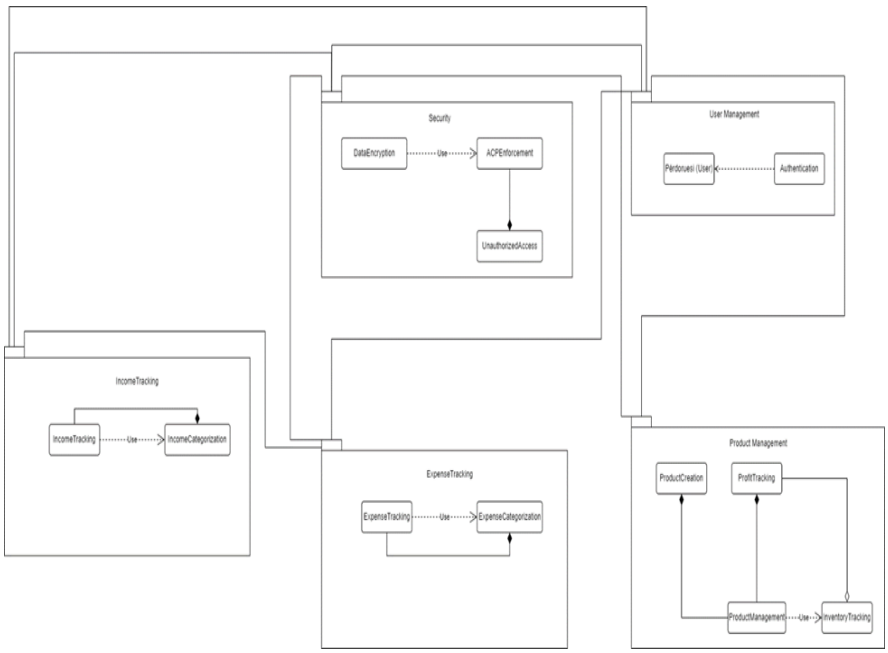

Figure 6. Diagram of Modules

6.4 Designing Classes

Description of System Classes and Objects

A class diagram represents the structure of the system by showing the main classes and objects, their attributes and methods, and the relationships between them.

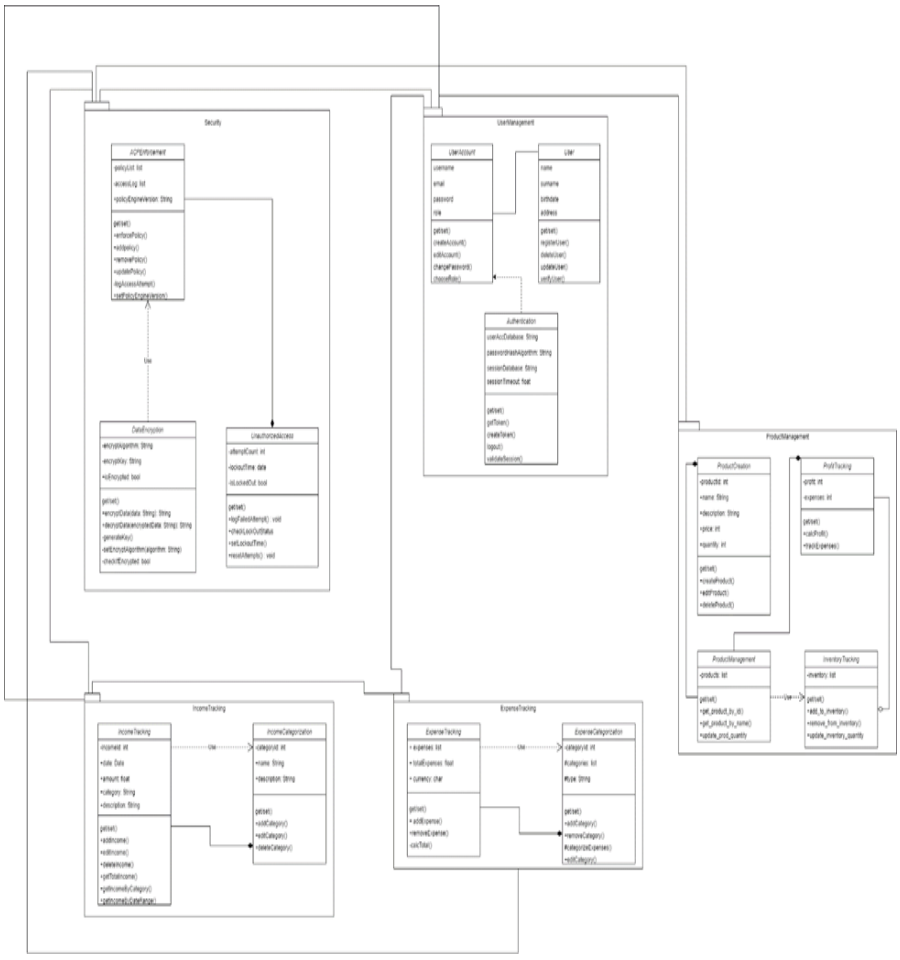

Figure 7. Class Diagram

Relationships and Dependencies Between Classes
The classes are linked together to provide a clear and manageable system structure. Some of the key links include:
• User Management and Security: Ensures the privacy and security of user data.
• Product Management and User Management: Ensures product data protection.
• Expense Tracking and Income Tracking: Provides accurate categorization and tracking of expenses and income.

Main Attributes and Methods for Each Class
• User: name, surname, email, address, methods getUser(), addUser(), deleteUser().
• Product: name, description, quantity, getProduct(), addProduct(), deleteProduct() methods.
• IncomeTracking: amount, date, category, addIncome(), getIncome() methods.
• ExpenseTracking: amount, date, category, addExpense(), getExpense() methods.
• Security: encryptData(), decryptData(), checkAccess().

6.5 Database Design

Conceptual and logical models of the database
Database design is an essential component in the development of an information system. Conceptual and logical models are two different phases of design that help structure data consistently and efficiently.

Conceptual Model
The conceptual model represents the logical structure of the data at a high level of abstraction, without technical concerns or implementation details. This model focuses on defining large entities (entities) and the relationships between them. An entity-relationship diagram (ERD) is a common tool for creating conceptual models.
In the attached diagram, the main entities are Products, User, Transaction, Category, Company, and Roles. These entities are linked in various ways to represent the relationships between them, as can be seen in the ERD diagram.

The Logical Model
The logic model includes the technical details and is an extension of the conceptual model. This model specifies the exact structure of the data, including fields, data types, and complex database connections.
In the attached diagram, each entity has its own clearly defined fields. For example, the Products entity has the fields Product ID, Name, Quantity, Remaining, and Description.

Data schema normalization and optimization
Normalization
Normalization is a process for partitioning tables in order to minimize data redundancy and improve data integrity. The normalization process goes through several normal forms (NF), each eliminating different types of redundancy.
• 1NF: Each field in a table must contain only a single value (be atomic).
• 2NF: All non-prime attributes must be fully dependent on the primary key.
• 3NF: All non-prime attributes must depend only on the primary key, and not on any other non-prime attributes.

Optimization
Data schema optimization includes techniques to improve query performance and data integrity. This includes creating indexes, using partial normalization when needed to improve query speed, and designing schemas to reduce unnecessary joins.

Definition of tables, relationships and data integrity
Tables and Links
Tables are defined for each logical model entity. Each table has specific fields that represent the attributes of the corresponding entity. For example:
• Products table contains the fields Product ID, Name, Quantity, Remaining, Description.
• User table contains fields User ID, Email, Password, Name, Surname.
Relationships between tables are represented through foreign keys. For example, the User table has a link to Company through the Company ID.

Data Integrity
Data integrity is ensured through primary keys, foreign keys, and other constraints. Primary keys uniquely identify each row in a table, while foreign keys link tables and ensure that references between tables are correct.
Referential integrity ensures that each foreign key corresponds to an existing primary key in the linked table. For example, the Company ID in User must correspond to a valid Company ID in Company.

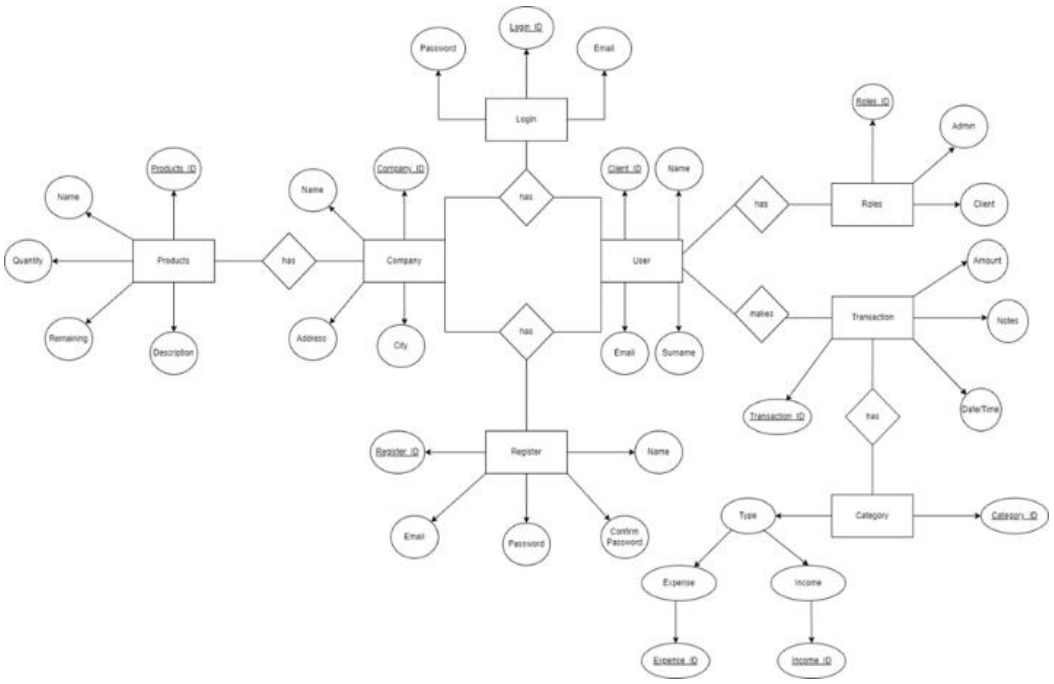

Figure 8. Database diagram

7. CONCLUSIONS

In conclusion, the development and implementation of the financial web application for budget and expense management has shown that modern technology can provide efficient and comprehensive solutions to financial management challenges. During this project, we managed to create a powerful platform, which not only addresses the current needs of users, but also creates a solid foundation for future improvements and extensions.

This project has demonstrated the importance of designing a usable and accessible interface for various users, including individuals and companies. The user interface built with Angular has ensured a smooth and integrated experience for users, while the server and database layers have provided a scalable and reliable performance for data processing and business logic.

In addition, the focus on security and data privacy is one of the app's strongest points. The use of advanced encryption technologies and security measures has ensured that user data remains secure and protected from any type of unauthorized access. This is a critical feature, given the sensitivity of financial information and the need to gain user trust.

Another important aspect of this project is the integration of data analytics to provide personalized recommendations and insights to users. These analyzes help users make more informed decisions and optimize the management of their finances, making the app an indispensable tool in everyday financial life.

In conclusion, this project has achieved its main objectives and has provided a powerful tool for financial management. It represents a significant advance in the field of financial applications, creating a strong foundation for future innovations. The application not only fulfills the needs of current users, but also shows the potential to be a leading solution in the future of financial management. As technologies and user needs evolve, this application will continue to improve and expand to meet new challenges that will arise.

REFERENCES

Fisher, J. & Lay, P. (2018). "Impact of Mobile Financial Applications on Personal Financial Management". Journal of Financial Management, 24(2), 123-136.

Riquelme, H. & Rios, R. (2019). "The Role of Technology in Business Financial Management". Small Business Economics, 36(4), 411-425.

Chen, S., Davis, T. & Wang, J. (2020). "User Interface Design and Its Impact on Financial Application Efficiency". International Journal of Human-Computer Studies, 142, 102456.

Kapoor, K. & Gunta, S. (2021). "Data Security and Privacy in Financial Applications". Cybersecurity Journal, 8(1), 78-89.

Brown, A. & Black, E. (2022). "Financial Education Through Mobile Applications: A New Paradigm". Journal of Financial Education, 15(3), 215-230.

Suryadevara, R., & Babu, G. (2020). "Personalized Financial Recommendations Using AI and Machine Learning". Journal of Financial Technology, 12(1), 89-103.

Kaczorowski, R., Lee, M., & Jackson, P. (2021). "Impact of Financial Apps on Financial Control and Stress Reduction". Journal of Behavioral Finance, 14(2), 112-127.

Johansson, K., & Olsson, M. (2021). "Financial Applications and Strategic Decision Making in Businesses". Strategic Management Journal, 32(3), 233-248.

Doe, J. (2020). Financial Management in the Digital Age. New York: Tech Press.

Johnson, K. (2021). Best Practices in Financial Technology. London: FinTech Publishers.

Angular Official Documentation, "Introduction to Angular," Angular.io

Microsoft .NET Documentation, "Introduction to .NET," Microsoft Docs

Microsoft SQL Server: https://docs.microsoft.com/en-us/sql/sql-server/

[Synchorus, "Syncfusion Dashboard Visualization," .NET, Xamarin, JavaScript, Angular UI components | Syncfusion

OAuth 2.0 Authorization Framework: https://oauth.net/2/

Kenichi Ohmae, "The Mind of the Strategist: The Art of Japanese Business", 1982.

User Interface Design Principles: https://www.interaction-design.org/literature/topics/ui-design.

Optimization and Characterization of Niaouli/Lavender Essential Oil Loaded Microcapsules

HÜLYA KESICI[*1], FUNDA CENGIZ ÇALLIOĞLU[1]

Abstract: In this study, it was aimed at the optimization and characterization of lavender essential oil (LEO) and niaouli essential oil (NEO) loaded microcapsules via the emulsion/solvent evaporation method. For this purpose, optimization studies were carried out between both the process parameters, such as stirring time and stirring speed, and the structure of the microcapsules, such as surfactant concentration, solvent ratio, and oil:polymer ratio, in terms of the most uniform microcapsule morphology obtained. For the production of microcapsules by the emulsion/solvent evaporation method, polyvinyl alcohol (PVA) and Eudragit RS 100 were used as shell polymers, chloroform and distilled water (DI water) as solvents, LEO and NEO as core materials, and Span20 as a surfactant. In the characterization studies, images were taken by scanning electron microscopy (SEM) to observe and determine the morphology of the microcapsules. Fourier Transform Infrared Spectroscopy (FT-IR) analysis was performed to determine the presence of core materials in the structure of the microcapsules. According to the results, while sticky structures were observed at low stirring speeds, fractures and cracks occurred in the microcapsules at high speeds. Similarly, as the stirring time decreased, the solvent could not evaporate, and uniform microcapsules could not be produced. Moreover, microcapsules were unable to be produced because the equilibrium in the emulsion was disturbed as the amount of surfactant increased. As the solvent concentration decreased, microcapsule shape was not possible. The drug-polymer ratio was found to be highly effective in morphology.

Keywords: Lavender Essential Oil, Niaouli Oil, Microencapsulation, Emulsion/solvent evaporation.

[1]**Address:** Süleyman Demirel University, Faculty of Engineering and Natural Sciences, Isparta/Turkiye

***Corresponding author**: kesicihulya@gmail.com

1. INTRODUCTION

It is widely acknowledged that sleep disturbances are a significant health and public health problem that has an impact on the physical, mental, and emotional well-being of individuals throughout the world. The inhalation of essential oils may serve as a safe alternative to pharmaceutical treatments for mild to severe sleep disorders (Lillehei and Halcon, 2014). Essential oils are fragrant substances derived from various parts of medicinal and aromatic plants (Hammer et al., 1999; Bakkali et al., 2008; Zhang et al., 2017). The lavender essential oil utilized in this study possesses antiseptic, antibacterial, sedative, tranquilizing, antioxidant, and relaxing characteristics therefore being applicable in perfumery, pharmacology, medicine, and particularly aromatherapy (Lis-Balchin et al., 1999; Cavangh et al., 2002; Hui et al., 2010). The efficacy of NEO in cosmetics and dermatology is well documented and often shows good synergistic effects in skin care formulations (Rakotondrazafy et al., 2023). In addition to its antibacterial and antiviral effects, it was used in this study because it increases transdermal penetration and facilitates the transition to sleep (Sang-Yun et al., 2008; Steflitsch and Steflitsch 2008; Yıldırım et al., 2025).

Eudragit RS 100 is a water-insoluble, biocompatible, inexpensive, and highly effective polymer that is frequently used as a wall material in extended-release microcapsules. It has a low permeability, which makes it useful for drug release. Moreover, Eudragit RS 100 is a user-friendly and readily processable polymer available in several forms, including aqueous dispersions, granules, organic solutions, powders, or pre-formulated powders (Bolourchian and Bahjat, 2019). The emulsion/solvent evaporation technique is the predominant method utilized for the microencapsulation of water-insoluble components. Moreover, the impermeability and structural integrity of oil-loaded microcapsules post-production enhance the benefits of this technique. The system does not require an addition, as the solvent can be quickly evaporated by itself, heat, or mixing during production, thereby simplifying and expediting the production process (Hong et al., 2005; Heiskanen et al., 2012).

The objective of the present study was to produce and characterize microcapsules that were loaded with LEO and NEO through the emulsion/solvent evaporation method.

2. MATERIAL AND METHOD

2.1. Materials

Eudragit ® RS 100 (Evonik Röhm GmbH) and Polyvinyl alcohol (Mn=88,000, 88% hydrolyzed) were used as shell materials. LEO and NEO (Botalife, Isparta, Turkey) were used as core materials. Chloroform (Sigma-Aldrich Corporation (St. Louis, MO, USA)) and distilled water were used as solvents.

2.2 Methods

A solvent/evaporation method was used to generate microcapsules. Initially, the oil phase and water phase were prepared to create an emulsion for microcapsule production. The Eudragit RS 100 polymer was solubilized in chloroform in order to generate an oil phase. The core ingredient LEO and NEO was then added. Concurrently, the watery phase was obtained by stirring PVA and the surfactant with distilled water in a high-speed mixer. Finally, washing, filtering, and drying processes were carried out. Table 1 presents microcapsules produced using different process parameters, compositions, and sample codes.

Table 1. Microcapsules codes, contents and process parameters

Sample Codes	Stirring Speed (rpm)	Stirring Time (h)	Surfactant (g)	Drug:Polymer Ratio	PVA Content (g)
M1	300	1	0.1	1:10	1
M2	300	3	0.1	1:10	1
M3	300	5	0.1	1:10	1
M4	100	3	0.1	1:10	1
M5	500	3	0.1	1:10	1
M6	300	3	0.5	1:10	1
M7	300	3	0.1	1:1	1
M8	300	3	0.1	1:10	-

3. RESULTS

Microcapsule production was achieved using the emulsion/solvent evaporation method. SEM images of NEO and LEO-loaded Eudragit RS 100-based microcapsules are shown in Figure 1, in order to understand the effect of process parameters on morphology. Figure 1 shows SEM images of the effect of production time.

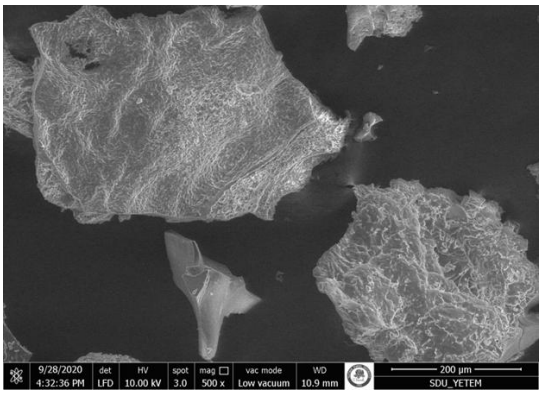

1 hour

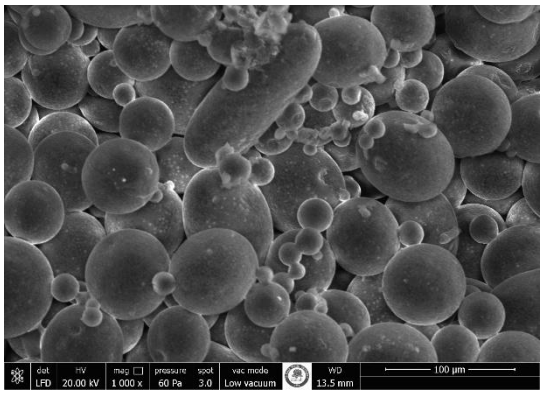

3 hours

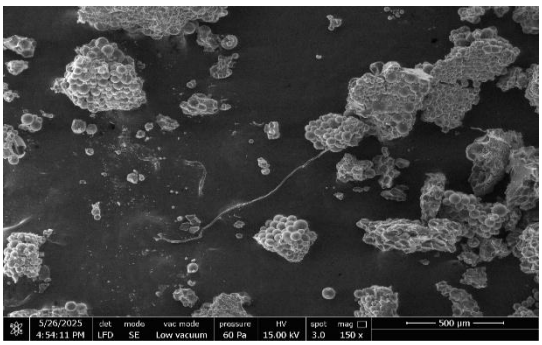

5 hours

Figure 1. SEM images of microcapsules with different production times

When Figure 1 is analyzed, it is clearly seen that microcapsule formation did not occur in 1 hour of production. At 5 hours of production, both the difference in the size of the microcapsules was noticeable and agglomeration occurred. However, it can be said that the microcapsules were spherical, homogeneous, uniform and smooth at 3 hours of production time. SEM images illustrating the effect of stirring speed are given in Figure 2.

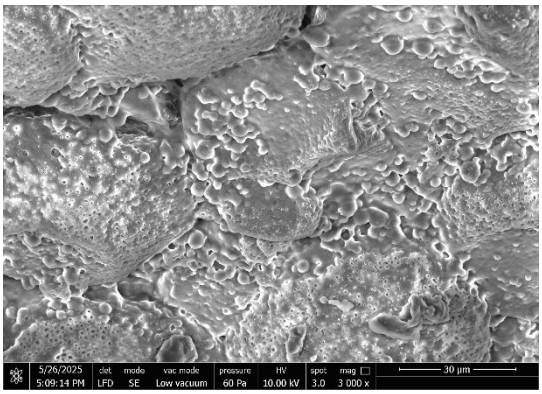

100 rpm

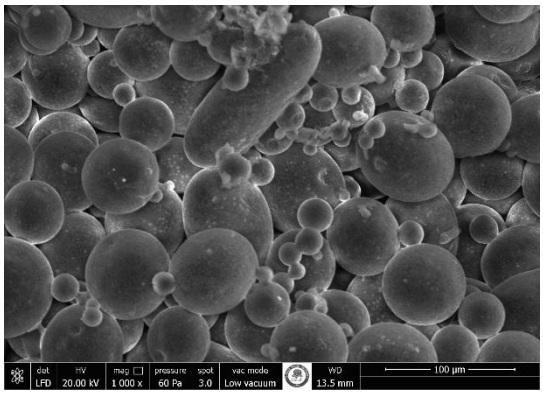

300 rpm

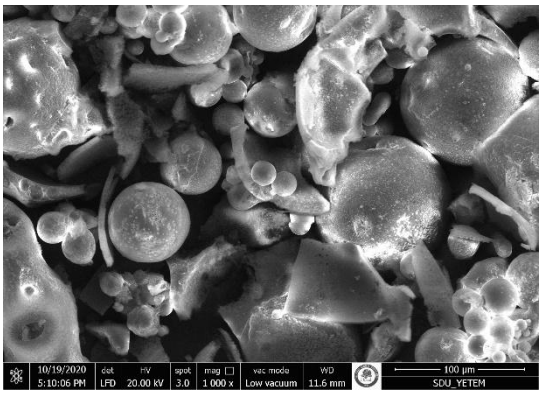

500 rpm

Figure 2. SEM images of microcapsules with different stirring speeds

As seen in Figure 2, microcapsule formation could not be realized at low stirring speed (100 rpm). At high stirring speed (500 rpm), it was observed that fractures occurred in the structure of microcapsules. Therefore, the optimum stirring speed was determined as 300 rpm. Figure 3 shows SEM images illustrating the effect of surfactant amount on microcapsule morphology.

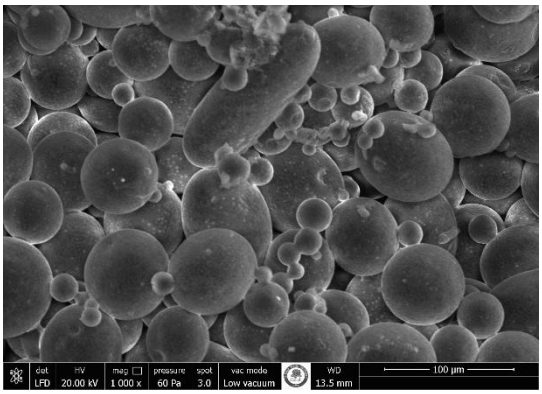

0.1 gram

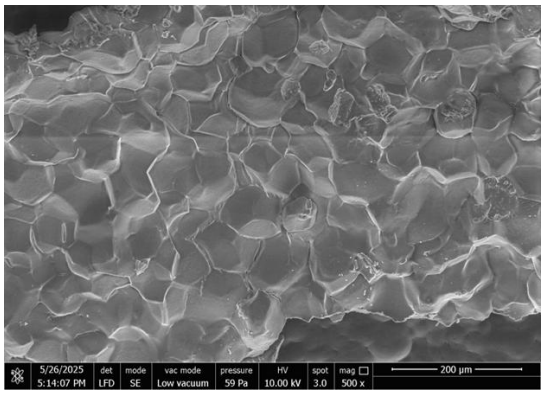

0.5 gram

Figure 3. SEM images of microcapsules with different surfactant concentrations

One of the most important success criteria in emulsion/solvent evaporation is to prepare stable emulsions. The amount of surfactant plays an important role in the preparation of stable emulsions. Therefore, in this step of the study, the effect of the amount of surfactant was investigated. As clearly seen in the SEM images, both circular and granular microcapsule structure could not be obtained because a stable emulsion could not be formed when 0.5 grams of surfactant was used. Another success criterion for emulsion/solvent evaporation is the ratio of the amount of core and shell material to each other. Figure 4 shows SEM images of microcapsules containing different ratios of core and shell material.

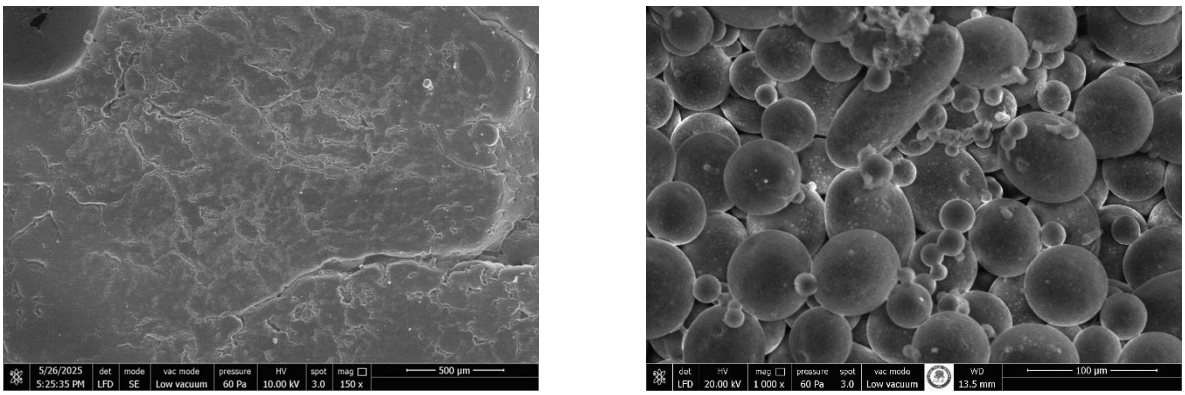

1:1 1:10

Figure 4. SEM images of microcapsules with different core:shell ratios

When both SEM images above were analysed, it was determined that the amount of polymer was insufficient for microcapsule formation at a 1:1 ratio and a stable emulsion could not be formed using this ratio. At last, the effect of the presence of PVA polymer in the shell structure on morphology was investigated (Figure 5).

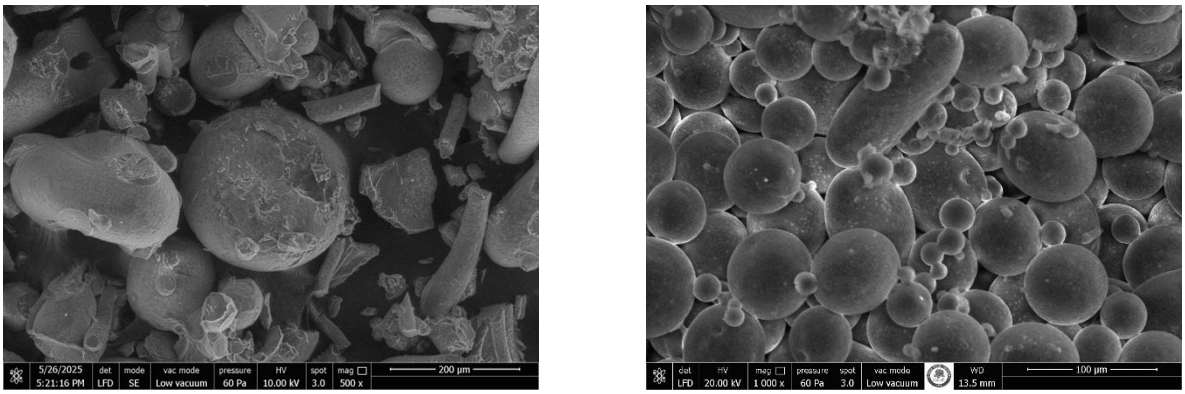

Without PVA With PVA

Figure 5. SEM images of microcapsules with and without PVA

When the images were analysed, it was clearly demonstrated that PVA polymer contributed highly to microcapsule formation and morphology when used in combination with Eudragit RS 100 polymer.

FT-IR analysis was performed to chemically verify the presence of components in the core and shell structure of the microcapsules and to demonstrate that no undesired chemical reactions occurred between the components during emulsion preparation (Figure 6).

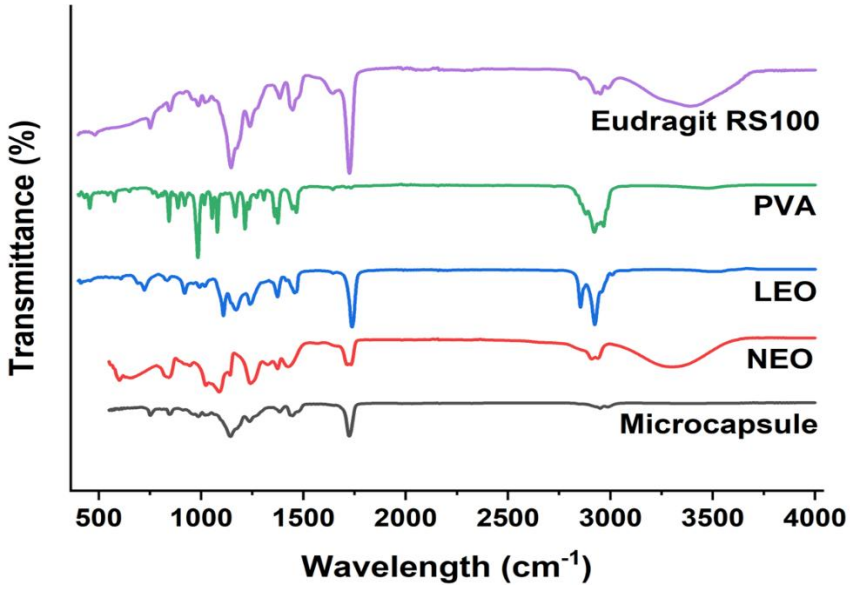

Figure 6. FT-IR spectra of PVA and Eudragit RS 100 polymers, LEO, NEO and microcapsules

The major peaks associated with PVA and the microcapsule are clearly seen in the PVA FT-IR spectrum. For example, the PVA polymer and microcapsule spectra showed the characteristic strong hydrogen bonded band at about 3400-3200 cm^{-1} wavelength. Due of the significant hydrophilic forces, intramolecular and intermolecular hydrogen bonding is anticipated to take place among PVA chains. Another important absorption peak was confirmed at 1141 cm^{-1}. The microcapsule spectra show that this peak appears at 1243 cm^{-1}. This vibrational band, which is associated with the carboxyl stretching band (C–O), is mainly caused by the crystallinity of PVA (Mansur et al., 2004; Eğri and Erdemir, 2019). The stretching bands of Eudragit RS 100 at 1143 cm^{-1} and 1237 cm^{-1} are caused by the carbonyl stretching vibration of the ester group. The stretching bands are assigned to 1237 cm^{-1} and 1145 cm^{-1} in the spectra of microcapsules. The most intense peaks in the spectrum of LEO and NEO are seen clearly for microcapsule spectra (Park and Park, 2010).

4. DISCUSSION AND CONCLUSIONS

This study was achieved to production and characterization of lavender essential oil (LEO) and niaouli essential oil (NEO) loaded microcapsules by the solvent/emulsion evaporation method successfully. Small, uniform and spherical microcapsules were produced under the optimum proses parameters such as 3 hours production time, 300 rpm mixing speed, 0.1 gram surfactant concentration, 1:10 oil:polymer ratio. FT-IR results indicated that there are no undesirable reactions in the emulsion between components and determined the presence of core materials in the structure of the microcapsules. As a result of this study, it is considered that the LEO and NEO loaded microcapsules has a high potential for end use as reduce stress and improve sleep quality in the pillowcase and bedclothes.

Acknowledgements
We would like to thank Evonik Röhm GmbH for their polymer supply.

Ethics Committee Approval
N/A

Peer-review
Externally peer-reviewed.

Author Contributions
Conceptualization: H.K and F.C.Ç.; Investigation: H.K.; Material and Methodology: H.K and F.C.Ç.; Supervision: F.C.Ç.; Visualization: H.K and F.C.Ç.; Writing-Original Draft: H.K; Writing-review & Editing: F.C.Ç.; Other: All authors have read and agreed to the published version of manuscript.

Conflict of Interest
The authors have no conflicts of interest to declare.

Funding
The authors declared that this study has received no financial support.

REFERENCES

Bakkali, F., Averbeck, S., Averbeck, D., Idaomar, M. (2008). Biological effects of essential oils-a review. Food and chemical toxicology. 46, 446-475.

Bolourchian, N., Bahjat, M. (2019). Design and In Vitro Evaluation of Eudragit-Based Extended Release Diltiazem Microspheres for Once-and Twice-Daily Administration: The Effect of Coating on Drug Release Behavior. Turk J Pharm Sci. 16, 340-347. https://doi.org/10.4274/tjps.galenos.2018.24861

Cavanagh, H., Wilkinson, J. (2002). Biological activities of lavender essential oil. Phytotherapy research. 16, 301-308.

Eğri, Ö., Erdemir, N. (2019). Production of Hyperivum Perforatum Oil-Loaded Membranes For Wound Dressing Material And in Vitro Tests Artificial Cells. Nanomedicine and Biotechnology An International Journal. 1404-1415.

Hammer, K. A., Carson, C., Riley, T. (1999). Antimicrobial activity of essential oils and other plant extracts. Journal of Applied Microbiology. 86, 985-990.

Heiskanen, H., Denifl, P., Pitkänen, P. (2012). Effect of Concentration and Temperature on The Properties of The Microspheres Prepared Using an Emulsion–Solvent Extraction Process. Adv Powder Technol. 23, 779-786. https://doi.org/10.1016/j.apt.2011.10.007

Hong, Y., Gao, C., Shi, Y. (2005). Preparation of Porous Polylactide Microspheres by Emulsion-Solvent Evaporation Based on Solution Induced Phase Separation. Polym. Adv. Technol. 16, 622-627. https://doi.org/10.1002/pat.629

Hui, L., He, L., Huan, L., Xiaolan, L., Aiguo, Z. (2010). Chemical composition of lavender essential oil and its antioxidant activity and inhibition against rhinitis-related bacteria. African Journal of Microbiology Research. 4, 309-313.

Lillehei, A. S., Halcon, L. L. (2014). A systematic review of the effect of inhaled essential oils on sleep. The Journal of Alternative and Complementary Medicine. 20, 441-451.

Lis-Balchin, M., Hart, S. (1999). Studies on the mode of action of the essential oil of LavenderLavandula angustifolia P. Miller. Phytotherapy Research: An International Journal Devoted to Pharmacological and Toxicological Evaluation of Natural Product Derivatives. 13, 540-542.

Mansur, H.S., Oréfice, R.L., Mansur, A.A. (2004). Characterization of poly (vinyl alcohol)/poly (ethylene glycol) hydrogels and PVA-derived hybrids by small-angle X-ray scattering and FTIR spectroscopy. Polymer. 45, 7193-7202.

Park, J.M., Park, S.J. (2010). Preparation and characterization of water-soluble microcapsule for sustained drug release using Eudragit RS 100. Macromolecular Research. 18, 1191-1194.

Rakotondrazafy, N., Farasoa, H. R., Ramanandraibe, V. V. (2023). Seed oil extraction of cucurbita maxima duchesne growing in Madagascar: impact of storage and use of a cineole–rich essential oil as a green solvent. Rec. Agric. Food. Chem. 3, 1-7.

Sang-Yun, Nam., Mi-Hye, Chang., Jeong-Su, Do., Hyo-Jung, Seo., Hong, Keun Oh. (2008). Essential Oil of Niaouli Preferentially Potentiates Antigen-Specific Cellular Immunity and Cytokine Production by Macrophages. Immunopharmacology and Immunotoxicology. 30, 459-474. DOI: 10.1080/08923970802135187

Steflitsch, W., Steflitsch, M. (2008). Clinical aromatherapy. Journal of Men's Health. 5, 74-85.

Yıldırım, M., Dogan, K., Yiğin, A., Cimentepe, M., Necip, A., Amangeldinova, M., Dellal, Ö. (2025). A breakthrough in infection control: niaouli oil–chitosan hydrogels for enhanced wound healing. Polymer Bulletin. 1-24.

Zhang, H, Dudley, E.G., Davidson, P.M., Harte, F. (2017). Critical concentration of lecithin enhances the antimicrobial activity of eugenol against Escherichia coli. Applied and Environmental Microbiology. 83, e03467-16.

Evaluation of Selected Fabric Properties Based on Yarn Type in Digitally Printed Knitted Fabrics

AYSEL KARA*[1], ENFAL KAYAHAN[2], DEMET YILMAZ[3]

Abstract: In recent years, the adoption of digital printing technology in the textile industry has expanded rapidly across the globe. This growth is primarily driven by the ability to transfer high-resolution photographic images onto textile surfaces, the increasing demand for environmentally friendly coloration methods, the rise of fast fashion, shorter lead times, and decreasing production volumes. These factors have positioned digital printing as a leading alternative to conventional printing techniques. This study aims to examine how different yarn production technologies influence the visual and functional properties of knitted fabrics after digital printing. For this purpose, single jersey fabrics were produced using the same fiber type (viscose) and yarn count (Ne 28/1) but with varying yarn structures: OE-rotor and vortex. All fabrics were subjected to an identical digital printing procedure under controlled industrial conditions.

Post-printing, the samples were assessed in terms of colorimetric properties such as color strength (K/S) and lightness (ΔL), along with various color fastness tests including resistance to washing, dry and wet rubbing, perspiration, water droplet exposure, and saliva. These measurements were carried out in accordance with standardized testing protocols. Furthermore, fabric performance such as fabric weight, seam slippage strength, pilling resistance and comfort-related parameters including water absorbency and drying time were also evaluated to determine the role of yarn structure in overall fabric behaviour. The results demonstrate that the yarn structure significantly affects not only the color yield and fastness characteristics but also the comfort and mechanical performance of the fabric. Notably, differences in yarn morphology influenced dye penetration during printing and contributed to observable variations in surface appearance and tactile properties. The findings of the study underscore the importance of considering yarn structure in digital printing processes and provide valuable scientific evidence regarding the relationship between yarn type and ink penetration, thereby contributing meaningfully to the existing body of literature.

Keywords: Digital textile printing, viscose yarn, yarn technology, fabric comfort, fastness properties.

[1]**Address:** Er-Ez Group Texco Boya Apre, 16245 Bursa/Türkiye
[2]**Address:** Pamukkale University, Faculty of Engineering, Department of Textile Engineering, Denizli/Türkiye
[2]**Address:** Süleyman Demirel University, Faculty of Engineering and Natural Science, Department of Textile Engineering, Isparta/Türkiye

***Corresponding author:** demetyilmaz@sdu.edu.tr

1. INTRODUCTION

As in other industrial sectors, the rising cost of energy continues to affect all stages of the supply chain in the textile industry, including raw materials such as fibers, dyes, and auxiliary chemicals. However, current market dynamics have also paved the way for new opportunities. The transformation process has accelerated globally across all markets and continents, particularly fostering the emergence of new business domains and innovation-driven models in the textile printing sector. Among these innovative approaches, digital printing stands out as a technology that transfers digital images directly onto fabric surfaces using extremely small ink droplets, without the need for color separation. In response to increasing consumer expectations, digital printing technology has gained prominence in the textile industry due to its advantages such as high production speed, cost efficiency, and design versatility (Mahbubur, 2021; Glogar et al., 2025).

When traditional and digital textile printing methods are compared, significant differences emerge in terms of process steps, customer response time, and cost. Inkjet printing technology eliminates time- and cost-intensive stages such as screen preparation and colorway development, offering considerable advantages particularly in sample production. While the number of printable colors is limited in conventional methods, digital printing does not impose such restrictions. Moreover, the need for screen preparation, associated costs, and storage requirements are eliminated. Patterns can be easily stored, modified, and transferred in digital environments, making them ready for immediate printing. The need for physical space to archive films, screens, and patterns is removed, and since screen, squeegee, and dye container cleaning is no longer necessary, water usage is significantly reduced—resulting in a lower environmental impact. In this respect, digital printing presents a cleaner, safer, and more environmentally friendly production method compared to traditional techniques.

In literature, many researches emphasized the advantages of digital textile printing. However, researchers widely focused on production parameters such as pre-treatment processes (Selçuk, 2009; 2010), ink formulation and print paste preparation techniques (Yuen, 2007; Supaporn Noppakundilograt, 2010; Çetin, 2019), as well as post-print fixation

conditions (Özomay Meral & Özomay, 2021; Özdemir & Doba Kadem, 2023). These studies also examined performance-related criteria such as print quality, color fastness, and environmental impact (Glogar et al., 2025).

Studies investigating the widespread adoption of digital textile printing technologies highlight the effects of technological developments on production processes in detail. Yılmaz and Cavuş (2018) analysed the key drivers behind the growing popularity of digital printing within the textile industry (Yılmaz and Cavus, 2018). Çetin (2019) evaluated the effects of digital print pastes prepared with thickeners of varying viscosities on silk fabrics, investigating their influence on color fastness, wash and rub resistance, and fabric handle (Çetin, 2019). Additionally, the study provided a comparative analysis of rotary and digital printing techniques in terms of pattern versatility and production costs. In a thesis study conducted by Rüzgar (2019), the environmental impacts of rotary and digital printing methods were examined using the Life Cycle Assessment (LCA) approach. The study emphasized that, unlike rotary printing—where the environmental burden increases with the number of colors—digital printing exhibits minimal change in environmental load regardless of color count (Ali Rüzgar, 2019). Yıldız (2018) approached digital printing within the broader context of printing technologies, detailing its functions in the production line, the parameters affecting print quality, and the reasons behind its growing preference in the industry (Yılmaz, 2018). In another study, Güleçer (2020), who studied digital transfer printing, examined the effects of transfer papers with different coating characteristics on the print quality and color yield of 100% polyester fabrics (Güleçer, 2020). The study concluded that the quality differences observed among primary colors were primarily due to the chemical and rheological properties of the dyes used. Focusing on ecological applications on natural textiles, Topoyan (2022) tested natural dyeing and eco-printing techniques on biodegradable linen and hemp knitted fabrics (Topoyan, 2022). Similarly, Toprak (2022) analyzed digital printing outcomes obtained under different resolutions, print passes, and color spaces (RGB/CMYK), reporting that RGB designs yielded better results in terms of color quality and that increasing the number of passes enhanced the depth of color (Toprak, 2022).

Distinct from previous studies, the present study aims to investigate the effects of yarn technologies used in the production of digitally printed fabrics—particularly on color properties, as well as on various other fabric characteristics. It is well known that yarn production technologies affect not only physical properties such as yarn irregularity, hairiness, strength, and elongation at break, but also aspects like appearance, luster, and absorbency. These characteristics, in turn, influence the visual appearance, color performance, and other functional properties of digitally printed fabrics. Based on this premise, the current study explores the impact of different yarn production technologies on various properties of digitally printed fabrics. Two commonly used yarn manufacturing technologies—OE-rotor (open-end rotor spinning) and vortex spinning—were selected, and fabrics made from these yarns were subjected to digital printing under identical conditions. The color and comfort performance of the samples produced with different yarn types were examined in detail following the digital printing process. Specifically, the study investigates how yarn structure affects not only color attributes such as color saturation and fastness, but also comfort-related properties like water absorption, and drying time, as well as performance metrics including seam strength and pilling resistance.

2. MATERIAL AND METHOD

In this study, OE-rotor and vortex yarn with Ne 28/1 yarn count was obtained from a yarn spinning factory. As known, OE-rotor and vortex yarn types are one of the widely used yarn production methods in textile practice. Both yarns were produced from the same fiber type (viscose). After yarn supply, single jersey knitted fabrics were produced from two different yarn technologies, namely OE-rotor and vortex spinning methods. The fabrics were subjected to the same digital printing recipe and process conditions to ensure consistency in application. The pre-treatment and digital printing processes were carried out at Er-Ez Group Texco Dyeing and Finishing Company (Bursa/Turkey), and all processing parameters were determined in accordance with the company's recommendations. The designs and colors to be printed on the fabrics were created and evaluated using Adobe Photoshop software. After finalizing the designs, the files were saved in Tagged Image File Format (TIFF), which is compatible with the digital printing machine.

The design was transferred to the printer using a RIP (Raster Image Processor) software, which was also used to adjust the repeat layout of the pattern based on the fabric dimensions. Before the printing process, the print head height of the digital printing machine was set to 3.5 mm, and the fabric height was adjusted to 0.5 mm. The print settings were configured according to the design to be printed.

The digital printing machine used was the EFI Reggiani Colors model, equipped with 24 heads and 11 color penetration capability. In the study, the printing process was performed using 12 colors in total, specifically 2 blue, 2 cyan, 2 orange, 2 scarlet, 2 magenta (Galibarda), and 2 yellow ink heads. The printing was conducted at 4-pass, 600 dpi (dots per inch) resolution. The machine operated with reactive dyes throughout the process.

Following the printing process, the samples were evaluated in terms of colorimetric properties and fastness performance. These assessments included measurements of color strength (K/S) and lightness (ΔL), based on the CIELAB color space standards, wash fastness (according to ISO 105 C06:2010), dry and wet rubbing fastness (ISO 105 X12:2016), perspiration fastness (acidic and alkaline, ISO 105 E04:2013), water droplet and saliva fastness, and water fastness under prolonged contact (ISO 105 E01:2013). In addition, to assess the influence of yarn structure on the post-printing fabric

performance, various fabric performance and comfort parameters were comparatively analyzed. These included pilling resistance (EN ISO 12945-2:2000), drying time, and water absorbency (AATCC 199).

3. RESULTS

3.1. Colour Properties and CIELAB Color Measurements

3.1.1. Color Properties and CIELAB Color Values Before Washing

Table 1 presents the color properties of fabrics made from Ne 28/1 OE-rotor and vortex yarns following the digital printing process. Color measurements were taken based on the dominant background color of the fabric.

Table 1. CIELAB Color Measurements

Yarn type	ΔL	A	b	C	h	K/S
OE-rotor	21,9316	4,1373	-18,2926	18,7547	282,7442	18,39274
Vortex	21,4664	4,4824	-18,039	18,5876	283,9546	18,85387

According to the measurements based on the navy blue reference color in the CIELAB color space, both fabric samples exhibit similar hue values. The h (Hue angle) values indicate bluish-violet tones, with a negligible difference between them. The b values confirm that both fabrics display bluish tones, although the fabric made from OE-rotor yarn appears slightly closer to blue. Examination of the a values reveals that both samples lean towards reddish hues; however, the fabric produced from vortex yarn shows a slightly higher red component.

The C (Chroma) value, which indicates color saturation, is slightly higher in the fabric made from OE-rotor yarn, suggesting that the color may be perceived as more vivid to the human eye. However, in terms of color depth and darkness, the fabric knitted from vortex yarn exhibits a higher K/S value and a lower L (lightness) value. This distinction is attributed to the smoother, shinier surface and lower hairiness of vortex yarns. Such surface characteristics result in reduced light scattering during spectrophotometric measurements, thereby reflecting light with less diffusion and contributing to greater perceived color depth. (Chae, 2022). These physical properties contribute to higher color depth in spectrophotometric measurements. Moreover, the smoother surface morphology of vortex yarns allows for greater accumulation of dye molecules on the fabric surface, enhancing both color intensity and uniformity (Özdemir & Oğulata, 2017).

Conversely, OE-rotor yarns are characterized by a looser structure, higher hairiness, and lower surface uniformity. While these properties allow dye molecules to penetrate more deeply into the fiber interior, the increased surface roughness leads to greater light scattering, resulting in lower K/S values and higher L* (lightness) readings in spectrophotometric evaluations.

3.1.2. Color Properties and CIELAB Color Values After Washing

To assess the color durability of printed fabrics, post-washing color properties were evaluated for knitted fabrics produced from two different yarn types. The results of color measurements for digitally printed fabrics made from Ne 28/1 OE-rotor and vortex yarns, after 1 and 5 washing cycles, are presented in Table 2.

Table 2. CIELAB Color Measurements

Yarn type	Washing Cycles	ΔL	a	b	C	ΔE	K/S
OE-rotor	1	0.1602	0.0300	0.1608	-0.1502	0.228956	17.953
	5	0.5973	0.0417	0.0145	-0.0049	0.598929	17.396
Vortex	1	0.3411	0.0895	-0.2782	0.2915	0.449171	18.244
	5	0.5947	-0.1623	0.4338	-0.4601	0.753785	17.601

Upon examining the repeated washing results of the CIELAB a and b values, it was observed that in the fabric produced from OE-rotor yarn, the color coordinates shifted toward red (increase in a*) and yellow (increase in b*) compared to the unwashed fabric. In the fabric made from vortex yarn, the a* value initially shifted toward red after the first wash, but by the fifth wash, it tended toward the green axis (decrease in a* or shift toward negative values). Similarly, the b* value initially moved toward blue (decrease in b*) after the first wash but subsequently shifted toward yellow (increase in b*) with repeated washes.

Overall, in both fabric types, b* values tended toward the yellow axis as the number of washing cycles increased. In contrast, a* values shifted toward red in OE-rotor fabrics and toward green in vortex fabrics. These findings indicate that color loss occurred primarily in the blue and green tones for OE-rotor fabrics, and in the red and blue tones for vortex fabrics.

In both fabrics, the ΔE values measured after repeated washing remained below 1, indicating that the color change was imperceptible to the human eye and that the degree of fading was negligible. However, the ΔE value was found to be slightly higher in the fabric produced from vortex yarn compared to that made from OE-rotor yarn. This can be attributed to the smoother and more uniform surface morphology of vortex yarns, which may result in dye accumulation on the fiber surface while limiting penetration into the yarn structure (Kireçci et al., 2009.). On the other hand, the looser and hairier structure of OE-rotor yarns allowed for easier penetration of the print paste into the inner parts of the fibers, leading to better dye fixation within the fiber. Consequently, less dye was removed from the surface during washing. Although the observed difference was not statistically significant, it is a relevant finding for optimizing the amount of print paste and application parameters in the printing process.

3.1.3. Color Fastness Properties

The color fastness values of fabrics produced from Ne 28/1 OE-rotor and vortex yarns are presented in Table 3. Upon examination of the data, it is observed that there is no significant difference between the fastness values of the samples, and both fabric types exhibit acceptable fastness to washing, rubbing, and perspiration. However, the fastness results for both acidic and alkaline artificial saliva conditions were found to be unfavorable in both samples.

Table 3. Fastness Properties

Yarn type	Rubbing Fastness		Wash Fastness	Perspiration Fastness	Saliva fastness	
	Wet	Dry			Acidic solution	Alkaline Solution
OE-rotor	4-5	3-4	4-5	4-5	-	-
Vortex	4-5	3-4	4-5	4-5	-	-

3.2. Fabric Performance Properties

3.2.1. Fabric Weight

The pre- and post-printing fabric weights of the knitted samples produced from Ne 28/1 OE-rotor and vortex yarns are presented in Table 4.

Table 4. Fabric weight before and after printing (g/m²)

Yarn Type	Before Printing	After Printing
OE-rotor	235	255
Vortex	234	228

Upon examining the data in the Table 4, it can be observed that fabrics made from OE-rotor yarns have slightly higher fabric weights compared to those made from vortex yarns. However, the difference between the fabric weights of OE-rotor samples before and after printing was not found to be statistically significant. In contrast, the change in fabric weight for vortex yarn fabrics was found to be statistically significant, showing a notable decrease after printing.

The reduction in fabric weight observed in vortex yarn fabrics following the printing process can be attributed to the distinct structural and physical characteristics of the yarn. This difference is associated with fiber packing within the yarn, lower hairiness, and differences in moisture retention behavior. According to the literature, fabrics made from vortex yarns tend to exhibit more shrinkage during thermal processes such as printing and fixation, resulting in a reduction in surface area and, consequently, a decrease in fabric weight. Additionally, due to the smoother surface and lower hairiness of vortex yarns, these fabrics tend to retain less moisture during the printing process. The rapid release of this moisture during drying and fixation stages may further contribute to the reduction in mass. On the other hand, OE-rotor yarn fabrics, with their looser and hairier structures, allow deeper penetration of the print paste into the fibers and display more stable dimensional behavior after thermal treatment (Kim & Kim, 2018).

3.2.2. Seam Slippage Strength (in Seamless and Seamed Conditions)

The seam slippage strength results of fabrics produced from Ne 28/1 OE-rotor and vortex yarns before and after digital printing are presented in Figure 1. In the seamless condition, it was observed that after the printing process, the seam slippage strength significantly decreased in the warp direction for both yarn types, while the strength significantly increased in the weft direction.

As expected, the fabrics produced from OE-rotor yarns exhibited higher seam slippage strength values compared to those produced from vortex yarns before and after printing. However, the differences in seam slippage strength between the two yarn types were found to be statistically insignificant (Figure 1).

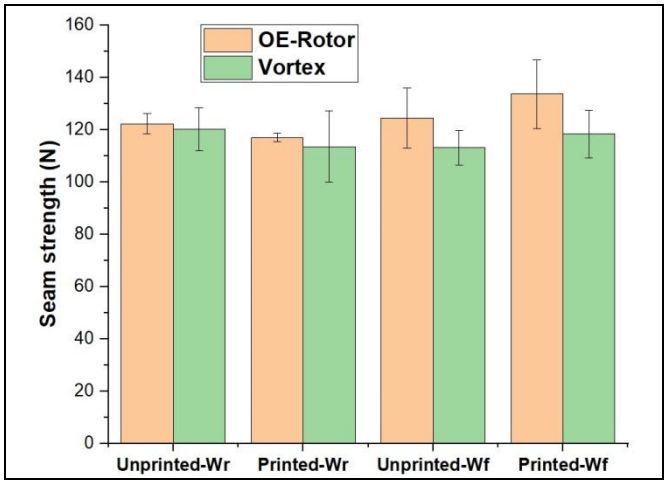

Figure 1. Seam slippage strength results in the seamless condition before and after printing for different yarn types.

When evaluating both directions, different tendencies were observed in the warp and weft directions. Following the printing process, OE-rotor yarn fabrics showed no significant change in the warp direction, whereas vortex yarn fabrics showed a tendency toward decreased seam slippage strength. However, this decrease was also statistically insignificant (Figure 2). In the weft direction, both yarn types demonstrated a significant increase in seam slippage strength after printing. While OE-rotor fabrics exhibited higher strength in the warp direction, vortex fabrics yielded higher strength values in the weft direction before and after printing. Except for the warp direction, differences in seam strength values were not statistically significant.

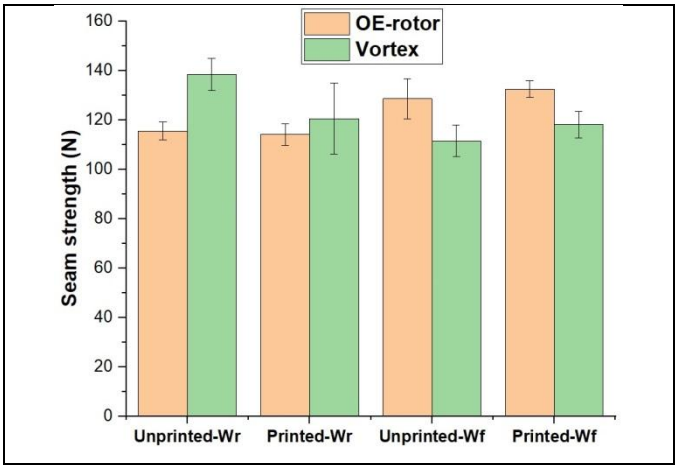

Figure 2. Seam slippage strength results in the seamed condition before and after printing for different yarn types.

The observed directional differences in seam slippage strength, regardless of yarn type, can be attributed to the different tensions experienced by warp and weft yarns during the production process, as well as their thermal behavior during the fixation process. Thermal treatments such as heat setting and drying significantly influence the dimensional stability of textile materials, often leading to greater shrinkage in the warp direction. It has been stated in the literature that the fabrics made from vortex-spun yarns tend to be more stable in the weft direction but are more susceptible to shrinkage in the warp, primarily due to their looser loop structure. During wet processing, fiber swelling and loop compression further contribute to these dimensional changes (Ortlek and Onal, 2008). While the weft yarns are relatively free, residual tension accumulating in the warp direction may lead to reduced or unchanged seam strength after printing and fixation, whereas fiber relaxation and rearrangement in the weft direction may cause increased seam strength. Supporting this, a recent study emphasized that seam strength differences between warp and weft directions are primarily due to the higher tension in warp yarns, and this difference becomes more pronounced after thermal treatment (Macit, 2024).

3.2.3. Pilling Resistance

The pilling resistance of the fabrics made from OE-rotor and vortex yarns tended to slightly decrease after the digital printing process. Fabrics produced from OE-rotor yarns were rated as “moderate” (grade 3), whereas those made from vortex yarns received a slightly higher rating of “moderate/good” (grade 3/4) (Table 5). As expected, vortex yarn fabrics exhibited better pilling resistance than OE-rotor fabrics by approximately one grade.

Table 5. Pilling resistance results of different yarn types before and after printing.

Fabric type	OE-rotor Yarn	Vortex Yarn
Unprinted fabric	3/4	4
Printed fabric	3	3/4

3.2. Fabric Properties Related to Fabric Comfort

3.2.1. Water Absorption

The water absorption results of the fabrics produced from OE-rotor and vortex yarns before and after the digital printing process are presented in Figures 3. Upon examination of the results, it is clearly observed that the fabrics made from vortex yarns exhibited higher water absorption values both before and after printing. The difference between the pre- and post-printing values in vortex yarn fabrics was found to be statistically significant. In contrast, water absorption in OE-rotor yarn fabrics showed a slight, statistically insignificant decrease after printing, while vortex yarn fabrics demonstrated a significant increase in water absorption following printing.

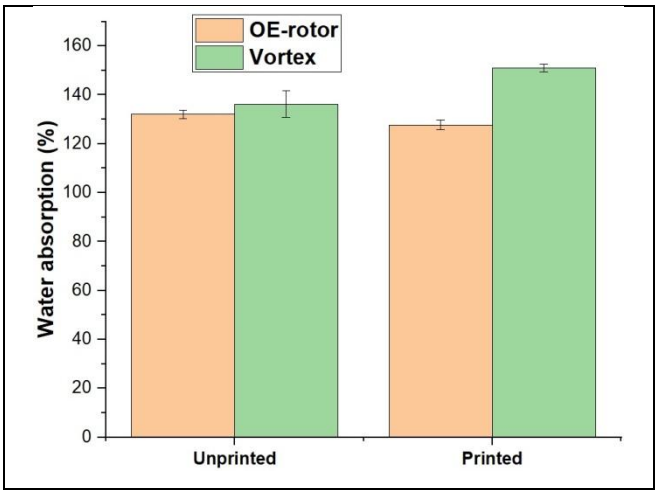

Figure 3. Water absorption results of fabrics made from different yarn types before and after digital printing.

3.2.2. Drying Behavior

Following the water absorption test, the fabrics were hung at room temperature and allowed to dry with their weights recorded at specific intervals. Based on the initially measured wet weights, the amount of water loss was calculated and evaluated as an indicator of drying rate. Upon reviewing the results presented in Figure 4.

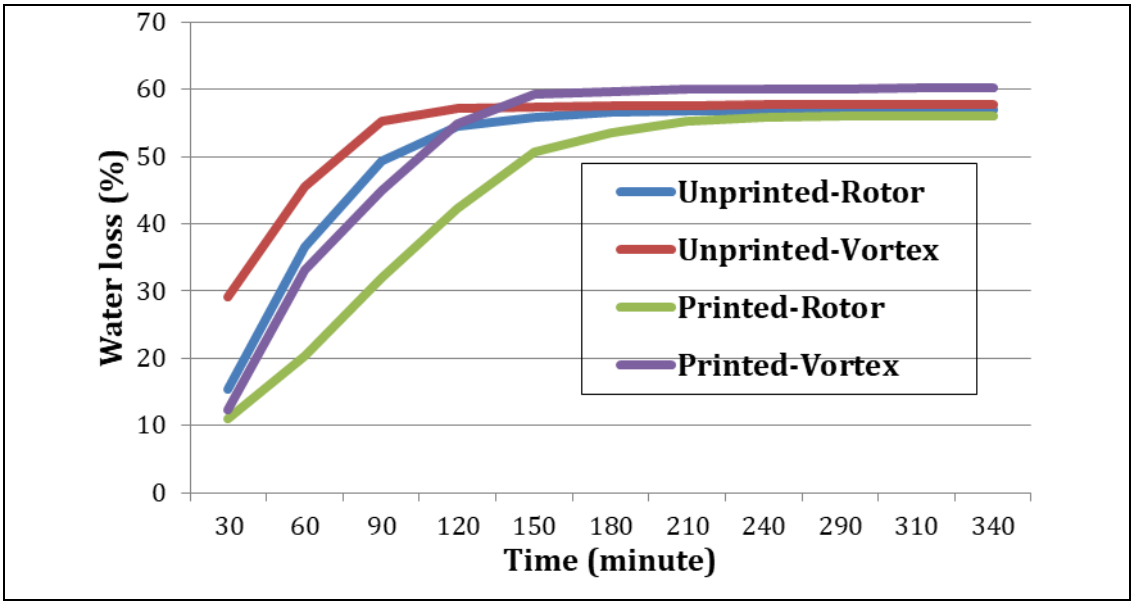

Figure 4. Water loss results of fabrics produced from different yarn types before and after digital printing.

It was observed that in unprinted fabrics, a high level of water loss occurred within the first 90 minutes, ranging from 15% to 55%. Between 90 and 120 minutes, water loss continued (54–57%), and after 120 minutes, the rate of water loss stabilized between 56% and 58% until the end of the test.

A similar trend was observed after printing. Depending on the yarn type, OE-rotor fabrics lost between 11% and 59% of their water content within 150 minutes, while vortex fabrics exhibited similar water loss within 120 minutes. During the relatively stable phase of water loss, between 120 and 180 minutes, the water loss ranged between 50% and 59%, and from 180 minutes until the end of the test, between 55% and 60%. It was determined that vortex yarn fabrics experienced higher water loss both before and after the printing process.

Fabrics made from vortex-spun yarns exhibit a more controlled and predictable drying profile in both printed and unprinted conditions. In contrast, OE-rotor yarn fabrics tend to dry faster but in a less uniform manner. This difference can be attributed to the compact and uniform structure of vortex yarns, their lower hairiness, and their ability to promote more even water distribution across the fabric surface.

4. DISCUSSION AND CONCLUSIONS

Digital printing stands out as one of the most advanced innovations in textile surface coloration, offering significant advantages such as high-resolution design flexibility, infinite color and pattern reproduction, and reduced environmental impact due to lower ink and water consumption (Gooby, 2020). However, the final appearance and performance of digitally printed textiles are closely influenced by the intrinsic characteristics of the substrate, including fiber type, surface morphology, fabric structure, and pretreatment conditions (Tkalec et al., 2024).
In this study, knitted fabrics produced from two different viscose yarn types (Ne 28/1 Vortex and OE-rotor spun) were comparatively evaluated in terms of color properties, fabric performance properties and comfort-related parameters following digital printing. The findings revealed that while the OE-rotor yarn offered slightly higher chroma values, vortex yarn-based fabrics demonstrated superior color uniformity, higher K/S values, and deeper shades. These results are attributable to the more compact and low-hairiness structure of vortex yarns, which enhances ink fixation and reduces light scattering during spectrophotometric analysis. Color fastness tests indicated no significant difference between the two fabric types.

However, vortex yarn fabrics exhibited superior results in terms of pilling resistance, water absorption and drying rate. The faster drying behavior of vortex-based fabrics—an outcome of lower moisture retention and tighter structure—may contribute to improved process efficiency and reduced energy costs during drying.

Overall, the results underscore the importance of yarn structure in determining digital print quality and fabric performance. The insights gained from this study provide valuable input for yarn selection and process optimization in digital textile printing. Future research may extend these findings by incorporating diverse knit structures, pre-treatment formulations, and ink systems to further explore material-performance relationships.

Acknowledgements
We would like to thank Er-Ez Group Texco Boya Apre (Bursa) company for carrying out this study.

Ethics Committee Approval
N/A

Peer-review
Externally peer-reviewed.

Author Contributions
Conceptualization: A.K., E.K., D.Y.; Investigation: A.K., E.K.; Material and Methodology: A.K., D.Y., E.K.; Supervision: D.Y.; Visualization: D.Y., E.K.; Writing-Original Draft: A.K., D.Y.; Writing-review & Editing: D.Y., E.K.; Other: All authors have read and agreed to the published version of manuscript.

Conflict of Interest
The authors have no conflicts of interest to declare.

Funding
The authors declared that this study has received no financial support.

REFERENCES

Chae, Y. (2022). Color appearance shifts depending on surface roughness, illuminants, and physical colors. Scientific Reports, 12, 1371. https://doi.org/10.1038/s41598-022-05409-2
Çetin, M. Y. A. (2019). Protein liflerinin baskısında ink jet baskı teknolojisinin kullanımı. [MSc Thesis]. Graduate School of Natural and Applied Sciences Pamukkale University.
Glogar, M., Petrak, S., Mahnić Naglić, M. (2025). Digital technologies in the sustainable design and development of textiles and clothing—A literature review. Sustainability, 17, 1371. https://doi.org/10.3390/su17041371.
Güleçer, M. (2020). Investigation of the effect of paper quality on color yield in digital transfer printing [Master's thesis]. Bursa Uludağ University, Institute of Science, Bursa,Türkiye.
Kim, H. A., & Kim, S. J. (2018). Mechanical Properties of Micro Modal Air Vortex Yarns and the Tactile Wear Comfort of Knitted Fabrics. Fibers and Polymers, 19, 211–218. https://doi.org/10.1007/s12221-018-7690-x
Kireçci, A., Parlakyiğit Erdal, P., İçoğlu, H.İ. 2009. Comparison of the fastness properties and color values of cotton fabrics knitted from air-vortex and ring spun yarns. Tekstil ve Konfeksiyon, 19, 227–233.
Noppakundilograt, S., Wongpisutpaisan, P., Kittinaovarat, C., Supaphol, P., Chotipradit, S. (2010). Modified chitosan pretreatment of polyester fabric for printing by ink jet ink. Carbohydrate Polymers, 82.
Ortlek, H.G., Onal, L. (2008). Comparative study on the characteristics of knitted fabrics made of vortex-spun viscose yarns. Fibers and Polymers, 9, 194–198.
Özdemir, H., Oğulata, R.T. (2017). Comparison of color values of packages wound from different spun yarns. Tekstil ve Muhendis, 24, 152–159. https://doi.org/10.7216/1300759920172410703
Özdemir, Ş., Doba Kadem, F. (2023). An eco-friendly approach: effect of fixation time on colour and comfort properties of digital printed fabric. Industria Textila, 74, 527–533. https://doi.org/10.35530/IT.074.05.2022122
Özomay Meral, Özomay, Z. (2021). The effect of temperature and time variables on printing quality in sublimation transfer printing on nylon and polyester fabric. European Journal of Science and Technology. https://doi.org/10.31590/ejosat.889147
Rahman, M.M. (2021). Applications of the digital technologies in textile and fashion manufacturing industry. Technium: Romanian Journal of Applied Sciences and Technology, 3, 114–121.
Rüzgar, A.. (2019). The Comparıson Of Envıronmental Impacts Between Rotary Screen And Dıgıtal Reactıve Prıntıng By Lıfe Cycle Assessment [MSc Thesis]. Graduate School of Natural and Applied Sciences.
Selçuk, E. (2009). Ink jet baskıda kumaşa uygulanan ön işlemlerin baskı kalitesi üzerine etkilerinin araştırılması [Master's thesis] Uludağ University, Bursa, Türkiye
Selçuk, E.K.M. (2010). Ön emdirme işleminde kullanılan kıvamlaştırıcı türünün reaktif ink jet baskı kalitesi üzerine etkileri. Uludağ Üniversitesi Mühendislik Fakültesi Dergisi, 15
Şevkan Macit, A. (2024). Investigation of seaming performance of dyed and finished polyester/viscose fabrics. Textile Research Journal, 94, 2095–2106. https://doi.org/10.1177/00405175241233215
Topoyan, Z. (2022). Sürdürülebilir tekstiller bağlamında doğal boyalar ve deneysel eko tasarım çalışmaları [Master's thesis] Dokuz Eylül University, İzmir, Türkiye
Toprak, G. (2022). Investigation of parameters affecting the print result in textile digital printing [Doctorate in Art]. Mimar Sinan Fine Arts University.
Yılmaz, S., Güler, C. (2018). Digital printing applications in textile and printing industry of Turkiye. https://www.efi.com/products/inkjet-printing-and-proofi
Yuen, C.W.M., Kan, C.W., Yip, J., Choi, K.C., Choi, P.S.R. (2007). A two-bath method for digital ink-jet printing of cotton fabric with chitosan. Fibers and Polymers, 8, 625–628. https://doi.org/10.1007/BF02875849.

Landslide Susceptibility Assessment Using Machine Learning Method around Gölbaşı (Adıyaman) and Doğanşehir (Malatya)

SENEM TEKİN*[1], TOLGA ÇAN[2]

Abstract: Landslides are complex geomorphic hazards that require localized analysis due to the diverse geological, geomorphological, and climatic conditions that influence their occurrence. This study presents a landslide susceptibility assessment in the region between Gölbaşı (Adıyaman) and Doğanşehir (Malatya), Türkiye, where numerous landslides were triggered following the February 6, 2023 Kahramanmaraş earthquake sequence. Using a logistic regression model and incorporating both historical and post-earthquake event-based landslide inventories, the study evaluates the spatial distribution and predictive capability of susceptibility zoning. The model integrates 14 environmental variables derived primarily from digital elevation data. The performance of the logistic regression model was assessed using the ROC curve, yielding an AUC value of 0.803. Results show that 71.53% of post-earthquake landslides were located in areas classified as high and very high susceptibility, validating the model's practical applicability. This study contributes to regional-scale risk assessment and land-use planning efforts in tectonically active and geomorphologically diverse regions of southeastern Türkiye.

Keywords: Landslide inventory, landslide susceptibility, machine learning method, geographic information systems

[1]**Address:** Remote Sensing and Geographic Information Systems Application and Research Center, Adiyaman University, 02040 Adiyaman, Türkiye
[2]**Address:** Department of Geological Engineering, Çukurova University, Adana, Türkiye

***Corresponding author**: senemtekin@adiyaman.edu.tr

1. INTRODUCTION

Despite advances in risk reduction and hazard mapping, landslides remain a significant natural threat in Türkiye, particularly in tectonically active and topographically complex regions. Effective landslide risk management requires comprehensive understanding of both preparatory and triggering factors, especially in the aftermath of major seismic events. Türkiye is situated along the Alpine-Himalayan orogenic belt, making it highly prone to landslides, particularly in proximity to major fault zones such as the East Anatolian Fault Zone. The February 6, 2023 earthquakes (Mw 7.7 and 7.6) triggered widespread landslides across southeastern Türkiye. In this context, landslide susceptibility maps, which delineate areas at relative risk of future landsliding, are critical tools for pre-disaster land use planning. This study focuses on (Figure 1) developing a logistic regression-based susceptibility model for the region between Gölbaşı and Doğanşehir, incorporating both historical landslide data and newly mapped landslides following the 2023 earthquakes.

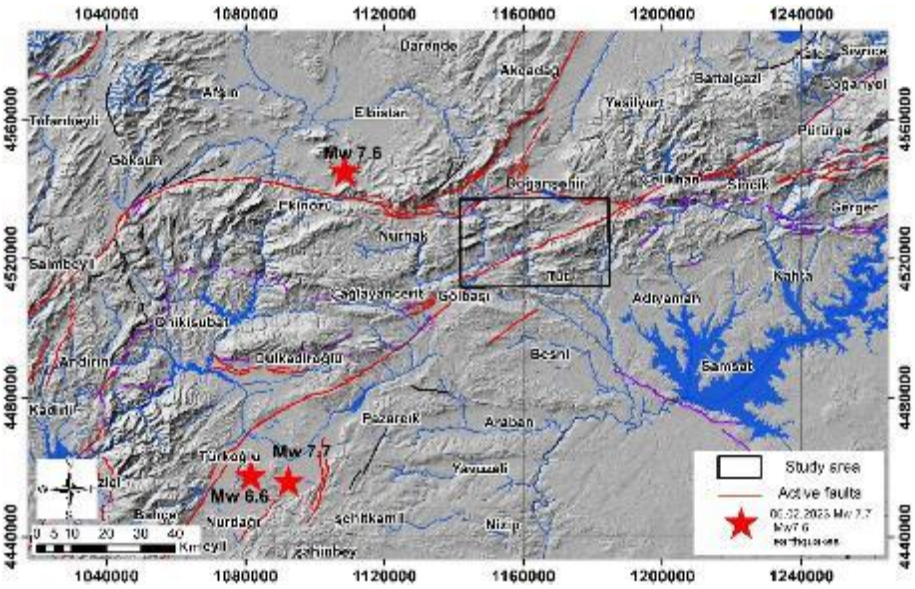

Figure 1. Study area

2. MATERIAL AND METHOD

The landslide inventory was created from both the historical landslide inventory and the landslides observed and mapped in the field following the Kahramanmaraş-centered earthquakes that occurred on February 6, 2023. The landslides that induced after the earthquake were digitized using satellite images, field observations, and various open source data. Thus, a comprehensive landslide inventory was obtained both temporally and event-based. According to the historical landslide inventory map, there are 144 landslides in the study area (Figure 2a). According to the event inventory map obtained using field observations and orthophoto images taken after the February 6, 2023 earthquakes obtained from the General Directorate of Mapping, 203 landslides were mapped (Figure 2a,b). 69 of the landslides that occurred after the February 6, 2023 earthquakes occurred in areas where old landslide masses were located. Especially the landslides in the Doğanşehir district and its surroundings, where deep slide type landslides are located, are seen to be active landslides again.

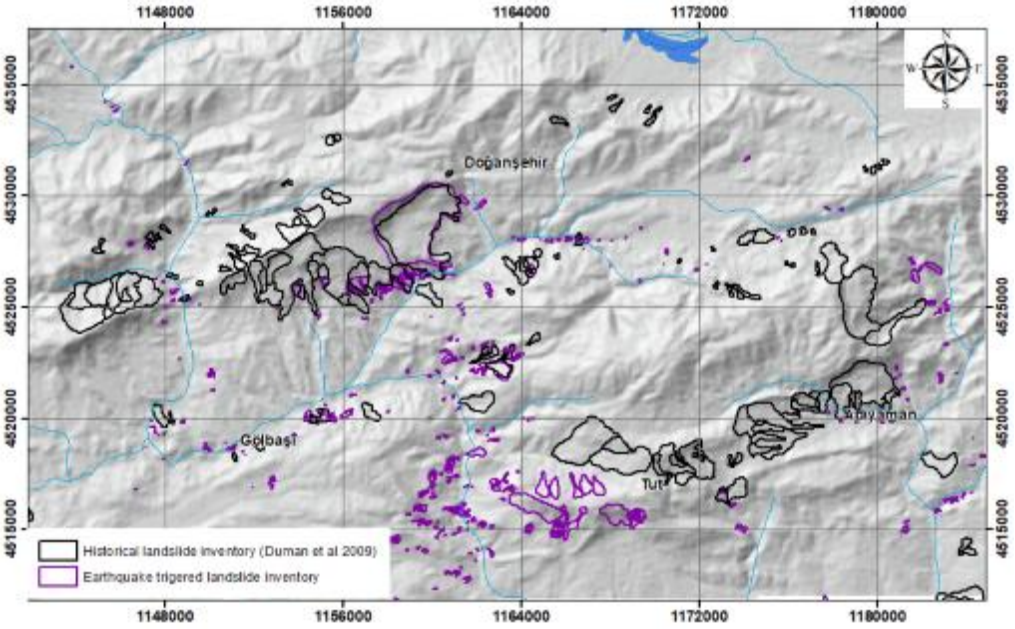

(a)

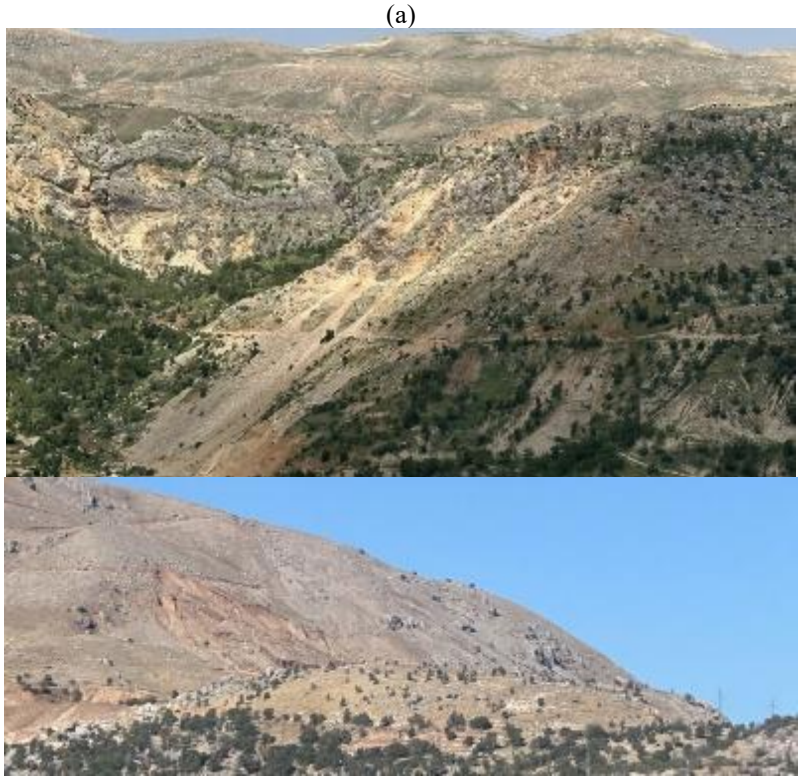

(b)

Figure 2. Landslide inventory map (a), sliding type landslides (b) of study area

As the environmental factors that prepare landslides, various parametric data widely used in the literature and known to affect land stability were used (Figure 3). Digital Elevation Model (DEM) was used as the main source in the calculation of 100 m resolution raster data (Figure 3a), The slope ranges between 0-57 degrees with an average of 15 degrees (Figure 3b, Table1). Profile and plan curvatures parameters which mainly control the ongoing erosion and deposition processes were also considered (Fig 3c,d,e). Positive and negative values in the curvature maps indicates convex (≅40%) and concave (≅40%) surfaces and the values close to the zeros (≅20%) are linear surfaces. Solar Radiation (Figure 3f) was included in the model due to fact that it affects the amount of solar energy by the topografy, which in turn affects soil moisture and drying patterns depending on slope orientation. Apart from these parameters, Compound Topographic Index (CTI), which represents the soil's potential for water saturation; Site Exposure Index (SITEEX), which calculates the extent to which a surface is exposed to environmental factors based on slope orientation and degree; Mean Curvature (MEANCUR), representing the average curvature of the slope; Slope Classification (SLPCLP), which expresses the slope parameter as a percentage; and Tangential Curvature (TANCUR), used to determine the direction and speed of water flow, channel formation, and flow path identification.

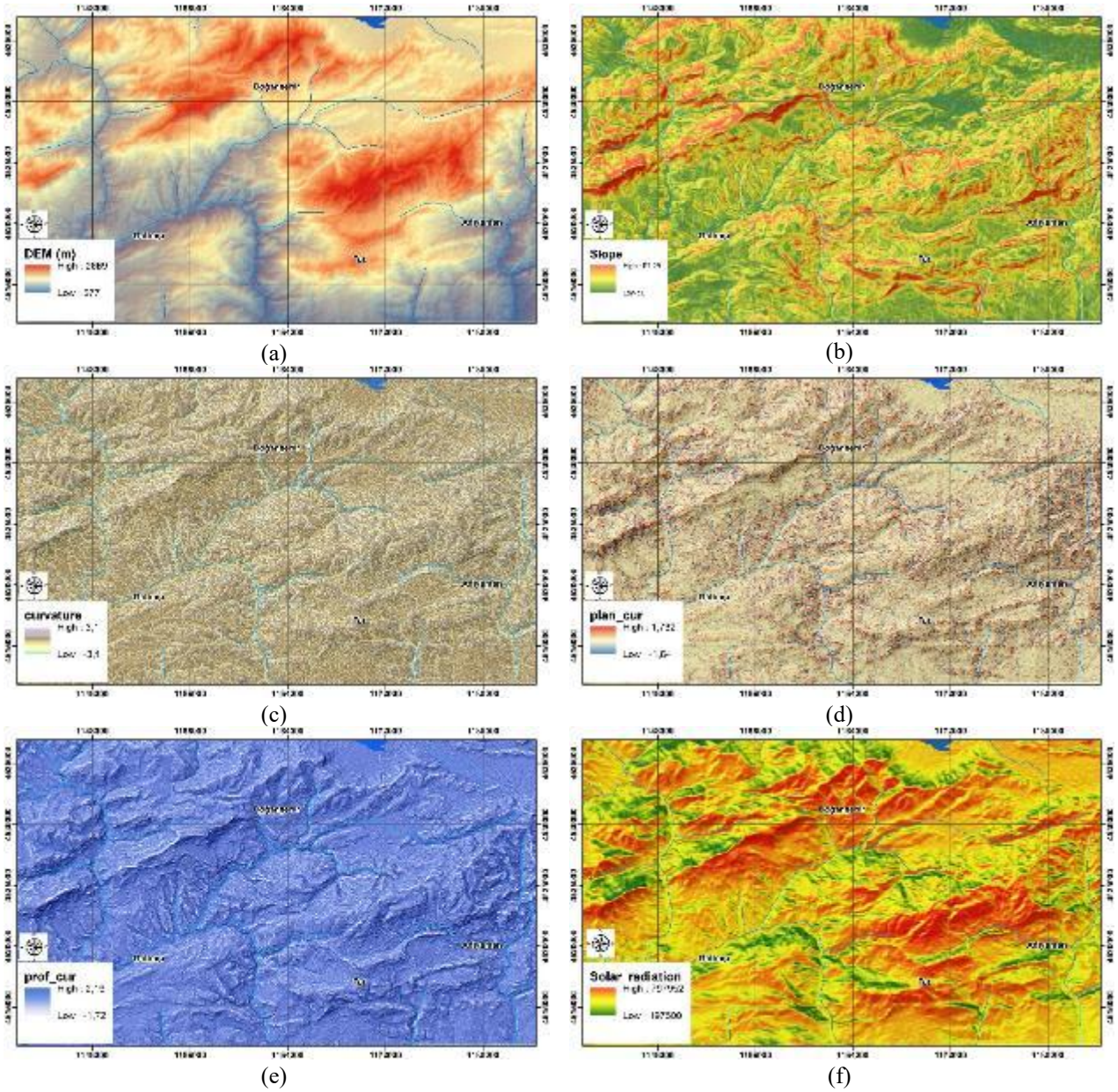

Figure 3. DEM (a), slope (b), Curvature (c), plan curvature (d), profile curvatyre (e), solar radiation (f) parameters

The study area between Doğanşehir (Malatya) and Gölbaşı (Adıyaman) has a rather heterogeneous geological structure characterized by lithological units belonging to various periods, which developed under a complex tectonic regime (Figure 4). The region is located within a tectonically active zone where sedimentary, volcanic and metamorphic rocks of different ages are found side by side. Quaternary alluvium and sediments, which are intensively exposed especially around Gölbaşı in the study area, consist of loosely structured materials and are generally located in alluvial plains, stream beds and plain bottoms. Upper Miocene–Pliocene terrestrial units are located southwest of Gölbaşı and around Tut. Paleocene–Miocene

terrestrial sediments and Eocene neritic limestones are also widespread throughout the region and present horizontal or gently sloping layering structures. In the eastern parts (northeast of Adıyaman), Upper Cretaceous, Upper Jurassic and Triassic carbonate platforms contain more mechanically resistant rocks. Ophiolite units and basalt-andesite lavas observed in limited areas within the area are more robust and impermeable units. However, slip planes are present along alteration and fracture zones. Paleozoic schists and gneisses consist of highly metamorphosed rocks.

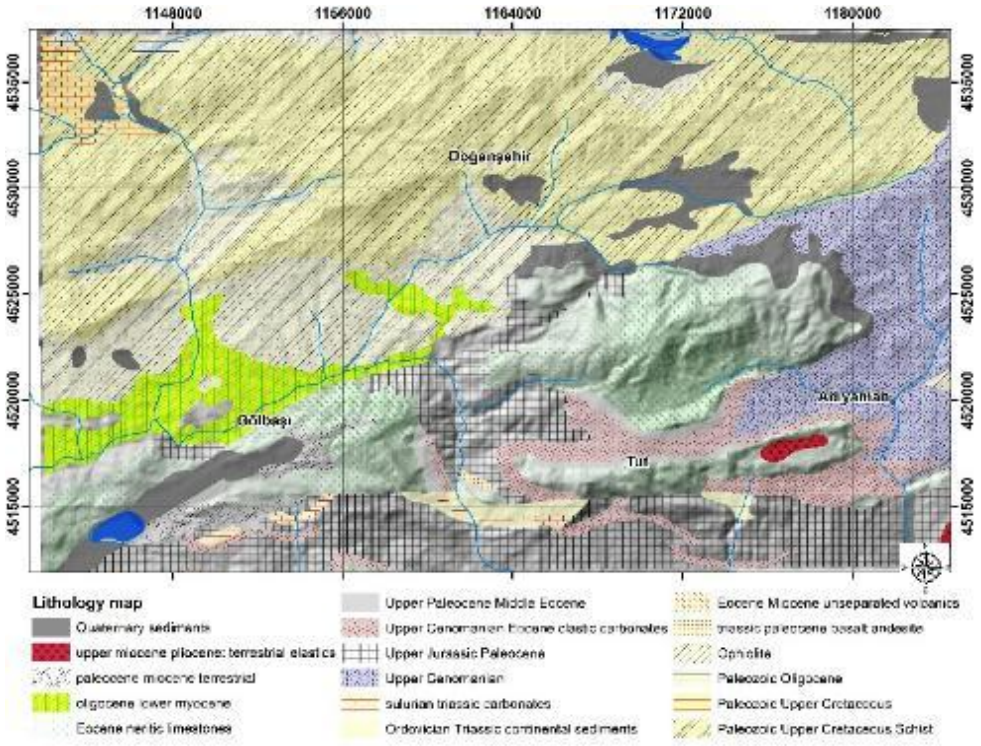

Figure 4. Geology of the study area (Aksay et al 2002)

2.1. Logistic regression

In this study, the logical regression method, which is one of the machine learning methods, was preferred. This method is widely used in modeling the relationships with independent variables when the dependent variable is categorical (mostly binary: landslide present/absent) (Hosmer et al., 2013). The aim of the model is to statistically evaluate the contribution of the determined environmental factors to the probability of landslide occurrence in each cell.

$$P(Y=1)=p_i=\frac{1}{1+e^{-(\beta_0+\beta_1X_1+\beta_2X_2+\cdots+\beta_nX_n)}} \quad (1)$$

$$\mathrm{MR}=\log\left[\frac{P_i}{1-P_i}\right]=z_i=\beta_0+\beta_1X_1+\beta_2X_2+\cdots+\beta_nX_n \quad (2)$$

While creating the model, pixels representing landslide areas were evaluated as "1" and landslide-free areas as "0". Landslide-free pixel areas were selected as many as landslide pixels. Since it is an effective tool in measuring the classification accuracy and discrimination power of the model, the success of the model was evaluated using the ROC curve and AUC value (Fawcett, 2006). The obtained susceptibility map was verified using both historical inventory data and new landslide events that occurred after the February 6, 2023 earthquakes, thus testing the predictive power of the model for both the past and the future.

3. RESULTS

The grid cell size of 100 m was used for terrain mapping unit where the landslide data set is represented by 5591 grid cells and the total study area has 107883 pixels. Landslide affected pixels data set considering the entire landslide polygons according to the sampling method proposed by Tekin and Çan (2018). Several logistic regression analyses were applied, and the final decision was made by two rules proposed by Can et al. (2005) that first, the majority of the landslides should locate in the high and very high susceptibility classes, and second, the high and very high susceptibility classes should cover the small percentages of the area. The variables entered in the best fit logistic regression model were summarized in Table 1. In regression model CLP100 and Meancur were found positively related to the presence of landslides.

Table 1. Variables in the Equation

Variables	B	S.E.	Wald	df	Sig.	Exp(B)
Solar	+0,000	,000	350,570	1	,000	1,000
Slope	-0,189	,011	295,592	1	,000	,828
1	+0,500	,117	18,242	1	,000	1,649
2	+1,355	,348	15,207	1	,000	3,877
5	-1,159	,106	119,757	1	,000	,314
6	+0,802	,199	16,242	1	,000	2,230
7	+1,325	,103	165,771	1	,000	3,764
9	+1,584	,088	326,779	1	,000	4,873
16	+0,952	,084	127,184	1	,000	2,590
17	+0,830	,244	11,546	1	,001	2,294
20	+0,265	,075	12,298	1	,000	1,303
402	-0,767	,395	3,773	1	,052	,465
Cti	+0,099	,019	27,980	1	,000	1,104
Siteex	-0,092	,006	227,765	1	,000	,912
Clp100	+5,090	1,458	12,187	1	,000	162,379
Meancur	-6,809	1,780	10,273	1	,001	,000
Slp	+0,341	,012	854,904	1	,000	1,406
Constant	-15,868	,753	443,592	1	,000	,000

**Quaternary sediments (1), upper miocene pliocene: terrestrial elastics (2), Eocene neritic limestones (5), Upper Paleocene Middle Eocene (6), Upper Cenomanian Eocene clastic carbonates (7), Upper Cenomanian (9), Ophiolite (16), Paleozoic Oligocene (17), Paleozoic Upper Cretaceous Schist (20), oligocene lower miocene (402).*

The landslide susceptibility map was given in figure 5a. According to the success and prediction rate curve the 17.80 % of the study area is located within the high – very high susceptibility classes comprising the 71.53 % of all landslides (Figure 5b). The area under Receiver Operating Characteristics (ROC) curve was found 0.803 indicating acceptable discrimination.

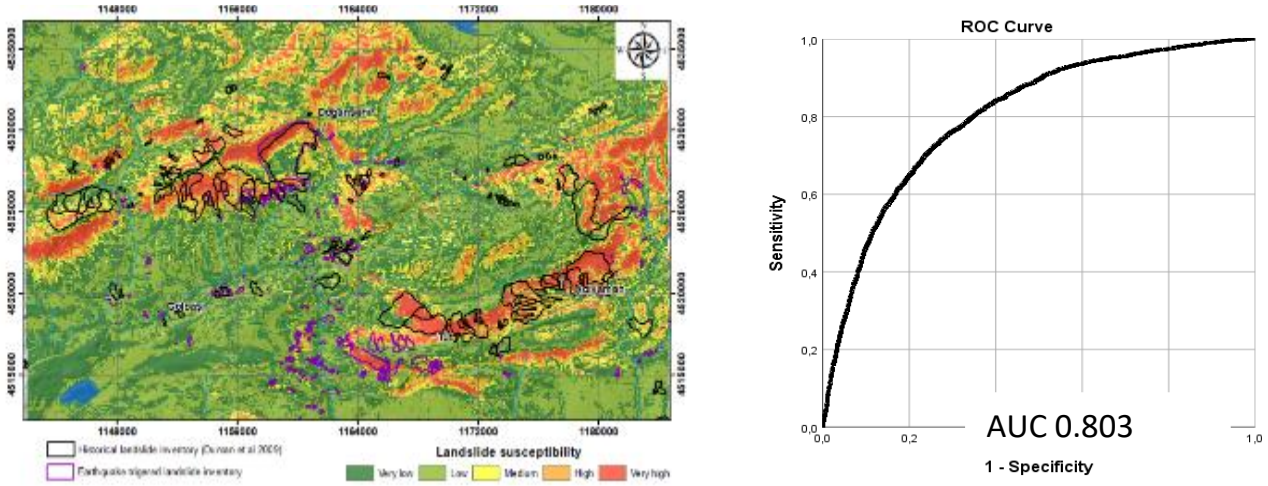

a b

Figure 5. Landslide susceptibility map (a) and ROC Curve (b).

4. DISCUSSION AND CONCLUSIONS

Landslides that develop in different movement mechanisms such asflowing, sliding, falling and toppling occur under the control ofregionally specific geological, morphological and physical factors.Factors such as the unit forming the landslide (soil, debris or rockmass), the areal and volumetric size of the moving mass, the rate of movement, the size of the study area and the scale of the studied map have mandatory and limiting effects to be considered in the studies to be carried out against landslides. The areas included in the "high" and "very high susceptibility" classes of the model largely coincide with the landslides that occurred after the February 6, 2023 earthquakes. The fact that the vast majority of the 203 new landslides mapped in the field after the earthquake (over 80%) are in these two susceptibility classes strongly supports the spatial validity and predictive power of the model. This demonstrates not only the model's statistical robustness but also its practical applicability following the disaster.

Author Contributions
Conceptualization: S.T.; T.Ç.; Investigation Material and Methodology, Analysis; Writing-Original Draft.

This research was funded by TÜBİTAK Project Number 123Y476.

REFERENCES

Aksay, A. Altun, İ. Arda, O. Aslaner, M., Aslantürk, M., Atabey, E., Atan, O., Ateş, Ş., Ayhan, A. Baskurt, M., et al., (2002), 1/500000 Ölçekli Türkiye Jeoloji Haritası Hatay Paftası. Maden Tetkik ve Arama Genel Müdürlüğü. Ankara (In Turkish).

Cruden, D. M., & Varnes, D. J. (1996). Landslide types and processes. In Turner, A.K., & Schuster, R.L. (Eds.), Landslides: Investigation and Mitigation (pp. 36-75). National Academy Press.

Emre, Ö., Duman, T. Y., Özalp, S., Elmacı, H., Olgun, Ş., & Şaroğlu, F. (2018). Active fault database of Turkey. Bulletin of the Mineral Research and Exploration, 157, 1–28.

Fawcett, T. (2006). An introduction to ROC analysis. Pattern Recognition Letters, 27(8), 861-874.

Gorum, T., et al. (2023). Earthquake-triggered landslides following the 6 February 2023 Kahramanmaraş (Türkiye) earthquakes: preliminary observations and inventory. Natural Hazards and Earth System Sciences Discussions.

Guzzetti, F., Reichenbach, P., Cardinali, M., & Galli, M. (2005). Landslide hazard assessment in the Staffora basin, northern Italian Apennines. Geomorphology, 72(1–4), 272–299.

Harp, E. L., & Jibson, R. W. (2002). Anomalous concentrations of seismically triggered landslides caused by liquefaction: 1994 Northridge, California earthquake. Bulletin of the Seismological Society of America, 92(4), 1128–1139.

Hosmer, D. W., Lemeshow, S., & Sturdivant, R. X. (2013). Applied Logistic Regression (3rd ed.). Wiley.

Lee, S., & Pradhan, B. (2007). Landslide hazard mapping at Selangor, Malaysia using frequency ratio and logistic regression models. Landslides, 4(1), 33–41.

Reichenbach, P., Rossi, M., Malamud, B. D., Mihir, M., & Guzzetti, F. (2018). A review of statistically-based landslide susceptibility models. Earth-Science Reviews, 180, 60–91.

Van Westen, C. J., Castellanos, E., & Kuriakose, S. L. (2008). Spatial data for landslide susceptibility, hazard, and vulnerability assessment: an overview. Engineering Geology, 102(3–4), 112–131.

Emulsion Electrospinning of PVA/Basil Essential Oil Nanofibers

MUSTAFA GEYSOĞLU*[1], FUNDA CENGIZ ÇALLIOĞLU[1]

Abstract: In this study, an oil-in-water emulsion electrospinning method was employed to fabricate nanofibers with potential applications in the medical field, particularly in wound dressings. Polyvinyl alcohol (PVA) was dissolved in deionized water to form the aqueous phase of the emulsion. Basil essential oil, renowned for its antimicrobial and antioxidant properties, was added at varying concentrations (0, 3, 6, 9, 12 wt%) to prepare emulsion solutions. These emulsions were characterized in terms of their viscosity, electrical conductivity, and surface tension to evaluate their spinnability and predict fiber formation behavior. Furthermore, the chemical composition of basil essential oil was analyzed using Gas Chromatography-Mass Spectrometry (GC-MS) in order to identify its major bioactive constituents. After electrospinning process; the resulting fibers were analyzed using Scanning Electron Microscopy (SEM) to examine their morphological features, such as fiber diameter, uniformity, and surface structure. The present study was systematically investigated the influence of basil oil concentration on fiber morphology and structural integrity. The objective of this study is to integrate the functional characteristics of basil oil with the high surface area and porosity of electrospun nanofibers. The integration of basil oil into nanofibers is expected to enhance their potential for use in biomedical applications, particularly as advanced wound dressings with inherent antimicrobial properties. The research will contribute to the development of novel functional nanofibrous materials for medical applications.

Keywords: Basil essential oil; Emulsion electrospinning; Nanofibers; Polyviny alcohol; Wound dressing.

[1]**Address:** Textile Engineering Department, Engineering&Natural Sciences Faculty, Süleyman Demirel University, Isparta, Türkiye,

***Corresponding author**: mgeysoglu@gmail.com

1. INTRODUCTION

Nanofibers are ultrafine fibers with diameters typically below 100 nanometers, exhibiting unique physicochemical properties such as high surface area-to-volume ratio, tunable porosity, and superior mechanical flexibility. These characteristics enable enhanced cell adhesion, efficient drug loading, and selective permeability, making nanofibers especially valuable in biomedical applications like wound healing, drug delivery, and tissue scaffolding. Electrospinning remains the most versatile technique for fabricating nanofibers with controlled morphology, composition, and functionalization. Additionally, nanofibers exhibit high thermal stability, optical tunability, and the ability to incorporate bioactive molecules, broadening their potential use in sensors, filtration systems, and energy storage devices (Zhang et al., 2023; Bhardwaj & Kundu, 2010).

Basil (*Ocimum basilicum*) essential oil contains bioactive components like linalool, methyl cinnamate, estragole, and eugenol, which contribute to its antioxidant, anti-inflammatory, antimicrobial, and anticancer properties (Kifer et al., 2023). Its potent free radical scavenging capacity (up to 96%) highlights its potential as a natural antioxidant (Elshafie & Camele, 2024). Furthermore, basil oil has demonstrated significant antimicrobial activity against pathogens such as *Staphylococcus aureus* and *Pseudomonas aeruginosa*, both commonly found in infected wounds (Abdelwahab et al., 2021). These bioactivities have led to its integration into medical textiles and wound dressings. Basil oil-loaded nanofibers and biopolymeric films have been developed for antimicrobial wound care, providing barrier protection and promoting healing without synthetic antibiotics (Ghosh et al., 2020).

The objective of this study is to fabricate a potential functional medical textile material for wound dressing applications through the emulsion electrospinning technique. The incorporation of basil (*Ocimum basilicum*) essential oil, recognized for its potent bioactive properties, into the nanofibrous matrix enhances its therapeutic functionality. It is anticipated that the inherent antimicrobial and anti-inflammatory properties of the essential oil will facilitate the wound healing process, thereby augmenting the biomedical efficacy of the material. The integration of basil essential oil into electrospun nanofibers has only been explored in a limited number of studies to date, emphasizing the novelty and scientific significance of the current research within the field of functional wound dressing.

2. MATERIAL AND METHOD

2.1. Materials

PVA, with a molecular weight ranging from 89,000 to 98,000 and a hydrolysis degree exceeding 99%, was utilized as the primary polymer, while distilled water was employed as the solvent medium. An oil-in-water emulsion was formulated using PEG-40 hydrogenated castor oil as the emulsifying agent, and Basil (*Ocimum basilicum*) essential oil was

incorporated as a functional additive. The PVA was sourced from Sigma-Aldrich (St. Louis, MO, USA), the surfactant was provided by Ersa Chemistry (Izmir, Türkiye), and the basil essential oil was obtained from Botalife (Isparta, Türkiye).

2.2. Methods

The experimental process was initiated with the preparation of emulsions intended for the fabrication of nanofibers through the process of emulsion electrospinning. The preparation was conducted in two sequential steps. Initially, an aqueous polymer solution was obtained by dissolving PVA in distilled water. In the subsequent step, varying proportions of basil essential oil and surfactant were incorporated into the PVA solution to form stable emulsions. The resulting mixtures were stirred at ambient temperature for approximately 24 hours to ensure homogeneity. Subsequently, the pivotal physicochemical properties of the emulsions, including electrical conductivity, viscosity, and surface tension, underwent comprehensive characterization. The detailed composition of the emulsions, including PVA, Basil and surfactant concentrations, was outlined in Table 1.

Table 1. The concentration of PVA, basil, and surfactant

Sample Codes	PVA (wt%)	Basil (wt%)	Surfactant (wt%)
B-0	10	0	5
B-3	10	3	5
B-6	10	6	5
B-9	10	9	5
B-12	10	12	5

The production of nanofiber was accomplished through the utilization of the emulsion electrospinning technique, a method that has been extensively employed for the fabrication of fine fibers with controlled morphology and functionality. During the process, critical electrospinning parameters were systematically optimized in preliminary experiments. These parameters included the applied voltage, the distance between the needle tip and the collector, and the flow rate of the polymer solution. Following optimization, these parameters given in Table 2 were consistently maintained throughout the entire spinning process to ensure uniform fiber formation. All electrospinning procedures were carried out under identical ambient conditions (e.g. temperature and humidity) in order to minimize variability between samples. The resulting nanofibers were collected directly onto aluminum foil substrates over a period of 15 minutes.

Table 2. Process parameters of emulsion electrospinning

Voltage (kV)	Distance Between Electrodes (cm)	Feed Rate (mL/h)	Humidity (%)	Temperature (°C)
20	20	0.2	43 (± 2)	22

The morphological characteristics of the nanofibers, including the average fiber diameter, the diameter distribution uniformity, and the surface of the fiber web, were examined using scanning electron microscopy (SEM). Quantitative measurements of fiber diameters were conducted using the ImageJ software. The statistical distribution of fiber diameters was evaluated, and diameter histograms were generated, using SPSS statistical software. Furthermore, the uniformity of the fiber diameters was assessed by calculating the fiber diameter uniformity coefficient, defined as the ratio of the weighted average diameter (Aw) to the number average diameter (An). A coefficient value approaching 1 indicates a high degree of uniformity among the fibers (Cengiz & Jirsak, 2009). The following formula was utilized to calculate the average fiber diameter uniformity coefficient values:

$$A_n = \frac{\sum n_i d_i}{\sum n_i} \quad \text{(Number average)} \tag{1}$$

$$A_w = \frac{\sum n_i d_i^2}{\sum n_i d_i} \quad \text{(Weight average)} \qquad (2)$$

ni=fiber number *di=fiber diameter*

In addition to the morphological characterization, the chemical composition of the basil essential oil employed in the study was identified through gas chromatography–mass spectrometry (GC-MS), a method that facilitated the detection and analysis of volatile compounds present in the oil.

3. RESULTS

As illustrated in Figure 1, the properties of the polymer solutions, which include viscosity, electrical conductivity, and surface tension, are influenced by the varying concentrations of basil essential oil. The findings indicate that basil concentration has a significant impact on all three parameters.

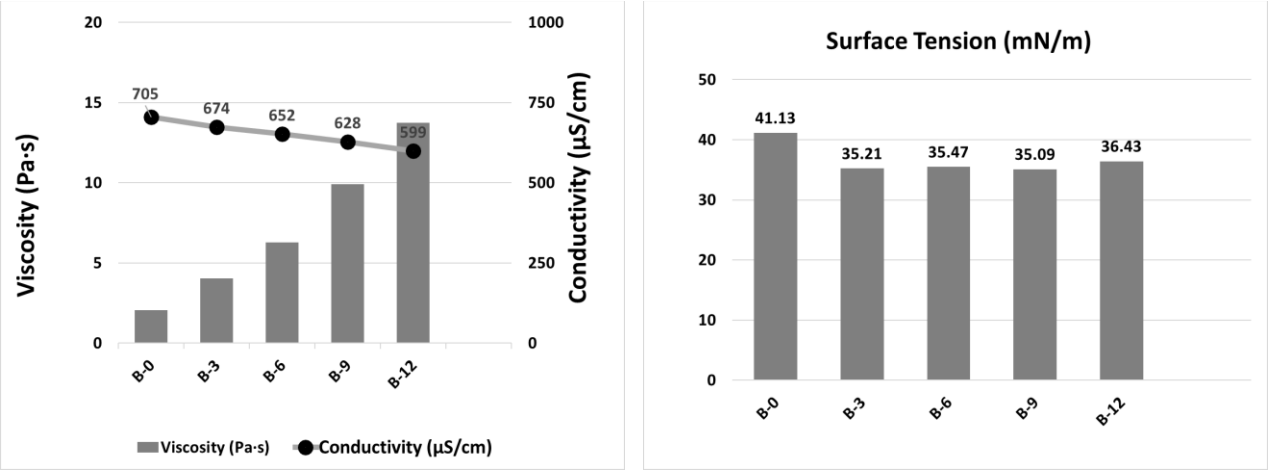

Figure 1. Results of polymer solutions properties with various concentrations of Basil

As anticipated, an increase in the viscosity of the polymer solutions was observed with rising concentrations of basil essential oil. The solution without basil (B-0) exhibited a viscosity of 2.042 Pa·s. The incorporation of 3% wt basil (B-3) resulted in an increase in viscosity to 4.035 Pa·s. The viscosity values of the B-6, B-9 and B-12 solutions with 6, 9 and 12 wt% basil content were measured as 6.267 Pa·s, 9.9 Pa·s and 13.75 Pa·s, respectively. This outcome is consistent with the findings from earlier studies that also demonstrated an increase in viscosity when herbal extracts or oils were incorporated into polymer matrices, such as poly(vinyl alcohol) (PVA), resulting from heightened molecular entanglement and intermolecular interactions (Bhardwaj & Kundu, 2010; Arıkan & Aksu, 2019).

Conversely, the electrical conductivity values exhibited a decreasing trend with elevated levels of basil content. The conductivity of the PVA solution (B-0) was measured at 705 µS/cm, while the solution containing 12% wt basil (B-12) exhibited a conductivity of 599 µS/cm. The decline in conductivity can be associated with the dilution effect of nonionic components present in the basil extract, which may reduce the number of free ions in the solution (Zamani et al., 2013). The presence of phenolic and essential oil compounds, which are predominantly non-conductive, could also contribute to this reduction. A similar phenomenon of conductivity suppression has previously been reported in polymer systems that incorporate essential oils (Rieger et al., 2013).

Surface tension analysis demonstrated that basil essential oil exerts a limited effect in reducing surface tension. The solution absents of basil exhibited a surface tension value of 41.13 mN/m. Following the incorporation of basil, a decline in surface tension values to a range of 35–36 mN/m was observed. However, an increase in the basil concentration beyond 3% wt did not result in any further significant changes in surface tension. This finding is consistent with the results of other studies, which demonstrated that essential oils surfactants initially reduced surface tension, subsequently stabilizing at concentrations that exceeded a critical value (Sill & von Recum 2008; Piletti et al., 2017).

The chemical composition of basil essential oil was analyzed using gas chromatography–mass spectrometry (GC–MS) method. The analysis yielded a total of 23 distinct chemical constituents, collectively accounting for 98.64% of the total oil composition, as detailed in Table 3. In the composition of the oil under scrutiny, the two most abundant compounds were determined to be *Estragole* (*allylanisole*), comprising 77.26%, and *α-Linalool*, comprising 15.99%. Collectively, these two components constituted over 93% of the total essential oil content, thereby underscoring their predominant role in the chemical profile of the basil extract (Yiğit et al., 2022).

Table 3. Components of basil essential oil by GC-MS analysis

Component Name	% Area
α-Pinene	0.15
Sabinene	0.11
α-Myrcene	0.07
o-Cymene	0.01
Dodecane	0.09
Linalool oxide	0.06
α-Linalool	**15.99**
I-Menthone	0.08
Menthol	0.67
p-Menth-1-en-8-ol	0.12
Estragole (allylanisole)	**77.26**
Z-Citral	0.54
E-Citral	0.76
Trans-Anethole	0.18
Trans-Caryophyllene	0.45
Trans-α-Bergamotene	0.38
α-Humulene	0.22
Trans-α-Farnesene	0.09
Germacrene-D	0.18
Bisabolene	1.12
Hexadecane	0.04
Heptadecane	0.03
Eicosane	0.04

Figure 2 presents the SEM images and histograms of fiber diameter of the nanofiber samples produced with different concentrations of basil. The SEM images are given at 1kx and 10kx magnifications. The morphological characteristics of the emulsion electrospun nanofibers were evaluated via SEM. Nanofibers produced using only PVA exhibited a smooth, bead-free, and homogeneous structure. The incorporation of basil did not significantly disrupt the fiber morphology. Fibers containing various concentrations of basil also displayed smooth and bead-free surfaces. Nevertheless, a slight change in surface morphology was observed in nanofibers loaded with basil, which exhibited a more adhesive appearance. This finding can be attributed to the presence of volatile and hydrophobic components in the basil essential oil, which may have interfered with the solvent evaporation during the emulsion electrospinning process. Fiber diameter analysis revealed an increase in standard deviation with rising basil concentration, indicating a broader diameter distribution. This suggests that while general fiber morphology remained intact, the addition of basil introduced some variability, probably due to changes in the rheological and electrical properties of the solution (Geysoğlu & Cengiz Çallıoğlu, 2024).

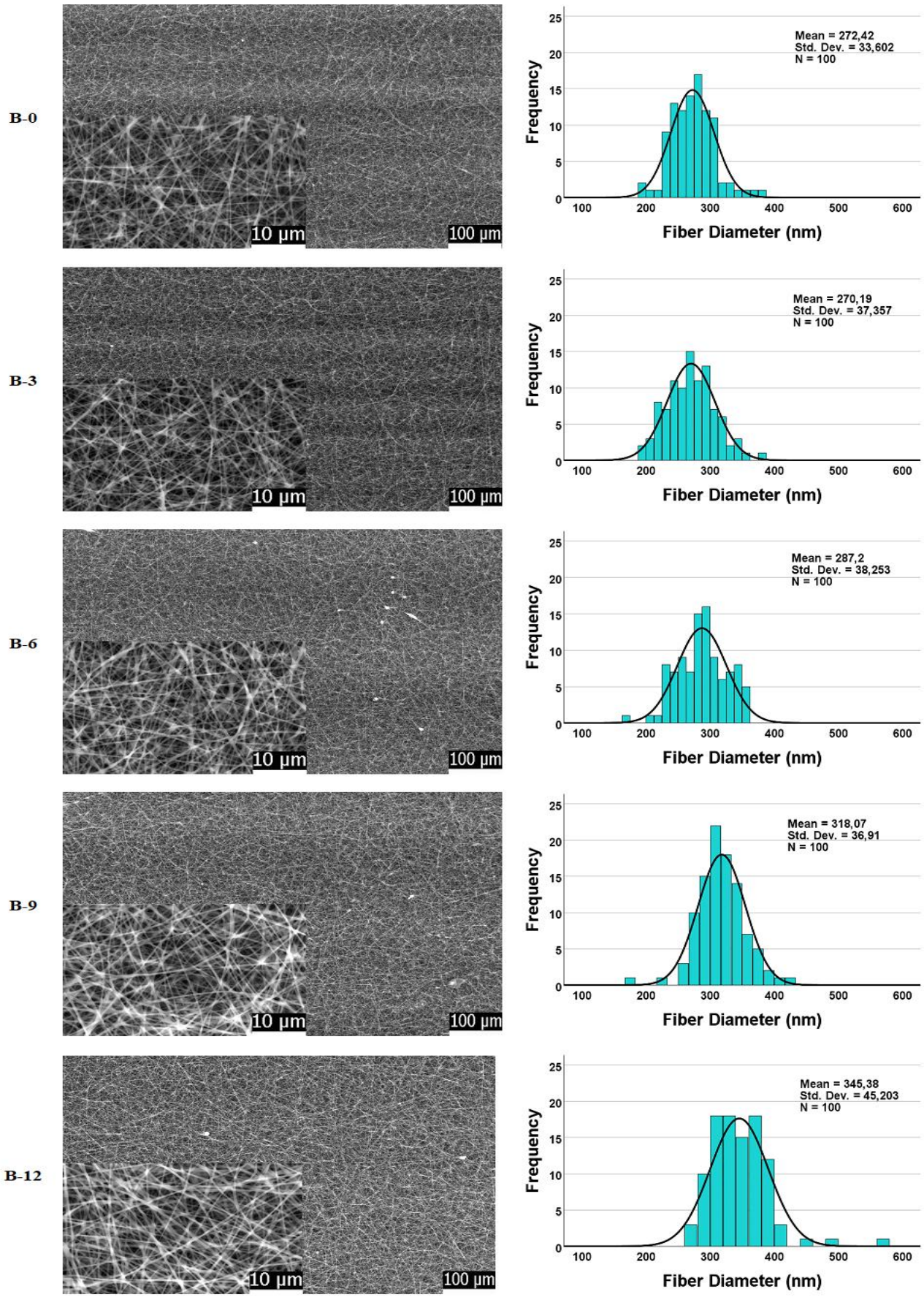

Figure 2. SEM images and fiber diameter histograms of basil based nanofiber samples produced with various concentrations (1kx, 10kx)

Figure 3 illustrates the influence of the concentration of basil essential oil on both the average fiber diameter and the fiber diameter uniformity coefficient.

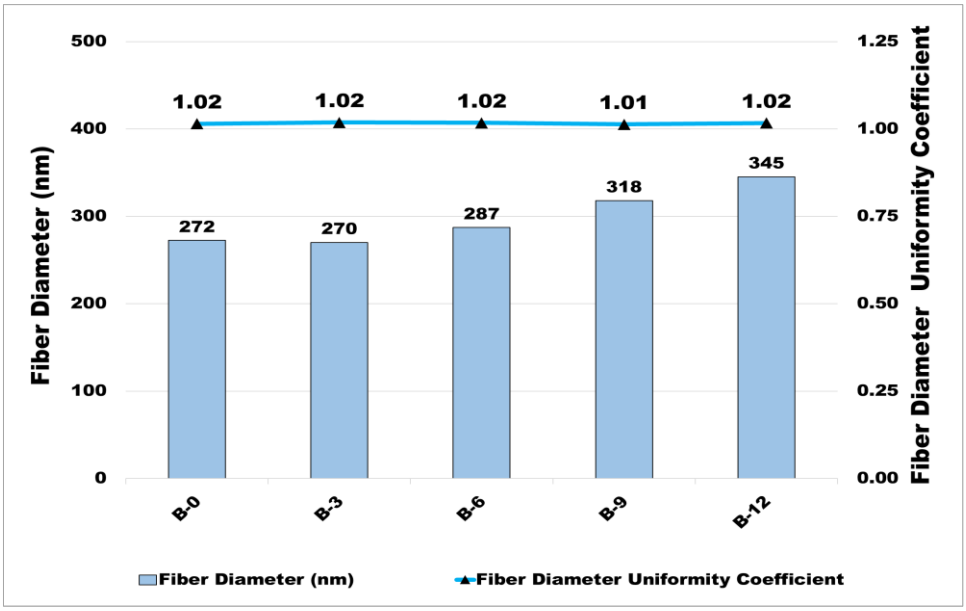

Figure 3. The effect of basil essential oil concentration on the average fiber diameter and fiber diameter uniformity coefficient of nanofibers

The average fiber diameter of nanofibers produced from PVA polymer alone was measured at 272 nm. The incorporation of basil essential oil into the polymer solution resulted in an increase in fiber diameter. This increase was found to be directly correlated with the concentration of basil added to the solution. Specifically, the nanofibers obtained from the solution containing 3 wt% basil (B-3) exhibited an average fiber diameter of 270 nm, which is comparable to the PVA-only sample. However, with further increases in basil concentration, an increase in the average fiber diameter was observed. The samples B-6, B-9, and B-12, which contained 6 wt%, 9 wt%, and 12 wt% basil, demonstrated average fiber diameters of 287 nm, 318 nm, and 345 nm, respectively. The results of this study indicate that the addition of basil to the electrospinning process contributes to an increase in solution viscosity. This, in turn, has the effect of reducing the stretching of the polymer jet during the electrospinning process, resulting in fibers that are thicker than those produced without basil. This finding is consistent with the results of previous studies on the incorporation of essential oils into electrospun fibers (Bhardwaj & Kundu, 2010).

Furthermore, the fiber diameter uniformity coefficients were analyzed in order to assess the consistency of fiber dimensions across all formulations. The findings suggest that the incorporation of basil exerted a negligible influence on fiber uniformity. It was demonstrated that all samples, including those with and without basil, exhibited uniformity coefficients ranging from 1.01 to 1.02. This finding indicates a relatively narrow and consistent fiber diameter distribution. This finding suggests that while the average diameter increased with basil concentration, the distribution of diameters around the mean remained stable.

4. DISCUSSION AND CONCLUSIONS

In this study, the emulsion electrospinning technique was used to successfully fabricate polyvinyl alcohol (PVA)-based nanofibers containing different concentrations of basil essential oil. The addition of basil essential oil resulted in significant changes to the properties of the solution, including increased viscosity and reduced conductivity. These changes subsequently influenced fiber formation during the electrospinning process.

SEM analysis revealed that all nanofibers maintained a smooth, bead-free and homogeneous morphology, regardless of basil content. However, nanofibers containing basil exhibited a slightly more adhesive surface structure, likely due to the interaction of volatile oil constituents with the fiber solidification process. An increase in the average fiber diameter was observed as the basil concentration increased, although fiber diameter uniformity coefficient remained within a narrow range.

GC-MS analysis of the basil essential oil showed that *α-Estragole* and *Linalool* were the dominant components, suggesting the potential for bioactivity, such as antimicrobial and antioxidant properties, in the nanofiber material. These findings suggest that not only do basil-loaded nanofibers retain their structural integrity, they also offer added value for use in active packaging, biomedical scaffolds, and wound dressings.

Overall, the results demonstrate that basil essential oil can be effectively incorporated into PVA nanofibers without compromising their structural integrity while imparting potential biofunctional properties. This approach presents a promising strategy for the development of multifunctional nanofibrous materials suitable for diverse applications, such as biomedical devices, packaging or wound dressings.

REFERENCES

Abdelwahab, S. I., Zainal, H., Sheikh, B. Y., & Taha, M. M. E. (2021). Antimicrobial and antioxidant properties of basil (*Ocimum basilicum*) essential oil: A review. *Natural Volatiles & Essential Oils, 8*(4), 1175–1183. Retrieved from https://www.nveo.org/index.php/journal/article/view/5214

Arikan, E. B., & Aksu, B. (2019). Electrospun PVA nanofibers incorporated with plant extracts for antimicrobial and antioxidant activity. *Journal of Applied Polymer Science, 136*(22), 47517.

Bhardwaj, N., & Kundu, S. C. (2010). Electrospinning: A fascinating fiber fabrication technique. *Biotechnology Advances, 28*(3), 325–347. https://doi.org/10.1016/j.biotechadv.2010.01.004

Cengiz, F., & Jirsak, O. (2009). The effect of salt on the roller electrospinning of polyurethane nanofibers. *Fibers and Polymers, 10*(2), 177–184.

Elshafie, H. S., & Camele, I. (2024). Basil (*Ocimum basilicum* L.) essential oil: Chemistry, biological activities, and applications. *Plants, 13*(1), 84. https://doi.org/10.3390/plants13010084

Geysoğlu, M., & Cengiz Çallıoğlu, F. (2024). Emulsion electrospinning of PVA/rosemary nanofibers. In *7th International Scientific Conference Contemporary Trends and Innovations in Textile Industry–CT&ITI 2024* (No. I Textiles & textile technol, pp. 116–125).

Ghosh, S., Mondal, A., & Mukhopadhyay, P. (2020). Basil essential oil-loaded PVA/gelatin nanofibrous scaffold promotes wound healing in diabetic mice model. *International Journal of Biological Macromolecules, 165*(Part B), 3006–3014. https://doi.org/10.1016/j.ijbiomac.2020.10.019

Kifer, D., Mandić, L., Klarin, B., Kosalec, I., & Vlainić, J. (2023). Chemical composition and biological activity of *Ocimum basilicum* L. essential oil: A review. *Molecules, 28*(12), 37160. https://doi.org/10.3390/molecules281237160

Manosroi, A., Dhumtanom, P., & Manosroi, J. (2011). Anti-proliferative activity of essential oils extracted from Thai medicinal plants on HeLa cancer cell lines. *American Journal of Applied Sciences, 8*(4), 293–300. https://doi.org/10.3844/ajassp.2011.293.300

Piletti, R., Monteiro, F. F., Costa, T. M. H., et al. (2017). Influence of essential oils on the physicochemical properties of electrospun PVA nanofibers. *Industrial Crops and Products, 108*, 749–757.

Rieger, K. A., Birch, N. P., & Schiffman, J. D. (2013). Designing electrospun nanofiber mats to promote wound healing—A review. *Journal of Materials Chemistry B, 1*(36), 4531–4541.

Sill, T. J., & von Recum, H. A. (2008). Electrospinning: Applications in drug delivery and tissue engineering. *Biomaterials, 29*(13), 1989–2006.

Yigit, N. O., Metin, S., Sabuncu, O. F., Didinen, B. I., Didinen, H., Ozmen, O., & Koskan, O. (2022). Efficiency of *Ocimum basilicum* and *Eucalyptus globulus* essential oils on anesthesia and histopathology of rainbow trout, *Oncorhynchus mykiss*. *Journal of the World Aquaculture Society, 53*(5), 1051–1061.

Zamani, M., Prabhakaran, M. P., & Ramakrishna, S. (2013). Advances in drug delivery via electrospun and electrosprayed nanomaterials. *International Journal of Nanomedicine, 8*, 2997–3017.

Zhang, C., Yu, S., & Wang, X. (2023). Recent advances in electrospun nanofibers for biomedical applications. *Materials Science and Engineering: C, 144*, 112242. https://doi.org/10.1016/j.msec.2023.112242

Evaluation of Mechanical and Tribological Properties of PTFE and MoS_2 filled Polyamide 66 Composites

HÜSEYIN EBEDİ[1], GÜRKAN ATAŞ[2], SALIH HAKAN YETGİN*[2]

Abstract: Polymer composites are used in tribological applications of industrial areas such as automotive, machinery, aerospace and medical with their properties such as low friction coefficient, high wear resistance and lightness. Polymers increase efficiency and prevent wear by reducing friction especially in brake systems, engine parts and bearings. Polyamide 66 (PA66) polymer is one of the thermoplastic materials used in industry due to its easy processability, corrosion resistance, very good resistance to solvents, self-lubricating and high wear resistance. In this study, the mechanical and tribological properties of polytetrafluoroethylene (PTFE) and molybdenum disulfide (MoS_2) filled PA66 composites were investigated. In order to determine the mechanical properties, tensile tests were carried out on samples produced by extrusion and injection moulding. MoS_2 filled to PA66 polymer increased the modulus of elasticity by 6.9%, tensile strength by 15.2% and decreased the elongation at break by 74.6%. On the other hand, PTFE filled PA 66 increased the modulus of elasticity by 14.5%, tensile strength by 16.9% and decreased the elongation at break by 66.8%. MoS_2 filled to PA 66 polymer increased the Shore A hardness by 5.7% and PTFE by 4.4%. Abrasion tests were carried out at room temperature with a pin on disc wear test at 0.5, 1.0 and 1.5 m/s sliding speed, 30 and 50 N force and 1000 m sliding distance. PTFE and MoS_2 solid lubricants filled to PA66 polymer significantly reduced the coefficient of friction and increased the wear resistance. PTFE was found to be a more effective solid lubricant in the development of tribological properties than MoS_2. It was determined that the transfer film layer affected the tribological behaviour depending on the applied sliding speed and load. The morphology of the fracture surfaces of the tensile test specimens was examined by scanning electron microscopy (SEM).

Keywords: friction, mechanical properties, polyamide, tribology, wear

[1]**Address:** Tarsus University, School of Graduate Studies, Mersin/Turkey
[2]**Address:** Tarsus University, Faculty of Engineering, Mersin/Turkey
[2*]**Address:** Tarsus University, Faculty of Engineering, Mersin/Turkey

***Corresponding author**: shakanyetgin@tarsus.edu.tr

1. INTRODUCTION

In recent years, polymer composites have used widespread application in tribological fields as replacements for traditional metallic materials, making the study of their friction and wear behavior commercially imperative (Palabiyik and Bahadur, 2002; Li et al., 2013; Lingesh et al., 2016; Zhang et al., 2020). Polymers and their composites are finding increasing use for a wide range of industrial applications such as bearing material, rollers, seals, gears, cams, wheels, and clutches (Pascoe, 1973; Demirci and Düzcükoğlu, 2014).

Polyamide 66 (PA66) polymer is a semi-crystalline thermoplastic with easy processability, a high melting point, corrosion resistance, very good resistance to solvents, self-lubricating and high abrasion resistance (Tjong et al., 2002; Lingesh et al., 2016; Rudresh et al., 2016). The good wear resistance and self-lubricating properties of PA66 polymer, as well as its good strength and stiffness, make these thermoplastics a promising candidate in bearing applications where two different housings are in contact under extreme sliding conditions (Pascoe, 1973; Chen et al., 2000; Demirci and Düzcükoğlu, 2014). Fillers, in particle and fiber form, are frequently used to improve the properties of PA 66 polymer. The incorporation of reinforcing fibers such as glass fibers, carbon fibers, or aramid fibers significantly enhances mechanical strength by effectively reduce deformation, but tend to break under heavy loading conditions and cause abrasion at the contact points (Basavaraj et al., 2012a). The addition of particles characterized as solid lubricants has the potential to reduce wear with low friction coefficient by forming a transfer film layer on the surface. Common solid lubricants used in thermoplastics are molybdenum disulfide (MoS_2), graphite (Gr) and polytetrafluoroethylene (PTFE) (Basavaraj et al., 2012b; Shangguan et al., 2021). Among these solid lubricants, PTFE is one of the commonly used solid lubricants with properties such as a low coefficient of friction, high thermal and chemical stability (Palabiyik and Bahadur, 2002; Demirci and Düzcükoğlu, 2014; Bijwe et al., 2016; Zhang et al., 2020). PTFE is also a highly crystalline engineering polymer known for its hardness and durability (Lı, 2010; Rudresh et al., 2016). The low coefficient of friction of PTFE arises from the ability of its extended-chain linear molecules, $-(CF_2\text{-}CF_2)_n-$, to form low shear-strength films both on its own surface and on opposing surfaces during sliding (Khedkar et al., 2002; Takeichi et al., 2008; Sun et al., 2016). Even at low PTFE amounts, PTFE debris that breaks off from the matrix due to the applied external force forms a continuous and smooth transfer film that is easily deformed due to low surface energy and poor creep resistance. At the same time PTFE retains its lubricating properties at high temperatures. (Zhang et al., 2008; Rodriguez et al., 2016). MoS_2 is a kind of solid

lubricant material with excellent performance, which can be used to extend the service life of machine elements under mechanical working conditions such as high pressure, high temperature, high load and high speed. (Shangguan et al., 2021). MoS_2 solid lubricant is in the form of black crystalline powder and has a layered structure. MoS_2 solid lubricant is in the form of black crystalline powder and has a layered structure. Due to its low friction properties, it is also widely used as a solid lubricant up to relatively high temperatures MoS_2 with particle sizes in the range of 1-100 μm, when added to polymer materials, forms composite structures with improved strength and reduced coefficient of friction. The self-lubricating properties are associated with the large area between the S-Mo-S sandwich layers and the weak Van der Waals forces and the pure positive charge on the surface, resulting in the propagation of electrostatic repulsion. Due to its low friction properties, it is also widely used as a solid lubricant up to relatively high temperatures. (Baş, 2023). MoS_2 is more easily subjected to shear stress parallel to the layers than along the layers and can easily deform parallel to the layers while being able to bear high forces at right angles to the layers. This property is effectively utilised for lubrication. The coefficient of friction is more or less equal to the shear stress parallel to the layers divided by the yield stress or hardness perpendicular to the layers. Since low friction only occurs parallel to the layers, it follows that these solid lubricants are only effective when the layers are parallel to the sliding direction (Basavaraj et al., 2012a; Basavaraj et al., 2012b).

In this study, the effect of solid lubricants such as PTFE and MoS_2 added to PA66 polymer, which has a wide range of applications in different areas of industry, especially in the automotive sector, on mechanical and tribological properties was investigated. In addition to tensile and hardness tests, tribological properties were investigated with pin-disc system at different loads and sliding speeds to determine the coefficient of friction and wear amount. The effect of sliding speed and load on the PA66 polymer was evaluated and the wear surfaces were examined by optical microscope.

2. MATERIAL AND METHOD

Tecomid®NA40-NL-E commercial code PA66 polymer, Tecomid®NA30-NL-RM commercial code PA66-MoS2 and Tecomid®NA40-NL-JA 0D commercial code PA66+PTFE composites produced by extrusion and injection moulding methods were obtained from Eurotech®. Test specimens were produced in accordance with the standards. Tensile tests were performed in accordance with ASTM D638 standard on a Zwick Roell Z-200 machine at room temperature and at a tensile speed of 5 mm/min. Shore D hardness tests were performed using the Tronic-PD801 device in accordance with the ISO 868 standard and the average of at least 10 measurements was taken. Tribological tests were carried out under dry sliding conditions at room temperature using a pin-disc abrasion tester. Table 1 shows the wear test parameters for the materials used in the study. AISI 1040 steel was used as the counter disc material. The surface roughness of the steel disc was determined as 0.32-0.50 R_a. Before each wear test, the steel disc and polymer composite pin surfaces were cleaned with acetone and dried. The sample pin weight (m_1) before each wear test and the pin weight (m_2) after the wear test were measured and the weight loss Δm (m_1-m_2) was determined. The specific wear rate (K_o) was calculated by the formula given in Equation (1). In the formula, L is the sliding distance (m), ρ is the density of the material (g/cm^3) and F is the applied load (N).

Table 1. Abrasion test parameters

Material	Test Temperature (°C)	Sliding Distance (m)	Applied Load (N)	Sliding Speed (m/s)
PA66			30	0.5
PA66/PTFE	22±2	1000	40	1.0
PA66/MoS_2			50	1.5

$$K_0 = \frac{\Delta_m}{L*\rho*F} \quad (1)$$

3. RESULTS

Figure 1 a-d shows the mechanical properties such as modulus of elasticity, tensile strength, elongation at break and Shore D hardness values of PA66 polymer and PTFE and MoS_2 filled PA66 composites after tensile test. While the modulus of elasticity, which is an indicator of the stiffness of the materials, was 2961 MPa for PA66 polymer, it increased by 6.9% with MoS_2 filling to 3165 MPa. PTFE additive added to PA66 polymer caused a 14.5% decrease in the modulus of elasticity. The modulus of elasticity of PA66/PTFE composite was obtained as 2531 MPa. Basavaraj et al. (2012) also stated that the mechanical properties increased depending on the amount of MoS_2 filling added to the PA66/Carbon black composite. (Basavaraj et al., 2012b). When the tensile strength results were examined, PTFE and MoS_2 added to PA66 polymer caused a decrease in tensile strength. This decrease was 16.9% for PTFE polymer and 15.2% for MoS2 additive. Similar results were obtained in studies by Zhao (Zhao et al., 2006), Zhang (Zhang et al., 2020) and Rudresh (Rudresh et al., 2016). It has been stated that particles dispersed in the matrix material (such as PTFE and MoS_2) may cause stress concentrations and this may reduce the tensile strength by reducing the interaction between polymer molecule chains

(Rudresh et al., 2016; Shangguan et al., 2021). In another explanation, it was stated that the poor interfacial interaction between such as PTFE and MoS_2 and the polymer matrix will cause the formation of voids and discontinuity defects in the structure and the mechanical properties will decrease (Rudresh et al., 2016; Zhang et al., 2020). The elongation at break value of PA66 polymer, which was 21.8%, decreased by 74.6% to 5.5% with MoS2 addition and decreased by 66.8% to 7.2% with PTFE addition. This is because MoS_2 (~240 GPa) filling is more rigid than PTFE (~0.5 GPa) filling (Bandaru et al., 2023; Srivastava et al., 2024) Similar results were obtained in studies by Shangguan (Shangguan et al., 2021) and Palabiyik (Palabiyik and Bahadur, 2002). When Shore D hardness values were examined, the hardness value of PA66 polymer increased significantly with the addition of MoS_2, while it decreased with the addition of PTFE. The hardness value of PA66 polymer, which was 78.6 Shore D, increased by 5.7% in PA66/MoS_2 composite and 83.1 Shore D was obtained, while it decreased by 1.0% in PA66/PTFE composite and 77.8 Shore D was obtained. The addition of PTFE, which is softer and self-lubricating, to PA66 polymer caused a slight decrease in Shore D hardness. Hard mineral-based fillers such as MoS_2 increased the hardness value of PA66 polymer (Basavaraj et al., 2012a; Rudresh et al., 2016). The effect of MoS_2 filling on mechanical properties compared to PTFE filling is related to the strength properties of MoS_2 filling itself. MoS_2 filling acted as strength and tribo-carrier during the performance of the composites (Rudresh et al., 2016).

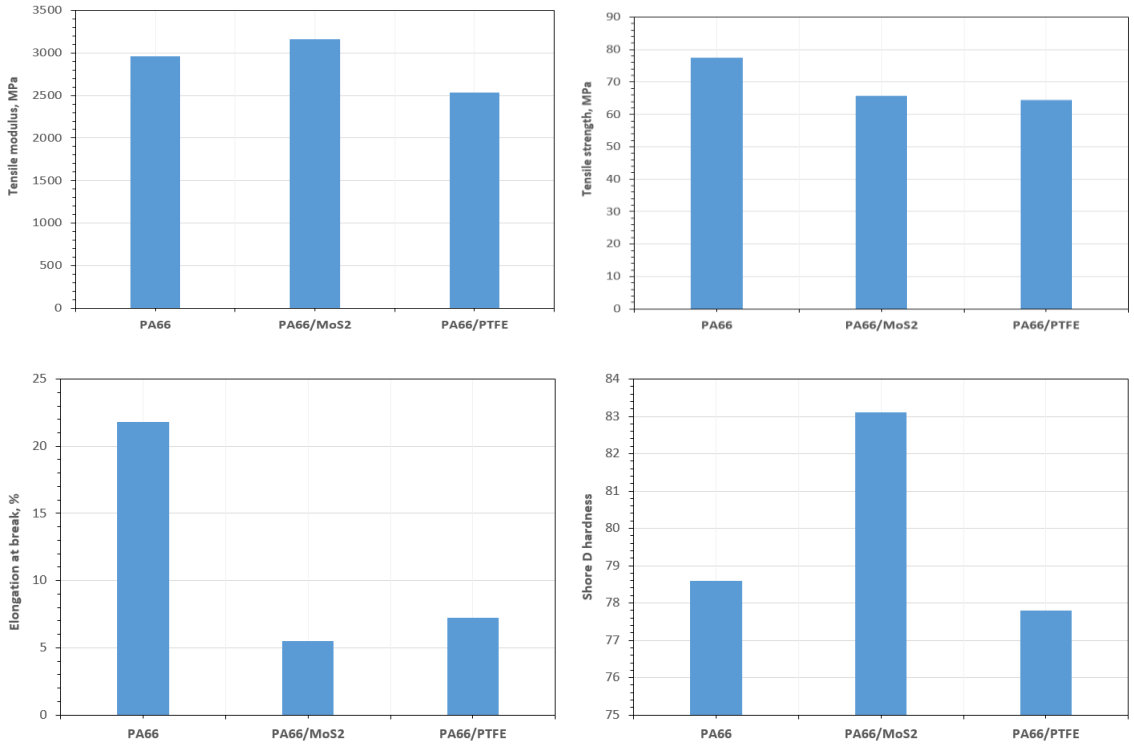

Figure 1. Mechanical properties and Shore D hardness test results **a)** modulus of elasticity **b)** tensile strength **c)** % elongation at break **d)** Shore D hardness value

Fracture surface images of PA66 polymer PA66/PTFE and PA66/MoS_2 composites obtained after tensile tests were taken using scanning electron microscopy (Figure 2). As seen in Figure 2, PA66 polymer has a ductile fracture surface image. MoS_2 and PTFE added to PA66 polymer transformed the fracture surfaces into brittle. This is supported by the elongation at break results. It was observed that PTFE and MoS_2 particles were homogeneously dispersed in the structure, but PTFE particles separated/detached from the matrix due to weak interfacial interaction. This explains why the mechanical properties of PTFE/PA66 composites are lower than MoS_2/PA66 composites. EDS analysis revealed the presence of Fluorine (F) atoms in the structure for PA66/PTFE composite and Molybdenum (Mo) atoms in the structure for PA66/MoS_2 composite.

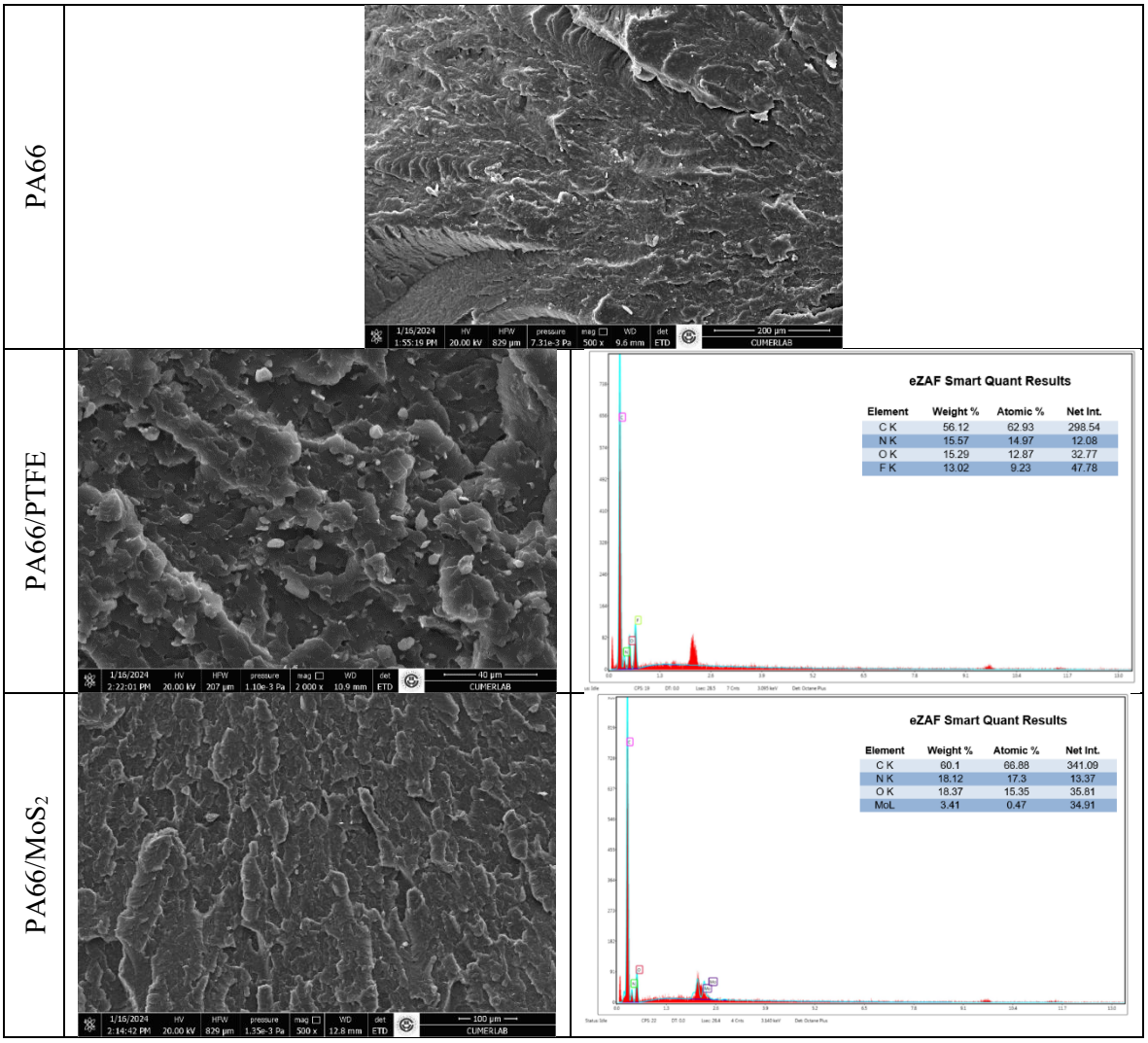

Figure 2. Fracture surface images of PA66 polymer and PA66/MoS_2 and PA66/PTFE composites after tensile test

Table 2 presents coefficient of friction values for PA66 and its composites tested at room temperature, at dry sliding conditions and under 30, 40 and 50N loads and at 0.5, 1.0 and 1.5 m/s sliding speed. Figure 3 presents the variation of the coefficient of friction with sliding distance for PA66 polymer, PA66/PTFE and PA66/MoS_2 composites materials tested under 50N load and 1.0m/s sliding speed. It is clear from this figure that for both PA66 polymer and PA66 composites, there are two flat stages in the coefficient of friction-sliding distance curves can be observed. This general behavior is observed for polymer composites. The coefficient of friction increased rapidly within the running-in period and attains a stable value within the steady state period. In the initial phase, the friction coefficients were at a minimum level. This may be due to less contact of rough surfaces due to the shorter test period. With the increase in sliding distance, the friction coefficient reached a steady state. The increase in sliding distance and asperity contacts may be related to the increase in the friction coefficient (Yetgin, 2020). When the roughness on the contact surfaces was balanced, the friction coefficient reached a steady state. The running-in period ended at 400-450 m for PA66 polymer with an increase of coefficient of friction values to 0.4. The friction coefficient of both PA66/PTFE and PA66/MoS_2 composites showed a similar change and reached steady state in a shorter sliding distance (150 m).

Table 2. Average coefficient of friction values for PA66 polymer, PA66/PTFE and PA66/MoS_2 composites tested at different load and sliding speed values.

Materials	Load (N)	Sliding speed (m/s)		
		0.5	1.0	1.5
		Coefficient of friction (μ)		
PA66	30	0.3269	0.3658	0.4118
	40	0.3473	0.3853	0.4336
	50	0.3718	0.4045	0.4587
PA66/PTFE	30	0.1951	0,2011	0.2135
	40	0.2025	0.2155	0.2312
	50	0.2175	0.2331	0.2451
PA66/MoS_2	30	0.1634	0.1722	0.1847
	40	0.1837	0.2014	0.2158
	50	0.2033	0.2175	0.2253

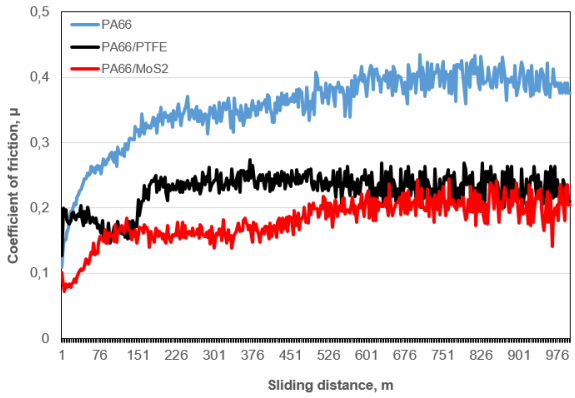

Figure 3. The variation of the coefficient of friction with sliding distance (Speed: 1.0 m/s, Load:50 N)

Figure 4a shows the change in the coefficient of friction of PA66 polymer and PA66/PTFE and PA66/MoS_2 composites depending on different sliding speeds under constant 40 N load. When the friction coefficient results are examined in Figure 4a, it is determined that the friction coefficient increases with increasing sliding speed. While the coefficient of friction of PA66 polymer was 0.3473 at 0.5 m/s sliding speed under constant 40 N load, the coefficient of friction was 0.3853 for 1.0 m/s and 0.4336 for 1.5 m/s sliding speed with increasing sliding speed. For PA66 polymer, the coefficient of friction increased by 24.8% with increasing the sliding speed by 200%. For PA66/PTFE composite, the coefficient of friction increased by 14.1% from 0.2025 to 0.2312 due to increasing sliding speed. For PA66/MoS_2 composite, the coefficient of friction increased by 17.4% from 0.1837 to 0.2158 for 0.5 m/s sliding speed. Figure 4b shows the friction coefficient results depending on the load applied at a constant sliding speed of 1.0 m/s. As seen in the figure, it is determined that the coefficient of friction increases with increasing load. The coefficient of friction for PA66 polymer increased by 10.5% from 0.3658 to 0.4045 with increasing load. For PA66/PTFE composite, the coefficient of friction increased by 15.9% and for PA66/MoS_2 composite by 26.3% with increasing load. In the applied sliding speed and load ranges, the highest coefficient of friction was obtained in the unfilling PA66 polymer with a value of 0.4587 at 1.5 m/s sliding speed and 50 N load, while the lowest coefficient of friction was obtained in the PA66/MoS_2 composite with a value of 0.1634 at 0.5 m/s sliding speed and 30 N load. When the effect of sliding speed and applied load values on the coefficient of friction was evaluated, it was determined that the most effective parameter on the coefficient of friction was the applied load.

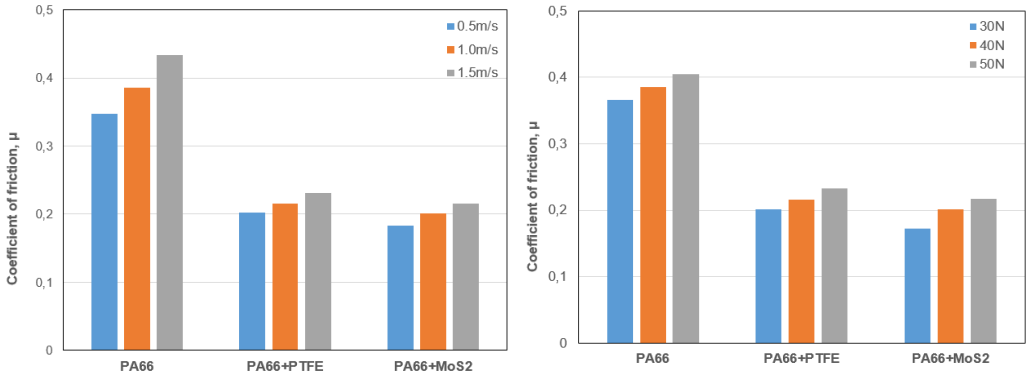

Figure 4. a) 40 N load, b) friction coefficient change depending on 1.0 m/s sliding speed

Table 3 presents specific wear rate values for PA66 and PA66 composites tested at room temperature, at dry sliding conditions and under 30, 40 and 50 N loads and at 0.5, 1.0 and 1.5 m/s sliding speed. Figure 5a and 5b shows the variation in wear rates for 40 N load and 1.0 m/s sliding speed. The specific wear rate for PA6 polymer and PA66/PTFE and PA66/MoS_2 composites was obtained around $10E^{-10}$ mm^3/Nm. When the specific wear rates under 40 N load are evaluated in Figure 5a, it is determined that the wear rates increase significantly with increasing sliding speed. The specific wear rate increased by 49.0% with 200% increase in the applied load for PA66 polymer, 44.6% for PA66/PTFE composite and 41.1% for PA66/MoS2 composite. As can be seen in Figure 5b, the wear rate increased by increasing the load from 30 N to 50 N at a sliding speed of 1.0 m/s. This increase was 32.8%, 28.2% and 33.9% for PA6 polymer and PA66/PTFE and PA66/MoS_2 composites, respectively. The highest wear rate was obtained for PA6 polymer at 1.5 m/s sliding speed and 50 N load. The wear rate value was determined as $5.8771E^{-10}$ mm^3/Nm. The lowest wear rate was obtained in PA66/MoS_2 composite at 0.5 m/s sliding speed and 30 N load. The wear rate was determined as $1.0233E^{-10}$ mm^3/Nm.

Table 3. Specific wear rate values for PA66 and PA66 composites tested at different load and sliding speed values.

Materials	**Load (N)**	**Sliding speed (m/s)**		
		0.5	1.0	1.5
		Specific wear rate (mm^3/Nm)		
PA66	30	$3,0117E^{-10}$	$3,4210E^{-10}$	$4,4444E^{-10}$
	40	$3,4429E^{-10}$	$3,9254E^{-10}$	$5,1315E^{-10}$
	50	$4,2982E^{-10}$	$4,5438E^{-10}$	$5,8771E^{-10}$
PA66/PTFE	30	$1,2146E^{-10}$	$1,4406E^{-10}$	$1,5536E^{-10}$
	40	$1,3771E^{-10}$	$1,6313E^{-10}$	$1,9915E^{-10}$
	50	$1,5593E^{-10}$	$1,8474E^{-10}$	$2,3389E^{-10}$
PA66/MoS_2	30	$1,0233E^{-10}$	$1,2573E^{-10}$	$1,3450E^{-10}$
	40	$1,1184E^{-10}$	$1,4035E^{-10}$	$1,5789E^{-10}$
	50	$1,3333E^{-10}$	$1,6842E^{-10}$	$1,9824E^{-10}$

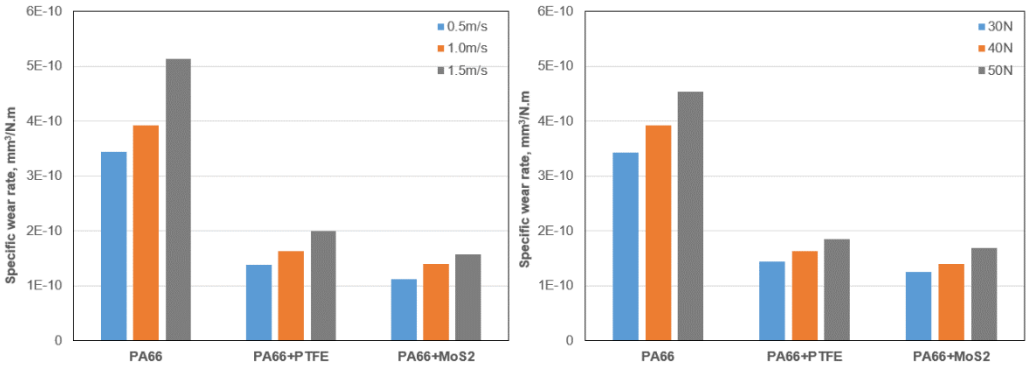

Figure 5. a) 40 N load, b) specific wear rate variation depending on 1.0 m/s sliding speed

Figure 6 shows the P.V factor plot showing the effect of load and velocity on wear rate and friction coefficient for PA66 polymer and PA66/PTFE and PA66/MoS_2 composites. The P.V factor is calculated by Equation 2 (Abdelbary, 2015).

$$P.V \text{ factor} = (\text{load } x \text{ velocity})/\text{pin area} \quad (2)$$

The coefficient of friction and wear rate were affected by the applied sliding speed and load. It was observed that the wear rate and coefficient of friction increased with the increase of the P.V factor. It was also determined that the wear rate and coefficient of friction varied depending on the PTFE and MoS_2. Friction coefficient and wear rate decreased with the addition of PTFE and MoS_2 to PA66 polymer. At 1.0 m/s sliding speed and 40 N load, PTFE and MoS_2 added to PA66 polymer reduced the coefficient of friction by 44.0% and 47.7%, respectively, while specific wear rates decreased by 58.4% and 64.2%. Ye et al. (2009) reported in their study that high load and frequency promote the formation of transfer films. It was stated that the high load carrying capacity of the transfer film layer and the superior wear resistance performance of solid film lubricants such as PTFE and MoS_2 affect the wear and friction behavior.

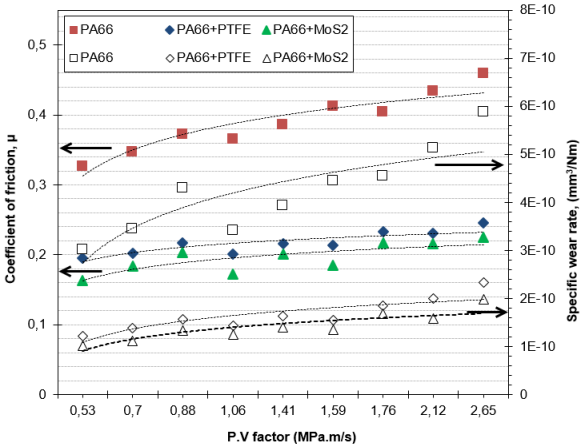

Figure 6. Variation of coefficient of friction and specific wear rate depending on P.V factor

Figure 7 shows the pin and disc optical images of PA66 polymer and PA66/PTFE and PA66/MoS_2 composite samples obtained after wear test. When the disc images were examined, it was observed that a transfer film layer was formed with wear particles that reduced the friction between the pin and disc. As is known, the characteristics of the transfer film layer formed for polymers and their composites play an important role in determining tribological properties. It was observed that the wear surfaces of the pure PA66 polymer had thin but numerous wear grooves in the sliding direction, while the steel disc had an irregular transfer film layer. In other words, abrasive wear mechanism was observed for the pure PA66 polymer. It was observed that the PTFE and MoS_2 added to the PA66 polymer resulted in fewer wear marks and a smooth surface on the wear surfaces. The transfer film layer formed on the disc surfaces interrupted the contact between the steel disc and the polymer pin, resulting in a decrease in the coefficient of friction and an increase in wear resistance. It has been reported that abrasive and adhesive wear mechanisms are observed during the contact of filler or reinforced polymer composites with the metal disc surface. The most important feature of adhesive wear is the transfer of the soft polymer to the harder metal disc surface (Palabiyik and Bahadur, 2002; Basavaraj et al., 2012a; Demirci and Düzcükoğlu, 2014). The reason why MoS_2 filled composites show lower coefficient of friction and wear rate than PTFE filled composites; This is mainly because the active element of MoS_2 has a strong adsorption on the bimetal atoms, the MoS_2 particles are easy to fall off and transfer to the metal surface to form a stable film layer, thus reducing the friction coefficient of PA66 composites (Shangguan et al., 2021).

	PA66	PA66/MoS_2	PA66/PTFE

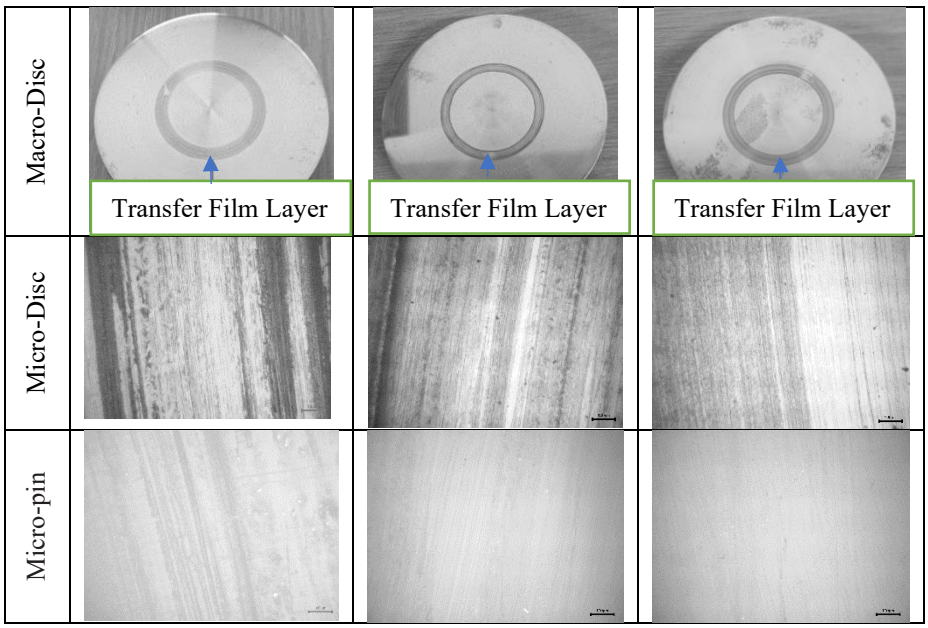

Figure 7. Optical microscope pictures (Sliding speed: 1.0 m/s, Load: 50N)

4. DISCUSSION AND CONCLUSIONS

As a result of the study in which the mechanical and tribological properties of PA66 polymer and PA66/PTFE and PA66/MoS_2 composites were investigated, the following results were obtained. MoS_2 added to PA66 polymer increased the modulus of elasticity by 6.9% and PTFE decreased it by 14.5%.

The addition of PTFE and MoS_2 to PA66 polymer caused the tensile strength to decrease by 16.9% and 15.2%. The elongation at break value of PA66 polymer, which was 21.8%, decreased by 74.6% to 5.5% with MoS_2 addition and decreased by 66.8% to 7.2% with PTFE addition. When the friction coefficient results were evaluated, it was determined that the friction coefficient increased with increasing load and sliding speed. In the applied sliding speed and load ranges, the highest coefficient of friction was obtained for the unfilled PA66 polymer at 1.5 m/s sliding speed and 50 N load, while the lowest coefficient of friction was obtained for the PA66/MoS_2 composite at 0.5 m/s sliding speed and 30 N load. The specific wear rate for PA6 polymer and PA66/PTFE and PA66/MoS_2 composites was obtained around $10E^{-10}$ mm^3/Nm. The lowest wear rate was obtained in PA66/MoS_2 composite at 0.5 m/s sliding speed and 30 N load. It was observed that the wear rate and friction coefficient increased with increasing P.V factor. While abrasive wear mechanism was observed in PA66 polymer, the transfer film layer formed on the disc surface caused adhesive wear mechanism in PA66/PTFE and PA66/MoS_2 composites. As a result of the study, it was determined that MoS_2 solid lubricant was the most effective solid lubricant in terms of tribological properties in the applied load and sliding speed ranges.

Ethics Committee Approval
N/A

Peer-review
Externally peer-reviewed.

Author Contributions / Yazar Katkıları
All authors contributed equally

Conflict of Interest / Çıkar Çatışması
The authors have no conflicts of interest to declare.

Funding / Finansal Destek
The authors declared that this study has received no financial support.

REFERENCES

Abdelbary, A. (2015). Wear of polymers and composites. Woodhead Publishing. https://doi.org/10.1016/C2014-0-03367-9

Bandaru, A. K., Khan, A. N., Durmaz, T., Alagirusamy, R., & O'Higgins, R. M. (2023). Improved mechanical properties of multi-layered PTFE composites through hybridisation. Construction and Building Materials, *374*, 130921. https://doi.org/10.1016/j.conbuildmat.2023.130921

Basavaraj, E., Ramaraj, B., & Siddaramaiah. (2012a). A study on mechanical, thermal, and wear characteristics of nylon 66/molybdenum disulfide composites reinforced with glass fibers. Polymer Composites, *33*(9), 1570–1577. https://doi.org/10.1002/pc.22293

Basavaraj, E., Ramaraj, B., Lee, J.-H., & Siddaramaiah. (2012b). Microstructure, thermal, physico–mechanical and tribological characteristics of molybdenum disulphide-filled polyamide 66/carbon black composites. Polymer Engineering & Science, *53*(8), 1676–1686. https://doi.org/10.1002/pen.23428

Baş, H. (2023). Tribological properties of MoS_2 particles as lubricant additive on the performance of statically loaded radial journal bearings. Turkish Journal of Engineering, *7*(1), 42–48. https://doi.org/10.31127/tuje.1016153

Bijwe, J., Naidu, V., Bhatnagar, N., & Fahim, M. (2006). Optimum concentration of reinforcement and solid lubricant in polyamide 12 composites for best tribo-performance in two wear modes. *Tribology Letters, 21*(1), 57–64. https://doi.org/10.1007/s11249-005-9010-7

Chen, Y. K., Kukureka, S. N., Hooke, C. J., & Rao, M. (2000). The wear mechanisms of polyethylene and polyamide bearing materials. Journal of Materials Science, *35*, 1269–1281. https://doi.org/10.1023/A:1004709125092

Demirci, M. T., Düzcükoğlu, H. (2014). Wear behaviors of polytetrafluoroethylene and glass fiber reinforced polyamide 66 journal bearings. Materials and Design, 57, 560–567. https://doi.org/10.1016/j.matdes.2014.01.013

Khedkar, J., Negulescu, I., & Meletis, E. I. (2002). Sliding wear behavior of PTFE composites. *Wear, 252(5–6),* 361–369. https://doi.org/10.1016/S0043-1648(01)00859-6

Lı, J. (2010). Friction and wear properties of PTFE composites filled with PA6. Polymer Composites, 31(1), 38–42. https://doi.org/10.1002/pc.20762

Li, D., Xie, Y., Li, W., You, Y., Deng, X. (2013). Tribological and mechanical behaviors of polyamide 6/glass fiber composite filled with various solid lubricants. Advances in Materials Science and Engineering, 9 pages. https://doi.org/10.1155/2013/320837

Lingesh, B. V., Ravikumar, B. N., & Rudresh, B. M. (2016). Investigation on the mechanical behavior of polyamide 66/polypropylene blends. Indian Journal of Advances in Chemical Science, 4(2), 168–171.

Palabiyik, M., Bahadur, S. (2002). Tribological studies of polyamide 6 and high-density polyethylene blends filled with PTFE and copper oxide and reinforced with short glass fibers. Wear, 253(3-4), 369–376. https://doi.org/10.1016/S0043-1648(02)00144-8

Pascoe, W. (1973). Plain and filled plastics materials in bearing: A review. Tribology, *6*(5), 184–190. https://doi.org/10.1016/0041-2678(73)90145-0

Rodriguez, V., Sukumaran, J., Schlarb, A. K., & De Baets, P. (2016). Influence of solid lubricants on tribological properties of polyetheretherketone (PEEK). Tribology International, 103, 45–57. https://doi.org/10.1016/j.triboint.2016.06.037

Rudresh, B. M., Ravikumar, B. N., & Madhu, D. (2016). Hybrid effect of micro fillers on the mechanical behavior of polyamide66/polytetrafluoroethylene blend. Indian Journal of Advances in Chemical Science, 4(1), 77-84.

Srivastava, M., Banerjee, S., Bairagi, S., Singh, P., Kumar, B., Singh, P., Kale, R. D., Mulvihill, D. M., & Ali, S. W. (2024). Recent progress in molybdenum disulfide (MoS_2) based flexible nanogenerators: An inclusive review. Chemical Engineering Journal, 480, 147963. https://doi.org/10.1016/j.cej.2023.147963

Sun, Y., Zhang, Q., Gao, L., Zhou, X., Cheng, Y., & Zhang, P. (2016). Experimental study on tribological properties of carbon/polytetrafluoroethylene hybrid fabric reinforced composite under heavy loads and oil lubrication. Tribology International, 94, 82–86. https://doi.org/10.1016/j.triboint.2015.08.019

Shangguan, J., Song, L., Lang, F., Yang, H., Li, D., Wang, J., Jiang, Q., & You, Y. (2021). Preparation and properties of MoS_2 modified polydimethylsiloxane/monomer casting nylon. Materials Research Express, 8(5), 055303. https://doi.org/10.1088/2053-1591/abfa47

Takeichi, Y., Wibowo, A., Kawamura, M., & Uemura, M. (2008). Effect of morphology of carbon black fillers on the tribological properties of fibrillated PTFE. *Wear, 264*(3–4), 308–315. https://doi.org/10.1016/j.wear.2007.03.013

Tjong, S. C., Shi-Ai, X., Robert, K., Yiu, L., Yiu-Wing, M. (2002). Short glass fiber reinforced polyamide 66 composites toughened with maleated SEBS. Composites Science and Technology, 62(15), 2017–2027. https://doi.org/10.1016/S0266-3538(02)00140-9

Ye, Y., Chen, J., & Zhou, H. (2009). An investigation of friction and wear performances of bonded molybdenum disulfide solid film lubricants in fretting conditions. We*ar, 266*(7–8), 859–864. https://doi.org/10.1016/j.wear.2008.12.012

Yetgin, S. H. (2020). Tribological properties of compatibilizer and graphene oxide-filled polypropylene nanocomposites. Bulletin of Materials Science, *43*(89). https://doi.org/10.1007/s12034-020-2061-4

Zhang, X., Liao, G., Jin, Q., Feng, X., & Jian, X. (2008). On dry sliding friction and wear behavior of PPESK filled with PTFE and graphite. Tribology International, 41(3), 195–201. https://doi.org/10.1016/j.triboint.2007.08.003

Zhang, H., Wu, Y., Liang, M., Wu, H., Zou, H., Chen, Y., Zhou, S. (2020). Comparative study on the mechanical, tribological, and thermal properties of POM composites filled with different PTFE. Journal of Thermoplastic Composite Materials, 1–23. https://doi.org/10.1177/0892705720932620

Zhao, R., Luo, W., Xiao, H., & Wu, G. (2006). Water-absorptivity and mechanical behaviors of PTFE/PA6 and PTFE/PA66 blends. Transactions of Nonferrous Metals Society of China, *16*(2), s498–s503. https://doi.org/10.1016/S1003-6326(06)60243-4

Energetic and Exergetic Performance Investigation of the Transcritical High-Temperature Heat Pump System

Fatih YILMAZ*[1]

Abstract: The uncertainty that has emerged due to the recent increase in natural gas prices and global problems has made heat pump systems important again. Heat pump systems are thermodynamic systems that take heat from a low-temperature side and transfer it to a higher-temperature side using a compressor and are used for heating purposes. In this study, the thermodynamic analysis of a heat pump system with a transcritical CO2 fluid and a flash tank is examined. This system consists of two compressors, a gas cooler, an evaporator, two throttle valves, and a flash tank. The cycle operates in transcritical phases form. By performing thermodynamic analysis, the heating capacity in this system and the energetic performance ecoefficiency (COPen) and exergetic performance coefficient (COPex) values are analyzed and determined. The evaporator temperature is analyzed according to 5 °C. Moreover, some system indicator values are changed parametrically and the change in system efficiency is observed. According to the analysis result, the COP value of this system is calculated as 2.4. If the refrigerants used in these systems are environmentally friendly, environmentally friendly systems will be designed for the future. To sum up, CO2 fluids are environmentally friendly fluids in terms of ODP and GWP values, and important studies are being carried out in these systems focused on both efficiency and marketing.

Keywords: CO2, heat pump, energy, exergy, COP

[1]**Address:** Isparta University of Applied Sciences, Faculty of Technology, Isparta/Turkiye
***Corresponding author**: fatiyilmaz7@mail.com

1. INTRODUCTION

Heat pumps play a crucial role in mitigating the effects of global warming and enhancing energy efficiency. Compared to conventional heating systems that rely on fossil fuels, heat pumps extract low-temperature heat from the environment (air, ground, or water) and provide heating with significantly lower primary energy consumption. When powered by electricity from renewable sources, these systems can substantially reduce carbon emissions, offering a sustainable heating solution. Moreover, with high COP (Coefficient of Performance) values, heat pumps can generate multiple units of heat energy for every unit of electricity consumed. With these advantages, heat pumps stand out as an effective technology in reducing the carbon footprint of buildings and combating global warming.

Heat pumps utilizing CO_2 (R-744) as a refrigerant have gained significant attention due to their environmental benefits and high efficiency, particularly in high-temperature applications such as domestic water heating and district heating systems. Unlike conventional synthetic refrigerants, CO_2 has an ultra-low global warming potential (GWP = 1) and does not contribute to ozone depletion, making it a sustainable alternative in the transition to low-carbon heating technologies (Kim et al., 2014). Additionally, transcritical CO_2 heat pump systems can achieve high COP values, especially in colder climates, due to their efficient heat transfer characteristics (Nekså, 2002). As energy policies and regulations increasingly favor low-GWP refrigerants, CO_2 heat pumps are expected to play a crucial role in reducing greenhouse gas emissions and enhancing the sustainability of heating systems. In recent years, transcritical CO_2 heat pumps (R-744) have become the focus of the search for environmentally friendly refrigerants offering high efficiency in heating systems. Unlike traditional refrigerants, CO_2 has attracted attention in many places in the literature due to its ability to operate in a transcritical cycle under certain conditions, especially at higher ambient temperatures.

Zhao et al (2025) developed a transcritical CO_2 heat pump system for heating loads. They carried out a comprehensive thermodynamic analysis, and then the results showed that COP increases by 1.6 to 2.5 with the increase in regenerator efficiency. Gambini et al (2024) studied the Energy and Exergy Analysis of Transcritical CO_2 Cycles for Heat Pump Applications. They revealed that the maximum coefficient of performance (COP) of the reference cycle ranged from 1.52-3.74. Liu et al. (2024) discussed transcritical-transcritical stage CO2 heat pump cycles for high-temperature heating: A numerical evaluation. It achieves a maximum COP of 2.22 for heating air (15 to 200 °C) from dryer exhaust heat.

This study presents the design and thermodynamic analysis of a CO_2 heat pump system with high-pressure and low-pressure compressors and flash tanks. Here, the energy and exergy performance coefficients of the system are examined and presented graphically.

2. MATERIAL AND METHOD

The proposed study aims to generate clean heating products with a transcritical CO2-based heat pump system (see Figure 1). The system consists of a low-pressure compressor (LPC), high-pressure compressor (HPC), gas cooler, expansion valves (EV), flash vapor separator tank, and evaporator. Heat can be released to the environment in the gas cooler section, and a house can be heated here. R744 refrigerant, which is heated to +5 degrees from the saturated vapor phase at point 1, enters the compressor, is compressed here, and cooled to some extent by vapor coming from point 7, then enters the HPC again. The high-temperature fluid heat can be transferred to the environment or intermediate water in the gas cooler, and a heating load can be obtained. Afterward, the pressure and temperature of the refrigerant entering the EV-1 at constant enthalpy decrease and enters the flash tank, where it separates into saturated liquid and vapor phases, enters the evaporator in saturated liquid form at point 8 and enters the system in gas phase again by drawing heat from the environment at point 1. The main purpose of performing double compressor intercooling here is to reduce the compressor load and increase system efficiency. In this way, the system works continuously in a closed loop.

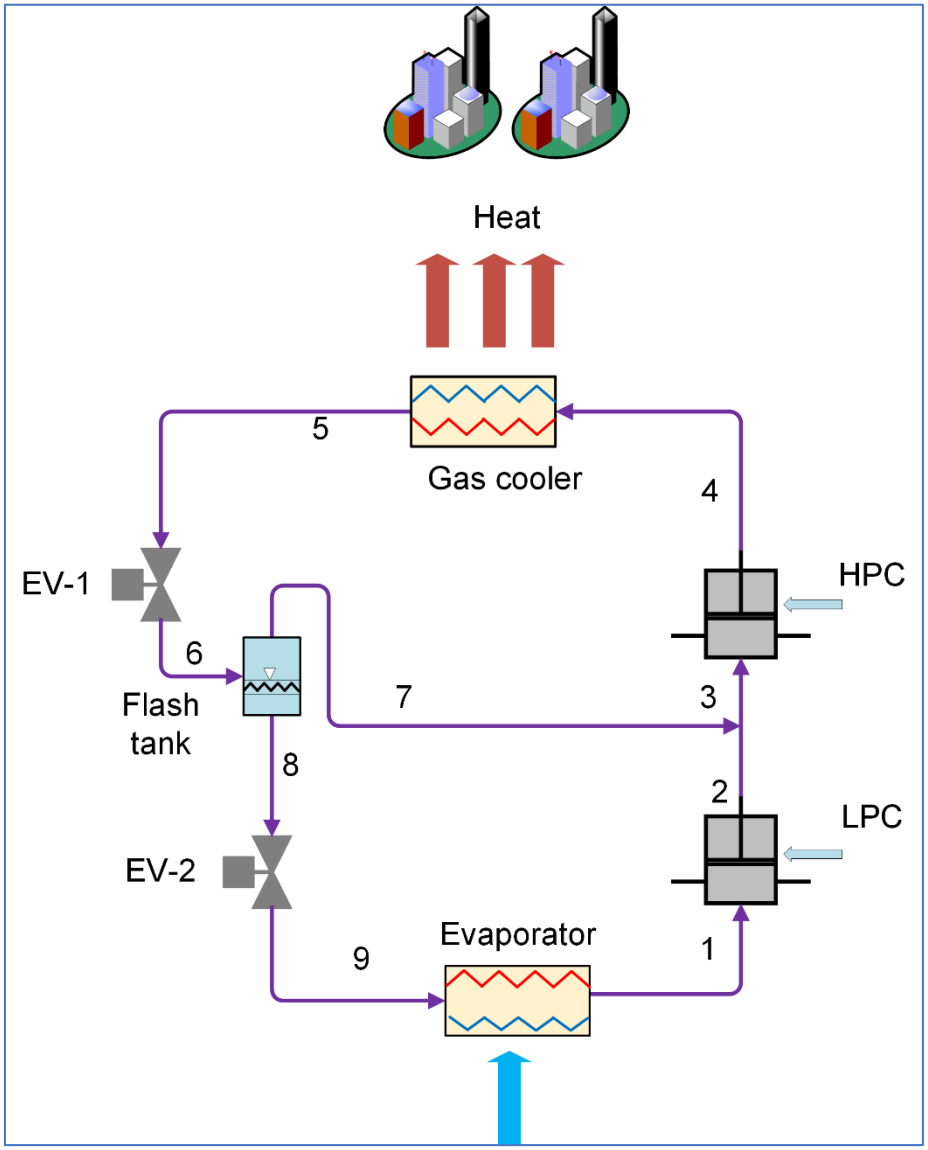

Figure 1. Schematic flow chart of the developed system

2.1. Thermodynamic analysis

This study performed a comprehensive thermodynamic analysis with the EES package program. The assumptions made before the thermodynamic analysis of the system are as follows:

- The system operates under steady-state flow conditions
- CO_2 is preferred as the refrigerant.
- Pressure and heat loss between the connection elements were not taken into account.
- The evaporator temperature was assumed to be 5 ℃.
- Compressors have isentropic efficiency.

In general, to conduct thermodynamic modeling, the four balance equations should be considered, which are mass, energy, entropy, and exergy formulations, and these can be written as (Cengel et al. 2011; Dincer 2020)

$$\dot{m}_{in} = \dot{m}_e \quad (1)$$

$$\dot{Q}_{in} + \dot{W}_{in} + \sum \dot{m}_{in} h_{in} = \dot{Q}_e + \dot{W}_e + \sum \dot{m}_e h_e \quad (2)$$

$$\sum \dot{m}_{in}\, s_{in} \sum \left(\frac{\dot{Q}}{T}\right) + \dot{S}_{gen} = \sum \dot{m}_e\, s_e \quad (3)$$

$$\dot{Ex}^{\dot{Q}_{in}} + \dot{Ex}^{\dot{W}_{in}} + \sum \dot{m}_{in} ex_{in} = \dot{Ex}^{\dot{Q}_e} + \dot{Ex}^{\dot{W}_e} + \sum \dot{m}_e ex_e + \dot{Ex}_{des} \quad (4)$$

The energetic performance coefficient ($\mathbf{COP_{en}}$) and exergetic performance coefficient ($\mathbf{COP_{ex}}$) of the developed system can be depicted as;

$$\mathbf{COP_{en}} = \frac{\dot{Q}_{\text{gas cooler (heating)}}}{\dot{W}_{LPC} + \dot{W}_{HPC}} \quad (5)$$

$$\mathbf{COP_{ex}} = \frac{\dot{Ex}_{\dot{Q}_{\text{gas cooler (heating)}}}}{\dot{W}_{LPC} + \dot{W}_{HPC}} \quad (6)$$

3. RESULTS AND DISCUSSION

The developed system is examined with thermodynamic energy and exergy analysis and presented graphically. The analysis results are given in Table 1. Here, a total power consumption of 1314.8 kW occurs in this system, while the heating load of the gas cooler is calculated as 3636 kW. The COP_{en} and COP_{ex} values of the system are calculated as 2.76 and 0.21. The data in this system with CO_2 fluid can be evaluated as logical and reasonable.

Table 1. Thermodynamic analysis results of the developed system

Parameters	Results
$\dot{W}_{LPC}$	181.8 kW
$\dot{W}_{HPC}$	1133 kW
$\dot{Q}_{heating}$	3636 kW
COP_{en}	2.76
COP_{ex}	0.21

The evaporator temperature (T_{ev}) changes had more important indicators in the heat pump and refrigeration systems. For this reason, the change in the T_{ev} (increases) effects on the system performance criteria are examined and presented in Figure 2. While the rise in the T_{ev} from 0 to 10 °C, leads to a decrease in the LPC and HPC power consumptions, and then system performance coefficiency for energy and exergy is inversely increased. COP_{en} increased from 2.4 to 3, and also COP_{ex} rose from 0.20 to 0.24.

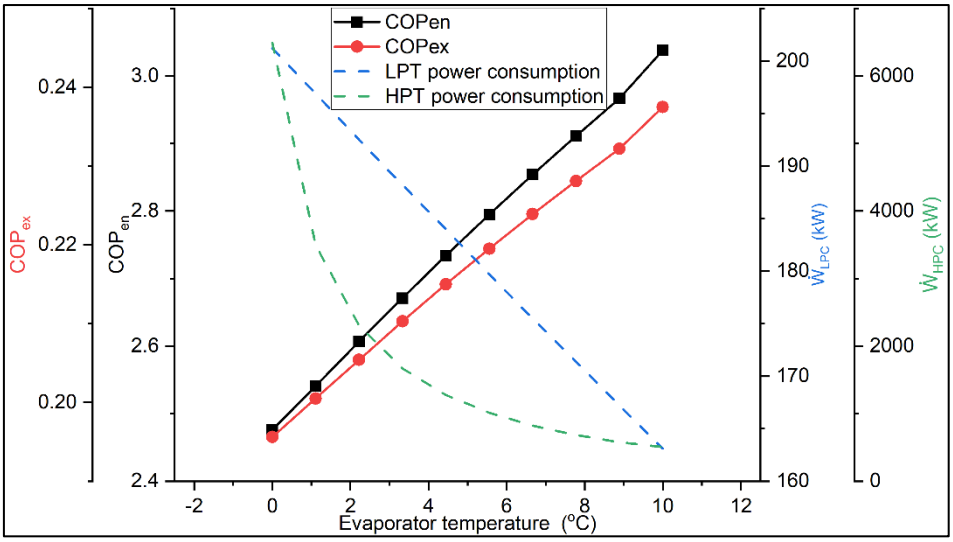

Figure 2. Effect of T_{ev} on system performance ratio and power consumption

The gas cooler temperature change is analyzed and its effect on the system is presented parametrically in Figure 3. This part is also an important indicator because it is the part where the heating load is realized. As the Tgs temperature increases

from 45 C to 65 C, the amount of energy consumed by the compressors increases and accordingly the COP values of the system decrease for energy and exergy. The increase in energy consumption negatively affects the system's efficiency.

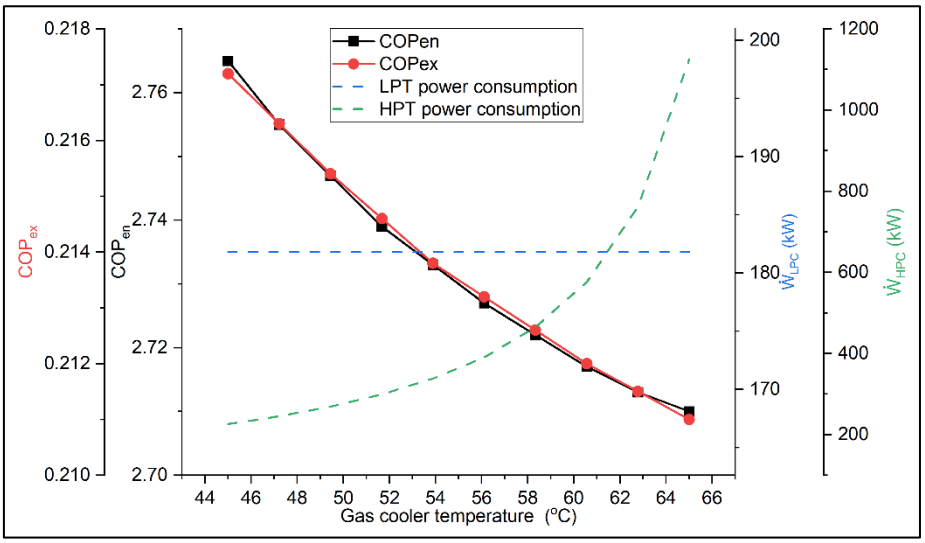

Figure 3. Effect of T_{gs} on system performance ratio and power consumption

In this study, the transcritical CO_2 fluid is investigated, and therefore the effects of evaporator pressure (P_{ev}) changes in the system efficiency are analyzed and illustrated in Figure 4. With the increase of the P_{ev} value from 2800 kPa to 3600 kPa, the amount of energy consumed by the compressors decreased, and in return, the energy and exergy COP values of the system increased. According to Equations 5 and 6, the system becomes more efficient with the decrease in energy consumption, i.e. the decrease in the denominators. In the opposite case, the effects of the change in the Gas cooler pressure (P_{gs}) are presented in Figure 5. Here, with the increase in the P_{gs} value, the amount of energy consumed by the system increases, and therefore the COP_{en} and COP_{ex} values decrease. High P_{gs} means more work consumption and lower efficiency. Therefore, optimum efficiencies can be achieved with these systems in optimum pressure ranges.

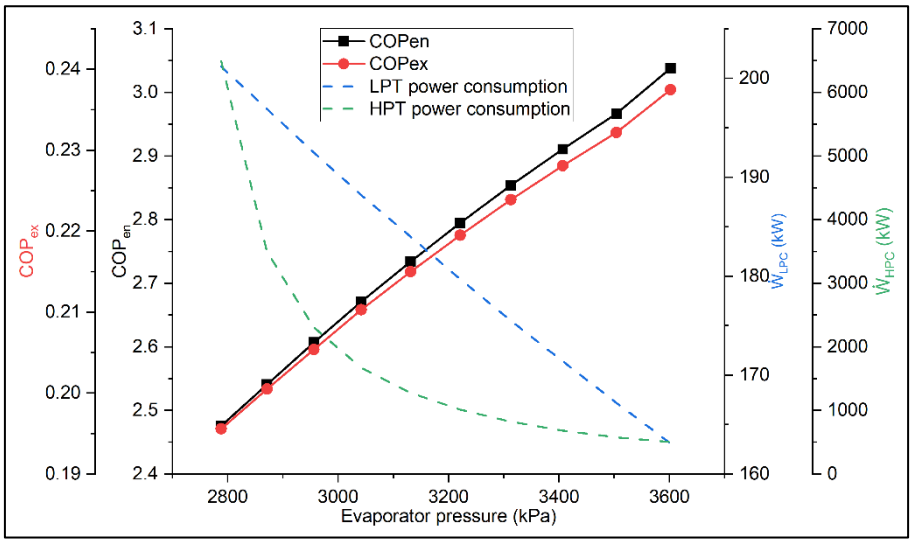

Figure 4. Relationship between P_{ev} and system efficiency indicators

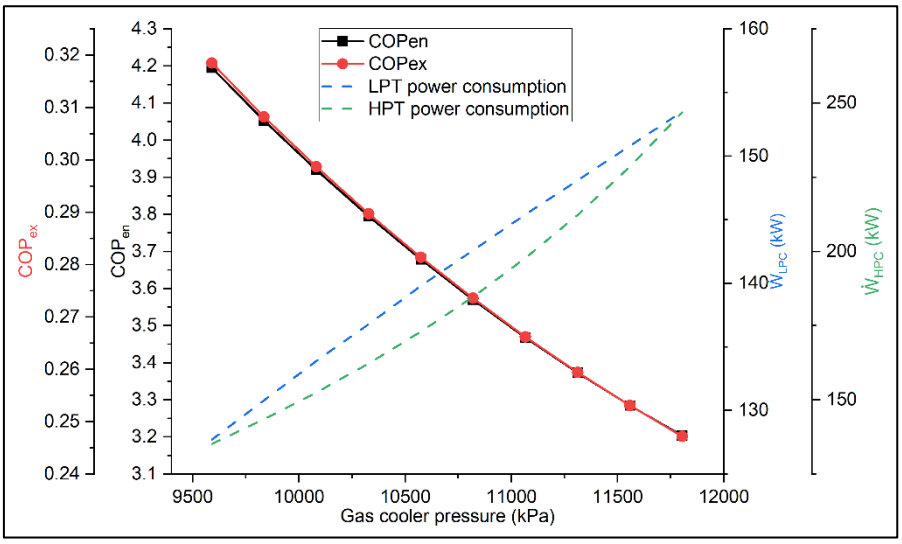

Figure 5. Relationship between P_{gs} and system efficiency indicators

To sum up, the effect of the change in the compression ratio of LPC and HPC compressors on the system efficiency is analyzed and shown graphically in Figure 6. As a result of the increase in the compression ratio (constant compressor input), the system reaches higher pressure values and consumes more energy. Therefore, the energy and exergy COP values of the system have decreased. Determining the optimum ranges by examining them more comprehensively with optimization methods will be positive for higher system efficiency.

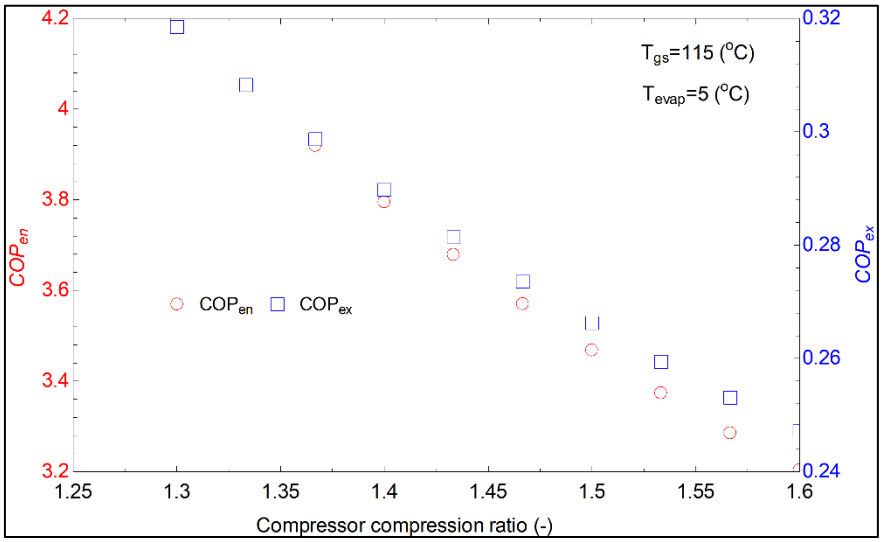

Figure 6. The impact of compressor compression ratio on COP_{en} and COP_{en}

4. CONCLUSIONS

Due to global warming and environmental problems, the use of environmentally friendly new-generation refrigerants has become important. In this study, an environmentally friendly CO2 fluid transcritical heat pump system has been designed, analyzed, and presented. To determine the system performance values and also compressor energy consumption, a comprehensive mathematical model has been made according to the first and second laws of thermodynamics.

According to the analysis results, a 3636 kW heating load can be obtained with this developed system. In addition, the total COP_{en} and COP_{ex} values of the system are calculated as 2.76 and 0.21, respectively. According to the parametric analysis results, the increase in the temperature and pressure of the P_{gs} value negatively affects the system's efficiency.

Author Contributions
Fatih YILMAZ; Conceptualization, Investigation, Material and Methodology, Writing-Original Draft, Writing-review & Editing.

Conflict of Interest
The authors have no conflicts of interest to declare.

Funding /
The authors declared that this study has received no financial support.

REFERENCES

Cengel, Y. A., Boles, M. A., & Kanoğlu, M. (2011). Thermodynamics: an engineering approach (Vol. 5, p. 445). New York: McGraw-hill.

Dincer, İ. (2020). Thermodynamics: a smart approach. John Wiley & Sons

Gambini, M., Manno, M., & Vellini, M. (2024). Energy and Exergy Analysis of Transcritical CO2 Cycles for Heat Pump Applications. *Sustainability*, *16*(17), 7511.

Kim, M. H., Pettersen, J., & Bullard, C. W. (2004). Fundamental process and system design issues in CO2 vapor compression systems. Progress in energy and combustion science, 30(2), 119-174.

Liu, X., Peng, X., Yang, Y., Qin, X., Wang, D., Wang, G., & Wang, D. (2024). Energetic analysis and performance improvement algorithm of transcritical CO2 heat pump water heater system. *Applied Thermal Engineering*, *236*, 121823.

Nekså, P. (2002). CO2 heat pump systems. International Journal of refrigeration, 25(4), 421-427.

Zhao, W., Zhang, Y., Sun, C., Li, L., Li, B., & Xu, J. (2025). Thermodynamic analysis of a transcritical CO2 heat pump for heating applications. *Energy*, 134896.

Development and Performance Analysis of Green Hydrogen Production with a Combined Hydropower System

Fatih YILMAZ*[1]

Abstract: Clean hydrogen production is among the most important issues for overcoming global warming and environmental problems and also for the transition into net zero emissions. Therefore, hydrogen production, transportation, and storage are important issues. Therefore, this study focuses on the design and analysis of a hydropower-integrated system for clean (green) hydrogen production, fresh water, and clean power. Here, the thermodynamic analysis of the integrated system is discussed. In line with the thermodynamic analysis, the hydrogen, electricity, and clean water production capacities of the system are examined. Also, energy and exergy efficiency analyses are thoroughly discussed. Moreover, comprehensive parametric analyses are performed and the variables affecting the system efficiency are examined and shown graphically. According to the analysis data, 15.8 MW of net electricity can be produced from a hydroelectric power plant with a gross height of 320 m, while 0.0256 kg/s of clean hydrogen is also produced. The total system efficiency is calculated as 74.31% Moreover, the exergy efficiency of the whole system was calculated as 62.69%. In the parametric analysis, as the height of the unit increased, the useful outputs obtained from the system increased clearly. It can be concluded that these systems have a good potential for hydrogen production due to their high electricity generation capacity and also due to their well-established technologies.

Keywords: Energy, exergy, hydropower, green hydrogen

[1]**Address:** Isparta University of Applied Sciences, Faculty of Technology, Isparta/Turkiye
***Corresponding author**: fatiyilmaz7@mail.com

1. INTRODUCTION

Fossil fuels such as coal, oil, and natural gas are one of the most important factors in the emergence of environmental problems. These carbon-based fuels emit large amounts of carbon dioxide (CO_2) into the atmosphere as a result of their combustion, which is one of the leading causes of global warming. The use of these fuels leads to environmental problems such as greenhouse gas emissions, air pollution, and acid rain. Therefore, the transition from fossil fuels to cleaner, renewable energy sources is essential to address environmental sustainability and reduce long-term impacts on the planet. Cleaner than fossil fuels, renewable energy reduces greenhouse gas emissions, mitigates environmental change, improves economic growth, and contributes to energy access. Renewable energy also helps address energy demand and the energy security that results from that demand (Adedoyin et al. 2021; Sharif et al. 2020). In this context, hydro energy—hydraulic power or water power is the power obtained from the energy of falling or fast-flowing water that can be used for a useful purpose—is a type of renewable energy source with established technology.

Another critical role in combating environmental problems is hydrogen. If hydrogen is produced by electrolysis and the electrical energy required for this electrolysis is renewable, this production method is called green hydrogen. In other words, hydroelectric energy produces green energy and the electricity produced technically has no pollution. The green energy obtained is converted into hydrogen. Since hydrogen is a completely green energy carrier, the entire process can be considered a green-green system (Karayel et al. 2023).

When we look at the open literature, many studies on renewable energy supported hydrogen production. Most of them are partially wind and solar energy-supported systems. Yilmaz (2024) discussed and examined the design and performance analysis of hydro and wind-based power and hydrogen production systems for sustainable development. Here, hydrogen production with a wind turbine-supported integrated system is aimed. Altayip and Dinçer (2020) studied the development and thermodynamic analysis of an integrated hydroelectric system with hydrogen and methanol production. They calculated the exergy efficiency of the whole system as 58.2%. The investigation of water electrolysis for green hydrogen production considering PV/wind/hybrid/hydroelectric/geothermal/tidal and wave/biogas energy systems, economic analysis, and applications was carried out by Wad et al. in 2024. Andrus et al (2023) investigated the case study of the Northwest Columbia River system for hydropower-assisted green hydrogen production. The study data highlights that hydrogen production from spilled hydropower and its use in the transportation sector is a viable opportunity to move the country towards a hydrogen economy.

In line with the brief literature review presented above, hydrogen production supported by hydropower emerges as a significant research area. The utilization of surplus electricity generated in these studies for hydrogen production is of particular importance. This study comprehensively examines a theoretical thermodynamic analysis of an integrated system that utilizes hydropower for the production of hydrogen, clean water, and electricity. The system's hydrogen

generation capacity is analyzed under various operating conditions, and an energy and exergy analysis is conducted to evaluate its overall performance.

2. MATERIAL AND METHOD

This system represents a hydroelectric power generation process that utilizes seawater and a Kaplan turbine to produce electricity (see Figure 1). Sea water is directed through an intake structure and flows down a penstock, gaining speed and pressure due to gravity. The high-pressure water strikes the blades of a Kaplan turbine, which is specifically designed for low-head and high-flow conditions. As the turbine rotates, it drives a generator that converts mechanical energy into electrical energy. After passing through the turbine, the water is discharged back into the sea, and the generated electricity is transmitted to the power grid for use.

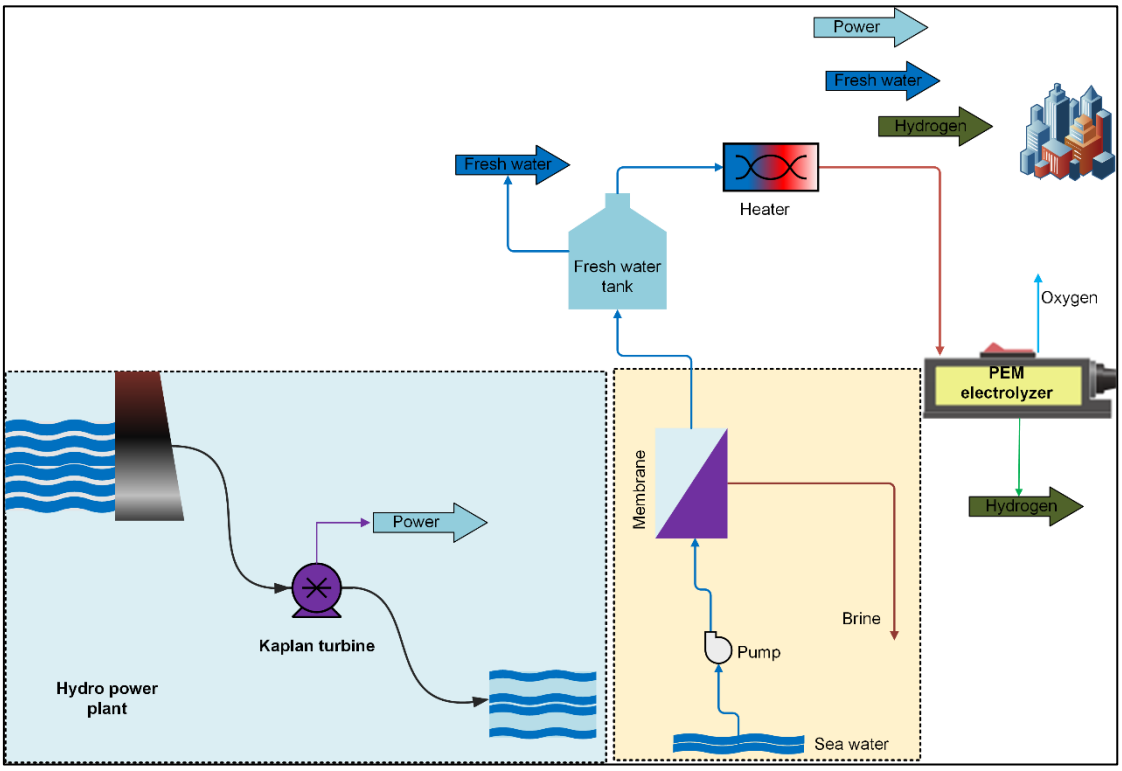

Figure 1. The working flow chart of the developed system

2.1. Thermodynamic analysis

The study deals with the thermodynamic analysis of the hydropower-based freshwater, power, and hydrogen generation system. To conduct the thermodynamic analysis, the following assumptions should be made:

- The system works as steady-state flow conditions
- the heat and pressure drops are not taken into computation
- Seawater inlet temperature and pressure is taken as 25 °C and 101 kPa
- The pump and turbines have isentropic efficiency
- PEM inlet temperature is assumed to be 80 °C.
- The required PEM power rate is taken as 25% of the net power load.

To apply the thermodynamic mathematical modeling of any thermal system, it should be taken into account the mass, energy, entropy, and exergy formulation, respectively ((Cengel, 2015; Dincer, 2020; Kotas, 1985);

$$\sum_i \dot{m}_i = \sum_e \dot{m}_e \quad (1)$$

$$\dot{Q}_i + \dot{W}_i + \sum_i \dot{m}\,(h) = \dot{Q}_e + \dot{W}_e + \sum_e \dot{m}\,(h) \quad (2)$$

$$\sum_i \dot{m}_i s_i + \dot{S}_{gen+} \sum_i \left(\frac{\dot{Q}_k}{T_k}\right) = \sum_e \dot{m}_e s_e \sum_e \left(\frac{\dot{Q}_k}{T_k}\right) \quad (3)$$

$$\sum_i \dot{m}_i ex_i + \dot{E}x^{\dot{Q}} + \dot{E}x^{\dot{W}} = \sum_e \dot{m}_e ex_e + \dot{E}x^{\dot{Q}} + \dot{E}x^{\dot{W}} + \dot{E}x_{dest} \quad (4)$$

For the overall system energy and exergy efficiency;

$$\eta_{sys} = \frac{\dot{W}_{net} + \dot{m}_{H_2} LHV_{H_2} + \dot{m}_{fw} h_{fw}}{\dot{E}_{in} + \dot{m}_{sw} h_{sw}} \quad (5)$$

$$\psi_{sys} = \frac{\dot{W}_{net} + \dot{m}_{H_2} ex_{H_2} + \dot{m}_{fw} ex_{fw}}{\dot{E}x_{in} + \dot{m}_{sw} ex_{sw}} \quad (6)$$

3. RESULTS AND DISCUSSION

This subsection presents the thermodynamic analysis results of the developed system. A comprehensive thermodynamic analysis is conducted and presented graphically to determine the best performance and operating conditions of the system. Table 1 presents the analysis results at 250 m water gross height. The system can generate 15.8 MW of clean power, 0.0256 kg/s of green hydrogen, and 3.26 kg/s of fresh water. The power generation capacity has too much potential compared to the other renewable energy source systems. To sum up, the sustainability index of the system is determined as 2.68. Finally, the energy and exergy efficiency of the developed integrated overall system are 74.31% and 62.69%, respectively.

Table 1. A case study analysis results of the developed system

Parameters	**Value**	**Unit**
Net power rate	15.8	MW
Hydrogen capacity	0.0256	kg/s
Fresh water capacity	3.26	kg/s
SI	2.68	-
Total exergy destruction rate	2466	kW
Energy efficiency	74.31	%
Exergy efficiency	62.69	%

The effects of changes in the parameters affecting the system efficiency are investigated parametrically and are presented here. In the first parametric investigation, the effects of the gross water height (H_{gross}) on the system outputs (a) and system efficiency (b) were investigated and are illustrated in Figure 2. Here, due to the high potential energy change in H_{gross}), the net work done in the system has increased by approximately 7500 kW as a result of its increase. (See Figure 2(a). At the same time, the energy and exergy efficiency of the system also increases due to this increase. However, there is also an increase in exergy efficiency. It is possible to operate these systems at optimum points by obtaining ideal H_{gross}) heights.

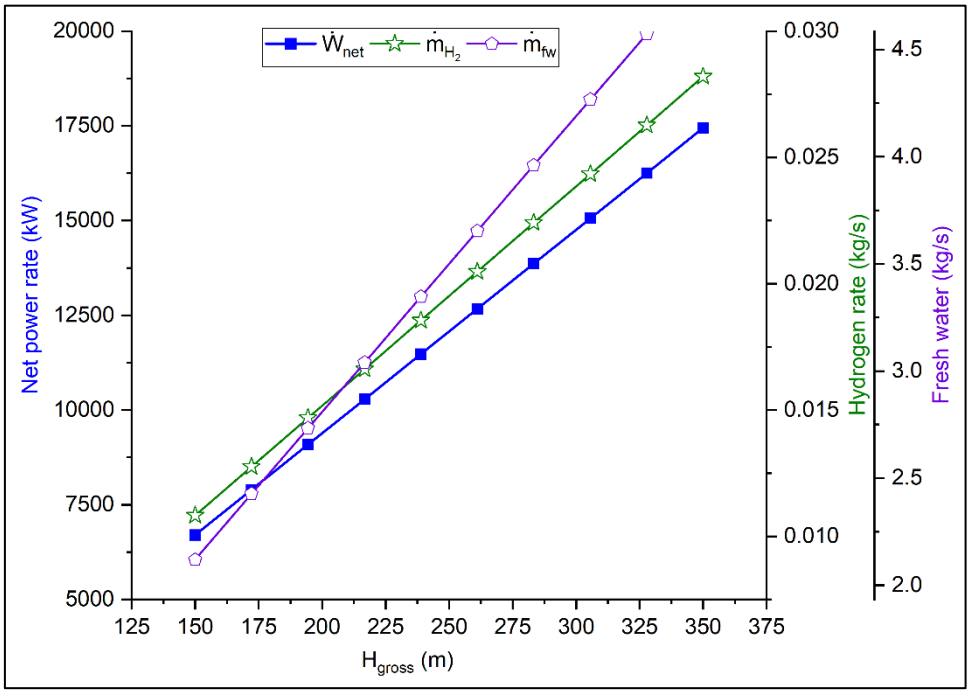

(a)

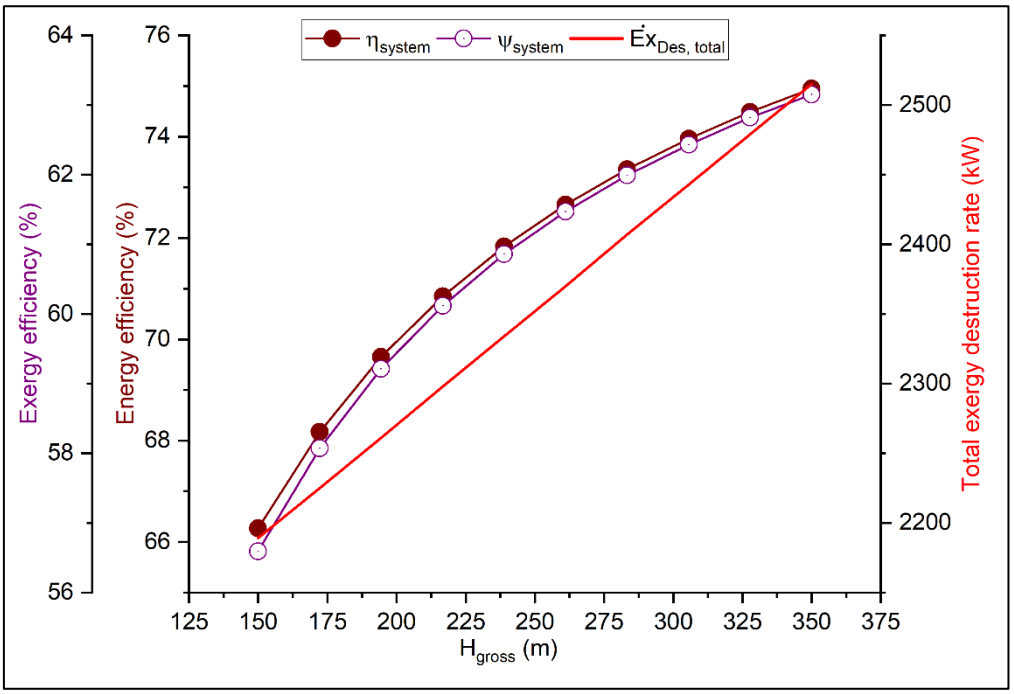

(b)

Figure 2. Effect of the water gross height on the system indicators

The increase in water flow rate ($\dot{Q}_{water}$) is another parameter that positively affects efficiency. In Figure 3(a-b), as a result of the increase in $\dot{Q}_{water}$ from 5 to 125 m^3/s, the system can obtain more output (electricity, clean water, and hydrogen), and also the energy and exergy efficiencies of the system have increased linearly. In this increased range, the green hydrogen rate obtained in the system has increased from 0.05 to 0.45 kg/s. With an increase of $\dot{Q}_{water}$ by 120 m^3/s, the energy efficiency of the system increases from 73% to 75% and the exergy efficiency increases from 62% to 68%.

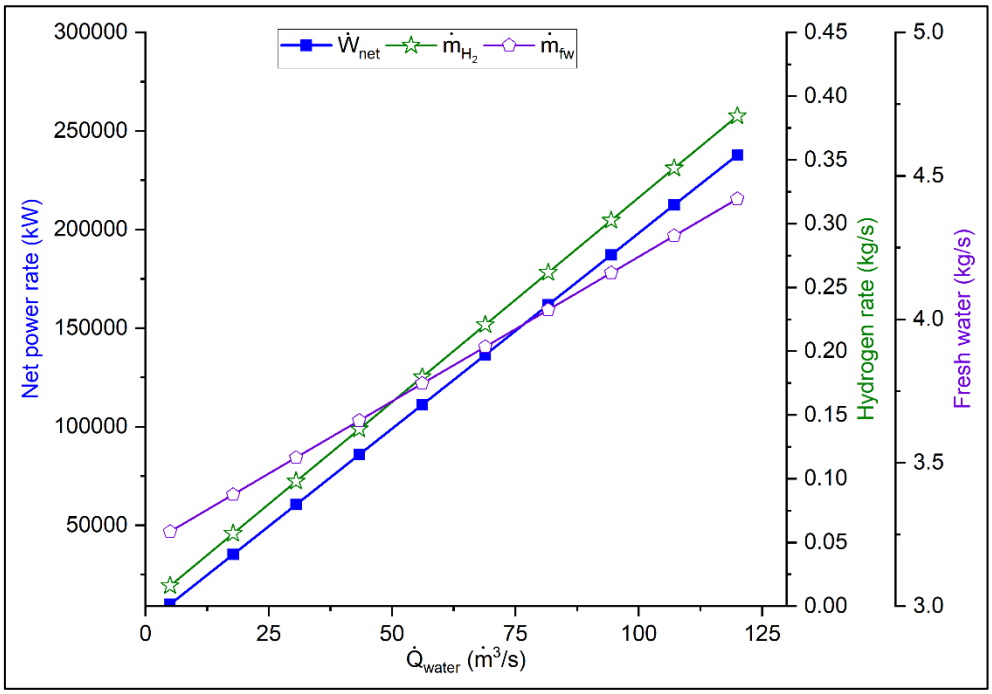

(a)

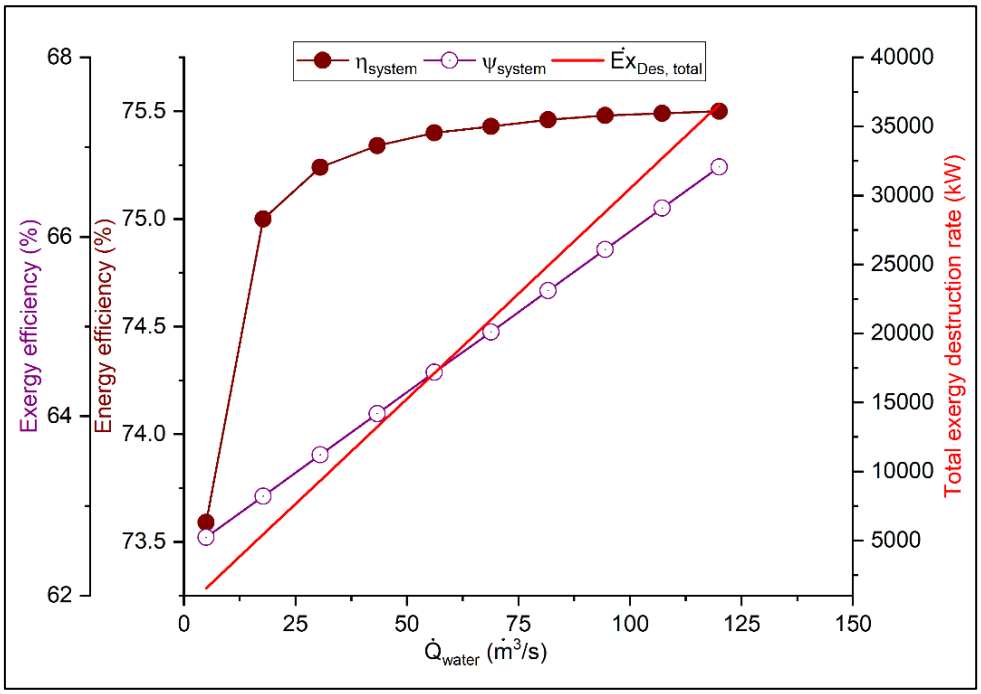

(b)

Figure 3. Relationship between water flow rate and system's outputs and efficiency

The effect of water temperature on the developed system products is analyzed and shown in Figure 4(a). When the water temperature is increased from 5 to 45 °C, the designed system produces less useful products. The net power production is reduced from 15900 kW to 15700 kW and due to this decrease, the green hydrogen generation is also reduced. The main reason for this decrease is the decrease in the density of water with increasing temperature and the decrease in net electricity production. Furthermore, under the same circumstances, the developed system's efficiency indicators decrease, as shown in Figure 4(b). Herein, the system performance indicators decreased as the water temperature rose.

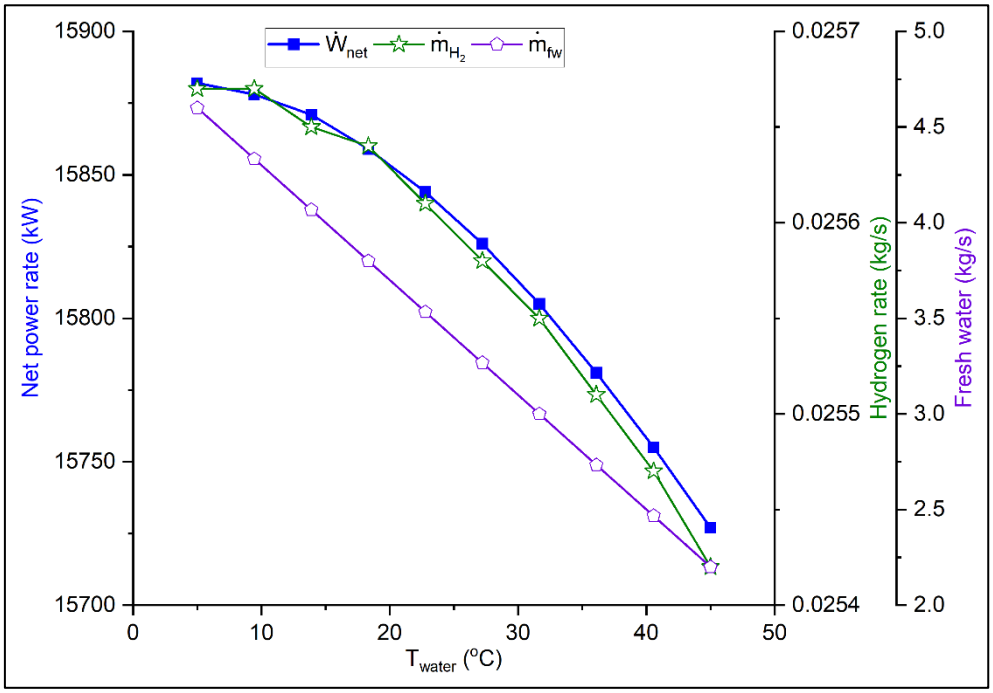

(a)

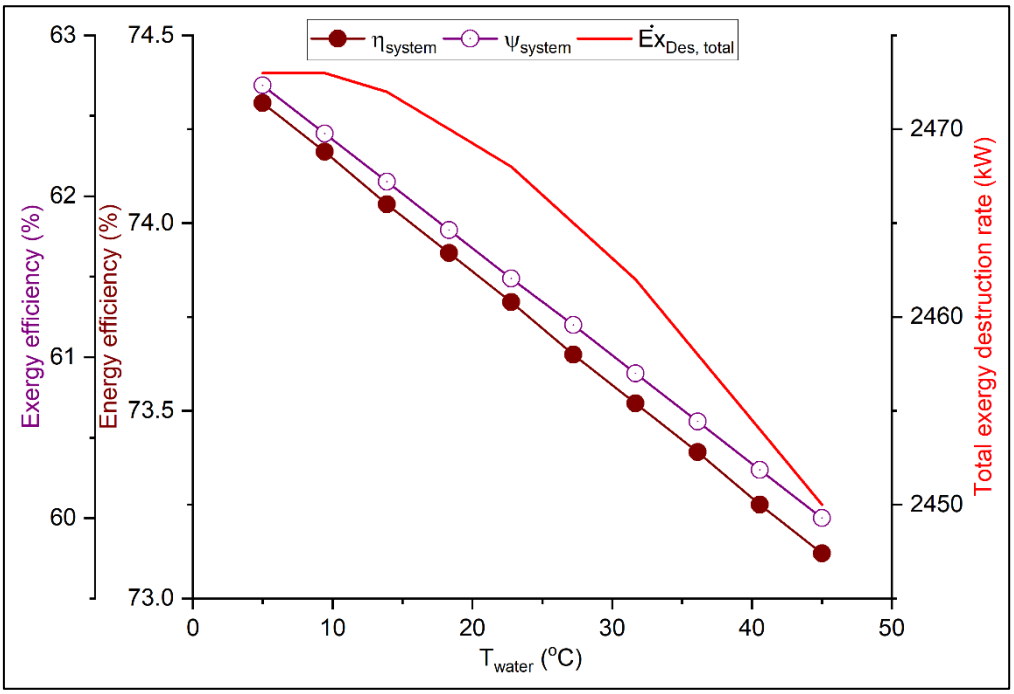

(b)

Figure 4. The impact of the water temperature on the generated products of the developed system

4. CONCLUSIONS

The production of important commodities such as renewable energy-supported power and hydrogen production is one of the most important tools in overcoming global environmental problems. In particular, it is possible to produce high-capacity electricity with hydropower plants with well-established technology among renewable energy sources. In this study, a hydropower-supported system is designed and aimed at the production of clean hydrogen, electricity, and drinking water. A comprehensive thermodynamic mathematical model is applied to determine the system's performance behavior. Moreover, energy and exergy analyses and also an exergy destruction examination are fulfilled, and a parametric analysis is conducted. The generated excess power aiming to send the PEM unit and hydrogen can be generated here. The foremost analysis results of this developed paper can be summarized as;

- With this system at a gross water level of 320 m, 15.8 MW of clean electricity, 0.0256 kg/s green hydrogen, and 3.26 kg7s clean (drinkable) water could be produced.
- The SI value of this designed study was calculated as 2.68, while the total exergy destruction was calculated as 2466 kW.
- The entire system has 74.31% energy efficiency and 62.69% exergy efficiency. It is an important and high value in terms of energy and exergy efficiency.
- According to the parametric analysis, with the increase in water flow rate and gross water level height, the system works with both more product and higher efficiency.

To sum up, especially in the future, green hydrogen will be the most indispensable issue. Because hydrogen only produces power and water vapor after the reaction, it is indispensable for the environment. At this point, hydrogen production with hydropower systems that produce high electricity will be thermodynamically promising.

Author Contributions
Fatih YILMAZ; Conceptualization, Investigation, Material and Methodology, Writing-Original Draft, Writing-review & Editing.

Conflict of Interest
The authors have no conflicts of interest to declare.

Funding /
The authors declared that this study has received no financial support.

REFERENCES

Adedoyin, F. F., Ozturk, I., Bekun, F. V., Agboola, P. O., & Agboola, M. O. (2021). Renewable and non-renewable energy policy simulations for abating emissions in a complex economy: evidence from the novel dynamic ARDL. *Renewable Energy*, *177*, 1408-1420.

Sharif, A., Mishra, S., Sinha, A., Jiao, Z., Shahbaz, M., & Afshan, S. (2020). The renewable energy consumption-environmental degradation nexus in Top-10 polluted countries: Fresh insights from quantile-on-quantile regression approach. *Renewable Energy*, *150*, 670-690.

Karayel, G. K., Javani, N., & Dincer, I. (2023). Hydropower for green hydrogen production in Turkey. International Journal of Hydrogen Energy, 48(60), 22806-22817.

Yilmaz, F. (2024). Design and performance analysis of hydro and wind-based power and hydrogen generation system for sustainable development. *Sustainable Energy Technologies and Assessments*, *64*, 103742.

Altayib, K., & Dincer, I. (2022). Development of an integrated hydropower system with hydrogen and methanol production. *Energy*, *240*, 122780.

Awad, M., Said, A., Saad, M. H., Farouk, A., Mahmoud, M. M., Alshammari, M. S., ... & Omar, A. I. (2024). A review of water electrolysis for green hydrogen generation considering PV/wind/hybrid/hydropower/geothermal/tidal and wave/biogas energy systems, economic analysis, and its application. *Alexandria Engineering Journal*, *87*, 213-239.

Andrus, S. R., Diffely, R. J., & Alford, T. L. (2023). Theoretical analysis of green hydrogen from hydropower: a case study of the Northwest Columbia River system. *International Journal of Hydrogen Energy*, *48*(22), 7993-8001.

Çengel YA, Boles MA. Thermodynamics : an engineering approach. 8th ed. Mc. New York: McGraw-Hil;2015; 2015.
Dincer I. Thermodynamics: A Smart Approach. USA: John Wiley & Sons Ltd; 2020.

Kotas TJ (Tadeusz J. The exergy method of thermal plant analysis. Butterworths; 1985.

Suitability Analysis of Wind Farm Site in the Marmara Region (Türkiye) Using Logistic Regression Method

SENEM TEKİN*[1], M. İSMAİL GÜRSOY[2], MÜGE ÜNAL ÇİLEK[3], AHMET ÇİLEK[4]

Abstract: In this study, the Logistic Regression Method was used for the suitability analysis of Wind Farm Site in the Marmara Region. Wind energy, as a sustainable and environmentally friendly energy source, has been gaining increasing global significance. However, for wind power plants to operate efficiently, identifying suitable locations is a critical necessity. Therefore, comprehensive analyses are required to determine the most suitable locations for wind energy plants. Within the scope of this study, meteorological, topographical, and environmental factors affecting wind energy potential were identified and integrated with Geographic Information Systems (GIS). During the modeling process, a suitability analysis was conducted by considering parameters such as Digital Elevation Model (DEM), slope, roughness, Capacity Factor International Electrotechnical Commission (IEC) Class III, Mean Wind Power Density (150 m and 200 m), and Air Density (150 m–200 m). The Maximum Entropy Method, a widely used statistical modeling technique in spatial analyses, provides reliable predictions, particularly in environmental suitability assessments. Through this method, the most suitable areas for Wind Farm Site installations were identified, establishing a scientific foundation for regional wind energy investments. The results obtained contribute to identifying high wind energy potential areas in the Marmara Region and optimizing investments in these areas. The findings provide essential data to support scientific-based decision-making in wind power site planning. This study not only contributes to the development of sustainable energy policies but also offers valuable insights for strategic planning in the energy sector. The analysis results present significant findings for planning wind energy investments effectively.

Keywords: Logistic Regression, Wind Energy, Suitability Analysis, GIS, Marmara Region.

[1]**Address:** Remote Sensing and Geographic Information Systems Application and Research Center, Adiyaman University, 02040 Adiyaman, Türkiye
[2]**Address:** Electrical and Electronics Engineering, Adıyaman University, 02040 Adıyaman, Türkiye
[3]**Address:** Landscape Architecture Department, Faculty of Architecture, Firat University, 23119 Elazig, Türkiye
[4]**Address:** Remote Sensing and GIS Lab, Landscape Architecture Department, Cukurova University, 01330 Adana, Türkiye

***Corresponding author**: senemtekin@adiyaman.edu.tr

1. INTRODUCTION

Nowadays, the rapid increase in global energy needs has brought about environmental sustainability problems. The depletion of fossil fuels and the environmental damage they cause have made it necessary to turn to alternative energy sources (IEA, 2021). Among renewable energy sources, wind energy stands out with its low carbon emission, sustainability and economic advantages (Tüysüz, 2020). Especially in recent years, investments in the development of wind energy have been increasing worldwide and in Türkiye.

Türkiye's wind energy potential is high, and the Marmara Region in particular is one of the areas where this potential is most intense. The Marmara Region (Figure 1) offers a very suitable area for wind power sites due to its strategic location, industrial infrastructure and high wind speeds (Erdem and Şen, 2019). According to the data of the Türkiye Electricity Transmission Company (TEİAŞ, 2023), wind power plants in the Marmara Region constitute a significant part of the country's total wind energy capacity. This situation reveals the critical role the region plays in energy production.

Correct location selection is of great importance for wind power farms to operate efficiently. In the selection of wind power farms, digital elevation model, slope, roughness, Capacity factor International Electrotechnical Commission (IEC) Class III, Mean wind power density (150 m and 200 m), Air density (150 m–200 m) parameters should be taken into consideration (Aydin and Kaya, 2021). Wrong location selections can cause decreased energy efficiency, negative effects on the ecosystem, and economic losses. In this context, scientifically based suitability analyses are of critical importance for decision makers and investors. Appropriate location selection for wind power farms is of great importance both technically and economically. Suitability analyses are a critical step in determining the areas where power plants can operate most efficiently. Wrong location selection can lead to low energy production, high maintenance costs, and increased environmental damage (Aydin and Kaya, 2021). Wind power farms can only operate efficiently in areas with sufficient wind potential. In addition to meteorological factors such as wind speed, wind direction, and turbulence, topographic factors that will ensure the efficient operation of turbines should also be taken into account. It is known that

wind turbines operate more efficiently, especially in high altitude, open areas (Erdem and Şen, 2019; Ünal et al 2024). In addition, factors such as terrain slope and surface roughness affect wind flow dynamics and determine the energy production capacity of turbines.

In this study, the Logistic Regression Method was used to determine areas suitable for wind power farms installation in the Marmara Region. Logical Regression is a statistical analysis method used in cases where the dependent variable is categorical and is frequently preferred in spatial suitability analyses (Hosmer and Lemeshow, 2000). In the modeling process, the current locations of the wind power plants were determined as dependent variables, and the digital elevation model, slope, roughness index, Capacity factor International Electrotechnical Commission (IEC) Class III, Mean wind power density (150 m and 200 m), Air density (150 m–200 m) parameters were included in the model as independent variables. In the study, spatial integration of the data was achieved using GIS and the analysis results were mapped.

Figure 1. Study area.

In this study; It is aimed to determine the most suitable areas for wind power farms installation in the Marmara Region using the Logistic Regression Method and to provide a scientific roadmap to decision makers in this direction. Investment costs of wind power plants are not limited to the installation of turbines, but also include infrastructure, energy transmission lines and maintenance costs. Selecting suitable areas minimizes transmission costs by ensuring that the plant is close to the grid connection points (Tüysüz, 2020). In addition, maintenance and repair costs can be reduced and economic efficiency can be achieved in the long term thanks to the selection of suitable areas. The results obtained will contribute to sustainable energy policies by providing important data for the evaluation of wind energy potential in the region.

2. MATERIAL AND METHOD

The impact of wind power farms on nature and settlements is also an important criterion in suitability analyses. Wrong location selection can lead to the destruction of agricultural lands, damage to natural habitats and negatively affect local people (Erdem and Şen, 2019). Factors such as noise pollution, visual impact and shadow flicker effect can also affect the quality of life of the people. For this reason, power plants should be established in locations away from natural conservation areas and densely populated areas. Suitability analyses also constitute the cornerstone of a planning process that minimizes environmental impacts in line with sustainable development goals. These analyses help determine power farm locations that comply with environmental sustainability principles by evaluating the impacts on the ecosystem. The Marmara Region is located in the northwest of Türkiye and has a high potential in terms of wind energy.

2.1. logistic regression

Logistic regression is a statistical analysis method used in cases where the dependent variable is categorical (available/ unavailable). In particular, it is used to model the probabilities of dependent variables divided into two or more categories (Hosmer and Lemeshow, 2000). Logistic regression can be considered as a generalization of linear regression, but since the dependent variable is not continuous but categorical (usually binary: 0 and 1), it is modeled using the logistic function (sigmoid function) instead of the linear function (Menard, 2002). The logistic function is defined as follows: In this model, the effects of independent variables (environmental variables used in the analysis) on determining whether they are suitable for Wind Farm sites are calculated with logistic regression coefficients (β) (eq. 1). The dependent variable used in the analysis is discrete and takes the values [0-1]. The value on the right side of the equation equation, which reveals the relationship between the dependent variable and the independent variables, varies between -∞ and +∞. Logit transformation is applied to convert the -∞ to +∞ curve into linear (Eq. 2). This transformation essentially approaches the probability of the situation as the probability value P approaches 0 to -∞, and approaches +∞ as it approaches 1. The effectiveness of the model is evaluated with the Receiver Operating Characteristic Curve (Roc Curve) and the Area Under the Curve (AUC). The logical regression method is one of the methods frequently used in spatial decision support systems

and RES suitability analyses by integrating with geographic information systems (GIS). In the application of the model, the inventory of existing wind power plants and wind turbines in these plants must be prepared in the first stage. Secondly, the spatial variables effective in the establishment of the plants must be prepared with the help of geographic information systems software.

$$P(Y=1)=p_i=\frac{1}{1+e^{-(\beta_0+\beta_1X_1+\beta_2X_2+\ldots+\beta_nX_n)}} \tag{1}$$

$$MR=\log\left[\frac{P_i}{1-P_i}\right]=z_i=\beta_0+\beta_1X_1+\beta_2X_2+\ldots+\beta_nX_n \tag{2}$$

Wind Atlas data contribute to the determination of the most suitable areas for wind power plant installation by providing long-term statistical analysis of wind speeds, directions and energy density in a certain region (Troen and Petersen, 1989). Marmara Region is one of the regions with the highest wind energy potential in Türkiye, especially coastal areas and high altitude areas have high wind speeds. In line with the analyses, Wind Atlas data was coordinated and an inventory was prepared by digitization process; wind energy potential in the region was evaluated. A total of 425 wind turbines were digitized (Figure 2). Many variables such as elevation model, land slope, proximity to residential areas were taken into consideration as the parameters that play an active role in the selection of suitable areas. The findings obtained show that Marmara Region has a strategic position in wind energy production. Turbines concentrated especially in Çanakkale, Balıkesir and Tekirdağ provinces meet the majority of the energy production capacity in the region.

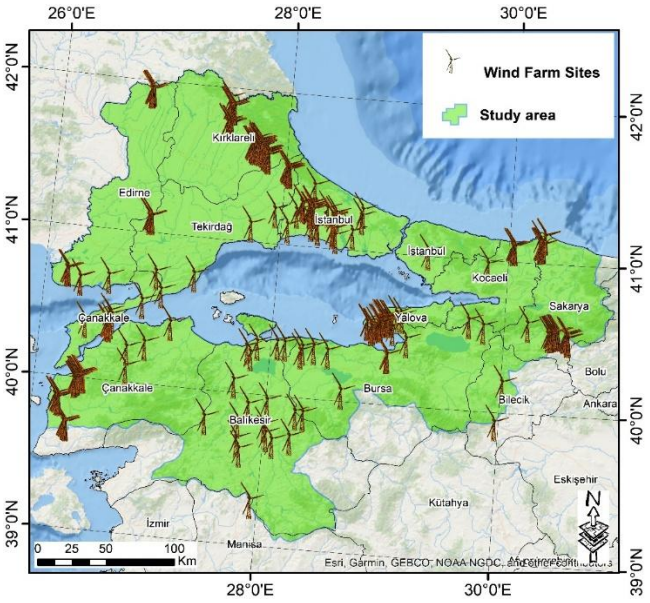

Figure 2. Marmara region wind power site locations.

In the suitability analyses performed with the logistic regression method, various geographical and meteorological parameters that are critical for the positioning of wind power plants (WPPs) were evaluated (Figure 3). Each of these parameters plays important roles in terms of the efficiency, structural stability and economic sustainability of wind turbines. The digital elevation model plays an important role in the evaluation of wind resources by providing a three-dimensional representation of the land surface. Elevation changes determine the energy production potential by directly affecting the wind speed and direction. It is known that wind speeds are generally higher in high altitude regions, therefore the use of DEM contributes to the determination of the most suitable turbine location points. Slope refers to the degree of land slope in a region and is an important topographic factor for wind power plants. While steeply sloped areas may limit the structural integrity and accessibility of turbines, areas with optimum slopes increase energy production by improving wind flow. In addition, slope analysis is one of the critical parameters in evaluating the stability of turbine foundations and construction costs. The roughness of the land surface is an important factor affecting the turbulence levels and speed distribution of the wind flow. While open areas with low roughness (e.g. sea coasts, plains) are more suitable for wind turbines, forested or mountainous areas with high roughness increase turbulence and negatively affect energy production. IEC Class III, which is among the wind classifications determined by the International Electrotechnical Commission (IEC) (CapFac3), is suitable for low to medium wind speeds. The capacity factor expresses the actual production rate compared to the maximum energy that a wind turbine can produce in a certain time period. wind energy sitesprojects are more economical and efficient in regions with high capacity factors. Wind power density is a critical parameter that indicates the amount of energy carried by the air flow at a certain altitude. Since this value is proportional to the cube of the wind speed, regions with high wind power density provide higher energy production. Measurements made at altitudes

of 150 m and 200 m are suitable for modern large-scale turbines and are a decisive factor in long-term investment decisions. Air density (AD150/AD200) has a direct effect on the power generated by wind turbines, since wind power increases linearly with air density. Air density decreases at high altitudes, while it can be higher at low altitudes and in cold regions. Therefore, air density data at altitudes of 150 m and 200 m is a critical variable to optimize the energy production capacity of wind turbines. The production efficiency of wind turbines (Ws 150/200) is directly dependent on wind speed. In regions where the average wind speed is high, energy production is more stable and economical. Near Surface Wind Speed is the measurement made at ground level to determine wind resources, but wind speeds measured at turbine height are more important. 150 m and 200 m Wind Speed: Since modern wind turbines are usually installed at altitudes of 100-200 m, determining the wind speed at these levels is necessary to estimate the energy production potential.

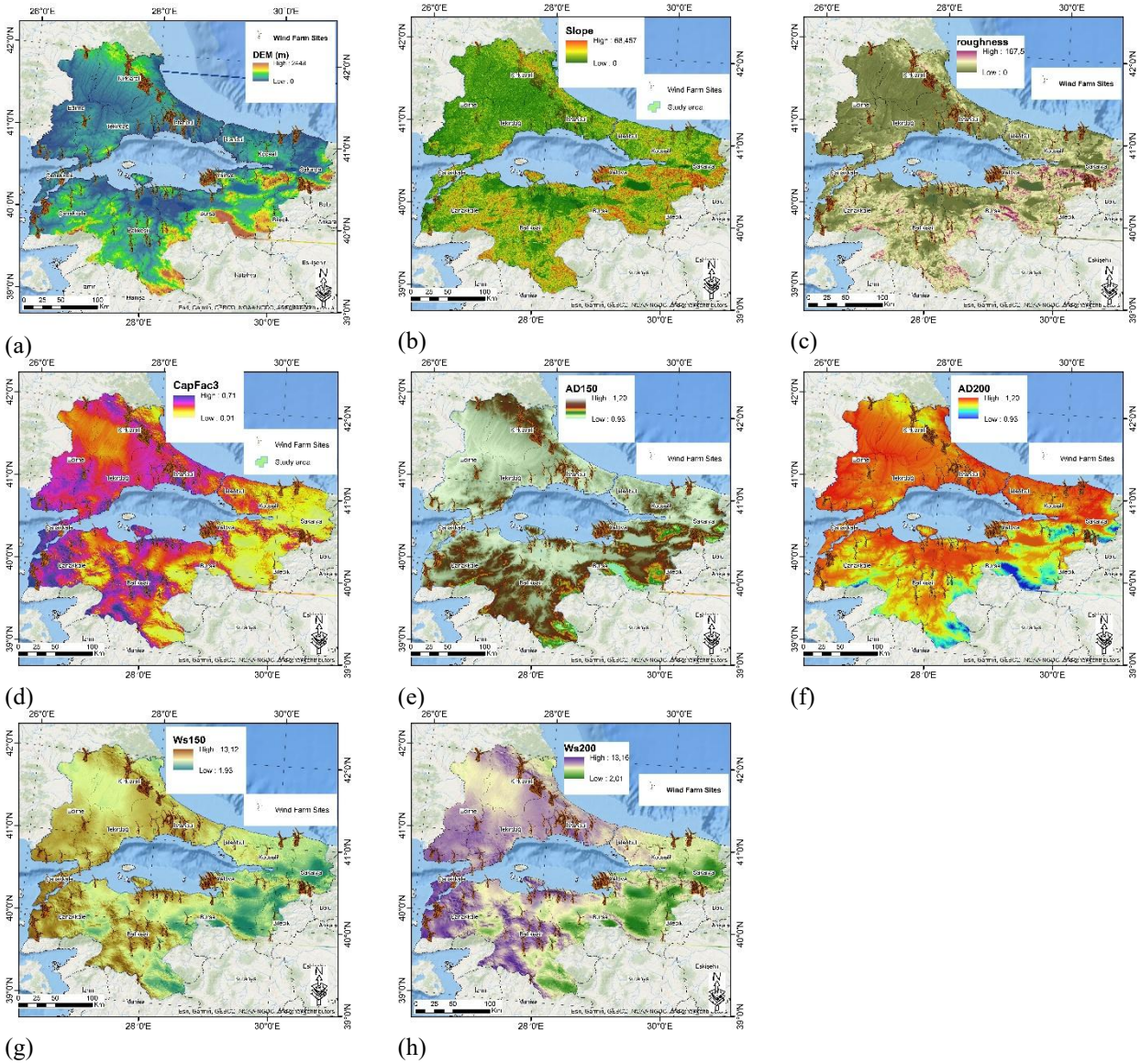

Figure 3. Environmental variables used in the analysis.

3. RESULTS

The selection of the area for wind power site installation was carried out by taking into account environmental, technical and economic factors. In this study, potential areas in the Marmara Region were determined by using the Logistic Regression Method in wind power plant suitability analysis. The study aims to provide a scientific roadmap to decision makers and investors. The obtained analysis results determined the most suitable areas for wind power sites in the Marmara Region. As a result of the modeling, regions where the wind speed is over 7 m/s show high suitability. It is seen that protected areas and areas far from settlements are more suitable in terms of minimizing environmental impacts. Table 1 shows the coefficients (B), standard errors (S.E.), Wald test values, degrees of freedom (df), significance levels (Sig.) and Exp(B) values of the variables belonging to the model made for the Suitability Analysis of Wind Power Plants in the Marmara Region (Türkiye) by using the Logistic Regression Method. The coefficient of the DEM variable is +0.170 and the significance level is determined as 0.000. Since the Exp(B) value is 1.185, the effect of DEM on the dependent variable is positive. The coefficient for the slope variable is -3.478 and is significant and the Exp(B) value is 0.031. This shows

that the effect of the slope on the dependent variable is decreasing. The coefficient of the roughness variable is -0.038 and Exp(B) is 0.963 and has a small effect in the model. The CapFac3 variable has an increasing effect on the dependent variable with a coefficient of +0.159 (Exp(B) = 1.172). The Ws150 and Ws200 variables have coefficients of -3.326 and -0.038, respectively. The Exp(B) values are 0.036 and 0.963, indicating that especially Ws150 strongly decreases the dependent variable. AD150 and AD200 variables have coefficients of +0.254 and +0.178, respectively, and are significant. Exp(B) values are 1.289 and 1.195, indicating an increasing effect on the dependent variable.

Table 1. Variables in the Equation

		B	S.E.	Wald	df	Sig.	Exp(B)
Variables	**DEM**	+0,170	,003	3513,250	1	0,000	1,185
	Slope	-3,478	,062	3100,778	1	0,000	,031
	Roughness	-0,038	,001	709,488	1	0,000	,963
	CapFac3	+0,159	,003	2836,911	1	0,000	1,172
	Ws150	-3,326	,063	2745,117	1	0,000	,036
	Ws200	-0,038	,001	683,400	1	0,000	,963
	AD150	+0,254	,019	186,111	1	0,000	1,289
	AD200	+0,178	,003	2694,339	1	0,000	1,195
	Constant	4,171	,989	17,782	1	0,000	64,771

The suitability analyses obtained as a result of the study were evaluated in 5 classes as Unsuitable, Marginally suitable, Moderately suitable, Suitable, Highly suitable at equal intervals. It is seen that Balıkesir, Çanakkale, Kırklareli in the Marmara region are regions where high/very high wind energy farms can be established. It is seen that the study area is 57.60% Unsuitable, 18.04% Marginally suitable, 16.73% Moderately suitable, 7.28% Suitable, 0.32 Highly suitable areas. It is seen that 92.56 percent of the existing wind energy plants are in high and very high suitable areas.

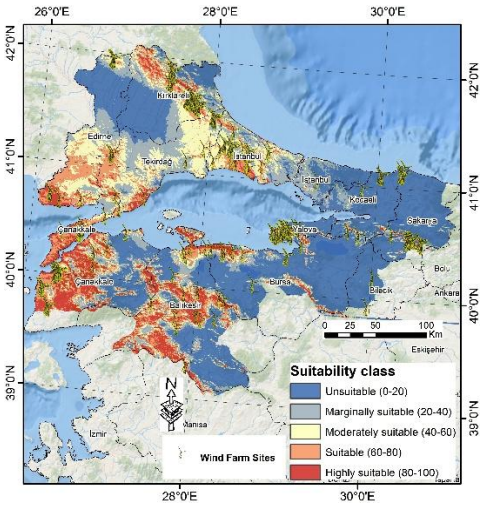

Figure 4. wind farm suitability maps.

The accuracy assessment for the suitability analysis model was performed using the Receiver Operating Characteristic Curve (ROC Curve). The ROC curve is one of the widely used methods for evaluating the classification performance of the model and particularly shows the relationship between the true positive rate and the false positive rate. The Area Under the Curve (AUC) value, which quantitatively expresses the performance of the model, was calculated as 0.92. AUC = 0.92 indicates that the model has a high discrimination power. In general, when the AUC value is between 0.90-1.00, it is accepted that the model exhibits a near-perfect classification performance. In this context, it is seen that the model has a successful prediction performance in terms of susceptible and specificity.

4. DISCUSSION AND CONCLUSIONS

In this study, the logistic regression Method was used to determine the most suitable areas for wind power sites installation in the Marmara Region. The results of the study provide important data for the evaluation of the wind potential in the region. Environmental impacts should be evaluated in detail in the planning of wind power plants. Such analyses will contribute to the formation of sustainable energy policies.

The increase in global energy demand and the environmental impacts of fossil fuels have increased the interest in renewable energy sources. Wind energy is considered as an important alternative in many countries due to its clean and sustainable source. Turkey is in an advantageous position in terms of wind energy potential, and it has been concluded that the Marmara Region in particular is a critical region in terms of the evaluation of this potential.

Author Contributions / Yazar Katkıları
Conceptualization: S.T.; M.İ.G., A.Ç.; M.Ü.Ç.; Investigation: A.Ç.; M.Ü.Ç. Material and Methodology: S.T.; M.İ.G., A.Ç.; M.Ü.Ç.; Analysis; Writing-Original Draft.

REFERENCES

Field, A. (2013). Discovering Statistics Using IBM SPSS Statistics. SAGE Publications.

Hosmer, D. W., & Lemeshow, S. (2000). Applied Logistic Regression. John Wiley & Sons.

Menard, S. (2002). Applied Logistic Regression Analysis. SAGE Publications.

TÜİK. (2023). Korunan alanlar ve yerleşim yerleri verileri.

Tüysüz, F. (2020). Türkiye'de rüzgar enerjisi potansiyeli ve yatırımlar. Enerji Dergisi, 15(2), 45-60.

Troen, I., & Petersen, E. L. (1989). European Wind Atlas. Risø National Laboratory.

Gökçek, M. (2010). "Evaluation of electricity generation and energy cost of wind energy conversion systems (WECSs) in Central Turkey." Applied Energy, 87(8), 2574-2584.

Unal, M.; Cilek, A.; Tekin, S. Maximum Entropy Method for Wind Farm Site Selection: Implications for river Basin Ecosystems Under climate Change. Water 2024, 16, 3679. https://doi.org/10.3390/w16243679

Integration of Photovoltaic Plant with Electric Vehicle and Battery System: A Case Study in Türkiye

FURKAN DİNCER*, AHMET SERDAR YILMAZ, MUSTAFA TORUN, OGUZ CEM TATAR

Abstract: The using of electric vehicles has become widespread in Türkiye as well as in the world. The main advantage of electric vehicles is that they do not pose a threat to the environment as fossil fuel vehicles. In addition, electric vehicles contain far fewer parts than internal combustion vehicles and maintenance costs are much lower. Another advantage of electric vehicles is that there is no CO_2 emission since there is no combustion process. In this study, a charging station for electric vehicles powered by a PV generation plant installed on open land is designed. In addition, it is aimed to transfer the unused portion of the electrical energy generated in the plant to the grid and generate income. At the same time, batteries are used to enable this charging station to serve at night hours when the PV system is not generating electricity.

Keywords: Solar Energy, Electric Vehicle, PV Systems, Kahramanmaras

[1]**Address:** Department of Electrical and Electronics Engineering, Faculty of Engineering and Architecture, Kahramanmaras Sutcu Imam University, Kahramanmaras/Türkiye
***Corresponding author**: furkandincer@ksu.edu.tr

1. INTRODUCTION / GİRİŞ (Times New Roman 10pt)

One of the most important needs of today's people is transportation. In our age of developing economic conditions and transportation facilities, people now meet their transportation needs largely with their own vehicles. Most of the vehicles used have internal combustion engines powered by petroleum derivatives. As of the end of December 2023, 35.6% of 15 million 221 thousand 134 cars registered to traffic was diesel, 33.5% was LPG, 28.7% were gasoline, 1.5% was hybrid and 0.5% was electric. The rate of cars with unknown fuel type was 0.2%. (Dinçer, 2021; Web 1, 2024)

Given the increase in fuel prices today, low fuel costs are one of the most important reasons why electric vehicles are preferred. The fact that electric car maintenance and fuel costs are lower than other vehicles provide support for consumers to purchase electric cars (Van Sloten, 2015). The charging costs of electric vehicles provide significant savings compared to fossil fuel vehicles. In addition, considering the foreign dependence of our country on oil derivatives, the use of electric cars becomes very attractive. Although the fuel cost of electric vehicles is lower than those of vehicles using petroleum-derived fuels, the use of electrical energy in our country is also quite expensive. The cost of electric cars is of great importance in electric car purchase intentions. (Carley 2013).

It would be even more advantageous to feed the charging station with solar panels to further reduce the cost of electricity. However, despite all these advantages, the use of electric cars in our country has remained at a very low rate of 0.5%, approximately. This shows that people are still distant from electric cars. In a study conducted in Europe on which reasons people consider when choosing an electric vehicle, the cost variable was the first preferred factor in France, Germany, Italy, Poland, Spain and the UK (Dinçer, 2025; Gomez et al., 2019).

2. MATERIAL AND METHOD

In order to realize the proposed research, a location is determined for numerical study. Figure 1 shows that the solar panel plant is located in Kilavuzlu Neighborhood of Onikisubat District of Kahramanmaras Province at 37.61° latitude and 36.80° longitude. The altitude of the region is 515 meters, the total annual insolation is 1878 kWh/m² and the average annual temperature is 18.0 °C. (Web 2, 2024). In this study, the PVSOL demo simulation program was used to design and analyze PV system with grid-connected electric vehicle and battery system. PVSOL is a simulation program that can calculate the design, cost calculation, efficiency and depreciation periods of photovoltaic systems.

Figure 1. Location of proposed the solar power plant (Web 3, 2024)

When Figure 2. is examined, it is seen that the facility is built on a wide and open land. There is no shadow factor such as structure or tree around it that would negatively affect the generation of electrical energy on the panels. In this study, the total installed power of the facility is 163,675 kWp and 188 solar panels with 550 W power were used. In addition, our facility has a surface area of 481 m². This facility is connected to the grid and the purpose of the installation is to charge the electric vehicle and the excess energy produced by charging the electric vehicle is stored in the battery systems and transferred to the grid. For this purpose, batteries were added to the proposed model.

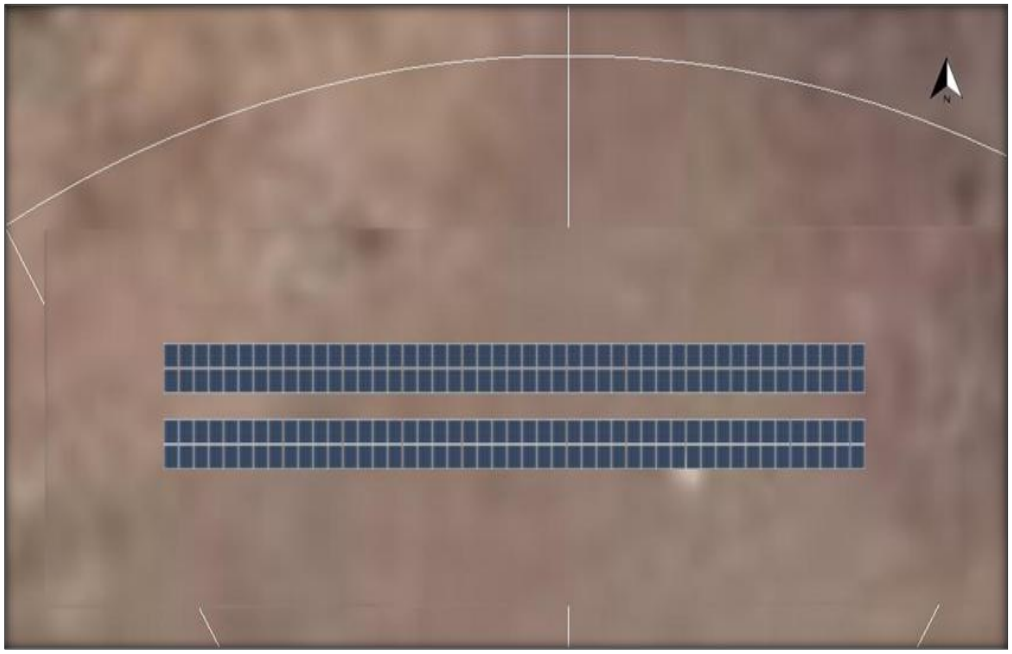
Figure 2. Modeling of the solar panel plant

When Figure 3 is examined, it is seen that the amount of irradiation required to generate electricity from the PV system in Kahramanmaras, the province where the plant is located, is at appropriate levels. The values next to the colors represent the kWh/m²-year values within the Figure 3.

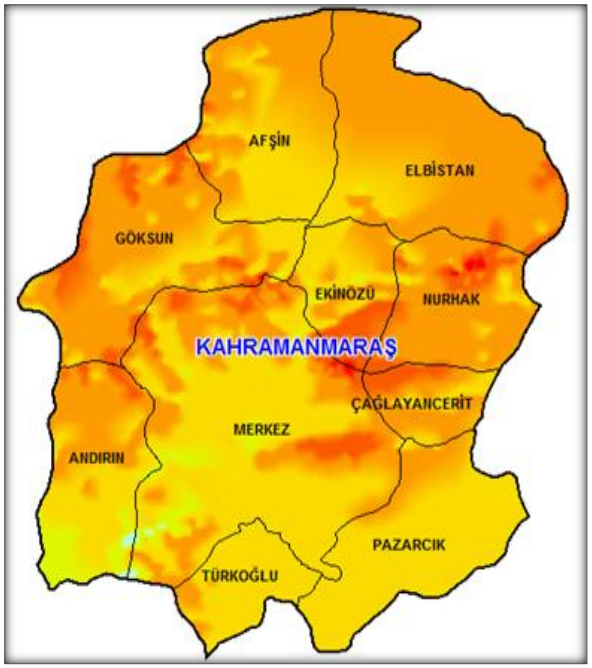

Figure 2. Solar distribution map for Kahramanmaras province (Web 4, 2024)

When Table 1 is examined, it is seen that the total annual electrical energy generation of the facility is 163,675 kWh and 1,152 kWh of this electrical energy is directly spent for self-consumption. 82,141 kWh was transferred to the grid and 80,382 kWh was used for electric vehicle charging.

Table 1. Simulation Results

PV generator energy (AC grid)	**163,675 kWh**
Direct-Self consuption	1,152 kWh
Electric vehicle charging	80,382 kWh
Grid supply	82,141 kWh
System utilization rate (PR)	87.3 %

Figure 4 shows the distribution of electrical energy generation throughout the year. It is seen that all the energy required for the electric vehicle is met by the PV system throughout the year. In addition, it is seen that in December and January, when the irradiance is at the lowest level, almost all of the electricity generated is used for electric vehicle charging, and the amount of electricity transferred to the grid drops to very low levels. In June and July, when the irradiance is high, this situation is on the contrary, and it is seen that the electrical energy transferred to the grid is more than the energy used for electric vehicle charging.

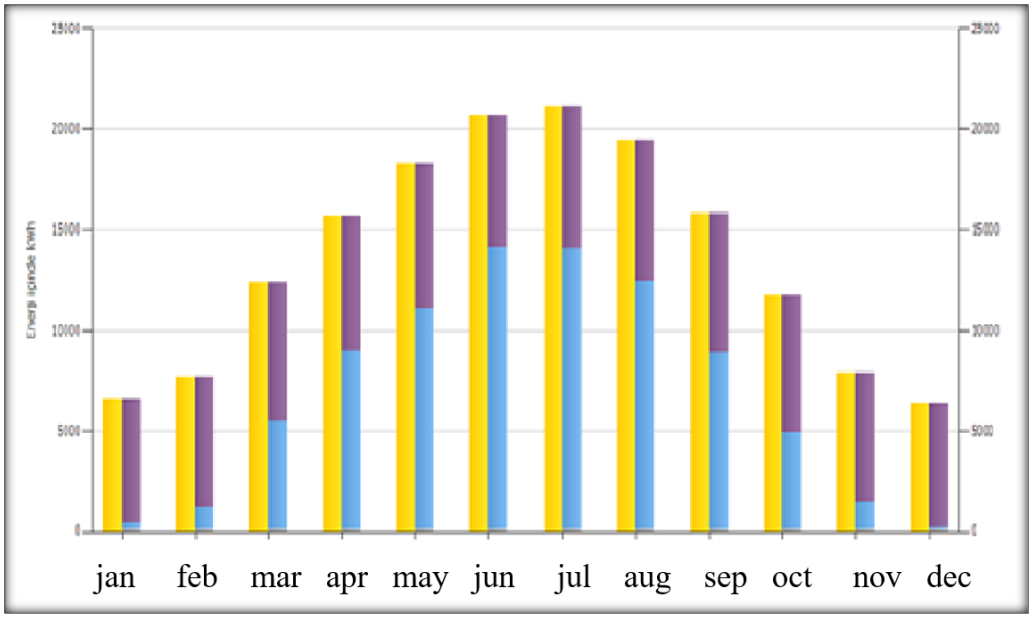

Figure 4. Utilization Distribution of Energy Generated by The PV System

Figure 5 shows coverage of total consumption. This figure shows how the total consumption is met. Although the PV system has produced the total energy required for self-consumption and EV charging throughout the year, it is seen that a certain amount of electricity is used from the grid every month. The main reason for this is that the charging station for electric vehicle charging is also active at night.

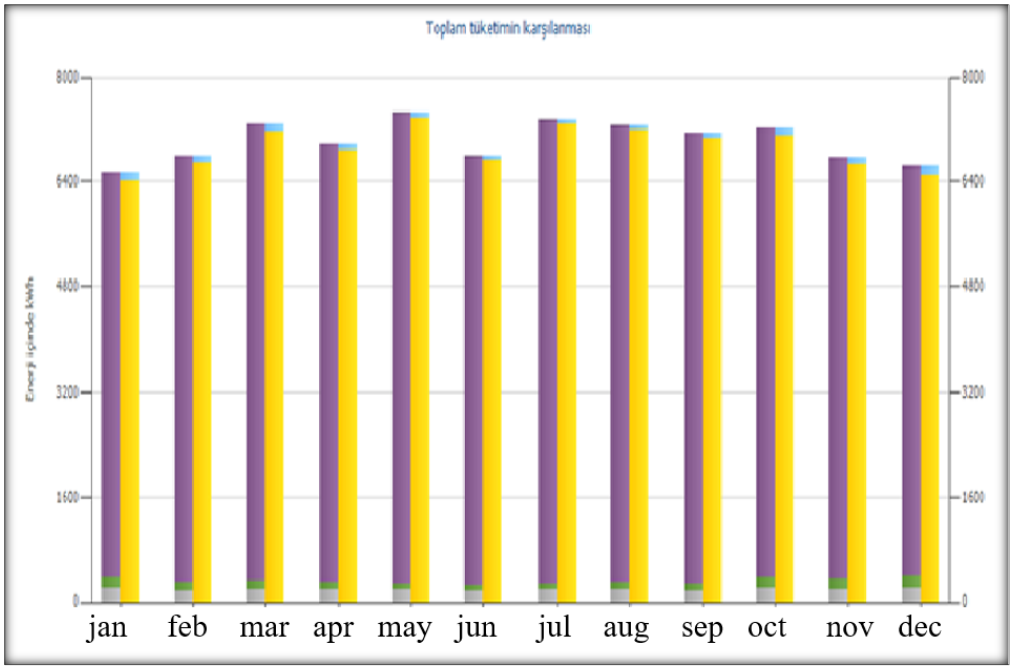

Figure 5. Coverage of Total Consumption

3. RESULTS

In accordance with the purpose of the facility, it was observed that the electrical energy required for electric vehicle charging was met by the facility throughout the year. The climatic conditions and the amount of irradiation on the location of the facility positively affected this situation. As the use of electric vehicles becomes more widespread, charging stations will operate more and the amount of electrical energy transferred to the grid will increase. This may lead to greater investments in renewable energy sources.

Table 2 shows that the annual charge of the EV is 80.383 kWh/year, the consumption per km traveled is 53.655 kWh/year and the annual distance traveled is 365.000 km. This shows that the approximate consumption per km on an annual basis is 147 W. In other words, an EV can travel an average of 8 km with 1 kWh of electrical energy.

Table 2. Electric vehicle charging kWh/year

Total charge of electric vehicle	**80,383 kWh/year**
Covered with PV and battery	80,383 kWh/year
Covered with grid	0
Consumption according to distance traveled	53,655 kWh/year
Distance traveled per year	365,000 km

Electric vehicles have great potential to reduce the harmful effects of vehicles with internal combustion engines on the environment and nature. Since electric vehicles do not have fuel tanks and exhaust fumes, they do not harm the environment. The electric vehicles charged at this facility traveled a total of 365,000 km during the year. This reduced the amount of carbon dioxide released into the environment. Thanks to this facility, electric vehicles have also benefited the environment as they do not use electricity from a coal-fired power generation plant. It is clear from this information that electric vehicles are environmentally friendly.

When Table 3 is examined, it is clearly seen how much and to what extent the generated electricity is used for which needs. The amounts stated in this table, which are transferred to the grid, used for EV charging and used for self-consumption, can be considered as income when calculating depreciation, while the amount of energy received from the grid can be considered as expense. The reason why self-consumption is considered as income is that the electricity required for this need is met by the facility.

Table 3. Generation Consumption Data

Months	**Taken from the grid**	**Transferred to the grid**	**Electric vehicle**	**Self-consumption**
Jan	120,6 kWh	369,8 kWh	6165,5 kWh	208,2 kWh
Feb	97,5 kWh	1175,8 kWh	6474,2 kWh	178,9 kWh
Mar	98,5 kWh	5353,1 kWh	6945,7 kWh	196,1 kWh
Apr	76,6 kWh	8872,4 kWh	6664,8 kWh	186,7 kWh
May	75,8 kWh	11041,7 kWh	7167,7 kWh	184,6 kWh
Jun	71,8 kWh	14020,7 kWh	6538,2 kWh	170,1 kWh
Jul	75,6 kWh	13907,2 kWh	7068,3 kWh	189,3 kWh
Aug	82 kWh	12362,9 kWh	6964,2 kWh	186,6 kWh
Sep	90,2 kWh	8803 kWh	6865,8 kWh	178,1 kWh
Oct	109,7 kWh	4787,6 kWh	6848,9 kWh	208,4 kWh
Nov	111,3 kWh	1386,5 kWh	6426 kWh	188,8 kWh
Dec	125,6 kWh	60,7 kWh	6553,2 kWh	211,1 kWh
Total	1.135,2 kWh	82.141,4 kWh	80.682,5 kWh	2286,9 kWh

4. DISCUSSION AND CONCLUSIONS

In this study, a solar power plant with an installed capacity of 103.4 kWp and a total annual electrical energy generation of 163,675 kWh is designed and modelled. Approximately half of the electricity generated is transferred to the grid and the remaining part is used for electric car charging. According to the calculations, a vehicle traveling 8 km needs 1 kWh of electrical energy. The electrical energy required for the vehicles fed from the Charging Station to travel an average of 365,000 km per year is calculated as 53,655 kWh/year.

Acknowledgements
This work was supported by a grant from the Kahramanmaraş Sütçü İmam University Scientific Research Projects Unit, Project Number: ....

Ethics Committee Approval
N/A

Peer-review
Externally peer-reviewed.

Author Contributions
Conceptualization: F.D.; Investigation: M.T.; Material and Methodology: A.S.Y, F.D.; Supervision: F.D.; Visualization: M.T.; Writing-Original Draft: O.C.T. Other: All authors have read and agreed to the published version of the manuscript.

Conflict of Interest
The authors have no conflicts of interest to declare.

Funding
This work was supported by a grant from the Kahramanmaraş Sütçü İmam University Scientific Research Projects Unit, Project Number: ....

REFERENCES

Carley, S., Krause, R. M., Lane, B. W., Graham, J. D., "Intent to purchase a plug-in electric vehicle: A survey of early impressions in large US cites. Transportation Research Part D: Transport and Environment", 18, pp. 39-45, 2013.

Dinçer, F., "Lifetime and performance alteration of photovoltaic panels, the case of Aerzen, Germany", DUJE (Dicle University Journal of Engineering) 12(4), pp. 591-594, 2021.

Dinçer, F., "Modeling And Simulation Analysis For Grid Connected Solar Power Plant Installation: A Case Study Of Ilgin/Konya", Kahramanmaras Sutcu Imam University Journal of Engineering Sciences, 28(1), 112-128, 2025.

Gomez Vilchez, J. J., Smyth, A., Kelleher, L., Lu, H., Rohr, C., Harrison, G., Thiel, C., "Electric car purchase price as a factor determining consumers' choice and their views on incentives in Europe", Sustainability, 11(22), 6357, 2019.

Sloten, R.V., "Niche-markets subsidy for effective diffusion of battery electric vehicles in Sweden", Mid Sweden University, 2015.

Web 1, TÜİK Data Portal, https://data.tuik.gov.tr/, Access Date: April 17, 2024.

Web 2, Republic of Turkey Ministry of Environment, Urbanization and Climate Change General Directorate of Meteorology, https://www.mgm.gov.tr/, Access Date: April 17, 2024.

Web 3, Google Maps, https://www.google.com/, Access Date: April 17, 2024.

Web 4, GEPA Atlas, https://gepa.enerji.gov.tr/MyCalculator/pages/46.aspx, Access Date: April 17, 2024.

Techno-Economic Analysis of A Micro PV System: A Case Study in Türkiye

AHMET SERDAR YILMAZ*[1], FURKAN DİNCER[1], OGUZ CEM TATAR[1], MUSTAFA TORUN[1]

Abstract: Human beings have started to live intertwined with nature by exploiting mountains, hills, plateaus, plateaus and plains without electricity. This beginning creates an indispensable need for electrical energy in addition to the most necessary needs such as water and roads. The distance to the nearest settlement no longer deprives people of this desire and need because it is very easy to generate electricity on-site with solar power plants. The ease of installation of solar panels provides a great advantage in order to meet this requirement very quickly. Solar power plants have become a widespread and preferred necessity all over the world. In this study, a micro solar power plant producing 3 kWe and 3,3 kWp power in city of Kahramanmaras, Türkiye was designed and the data were examined. The results were analyzed. Depreciation calculations were made based on the values calculated in the design and current electrical energy prices. Return periods of the system were determined. In addition, the environmental impacts of the installed system were analyzed and the extent to which emissions were prevented was also realized.

Keywords: Solar Energy, Photovoltaic Panel, Kahramanmaras, Micro PV System

[1]**Address:** Department of Electrical and Electronics Engineering, Faculty of Engineering and Architecture, Kahramanmaras Sutcu Imam University, Kahramanmaras/Türkiye
***Corresponding author**: asyilmaz@ksu.edu.tr

1. INTRODUCTION / GİRİŞ (Times New Roman 10pt)

The rapid increases in the world population and the need for energy in the industrial sectors have accelerated the search for new resources in the energy sector every day. Since the majority of the current electrical energy production is supplied from non-renewable energy sources, both the rapid decrease in resources and the negative effects of the use of these resources cause great and irreversible damage to our world. Due to the fact that the formation of fossil resources take many years and the existing ones are rapidly depleting, their high cost, as well as the damage caused to the natural environment by CO2, sulfur and nitrogen gases released into the atmosphere after the use of these resources, mankind needs to utilize clean and renewable energy sources (Aracı, 2013).

One of the main reasons for the search for energy is the attempt to reduce greenhouse gas emissions. According to the evaluations of greenhouse gas emission measurement results, the energy sector is the sector that causes the highest greenhouse gas emissions. Carbon dioxide (CO2) gas released as a result of the use of fossil fuels, together with the decrease in forests, causes the greenhouse gas effectby preventing the reflection of sunlight in the atmosphere. As a result of the increase in the greenhouse gas effect in the atmosphere, the temperature rises, resulting in global warming, this in turn results in environmental disasters (floods, forest fires). All this information has caused states to create new energy policies and turn to renewable energy sources (Yılmaz, 2022). Today, within the scope of renewable energy, solar energy is widely used due to its cleanliness, persistence and being low cost. The sun is a source that directly affects natural processes and events on the earth and in the atmosphere, and matter and energy cycles on earth can only occur with solar energy (Varınca and Gönüllü, 2006; Külekçi 2009)

The sun is a preferred energy source due to its inexhaustible nature and easy accessibility. In this regard, the significance of sustainable, clean, and environmentally friendly renewable energy sources has become increasingly evident. The use of solar energy for electricity generation has gained traction because it is renewable, eco-friendly, and provides a stable power supply. Additionally, its portability and the ability to be designed and installed in various capacities make it an attractive option (Şahin et. al. 2022).

There are various programs available for the analysis of PV systems, such as PVsyst, RETScreen, PVGIS, PVSOL, etc. PVsyst program was used in this study because it has a wide range of applications. It offers easy adaptability by incorporating PV system components. It can present the data of gains and losses in PV simulation as a document, the preferred materials can be used in daily life, shading factors can be observed with 3D view feature, cost calculation can be made and there is almost no difference between the actual results and design results.

In this study, with the use of PVsyst simulation software, the performance and efficiency of a 3,3 kWp domestic micro solar power plant is analyzed in detail. The aim of this study is to determine the performance, shading, generation rate, evaluate the potential, economic analysis and environmental impacts of solar power plants by using PVsyst simulation software.

2. MATERIAL AND METHOD

Proposed PV system is located at 37.62° latitude and 36.81° longitude in the Kilavuzlu Neighborhood of Onikisubat District of Kahramanmaras Province. It is high solar radiation potential city in Türkiye. The climatic data in this area shows that the altitude is 515 meters, the total annual insolation is 1878 kWh/m² and the average annual temperature is 18.0 °C. Figure 2 shows the location of the solar power plant.

Figure 1. Location of the solar power plant

With the PVsyst program, it is possible to obtain data such as location information, insolation and shading, losses, efficiency, performance ratios, three-dimensional view and cost analysis. For this reason, PVsyst program was used for the design of a domestic micro solar power plant at a location in Kahramanmaras. Table 1 shows simulation input parameters. Also, Figure 2 shows the southwestern view of the installed rooftop SPP plant. As shown in Fig. 2, simulation parameters are taken as inclination/Azimuth 37/ 0°, shading angle limit (profile angle limit) 15.2° and horizon average height 26.9°.

Table 1. Simulation Report Table

Title	Parameters
System Type	On-Grid
Project	3,3 kWp Micro Power Plant
System Power	3300 Wp
Number of config. modules	6 pieces (3,3 kWp)
Location	Kahramanmaras, Türkiye
Latitude	37.62° N
Longitude	36.81°E
Altitude	516 m

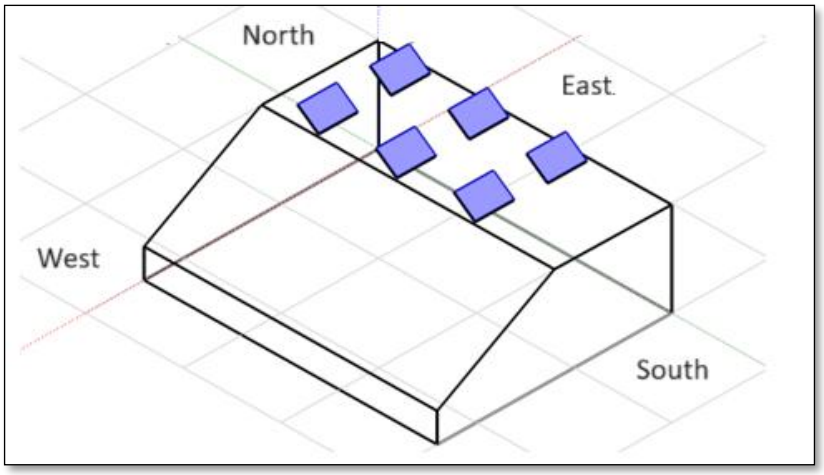

Figure 2. Installation roof view and shading angle

As can be seen in the Single Line Diagram of the installed system, CW brand 550 Wp Panels, CWT550-108PM12(6 pieces) and 1 Huawei brand SUN2000-3KTL-M1 Inverter were used.

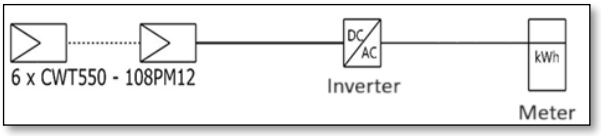

Figure 3. Single line schematic of the proposed model

3. RESULTS

In the rooftop solar power plant designed for Kahramanmaras Kilavuzlu location, PV power is 3,3 kWp and AC power is 3 kWe. The performance ratio of the designed plant is given in Figure 4. Considering the results obtained from the graphs, it is seen that the highest performance ratio is in January and December, while the lowest is in July and August.

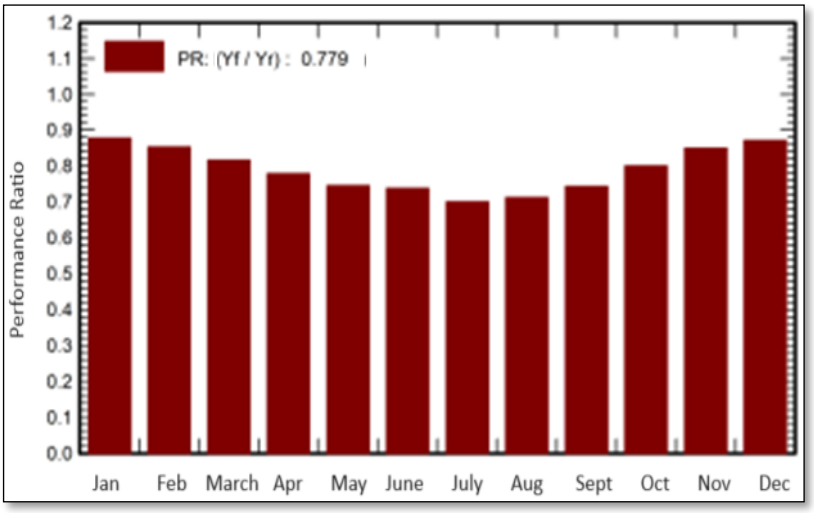

Figure 4. Performance ratio

In the normalized production graph given in Figure 5, the months with the highest production are August-September, while the months with the lowest production are December-January. The months with the highest and lowest collectors and system losses are directly proportional to the production rate. The sum of system and collector losses is 1.26kWh/kWp/day and the useful energy generated is 4.43 kWh/kWp/day.

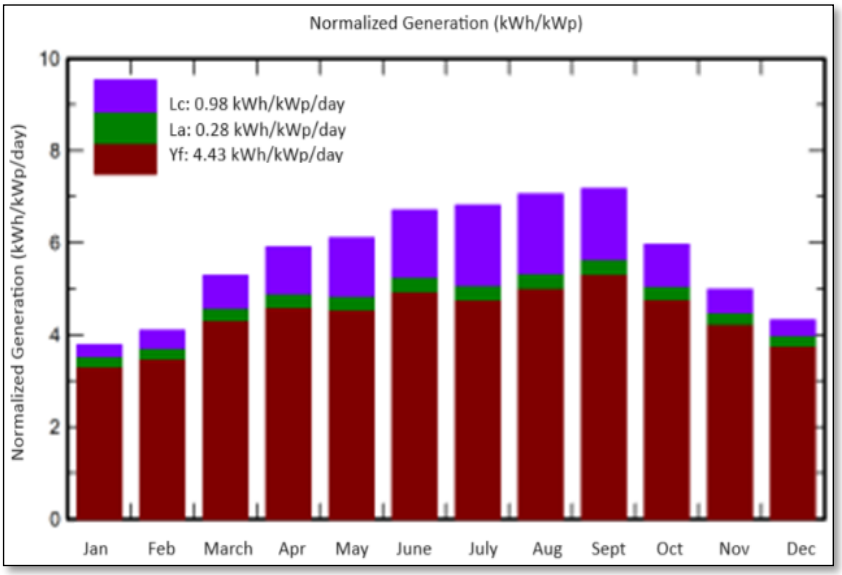

Figure 5. Normalized production

Table 2 shows the monthly and annual irradiation rate, the distribution of the energy reflected in the collectors per square meter, the amount of effective energy at the output of the array and the average performance ratio of the plant.

Table 2. Simulation Results

	GlobHor kWh/m²	DiffHor kWh/m²	T_Amb °C	GlobInc kWh/m²	GlobEff kWh/m²	EArray kWh	PR oran
Jan.	71.4	33.10	4.86	117.2	114.1	361.7	0.878
Feb.	82.6	39.90	7.32	114.6	110.4	343.9	0.853
March	134.1	63.50	12.01	164.0	153.6	469.7	0.817
Apr.	167.5	65.70	16.05	177.3	163.1	485.0	0.779
May.	202.5	77.00	21.03	189.3	169.5	495.6	0.745
June	226.5	68.60	26.74	201.2	182.9	521.1	0.737
July	231.9	66.00	31.30	211.1	187.7	519.9	0.701
Ağst.	213.9	54.20	31.65	218.6	198.4	546.5	0.712
Sept.	177.7	38.80	26.59	215.0	199.5	559.0	0.743
Oct.	130.1	38.60	19.49	184.9	177.1	517.9	0.801
Nov.	89.3	29.50	12.21	149.5	146.3	444.7	0.850
Dec.	72.1	24.50	7.24	133.8	130.6	408.5	0.871
Year	1799.6	599.40	18.10	2076.5	1933.3	5673.5	0.779

As can be seen in Table 2, the highest production is observed between June and September. From September onwards, production gradually decreases towards the end of the year. Likewise, after January, the beginning of the year, production increases in spring and reaches its highest level in summer. Similarly, radiation values increase in spring and reach their highest level in summer.

In Kahramanmaras Kilavuzlu micro-rooftop Ges design, the annual production of the system is 5673.5 kWh/year, 77.88% in terms of performance, and the cost is calculated as 1500 USD. The values given in Table 3 are based on the following calculations and are calculated in the light of the Low Voltage Single Term tariff and Distribution Fee data obtained from EPDK (Türkiye Energy Market Regulatory Authority). The calculation is made as all of the generated electricity will be sold.

Table 3. Depreciation Account (Web 1, 2024)

Installation Cost (USD)	**1500 USD**
Annual Energy Generated	5673,5 kWh/year
Installed Power	3,3 kWp
Residential (over 8 kWh/day) (Electricity Authority)	0,036 USD/kWh
Distr. Fee (EPDK)	0,009 USD/kWh
Annual Earnings	(0,036-0,009)x5673,5=153,18 USD
Depreciation Period	1500/153,18= 9,8 year

Moreover, the total greenhouse gas emission value is calculated as -5.7 tCO_2 over time. In the designed solar energy system, the total generated emission value is 5.65 tCO_2, the avoided emission value is 5673.5 kWh/year, the emissions due to grid energy are 0 gCO_2/kWh, and the degradation value is 1.0%. In the designed system, the emission per module is 1713 kgCO2 and the emission for total power 3.30 kWp is 5652 kgCO2. Table V shows that the total emission for the stands is 0.40 kgCO2 and 0.66 for the inverter.

4. DISCUSSION AND CONCLUSIONS

A location was preferred for the installation of the facility. 6 panels with 550 W power were used. The facility produced 5673.5 kWh of electrical energy annually. The installation cost was calculated as 1500 USD, the approximate amortization period is 9,8 years and the performance ratio is 77.88%. When the PV system is evaluated in terms of kgCO2 emission, it is seen that its negative environmental impacts are at a minimum level. In this study, it was observed that the micro-facility installed met the electrical energy needs of a rural household at a minimal level. The necessary calculations have been made to make it available to humanity without requiring large costs.

Such a study can be adapted for different locations. Such studies should be carried out before the installation of the power plant. Pre-installation feasibility studies are of great importance. With the necessary feasibility studies, pre-installation cost and performance values can be derived in detail. Thus, it can be determined how long the investment will pay for itself.

Acknowledgements
This work was supported by a grant from the Kahramanmaraş Sütçü İmam University Scientific Research Projects Unit, Project Number: ....

Ethics Committee Approval
N/A

Peer-review
Externally peer-reviewed.

Author Contributions
Conceptualization: A.S.Y.; Investigation: O.C.T.; Material and Methodology: A.S.Y, F.D.; Supervision: F.D.; Visualization: M.T.; Writing-Original Draft: M.T. Other: All authors have read and agreed to the published version of manuscript.

Conflict of Interest
The authors have no conflicts of interest to declare.

Funding
This work was supported by a grant from the Kahramanmaraş Sütçü İmam University Scientific Research Projects Unit, Project Number: ....

REFERENCES

Aracı, F., "Yenilenebilir Enerji Kaynakları ve Termal Enerji Kaynaklarından Yararlanma", İstanbul Teknik Üniversitesi Fen Bilimleri Enstitüsü, Yüksek Lisans Tezi, İstanbul, 2013.

Dinçer, F., "Modeling And Simulation Analysis For Grid Connected Solar Power Plant Installation: A Case Study Of Ilgin/Konya", Kahramanmaras Sutcu Imam University Journal of Engineering Sciences, 28(1), 112-128, 2025.

Külekçi Ö.C., "Yenilenebilir Enerji Kaynakları Arasında Jeotermal Enerjinin Yeri ve Türkiye Açısından Önemi", Ankara Üniversitesi Çevrebilimleri Dergisi. 1(2), 83-91, 2009.

Şahin, Z. R., Dinçer, F., & Yılmaz, A. S., "Desıgn And Sımulatıon Of Grıd Connected Solar Power Plant For The Electrıcal Energy Needs Of A Famıly Of Four People. Kahramanmaraş Sütçü İmam Üniversitesi Mühendislik Bilimleri Dergisi, 25(Özel Sayı), 46-56", 2022.

Yılmaz, N., "Türkiye deki yenilenebilir enerji kaynakları ve diğer enerji kaynaklarının durum analizi, çevresel etkileri, karşılaştırılması", Sakarya Üniversitesi, Fen Bilimleri Enstitüsü, Yüksek Lisans Tezi, 2022.

Varınca, B.K., Gönüllü, M.T., "Türkiye'de Güneş Enerjisi Potansiyeli ve Bu Potansiyelin Kullanım Derecesi, Yöntemi ve Yaygınlığı Üzerine Bir Araştırma", I. Ulusal Güneş ve Hidrojen Enerjisi Kongresi, Eskişehir, 270-275, 2006.

Web 1, Tariff Tables for Electricity Bills, https://www.epdk.gov.tr/Detay/Icerik/3-1327/elektrik-faturalarina-esas-tarife-tablolari, Accessed on April 15, 2024.

Oncohydrogel for Early Skin Cancer Diagnosis

JULIA GODZWON*[1], NATALIA PAŁKA[1], JOANNA SZCZEPAŃSKA[1], LIWIA CICHOŃ[2], URSZULA KLIMCZAK[2]

Abstract: The OncoHydrogel project focuses on developing a modern, non-invasive diagnostic system that enables the early detection of skin cancers. The innovation of this method lies in the use of a hydrogel that reacts to specific biological changes in cancerous tissue, allowing for quick and easy recognition of pathological skin changes. As part of the research, various hydrogel matrices will be tested, such as sodium alginate and Gelma, which is modified gelatin. Each of these matrices has unique physicochemical properties that may influence the sensitivity and effectiveness of detecting cancerous skin changes. A key element of the detection mechanism is the use of L-Dopa, which reacts with the enzyme tyrosinase – a marker characteristic of cancer cells. This interaction triggers a color change in the hydrogel, enabling a rapid and visual detection of abnormalities on the skin's surface. Additionally, the project includes the analysis of pH changes in the cancerous lesion area, as cancer cells often alter the microenvironment by acidifying the surrounding tissues. Monitoring this parameter may provide an additional method for identifying skin cancers, increasing the diagnostic accuracy of the OncoHydrogel system. Another important aspect of the research is the detection of biomarkers characteristic of melanoma, such as S100 proteins, gp100, and MIA. Their presence in the tested area could further confirm the diagnosis and provide valuable information about the nature of the skin changes. OncoHydrogel aims to create a diagnostic method accessible to a wide range of patients, including the elderly and children. Due to the simple and intuitive interpretation of results based on the hydrogel's color change, this system could be an appealing alternative to traditional diagnostic methods, such as biopsies or imaging studies. Standard techniques are often invasive, require advanced equipment, and can be stressful for patients. In contrast, the proposed solution offers a quick, comfortable, and effective diagnosis, which may contribute to the earlier detection of skin cancers and, consequently, improve the effectiveness of treatment. The use of innovative hydrogel in skin cancer diagnostics could revolutionize the approach to early detection of neoplastic lesions, enabling an easier, more accessible, and more efficient method for monitoring skin health. Implementing this solution could not only increase the chances of successful treatment but also improve the quality of life for patients by eliminating the need for invasive diagnostic tests.

Keywords: biopolymers, diagnostic materials, hydrogel, material engineering, skin cancer

[1]**Address:** AGH University of Krakow, Faculty of Materials Science and Ceramics, Cracow/Poland
[2]**Address:** AGH University of Cracow, Faculty of Electrical Engineering, Automation, Computer Science and Biomedical Engineering, Cracow/Poland

***Corresponding author**: juliagodzwon@student.agh.edu.pl

1. INTRODUCTION

Melanoma is currently the most dangerous type of skin cancer that accounts for 90% of skin cancer-related deaths. The first step in diagnosing melanoma-induced lesions is a macroscopic skin assessment of the entire body using the ABCDE rule. "A" stands for asymmetry of the lesion, "B" for irregular borders, "C" for uneven coloration, "D" for diameter, indicating an enlarged size, and "E" for the evolution of the lesion. This method can be used by individuals without specialized medical knowledge; however, it should only serve as an initial screening tool for further diagnostics. A more precise examination for determining the nature of a skin lesion is dermatoscopy, conducted by a specialist. A more invasive diagnostic method is histopathological examination, which requires a skin biopsy. Histopathology provides detailed information regarding the subtype of the disease, lesion thickness, the presence of ulceration, and whether the lesion infiltrates nearby nerves and blood vessels. Complementing traditional diagnostic methods is immunohistochemistry, a technique based on detecting specific tumor markers using labeled antibodies. Although used less frequently, it can offer valuable insights into the molecular characteristics of the tumor and its potential malignancy (Milanowska et al., 2023).

Diagnostic technologies based on biomaterials, especially hydrogels, have garnered growing interest in recent years. Hydrogels represent a promising platform for modern biosensors due to their high water content, flexibility, and ability to immobilize biomolecules, while preserving their biological activity. Their structure can dynamically respond to chemical or physical stimulation, making them ideal materials for detecting disease biomarkers. Thanks to these properties, hydrogels can be functionalized to selectively recognize specific biological substances, such as metabolites, toxins, or drugs, making them highly useful in medical diagnostics.

The use of aptamers as recognition elements in hydrogel-based biosensors enables the selective detection of target analytes through structural changes in the hydrogel. For example a biosensor that detects ochratoxin A (OTA), in which DNA aptamers stabilize the hydrogel network, and contact with the toxin leads to its degradation and the release of gold nanoparticles, allowing for optical detection. Such solutions are not only highly sensitive but also adaptable for portable and cost-effective diagnostic systems. A similar principle has been applied in microfluidic paper-based devices (μPADs) for cocaine detection. The presence of the drug induces hydrogel degradation, altering fluid flow within the system. Additionally, graphene oxide-based hydrogels functionalized with fluorescently labeled aptamers have been developed, enabling the sensitive detection of antibiotics through the Förster resonance energy transfer (FRET) phenomenon (Jung et al., 2017).

The use of hydrogels for detecting disease biomarkers opens new possibilities in diagnostics, especially skin cancer detection. *OncoHydrogel* is a project aimed at developing a hydrogel-based biosensor in the form of a patch, enabling non-invasive, rapid, and cost-effective melanoma diagnosis. The patch will function by detecting the concentration of tumor-specific proteins that serve as biomarkers for the disease. The ease of application and low cost of this solution could significantly improve diagnostic accessibility for individuals with limited access to medical care while also raising public awareness of melanoma prevention.

Although this technology is still in development, the concept of using hydrogels in skin cancer diagnostics is reflected in existing solutions. Currently, reports describe a material called *OncoGel*, which serves as a drug delivery system for cancer therapy. This material is based on the *ReGel*™ copolymer matrix, composed of poly(d,l-lactic-co-glycolic acid) and polyethylene glycol. *ReGel*™ transitions from a low-viscosity state (between 2 and 15°C) to a gel form at body temperature, allowing for controlled drug release (Elstad, Fowers, 2009).

2. MATERIAL AND METHOD

The development of hydrogel matrices is planned, utilizing both natural polymers, such as sodium alginate and gelatin methacrylate (GelMA), as well as synthetic components, including poly(2-hydroxyethyl methacrylate) (pHEMA) and polyethylene glycol diacrylate (pEGDA). Sodium alginate, derived from brown seaweed, will be employed in the preparation of biofilaments through ionic crosslinking with calcium chloride.

GelMA, a modified form of gelatin characterized by excellent cytocompatibility and tunable physicochemical properties, will be utilized in conjunction with photoinitiators to fabricate crosslinked three-dimensional structures. In contrast, synthetic hydrogels such as pHEMA and PEGDA offer enhanced control over mechanical properties and degradation kinetics. The structural diversity and functionalization potential of these materials establish a robust platform for the development of intelligent detection carriers capable of selectively responding to melanoma biomarkers. The incorporation of specific reagents into the hydrogel matrix will facilitate the creation of a system capable of rapid and non-invasive detection of malignant skin lesions (Slaughter et al., 2009).

One of the key biomarkers of melanoma is tyrosinase—an enzyme involved in melanin biosynthesis, whose activity is elevated in melanocytic-derived cancer cells. To detect the presence of this enzyme, 3,4-dihydroxyphenylalanine (L-DOPA), a natural substrate of tyrosinase, has been selected for use. Upon enzymatic action, L-DOPA undergoes oxidation to dopachrome, triggering a series of polymerization reactions that result in the formation of dark-colored compounds. This process can also be effectively conducted using immobilized tyrosinase, which enhances enzyme stability and enables its repeated use in the reaction system. In the context of the proposed biosensor, this mechanism is adapted into a hydrogel containing L-DOPA, which undergoes a visible color change in the presence of active tyrosinase. This approach enables rapid, non-invasive, and visually interpretable detection of potential malignant skin lesions, facilitating early melanoma diagnosis without the need for complex diagnostic tools (Carvalho et al., 2000).

Additional key biomarkers of melanoma include the S100B protein and the HMB-45 antibody. S100B, a member of the S100 protein family, plays a regulatory role in cell cycle processes, melanocyte differentiation, and cellular stress response. Its elevated concentration is strongly correlated with the presence and progression of malignant melanoma, particularly in metastatic cases, making it one of the most well-documented biomarkers of this cancer. Detection of S100B in the analyzed material will be achieved through the use of specific anti-S100 antibodies, such as rabbit-derived antibodies, immobilized within the hydrogel matrix. HMB-45, on the other hand, is a monoclonal antibody that recognizes the PMEL antigen (also known as gp100), which is present in the melanosomes of melanoma cells. Its expression is characteristic of melanocytic lesions with high malignant potential and is widely used in histopathology as a melanoma marker. In the proposed biosensor, the detection of this antigen will be accomplished using an anti-PMEL antibody (HMB-45 clone), allowing for the identification of cancerous cells in the tested sample (Harpio & Einarsson, 2004).

To ensure precise detection of changes in the chemical environment, pH indicators such as litmus (at a concentration of 0.1%) and bromothymol blue will be incorporated into the hydrogels. These compounds will enable the monitoring of local pH changes occurring in response to the presence of cancer biomarkers. A decrease or increase in pH within the

skin lesion—characteristic of the tumor microenvironment—can result in a change in the hydrogel's reaction, producing a clear visual signal in the form of a color shift. On the detection plate, solutions with known pH values will be applied, which will interact with the hydrogel. This will allow for easy and unambiguous interpretation of results—without the need for specialized laboratory equipment.

As part of the planned tests, we intend to conduct a series of experiments using multi-well plates, starting with the assessment of pH changes in the hydrogel using the previously mentioned color indicators. The aim of this stage will be to determine the sensitivity and the range of color changes in response to pH modifications. In the subsequent phase of the research, we will focus on analyzing the hydrogel's reaction containing L-DOPA in the context of its interaction with tyrosinase. This will allow us to assess whether the presence of the enzyme leads to a clear and noticeable color change, which forms the basis for enzymatic detection.

In the final stage of the tests, we also plan to evaluate the performance of hydrogels functionalized with antibodies, including the HMB-45 antibody, which enables the detection of the PMEL antigen. Concurrently, tests will be conducted using the anti-S100 antibody, which is used for detecting the S100B protein. The use of both antibodies will allow for the assessment of the system's specificity with respect to different cancer biomarkers. The entirety of the experiments will provide a comprehensive validation of the developed biosensor and its potential application as a diagnostic platform for the early detection of melanoma.

2.1. Simulation

In our study, we have assumed that the physiological conditions present in the human body—particularly concerning the tumor microenvironment—will be replicated as closely as possible to ensure realistic and reliable results. A key parameter controlled during the experiments will be temperature, maintained at approximately 37°C, which corresponds to the average body temperature. Such conditions enable chemical and enzymatic reactions to occur in a manner similar to biological processes in vivo. Additionally, we have taken into account that the local pH within skin tumor lesions may differ from that of healthy skin—usually trending towards a more acidic environment, which is linked to the metabolic activity of cancer cells. Therefore, pH indicators such as litmus and bromothymol blue have been incorporated into the hydrogels, allowing real-time detection of these subtle pH changes. This approach enables visual assessment of the hydrogel's pH shift after contact with the sample, without the need for specialized equipment. When detecting melanoma biomarkers such as tyrosinase, S100B, or the PMEL antigen, maintaining physiochemical conditions close to natural ones will be essential—specifically a temperature of 37°C and a neutral pH range. Enzymes like tyrosinase require specific conditions for catalyzing reactions with L-DOPA, while antibody-antigen interactions (e.g., HMB-45 and S100) occur most efficiently in an isotonic environment with stable pH. Moreover, the materials used to create the hydrogels, such as sodium alginate and GelMA, were selected due to their high biocompatibility and ability to form stable, hydrated structures that facilitate molecular exchange. These properties make it safe to use the system in contact with the skin, without the risk of toxic reactions or irritation. The use of realistic experimental conditions increases the likelihood of developing an effective, non-invasive tool for the early diagnosis of skin melanoma.

3. RESULTS

The detailed results of our research will be published upon the completion of the experiments and the full analysis of the obtained data. At this stage, in line with our hypotheses, we expect that local pH changes within tumor lesions will induce a noticeable color change in the hydrogel, providing a clear signal of the presence of cancer biomarkers. We anticipate that the best results will be achieved using sodium alginate-based hydrogel, due to its high biocompatibility and rapid response to environmental changes. Regarding the active substances incorporated into the matrix, we assume that the combination of pH indicators (such as bromothymol blue and litmus) with the detection of tyrosinase and the S100B protein will provide the most precise and sensitive results. We expect that such a combination of components will create an effective system for rapid and non-invasive skin cancer detection, forming the foundation for an innovative diagnostic technology. environments, such as detecting glucose concentration, hydrogen ions, or various chemical compounds. For instance, hydrogels modified with aptamers have been used for detecting toxins or drugs, where the hydrogel's structural change in response to the presence of a specific analyte resulted in noticeable color shifts, enabling the detection and quantification of the analyte. While our research is pioneering in the context of detecting cancer biomarkers, it will rely on the same principles—using pH changes in response to the presence of cancer markers, which has proven effective in detecting other biomolecules. Therefore, although our approach may be among the first to detect specific cancer biomarkers using hydrogels, our methodology and technology are closely aligned with those used in other fields of biomedicine, providing a solid foundation for predicting the success of our planned tests. The properties of pH-sensitive indicators, such as bromothymol blue, combined with suitable hydrogel materials, have the potential to effectively detect changes related to skin cancers, much like in other applications where pH changes serve as a basis for monitoring alterations in living organisms.

4. DISCUSSION AND CONCLUSIONS

Although research on the use of hydrogels for the detection of cancer biomarkers is still limited, there are several similar studies that utilize hydrogels in the diagnosis of other biological substances, such as toxins, drugs, or bacteria. The literature includes examples of using hydrogels to detect pH changes associated with enzymatic reactions or the presence of specific biomarkers. pH-indicator-based hydrogels have been employed to monitor pH variations in various biological

Acknowledgements

We would like to sincerely thank Juliusz Leszczyński, BEng, PhD, the supervisor of our Student Research Group, for his invaluable help, support, and insightful guidance, which have been crucial to the successful implementation of our project.

Ethics Committee Approval

No ethical approval was required for this study.

Peer-review

This study has not undergone peer-review, as it is a part of an ongoing research project or internal report. Further peer-review will be conducted prior to publication.

Author Contributions

Conceptualization: J.G., A.S, U.K., L.C, N.P.; Investigation: J.G., A.S, U.K., L.C.; Material and Methodology: J.G., A.S, U.K., L.C.; Writing-Original Draft: J.G., A.S, U.K., L.C.;
All authors have read and agreed to the published version of manuscript.

Conflict of Interest

The authors have no conflicts of interest to declare.

Funding

This research was funded by the IDUB project at AGH University of Cracow.

REFERENCES

Carvalho, G. M. J., Alves, T. L. M., & Freire, D. M. G. (2000). L-DOPA Production by Immobilized Tyrosinase. *Applied Biochemistry and Biotechnology*, *84–86*(1–9), 791–800. https://doi.org/10.1385/ABAB:84-86:1-9:791

Elstad, N. L., Fowers K. D., (2009). *OncoGel (ReGel/paclitaxel)* — Clinical applications for a novel paclitaxel delivery system. *Advanced Drug Delivery Reviews,* 61, 785-794. https://doi.org/10.1016/j.addr.2009.04.010

Harpio, R., & Einarsson, R. (2004). S100 proteins as cancer biomarkers with focus on S100B in malignant melanoma. *Clinical Biochemistry*, *37*(7), 512–518. https://doi.org/10.1016/j.clinbiochem.2004.05.012

Jung, I. Y., Kim, J. S., Choi, B. R., Lee, K., & Lee, H. (2017). Hydrogel Based Biosensors for In Vitro Diagnostics of Biochemicals, Proteins, and Genes. In *Advanced Healthcare Materials* (Vol. 6, Issue 12). Wiley-VCH Verlag. https://doi.org/10.1002/adhm.201601475

Milanowska, M., Grudzińska, A., Jarosz, D., Tsitko, H., & Dudzińska, P. (2023). Skin cancer's prevention in the light of current medical knowledge. *Journal of Education, Health and Sport,* 35-39 (Vol. 23, No. 1) https://doi.org/10.12775/JEHS.2023.23.01.004

Slaughter, B. V., Khurshid, S. S., Fisher, O. Z., Khademhosseini, A., & Peppas, N. A. (2009). Hydrogels in Regenerative Medicine. *Advanced Materials*, *21*(32–33), 3307–3329. https://doi.org/10.1002/adma.200802106

Prevalence and Awareness of Diabetic Retinopathy among Diabetic Patients in Tirana Healthcare

MARSİDA KRASNİQİ*[1]

Abstract: This cross-sectional study aimed to assess the prevalence of diabetic retinopathy (DR) and the level of awareness among diabetic patients attending healthcare clinics in Tirana. A total of 279 patients participated, comprising 176 males (63%) and 103 females (37%), with a mean age of 57.3 years (SD = 12.3). The study utilized a questionnaire administered by medical staff to collect demographic data, diabetes-related complications, and sources of information about diabetes and its complications. Participants were classified based on the duration of diabetes into three groups: <5 years, 6-10 years, and >10 years. Medication use was categorized into three types: oral tablets, insulin, and a combination of both. The study also included questions regarding previous diagnoses of diabetic retinopathy. The results revealed that 3% of participants were diagnosed with diabetic retinopathy. Furthermore, it was observed that patients with lower levels of education showed significantly less awareness about diabetic retinopathy and its potential complications, with many reporting insufficient or no information. The findings highlight a gap in education regarding diabetic retinopathy, particularly among less-educated individuals. The study emphasizes the importance of improving awareness and providing targeted education for diabetic patients, particularly in settings with limited access to specialized healthcare resources.

Keywords: Diabetic Retinopathy, Cross-Sectional Study, Tirana Healthcare, Complications

[1]**Address:** Department of Medical Technical Science, Faculty of Professional Studies, University Aleksander Moisiu, Durrës, Albania.

***Corresponding author**: marsidakrasniqi@uamd.edu.al

1. INTRODUCTION

W Diabetic retinopathy (DR) remains one of the most common and serious complications associated with long-standing diabetes, often leading to vision impairment and blindness[1] if left undetected or untreated. As the global prevalence of diabetes continues to rise, especially in urban populations, addressing the complications of this condition has become a public health priority [2]. Early detection and awareness of DR are essential for preventing irreversible visual damage[3], yet levels of understanding about the condition vary widely among patients.

In Albania, particularly in Tirana, data on the awareness and prevalence of diabetic retinopathy among diabetic individuals is limited. This lack of information hinders the development of effective educational and preventive strategies[4]. Assessing the extent to which patients are informed about DR, as well as identifying groups at higher risk of lacking awareness, can help shape targeted interventions[5,6]. This study investigates both the prevalence of diabetic retinopathy and the awareness levels among diabetic patients attending healthcare centers in Tirana, with the aim of identifying educational gaps and promoting better management practices.

2. METHODOLOGY

A descriptive cross-sectional study was conducted to evaluate the presence of diabetic retinopathy and the extent of patient awareness regarding this complication. The study population included 279 diabetic patients who attended various healthcare clinics in Tirana. Participants were selected using a non-probability sampling method and included both male and female patients diagnosed with diabetes.

Data collection was carried out through a structured questionnaire administered by trained medical personnel. The questionnaire was designed to gather comprehensive information including demographic characteristics, diabetes duration, treatment modalities, awareness of diabetic complications, and specifically any history of diabetic retinopathy diagnosis.

Participants were categorized based on the length of time they had been living with diabetes into three groups: less than 5 years, 6–10 years, and more than 10 years. In terms of treatment, patients were grouped into those using oral medication, insulin therapy, or a combination of both. To assess awareness, the questionnaire included items related to the sources of diabetes-related information and knowledge about potential complications, including DR.

The data obtained were analyzed to determine both the prevalence of diagnosed diabetic retinopathy and patterns of awareness across demographic and treatment subgroups. Ethical approval was obtained, and informed consent was collected from all participants before their involvement in the study.

3. RESULTS

The study participants were predominantly male (63.1%), with a mean age of 57.3 years. In terms of education, most participants had secondary or higher education, with 22.9% having primary education or less. These demographic details presented in Table 1 are important as they can influence the awareness and prevalence of complications such as diabetic retinopathy.

Characteristic	Category	Frequency (n)	Percentage (%)
Gender	Male	176	63.1
	Female	103	36.9
Mean Age (Years)	57.3 (SD ± 12.3)		
Education Level	Primary or less	64	22.9
	Secondary	102	36.6
	Higher	113	40.5

Table 1: Demographic Characteristics of Participants

From Table 2, we can see that the prevalence of diabetic retinopathy (DR) was low overall, with only 2.9% of the participants diagnosed with DR. The highest prevalence was observed in the group with more than 10 years of diabetes (4.8%), while the group with less than 5 years of diabetes had the lowest rate (1.1%). These findings suggest that DR is more likely to develop with longer durations of diabetes.

Duration of Diabetes	Diagnosed with DR (n)	Not Diagnosed with DR (n)	Total (n)	Prevalence of DR (%)
< 5 years	1	91	92	1.1
6–10 years	3	100	103	2.9
> 10 years	4	80	84	4.8
Total	8	271	279	2.9

Table 2: Period of Diabetes and Prevalence of Diabetic Retinopathy

4. DISCUSSION

The results of this study indicate a relatively low overall prevalence of diabetic retinopathy (DR) among the diabetic patients in Tirana, with only 2.9% of participants reporting a diagnosis of DR. This is somewhat surprising given the well-established association between prolonged diabetes duration and an increased risk of diabetic complications[7]. However, the observed prevalence aligns with the notion that underdiagnosis and limited screening may be factors contributing to this lower-than-expected figure.

The study also highlights an important trend where the duration of diabetes is positively correlated with the prevalence of DR. Participants with diabetes for more than 10 years had a DR prevalence of 4.8%, which is consistent with previous literature that suggests longer diabetes duration significantly increases the likelihood of developing diabetic retinopathy[8]. In contrast, participants with less than 5 years of diabetes had a DR prevalence of just 1.1%. This finding supports the idea that early-stage diabetes, while still requiring close monitoring, is less likely to present serious complications like DR.

In terms of demographic characteristics, the study revealed a predominance of male participants (63.1%) with a mean age of 57.3 years. The age and gender distribution reflect the typical demographics of individuals most affected by diabetes. Additionally, the educational level of participants played a critical role in awareness levels. Although not directly measured in the results, education level can be inferred to influence the participants' knowledge of their disease and its complications[9,10]. Those with higher education were likely more aware of the need for eye examinations and monitoring for DR, even though the overall awareness of DR in this sample remains unclear.

A key limitation of the study lies in the relatively small number of DR diagnoses, with only 8 cases reported. This may point to an underrepresentation of those at risk for DR, as the sample likely did not include enough patients with advanced or more severe forms of diabetes or retinopathy. Future studies could benefit from larger sample sizes and better screening practices to determine a more accurate prevalence of DR.

5. CONCLUSION

This study provides valuable insights into the prevalence of diabetic retinopathy and the potential influencing factors, such as diabetes duration, among diabetic patients in Tirana. While the overall prevalence of DR was low (2.9%), the data suggest that individuals with longer durations of diabetes are at greater risk for developing this complication. Furthermore, the study highlights a potential gap in screening and education, especially for individuals with shorter durations of diabetes or those with less education.

Given the correlation between the duration of diabetes and the prevalence of DR, it is crucial for healthcare providers to focus on regular screening, particularly for patients with longer diabetes durations. Additionally, improving patient education, especially for those with lower education levels, can help raise awareness about the importance of regular eye exams and the risks associated with DR. Expanding access to ophthalmologic screenings in Tirana, particularly in underserved populations, could contribute to earlier detection and prevention of vision-related complications in diabetic patients.

REFERENCES

1. Krasniqi, M., & Trebicka, B. (2020). Visual impairment and quality of life, a cross-sectional study. International Journal of Psychosocial Rehabilitation, 24(7), 10234-10240.
2. Kropp M, Golubnitschaja O, Mazurakova A, Koklesova L, Sargheini N, Vo TKS, de Clerck E, Polivka J Jr, Potuznik P, Polivka J, Stetkarova I, Kubatka P, Thumann G. Diabetic retinopathy as the leading cause of blindness and early predictor of cascading complications-risks and mitigation. EPMA J. 2023 Feb 13;14(1):21-42. doi: 10.1007/s13167-023-00314-8. PMID: 36866156; PMCID: PMC9971534.
3. Upadhyay T, Prasad R, Mathurkar S. A Narrative Review of the Advances in Screening Methods for Diabetic Retinopathy: Enhancing Early Detection and Vision Preservation. Cureus. 2024 Feb 4;16(2):e53586. doi: 10.7759/cureus.53586. PMID: 38455792; PMCID: PMC10918290.
4. Khalaf FR, Fahmy HM, Ibrahim AK, Mohamed GA, El Sayed Ez Eldeen M, Elkady A, Hetta HF. Does a diabetic retinopathy educational program raise awareness among elderly diabetic patients? Diabetes Metab Syndr Obes. 2019 Sep 20;12:1867-1875. doi: 10.2147/DMSO.S208072. PMID: 31571961; PMCID: PMC6759836.
5. Bhattad PB, Pacifico L. Empowering Patients: Promoting Patient Education and Health Literacy. Cureus. 2022 Jul 27;14(7):e27336. doi: 10.7759/cureus.27336. PMID: 36043002; PMCID: PMC9411825.
6. Trebicka, B., Harizi, A., Krasniqi, M., Kalaja, R., & Tartaraj, A. (2024). FINANCIAL DEVELOPMENT AND ECONOMIC GROWTH: EXPLORING THE IMPACT OF FINANCIAL SYSTEMS, STABILITY, AND INSTITUTIONAL QUALIT ON ECONOMIC PERFORMANCE. Risk Governance & Control: Financial Markets & Institutions, 14(3).
7. Wu Y, Ding Y, Tanaka Y, Zhang W. Risk factors contributing to type 2 diabetes and recent advances in the treatment and prevention. Int J Med Sci. 2014 Sep 6;11(11):1185-200. doi: 10.7150/ijms.10001. PMID: 25249787; PMCID: PMC4166864.
8. Vashist P, Senjam SS, Gupta V, Manna S, Gupta N, Shamanna BR, Bhardwaj A, Kumar A, Gupta P. Prevalence of diabetic retinopahty in India: Results from the National Survey 2015-19. Indian J Ophthalmol. 2021 Nov;69(11):3087-3094. doi: 10.4103/ijo.IJO_1310_21. PMID: 34708747; PMCID: PMC8725073.
9. Krasniqi, M., & Nallbani, G. (2022). The effect of corticosteroids on macular edema in patients with noninfective uveitis. Journal of Advanced Pharmacy Education & Research| Apr-Jun, 12(2).
10. Hoffmann R, Lutz SU. The health knowledge mechanism: evidence on the link between education and health lifestyle in the Philippines. Eur J Health Econ. 2019 Feb;20(1):27-43. doi: 10.1007/s10198-017-0950-2. Epub 2018 Jan 3. PMID: 29299763; PMCID: PMC6394601.

Critical cooperativity in two urban development case studies from Budapest

CSILLA MILE*[1], ZOLTÁN BODROG*[2]

Abstract: Nowadays, when the whole of humanity seems to be paralyzed in the struggle for global sustainability, every step towards sustainability should be thoroughly considered; every possible step has to be realized as quickly as possible. In turn, steps against sustainability and procrastination in steps for sustainability should be identified and avoided. This calls for the most intensive attention in cases when there seem to be parallel sustainability development projects rivalling for resources, but the reality is the contrary: a cooperative process is possible. Another aspect of false rivalry between such projects is that motivation and readiness are extremely important development resources; therefore they must not be wasted, especially because of falsely apparent reasons. We show two current project debates from the inventory of urban development in Budapest; each in a speculative, propositional stage, but in this embryonic state already showing illusionary conflicts which effectively hinder further evolution of concepts into actual development steps. The first small "case study" is laying the foundations of a new, larger pedestrian zone in the seventh district. The political actors have already set up against each other along the lines of "Whose goals will be served by this project, tourism or the residents?". The real question is: what goals can be served by quality urban space in parallel? Are there conflicting interests? Is it at all possible to have conflicting interests here (at least until a certain basic development of quality)? The second small story is the further continuation of a still planned (not even under construction) tramway extension project. While all the actors in the story seem to feel some rivalry between two 'alternatives', we show that these are not alternatives to each other, but independent, or even possibly cooperative further development stages. This 'case study' serves also as a typical situation: development projects often generate sentiments of engineering personnel around them, and this exaggerates perceived rivalries between such projects, hindering consistent evolution of further planning.

Keywords: Urban planning, cooperative resource usage, zero-sum fallacy, sustainability management

[1]**Address:** Óbuda University, Keleti Károly Faculty of Business and Management, Budapest, Hungary
[2]**Address:** Óbuda University, Keleti Károly Faculty of Business and Management, Budapest, Hungary

***Corresponding author**: mile.csilla@uni-obuda.hu

1. INTRODUCTION

Sustainability has become the most prominent task and goal for humanity in the (first half of the) 21st century; this is now a trivial statement. As for urban planning, this means that we have no freedom of choice when we choose between sustainable and unsustainable development, or when we carry out a (really) sustainable development project or not. The choice should be trivial, our hands should be tied. In everyday practice, however, this triviality does not seem to prevail. Sustainable projects, sustainable transformations are delayed infinitely or simply not done, [1,2,3] moreover, projects of unsustainability are frequently chosen over sustainable ones. This is why we stand where we stand in the global struggle for sustainability.

In this paper, we show two tiny case studies where sustainability does not prevail for an especially awkward reason: different kinds of perceived conflicts which are based on interpersonal or intergroup competition which in turn originate from personal feelings or interest. The factors which turn out to be prohibitive to cooperation are artificial and subjective. Nonetheless they appear as rational motivations, and this is what makes them worrying and worth studying.

What are the apparent rational motivations behind the false competitive situations? This is very important to study, [4] because we should be prepared for these typical interpersonal or intercommunity, etc. processes, and we should be able to identify and stop (or at least dominate) them. [5] In the two case studies we bring here, there will be two main sources of apparent competition:

1. political tensions and searching for political utility (this is a kind of intercommunity competition),
2. idées fixées of urban design strategists or experts (as interpersonal obstacles against naturally feasible cooperation).

The former one will appear behind the first case study, while the latter will drive the second. Before we step further to study them, let us reiterate how they appear as rational obstacles of cooperation. First, political tensions, especially when they relate to a certain (e.g. development) question, appear as doing the best for the citizens concerned. At least, the communicated goal of political battles is that. Second, preliminary biased thoughts in minds of urban planning strategists and experts come by their nature as reasons behind doing this and that. The lack of *intradisciplinary* communication and joint planning efforts efficiently prohibit cooperation, and the reason of last resort remains: what to analyse further when the experts in charge do not have motivation for a thorough and unbiased analysis?

2. Review of the pseudoconflicts

We now introduce the two cases; each one is about an urban development project. The first is a typically cheap one (if properly realized), the second is expensive, and their contents are also quite different. The stories, though, will be rather similar if we look at the progress towards a sustainable end: sustainability is difficult enough on its own; and adding some artificial conflict will effectively stop development. [6]

2.1. Case 1: pedestrian streets in the 7th district

Budapest is very poorly equipped with pedestrian-dominated public spaces. This is mainly the result of a very slow transition and development period (until 2010) after the fall of the communism (1990), [7,8] when earlier paradigms of transportation and city planning remained active; and since then, though all the new candidates for the mayorship have run with agendas humanizing the city, the level of very action towards this has stalled. While there is a steady but slow evasion from this situation, e.g. in the 8th district recently, the landscape changes very slowly, and especially in the 7th district, which somehow emerged as the tourist and night-life centre of Budapest in the last two decades, car-oriented accessibility of every part of the city, even when not feasible, remained a central policy goal.

Given this, and the apparent world trend of making cities more and more livable by extending pedestrian-dominated areas, [9] it is not a surprise that walkability and pedestrian-oriented transformation appeared even as a central offer of a non-partisan mayor candidate in 2019 (no particular breakthrough with a centrist, 'deep green' agenda, because Hungarian political life is extremely fixed to a two-bloc, two-ideology dichotomy), and the most successful, most well-organized still active district-level NGO for urban development originates from the 7th district (*Színes Erzsébetváros*, lit. 'Colorful Elizabethtown'; one seat in the local assembly).

The above civilian activity, complete with a fragmented political landscape in the council of Budapest, and the activity of a strong independent mayor candidate who has lost the most recent election by an extremely narrow margin (less than 0,1%), has led to the promulgation of a pedestrianization plan in the Budapest city council for the inner part of district 7., [10] the most affected area of Budapest by tourism, night life, and unsustainability of any level of car traffic. The origins of the plan were then already perfect to make this issue a political one, thus hindering a solution-oriented discussion from the beginning. As we have pointed it out in the abstract already, the pseudoconflict has come about the priority of residents over tourism and nightlife, or vice versa.

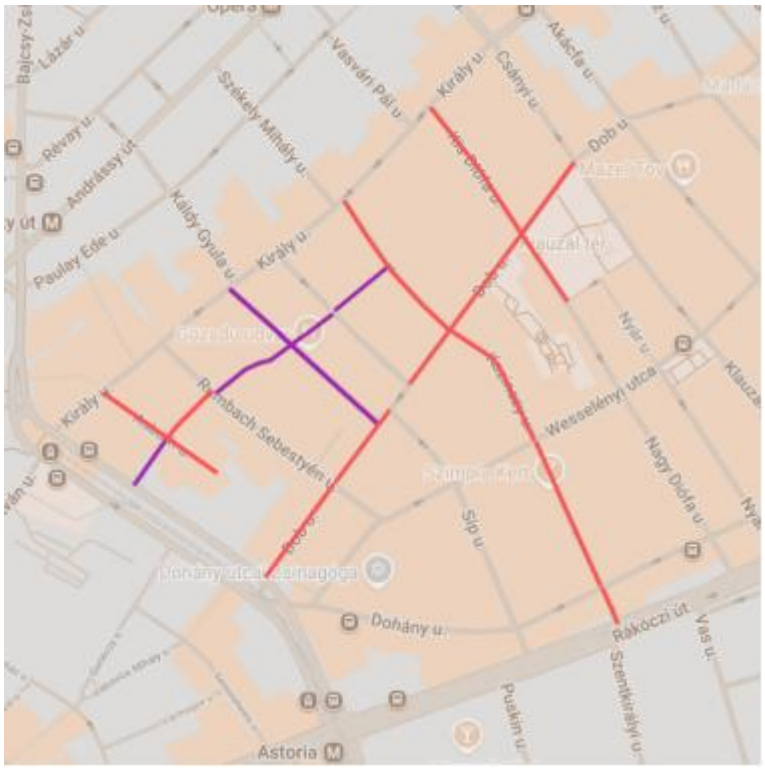

Figure 1. The network of pedestrian streets (red and purple) originally proposed for the inner part of district 7. Purple are the streets already freed from cars. (Picture from the original proposal. [10])

But what would be the content of a meaningful discussion? The common usage of public space, especially pedestrianized streets by tourism and night life on one hand, being residents on the other. [11] Which 'half of city life' in district 7 shall

take precedence? By our opinion, in this case cooperative usage would have been not only possible but almost determined as the single outcome of a pedestrianization programme. Our opinion is based on two arguments.

First, the ‘quality usage’ of public spaces in the 7th district (and in Budapest, generally) is so sparse and untypical, that going into this direction would have no chance to reach such saturation effects like conflicts between several different advantages of it. This can be visualized by imagining the production function [12] of public space humanization both in residential usage, and in tourism and night-life usage. Since only the first bits of production were set to appear, we would have been in well the so-called first stage of it (increasing marginal product), very far from exhausting possibilities of growth, e.g. by having conflicting interests of utilizations. Simply told, there are so few quality public spaces in the 7th district, and in Budapest at all, that by taking the first steps of pedestrianization, we do not have a chance to reach, and run into adverse effects.

There is still conflict between living in the 7th district as a resident (seeking for peace and silence in the night, for example), and using it as a tourist, a visitor or an entrepreneur serving them. These conflicts arise, however, from the number and mismanagement of visitor masses. The 7th district suffers from overtourism, which is rather a relative one: not exhausting the resources absolutely, but allocating them suboptimally, due to deficient management. [13] In this situation, direct management of the tourist and night-life problem, as well as a better monitoring of the number of visitors would solve the existing problems. [14] Moreover, the number of visitors is in connection with other factors of the industry (number of beds offered in the district, open hours of bars, restaurants, pubs, etc.), and debate about these factors are a part of local politics, but this has to be clarified independent of the problem of quality public spaces.

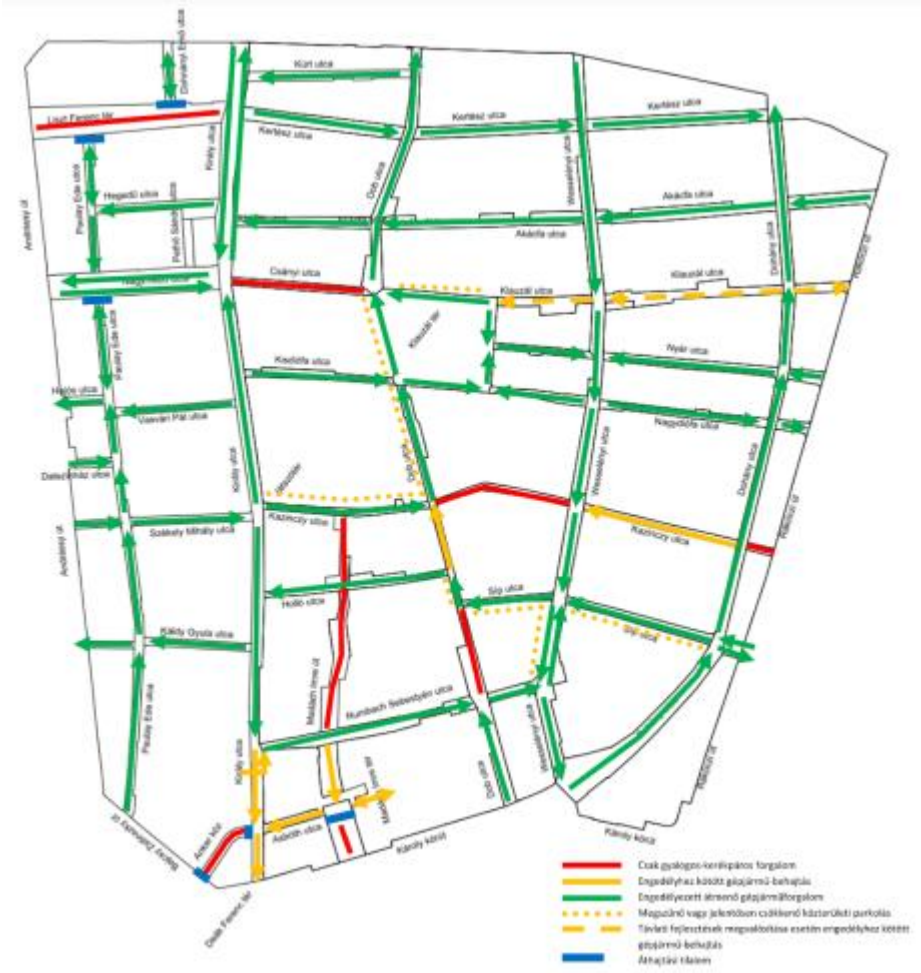

Figure 2. The City Council bill reappeared in May, [15] modified according to the requests of the ‘pro-residents’ mayor of the 7th district, and his ally, the mayor of Budapest. It is basically a watered-down version of the original, it fails to show the integrated, networked characteristics of it. Moreover, the red streets in the lower left quarter are already pedestrian streets (cf. the map from the former proposal). (Picture from the proposal. [15])

In short, there were enough political motivations to construct a false conflict around the quality public spaces problem i.e. the pedestrianization of the inner 7th district; and this conflict materialized as a conflict of residents and the local hospitality industry. Nonetheless, we have the underpinned opinion that this conflict cannot come from the question of

public spaces. First, because there are other, well-identifiable factors which result in this conflict; and second, because the sparsity of actual quality public spaces effectively prohibits a conflict between two such usages of them.

The apparent conflict was nonetheless able to water down the proposal; thus missing a chance to take a step in a long-stalled problem of Budapest.

2.2. Case 2: whither to extend a still not built tramline extension?

The second case of false conflict is similarly about an urban development project, but in most aspects totally different. Maybe, the most important difference is that here no 'real', near-implementation steps are under consideration. The object of debate is a hypothetic extension of a tram section which itself is not yet under construction. Thus, we are now on the other extremity of the imminence spectrum. This debate about a distant project element is also able to show how the life of a city depends on false conflicts. This is because if this project element fails to build some consensus, there is no chance for it to become agreed-upon, and then a plan, ultimately reaching realization.

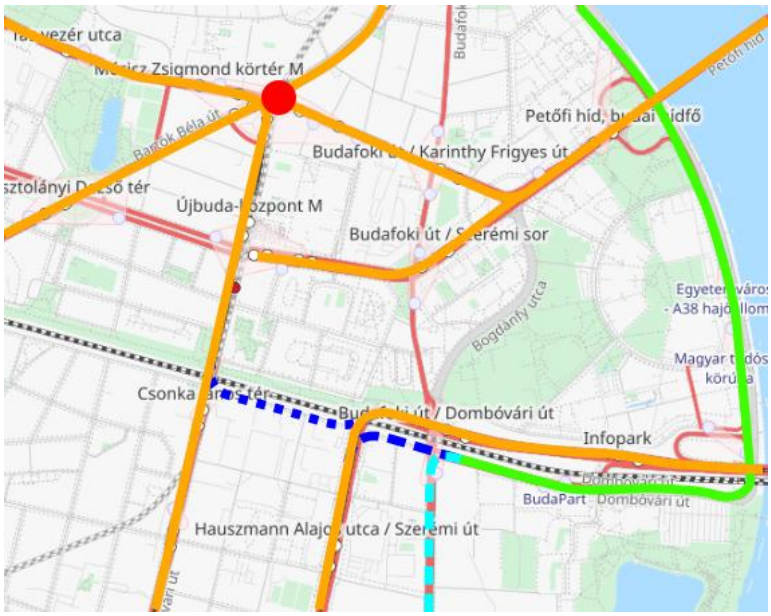

Figure 3. The planned „Budai fonódó 2." tram network extension (green) to which we discuss further increments. Cyan-dashed is the primarily contemplated long-term southward extension, blue-dashed is a short connection to a neighbouring line (blue-dotted is a connection of that line to the central hub of southern Buda, red dot). Yellow: other (existing) lines.

Let us see what the question is! In Fig 3. we see the well-planned and procrastinated so-called "Buda-Intertwined-2" (Hungarian: „Budai fonódó 2.") [16] tram section (green), which as an inconsistency to its name, does intertwine only on one end to the tram network, as a branch, and does not intertwine on the other end. This 'dangling' nature of this section is thanks to the contemplated extensions of it. This contemplation is directed primarily to the south, thus envisioning a parallel axis to an existing tram axis (cyan, dashed on Fig 3.), but strictly in the long run (note that this parallelism can seem superfluous, but if cities go more sustainable, denser public transit networks will be necessary).

There arises, however, a very cheap extension which gives an intertwining closure of this tram section by directing it back into the existing southward axis mentioned above (blue, dashed on Fig. 3). This would be possible in the short run (infrastructure conflicts with the district heating clarified [17]), because of its relatively low cost, and giving the double intertwining, it would instantaneously double the social benefit of the fundamental project (Buda-Intertwined-2), roughly said. Other benefits also realized, e.g. reducing congestion at the main tram hub of southern Buda (called "Móricz Zsigmond körtér", marked with a red dot in Fig 3.), or giving an alternative terminus to tram line 1 also there; a long-faded dream of transit network planning in this region (historically planned in parallel to heavy road development, which has been cancelled, and the tram connection faded together with it).

Shall then the short-run, multiple-advantage, cheap extension considered by the urban design and strategic community overseeing the fundamental project? Of course, but motivation lacks, due to an apparent conflict between the southern long-term extension and the simpler one. If resources are allocated to the latter, and trams run into that direction, it will be impossible to allocate resources and have trams run to the other; a fine example of the zero-sum fallacy. [18] Why would direction A prohibit direction B, especially when they are so different both in alignment and function? Moreover, the short-term extension would be built long ago when the long-term becomes a real question, and the short-run section would then give the opportunity to connect the new southward axis to the busiest southern-Buda hub of the network.

3. The apparent solution, and conclusion

Up to this point, both the stories are something straightforward and happening every-day. Perceived conflicts, instead of real ones, hinder some development projects. Policymakers, urban planners, etc., and strategists shall be aware of this possibility, and try to discuss, mitigate and solve conflicts. In the two cases we treated, we have shown, in a sketched way, that this is possible, as for the real content of the projects. The way is by all our knowledge open for this.

This unused opennes leads us to the identification of an extremely important resource of urbanism: real short-term determination and motivation. The basic strategic flaw in both cases is letting the moment fly away, which means not using the political and other motivations that are present for a very short time. No difference if it is about realizing a change which can be realized, or putting a theoretical answer to a theoretical problem on the way of realization, if short moments of widespread support to the project elements is not used, the development of whole city regions of districts can become (or remain) stalled.

In the question of sustainability, and urban mobility development projects towards sustainability, [19] this is even more important, because sustainability projects should be done in time (all related somehow to the global sustainability trajectory), and they should not lose hard-earned societal support behind them.

References

Budapest City Council. (2025, March) Javaslat Belső-Erzsébetvárosban gyalogosbarát forgalmi rend bevezetésére (translated to English: proposal for a pedestrian-friendly traffic order in the inner part of Erzsébetváros) https://einfoszab.budapest.hu/list/fovarosi-kozgyules-nyilvanos-ulesei;id=126232;type=3;parentid=18440;parenttype=2

Budapest City Council. (2025, March) Javaslat Belső-Erzsébetvárosban gyalogosbarát forgalmi rend bevezetésére (translated to English: proposal for a pedestrian-friendly traffic order in the inner part of Erzsébetváros) https://einfoszab.budapest.hu/list/fovarosi-kozgyules-nyilvanos-ulesei;id=127451;type=3;parentid=18448;parenttype=2

Chambers, Robert. Transforming power: from zero-sum to win-win? (2023).

ÉDES Balázs. State of play of transport in Budapest metropolitan area, transport development plans to be financed by EU. Budapest Transit Authority, BKK (2015).

Gautam, L., Sahu, V., Singh, R., Thiyagarajan, S. V., & Suseelan, A. Sustainable Solutions for Metro Project Delays: Lean Practices for Enhanced Resource Efficiency and Cleaner Production. Sustainability, 16(24), 10897. (2024)

Hussain, S., Shahzad, M., Appolloni, A., & Xuetong, W. (2023). The impact of public infrastructure project delays on sustainable community development. Environmental Science and Pollution Research, 30(14), 40519-40533.

Khahro, S. H., Shaikh, H. H., Zainun, N. Y., Sultan, B., & Khahro, Q. H. Delay in decision-making affecting construction projects: a sustainable decision-making model for mega projects. Sustainability, 15(7), 5872. (2023)

Kocsis, János B. Patterns of urban development in Budapest after 1989. Hungarian Studies, 2015, 29.1-2: 3-20.

Kovács, Zoltán, and Reinhard Wießner. Budapest: restructuring a European metropolis. Europa regional 12.1 (2004): 22-31.

Memon, A. H., Memon, A. Q., Khahro, S. H., & Javed, Y. Investigation of project delays: Towards a sustainable construction industry. Sustainability, 15(2), 1457. (2023)

Niella, Tamara, Nicolas E. Stier-Moses, and Mariano Sigman. Empirical evidence of the zero-sum game fallacy. Available at SSRN 2586195 (2015).

Plichta, Jaroslaw. The co-management and stakeholders theory as a useful approach to manage the problem of overtourism in historical cities–illustrated with an example of Krakow. International Journal of Tourism Cities 5.4 (2019): 685-699.

Shephard, Ronald William. Theory of cost and production functions. (2015): 1-322.

Sisman, Elif Ebru. Pedestrian zones. In: Advances in Landscape Architecture. IntechOpen, 2013.

Tibor Sipos, Cognitive Dissonance on Sustainable Mobility, Acta Polytechnica Hungarica 20.5:31 (2023), doi:10.12700/APH.20.5.2023.5.3

Tsaur, Sheng-Hshiung, Chang-Hua Yen, and Hsiu-Yu Teng. Tourist–resident conflict: A scale development and empirical study. Journal of Destination Marketing & Management 10 (2018): 152-163.

Żemła, Michał. Reasons and consequences of overtourism in contemporary cities—Knowledge gaps and future research. Sustainability 12.5 (2020): 1729.

Zhuo, C., Xie, Y., Mao, Y., Chen, P., & Li, Y. Can cross-regional environmental protection promote urban green development: Zero-sum game or win-win choice?. Energy Economics, 106, 105803. (2022)

Zoltán Bodrog (Pedestrian's Budapest Initiative), Hogyan lehet a Műegyetem rakparti villamos sokkal jobb? (translated to English: How can the tram on the Technical University Quay be much better?), preliminary feasibility study, Budapest, 2020, https://drive.google.com/file/d/1xoQKgxWLljvTBmxE7alxW-od3bNg-dyJ/

Assessment and Validation of Wildfire Susceptibility Map in İzmir City (Aegean Coast of Türkiye) Using Maximum Entropy (MaXEnt) Model

OSMAN ORHAN*[1], SENEM TEKİN[2], ÇAĞRI KAPUSUZ[1]

Abstract: In this study, a wildfire susceptibility map was generated using the maximum-entropy method (MaxEnt) based on fire locations derived from MODIS Active Fire and Burned Area Products for İzmir, located on the Aegean coast of Türkiye. First of all, a total of 383 wildfires were determined, of which 70% of the fire locations were used to train the model and 30% were used for the validation stage. Second, fourteen conditioning factors, namely elevation, slope, aspect, plan curvature, topographic wetness index (TWI), distance from roads, distance from settlements, distance from streams, precipitation, maximum temperature, solar radiance, wind speed, land use/land cover, normalized difference vegetation index (NDVI) were determined for wildfire susceptibility analysis. After that, the MaxEnt method was utilized to evaluate the relationships between the locations of wildfires and associated conditioning factors. As a result of the study, Izmir city's wildfire susceptibility map was created.

Keywords: Wildfire, Susceptibility Map, Aegean, MaxEnt

[1]**Address:** Department of Remote Sensing and GIS, Institute of Science and Technology, Mersin University, 33343 Mersin, Türkiye
[2]**Address:** Remote Sensing and Geographic Information Systems Application and Research Center, Adiyaman University, 02040 Adiyaman, Türkiye

***Corresponding author**: senemtekin@adiyaman.edu.tr

1. INTRODUCTION

Forests are one of the most critical ecosystems in the world. In its most general and comprehensive definition, a forest is an ecosystem in which trees, plants and animal communities interact. In this ecosystem, there is a mutual balance between invisible or-ganisms in the soil and the inanimate environment. As a result of events such as people's destruction of nature, unconscious use, and fires, forest areas are being destroyed and are decreasing in area (Sabuncu & Özener,2019; Hong et al., 2019).

According to the US space agency NASA's Fire Information for Resource Manage-ment System, wildfires spread to numerous parts of the world in 2021 (FIRMS, 2023). Wildfires that occurred this year have affected most of North and South America, the South African plateau, the northern part of the Arabian Peninsula, the Mediterranean coast of Europe, the Eastern parts of Asia as well as Northern and Eastern Europe. Tur-key's Mediterranean coast is one of the regions most affected by these fires.

Therefore, revealing the relationships between past wildfire records and triggering factors and identifying locations with wildfire potential are essential in terms of develop-ing the right policies against such catastrophic disasters.

Due to its Mediterranean climate zone, Türkiye experiences many wildfires. The General Directorate of Forestry reports that there were 23.1 million hectares of forest in 2021. In 2017, 139503 hectares of forest area were destroyed by wildfire in 2793 fires (OGM,2022).

Data on past and present wildfires, including their start date, location, amount of burned area, and duration, are collected to understand the mechanisms of occurrence of wildfires and to reveal their relationship with influencing factors. This data is then used to develop planning programs to prevent and respond to wildfires (Tonini et al.,2020). The information from these inventories is critical for creating a map of hazards, risks, and susceptibilities (Bustillo et al.,2021; Nur et al.,2022). Susceptibility mapping can be used to identify wildfire-prone areas. Wildfire susceptibil-ity mapping uses a wide variety of methods that take advantage of Geographic Infor-mation System (GIS) and Remote Sensing (RS) integration. In many places in the world, wildfire susceptibility maps are created using a variety of techniques, including Analyti-cal Hierarchy Process (AHP) (Hong et al.,2019), Logistic Regression (Shmuel & Heifetz,2022), Random Forest (Bustillo et al.,2021) and Artificial Neural Network (ANN) (Cao et al.,2017).

Firstly, it aims to create a wildfire susceptibility map to identify potential forest fire areas in the city of İzmir, located on the Aegean coast of Türkiye and has a significant for-est asset. For this purpose, past forest fire records of the region and fourteen conditioning factors known to be effective on wildfires were used. The secondary purpose of this study is to investigate the performance of the maximum entropy (MaxEnt) model, which is widely used in ecological modeling

studies, such as habitat suitability and species distri-bution modeling in different parts of the world, in wildfire susceptibility studies.

2. STUDY AREA

İzmir is located at latitude 37o 40'-39o 15' N and longitude 26o 15'-28o 20' E East on Türkiye's Aegean coast. Additionally, the study area's altitude ranges from sea level to 2200 meters above it (Figure 1). The city, situated in the Mediterranean climate zone, expe-riences mild, rainy winters and hot, dry summers. Izmir's annual average temperature is 16.7 ° C, although there is 687 mm of precipitation on average annually (tr.climate-data.org). Almost all of the mountainous parts of the study area are covered with forests. According to CORINE 2018 LULC data, there is a forest area of approximate-ly 250 000 hectares in study area.

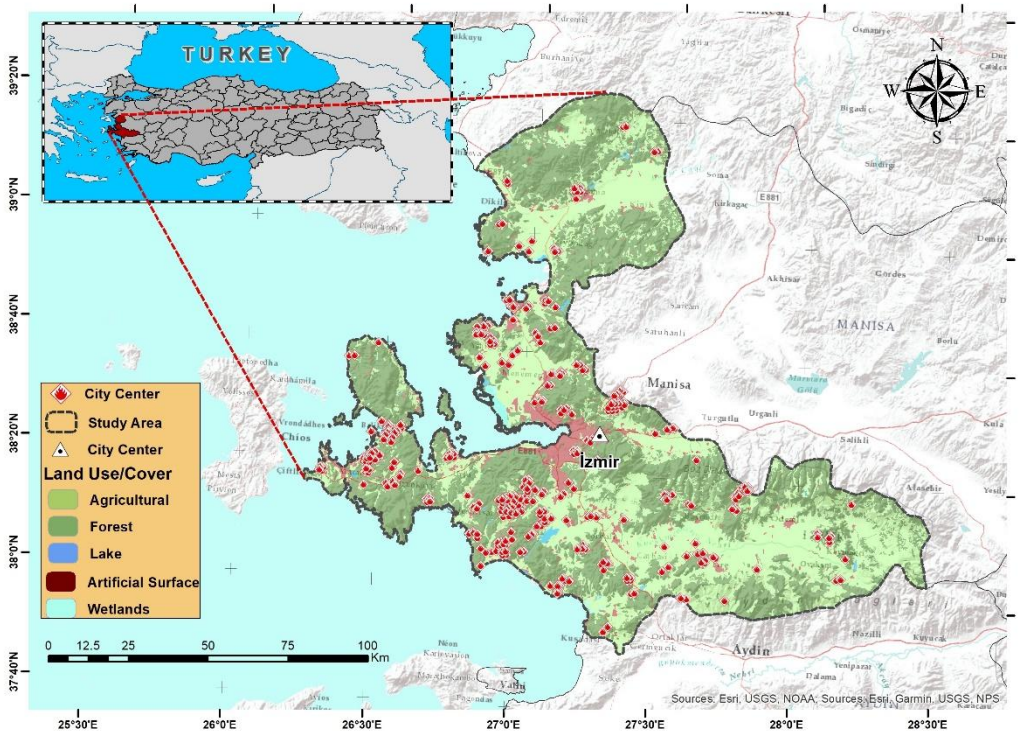

Figure 1. this is a figure. schemes follow the same formatting.

3. MATERIAL AND METHOD

3.1. Wildfire inventory and conditioning factors

Firstly, we need historical wildfire inventory data to predict potential wildfire areas. Therefore, MODIS active fire product (https://firms.modaps.eosdis.nasa.gov/), which con-tains historical forest fire data, was used. The MODIS Collection 6.1 active fire product de-tects fires in 1-km pixels that are burning at the time of overpass under relatively cloud-free conditions. This data set, which includes historical fire data from 2000 to the present, was used as training and test data to determine potential wildfire areas within the scope of the study. Also, this MODIS data has been subjected to a filtering process since it contains fire data due to various reasons in the study area. As a result of filtering, a total of 383 fires occurred in the vegetation and forest areas in the study area. In addition, pixels with low confidence values (<0.95) in the data set were eliminated for reliable wild-fire susceptibility map.

There is still no clear consensus on which environmental variables (conditioning factors) are the most effective for modeling fire prediction due to the complexity of wildland fire causes (Fischer et al.,2016). Based on a review of the corresponding literature (e.g., (Jaafari & Pourghasemi; Nur et al.,2022) and available data, we obtained fourteen potential conditioning factors namely elevation, slope, aspect, plan curvature, topographic wetness index (TWI), distance from roads, dis-tance from settlements, distance from streams, precipitation, maximum temperature, solar radiance, wind speed, land use/land cover, normalized difference vegetation index (NDVI) and they were included in the analysis along with the inventory data. Table 1 summarizes the data types and sources for wildfire conditioning factors used in this study.

Table 1. Data types and sources used in this study

Factors	Data type	Scale/Resolution (Final Res.)	Explanation	Source
Elevation	Raster	30 m	DEM from AW3D data	AW3D data
Slope	Raster	30 m	Calculated from DEM	AW3D data
Aspect	Raster	30 m	Calculated from DEM	AW3D data
Plan curvature	Raster	30 m	Calculated from DEM	AW3D data
TWI	Raster	30 m	Calculated from DEM	AW3D data
Distance from roads	Vector	1/100.00 (30 m)	Euclidean distance analys.	Environmental Plan
Distance from settlements	Vector	1/100.00 (30 m)	Euclidean distance analys.	Environmental Plan
Distance from streams	Vector	1/100.00 (30 m)	Euclidean distance analys.	Environmental Plan
Precipitation	Raster	30 arc second-(30m)	WorldClim v.2.1 database	Fick and Hijman(2017)
Maximum temperature	Raster	30 arc second-(30m)	WorldClim v.2.1 database	Fick and Hijman(2017)
Solar radiance	Raster	30 arc second-(30m)	WorldClim v.2.1 database	Fick and Hijman(2017)
Wind speed	Raster	30 arc second-(30m)	WorldClim v.2.1 database	Fick and Hijman(2017)
Land use/Land cover	Raster	100 m – (30 m)	Level 1 classification	CORINE - 2018
NDVI	Raster	(30 m)	Derived from Landsat data	Landsat 8 OLI

3.2. Maximum Entropy (MaxEnt)

With limited information and the link between this knowledge and environmental variables, the maximum entropy technique generates a probability distribution with the least biased estimation feasible. By creating connections between just "accessible" data and local attributes, the MaxEnt method creates distribution models for the studied area (Elith et al.,2006). By using just "available" data, or inventory data, the issue of unreliable "unavailable" data loss is avoided. Particularly, the power of environmental interactions and dispersion limits carried by "missing" data can prevent the prediction of potential dispersion (Jiménez-Valverde et al.,2008).

4. RESULTS AND DISCUSSION

Figure 2 displays the wildfire susceptibility result map that was created as a conse-quence of the MaxEnt analysis and determined using levels of the wildfire potential index. As a result of the analysis, the map showing the distribution of wildfire potential was sorted into five classes, namely very low (0-0.15), low (0.15-0.31), moderate (0.31-0.46), high (0.46-0.63) and very high (0.63-1.0) using the natural breaks classification technique. The red, yellow, and green color zones on the wildfire susceptibility map in Figure 2 show the high, moderate, and low potential degrees for wildfire, respectively.

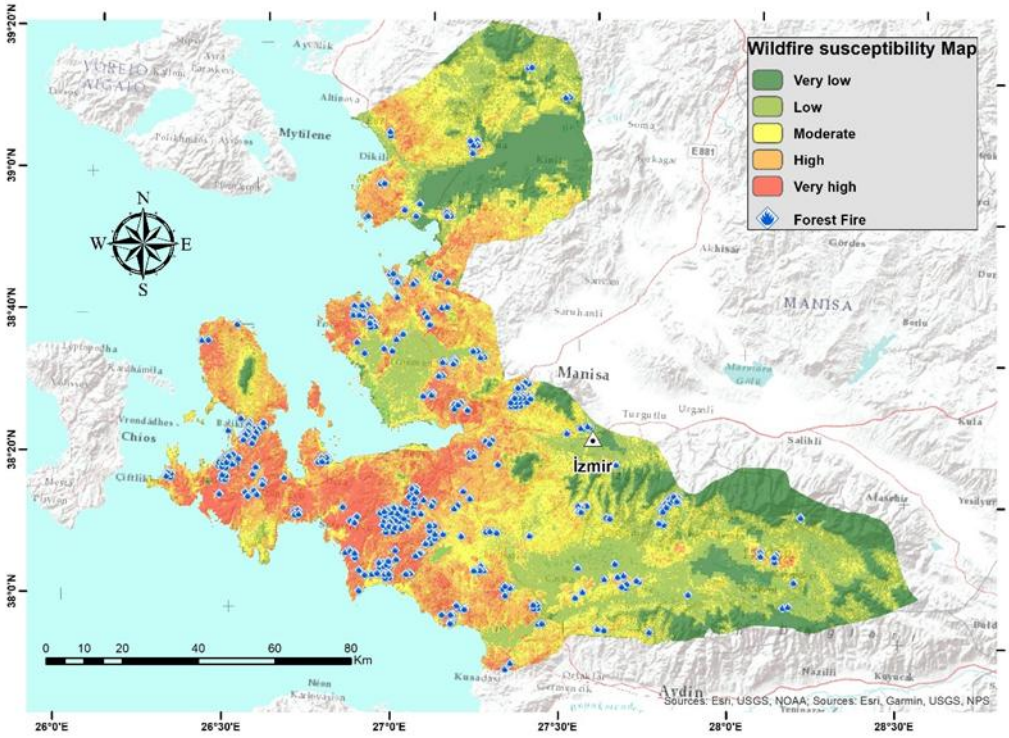

Figure 2. wildfire susceptibility map.

The The MaxEnt-based wildfire susceptibility map specifies that 16.30 % (1 991 km2) and 26.60 % (3 249 km2) of the study area have very high and high potential for wildfire, respectively. In comparison, nearly 22.18 % (2 709 km2), 21.36 % (2 609 km2) and 13.57 % (1 657 km2) of the region comes under moderate, low and very low potential classes, respectively (Figure 3).

In the wildfire susceptibility analysis with the maximum entropy method, 70% of the fire records were used in the analysis and 30% were evaluated as test data. Elevation, Slope, Aspect, Plan curvature, TWI, Distance from roads, Distance from settlements, Dis-tance from streams, Precipitation, Maximum temperature, Solar radiance, Wind speed, Land use/Land cover, NDVI parameters were used in fire susceptibility evaluations. Ac-cording to the analyzes made, it was determined that the importance levels of all parame-ters in the fire formation were high in the result susceptibility map.

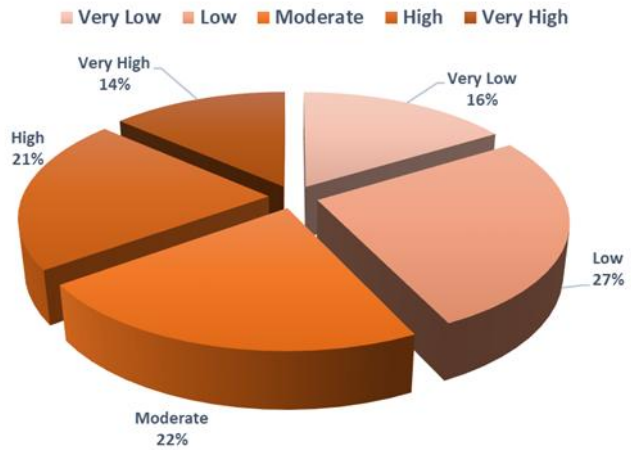

Figure 3. percentages of the different wildfire susceptibility classes.

The The accuracy analysis was performed using the receiver operating characteristic (ROC) curve for the wildfire model and an accuracy rate of 77% was obtained (Figure 4). The MaxEnt model's value is above 0.5, and the area under the ROC curve is close to 1. This score indicates that the wildfire susceptibility map developed in this study per-formed as acceptable and consistently.

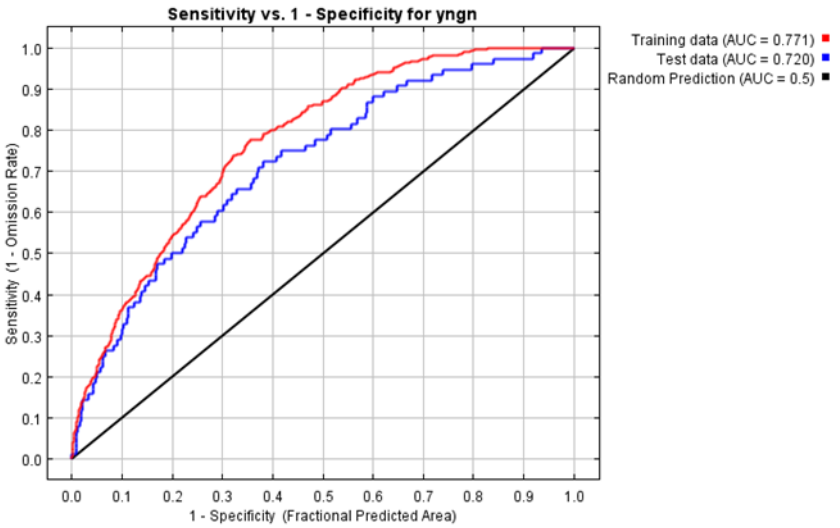

Figure 4. Percentages of the different wildfire susceptibility classes.

5. CONCLUSIONS

İzmir city has recently been plagued by catastrophic wildfires that have caused sig-nificant economic damages and put residents' safety in danger. In order to avoid, mitigate, and control wildfires, it is essential to determine their susceptibility to wildfires. Therefore, a wildfire susceptibility map showing potential wildfire areas of the study area was pro-duced using the MaxEnt method. It depends on the spatial distribution of fires in a region as well as the factors that predispose and cause fires. The regions in İzmir city where po-tential wildfire events would occur have been mapped using the fire locations experienced there so far, and a modeling research was conducted along with the variables assumed to have caused the fire. The findings of this study will probably give policymakers a better knowledge of wildfires in Aegean coast of Türkiye.

Author Contributions
Conceptualization, O.O. and S.T.; methodology, O.O., S.T. and C.K. ; validation, O.O. and S.T.; O.O., S.T. and C.K.; writing-review and editing, O.O. and S.T.

REFERENCES

Bustillo Sánchez, M.; Tonini, M.; Mapelli, A.; Fiorucci, P. Spatial assessment of wildfires susceptibility in Santa Cruz (Bolivia) using random forest. Geosciences, 2021, 11(5), 224.

Cao, Y.; Wang, M.; Liu, K. Wildfire susceptibility assessment in Southern China: A comparison of multiple methods. International Journal of Disaster Risk Science, 2017, 8(2), 164-181.

Elith, J.; H. Graham, C.; P. Anderson, R.; Dudík, M.; Ferrier, S.; Guisan, A.; ... & E. Zimmermann, N. (2006). Novel methods improve prediction of species' distributions from occurrence data. Ecography, 2006, 29(2), 129-151.

Fick, S.E.; Hijmans, R.J. WorldClim 2: new 1km spatial resolution climate surfaces for global land areas. International Journal of Climatology, 2017, 37 (12): 4302-4315.

Fischer, A. P.; Spies, T. A.; Steelman, T. A.; Moseley, C.; Johnson, B. R.; Bailey, J. D.; ... & Bowman, D. M. Wildfire risk as a socioecological pathology. Frontiers in Ecology and the Environment, 2016, 14(5), 276-284.

Hong, H.; Jaafari, A.; Zenner, E. K. Predicting spatial patterns of wildfire susceptibility in the Huichang County, China: An integrated model to analysis of landscape indicators. Ecological Indicators, 2019, 101, 878-891.

Jaafari, A.; Pourghasemi, H. R. Factors influencing regional-scale wildfire probability in Iran: an application of random forest and support vector machine. In Spatial modeling in GIS and R for Earth and environmental sciences, 2019, (pp. 607-619). Elsevier.

Jiménez-Valverde, A.; Lobo, J. M.; Hortal, J. Not as good as they seem: the importance of concepts in species distribution modelling. Diversity and distributions, 2008, 14(6), 885-890.

Nur, A. S.; Kim, Y. J.; Lee, C. W. Creation of Wildfire Susceptibility Maps in Plumas National Forest Using InSAR Coherence, Deep Learning, and Metaheuristic Optimization Approaches. Remote Sensing, 2022, 14(17), 4416.

OGM. 2022, Available online: https://www.ogm.gov.tr/tr/e-kutuphane/resmi-istatistikler (accessed on 26/09/2022)

Sabuncu, A.; Özener, H. Uzaktan algılama teknikleri ile yanmış alanların tespiti: İzmir Seferihisar orman yangını örneği. Doğal Afetler ve Çevre Dergisi, 2019, 5(2), 317-326.

Shmuel, A.; Heifetz, E. Global Wildfire Susceptibility Mapping Based on Machine Learning Models. Forests, 2022, 13(7), 1050.

Tonini, M.; D'Andrea, M.; Biondi, G.; Degli Esposti, S.; Trucchia, A.; Fiorucci, P. A machine learning-based approach for wildfire susceptibility mapping. The case study of the Liguria region in Italy. Geosciences, 2020, 10(3), 105.

Influence of 3D Printing Flow Rate on the Modal Characteristics of Railway Sleeper Prototypes

FERHAT ÇEÇEN*[1], MEHMET SALTAN[2]

Abstract: This study investigates the influence of extrusion flow rate on the modal characteristics of 3D-printed railway sleeper prototypes fabricated using fused deposition modeling (FDM). In FDM processes, flow rate refers to the volume of filament extruded per unit time, directly affecting material density, internal void ratio, and interlayer bonding quality. Variations in flow rate can significantly modify the specimen's unit weight, porosity, modal mass, mechanical strength, and consequently its elastic and shear moduli. To explore these effects, semi-functional miniature sleeper models were fabricated at different flow rate settings (0.926, 0.960, and 1.050), while maintaining constant printing parameters such as 0.08 mm layer height, 0.42 mm layer width, aligned seam positioning, 0.0006 mm resolution, two perimeter walls, and monotonic surface and infill patterns. As a case study, a miniature model of a B70-type railway sleeper—a widely used prestressed concrete sleeper model across the railways of Europe, Türkiye, and other countries—was utilized. Modal impact testing was conducted to obtain frequency response functions (FRFs), from which resonance frequencies and damping ratios were identified using the Least Squares Complex Frequency (LSCF) algorithm, Complex Mode Indicator Function (CMIF) plots, and Auto Modal Assurance Criterion (AutoMAC) correlations. Results reveal that flow rate has a notable influence on dynamic behavior: resonance frequencies generally increase with modal mass, while damping ratios tend to be lower near the optimal flow rate and higher at both lower and higher flow settings. These findings underline the necessity of precise flow rate control for achieving geometrically accurate and dynamically stable prototypes, thereby promoting sustainable prototyping practices through reduced material waste and enhanced experimental reliability and sustainability.

Keywords: 3D Printing, Fused Deposition Modeling, Railway Sleeper Prototype, Modal Testing, Flow Rate Optimization.

[1]**Address:** Suleyman Demirel University, Göller Bölgesi Teknokent Coordinatorship, Isparta/Türkiye
[2]**Address:** Suleyman Demirel University, Faculty of Engineering and Natural Sciences, Civil Engineering Department, Isparta/Türkiye

***Corresponding author**: cecenferhat@sdu.edu.tr

1. INTRODUCTION

The adoption of additive manufacturing (AM) techniques, particularly fused deposition modeling (FDM), has revolutionized the fabrication of complex geometries across multiple engineering sectors (Gardan, 2016; Mohamed et al., 2015). In railway and other engineering fields, 3D printing facilitates the rapid prototyping of structural components, enabling cost-effective design iterations and experimental validations. However, the mechanical and dynamic properties of FDM-printed parts are highly sensitive to printing parameters, necessitating a comprehensive understanding of how these parameters influence structural performance.

Extensive research has investigated the influence of FDM process parameters such as layer thickness, infill density, and print orientation on the mechanical properties of printed parts (Ahn et al., 2002; Domingo-Espin et al., 2015). Experimental modal analysis (EMA) has also revealed that printing conditions can alter the dynamic behavior, including natural frequencies and damping characteristics of additively manufactured polymers (Nguyen et al., 2022). In railway-related applications, 3D printing technologies have mainly been utilized for geometric replication and surface treatments, and their use remains largely at the exploratory stage (Fu and Kaewunruen, 2022). Although additive manufacturing offers considerable potential, systematic investigation into the dynamic mechanical characterization of semi-functional 3D-printed railway components remains limited.

Among the various FDM parameters, extrusion flow rate (also referred to as the extrusion multiplier) — which defines the volume of filament extruded per unit time — plays a critical role in determining density, porosity, and interlayer bonding (Gajjar et al., 2025). While many slicer programs default to a flow rate near 1.0 (100%), factory-calibrated settings can vary significantly depending on the printer model, with initial flow rates as low as 0.92 commonly observed; practical tuning typically ranges between 0.90 (90%) and 1.10 (110%) (All3DP, 2024). Maintaining a sufficiently low extrusion flow rate is important not only for material efficiency but also to mitigate thermal expansion and contraction effects during FDM printing. In thermoplastics such as PLA and ABS, the filament undergoes significant thermal expansion upon extrusion and contracts during cooling; deviations from optimal flow settings — particularly excessive flow rates — can lead to material overaccumulation, internal stresses, and dimensional instability, whereas insufficient flow rates can exacerbate interlayer voids and mechanical weakness (Wevolver, 2024). Although the impact of extrusion

flow rate on static properties is relatively well understood, its effect on dynamic characteristics — particularly modal behavior — has yet to be systematically explored.

This study aims to investigate the influence of extrusion flow rate on the modal characteristics of 3D-printed railway sleeper prototypes produced using FDM. A miniature model of a B70-type prestressed concrete sleeper was fabricated under three different flow rate settings, while maintaining other printing parameters constant. Through modal impact testing, frequency response functions (FRFs) were obtained and used to identify resonance frequencies and damping ratios. The findings are expected to provide valuable insights into optimizing FDM process settings for reliable and dynamically stable prototypes in railway and broader engineering applications.

2. MATERIAL AND METHOD

2.1. Specimen fabrication via 3D printing

Three-dimensional (3D) printing in this study was performed using a Creality K1C 3D printer operated through Creality Print V.6.0 software. The filament material was CR-ABS with a diameter of 1.75 mm. Printing parameters were carefully selected, utilizing a 0.4 mm nozzle with a nozzle temperature set at 260 °C, while the build chamber temperature was maintained at a maximum of 60 °C. Cooling was disabled for the first three layers to enhance adhesion. Retraction settings were configured with a retraction distance of 2.5 mm and a Z-hop height of 0.4 mm during retraction movements. The initial layer height was set to 0.2 mm to promote better adhesion to the build plate, followed by a layer height of 0.08 mm for subsequent layers. All printing parameters, except for the extrusion flow rate, were kept constant across all specimens. These parameters included a 0.42 mm layer width, aligned seam positioning, a resolution of 0.0006 mm, two perimeter walls, and monotonic patterns for both the surface and infill. Three different flow rate values (0.926, 0.960, and 1.050) were employed to investigate the influence of material deposition rates on printing performance. The flow rate of 0.926 corresponds to the default setting provided by Creality Print software for CR-ABS, representing the lowest flow rate capable of achieving stable prints without inducing under-extrusion, thus promoting filament economy. Conversely, the flow rate of 1.050 was identified through preliminary trials as the highest feasible setting that could be used without damaging the nozzle. The intermediate flow rate of 0.960 was selected based on macro photography analysis, which revealed optimal contact between deposited layers during the printing process (prior to cooling), minimizing interlayer voids while avoiding the formation of positive texture that could lead to nozzle collisions with previously deposited layers. Although slightly higher flow rates such as 0.980 could potentially reduce voids after cooling, they were observed to promote positive texture formation during printing, increasing the risk of nozzle interference. Given that railway superstructures are predominantly subjected to dynamic loads, sleepers are among the most critical components influencing track performance. To represent such conditions accurately and meaningfully in this study, a sleeper model was selected as the test geometry. Specifically, the B70-type prestressed concrete sleeper, which is widely used in Türkiye, Europe, and many other regions worldwide, was chosen due to its characteristic geometric details that facilitate the observation of flow rate-induced effects on printed structures. The slicing of the B70-type sleeper geometry in Creality Print software and selected perspective views of certain layers are presented in Figure 1. The printed B70-type sleeper specimens are shown in Figure 2. Additionally, macro-scale views illustrating the layer structure and interlayer void variations across different flow rates are presented in Figure 3.

After fabrication, the miniature models were weighed using a precision scale, with the measurements for flow rates of 0.926, 0.960, and 1.050 presented from left to right in Figure 4. The specimens were produced by scaling down actual B70-type railway sleepers at a ratio of 7.5:100 (i.e., 1:13.33), resulting in a model length of 195 mm compared to the original 2600 mm. The average recorded weights for each flow rate were 46.2 g, 48.6 g, and 51.1 g, respectively. Based on the fixed specimen volume of 48,480 mm³, the corresponding unit weights were calculated as approximately 0.953 g/cm³, 1.003 g/cm³, and 1.054 g/cm³ for the 0.926, 0.960, and 1.050 flow rates, respectively. Figure 5 presents a comparison between these measured unit weights and the nominal unit weight of 1.050 g/cm³ for the CR-ABS filament used in this study, as specified by the manufacturer (Creality, 2023). The unit weight measured at a flow rate of 0.926 is slightly below the nominal material value; however, this setting corresponds to the default value defined by Creality Print software for CR-ABS and represents the lowest flow rate that still ensures stable prints without signs of under-extrusion. In contrast, the sample produced at a flow rate of 1.050 shows a more pronounced increase, suggestive of potential over-extrusion. While it may seem counterintuitive for the calculated unit weight (1.054 g/cm³) to exceed the nominal material density (1.050 g/cm³), this apparent increase is likely due to surface bulging and material overflow, which slightly expands the specimen beyond its intended volume. As the weight increases while the nominal volume remains fixed for calculation, the resulting unit weight appears artificially elevated. Consequently, the unit weight at 0.960 remains the closest to the nominal CR-ABS value.

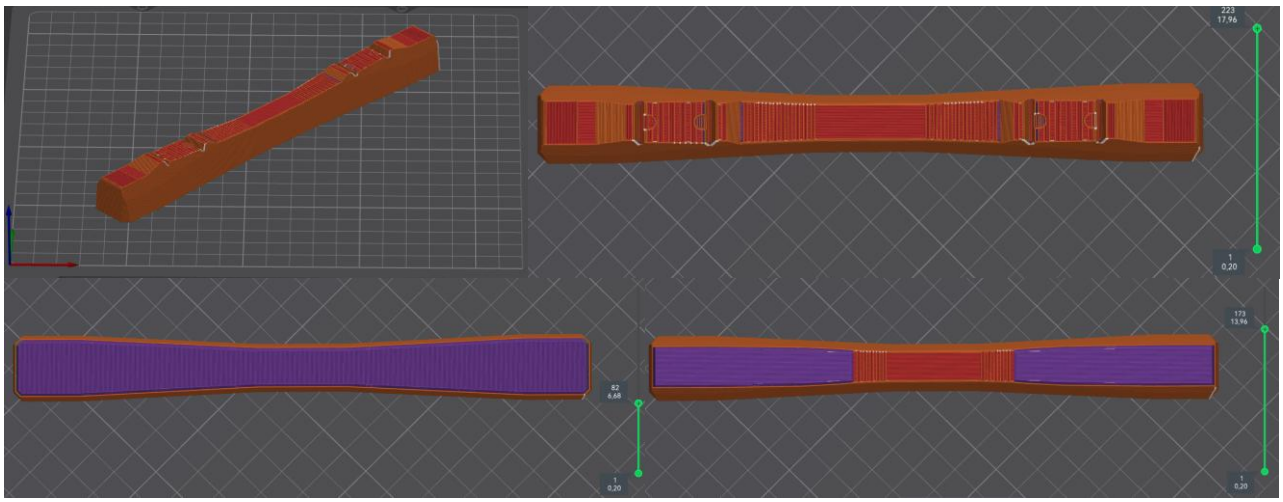

Figure 1. Slicing visualization and sliced perspectives of selected layers for the B70-type sleeper geometry generated in Creality Print 6.0.

Figure 2. Miniature 3D-printed B70-type railway sleeper models fabricated at different flow rates (from top to bottom: 1.050, 0.960, and 0.926)

Figure 3. Zoomed-in views of the miniature 3D-printed B70-type railway sleeper models (flow rates from top to bottom: 1.050, 0.960, and 0.926)

Figure 4. Miniature B70-type sleeper models being weighed on a precision scale, showing weight readings for flow rates of 0.926, 0.960, and 1.050 (left to right)

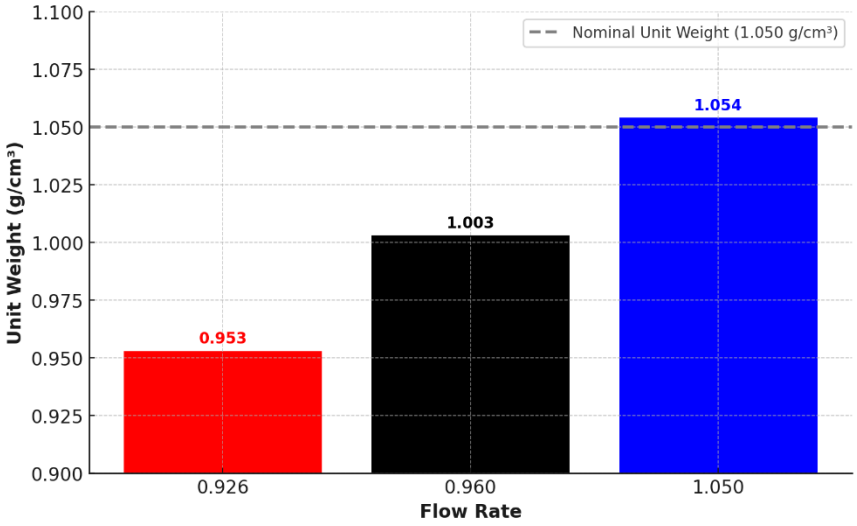

Figure 5. Comparison of measured unit weights at different extrusion flow rates with the nominal unit weight of solid CR-ABS filament.

2.2. Modal testing configuration and data processing

Modal testing was conducted using a Dytran 5800 SL miniature modal hammer and an MMF KS95C100 miniature accelerometer, as illustrated in Figure 6. The Dytran hammer was equipped with a 9.8 g head and a 2.54 mm diameter tip, and was capable of measuring impact forces up to 200 N. The accelerometer featured a mass of 3.2 g, a noise density of 1 µg/Hz^0.5 at 1 kHz, and a dynamic measurement range of ±60 g over a frequency bandwidth from 1 Hz to 18 kHz, with an accuracy better than 5%. Data acquisition was performed using a Dewesoft Sirius Mini DAQ system, while test execution and subsequent analysis were carried out through Dewesoft X software utilizing the dedicated Modal Test and Modal Analysis modules. To simulate free-free boundary conditions, specimens were suspended on soft elastic cords. Each specimen was marked with 19 degrees of freedom (DOFs). One DOF was allocated for accelerometer attachment, while the remaining points were designated for vertical axis impact excitations. Acceleration responses (m/s²) were normalized by the applied impact forces (N) to compute Frequency Response Functions (FRFs), expressed in m/s²/N. The accelerometer was mounted using a thin layer of softened beeswax to minimize mass loading and preserve high-frequency response. Testing was configured in a Single Input Single Output (SISO) scheme. A 6 kHz sampling frequency was selected based on preliminary evaluations to fully capture the relevant frequency content of interest. Using the roving hammer method, a total of 90 FRF measurements were obtained for each specimen. The collected FRFs were synthesized using the peak-to-peak method and subsequently analyzed with the Least Squares Complex Frequency-domain (LSCF) fitting algorithm. Stabilization diagrams were generated using up to 11 polynomial orders within the 0–2 kHz frequency band. Polar points were identified under stringent selection criteria, allowing a maximum frequency error of 0.1% and a maximum damping ratio error of 1%.

Figure 6. Experimental modal testing setup

3. RESULTS AND DISCUSSION

After the modal tests, stabilization diagrams corresponding to the specimens fabricated at flow rates of 0.926, 0.960, and 1.050 are presented in Figures 7–9, respectively. In these diagrams, stabilized poles are shown as green circles, and non-stabilized poles as red crosses. Resonance frequencies were visually correlated with peaks in the Complex Mode Indicator Function (CMIF) curves, which are overlaid on the diagrams. The left-hand plots display the distribution of resonance magnitudes with respect to the modal order, while the right-hand plots show the distribution of damping ratios and magnitudes independent of order. In all three specimens, the first resonance frequencies and damping ratios appear well-aligned and tightly clustered, indicating that the applied modal testing and analysis method is both accurate and representative. Subsequent resonance modes were excluded from the analysis due to the lower accuracy observed at higher frequencies.

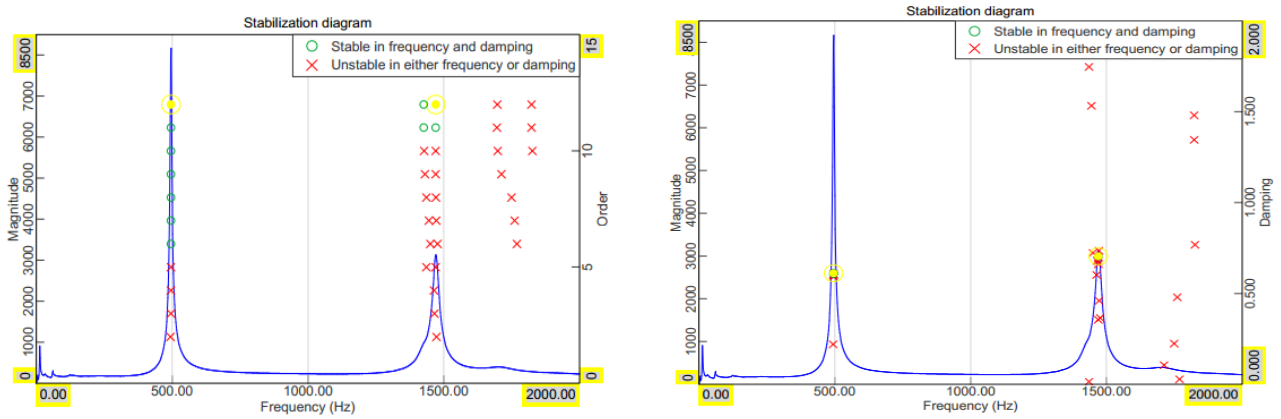

Figure 7. Stabilization diagrams of the B70-type miniature prototype fabricated at a 0.926 flow rate (left: order-based diagram; right: damping ratio-based diagram).

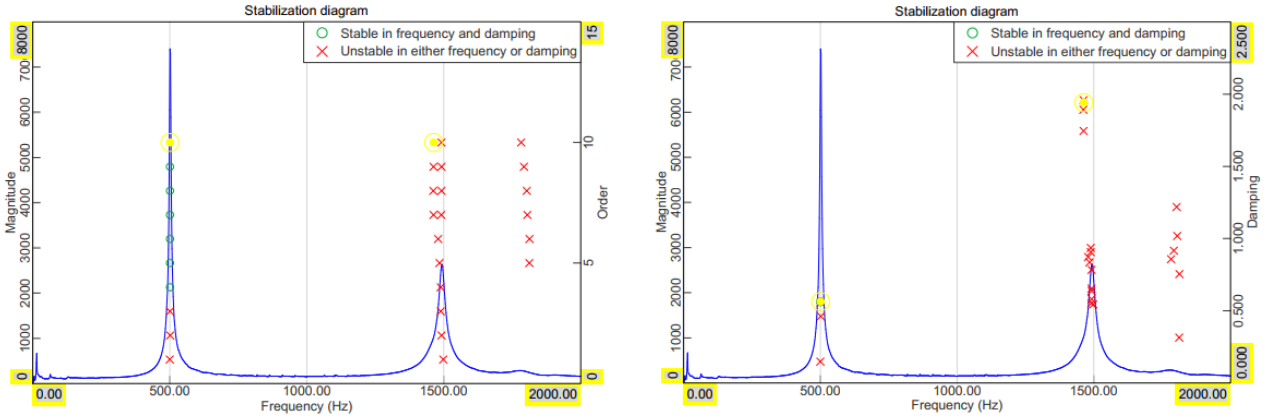

Figure 8. Stabilization diagrams of the B70-type miniature prototype fabricated at a 0.960 flow rate (left: order-based diagram; right: damping ratio-based diagram)

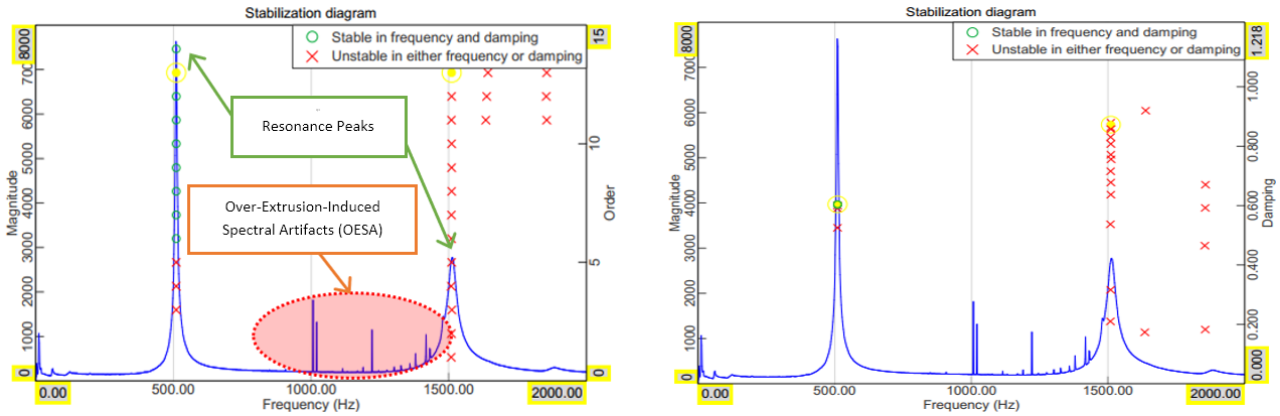

Figure 9. Stabilization diagrams of the B70-type miniature prototype fabricated at a 1.050 flow rate (left: order-based diagram; right: damping ratio-based diagram)

Figure 10 presents the Auto Modal Assurance Criterion (AutoMAC) matrices for the specimens fabricated at flow rates of 0.926, 0.960, and 1.050, shown from left to right, respectively. The AutoMAC analysis clearly confirms the separation between the first and second vertical resonance modes, as indicated by distinct red diagonals aligned with the selected stabilized poles.

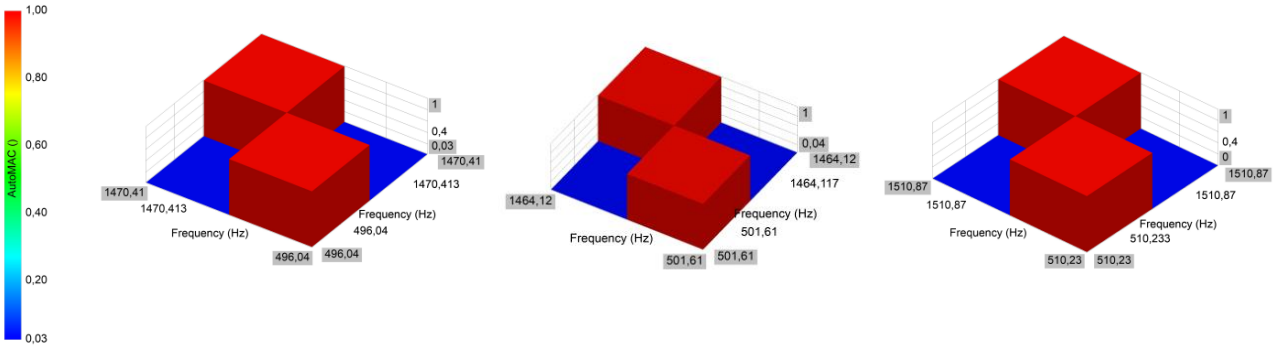

Figure 10. Representative AutoMAC correlation diagrams for the B70-type miniature prototypes, presented from left to right for specimens fabricated at flow rates of 0.926, 0.960, and 1.050, respectively

Additionally, Figure 11 provides a comparative plot where the CMIF curves obtained from the specimens at all three flow rates are superimposed on a single graph. This comparative visualization enables the evaluation of peak frequency shifts and magnitude changes among the different prototypes. The key findings derived from the fabrication, testing, and analysis stages are summarized in Table 1, which includes the average values of the first resonance frequency (Hz), the first mode damping ratio (ζ, %), and the CMIF peak magnitude (m/s²/N). Furthermore, Figure 12 was generated to visualize these summarized values graphically, providing a clearer understanding of how modal characteristics evolve as a function of flow rate.

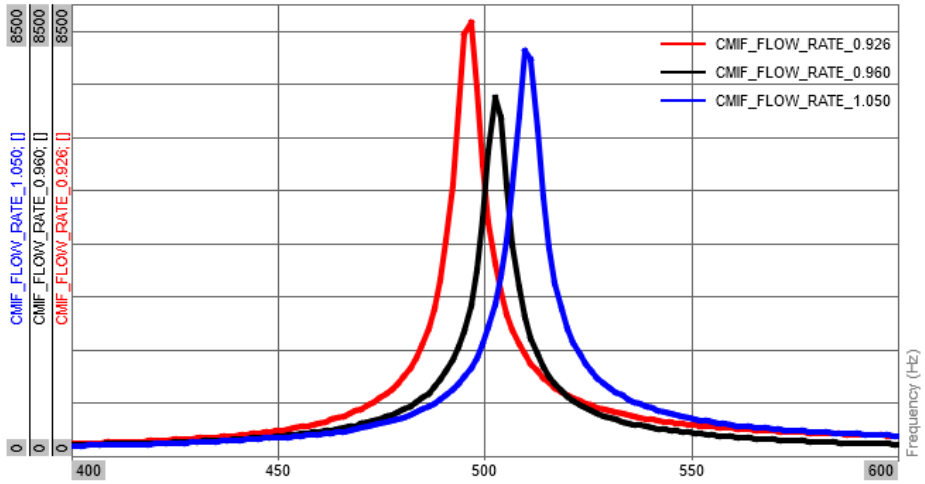

Figure 11. Comparison of CMIF curves for the miniature prototypes within the 400–600 Hz frequency bandwidth

Table 1. Modal analysis findings of B70-type miniature prototypes fabricated at different flow rates

3D-Printing Extrusion Flow Rate	Average 1st Resonance Frequency (Hz)	Average 1st Resonance Damping Ratio (ζ%)	Average CMIF Magnitude ($m/s^2/N$)
0.926	496.04	0.612	8,164
0.960	502.51	0.582	6,740
1.050	510.23	0.605	7,629

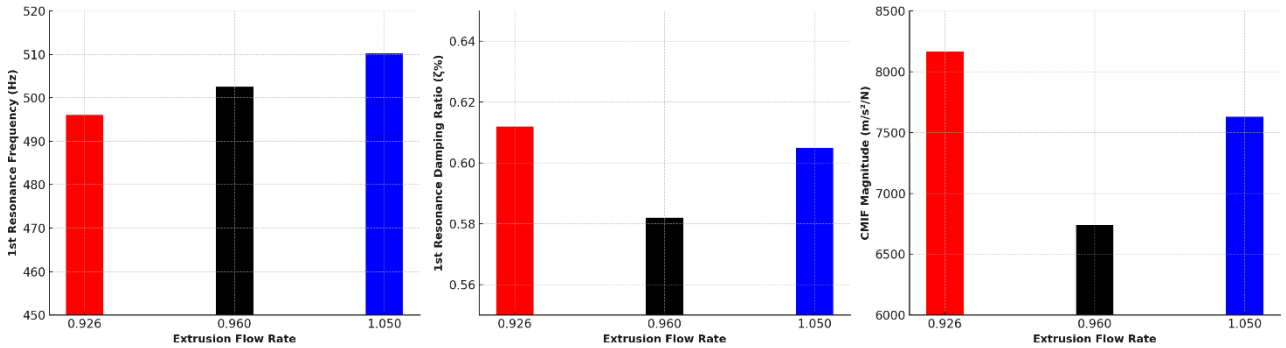

Figure 12. Variation of the first resonance frequency, damping ratio, and CMIF peak magnitude of B70-type miniature prototypes as a function of extrusion flow rate

As observed in Figure 12, The first resonance frequency increased by approximately 2.9%, from 496.04 Hz at 0.926 flow rate to 510.23 Hz at 1.050, demonstrating a relatively linear correlation with increasing flow rate. This behavior is consistent with established empirical relationships, whereby an increase in unit weight primarily contributes to higher modal mass and may also be associated with increased structural stiffness—both of which can lead to elevated resonance frequencies, as reported in classical material studies (Çeçen et al., 2023). Correspondingly, the unit weights of the specimens were calculated as approximately 0.953 g/cm³, 1.003 g/cm³, and 1.054 g/cm³ for the flow rates of 0.926, 0.960, and 1.050, respectively. As a result, the CMIF peaks systematically shift toward higher frequencies with increasing flow rate.

Another significant observation concerns the damping ratio. Unlike the resonance frequency, the damping ratio exhibits a non-monotonic trend: it initially decreases with increasing flow rate, reaches a minimum at the intermediate value of 0.960, and then increases again at the highest flow rate. The initial decrease in this trend reflects the influence of filament deposition quality on the formation of internal microstructures. As the flow rate increases, the spacing between adjacent filament tracks within each layer decreases, improving inter-track fusion and reducing intra-layer air void content. This enhanced material continuity contributes to lower damping due to fewer internal discontinuities. However, at the highest flow rate of 1.050, over-extrusion effects such as filament overflow, surface bulging, and irregular bead formation can introduce local inconsistencies, increasing the effective damping ratio. Additionally, excess material accumulation may cause the nozzle to intermittently interfere with previously deposited and partially solidified layers. This mechanical dragging effect can lead to localized surface disruption, residual interfacial stress accumulation, and geometric imperfections—factors that collectively contribute to elevated damping ratio.

The evolution of CMIF peak magnitudes further enhances the understanding of the system's dynamic behavior. As shown in the final column of Table 1 and the rightmost plot in Figure 12, CMIF peak magnitudes initially decrease with increasing flow rate, reaching a minimum at 0.960, and then increase again at 1.050—a trend that generally parallels that of the damping ratio. The initial decrease in this trend can be attributed to increased modal mass and improved material continuity, both of which suppress the amplitude of the system's acceleration response under constant excitation—consistent with classical vibration theory. However, the behavior of the 0.960 specimen compared to the 1.050 specimen is particularly noteworthy. Despite having the lowest damping ratio and a lower modal mass compared to the 1.050 specimen, it exhibits the lowest CMIF peak magnitude overall. Given that all specimens share nearly identical geometry, sensor placement, and excitation direction, this counterintuitive result cannot be explained by variations in modal projection. Instead, it is likely that specific microstructural factors—such as optimal inter-track fusion and minimal porosity—redistributed the dynamic response in a way that reduced observable peak amplitude.

Additionally, the CMIF curve of the 1.050 specimen (Figure 9) exhibits not only a broader main resonance but also minor off-resonance peaks. These features are not attributed to the noise measurement or external disturbances but are more plausibly explained as over-extrusion-induced spectral artifacts (OESA), stemming from microstructural irregularities in filament deposition. Such non-uniformities may give rise to local resonant effects, caused by localized stiffness variations and geometric asymmetries introduced during printing. These findings underscore the complex interplay between process parameters and dynamic response in layered, additively manufactured components.

4. CONCLUSIONS

This study investigated the influence of extrusion flow rate on the modal characteristics of 3D-printed B70-type miniature railway sleeper prototypes manufactured via fused deposition modeling (FDM). Understanding the relationship between flow rate and dynamic behavior is essential for optimizing the mechanical performance of printed structural components, particularly in applications subjected to dynamic loading conditions such as railway systems. To this end, experimental modal testing and detailed analyses were performed on specimens fabricated at three different flow rate settings: 0.926, 0.960, and 1.050. Based on the experimental findings, the key conclusions are summarized as follows:

a. Resonance frequencies increased almost linearly with extrusion flow rate, rising progressively across the tested values of 0.926, 0.960, and 1.050, primarily due to increased unit weight, which in turn contributes to higher modal mass.
b. The damping ratio exhibited a non-monotonic trend across the flow rates, decreasing to a minimum at 0.960 as a result of improved inter-track fusion and reduced intra-layer air voids, and increasing again at 1.050 due to over-extrusion-related effects—such as surface bulging, filament irregularities, and nozzle interference with previously deposited layers—that introduced local microstructural inconsistencies and thereby led to increased energy dissipation.
c. CMIF peak magnitudes also followed a non-monotonic trend, decreasing to a minimum at 0.960 due to increased modal mass and improved material continuity, then increasing again at 1.050 in line with the observed increase in damping behavior.
d. Despite having lower damping and modal mass than the 1.050 specimen, the 0.960 specimen exhibited the lowest CMIF peak magnitude overall. Furthermore, the CMIF curve of the 1.050 specimen exhibited additional minor off-resonance peaks, attributed to over-extrusion-induced spectral artifacts (OESA) caused by filament deposition irregularities. These non-uniformities may have introduced local resonant effects through stiffness variations and geometric asymmetries, reflecting the complex interaction between process parameters and dynamic response in layered printed components.
e. Among the evaluated modal parameters, the damping ratio and CMIF curve characteristics—specifically peak magnitude and the presence or absence of OESA—emerged as the most sensitive and reliable indicators of extrusion flow rate. While resonance frequency showed a near-linear trend, the 0.960 flow rate yielded both the lowest damping ratio and CMIF peak magnitude. Notably, no observable OESA was present at this setting, indicating an optimal balance between under- and over-extrusion regimes for modal-quality specimen production.
f. Overall, these findings confirm that the extrusion flow rate significantly influences the dynamic performance of 3D-printed components by altering modal mass, stiffness, damping behavior, and internal microstructural uniformity. Among the tested settings, a flow rate of 0.960 yielded the most favorable results, reinforcing its suitability as a reference point for producing consistent and modal-quality specimens.

The experimental and analytical framework developed in this study provides a non-destructive, rapid, economical, and sufficiently accurate approach for evaluating and optimizing flow rate parameters in FDM-based structural prototyping. However, as with any initial case study, certain limitations should be acknowledged. This work was conducted using a single printer model (Creality K1C) and a specific filament type (CR-ABS). Variations in printer hardware, filament properties, nozzle geometry, extrusion temperature, layer height, ambient conditions, etc., may all affect the outcomes. Therefore, further studies are encouraged to validate and expand the proposed methodology across a wider range of printing conditions to enhance its general applicability.

Acknowledgements
This study was supported by the Scientific and Technological Research Council of Turkey (TÜBİTAK) under project number 1005/124M258, and the authors would like to express their gratitude for this support.

Ethics Committee Approval
N/A

Peer-review
Externally peer-reviewed.

Author Contributions
Conceptualization: F.Ç.; Investigation: F.Ç.; Material and Methodology: F.Ç., M.S.; Supervision: M.S.; Visualization: F.Ç.; Writing-Original Draft: F.Ç.; Writing-review & Editing: F.Ç., M.S.; Other: All authors have read and agreed to the published version of the manuscript.

Conflict of Interest
The authors have no conflicts of interest to declare.

Funding
This study was supported by the Scientific and Technological Research Council of Turkey (TÜBİTAK) under project number 1005/124M258.

REFERENCES

Ahn, S.-H., Montero, M., Odell, D., Roundy, S., Wright, P.K. (2002). Anisotropic material properties of fused deposition modeling ABS. Rapid Prototyping Journal. 8, 248–257. https://doi.org/10.1108/13552540210441166

All3DP, (2024). Cura extrusion multiplier: How to improve your prints. https://all3dp.com/2/extrusion-multiplier-cura-ways-to-improve-your-prints/ (accessed 29 April 2025).

Creality. (2023). What is ABS 3D printing filament? Creality Official Blog. https://store.creality.com/blogs/all/what-is-abs-3d-printing-filament

Çeçen, F., Özbayrak, A., & Aktaş, B. (2023). Experimental modal analysis of fly ash-based geopolymer concrete specimens via modal circles, mode indication functions, and mode shape animations. Cement and Concrete Composites, 137, 104951. https://doi.org/10.1016/j.cemconcomp.2023.104951

Domingo-Espin, M., Puigoriol-Forcada, J.M., Garcia-Granada, A.A., Llumà, J., Borros, S., Reyes, G. (2015). Mechanical property characterization and simulation of fused deposition modeling Polycarbonate parts. Materials & Design. 83, 670–677. https://doi.org/10.1016/j.matdes.2015.06.074

Fu, H., & Kaewunruen, S. (2022). State-of-the-Art Review on Additive Manufacturing Technology in Railway Infrastructure Systems. Journal of Composites Science, 6(1), 7. https://doi.org/10.3390/jcs6010007

Gajjar, T., Yang, R., Ye, L. et al. (2025). Effects of key process parameters on tensile properties and interlayer bonding behavior of 3D printed PLA using fused filament fabrication. Prog Addit Manuf. 10, 1261–1280. https://doi.org/10.1007/s40964-024-00704-y

Gardan, J. (2016). Additive manufacturing technologies: State of the art and trends. International Journal of Production Research. 54, 3118–3132. https://doi.org/10.1080/00207543.2015.1115909

Mohamed, O.A., Masood, S.H., Bhowmik, J.L. (2015). Optimization of fused deposition modeling process parameters: A review of current research and future prospects. Advances in Manufacturing. 3, 42–53. https://doi.org/10.1007/s40436-014-0097-7

Nguyen, H. T., Crittenden, K., Weiss, L., & Bardaweel, H. (2022). Experimental modal analysis and characterization of additively manufactured polymers. Polymers, 14(10), 2071. https://doi.org/10.3390/polym14102071

Wevolver, (2024). How to fix under extrusion: Maintenance and print settings. https://www.wevolver.com/article/under-extrusion (accessed 29 April 2025).

Long-Term Strength Development of Mortars Containing Rice Husk Ash

EREN GÖDEK*[1], SERHAT OĞUZHAN KIVRAK[1], JULİDE ERKAL KIVRAK[1]

Abstract: The incorporation of rice husk ash (RHA) into mortars as a supplementary binding material is common due to its potential to enhance the strength and durability properties. Studies have shown that RHA blended mortars exhibit increased compressive strength after a standard curing period of 28 days. In this experimental study, a reference mortar and several cement mortars were prepared substituting RHA with cement at the rates of 5, 10, 15, 20, and 25% by weight of cement. 6 prismatic specimens of 40x40x160 mm^3 were taken from each replacement ratio. Half of the specimens were cured in water for 28 days, while the other half was subjected to an extended water curing period of 720 days. Flexural and compressive strength tests were performed on the specimens at stated curing periods. Results showed that an extended curing period greatly enhanced the flexural strength and compressive strength up to 388% and 253%, respectively. Although the replacement of cement with RHA negatively affected the strengths at 28 days, it was observed that this effect completely disappeared in the long term (720 days), and higher mechanical performance was obtained compared to the reference mortar. These findings suggest that mortars containing RHA have the potential to be used instead of traditional mortars, contingent upon the acceleration of RHA reactivity.

Keywords: Rice Husk Ash, Long-Term, Strength, Flexural, Compressive

[1]**Address:** Hitit University, Vocational School of Technical Sciences, Department of Construction, Çorum/Türkiye

***Corresponding author**: erengodek@hitit.edu.tr

1. INTRODUCTION

The use of rice husk ash (RHA) as a pozzolanic material has been extensively researched due to its potential to enhance strength and durability properties of cement based materials with reduced environmental effects. Rice husk ashes with desired high amorphous silica content can be obtained with the incineration of rice husk under controlled heating and duration. The use of RHA in cement-based materials can prolong the strength development due to late pozzolanic reactions with $Ca(OH)_2$ beyond the standard curing duration of 28 days (Ganesan et al., 2008).

Marthong (2012) investigated the effect of RHA replacement ratio on the concrete properties prepared with three different grades of cements up to 90 days. Test results indicate that RHA incorporating concretes can attain the same order of strength as reference concrete at longer curing periods. Barua et al. (2018) prepared concretes replacing cement with RHA and investigated their compressive strengths between 7 and 90 days. They reported that increasing the RHA replacement ratio decreased the compressive strength and optimal use of RHA is declared as 0-15%. Additionally, all compressive strengths were obtained below the compressive strength of reference concrete for all curing periods. In a similar research by Rasoul et al. (2018) showed that substituting RHA with cement at 20% performed higher compressive strength at 28 days and all RHA blended specimens up to 40% exhibited higher compressive strength at 90 days. Madandoust et al. (2011) investigated the mechanical properties of RHA concrete up to 360 days. They concluded that RHA filled up the pores with ongoing pozzolanic reactions over time which resulted higher compressive strength compared to reference concrete at 270 and 360 days. Thiedeitz et al. (2022) compared the compressive strength of RHA and fly ash blended mortars (25% by weight of cement) up to 90 days and RHA blended mortars exhibited higher compressive strength between 7 and 90 days. Additionally, RHA blended mortars performed higher compressive strength than reference mortar (including only cement) prepared with lower water to binder ratio. Another study investigated the effect of curing conditions (air and water) on the properties of RHA containing concrete cubes at different curing ages (Abalaka and Okoli, 2013). This study declared that the air-cured specimens incorporating RHA exhibited greater compressive strength reductions at 90 days compared to control specimens without RHA; however, RHA specimens demonstrated compressive strength gains exceeding the control only when subjected to water curing. A comprehensive study by Ettu et al. (2013) investigated the RHA replacement ratio (from 0 to 20%) and prolonged curing (from 7 to 210 days) combinations with 165 concrete cube. This study reported that the initially lower compressive strength of RHA replaced cement composites during early curing (up to 14 days) was subsequently surpassed by sustained pozzolanic activity between 28 and 210 days, resulting in comparable or even greater strength than the control samples at later ages. They also inferred that the compressive strengths can be increased due to the possible ongoing pozzolanic activity at later curing periods.

In the existing literature, the positive effects of RHA have been demonstrated at 28-day curing periods, generally. Besides, the mechanical performance observations for 60 and 90 days were found to be remained limited. This lack of long-term data increases uncertainties regarding the reliable use of RHA in practical applications. The aim of this study is to

systematically investigate the long-term (720-day) mechanical performance of mortar mixtures containing RHA at various replacement levels.

2. MATERIAL AND METHOD

In this study, reference mortar was prepared using CEM I 42.5R type cement, standard sand and water with a cement-to-sand-to-water ratio of 1:3:0.6 by weight. Subsequently, cement was partially replaced with RHA at substitution levels of 5%, 10%, 15%, 20%, and 25% by weight. The physical and chemical characteristics of RHA, previously determined in the authors' earlier investigations, are presented in Figure 1 and Table 1 (Kıvrak et al., 2019).

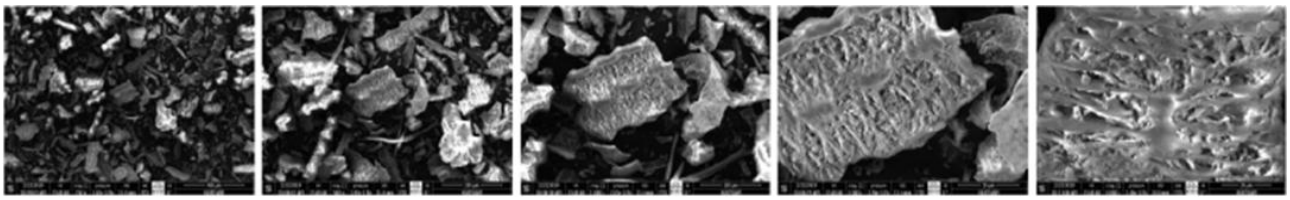

x250 x500 x1000 x2000 x4000

Figure 1. SEM images of RHA at different magnifications (Kıvrak et al., 2019)

Table 1. Chemical and physical properties of RHA (Kıvrak et al., 2019)

Basic Oxides (%)	
SiO_2	85.82
Al_2O_3	0.35
Fe_2O_3	3.40
CaO	2.37
MgO	0.33
SO_3	0.58
Na_2O	0.17
K_2O	6.33
Physical Properties	
Density (gr/cm^3)	1.51
Residue on 75 µm sieve	<0.1

All mixing procedures and mechanical tests adhered to the guidelines specified in the TS EN 196-1 (2016) standard. 6 prismatic specimens of 40x40x160 mm^3 were taken from each replacement ratio. One day after casting, specimens demolded and half of the specimens were cured in water for 28 days, while the other half was subjected to an extended water curing period of 720 days. Mechanical properties were investigated under flexural and compression tests. The flexural tests were performed with a support span of 130 mm under three-point flexural loading (Figure 2a). Compressive strengths were determined using the broken parts of 40x40x160 mm^3 test specimens following ASTM C349-18 (2018) standard (Figure 2b). During the flexural and compression tests, the load at the break is determined, and related strengths were calculated following the TS EN 196-1 (2016) standard.

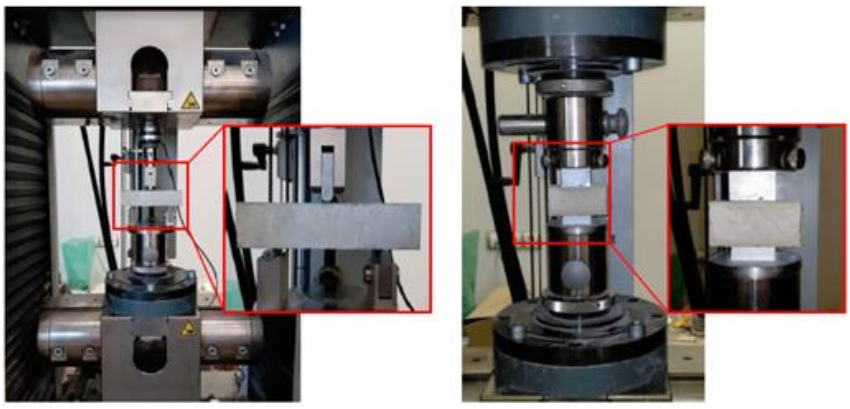

(a) (b)

Figure 2. a) Three-point flexural test setup, b) Compressive test setup

3. RESULTS

The flexural strengths of all mortars calculated at 28 and 720 days are presented in Figure 3. In the case of flexural strengths, reference mortar exhibited higher flexural strength than the RHA-substituted mortars at the age of 28 days. Besides, increasing the RHA substitution ratio gradually decreased the flexural strengths. The flexural strengths decreased by 17.35% to 25.43% depending on the RHA substitution ratio between 5% and 15%. This reduction increased up to 64.71% when the substitution ratio increased to 25%. On the other hand, when the curing age is 720 days, RHA-substituted specimens performed higher flexural strengths than the reference mortar, except in the case of 25% RHA. Incorporation of RHA into the mortar increased the flexural strengths by 11.92%-13.22%, depending on the substitution ratio up to 20%.

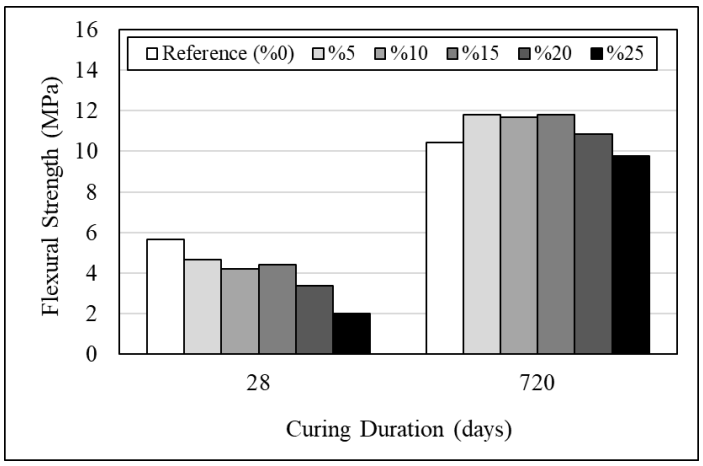

Figure 3. Flexural strengths of specimens considering both RHA substitution ratio and the curing duration.

The compressive strength data obtained are shown in Figure 4. At 28 days, the compressive strength of reference mortar was calculated as 34.9 MPa on average. The RHA incorporating specimens exhibited lower compressive strengths than the reference mortar. Reduction in the compressive strengths ranged between 28.93%-68.80%, depending on the RHA substitution ratio. The specimens with the 25% RHA substitution ratio showed a compressive strength of only about 11 MPa, which is 68.80% lower compared to reference mortar. On the other hand, by the end of the 720-day curing period, all RHA-containing mortar mixes exhibited notable improvements in compressive strength. Mortar with the RHA substitution rates of 5% and 10% marginally surpassed the performance of the reference mix, achieved compressive strengths slightly above 45 MPa. Higher substitution rates (15%–25%) still resulted in lower compressive strengths compared to the control, however, the difference in compressive strengths diminished significantly over time.

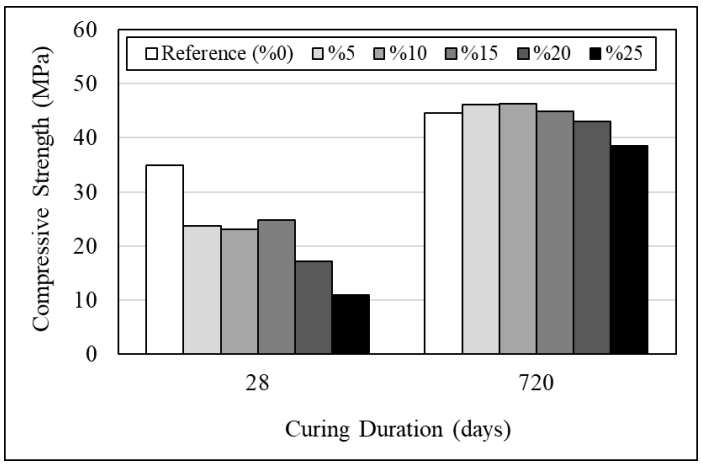

Figure 4. Compressive strengths of specimens considering both RHA substitution ratio and the curing duration.

4. DISCUSSION AND CONCLUSIONS

This study investigated the combined effect of rice husk ash (RHA) incorporation on the mechanical behavior of cement mortars at both early and extended curing ages. At 28 days, mortars containing RHA showed decrease in flexural and compressive strengths relative to the control specimen. These early-age deficiencies result predominantly from the dilution of the cementitious phase and the inherently slower pozzolanic reactivity of RHA, which delays the generation of calcium silicate hydrate and impedes matrix consolidation. However, a markedly different trend emerged at 720 days. The flexural strength of mortars with RHA substitution ratios up to 20% surpassed that of the reference mix, indicating

the development of a denser and more refined microstructure over time due to ongoing pozzolanic reactions. The compressive strength followed a similar trend, with mixes containing 5% and 10% RHA achieving higher strengths than the control mix. Even for higher substitution rates (15% and 20%), the gap in compressive strength diminished substantially, highlighting the long-term reactivity and beneficial contribution of RHA to strength development.

In conclusion, while RHA adversely affects early-age strength, especially at high substitution levels, its long-term contribution to both the flexural and compressive strength can be significant at moderate dosages. Optimal performance was observed in mortars containing 5–20% RHA, which eventually outperformed the reference mix in the long term. Therefore, for applications where long-term durability and strength development are prioritized over early-age strength, RHA can be considered a sustainable and effective partial cement replacement material within appropriate substitution limits.

Acknowledgements
The authors would like to thank Hitit University Scientific and Technological Application and Research Center (HÜBTUAM) for their assistance during the experimental tests.

Ethics Committee Approval
N/A

Peer-review
Externally peer-reviewed.

Author Contributions
Conceptualization: S.O.K.; Investigation: E.G., J.E.K., S.O.K.; Material and Methodology: E.G., S.O.K.; Testing: E.G., J.E.K., Supervision: S.O.K.; Visualization: J.E.K; Writing-Original Draft: E.G.; Writing-review & Editing: E.G., S.O.K.; Other: All authors have read and agreed to the published version of the manuscript.

Conflict of Interest
The authors have no conflicts of interest to declare.

Funding
The authors declared that this study has received no financial support.

REFERENCES

Abalaka, A.E., Okoli, O.G. (2013). Comparative effects of air and water curing on concrete containing optimum rice husk ash replacement. Journal of Emerging Trends in Engineering and Applied Sciences. 4(1), 60-65.

ASTM C349-18. (2018). Standard Test Method for Compressive Strength of Hydraulic-Cement Mortars (Using Portions of Prisms Broken in Flexure), ASTM International.

Barua, D., Rahman, M.M., Chowdhury, M.W.R., Arif, M.M., Hasan, M.A. (2018). Effectiveness of rice husk ash (RHA) as a partial replacement of cement in concrete. In International Conference on Civil Engineering for Sustainable Development (ICCESD 2018), February (pp. 3-9).

Ettu, L.O., Mbajiorgu, M.S.W., Nwachukwu, K.C. (2013). Variation of OPC-Rice Husk Ash Composites Strength Under Prolonged Curing. International Journal of Engineering Research and Technology (IJERT). 2(7), 2276-2283.

Ganesan, K., Rajagopal, K., Thangavel, K. (2008). Rice husk ash blended cement: Assessment of optimal level of replacement for strength and permeability properties of concrete. Construction and building materials. 22(8), 1675-1683. https://doi.org/10.1016/j.conbuildmat.2007.06.011

Kıvrak, S.O., Gödek, E., Kıvrak, J., Öbekcan, H. Characterization of Rice Husk Ashes Produced from Paddy Wastes in Osmancık Region. 2nd International Turkish World Engineering and Science Congress, Alanya, 133-141, 2019.

Madandoust, R., Ranjbar, M.M., Moghadam, H.A., Mousavi, S.Y. (2011). Mechanical properties and durability assessment of rice husk ash concrete. Biosystems Engineering. 110(2), 144-152. https://doi.org/10.1016/j.biosystemseng.2011.07.009

Marthong, C. (2012). Effect of rice husk ash (RHA) as partial replacement of cement on concrete properties. International Journal of Engineering Research & Technology. 1(6), 1-9.

Rasoul, B.I., Günzel, F.K., Rafiq, M.I. (2018). Effect of rice husk ash properties on the early age and long term strength of mortar. In High Tech Concrete: Where Technology and Engineering Meet: Proceedings of the 2017 fib Symposium, held in Maastricht, The Netherlands, June 12-14, 2017 (pp. 207-214). Springer International Publishing.

Thiedeitz, M., Ostermaier, B., Kränkel, T. (2022). Rice husk ash as an additive in mortar–Contribution to microstructural, strength and durability performance. Resources, Conservation and Recycling. 184, 106389. https://doi.org/10.1016/j.resconrec.2022.106389

TS EN 196-1. (2016). Methods of testing cement - Part 1: Determination of strength, Turkish Standardization Institute. (in Turkish)

Linking Indoor Air Quality Measurements with Occupant Satisfaction: A Case Study from a University Architecture Studio

DAMLA YAĞMUR SAĞ BAYRAM *[1], DENİZ ERDOĞAN ÖLÇER[2], TUĞÇE PEKDOĞAN[3]

Abstract: This study investigates the indoor air quality of the Architecture Studio at Adana Alparslan Türkeş Science and Technology University during December 2024. Measurements were planned for four separate days -once per week- on the studio's busiest weekday, at 09:00, 12:00, and 15:00. A hybrid approach combining objective field measurements with subjective user satisfaction surveys was employed. Measurements of $PM_{2.5}$, PM_{10}, carbon dioxide (CO_2), temperature, and relative humidity were conducted. Daily average $PM_{2.5}$ concentrations ranged between 12.13 µg/m³ and 27.20 µg/m³, frequently exceeding the 15 µg/m³ 24-hour limit recommended by WHO 2021 Air Quality Guidelines. PM_{10} values varied between 17.60 µg/m³ and 38.60 µg/m³, remaining within the WHO's 45 µg/m³ 24-hour limit. Hourly CO_2 concentrations ranged from 524 ppm to 1236 ppm. Although most hourly readings complied with the ASHRAE 62.1 guideline of 1000 ppm for acceptable indoor air quality, temporary peaks exceeding this limit were observed during high occupancy periods, suggesting periods of inadequate ventilation. Hourly temperature measurements fluctuated between 19.22°C and 27.35°C. While 12:00 and 15:00 measurements generally complied with ASHRAE Standard 55 (acceptable range 20–24°C for winter), 09:00 readings occasionally fell below 20°C, and some afternoon values exceeded 24°C, indicating transient thermal discomfort. Relative humidity levels ranged from 31.5% to 51.9%, remaining within the 30–60% comfort range recommended by ASHRAE Standard 55.A user satisfaction survey with 34 participants revealed that only 44.1% were satisfied with indoor air quality, while 41.2% were neutral and 14.7% dissatisfied, falling significantly below the 80% satisfaction benchmark. The findings underscore the need for improved particulate control, ventilation enhancement, and better thermal comfort strategies in the architecture studio.

Keywords: Indoor Air Quality, Occupant Satisfaction, $PM_{2.5}$ and PM_{10}, CO_2 Levels, Relative Humidity Levels.

[1]**Address:** Adana Alparslan Türkeş Science and Technology University , Faculty of Design and Architecture, Adana/Turkiye
[2]**Address:** Adana Alparslan Türkeş Science and Technology University , Faculty of Design and Architecture, Adana/Turkiye
[3]**Address:** Adana Alparslan Türkeş Science and Technology University , Faculty of Design and Architecture, Adana/Turkiye

***Corresponding author**: damlayagmursag@gmail.com

1. INTRODUCTION

Indoor Air Quality (IAQ) plays a vital role in ensuring the health, comfort, and cognitive performance of building occupants. Poor IAQ has been consistently associated with a range of adverse outcomes, including fatigue, headaches, respiratory discomfort, and reduced productivity (Fisk et al., 2009; Wargocki et al., 1999). Educational environments, particularly architecture studios, are especially critical in this regard due to their prolonged occupancy periods, high user density, and the demand for continuous cognitive engagement. These studios also present unique challenges due to their open-plan spatial arrangements, intensive use of materials and equipment, and typically extended working hours.

Previous research has highlighted the influence of key IAQ parameters—such as particulate matter PM2.5 (fine particulate matter smaller than 2.5 µm in diameter) and PM10 (inhalable particulate matter smaller than 10 µm in diameter), carbon dioxide (CO_2), temperature, and relative humidity—on both physical health and perceived comfort (Frontczak & Wargocki, 2011; Al Horr et al., 2016). For instance, CO_2 concentrations above 1000 ppm have been linked to reduced cognitive performance and impaired decision-making (Satish et al., 2012), while PM2.5 exposure is known to cause respiratory distress and long-term health risks. The World Health Organization's (2021) air quality guidelines and the ASHRAE standards (55 and 62.1) provide reference thresholds for these parameters. However, real-world conditions in educational buildings often deviate from such recommendations due to design limitations and fluctuating occupancy.

Recent studies have increasingly drawn attention to IAQ in educational settings, including architecture studios where students spend extended hours under intensive cognitive and physical workloads.

In their pilot study, Erlandson et al. (2019) examined indoor air quality (IAQ) across different building types in a university setting and found that occupancy status and building zones had a significant impact on pollutant levels, including CO_2, formaldehyde, and various sizes of particulate matter ($PM_{2.5}$, PM_4, PM_{100}). The study highlighted that occupied spaces consistently exhibited higher pollutant concentrations than unoccupied ones, emphasizing the role of human presence and activity in indoor air dynamics. These findings contribute valuable insight into the relationship between indoor environmental conditions and potential effects on health and cognitive function in educational spaces.

Eltaweel et al. (2023) explored IEQ factors—such as air quality, thermal conditions, lighting, and acoustics—across eight design studios, revealing that students expressed the lowest satisfaction with air quality and thermal comfort.

Furthermore, existing literature often prioritizes objective IAQ measurements while overlooking users' subjective experiences. As emphasized by Kim and de Dear (2012), integrating perceptual assessments is essential for a holistic understanding of indoor environmental quality.

Al-Jokhadar et al. (2023) conducted a study investigating indoor environmental quality (IEQ) in architecture design studios, focusing on how factors such as air quality, thermal conditions, lighting, and acoustics influence student comfort and academic performance. Based on measurements and student surveys conducted across eight design studios, their findings revealed generally low satisfaction levels with overall comfort—particularly with noise, humidity, and temperature conditions—while lighting and air quality also received mixed responses. The study highlights the critical role of IEQ in shaping health outcomes and concentration levels, with over 77% of students believing that improving IEQ would positively impact their academic performance.

Ranjbar (2019) conducted an experimental study to investigate the effects of different ventilation modes—natural, mechanical (HVAC), and no ventilation—on thermal comfort, indoor air quality (IAQ), and student performance in design studios and classrooms. Measurements of CO_2 concentration, temperature, and humidity were accompanied by thermal comfort surveys and cognitive performance tests (Kraepelin and Prague) to assess students' responses under varying environmental conditions. Results indicated that the mechanical ventilation mode provided the most favorable indoor environment and led to significantly higher performance scores, especially during the winter term. The study emphasized the importance of effective ventilation in maintaining acceptable IAQ and supporting student productivity in design education environments.

Tunalı Kayılı and Yetiş (2023) investigated indoor air quality (IAQ) and thermal comfort in architectural studios during model-making activities. Measurements based on ASHRAE standards and student surveys revealed that despite ongoing natural ventilation, pollutant concentrations—particularly CO_2 and TVOCs—rose to levels that may threaten health, especially in smaller studio volumes. Symptoms such as fatigue, headache, and shortness of breath were frequently reported, with female students experiencing more discomfort. The study highlighted the critical role of studio size, material use, and ventilation design in ensuring student comfort and health in educational settings.

Building on prior research that has explored IAQ and occupant satisfaction in educational settings, this study contributes to the growing body of literature by providing a detailed case analysis of an architecture studio at Adana Alparslan Türkeş Science and Technology University. By integrating objective field measurements with subjective user evaluations, the study offers nuanced insights into the alignment between environmental performance and occupant perception. The findings are intended to support evidence-based strategies for improving indoor environmental conditions in studio-based learning environments.

2. MATERIAL AND METHOD

The research was conducted in the architecture studio of Adana Alparslan Türkeş Science and Technology University throughout December 2024. The studio measures approximately 14.40 m by 14.40 m and has a square-plan, open-layout design, which is heavily occupied by students and instructors during weekdays (see Figure 1). It is equipped with a split-type air-conditioning system that provides mechanical cooling, and two façades are lined with operable windows, enabling natural ventilation. These features allow for both mechanical and natural ventilation, making the studio a representative setting for evaluating IAQ in educational environments.

Figure 1. General views of the architecture studio

A hybrid methodology was implemented, combining field measurements with subjective feedback. Data collection took place on four consecutive Wednesdays—identified as the studio's busiest days. Measurements were performed at three specific time points (09:00, 12:00, and 15:00) each day. CO_2 concentration, temperature, and relative humidity were measured using a Testo 435 multifunctional IAQ meter (see Table 1), with readings taken at four locations within the studio and averaged for each time slot. In parallel, $PM_{2.5}$ and PM_{10} concentrations were measured using a Triplett EPC175 particle counter (see Table 1) at five different locations, with daily averages calculated for analysis.

Table 1. Properties of measurement devices used in the study

Device Name	Measured Parameter	Measurement Range	Resolution / Accuracy
Testo 435	CO_2	0–10,000 ppm	1 ppm
	Temperature	-50–150 °C	±0.2 °C (within -25 to +74.9 °C)
	Relative Humidity	0–100% RH	±2% RH (+2 to +98 %RH)
Triplett EPC175	$PM_{2.5}$	0–999 µg/m³	1 µg/m³
	PM10	0–999 µg/m³	1 µg/m³

As Table 2 shows, the measured values were evaluated against international standards. WHO (2021) guidelines define a 24-hour limit of 15 µg/m³ for $PM_{2.5}$ and 45 µg/m³ for PM_{10}. ASHRAE Standard 62.1 sets an upper limit of 1000 ppm for CO_2, while ASHRAE Standard 55 recommends maintaining indoor temperatures between 20–24 °C in winter and relative humidity between 30–60% for optimal comfort.

Table 2. Reference standards for ındoor environmental quality

Parameter	Standard	Recommended Limit	Source
PM2.5	24-hour average	≤ 15 µg/m³	WHO (2021)
PM10	24-hour average	≤ 45 µg/m³	WHO (2021)
CO_2	Instantaneous	≤ 1000 ppm	ASHRAE Standard 62.1
Temperature (winter)	Operative temperature	20–24 °C	ASHRAE Standard 55
Relative Humidity	Comfort range	30% – 60%	ASHRAE Standard 55

Additionally, a structured user satisfaction survey was administered to 34 studio users, comprising students and instructors. The survey included Likert-scale items to assess perceptions of air quality, thermal comfort, and dust sensation. These data were analyzed to explore the alignment between measured environmental conditions and users' subjective evaluations.

3. RESULTS

Environmental measurements collected over the four-day period revealed several patterns across the IAQ parameters. Daily average $PM_{2.5}$ concentrations ranged from 12.13 µg/m³ to 27.20 µg/m³, exceeding the WHO threshold of 15 µg/m³ on multiple occasions. PM10 levels, in contrast, remained within the acceptable range, varying between 17.60 µg/m³ and 38.60 µg/m³.

Hourly measurements of CO_2 showed fluctuations based on occupancy patterns. Morning values at 09:00 were generally below the ASHRAE 62.1 guideline of 1000 ppm, ranging from 524 ppm to 910 ppm. However, during later time points, peak values reached up to 1236 ppm, indicating temporary ventilation inadequacies.

Temperature readings followed a similar diurnal pattern. Early morning values fell as low as 18.7 °C, below the ASHRAE thermal comfort range, while midday and afternoon readings approached 23.7 °C, staying within acceptable limits. Relative humidity levels remained within the recommended 30–60% range throughout the measurement period, with values between 31.5% and 51.9% (see Table 3 and Figure 2).

Table 3. Minimum and maximum values of IAQ parameters measured in the architecture studio

Parameter	Minimum Value	Maximum Value	Unit
$PM_{2.5}$	12.13	27.20	µg/m³
PM10	17.60	38.60	µg/m³
CO_2	524.50	1236.00	ppm
Temperature	18.70	23.72	°C
Relative Humidity	31.50	51.90	%

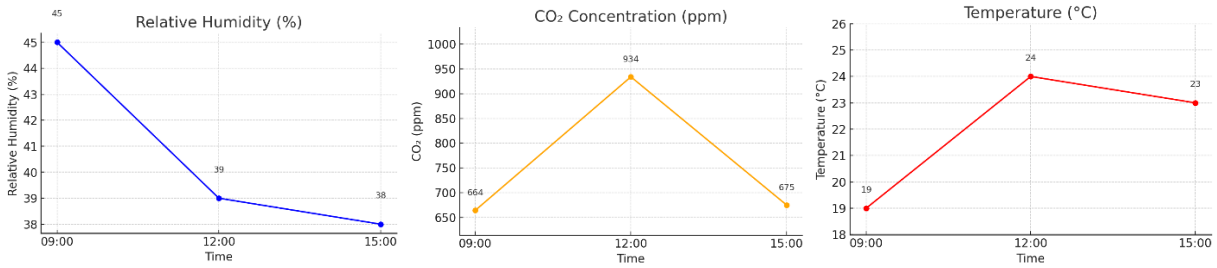

Figure 2. Indoor environmental parameters: Monthly mean CO_2, temperature, and relative humidity levels

Survey results aligned with many of these observations. In terms of dust perception, 54.5% of the participants reported perceiving a dusty environment either "rarely", "occasionally", "frequently", or "always", while only 9.1% stated that they never experienced such a sensation. This subjective perception aligns partially with the measured PM2.5 levels, suggesting that even low-frequency exposure may contribute to users' awareness of particulate matter in the studio environment.

Regarding thermal comfort, 52.9% of respondents expressed satisfaction ("satisfied" or "very satisfied"), while 41.2% reported a neutral stance. Only 5.9% indicated dissatisfaction. This distribution suggests that although most participants were content with the thermal conditions, a considerable portion remained indifferent, potentially due to temperature fluctuations throughout the day (see Figure 3).

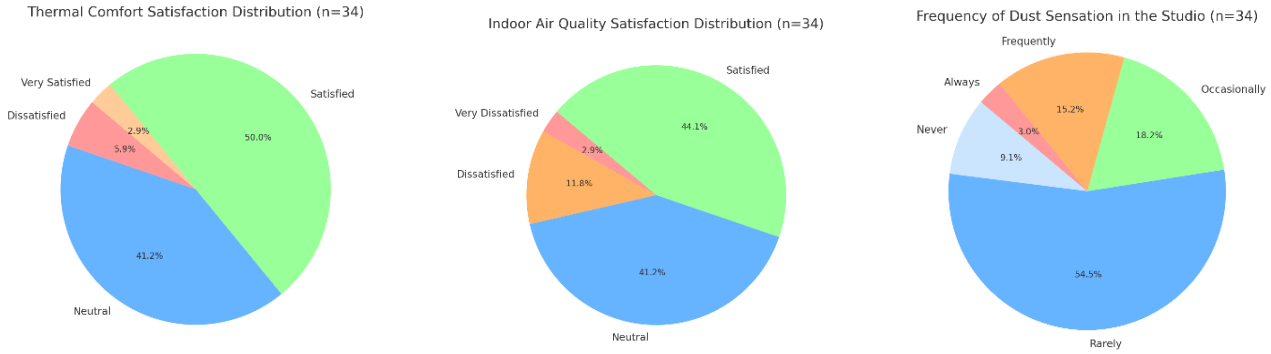

Figure 3. User-reported assessments of thermal conditions, air quality, and dust perception in the studio

To evaluate the sufficiency of user satisfaction in indoor environments, ASHRAE Standard 55 (2020) suggests that at least 80% of occupants should be satisfied with the thermal environment. In this study, however, satisfaction levels fell short of that benchmark across all IAQ dimensions. This discrepancy underscores the need for targeted interventions in ventilation and thermal management.

Regarding indoor air quality, 44.1% of the participants reported being satisfied, while 41.2% maintained a neutral opinion. A smaller portion—14.7%—expressed dissatisfaction ("dissatisfied" or "very dissatisfied"). This distribution suggests a generally acceptable level of perceived air quality, though nearly half of the respondents were either indifferent or dissatisfied, potentially indicating areas for ventilation or filtration improvements.

4. DISCUSSION AND CONCLUSIONS

This study assessed the indoor air quality of a university architecture studio through environmental measurements and user surveys. PM2.5 concentrations consistently exceeded WHO limits, while PM10 remained within acceptable thresholds. CO_2 levels occasionally surpassed ASHRAE guidelines during periods of high occupancy, whereas temperature fell below the recommended lower limit only in the morning hours. Relative humidity remained within the acceptable comfort range throughout.

User feedback aligned with the measured data, with many respondents reporting neutral or negative perceptions regarding air quality, thermal comfort, and dust presence.

These findings emphasize the need for improved ventilation strategies and the potential benefit of localized air purification and adaptive thermal regulation. Future research should include long-term monitoring and additional IAQ indicators to support evidence-based improvements in studio environments.

Acknowledgements
This study was supported by TÜBİTAK under Project Number 323K112. We sincerely thank TÜBİTAK for providing the financial support. Additionally, we thank the organizers of ICONST-2024 for their support.

Ethics Committee Approval
This study was approved by the Ethics Committee of Adana Alparslan Türkeş Science and Technology University

Peer-review
Externally peer-reviewed.

Author Contributions
Conceptualization: T.P..; Investigation: D.Y.S.B., D.E.Ö.; Material and Methodology: T.P., D.Y.S.B.; D.E.Ö.; Supervision: T.P.; Visualization: D.Y.S.B.; Writing-Original Draft: D.Y.S.B.; Writing-review & Editing: T.P.; Other: All authors have read and agreed to the published version of the manuscript.

Conflict of Interest
The authors have no conflicts of interest to declare.

Funding
This study was financially supported by TÜBİTAK.

REFERENCES

Al Horr, Y., Arif, M., Katafygiotou, M., Mazroei, A., Kaushik, A., & Elsarrag, E. (2016). Impact of indoor environmental quality on occupant well-being and comfort: A review of the literature. *International Journal of Sustainable Built Environment*, 5(1), 1–11. https://doi.org/10.1016/j.ijsbe.2016.03.006

Al-Jokhadar, A., Alnusairat, S., Abuhashem, Y., & Soudi, Y. (2023). The impact of indoor environmental quality (IEQ) in design studios on the comfort and academic performance of architecture students. *Buildings, 13*(11), 2883. https://doi.org/10.3390/buildings13112883

ASHRAE. (2022). *ANSI/ASHRAE Standard 62.1-2022: Ventilation for acceptable indoor air quality*. American Society of Heating, Refrigerating and Air-Conditioning Engineers. https://www.ashrae.org/technical-resources/bookstore/standards-62-1-62-2

ASHRAE. (2020). *ANSI/ASHRAE Standard 55-2020: Thermal environmental conditions for human occupancy*. American Society of Heating, Refrigerating and Air-Conditioning Engineers. https://www.ashrae.org/technical-resources/bookstore/standard-55-thermal-environmental-conditions-for-human-occupancy

Erlandson, G., Magzamen, S., Carter, E., Sharp, J. L., Reynolds, S. J., & Schaeffer, J. W. (2019). Characterization of indoor air quality on a college campus: A pilot study. International Journal of Environmental Research and Public Health, 16(15), 2721. https://doi.org/10.3390/ijerph16152721

Fisk, W. J., Black, D., & Brunner, G. (2009). Benefits and costs of improved IEQ in U.S. offices. *Indoor Air*, 19(4), 357–372. https://doi.org/10.1111/j.1600-0668.2009.00615.x

Frontczak, M., & Wargocki, P. (2011). Literature survey on how different factors influence human comfort in indoor environments. *Building and Environment*, 46(4), 922–937. https://doi.org/10.1016/j.buildenv.2010.10.021

Kim, J., & de Dear, R. (2012). Nonlinear relationships between individual IEQ factors and overall workspace satisfaction. *Building and Environment, 49*, 33–40. https://doi.org/10.1016/j.buildenv.2011.09.022

Ranjbar, A. (2019). Analysing the effects of thermal comfort and indoor air quality in design studios and classrooms on student performance. IOP Conference Series: Materials Science and Engineering, 609(1), 042086. https://doi.org/10.1088/1757-899X/609/4/042086

Satish, U., Mendell, M. J., Shekhar, K., Hotchi, T., Sullivan, D., Streufert, S., & Fisk, W. J. (2012). Is CO_2 an indoor pollutant? Direct effects of low-to-moderate CO_2 concentrations on human decision-making performance. *Environmental Health Perspectives*, 120(12), 1671–1677. https://doi.org/10.1289/ehp.1104789

Tunalı Kayılı, M., & Yetiş, C. (2023). Determination of the indoor air quality and occupancy satisfaction in architecture studios during model making process. *GRID Architecture, Planning and Design Journal*, *6*(1), 30–55. https://doi.org/10.37246/grid.1031184

Wargocki, P., Wyon, D. P., Sundell, J., Clausen, G., & Fanger, P. O. (1999). The effects of outdoor air supply rate in an office on perceived air quality, Sick Building Syndrome (SBS) symptoms and productivity. *Indoor Air*, 9(3), 165–179. https://doi.org/10.1111/j.1600-0668.1999.00003.x

World Health Organization. (2021). *WHO global air quality guidelines: Particulate matter (PM2.5 and PM10), ozone, nitrogen dioxide, sulfur dioxide and carbon monoxide*. https://www.who.int/publications/i/item/9789240034228

A Rehabilitation Project for the Valorization of Built Heritage. Platamone Castle in Rosolini in Sicily

FERNANDA CANTONE *[1]

Abstract: Rehabilitation is the process which seeks to preserve the historical portions or features of a building while making the building compatible with a new use. In Italy, Rehabilitation has a 70-year history that has become the most widespread tool in construction. Rehabilitation interventions are performed on all existing buildings, regardless of age, property, cultural or economic value. Abandoned buildings, not yet rehabilitated, are the only ones which hold the power of memory and characterization of urban space. The research aims to propose a case study on the theme of rehabilitation which expresses all the value of abandoned buildings. These are buildings that have a strong historical value and that transmit important moments of the history of Italian cities. The abandonment, transformations and improper uses make it a perfect case study to propose a rehabilitation project based on an in-depth documentary phase (survey, historical research, analysis of potential, regulatory tools) followed by a valorisation project. The case study is the Platamone Castle of Rosolini, a building built in 1606 and around which the city was born in 1673. It was the castle of the Prince Platamone, built near a hypogeic basilica of the IV century. The castle has undergone many modifications, demolitions, elevations that have transformed it. It belongs to various owners who have used it in many ways, oil mill, warehouse, stable. The objective is a path of deepening the components of the project sensitive to past values and load reference elements for the future.

Keywords:

[1]**Address:** Catania University, SDS Architecture and Cultural Heritage, Siracusa/Italy

***Corresponding author**: fernanda.cantone@unict.it

1. INTRODUCTION

The preservation of architectural heritage is taking on an urban dimension worldwide. It is concerned with wider issues than the rehabilitation of individual buildings or their cultural value. During this period, Italy, through the PNRR instrument, has had the opportunity to carry out concrete actions for the conservation and/or recovery of its historical cultural heritage. Project interventions, except for the striking cases of large cities such as Rome, have not had an agreed planning and design, but often they were dictated more by the presence of ready-made projects in municipal administrations than by a real decision phase. In fact, despite regulatory efforts, in Italy there is no national project for the conservation (Ministry of Culture, 2018), protection and enhancement of the building heritage and this prevents to observe, analyze and intervene on the relationship between culture, Urban historical landscape and future. The presence of this tool would lead to a contemporary vision of the public project of re-use of our goods and spaces, cities and territories, with a time and economic planning of the interventions to be implemented, with a clear vision of a strategy, of an end, a goal.

«If you want to relaunch a territory you don't have to invent weird things. You must start from what we have. At the same time, we cannot be satisfied with what is there but we must add the drive of transformation, that is we must innovate» (Barca, 2017), this wrote Fabrizio Barca in 2017. The objective is to transmit the identity of the territory and the possible ways of use, to be imagined flexible for the ever more rapid change of needs and social and economic organization. In this sense, enhance must imagine a new relationship between local needs and prospects, from the concept of urban historical heritage (Unesco, 2019).

The starting point for the exploitation of existing heritage is the concept of urban historical heritage (UNESCO, 2019). It comprises all the elements, both material and immaterial, which characterise an urban area over time and reflect its history, culture and identity. These elements include historical buildings, monuments, archaeological sites, but also traditions, customs and social and cultural practices that characterize a given place (START, 2024).

Through this concept, UNESCO has issued Recommendations on the Historic Urban Landscape (United Nations Educational, Scientific and Cultural Organization, 2011-2020). This paper proposes a model for analysing interventions on existing buildings, to understand and incorporate the complexity of the subject into the project. The new approach proposes coordination of all conservation disciplines. It is a matter of proposing actions that can transform, integrate and improve the potential of these places to offer spaces of great cultural impact, rethinking of public space, aggregation for the community.

We know that Italy has a great amount of historical and landscape resources. Some of them have been abandoned or profoundly transformed because they did not respond to the new needs of society. This is referred to as "functional deficits". In architecture, the lack of functionality refers to existing spaces that do not meet the needs of users, being inadequate or inaccessible (Manzione, 2025). This problem manifests itself mainly in cases of changing economic conditions and the absence of essential services that guarantee comfort and safety. The valorisation of these areas could be summed up with a slogan: memory of the old for a community of the future. This is an important heritage, often in a state of ruin, now forgotten.

In the rehabilitation and enhance project, it is essential to include analysis to recognize types of deficits. They manifest themselves express inefficiencies and limitations that affect not only the functionality but also the sustainability of buildings and public spaces. The three main categories of deficits are structural deficit, appearance deficit and environmental deficit. The first refers to deficiencies in the physical components of a work, which can be manifested through cracks or collapses, the second concerns the lack of an architectural perception of the building and concerns the choice of materials, the coherence of style and integration with the urban fabric. Finally, the environmental deficit manifests itself in buildings of the past that offered a poor management of resources such as poor water management and inadequate thermal insulation (Carta et al., 2022). Understanding and addressing these types of deficits becomes, therefore, fundamental to raise design standards increasingly ethical and responsible.

2. MATERIAL AND METHOD

The research proposes a path of analysis that starts from the historical, dimensional and technological knowledge of abandoned artifacts and proposes an approach based on the characteristics of buildings, their context and the analysis of the functional deficit.
It has been implemented in phases:

- Historical and documentary analysis;
- Technology analysis;
- Qualitative analysis of the building and its context:
    - Structural deficit
    - Deficit of appearance and perception
    - Environmental deficit;
- Community interviews.

This articulation allows to have a series of information of which it is possible to understand the weight and importance. It is a procedure that aims to enhance the values of the built and the needs of the community.
The initial analyses (historical, technological and perceptive) allow to know the events of the building and to frame the construction in the right perspective. They define the main historical and technological events, the transformations that took place on the building, the characteristics of the technologies used. This framework serves to provide the starting information for the analysis of the building's functional deficit.
Once the lack of functionality was identified, it was possible to identify the components of the intervention project and propose a project that is participatory and sensitive to the past of the building.
The involvement of stakeholders in the analysis phase measures the effectiveness of design solutions and guides intervention phases, contributing to solutions to improve the adequacy of existing buildings for current and future needs. Therefore, the analysis of the functional deficit is not only an objective of evaluation but also a design imperative, aimed at ensuring sustainable livability and universal dignity in built environments.

3. THE CASE STUDY

The object of research is a building system composed of the vestiges of a castle and the ruins of the production area (warehouses, mill, stables). It is located at the entrance of Rosolini, a town of 20,000 inhabitants, in the district of Syracuse, on the border with the district of Ragusa. Rosolini has an old history but not at all valued and known and is outside the most well-known tourist circuits. The case study is a set of ruins, abandoned for decades, located at the entrance to the town of Rosolini, near a large and horrible elevated roundabout, recently built. This castle was the control building of an area owned by the Platamone family. It became the first foundation of Rosolini. The castle includes several buildings, now distant from each other. The representative areas of the castle, partly disappeared, partly in a state of ruins, are private property and have undergone enormous transformations, elevations and extensions. The productive part, which is also in a ruinous state, does not seem to have been transformed. There are large rooms, some carved in the rock, which preserve the signs of their past: amphorae embedded in the ground to collect the freshly pressed oil, stone pipes that cross the various environments and old places with a history to discover. The project to enhance these places starts from this.
The complex of buildings that make up the castle system is a unique example of the buildings of the time that strongly characterized the historical urban structure of the city. The district on which the castle insisted was densely built in later eras and has an articulated spatial organization, developed over time.

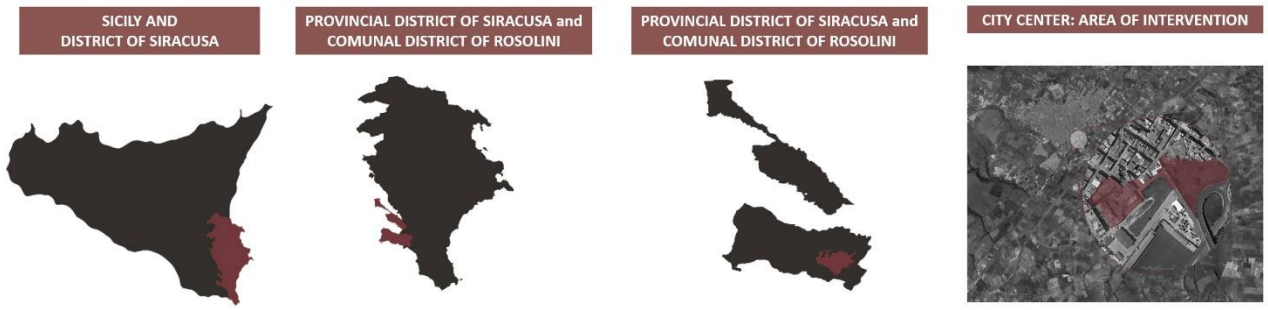

Figure 1. Territorial framing

4. THE RESEARCH

The research identified the following results:

4.1 Historical analysis

The historical investigations carried out at the state archives of the area have revealed an extremely interesting reality: the ruins belong to the first foundation of Rosolini that was born from 1485 with the realization of a castle, built only in part, following a building license requested by the Platamone family, first granted and then withdrawn for the hostility of the nearby and powerful city of Noto.

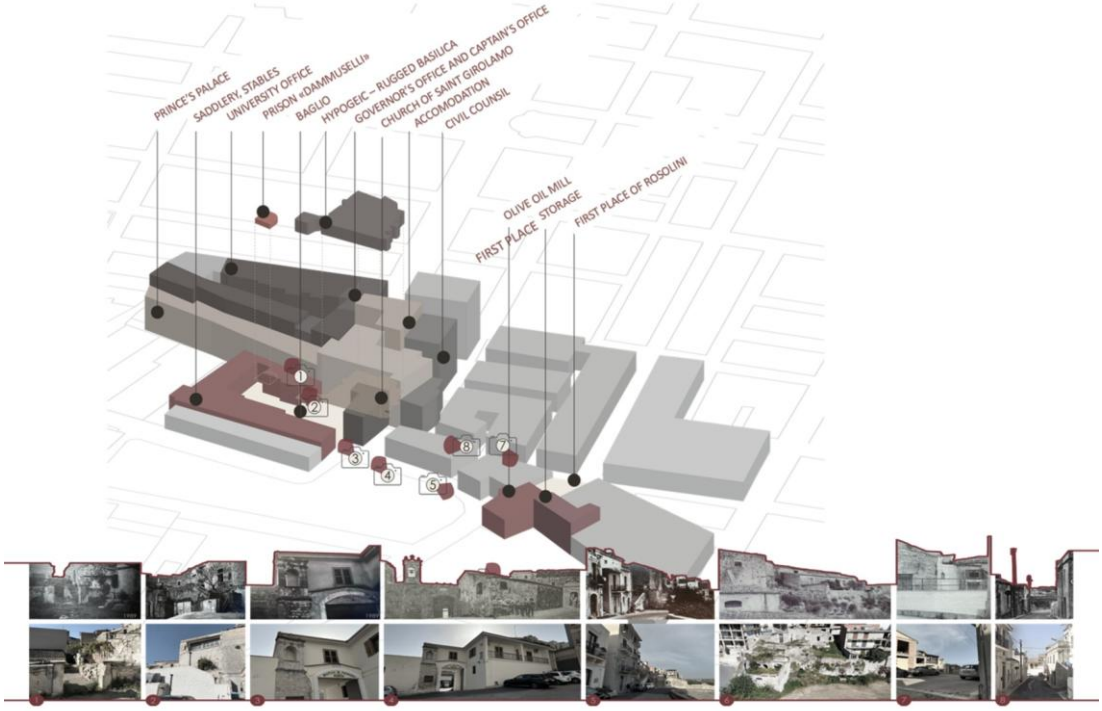

Figure 2. Reconstruction of the castle system with original functions

The site chosen, a hill overlooking a large area, was an important site, chosen in the fourth century to build an underground basilica with three naves, in use until the twelfth century and today used as a deposit. In the following two centuries, the Platamone family again applied for a license to build a new town, which was always rejected. The castle will be completed in 1606 but will remain an isolated garrison, without a settlement around. We must wait 228 years to arrive at 19 December 1673 when finally, Baron don Francesco Platamone Gantes became prince of Rosolini and received the "building license" from the Viceroy in office (Savarino, 1995). The earthquake of 1693 caused extensive damage to the castle and the first buildings built. In 1696 the adjacent warehouses and the mill were built. For two centuries these places have been used and lived. Then the change in production habits, new machinery and simplification of processes have led to changes and transformations in buildings and subsequently abandonment. Some parts have been demolished, such as the church, of which only part of the bell tower remains and on which a new building has been built, others have been transformed and elevated, losing the original configuration of the castle system, others have been abandoned and have become ruins, such as the warehouses and the mill.

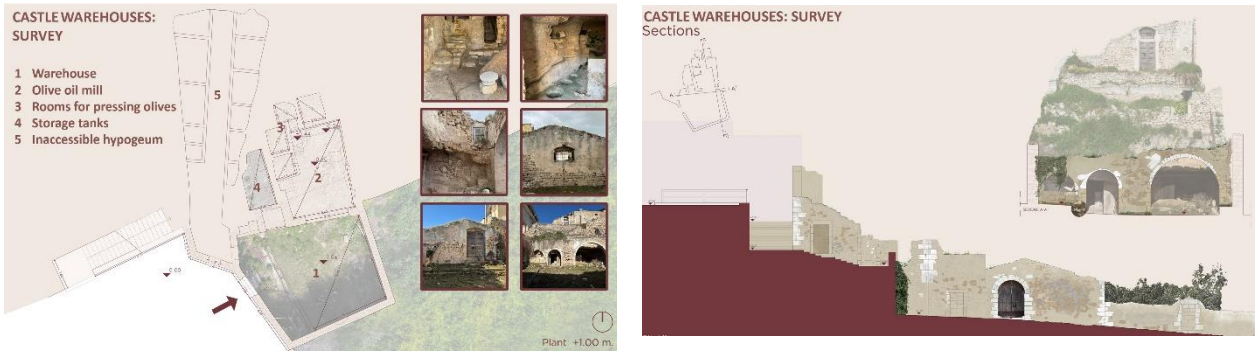

Figure 3. Survey: ground floor plant and section

4.2 Technological analysis

From a technological point of view, studies have been carried out on masonry, wall connections, the construction characteristics of mortar and the resistance system. The historical analysis confirms the technological characteristics of the buildings. The local building tradition is in perfect harmony with the state of the buildings.

The complex of buildings in a state of ruins has calcarenite masonry of thickness varying between 50 and 80 cm, with irregular blocks and just rough, bound with lime mortar, almost entirely disappeared. The stones are of various sizes and shapes and do not have layers of levelling. In some parts remains traces of lime plaster. The ceilings, vaults and roofs have collapsed long ago. The fixtures are deteriorated and present only in the entrance opening. We can see traces of wooden frames. There are no traces of paving.

In this analytical framework, the results provide important knowledge regarding the original volumes, use and materials used for construction. They are essential information for the realization of a project adhering to the new needs of the community, sensitive to the past, attentive to traditional technologies and technological innovation.

4.3 Functional deficit analysis

- Structural deficit: The buildings have suffered major collapses. The walls appear disintegrated and not tenacious. Prolonged exposure to atmospheric agents has accelerated the phenomenon. Buildings need major consolidation.
- Deficit of the appearance: the buildings present an extremely interesting material unity. The walls, made of white stone blocks, are perceptively imposing and bright, consistent with the historical - cultural context in which they were made. The openings have white stone frames, typical of nineteenth-century productive buildings. The whole is harmonious and refers to an architectural and cultural past of value. It is the aspect most to be valued.
- Environmental deficit: No environmental aspects can be identified due to the state of ruin. The time of construction and use in the distant time make the building to adapt.

4.4 Project objectives for the community

We conducted an in-depth study of the economic and social needs of the local community. The surveys involved 50 people of different ages and levels of education: interviews and questionnaires, conducted among residents and visitors to the neighbourhood, have shown a broad awareness of the potential of the territory and a widespread orientation towards urban regeneration interventions in the area. In summary, the elderly population shows the need for services that improve daily well-being, with particular attention to public spaces and activities to enhance the urban centre. Younger people want childcare services and measures to improve urban safety. Regardless of age, there is a shared demand for social spaces that promote integration and active participation in the community. Despite the problems related to the degradation of buildings, the inhabitants recognize in the neighbourhood a possible pole of cultural and social aggregation. We also found that many subjects do not know the history of their city and the presence of the remains of the old castle. The information gathered provides a clear picture of the needs and aspirations of the local community, providing an additional element for the development of redevelopment strategies. The community stresses the need for targeted interventions that on the one hand can enhance an important part of the history of Rosolini, on the other that can stimulate the development of new economic opportunities (especially tourism), the strengthening of services and the strengthening of social cohesion.

In conclusion, through the analysis of the lack of functionality, the impression of the inhabitants regarding the district where the castle is located emerged. This area is marginal to the old town and, in some parts, has some buildings marked by a progressive abandonment of housing and the loss of productive vitality that characterized it in the past. The widespread abandonment and deterioration of buildings negatively affects the overall perception of the area, accentuating the marginalization of the neighbourhood in the urban context and endangering its historical identity. Around the castle there are few commercial activities and services, creating a functional vacuum that hinders the social and cultural revival of the area.

Figure 4. Urban and perceptual analysis

5. THE PROJECT

It is well known that community support is needed to trigger redevelopment/regeneration processes. The analyses carried out highlighted the physical component of the building, its technology and its spatial configuration, but above all the strong desire of the community to bring back to life a significant place from the past, giving it a cultural and social function. This request has become the main objective of the project especially after discovering that many inhabitants of Rosolini do not know the site and its history.

In addition, given the demand for social spaces, the project was also based on the concept of "third places", a definition given by sociologist Oldenburg in 1989, but now extremely relevant. The concept of "third place" (Oldenburg, 1989) was introduced in the 1980s and identifies a social space which is neither home nor work, but which favours relationships and communities. It is a great where people from different backgrounds and perspectives can mix in a comfortable, unpretentious and low-cost environment. This category of buildings includes places of worship, museums and exhibition spaces, recreation centres, parks and social clubs, as well as bars, gyms and shopping malls. These are hybrid spaces that are constantly evolving, integrating different dimensions of social life, playing a crucial role in the growth of society and in creating real civic engagement. These places are important for building a strong community, promote socialization and can be fundamental to a person's social life. In a small, unstimulated community, the activation of a third place is essential for the effectiveness of the intervention.

In this perspective, the objectives of the project are the valorisation of the castle system, its recovery and the possibility of being visited, the recovery of warehouses and their reuse, allocating them to social spaces and communication. Regarding the warehouses, the project sees the integration of the lower environments with those above and the realization of a path of visit and enjoyment, in an alternation of internal and external paths, where the simple visit can be associated with the experience of augmented reality, co-working, experiential activities of various kinds.

In general, the measures identified include the elimination of overcrowding which, over time, has largely transformed the buildings, the consolidation of existing portions of masonry, a new coverage for warehouses and their recovery in terms of accessibility, functionality and adaptability.

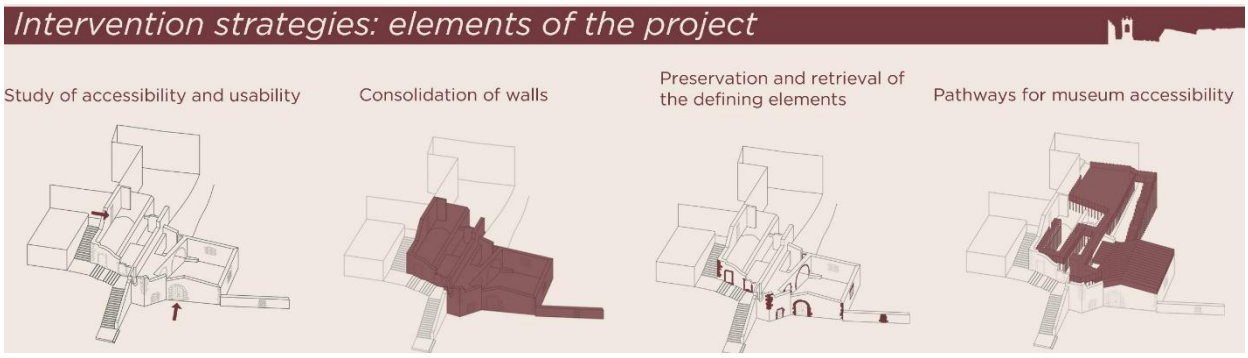

Figure 5. Valorization project for the warehouses

In particular, the project involves the construction of an elevated and continuous path between the various levels, a kind of Corten steel tape that runs through a series of buildings at different altitudes and reaches open spaces for socialization and places rich in innovation, related to visual communication. It rests on thin and thick pillars that rise above the floor to form the parapet. A ribbon that unrolls memories of the past.

Figure 5. Valorization project for the warehouses

6. DISCUSSION AND CONCLUSIONS

The Platamone Castle complex is an important historical witness for the town of Rosolini. In this direction, the research proposes cultural promotion initiatives to involve the community and stimulate tourism. These strategies aim to ensure the preservation of the Platamone Castle complex while respecting its historical identity, promoting at the same time a new function within the urban and cultural context of Rosolini.
The lack of services, places of aggregation, of interest in its past make Rosolini the perfect place to implement strategies of requalification and economic and social development.
The research aims to give a significant example of validation of the heritage abandoned and forgotten, without forgetting social sustainability, motor of the evolution of communities.
The proposed approach responds to the needs of the territory by enhancing its own forgotten heritage and proposing a project sensitive to the demands of the community. This project could be perfectly integrated into a strategy of sustainable cultural, social and economic development which would bring significant social and economic improvements.

Acknowledgements
Interventions on the Platamone Castle in Rosolini and relative images are taken from the degree thesis of Mariatina Cataudella and Adriana Cerruto entitled: *Reflorebunt. Rehabilitation of the Platamone Castle system in Rosolini (SR).* Supervisor: Prof. F. Cantone, Catania University, SDS of Architecture, Syracuse, Sicily. Academic year 2023/24.

Peer-review
Externally peer-reviewed.

Conflict of Interest
The authors have no conflicts of interest to declare.

REFERENCES

Barca, F. (2017). I borghi d'Italia. Dalla visione alla rigenerazione. In ANCE, 2017, p. 8. https://www.ance.it/docs/docdownload.aspx?id=41557 (accessed 12 January 2025).

Carta, M. Lino, B. Ronsivalle, D. (2022). Alimentare la resilienza. Approcci e metodi per alimentare un modello di sviluppo orizzontale nelle aree interne siciliane. In And-architettura n. 40. www.and-architettura.it (visited 2 February 2025).

Manzione, F. (2025). The nature of living spaces. Strategies for psycho-physical well-being. Degree thesis under Prof. F. Valpreda. Polytechnic University of Turin. https://webthesis.biblio.polito.it/secure/34384/1/tesi.pdf, (accessed 11 April 2025).

Grion. C. Sabbatini, E. (2025). Regenerating spaces, building dignity: A Place Identity and Wayfinding project. Degree thesis under Prof. C. Campagnaro. Polytechnic University of Turin. https://webthesis.biblio.polito.it/secure/34460/1/tesi.pdf (accessed 11 April 2025).

Ministero della Cultura (2018). Piano Straordinario Nazionale di Monitoraggio e Conservazione dei Beni Culturali Immobili. https://dgspatrimonioculturale.beniculturali.it/attivita-direzione-generale-sicurezza-del-patrimonio-culturale/bozza-automaticapiano-straordinario-di-monitoraggio-e-conservazione-dei-beni-culturali-immobili, (accessed 11 April 2025).

Oldenburg, R. (1989). The great good place. Cafes, coffee shops, bookstores, bars, hair salons, and other hangouts at the heart of a community. New York: Marlowe & Company.

Savarino, G., Milceri Oddo, G. (1995). Rosolini, un secolo di storia. Rosolini: Edizioni Archeoclub, pp. 41, 42.

START (2024). The importance of the recovery of historic urban heritage in a modern context, 24 May 2024, https://www.masterin.it/start/3389-l'importanza-del-recupero-del-patrimo-urbano-storico-nel-contesto-moderne/ (accessed 11 April 2025).

Unesco (2019). Global Report on culture for sustainable urban development, on line, p. 3, (accessed 11 April 2025).

United Nations Educational, Scientific and Cultural Organization (2011-2020), Recommendation on the historic urban landscape, 2011-2020 in https://whc.unesco.org/uploads/activities/documents/activity-638-98.pdf.

Linearization of NTC Thermistor Using the Newton-Raphson Method and Modified Nodal Analysis

YALÇIN BINICI*[1], ALI BEKIR YILDIZ[2]

Abstract: In this study, the temperature-resistance characteristic of a Negative Temperature Coefficient (NTC) thermistor is modeled within the temperature range of 248.15 K to 378.15 K using the Basic Equation, the Steinhart-Hart Equation, and the Hoge-3 Equation. These models contain different error rates depending on their usage. The Basic Equation shows a higher error rate compared to the other models due to its dependence on the beta parameter. The Hoge-3 Equation provides the lowest error rate. In this study, the non-linear behavior of the thermistor is linearized using the Newton-Raphson method, and the resulting models are integrated into an operational amplifier (op-amp) based circuit analyzed using Modified Nodal Analysis (MNA). As the temperature of the thermistor changes, the output voltage of the circuit changes. Although different approaches exist for linearizing, the effects of the models used in this study on the circuit output due to temperature changes are analyzed using the MNA method. Additionally, the theoretical output voltages obtained with MNA are validated by comparing them with circuit simulation results carried out in the LTspice environment. The results obtained contribute to the literature both technically and practically by demonstrating the linear modeling of NTC thermistors and their applicability in MNA-based circuit analysis.

Keywords: NTC thermistors, Steinhart-Hart, Newton-Raphson Method, Modified Nodal Analysis, MNA.

[1]**Address:** Sarsılmaz Silah Sanayi A.Ş., Düzce, Türkiye
[2]**Address:** Department of Electrical Engineering, Institute of Science, Kocaeli University, Kocaeli, Türkiye

***Corresponding author**: bncyalcinn@gmail.com

1. INTRODUCTION

NTC (Negative Temperature Coefficient) thermistors are sensors capable of accurately detecting temperature changes. These components, whose resistance decreases as temperature increases, are widely used in various fields such as medicine, engineering and industry. In this study, the steady-state behavior of an NTC thermistor is investigated. The term “steady-state” refers to the condition in which the current, voltage, and temperature values of the thermistor remain constant over time. In the literature, the steady-state current-voltage characteristic of NTC thermistors has been modeled using ideal diodes, current sources, and both negative and positive resistance elements. During the modeling process, the nonlinear current-voltage behavior of the thermistor is represented using a piecewise-linear (PWL) approach to facilitate analysis (Keskin and Yanar, 2004). Furthermore, more practical linearization techniques have been introduced by adding a parallel resistor to the NTC element (Keskin, 2005).

In an earlier study, seven calibration equations were evaluated to model the resistance-temperature (R-T) relationship of NTC thermistors. The Beta equation, the Steinhart-Hart equation, and Hoge equations were tested on four thermistors, and the coefficients were calculated using the least squares method. Among them, the Hoge-3 equation exhibited the best performance with the lowest errors across all thermistors. Notably, the Newton-Raphson method was not employed in this study (Chen, 2009).

The findings revealed that the Hoge-3 Equation achieved the lowest error rates across the entire temperature range (0.000%–0.010%), while the Steinhart-Hart Equation produced the second-best results with error rates ranging from 0.012% to 0.075%. On the other hand, the Basic Equation exhibited significantly higher errors, particularly at lower temperatures (e.g., a 13.681% error at 248.15 K). The primary reason for this deviation is that the Basic Equation relies on a beta (β) parameter typically measured over a limited temperature range (usually 25°C–85°C). Consequently, at lower temperatures, the Basic Equation fails to accurately capture the complex nature of the temperature-resistance relationship, leading to a loss of precision. These findings underscore the necessity of using multi-parameter models (such as the Steinhart-Hart and Hoge-3 Equations) over wide temperature ranges.Another linearization approach involved analytically deriving the temperature (T) from the resistance (R) using the Steinhart-Hart equation. This was
achieved through methods such as the three-point technique, least squares fitting with multiple data points, or using Chebyshev polynomials. For the Chebyshev method, an adaptive algorithm was used to optimize the polynomial degree (Cong et al., 2011). In a more recent method, the R-T relationship of NTC thermistors is modeled in two stages. In the first stage, a VCO-SCC circuit partially linearizes the exponential R-T behavior of the thermistor. In the second stage, an LSTM-MLSA model compensates for the remaining nonlinear characteristics. This method does not employ the Steinhart-Hart equation (Thangamalar et al., 2025).

The aim of this study is to analyze the NTC thermistor element using different equations and to calculate the node voltages in an electrical circuit based on the thermistor's temperature using the Modified Nodal Analysis (MNA) method. Furthermore, the previously reported high performance of the Hoge equation is re-evaluated using the Newton-Raphson method to conduct a comparative analysis.

2. FUNDAMENTAL CONCEPTS AND METHODS

The equations used for thermistors, mathematical approaches, and fundamental definitions related to circuit analysis are presented below to improve the understanding of this paper.

(a) Steinhart-Hart Equation : A function for use in interpolating thermistor calibrations has been found which is suitable for use with a wide variety of thermistors for ranges of a few degrees to a few hundred degrees (Steinhart and Hart, 1968).

$$\frac{1}{T} = A + B(lnR) + C(lnR)^3 \tag{1}$$

Where *T* is the Kelvin temperature, *R* the resistance, and A, B and C constants.

The coefficients A, B and C in the Steinhart-Hart equation can be determined through measurements taken over specific temperatures ranges. For example, if the resistance values of an NTC thermistor are measured at three different temperatures (in Kelvin), these data can be substituted into the Steinhart-Hart equation to calculate the corresponding coefficients.

The coefficients of the Steinhart-Hart equation are determined as shown below. The matrix representation used for calculating these coefficients is given (Eq.2).

$$\begin{bmatrix} 1 & (lnR1) & (lnR1)^3 \\ 1 & (lnR2) & (lnR2)^3 \\ 1 & (lnR3) & (lnR3)^3 \end{bmatrix} . \begin{bmatrix} A \\ B \\ C \end{bmatrix} = \begin{bmatrix} \frac{1}{T1} \\ \frac{1}{T2} \\ \frac{1}{T3} \end{bmatrix} \tag{2}$$

(b) Basic Equation : The Basic equation is also called as the two-term exponential equation (Chen, 2009).

$$R_T = R_{T0}\exp\left(ß\left(\frac{1}{T} - \frac{1}{T_O}\right)\right) \tag{3}$$

Where R_T is the resistance of thermistor at temperature T(K), R_{T0} is the resistance of thermistor at the nominal operating temperature at T_O, ß is the coefficient.

(c) Hoge-3 Equation : This equation is another form of the Steinhart-Hart equation.

$$\frac{1}{T} = A_0 + A_1 lnR + A_2(lnR)^2 + A_3(lnR)^3 + A_4(lnR)^4 \tag{4}$$

where A_0, A_1, A_2, A_3, and A_4 are constants.

2.1 Newton-Raphson Method

In numerical analysis, the Newton-Raphson method is a method used to find successively better approximations to the roots (or zeroes) of a real-valued function.Geometrically, the point $(x_1, 0)$ is the intersection with the x-axis of the tangent to the graph of f at $\left(x_0, f(x_0)\right)$ (Akram and Ann, 2015).

$$x_{n+1} = x_n - \frac{f(x_n)}{f'(x_n)} \tag{5}$$

2.2 Modified Nodal Analysis (MNA)

In computer-aided system analysis, the way circuit equations are formulated is a significant factor that determines the power, speed, and memory requirements of the method. The Modified Nodal Analysis (MNA) method meets these expectations effectively. In the classical nodal analysis, certain circuit elements such as voltage sources and controlled sources could not be included in the system equations. To overcome these limitations, the MNA method was developed, and over time, many circuit elements (such as transformers, mutual inductances, operational amplifiers, and semiconductor switching elements) have been incorporated into this representation, further enhancing the method (Çınar and Yıldız, 2006).

The circuit equations in operational corresponding to the modified nodal analysis method, have the following from (Erdei et al., n.d.):

$$\begin{bmatrix} G_d & A_2 \\ A_2^T & Z_2 \end{bmatrix} . \begin{bmatrix} V_n \\ I_2 \end{bmatrix} = \begin{bmatrix} J \\ E \end{bmatrix} \tag{6}$$

The unknown vector containing the node voltages and source currents is represented as the [X] matrix. These relationship are summarized in the matrix equation shown below as (Eq.7);

$$[K].[X] = [B] \quad (7)$$

2.3. The Characteristic Parameters of the NTC Thermistors

The technical specifications of the selected NTC thermistor are provided in Table 1, while the temperature-resistance characteristics are given in Table 2 (Vishay Intertechnology, 2024).

Table 1

Parameter	Value	Unit
Resistance value at 25 °C	10K	Ω
Tolerance on R25-value	± 3	%
ß25/85-value	3984	K
Tolerance on ß25/85-value	± 0.5	%
Operating temperature range at zero dissipation	-25 to 105	°C

Table 2

Temperature (°C)	Temperature (K)	Resistance (Ω)
-25	248.15	129 900
-5	268.15	42 268
0	273.15	32 624
15	288.15	15 711
40	313.15	5323.9
55	328.15	2982.3
65	338.15	2078.7
75	348.15	1475.9
90	363.15	911.59
105	378.15	582.84

3. APPLICATION OF NEWTON-RAPHSON METHOD

3.1 Application to the Steinhart-Hart Equation

The Steinhart-Hart equation is a third-order logarithmic expression that defines the relationship between temperature and resistance. Therefore, NTC thermistors are nonlinear components. Due to their nonlinear nature, they cannot be directly incorporated into the conductance matrix when using the Modified Nodal Analysis (MNA) method. This issue can be addressed by employing the Newton-Raphson method. In this approach, the nonlinear characteristic of the

thermistor is linearized as a result of the iteration, and the updated resistance value is integrated into the MNA equation system. The Steinhart-Hart Equation (Eq.1) is given again as follows.

$$\frac{1}{T} = A + B(lnR) + C(lnR)^3$$

All terms of this equation are collected on one side and rearranged as a function of R.

$$f(R) = A + B(lnR) + C(lnR)^3 + A - \frac{1}{T} \quad (8)$$

According to the Newton-Raphson method, the derivative of the defined $f(R)$ function is calculated.

$$f'(R) = \frac{B}{R} + \frac{3C(lnR)^2}{R} \quad (9)$$

$$R^{n+1} = R^n - \frac{f(R^n)}{f'(R^n)} \tag{10}$$

The resistance value of the thermistor at the desired temperature is given in (Eq.10). With an appropriate initial value R^0, the equation converges to the actual R value. The coefficients of the Steinhart-Hart equation can be calculated using the temperature-resistance data provided in the thermistor's datasheet. At least three temperature-resistance pairs are required to determine the coefficients A, B and C.

$$\frac{1}{T} = A + B(lnR) + C(lnR)^3$$

$$\begin{bmatrix} 1 & (lnR1) & (lnR1)^3 \\ 1 & (lnR2) & (lnR2)^3 \\ 1 & (lnR3) & (lnR3)^3 \\ 1 & (lnR4) & (lnR4)^3 \end{bmatrix} \begin{bmatrix} A \\ B \\ C \end{bmatrix} = \begin{bmatrix} \frac{1}{T1} \\ \frac{1}{T2} \\ \frac{1}{T3} \\ \frac{1}{T4} \end{bmatrix} \tag{11}$$

$$\begin{bmatrix} 1 & \ln(129900) & (ln129900)^3 \\ 1 & \ln(15711) & (ln15711)^3 \\ 1 & \ln(2982.3) & (ln2982.3)^3 \\ 1 & \ln(582.84) & (ln582.84)^3 \end{bmatrix} \begin{bmatrix} A \\ B \\ C \end{bmatrix} = \begin{bmatrix} \frac{1}{248.15} \\ \frac{1}{288.15} \\ \frac{1}{328.15} \\ \frac{1}{378.15} \end{bmatrix} \tag{12}$$

Table 3

Coefficient	Value
A	0.001140955366834
B	0.000232270224406
C	0.000000094355015

The coefficients A, B, and C of the Steinhart-Hart equation, derived from the solution of the selected temperature-resistance pairs shown in (Eq.12), are presented in Table 3.

3.2 Application to the Hoge-3 Equation

The method previously applied to the Steinhart-Hart equation can also be used for the Hoge-3 equation. In this approach, the nonlinear characteristic of the thermistor is transformed into a linear form as a result of the iteration.

$$\frac{1}{T} = A_0 + A_1 lnR + A_2(lnR)^2 + A_3(lnR)^3 + A_4(lnR)^4$$

All terms of this equation are collected on one side and rearranged as a function of R.

$$f(R) = A_0 + A_1 lnR + A_2(lnR)^2 + A_3(lnR)^3 + A_4(lnR)^4 - \frac{1}{T} \tag{13}$$

According to the Newton-Raphson method, the derivative of the defined $f(R)$ function is calculated.

$$f'(R) = \frac{A_1}{R} + \frac{2A_2(lnR)}{R} + \frac{3A_3(lnR)^2}{R} + \frac{4A_4(lnR)^3}{R} \tag{14}$$

$$R^{n+1} = R^n - \frac{f(R^n)}{f'(R^n)}$$

The resistance value of the thermistor at the desired temperature is given in (Eq.10). With an appropriate initial value R^0, the equation converges to the actual R value. Previously, we obtained four temperature-resistance pairs from the thermistor datasheet to calculate the coefficients of the Steinhart-Hart equation. However, since the Hoge-3 equation has five coefficients, at least five temperature-resistance pairs are required.

$$\frac{1}{T} = A_0 + A_1 lnR + A_2(lnR)^2 + A_3(lnR)^3 + A_4(lnR)^4$$

$$\begin{bmatrix} 1 & (lnR1) & (lnR1)^2 & (lnR1)^3 & (lnR1)^4 \\ 1 & (lnR2) & (lnR2)^2 & (lnR2)^3 & (lnR2)^4 \\ 1 & (lnR3) & (lnR3)^2 & (lnR3)^3 & (lnR3)^4 \\ 1 & (lnR4) & (lnR4)^2 & (lnR4)^3 & (lnR4)^4 \\ 1 & (lnR5) & (lnR5)^2 & (lnR5)^3 & (lnR5)^4 \end{bmatrix} \cdot \begin{bmatrix} A_0 \\ A_1 \\ A_2 \\ A_3 \\ A_4 \end{bmatrix} = \begin{bmatrix} \frac{1}{T1} \\ \frac{1}{T2} \\ \frac{1}{T3} \\ \frac{1}{T4} \\ \frac{1}{T5} \end{bmatrix} \quad (15)$$

Table 4

Coefficient	Value
A_0	0.001179345270652
A_1	0.000216702267954
A_2	0.000002266287993
A_3	-0.000000045569392
A_4	0.000000003074864

While performing these calculations, the beta (β) value was taken as a constant 3984.

3.3. Application of the Basic Equation

The Basic Equation (Eq.3) is given again as follows

$$R_T = R_{T0}\exp\left(ß\left(\frac{1}{T} - \frac{1}{T_O}\right)\right)$$

Where R_T is the resistance of thermistor at temperature T(K), R_{T0} is the resistance of thermistor at the nominal operating temperature at T_O, ß is the coefficient (Chen, 2009). Some resistance values of the NTC thermistor between 25°C and 85°C have been calculated in Table 5.

Table 5

Temperature (K)	Calculated Resistance (Ω)	Nominal Temperature T0 (K)	Nominal Resistance R0 (Ω)
313.15	5272,59	298.15	10000
328.15	2947,55	298.15	10000
338.15	2058,42	298.15	10000
348.15	1467.45	298.15	10000

While performing these calculations, the beta (β) value was taken as a constant 3984.

4. COMPARISON OF EQUATION RESULTS

The resistance values and error rates of three different equations used for the NTC thermistor over a specific temperature range are presented in Table 6. Due to the constant beta value used in the Basic equation, the error rate is significantly higher at lower temperatures compared to the Steinhart-Hart and Hoge-3 equations. Among all the equations, the Hoge-3 equation provided the most accurate results with the lowest error rate.

Table 6

Temperature (K)	Actual Resistance (Ω)	Resistance from Basic Equation (Ω)	Resistance from Steinhart-Hart Equation (Ω)	Resistance from Hoge-3 Equation (Ω)	Error of Basic Equation (%)	Error of Steinhart-Hart Equation (%)	Error of Hoge-3 Equation (%)
248.15	129900,00	147671,35	129884,9	129899,99	13,681	0,012	0,000
253.15	96761	107542,76	96780,74	96762,07	11,143	0,020	0,001
258.15	72765	79286,79	72796,08	72765,44	8,963	0,043	0,001
268.15	42268	44591,34	42295,91	42267,99	5,497	0,066	0,000
273.15	32624	33973,35	32646,54	32624,13	4,136	0,069	0,000
288.15	15711	15899,95	15718,72	15710,99	1,203	0,049	0,000
313.15	5323,9	5272,59	5322,56	5323,89	0,964	0,025	0,000
328.15	2982,3	2947,55	2980,48	2982,36	1,165	0,061	0,002
338.15	2078,7	2058,42	2077,15	2078,73	0,976	0,075	0,001
348.15	1475,9	1467,45	1474,87	1475,98	0,573	0,070	0,005
363.15	911,59	914,71	911,19	911,58	0,342	0,044	0,001
378.15	582,84	591,96	582,97	582,78	1,565	0,022	0,010

5. MNA-BASED CIRCUIT SOLUTION USING THE LINEARIZED MODEL OF AN NTC THERMISTOR

The NTC thermistor is used in an op-amp circuit to control the output voltage based on temperature. In the circuit built with an OP07 op-amp powered by a 6V supply, all components except for the NTC thermistor's resistance value are kept constant. This allows the output voltage of the op-amp and thus the circuit's output voltage to be controlled solely by the temperature variation of the thermistor. The circuit used in this study is shown in Figure 1.

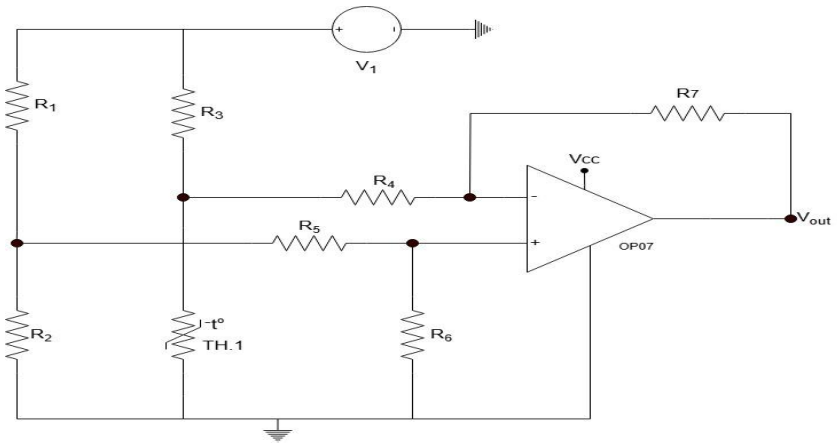

Figure 1.

Table 7

Circuit Parameters	Value	Unit
R_1	10K	Ω
R_2	10K	Ω
R_3	30K	Ω
R_4	100K	Ω
R_5	100K	Ω
R_6	220K	Ω
R_7	150K	Ω
Vcc	6	V
V_1	6	V

By keeping the circuit parameters provided in Table 7 constant, the effect of the temperature change of the TH.1 thermistor between 5°C and 105°C on the output voltage has been investigated. First, a simulation was performed, and the output voltage of the circuit was observed at the corresponding temperature values. Then, the output voltage was observed at the same temperature values using the MNA method. The matrix equation created for the MNA method is shown in Eq.(16).

$$\begin{bmatrix} G_{R3}+G_{R1} & -G_{R1} & -G_{R3} & 0 & 0 & 0 & 0 & -1 \\ -G_{R1} & G_{R1}+G_{R2}+G_{R5} & 0 & 0 & -G_{R5} & 0 & 0 & 0 \\ -G_{R3} & 0 & G_{R3}+G_{R4}+G_{R_{ntc}} & -G_{R4} & 0 & 0 & 0 & 0 \\ 0 & 0 & -G_{R4} & G_{R4}+G_{R7} & 0 & -G_{R7} & 0 & 0 \\ 0 & -G_{R5} & 0 & 0 & G_{R6}+G_{R5} & 0 & 0 & 0 \\ 0 & 0 & 0 & -G_{R7} & 0 & G_{R7} & -1 & 0 \\ 1 & 0 & 0 & 0 & 0 & 0 & 0 & 0 \\ 0 & 0 & 0 & 1 & -1 & 0 & 0 & 0 \end{bmatrix} \cdot \begin{bmatrix} V_a \\ V_b \\ V_c \\ V_d \\ V_e \\ V_f \\ I_o \\ I_{V1} \end{bmatrix} = \begin{bmatrix} 0 \\ 0 \\ 0 \\ 0 \\ 0 \\ 0 \\ 1 \\ 0 \end{bmatrix} \cdot \begin{bmatrix} V_1 \end{bmatrix} \tag{16}$$

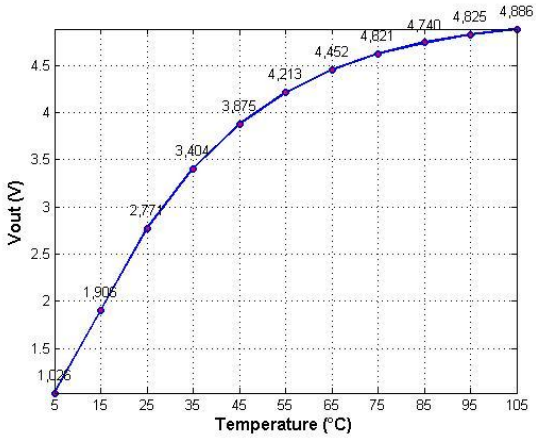

Figure 2. The effect of temperature change on the output voltage obtained using the MNA method with the Basic Equation.

Table 8. LTspice simulation results showing the effect of temperature change on the output voltage using the Basic Equation.

Temperature	Vout	Unit
5 °C	1,026	V
15 °C	1,966	V
25 °C	2,771	V
35 °C	3,404	V
45 °C	3,875	V
55 °C	4,213	V
65 °C	4,452	V
75 °C	4,620	V
85 °C	4,740	V
95 °C	4,825	V
105 °C	4,886	V

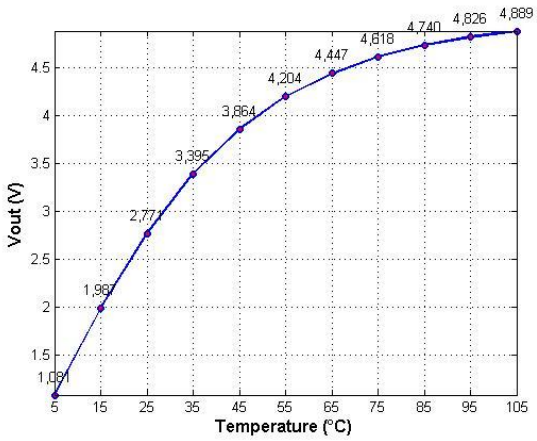

Figure 3. The effect of temperature change on the output voltage obtained using the MNA method with the Steinhart-Hart Equation.

Table 9. LTspice simulation results showing the effect of temperature change on the output voltage using the Steinhart-Hart Equation.

Temperature	Vout	Unit
5 °C	1,081	V
15 °C	1,987	V
25 °C	2,771	V
35 °C	3,395	V
45 °C	3,864	V
55 °C	4,204	V
65 °C	4,447	V
75 °C	4,618	V
85 °C	4,740	V
95 °C	4,826	V
105 °C	4,889	V

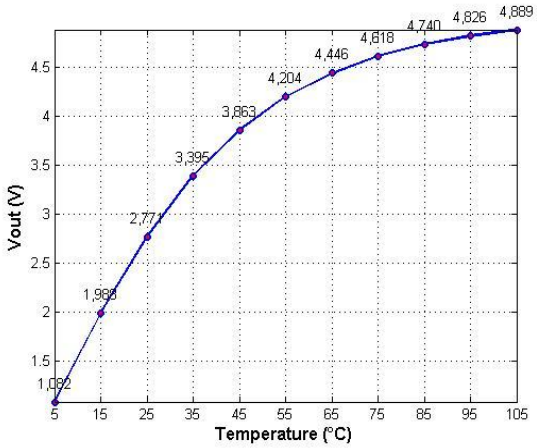

Figure 4. The effect of temperature change on the output voltage obtained using the MNA method with the Hoge-3 Equation.

Table 10. LTspice simulation results showing the effect of temperature change on the output voltage using the Hoge-3 Equation.

Temperature	Vout	Unit
5 °C	1,082	V
15 °C	1,988	V
25 °C	2,771	V
35 °C	3,395	V
45 °C	3,863	V
55 °C	4,204	V
65 °C	4,446	V
75 °C	4,618	V
85 °C	4,740	V
95 °C	4,826	V
105 °C	4,889	V

6. CONCLUSIONS AND DIRECTIONS FOR FUTURE RESEARCH

In this study, the nonlinear behavior of a Negative Temperature Coefficient (NTC) thermistor is successfully linearized using the Newton-Raphson method. Error rates of three different equations (Basic Equation, Steinhart-Hart Equation, and Hoge-3 Equation), which describe the temperature-resistance relationship of the thermistor, are calculated and analyzed over a specific temperature range using the Modified Nodal Analysis (MNA) method on an operational amplifier-based circuit. The theoretical results obtained through MNA closely match the simulation data, and among the models examined, the Hoge-3 Equation demonstrates the highest accuracy with the lowest error rates. The integration of the NTC thermistor into the MNA-based circuit analysis makes this study distinctive. In future work, the performance of the NTC thermistor in combination with various circuit elements can be explored, enabling the design of advanced circuits for highly sensitive temperature measurement and control applications..

Funding
The authors declared that this study has been supported by Sarsılmaz Silah Sanayi A.Ş.

REFERENCES

Akram, S., & Ann, Q. U. (2015). Newton Raphson Method. *International Journal of Scientific & Engineering Research*, 6(7), 1748. ISSN 2229-5518.

Analog Devices, Inc. (2024). LTspice (Version 24.0.12) [Computer software]. https://www.analog.com/en/design-center/design-tools-and-calculators/ltspice.html

Chen, C. (2009). Evaluation of resistance–temperature calibration equations for NTC thermistors. *Measurement*, 42(7), 1103–1111. https://doi.org/10.1016/j.measurement.2009.03.004

Çınar, M. A., & Yıldız, A. B. (2006). Time-domain analysis of transformers using generalized nodal equations. *IEEE Proc., Power Systems Conference and Exposition (PSCE 2006)*, Nov. 2006, Atlanta-USA.

Cong, Y., Wang-Chao, Z., Bin, S., & Hang-Xia, Z. (2011). Study on NTC thermistor characteristic curve fitting methods. *2011 International Conference on Computer Science and Network Technology*, China Jiliang University, Hangzhou, China.

Erdei, Z., Disco, A., Neamt, L., & Chiver, O. (n.d.). Symbolic equation using Modified Nodal Analysis for linear electrical circuit using Matlab. *Proceedings of the 4th European Computing Conference*, 430083. North University of Baia Mare.

How2Electronics. (2022). Temperature to Voltage Converter using Thermistor & Op-Amp 741. Retrieved from https://how2electronics.com/temperature-to-voltage-converter-using-thermistor-741/

Keskin, A. Ü. (2005). A simple analog behavioural model for NTC thermistors including self-heating effect. *Sensors and Actuators A: Physical*, 118(2), 244–247.

Keskin, A. Ü., & Yanar, T. M. (2004). Steady-state solution of loaded thermistor problems using an electrical equivalent circuit model. *Measurement Science and Technology*, 15, 2163.

Steinhart, J. S., & Hart, S. R. (1968). Calibration curves for thermistors. *Deep-Sea Research*, 15, 497–503.

The MathWorks, Inc. (2013). MATLAB (Version R2013a) [Computer software]. https://www.mathworks.com/products/matlab.html

Thangamalar, J. B., Gomathi, R., Gopalakrishnan, S., & Jackson, B. (2025). A two-stage linearized model for thermistor circuit linearization using LSTM-based multi-layer self-attention model. *Measurement*, 246, 116733.

Vishay Intertechnology, Inc. (2024). NTC thermistor datasheet (Document Number: 29131). Retrieved April 17, 2025, from https://www.vishay.com/docs/29131/ntcaimme3c90373.pdf

Yıldız, A. B. (2024). *Numerical methods for analyzing electrical circuits: Graduate course notes*. Kocaeli University, Department of Electrical Engineering.

Application of Electrical Filtering Techniques to Mechanical Filtering System by Analogy

ÇAĞATAY GÜLER[1], ALI BEKIR YILDIZ[2]

Abstract: Analogy is the establishment of similarities between systems. Through these analogies, systems become more understandable for both sides. There are many similarities between electrical systems and mechanical systems. In this study, an analogy will be established between an electrical system and a mechanical system, and mathematical and physical relationships will be obtained. To make these relationships more solid, practical electrical systems will be applied in mechanical systems through the obtained relationships. Another goal of the study is to demonstrate the positive effect of analogy in teaching a concept. Firstly, an analogy will be made between a tank circuit and a simple spring system, which have very similar operating principles, and relationships will be obtained. With the help of these relationships, electrical filtering techniques such as low-pass filters and harmonic filters will be applied to mechanical filtering systems. The results in both systems will be analyzed in detail, and the consistency of the applications will be tested.

Keywords: Analogy, Frequency Selector, Resonance, Filtering.

[1]**Address:** Kocaeli University, Faculty of Engineering, Kocaeli/Turkiye
[2]**Address:** Kocaeli University, Faculty of Technology, Kocaeli/Turkiye

***Corresponding author**: cagatayguler43@gmail.com

1. INTRODUCTION

Analogies are frequently drawn between electrical and mechanical systems. Establishing correlations between electrical and mechanical elements is among the most commonly used methods (Akbaba et al., 2022; Bloch, 1945; Akbaba 2021; Lopez-Martinez et al., 2021). In this study, practical counterparts of physical electrical systems will be adapted to mechanical systems using the correlations obtained. Similarly, many electrical and mechanical systems are analyzed using these analogies. Following this approach, equivalent models of complex rotational systems have also been developed (Tchakoua et al., 2015a, 2015b; Yildiz, 2012). In addition, the dynamics of mechanical systems have been investigated using electrical-mechanical analogies (Antonio, 2008). This study will particularly explore how closely the behaviors observed in electrical circuits align with the dynamic characteristics of mechanical systems. Moreover, there are studies analyzing practical systems through such analogical approaches (Nasim, 2023). The analogy method has also been applied in various fields such as the modeling and control of dampers Pehlivan, 2018; Xu, 2013; Jiamei 2010).

This study primarily aims to focus on theoretical foundations, although its practical applicability is also acknowledged. The purpose of the analogy is to demonstrate that a physical phenomenon in one system can be meaningfully applied to another system based on fundamental principles. In this study, with the help of analogical relationships, electrical low-pass/high-pass filter systems will be applied to mechanical filtering systems, and the feasibility and consistency of such designs will be demonstrated. A common physical phenomenon such as resonance, along with the filtering function in electrical systems, will likewise be applied to mechanical systems. Another aim of this study is to show that this approach can be beneficial in educational contexts, particularly in helping individuals with a mechanical background to understand electrical systems more effectively. Initially, an analogy will be drawn between two systems with highly similar operating principles: the tank (LC) circuit and a simple spring-mass system. These systems are highly suitable for analogy due to similarities such as capacitor charging versus spring compression, kinetic energy stored by a moving mass versus magnetic energy stored by current in an inductor, and so on. Non-ideal models of both systems will be addressed. This approach will also facilitate easier investigation of phenomena such as energy transfer and energy damping. In doing so, all necessary relationships will be obtained more clearly. Subsequently, to reinforce these correlations and the analogy itself, two electrical filtering techniques will be applied to mechanical filtering systems using the derived relationships. These applications will include low-pass filtering and harmonic filtering. The systems will be analyzed for all major states, simultaneous simulations will be presented, and all results will be compared and interpreted.

2. ANALOGY BETWEEN THE TANK CIRCUIT AND THE SPRING-MASS SYSTEM

In order to apply electrical filtering techniques to mechanical filtering systems, an analogy will first be drawn between two highly similar systems. The tank circuit (parallel LC circuit) and the spring-mass system both operate as oscillators. Their similar operating principles facilitate the development of an analogical approach. The practical (non-ideal) models of both systems will be considered, in order to account for all influencing factors in each system. For this reason, effects such as the internal resistance of the inductor and frictional forces will be taken into account. Initially, the state-space

equations of the two systems will be derived, followed by their time-dependent simulations. Using the similarity between their equations, corresponding relationships will then be established and presented in a tabular format.

The systems in question are illustrated in Figures 1 and 2. The state equations will be obtained based on the charged state of the capacitor and the compressed state of the spring—that is, the configurations in which the systems have reached certain potential energy levels. First, the electrical system will be analyzed, followed by the mechanical system.

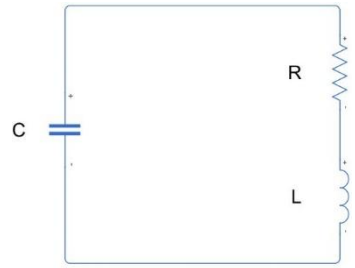

Figure 1. Tank Circuit

Figure 2. Mass-Spring System

State-space equations for the electrical system:

$$\begin{aligned} C\frac{dU_C}{dt} &= I_L \\ L\frac{dI_L}{dt} &= -U_C - U_R \end{aligned} \tag{1}$$

By considering the voltage drop across the resistor $U_R=R.I_L$, the equation is rearranged as follows:

$$\begin{aligned} C\frac{dU_C}{dt} &= I_L \\ L\frac{dI_L}{dt} &= -U_C - I_L \end{aligned} \tag{2}$$

In the state-space equations in Eq. (2), the values used are: $U_C(0)$= 10V, R=1Ω, L=1H, C=1F.

The time-dependent behaviors of the capacitor voltage and the inductor current are shown in Figure 3.

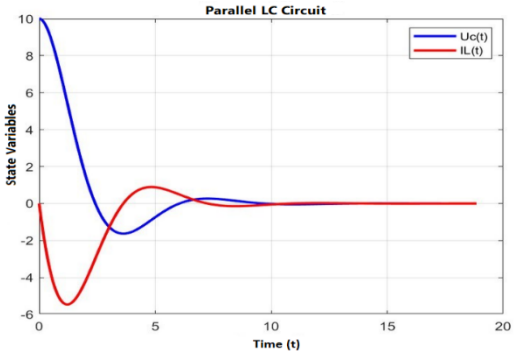

Figure 3. Time-Domain Simulation of the Tank Circuit

As expected, the system exhibits oscillatory motion for a certain period, and this oscillation gradually damps out over time.

The spring-mass system shown in **Figure 2** will be analyzed using its corresponding state-space equations. It is known that the derivative of position (x) corresponds to velocity. Accordingly, the state-space equations for the mechanical system are given in **Equation (3)**.

$$\begin{aligned} \frac{dx}{dt} &= v \\ F - F_S &= -kx \\ F_S &= -cv \\ m\frac{dv}{dt} &= -kx - cv \end{aligned} \tag{3}$$

The values used in the state-space equations in **Equation (3)** are as follows:

x(0)= 10m, c=1N.s/m, m=1kg, k=1 N/m

The time-dependent behaviors of the position and velocity are shown in **Figure 4**.

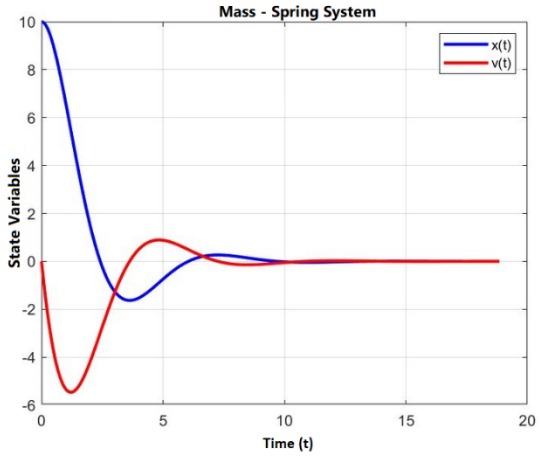

Figure 4. Time-Domain Simulation of the Spring-Mass System

The system's response is identical to that of the electrical system. The fact that the behaviors of both systems are the same forms the foundation of our analogical approach. Using loop equations for the electrical system and force equations for the mechanical system, the corresponding analogies will be established. These analogies will then be presented in tabular form.The loop equations for the tank circuit and the force equations for the mechanical system werepreviously derived.

If both equations are rearranged to allow for direct comparison and analogy:

$$\begin{aligned} \frac{dv}{dt} &= -\frac{kx}{m} - \frac{cv}{m} \\ \frac{dI_L}{dt} &= -\frac{q_C}{LC} - \frac{RI_L}{L} \end{aligned} \tag{4}$$

As clearly seen in **Equation (4)**, the characteristics of the equations are entirely analogous. The only noticeable difference is the inverse relationship between the capacitance and the spring constant. Taking this into consideration, the corresponding analogies are presented in **Table 1**.

Table 1.

Electrical	Mechanical
Voltage (U)	Force (F)
Current (I)	Velocity (v)
Electric Charge (q)	Position (x)
Inductance (L)	Mass (m)
Capacitance (C)	Inverse Spring Constant (k^{-1})
Resistance (R)	Damping Coefficient (c)

3. LOW-PASS FILTER APPLICATION

Filter circuits are widely used in electrical systems. These circuits generally have the ability to filter signals by selecting specific frequency ranges. Physical phenomena such as resonance are utilized in frequency selection. In this section, low-pass filters will be addressed. In general terms, low-pass filters are circuits that allow the passage of signals with low frequencies while attenuating high-frequency components. In a filtered signal, the frequency range that is blocked is called the stop band, whereas the range that is allowed to pass is called the pass band. The mechanical system will be designed based on an RC low-pass filter. The frequency that separates the pass band and stop band is referred to as the cutoff frequency. At this frequency, the output voltage is equal to 0.707 times (or $1/\sqrt{2}$ of) the input/source voltage. The cutoff frequency formula:

$$f_C = \frac{1}{2\pi RC} \tag{5}$$

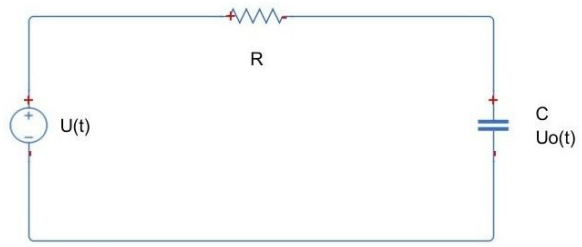

Figure 5. RC Low-Pass Filter

Figure 5 shows the RC low-pass filter. This RC low-pass filter will initially be examined for three different frequencies. Then, the equivalent mechanical filter will also be analyzed for the same frequencies, and the results will be compared with each other.The circuit will be analyzed for R = 100 Ω and C = 100 µF. In this case, according to Equation (5), the corner frequency (wc) will be 100 rad/s. In addition to this frequency, a low frequency (w = 20 rad/s) and a high frequency (w = 500 rad/s) will be considered. The three sources with these three different frequencies are:

$U_1(t) = 100\sin(20t)$ V
$U_2(t) = 100\sin(100t)$ V
$U_3(t) = 100\sin(500t)$ V

The circuit will be analyzed in the s-domain. The source voltage, circuit impedance, and circuit current will be expressed in the s-domain. Then, the voltages across the capacitor and resistor will be calculated. **Initially, the low-frequency source U1(t) will be examined.** The voltage source, circuit impedance, and current, as well as the voltages across the capacitor and resistor, will be expressed in the s-domain as follows:

$$U_1(s) = \frac{2000}{s^2+400}\ V$$
$$Z_C(s) = \frac{10^4}{s}\ \Omega\ ,\ R = 100\ \Omega$$
$$Z_1(s) = \frac{10^4}{s} + 100\ \Omega \tag{6}$$
$$I_1(s) = \frac{U_1(s)}{Z_1(s)}$$
$$U_R(s) = I_1(s).R\ V,\ U_C(s) = I_1(s).Z_C(s)\ V$$

The time-dependent variations of the voltages across the capacitor and resistor are shown in Figure 6.

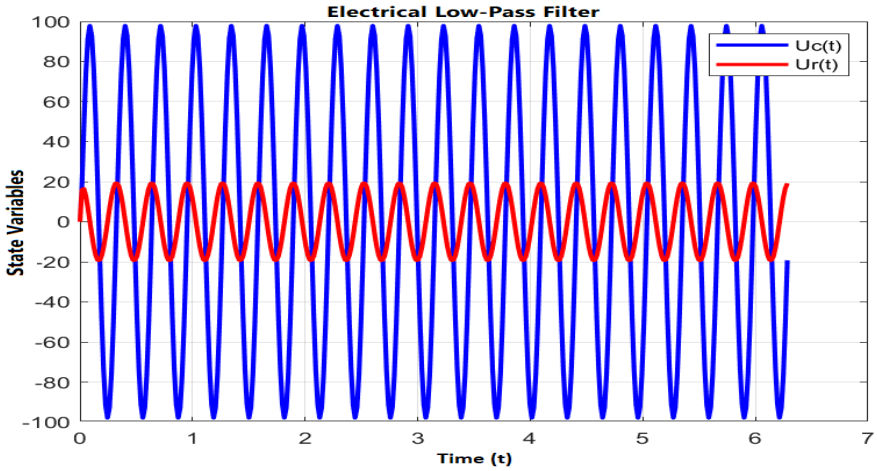

Figure 6. Low-Frequency Response of the RC Low-Pass Filter Circuit

Low-Frequency Response of the RC Low-Pass Filter CircuitAccording to Figure 6, the low-frequency voltage has been predominantly transferred to the output.

Now, the source U2(t) with the cutoff frequency component will be examined. The voltage source, circuit impedance, and current, as well as the voltages across the capacitor and resistor, will be expressed in the s-domain as follows:

$$U_2(s) = \frac{10^4}{s^2+10^4}\ V$$
$$Z_C(s) = \frac{10^4}{s}\ \Omega\ ,\ R = 100\ \Omega$$
$$Z_2(s) = \frac{10^4}{s} + 100\ \Omega \tag{7}$$
$$I_2(s) = \frac{U_2(s)}{Z_2(s)}$$
$$U_R(s) = I_2(s).R\ V,\ U_C(s) = I_2(s).Z_C(s)\ V$$

The time-dependent variations of the voltages across the capacitor and resistor are shown in Figure 7.

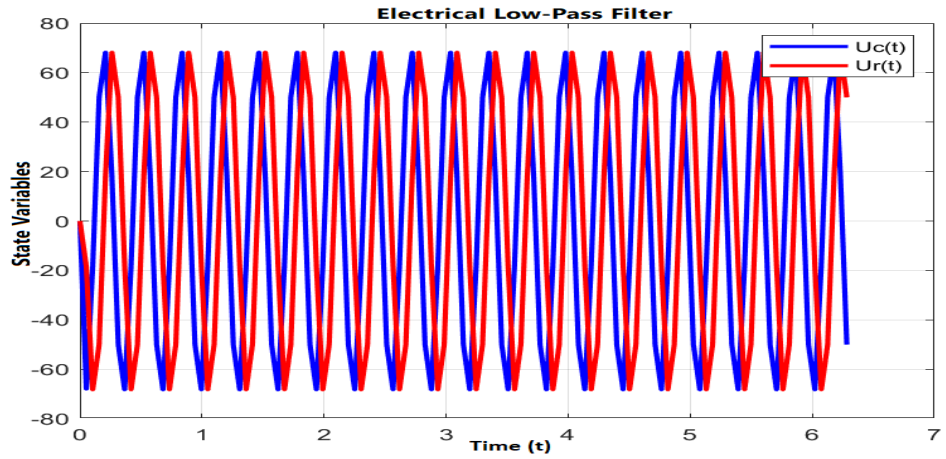

Figure 7. Cutoff Frequency Response of the RC Low-Pass Filter Circuit

Cutoff Frequency Response of the RC Low-Pass Filter CircuitAccording to Figure 7, the voltages across the two components are equal to each other, and these voltages are approximately equal to 0.707 times the source voltage. In this case, we can say that the cutoff frequency serves as a boundary. Now, the source U3(t) with the high-frequency component will be examined. The voltage source, circuit impedance, and current, as well as the voltages across the capacitor and resistor, will be expressed in the s-domain as follows:

$$U_3(s) = \frac{5.10^4}{s^2+25.10^4}\ V$$
$$Z_C(s) = \frac{10^4}{s}\ \Omega\ ,\ R = 100\ \Omega$$
$$Z_3(s) = \frac{10^4}{s} + 100\ \Omega \quad (8)$$
$$I_3(s) = \frac{U_3(s)}{Z_3(s)}$$
$$U_R(s) = I_3(s).R\ V,\ U_C(s) = I_3(s).Z_C(s)\ V$$

The time-dependent variations of the voltages across the capacitor and resistor are shown in Figure 8.

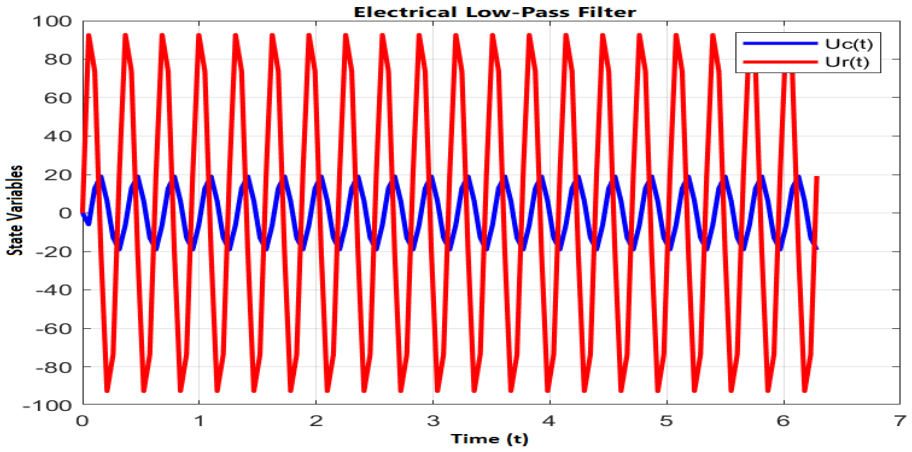

Figure 8. High Frequency Response of the RC Low-Pass Filter Circuit

According to Figure 8, the high-frequency component has not been allowed to pass to the output, effectively filtering out the high-frequency component. These analyses have been conducted to compare the operation principle of the low-pass filter with the results of the mechanical design analyses. Now, the design of the mechanical low-pass filter will be made.

The mechanical low-pass filter will be designed with the help of analogical relationships. From Table 1, the corresponding elements of the RC low-pass filter in mechanical systems will be selected. As a series circuit, a mechanical reference, a damper (c), a spring (k), and finally a sinusoidal force (F) with specific frequency components will be used. Each element will be connected in series. The schematic of the system is shown in Figure 9.

Figure 9. Mechanical Low-Pass Filter Design

$$f_c = \frac{k}{2\pi c} \quad (9)$$

The cutoff frequency of the system will be equal to the cutoff frequency of the RC filter, as expected. In this case, the three different forces applied to the system will be numerically equal to the sources in the electrical system.

$F_1(t) = 100\sin(20t)$ N
$F_2(t) = 100\sin(100t)$ N
$F_3(t) = 100\sin(500t)$ N

The system will be analyzed in the s-domain. The applied force, mechanical impedance, and velocity will be expressed in the s-domain. Then, the forces applied to the spring and damper elements will be calculated. Initially, the low-frequency force source F1(t) will be examined. The expressions of the force, mechanical impedance, velocity, and the forces applied to the spring and damper elements in the s-domain are:

$$
\begin{aligned}
F_1(s) &= \frac{2000}{s^2+400}\ N \\
Z_k(s) &= \frac{10^4}{s}\ \Omega\ ,\ c = 100\ N.s/m \\
Z_1(s) &= \frac{10^4}{s} + 100\ N.s/m \\
V_1(s) &= \frac{F_1(s)}{Z_1(s)} \\
F_c(s) &= F_1(s).R\ N,\ F_k(s) = F_1(s).Z_k(s)\ N
\end{aligned}
\tag{10}
$$

The time-dependent variations of the forces applied to the spring and damper elements are shown in Figure 10.

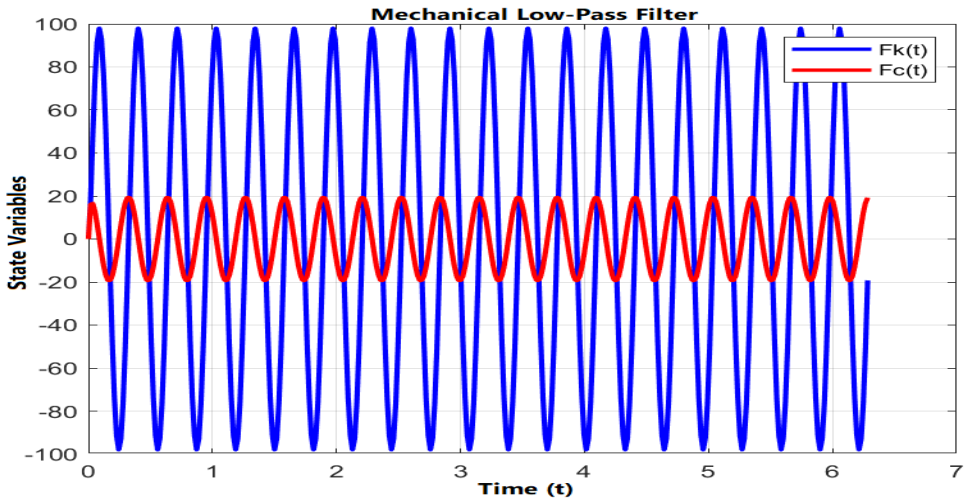

Figure 10. Low-Frequency Response of the Mechanical Low-Pass Filter

According to Figure 10, the low-frequency response of the mechanical low-pass filter is exactly similar to the response of the electrical low-pass filter. The force applied to the spring is much greater than that applied to the damper. The low-frequency force has been predominantly transferred to the output. Now, the force F2(t) with the cutoff frequency component will be examined. The expressions of the force, mechanical impedance, velocity, and the forces applied to the spring and damper elements in the s-domain are:

$$
\begin{aligned}
F_2(s) &= \frac{10^4}{s^2+10^4}\ N \\
Z_k(s) &= \frac{10^4}{s}\ \Omega\ ,\ c = 100\ N.s/m \\
Z_2(s) &= \frac{10^4}{s} + 100\ N.s/m \\
V_2(s) &= \frac{F_2(s)}{Z_2(s)} \\
F_c(s) &= F_2(s).R\ N,\ F_k(s) = F_2(s).Z_k(s)\ N
\end{aligned}
\tag{11}
$$

The time-dependent variations of the forces applied to the spring and damper elements are shown in Figure 11.

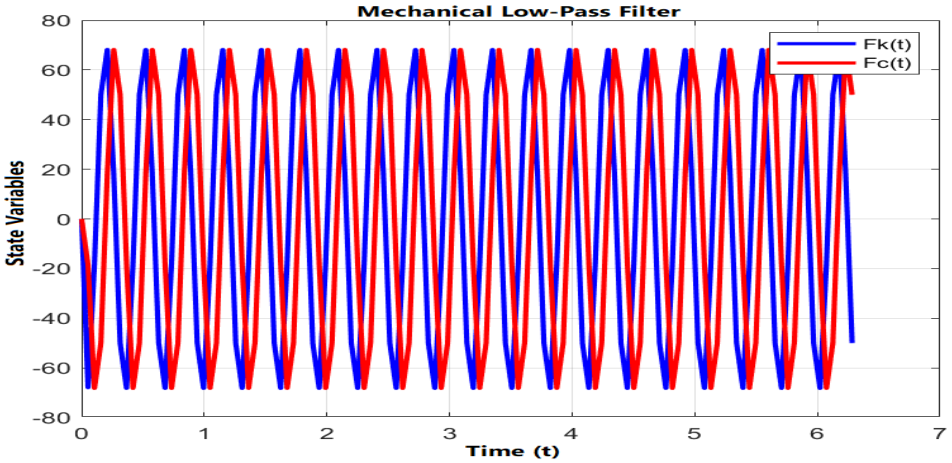

Figure 11. Cutoff-Frequency Response of the Mechanical Low-Pass Filter

According to Figure 11, the cutoff frequency response of the mechanical low-pass filter is exactly similar to the cutoff frequency response of the electrical filter. The forces applied to both elements are equal to each other. As in the electrical system, the cutoff frequency acts as a boundary between the passband and the stopband. Now, the force F3(t) with the high-frequency component will be examined. The expressions of the force, mechanical impedance, velocity, and the forces applied to the spring and damper elements in the s-domain are:

$$F_3(s) = \frac{5.10^4}{s^2+25.10^4}\ N$$
$$Z_k(s) = \frac{10^4}{s}\ \Omega\ ,\ c = 100\ N.s/m \tag{12}$$
$$Z_3(s) = \frac{10^4}{s} + 100\ N.s/m$$
$$V_3(s) = \frac{F_3(s)}{Z_3(s)}$$
$$F_c(s) = F_3(s).R\ N,\ F_k(s) = F_3(s).Z_k(s)\ N$$

The time-dependent variations of the forces applied to the spring and damper elements are shown in Figure 12.

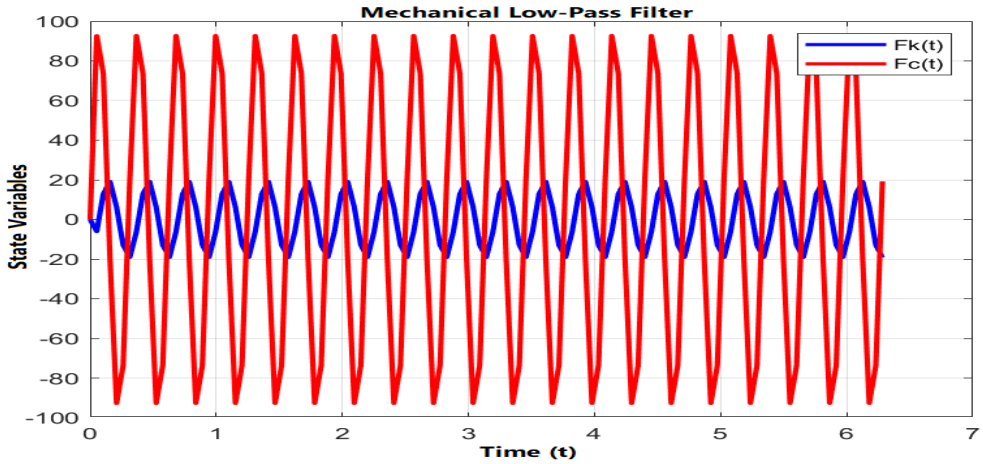

Figure 12. High Frequency Response of the Mechanical Low-Pass Filter

The high-frequency response of the mechanical low-pass filter, as expected, matches that of the electrical filter. The system has not allowed the passage of the high-frequency component, effectively filtering it out.

The mechanical low-pass filter serves the purpose of the design. The system has the ability to filter out high frequencies. The success of this design is based on analogical relationships. By using analogical relationships, it is also possible to design high-pass filters and even RL filters in the same way.

4. HARMONIC FILTER APPLICATION

In this section, the corresponding mechanical systems of harmonic filters designed by utilizing the resonance phenomenon in electrical systems will be discussed. The systems exhibit higher amplitude movements at certain frequencies. These frequencies are referred to as the resonance moment or resonance frequency. In a series circuit consisting of an inductor and a capacitor, the system achieves minimum impedance and maximum current by equalizing the capacitive and inductive reactances at certain frequencies. In this way, the entry of the harmonic component with the resonance frequency into the system is prevented.

The resonance frequency is:

$$f_r = \frac{1}{2\pi\sqrt{LC}} \tag{13}$$

By using analogical relationships, the mechanical resonance expression is:

$$f_r = \frac{1}{2\pi\sqrt{\frac{m}{k}}} \tag{14}$$

To better highlight their behavior at the resonance point, both systems will be examined as third-order filters. The third-order electrical harmonic filter and the third-order mechanical resonance filter are shown in Figure 13 and Figure 14.

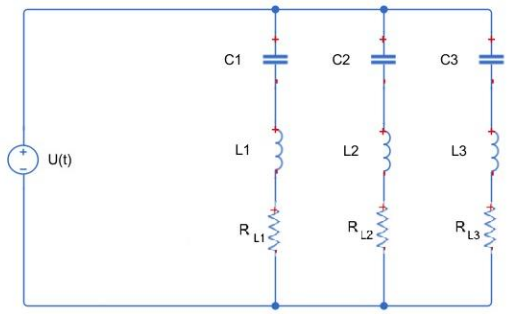

Figure 13. Third-Order Electrical Harmonic Filter

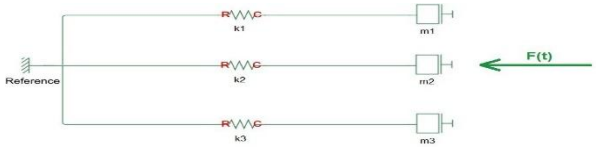

Figure 14. Third-Order Mechanical Harmonic Filter

Firstly, the electrical filter system will be analyzed, followed by the mechanical filter system, and the results will be compared. Simultaneously, analyses will be conducted based on the reduced form of the superposition theorem for the unwanted harmonic components of the systems. Since a common value selection method is used for both systems, the frequencies of the sources and forces (frequencies to be filtered, resonance frequencies) are determined to be the same. In the electrical system, simulations of the filter and output current will be obtained, while in the mechanical system, simulations of the filter (spring-mass) and output (damper) velocities will be obtained. The systems will be analyzed in the s-domain. Additionally, to make the system practical, the internal resistance of the coil and the friction acting on the masses will be considered. In the analysis, the internal resistance of the coil is taken as Riç = 1Ω. Due to the analogical relationships, the counterpart of this internal resistance will be a damper connected in series with the spring and mass, and the value of the damper will be c = 1 N.s/m. Three different harmonic frequencies have been selected for the electrical system:

$U_{h1}(t) = 10\sin(50t)$ V
$U_{h2}(t) = 10\sin(100t)$ V

$U_{h3}(t) = 10\sin(200t)$ V

The values of the capacitor and inductor for each harmonic are given below:

$L_1 = 1H,\ C_1 = 400$ uF

$L_2 = 1H,\ C_2 = 100$ uF

$L_3 = 1H,\ C_3 = 25$ uF

The corresponding harmonic representations of the system in the s-domain are given in equation (15). The circuit impedances and currents for each harmonic are expressed in equation (16).

$$U_{h1}(s) = \frac{500}{s^2+2500}\ V$$
$$U_{h2}(s) = \frac{1000}{s^2+10000}\ V \quad (15)$$
$$U_{h3}(s) = \frac{2000}{s^2+40000}\ V$$

$$Z_{f1}(s) = \frac{2500}{s}+s+1\ \Omega$$
$$Z_{f2}(s) = \frac{10^4}{s}+s+1\ \Omega \quad (16)$$
$$Z_{f3}(s) = \frac{4.10^4}{s}+s+1\ \Omega$$
$$I_{f1}(s) = \frac{U_h(s)}{Z_{f1}(s)}\ A,\ I_{f2}(s) = \frac{U_h(s)}{Z_{f2}(s)}\ A,\ I_{f3}(s) = \frac{U_h(s)}{Z_{f3}(s)}\ A$$

The time-dependent graphs of the steady-state circuit currents for each harmonic are shown in Figures 15, 16, and 17.

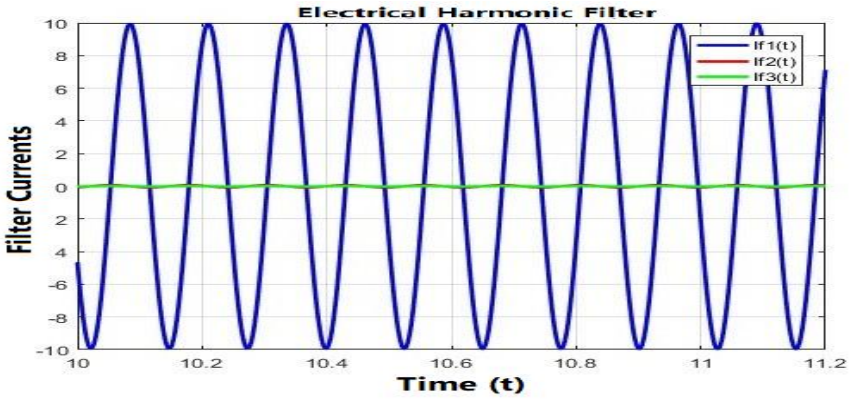

Figure 15. Steady-State Response of the Circuit at Resonance for Filter 1

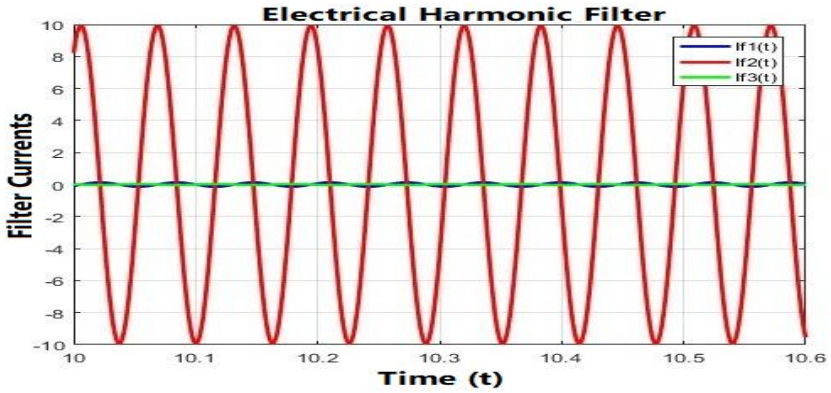

Figure 16. Steady-State Response of the Circuit at Resonance for Filter 2

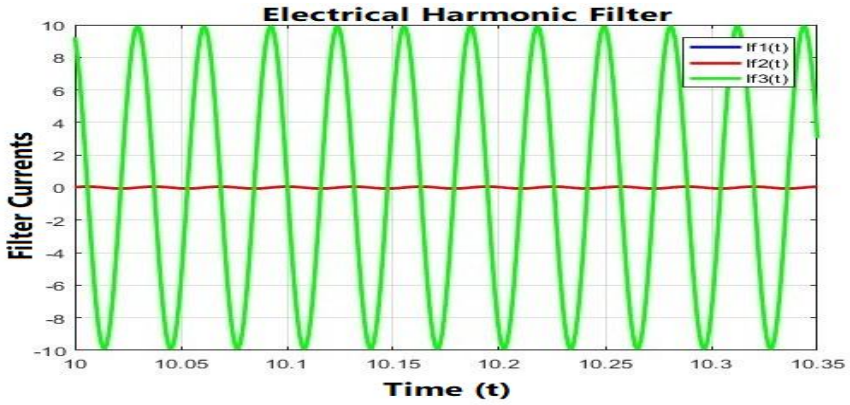

Figure 17. Steady-State Response of the Circuit at Resonance for Filter 3

As can be seen from the figures, each filter branch has passed the harmonic component at its respective frequency.

The same steps will be applied to the mechanical filter system, and the harmonic components and element values to be applied to the system are given below.

$F_{h1}(t) = 10\sin(50t)$ N
$F_{h2}(t) = 10\sin(100t)$ N
$F_{h3}(t) = 10\sin(200t)$ N

$m_1 = 1$ kg, $k_1 = 2500$ N/m

$m_2 = 1$ kg, $k_2 = 104$ N/m

$m_3 = 1$ kg, $k_3 = 4.104$ N/m

The corresponding expressions of the system's harmonics in the s-domain are given in equation (17). The mechanical impedances and velocities for each harmonic are expressed in equation (18).

$$F_{h1}(s) = \frac{500}{s^2+2500}\ N$$
$$F_{h2}(s) = \frac{1000}{s^2+10000}\ N \quad (17)$$
$$F_{h3}(s) = \frac{2000}{s^2+40000}\ N$$

$$Z_{f1}(s)=\frac{2500}{s}+s+1\ \ N.s/m$$
$$Z_{f2}(s)=\frac{10^4}{s}+s+1\ \ N.s/m \tag{18}$$
$$Z_{f3}(s)=\frac{4.10^4}{s}+s+1\ \ N.s/m$$
$$V_{f1}(s)=\frac{F_h(s)}{Z_{f1}(s)}\ m/s\ ,\ V_{f2}(s)=\frac{F_h(s)}{Z_{f2}(s)}\ m/s\ ,\ V_{f3}(s)=\frac{F_h(s)}{Z_{f3}(s)}\ m/s$$

The time-dependent graphs of the steady-state velocity responses for each harmonic are shown in Figures 18, 19, and 20.

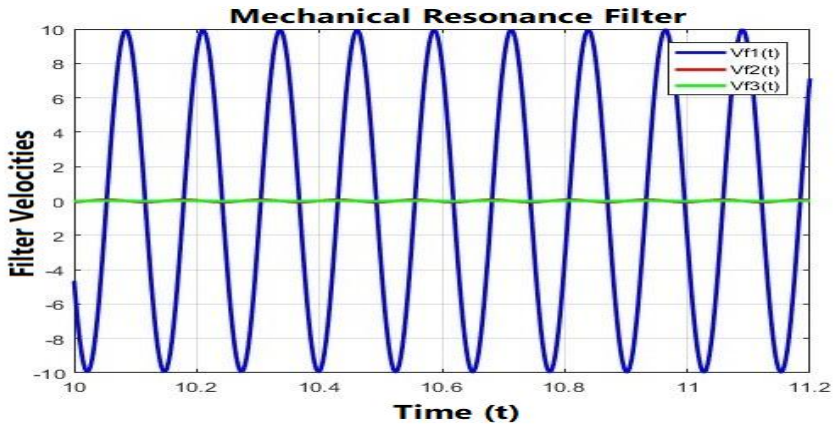

Figure 18. Steady-State Response at Resonance for Filter 1

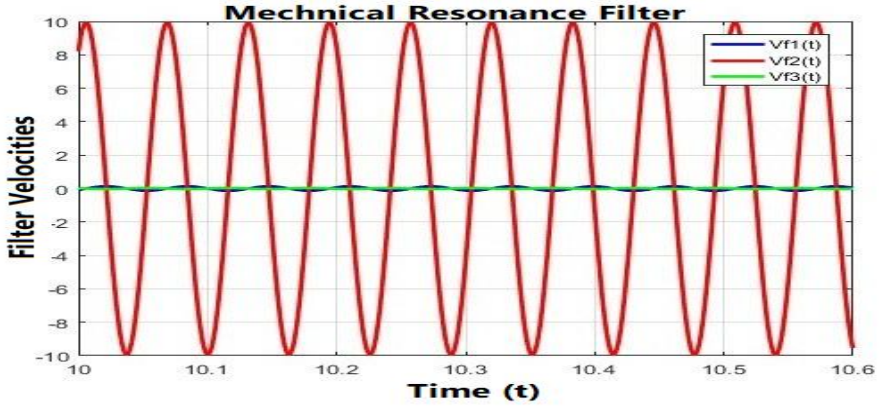

Figure 19. Steady-State Response at Resonance for Filter 2

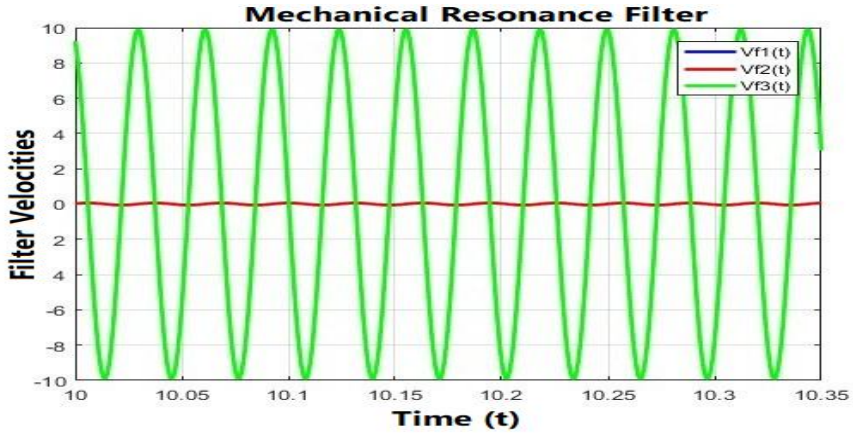

Figure 20. Steady-State Response at Resonance for Filter 3

As a result, the mechanical resonance filter operates similarly to electrical systems. It successfully selects unwanted or desired frequencies. Filters at resonance absorb all the energy.

5. CONCLUSION

The analyses and comparisons of the systems demonstrate the power of the analogical approach. It is also evident that many theoretical systems can be designed through analogy. The relationships between electrical and mechanical quantities and parameters have been established through analogy. Many electrical techniques can be applied to the design of mechanical systems using these methods. Beyond spring systems, similar approaches can be followed in other linear, rotational, and mechanical systems. Specifically for spring systems, filtering techniques can be combined to design more selective and complex filters. Additionally, this study clearly shows that analogy is an effective tool in the teaching phase of a concept.

REFERENCES

Mehmet A., Omar D., Byung-Seo K., Adnan Ç., Shahrudin Awang N. (2022). Electric Circuit-Based Modeling and Analysis of the Translational, Rotational Mechanical and Electromechanical Systems Dynamics, IEEE Access.

M. Akbaba, (2021). `Modeling and simulation of dynamic mechanical systems using electric circuit analogy, Turkish J. Eng., vol. 5, no. 3, pp. 111_117.

A. Bloch, (1945)., Electromechanical Analogies And Their Use For The Analysis of Mechanical And Electromechanical Systems, J. Inst. Electr. Eng., I, Gen.,vol. 92, no. 52, pp. 157_169.

J. Lopez-Martinez, J. C. Martinez, D. Garcia-Vallejo, A. Alcayde, and F. G. Montoya, (2021). A new electromechanical analogy approach based on electrostatic coupling for vertical dynamic analysis of planar vehicle models, IEEE Access, vol. 9, pp. 119492_119502,

Antonio P., Angelo P, Giovanni F., Ferdinando De C., Fabio G., Luigi G., (2008). A modeling approach for engine dynamics based on electrical analogy, 17th World Congress The International Federation of Automatic Control.

Pierre T., Mohand O., Tommy Andy T. Gabriel E., ReneW., Fouad S., (2015a). “Basis of Theoretical Formulations for New Approach for Modelling Darrieus-Type Vertical Axis Wind Turbine Rotors using Electrical Equivalent Circuit Analogy”,2015 3rd International Renewable and Sustainable Energy Conference (IRSEC).

Pierre T., Mohand O., Tommy Andy T. Gabriel E., ReneW., Fouad S., (2015b). Development of Equivalent Electric Circuit Model for Darrieus-Type Vertical Axis Wind Turbine Rotor using Mechanic - Electric Analogy Approach, 2015 3rd International Renewable and Sustainable Energy Conference (IRSEC).

Ali Bekir Y., (2012).“Electrical equivalent circuit based modeling and analysis of direct current motors“, International Journal of Electric Power & Energy Systems, Vol.43, pp.1043-1047, Elsevier.

Development of a GUI for EMI Filter Insertion Loss and Transfer Function Modeling

ÇAĞATAY GÜLER[1], ERSOY KELEBEKLER[2]

Abstract: Electromagnetic compatibility (EMC) is one of the biggest problems in modern electrical devices, while the size of the electronic component is getting smaller and the clock speed is increasing. The clock frequencies have exceeded gigahertz in many applications. These conditions cause electronic devices to interact more with each other, and the signals required for their operation are perceived as noise by other circuits. The common and the most effective method to suppress electromagnetic noise is to use electromagnetic interference (EMI) filter, especially for conducted emission noise. The characteristics of filters are defined by their attenuation, also known as insertion loss (IL), which is function of frequency and expressed in decibels (dB). Most filter manufacturers provide graphs showing the frequency response of the insertion loss for matched source and load condition, 50 Ω. But, in reality, the source and load impedances are mismatched. In this study, for different kinds of EMI filters like RL Low-Pass, RC High-Pass, LC Band-Pass, and LC Band-Stop, analytic expressions of IL have been obtained in mismatched source/load impedances, and a graphic user interface has been designed to enable the analysis of the different impedance values observed in real-world applications. Other important parameters for EMI filters are the transfer function and bode diagram which supply phase and magnitude characteristics depending on the frequency. The transfer function and bode diagram for related EMI filters have been included on the GUI, as well. The designed GUI enable the user to change dynamically component values of the EMI filter in mismatched source/load impedances and to see the characteristics of the filter in these specific conditions.

Keywords: EMC, EMI Filter, Insertion Loss, Transfer Function, Mismatched Load

[1]**Address:** Kocaeli University, Faculty of Engineering, Kocaeli/Turkiye
[2]**Address:** Kocaeli University, Faculty of Technology, Kocaeli/Turkiye

***Corresponding author**: cagatayguler43@gmail.com

1. INTRODUCTION

Modern electrical devices generally require multiple power circuits that may demand different voltage levels. To ensure the proper operation of all systems, each of these circuits must either be supplied by a separate power source or the output voltage levels must be regulated in some manner from a common power source. This can be accomplished using either linear power converters or switched-mode DC-DC converters. However, linear converter topologies come with the disadvantage that the power to be dissipated must necessarily be converted into heat. A major issue with this is the need for large surface areas to dissipate the generated heat. If there is insufficient physical space available for cooling via heat transfer, or if it is necessary to reduce the negative impacts of this heat on the electronic board within the power conversion system, the topology must be changed. In switched-mode DC-DC converters, there are various design topologies such as buck, boost, buck-boost, boost-buck, flyback, Ćuk, and SEPIC. Compared to linear converters, these topologies require less physical space and reduce the amount of power dissipated across electronic components (Rashid, 2019). Therefore, switched-mode DC-DC converter topologies are more efficient than linear converters. However, despite these advantages, DC-DC converter topologies have greater electromagnetic compatibility (EMC) challenges due to the switching elements used. The noise generated by switched-mode power converters can adversely affect electronic circuits either through conducted emissions on transmission lines or through radiated emissions as electromagnetic waves.

Electromagnetic compatibility (EMC) is defined as the ability of a system or device to perform its intended functions within its electromagnetic environment without causing or suffering from unacceptable electromagnetic disturbances (Sevgi, 2009). EMC standards include measurement methodologies to assess whether devices can operate compatibly without interfering with each other or with the surrounding environment and nature, either through conducted transmission paths or radiation. A product's EMC capability — meaning its levels of conducted and radiated emissions and its immunity against external sources of interference — can only be evaluated through EMC testing. Devices that operate without being affected by the environment and other systems, and which likewise do not adversely affect other systems, are considered electromagnetically compatible. Electromagnetic interference (EMI) is the primary cause of EMC problems. EMI is defined as the phenomenon where disturbing electromagnetic signals generated by devices, systems, or natural sources cause temporary or permanent adverse effects on other devices and systems (Yıldız, 2020). Techniques such as filtering, grounding, shielding, and termination are employed to eliminate electromagnetic problems caused by EMI. Among these methods, filtering is the most effective technique used to suppress conducted noise. Filters are circuit elements that allow useful signals to pass through by remaining ineffective over a certain frequency range while attenuating unwanted signals in another frequency range (Ott, 2005; Paul, 2005). A general filter structure is shown in Figure 1.1.

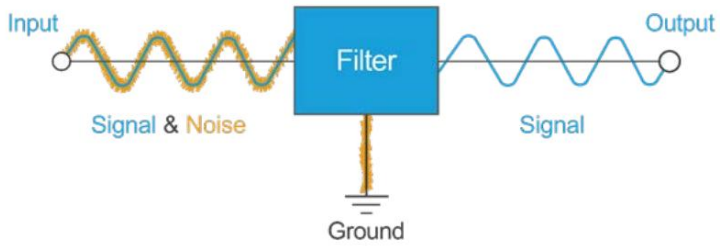

Figure 1.1. Basic EMI Filter Model

Power line EMI filters are the most effective tools for suppressing electromagnetic interference (EMI) occurring in power supply networks. Generally, the characteristics of filters are defined by their attenuation, also known as insertion loss, which is expressed in decibels (dB). Insertion loss corresponds to the reduction in load voltage at a particular frequency due to the insertion of the filter into the circuit. Typically, insertion loss is presented as a function of frequency. To determine the attenuation, a defined source and load are connected, and the signal coming from the source is measured. Then, the filter is inserted into the circuit, and the measurement is repeated. Insertion loss corresponds to the decrease in load voltage at the related frequency due to the addition of the filter. It is generally presented as a function of frequency. The insertion loss of a specific filter depends on the source and load impedances. Therefore, it cannot be expressed independently of the termination impedances. Most filter manufacturers provide graphs showing the frequency response of the insertion loss for a given filter. Since the insertion loss of a filter depends on the source and load impedances, manufacturers typically present the frequency-dependent insertion loss for cases where both the source and load impedances are equal to 50 ohms (Paul, 2005) . However, in practical applications, the source and load impedances are generally mismatched. In this study, insertion losses dependent on source and load impedances have been derived for different types of filters. In this way, unlike the ideal measurements with matched impedances provided by EMI filter manufacturers, the impedance mismatches commonly encountered in power line applications can be analyzed through the presented GUI application. In power lines, the ideally desired 50 Ω impedance cannot be achieved in most cases. Nicholson and Malack measured the impedance of an unfiltered AC power line at different locations in the United States within the 100 kHz–30 MHz range, as given below (Nicholson, Malack, 1973).

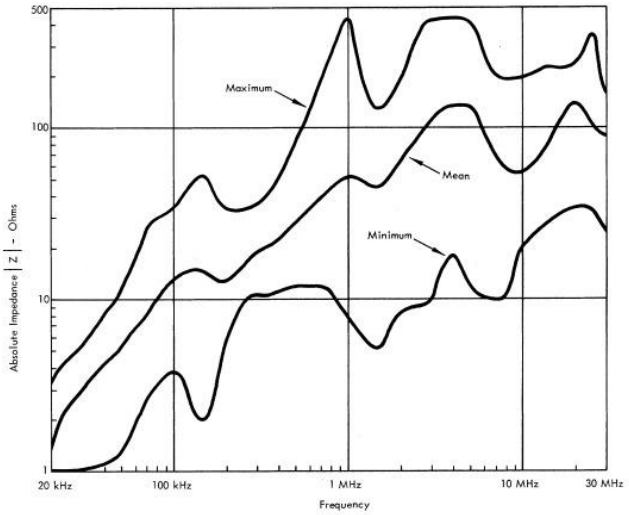

Figure 1.2. Impedance-Frequency Characteristic

As shown in the figure, power line impedance values vary approximately between 2 and 450 Ω. Considering this situation, the insertion loss characteristics provided by power line filter manufacturers for a 50 Ω matched source and load impedance become insufficient. The main objective of this study is to enable the analysis of the different impedance values observed in real-world power lines, which deviate from ideal conditions, as well as the mismatched load resistance conditions, through a designed graphical user interface (GUI). In this study, insertion loss expressions dependent on the source and load impedances have been obtained for different types of filters. Thus, unlike the ideal measurements provided by EMI filter manufacturers for matched conditions, the mismatches commonly encountered in power line applications can be modeled using the presented GUI tool.

2. EMC FILTERS AND INSERTION LOSS

EMC filters are designed to ensure the electromagnetic compatibility of devices and to block unwanted interference, and they play a critical role in increasing system efficiency. In many EMC suppression circuits, low-pass filters are commonly used to prevent the transmission of high-frequency interference (Roberts, Lametschwandtner, 2023). An electrical filter may be passive, active, analog, or digital. In general, there are four basic types and classifications of filters: low-pass filters, high-pass filters, band-pass filters, and band-stop filters (SCHAFFNER).
In this study, four different filter topologies will be examined: RL Low-Pass, RC High-Pass, LC Band-Pass, and LC Band-Stop. There is a LC Band-Pass filter in the Figure 2.1.

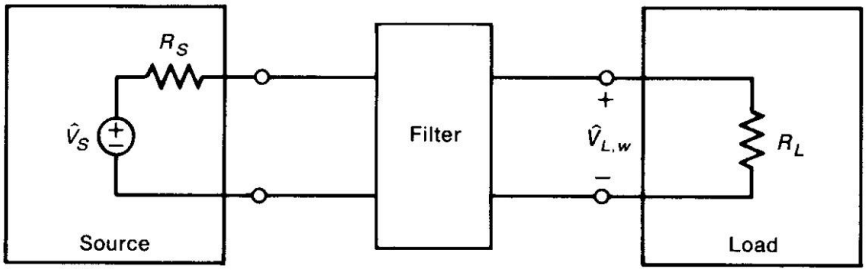

Figure 2.1. LC Band-Pass Filter

A fundamental characteristic of an EMC filter is typically defined by its insertion loss (IL). This characteristic is generally frequency-dependent and represents the attenuation provided by the EMC filter. When a component or group of components is placed between a source and a load, a portion of the signal from the source is absorbed by these components due to their internal resistive losses. Consequently, the signal delivered to the load is not as strong as it would be if the load were connected directly to the source. The resulting attenuation is referred to as insertion loss, and it is expressed in decibels (dB) (Bowick, 2008). Measuring insertion loss is complex from several perspectives. The configuration of the input and output terminals of the EMI filter varies depending on the measurement setup, which complicates the measurement process. Another issue arises from undefined impedance terminals on the input and output sides of the filter. The impedance of the power supply network is connected to the input terminals of the EMI filter. The actual impedance value of the power supply network depends on the type of power grid, the current load, and the operating frequency of the test signal. The output of the filter is typically terminated with an impedance, which is often unknown and not constant in the time domain (Ozenbaugh, Pullen, 2001). Insertion loss is the logarithm of a ratio. Specifically, it is the ratio between the output power without the filter and the output power with the filter inserted. The general formula derived from this relationship is given below.

$$IL_{dB} = 10\log\left(\frac{P_{L,wo}}{P_{L,w}}\right) \tag{1}$$

In fact, output power is the ratio of the square of the output voltage to the load resistance. Taking this into account, the equation can be rearranged, and the generalized formula becomes as follows:

$$IL_{dB} = 20\log\left(\frac{V_{L,wo}}{V_{L,w}}\right) \tag{2}$$

Adapting the general formula to the circuit models given above (Figures 2.1, 2.2, 2.3, 2.4) will facilitate our analysis of the respective filter configurations. For the RL Low-Pass Filter, the general formula will be derived step by step in order to demonstrate the underlying logic and methodology. For the other three topologies, the derivations will be omitted, and only their respective general formulas will be provided.

$$V_{L,wo} = U(t).\frac{R}{R+R_S}$$
$$V_{L,w} = U(t).\frac{R}{R+R_S+jwL} \tag{3}$$

The two different output voltages, which depend on the presence of the filter, are given in Equation (3). The result obtained by taking the ratio of both expressions is given below.

$$\frac{V_{L,wo}}{V_{L,w}} = \frac{jwL+R+R_S}{R+R_S} \tag{4}$$

The expression will be separated into its real and imaginary components. Then, the magnitude of the separated expression will be calculated, and the specific formula for the topology will be derived in a manner similar to that in Equation (2).

$$IL_{dB} = 20\log\left(\sqrt{\left(1+\left(\frac{wL}{R+R_S}\right)^2\right)}\right) \tag{5}$$

The square root term will be extracted, and the final form will be written.

$$IL_{dB} = 10\log\left(1+\left(\frac{wL}{R+R_S}\right)^2\right) \tag{6}$$

The insertion loss formula for the RL Low-Pass Filter, under the specified conditions, is given in Equation (6). Using the same method, the insertion loss formulas for the RC High-Pass, LC Band-Pass, and LC Band-Stop topologies under the specified conditions are presented below, respectively.

$$IL_{dB} = 10\log\left(1+\left(\frac{1/wC}{R+R_S}\right)^2\right) \tag{7}$$

$$IL_{dB} = 10\log\left(1+\left(\frac{wL-(1/wC)}{R+R_S}\right)^2\right) \tag{8}$$

$$IL_{dB} = 10\log\left(1+\left(\frac{wL}{(R+R_S)-(R+R_S)w^2LC}\right)^2\right) \tag{9}$$

3. DERIVATION OF TRANSFER FUNCTIONS OF EMC FILTERS

In the previous section, insertion loss formulas were derived using the defined circuit models for each filter topology. In this section, the same circuit models will be used to derive the transfer functions of the topologies. As in the previous section, general formulas will be written separately for each filter under the specified conditions. These transfer functions will be used to construct the Bode diagrams of the filters. As before, the procedure will be shown step by step for the RL Low-Pass Filter, followed by the general formulas for the other topologies, which will be presented without detailed derivation. In this analysis, the distinction between filtered and unfiltered states will not be made; instead, the transfer function of the circuit shown in Figure 2.1 will be directly obtained. The system will be analyzed based on the dynamic model of the circuit. The s-domain expressions for the output voltage and the input voltage are given below.

$$V_o(s) = R.I(s)$$
$$V_i(s) = I(s).((R_S+R)+sL) \tag{10}$$

The output and input voltages will be expressed in the form of Vo(s)/Vi(s), thereby allowing the transfer function to be obtained.

$$H(s) = \frac{V_o(s)}{V_i(s)} = \frac{R}{(R_S+R)+sL} \tag{11}$$

The transfer function has thus been obtained. Next, the transfer functions for the RC High-Pass, LC Band-Pass, and LC Band-Stop topologies will be presented in order.

$$H(s)=\frac{V_o(s)}{V_i(s)}=\frac{R}{(R_S+R)+(1/sC)} \tag{12}$$

$$H(s)=\frac{V_o(s)}{V_i(s)}=\frac{R}{(R_S+R)+(1/sC)+sL} \tag{13}$$

$$H(s)=\frac{V_o(s)}{V_i(s)}=\frac{R}{(R_S+R)+(\frac{sL}{s^2LC+1})} \tag{14}$$

4. TABLE AND BODE ANALYSES

The general formulas obtained in the previous sections will be presented in tabular form. Subsequently, Bode analyses will be carried out based on the transfer functions. The formulas of the transfer functions and insertion losses, derived from the circuit models, are collectively provided in the table below.

Table 1. The expressions of transfer functions and insertion losses for the filters

FILTER	TRANSFER FUNCTION	INSERTION LOSS
RL LOW-PASS	$H(s)=\frac{R}{sL+(R_S+R)}$	$IL_{dB}=10\log\left(1+\left(\frac{wL}{R+R_S}\right)^2\right)$
RC HIGH-PASS	$H(s)=\frac{RCs}{(R_S+R)Cs+1}$	$IL_{dB}=10\log\left(1+\left(\frac{1/wC}{R+R_S}\right)^2\right)$
LC BAND-PASS	$H(s)=\frac{RCs}{s^2LC+(R_S+R)Cs+1}$	$IL_{dB}=10\log\left(1+\left(\frac{wL-(1/wC)}{R+R_S}\right)^2\right)$
LC BAND-STOP	$H(s)=\frac{RLCs^2+R}{(R_S+R)LCs^2+sL+(R_S+R)}$	$IL_{dB}=10\log\left(1+\left(\frac{wL}{(R+R_S)-(R+R_S)w^2LC}\right)^2\right)$

Each equation presented in the table forms the foundation of the GUI to be developed. The transfer functions will be utilized for generating Bode diagrams, while the insertion loss expressions will be used to illustrate frequency-dependent variations. Additionally, each of these equations will be incorporated into the corresponding topology tab in an updatable format.

5. GUI DESIGN AND INTRODUCTION

Based on the obtained results, a GUI has been developed in the Python environment. Through this GUI, EMC engineers will have the opportunity to view the Bode diagrams and transfer functions of the filters as they wish. The values and graphs for presented filters can be obtained via sliders by users. After the user selects the values using the slider, the Bode diagram, insertion loss-frequency function, Insertion Loss and Transfer Function dynamically change. In this way, the desired filter topology, with the specified values of circuit elements, input resistance and the output load can be analyzed. Furthermore, a display box is embedded within the graphical outputs, allowing the corresponding Transfer Function or Insertion Loss equations to be presented upon user interaction with the adjacent buttons. Additionally, the insertion loss is calculated in decibels (dB) based on the frequency value entered by the user.
As an example of the GUI's operation, RC High-Pass and LC Band-Stop filters will be demonstrated in Figure 5.1 and 5.2, respectively. In the designed GUI, the values of source resistance Rs, presenting the power line impedance can be taken between 2 Ω and 450 Ω because of the impedance characteristic of the power line. The L and C can be taken as 0-0.1 H/F. These values can be customized by the user as desired. For the RC High-Pass filter given in Figure 5.1, Rs = 50 ohms, R = 50 ohms, C = 10 µF. For the LC Band-Stop filter given in Figure 5.2, Rs = 50 ohms, L = 0.01 H, C = 1 µF, R = 100 ohms. Furthermore, by entering 1 kHz in the frequency tab, the insertion losses of the corresponding filters at the specified frequency have been calculated in decibels (dB).

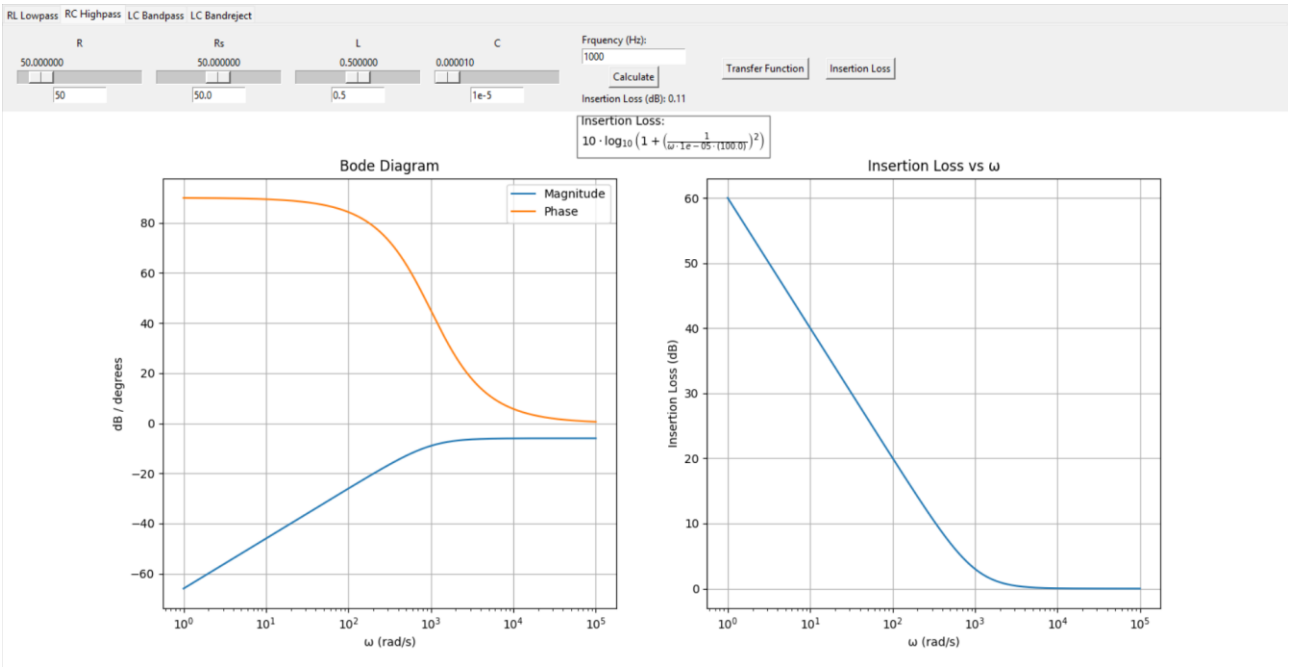

Figure 5.1 RC High-Pass

The RC High-pass topology for a 50-ohm matched load condition is presented in the figure above. As clearly shown in the figure, all elements have been updated according to the user's selections. Moreover, the 'Insertion Loss' button is active; therefore, the logarithmic frequency-dependent expression corresponding to the relevant filter is displayed within the designated box.

Next, the LC Band-Stop tab of designed GUI topology is presented in 5.2. The Transfer Function button can be activated, and the corresponding transfer function of the filter can be displayed within the designated box as shown in the figure.

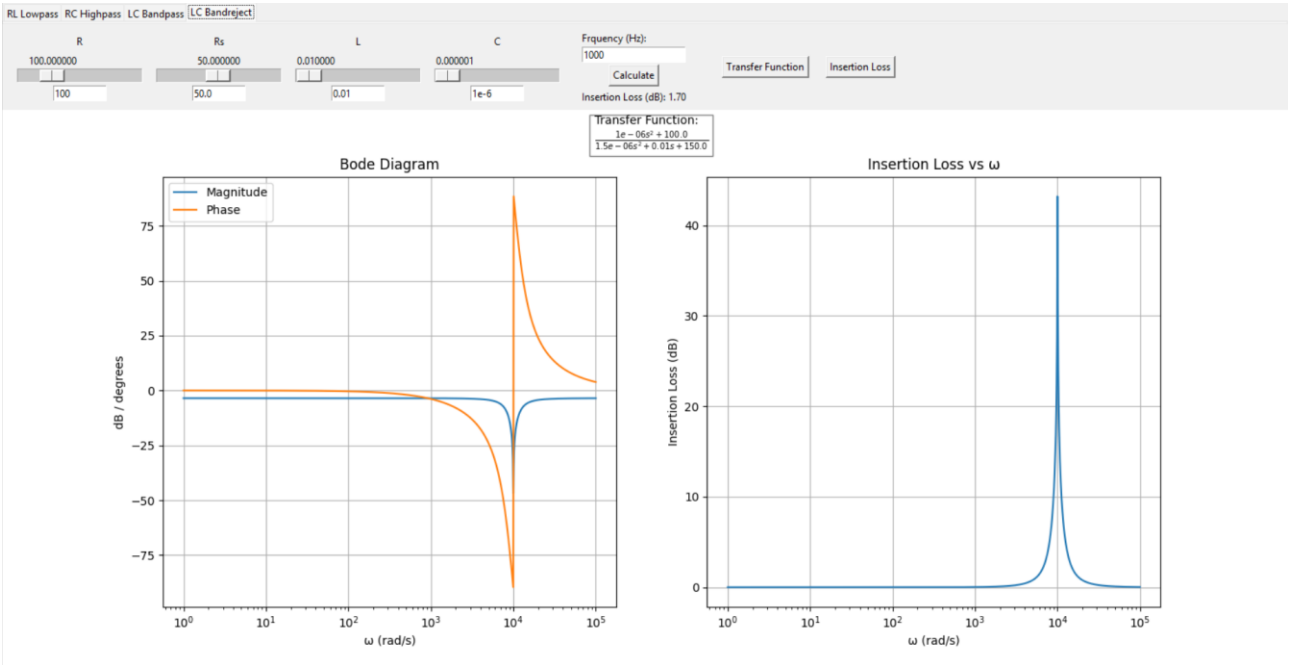

Figure 5.2 LC Band-Stop

The LC Band-Stop case for a 100-ohm mismatched load condition is illustrated in the figure. As anticipated, the simulation outputs align well with theoretical expectations, demonstrating the characteristic attenuation behavior of the filter within the stopband. For chosen source and load impedance and circuit elements, the cutoff frequency of the band stop circuit is about 10 KHz as shown in the figure.

6. CONCLUSION AND RECOMMENDATIONS

In this study, analytical expressions of insertion loss, transfer function, and Bode diagram of different type filters, such as low-pass, high-pass, band-pass, and band-stop filters, have been obtained. Additionally, a GUI has been designed to calculate numerical results of the obtained expressions and see graphically the characteristics of them. The insertion loss of any EMI filter is crucial parameter of the filter. It defines the frequency-dependent attenuation characteristics of the filter in decibels (dB). Most filter manufacturers provide the insertion loss frequency characteristics of a particular filter based on a 50-ohm matched load condition. However, in AC power line applications, the source impedance and load impedance are typically mismatched. In the study, expressions of the insertion losses for the filter structures given above have been obtained analytically for the condition of mismatched load. The filter insertions loss characteristic can be analyzed numerically and graphically by using the designed GUI for mismatched condition between source and load impedances, which are generally encountered in power line applications, differing from the ideal measurements with matched loads offered by EMC filter manufacturers.
Transfer functions and Bode diagram are other vital parameters which determine any filter characteristics. It is possible to analyze these characteristics of the presented filters with the designed GUI. The frequency-dependent phase and magnitude characteristics of the filter can be obtained simply changing the slider of the related components. In the future studies can effort to measure and determine the power line impedance and the input impedance of the circuit, and to obtain the insertion loss of the relevant filter circuits under real-world conditions.

REFERENCES

C. Bowick, (2008). RF Circuit Design, second ed., Elsevier, Oxford.

J. R. Nicholson, J. A. Malack, (1973). RF Impedance of Power Lines and Line Impedance Stabilization Networks in Conducted Interference Measurements, IEEE Transactions on Electromagnetic Compatibility.

H. W. Ott, (2005). Electromagnetic Compatibility Engineering, first ed., CRC Press, Florida.

Richard Lee Ozenbaugh, Timothy M. Pullen (2001). EMI Filter Design, third ed. CRC Press, Florida.

C. R. Paul (2005). Introduction to Electromagnetic Compatibility, John Wiley & Sons, New Jersey.

Muhammad H. Rashid, (2019). Power Electronics, fourth ed., Pearson, New Jersey.

Steve Roberts, Josefine Lametschwandtner, (2023). EMC BOOK OF KNOWLEDGE – Practical Tips for the User, RECOM.

SCHAFFNER, The Engineer's Guide to Designing Your EMI Filter, www.schaffnerusa.com

SCHAFFNER, Shaping Electrical Power, www.schaffnerusa.com

L. Sevgi (2009), From Design to Market of Electronic Systems: EMC Engineering Preface Electromagnetic Compatibility, Turkish Journal of Electrical Engineering and Computer Sciences.

C. M. Yıldız, (2020). Techniques For Increasing Immunity To Conducted Electromagnetic Interference And Reducing Conducted Emissions For Electromagnetic Compatibility, Halic University.

Production of Activated Carbon From Sumac Seeds Using The Vacuum Pyrolysis Method

SENA ÇİÇEK[1], SAID HARITS ALAYDRUS,[1] ALİ YALÇIN[*1]

Abstract: In this work, activated carbons with various surface properties were produced from sumac seeds by $ZnCl_2$-chemical activation using the vacuum pyrolysis method. The experiments in this study were performed with various SS-to-$ZnCl_2$ ratios and activation temperatures when the pretreatment time, the pretreatment temperature, and the activation time were kept constant for all experimental studies. The pyrolysis of sumac seeds was performed at elevated activation temperatures of 400–700°C and the SS-to-$ZnCl_2$ ratios of 1:0.5 to 1:2. The highest iodine number and BET surface area between the prepared activated carbons were 1103.2 mg/g and 1374.55 m^2/g for activation temperature of 600°C and the SS-to-$ZnCl_2$ ratio of 1:1. Surface of sumac seeds was changed from a flat surface with micron-sized particles to an irregular, rough surface texture with a heterogeneous surface due to pyrolysis. FTIR analysis demonstrates that the aromatic/aliphatic structures in sumac seeds were removed by degradation due to high activation temperature. This study demonstrates the potential to prepare activated carbon with a high BET surface area from sumac seeds.

Keywords: Activated carbon, Iodine number, Sumac seeds, Vacuum pyrolysis method

[1]Address: Süleyman Demirel University, Faculty of Engineering and Natural Sciences, Department of Chemical Engineering, Isparta/Türkiye
***Corresponding author**: ali.yalcin@sdu.edu.tr

1. INTRODUCTION / GİRİŞ (Times New Roman 10pt)

Activated carbon is commonly utilised as an effective adsorbent due to its highly porous structure and large surface area (typically 500–1500 m^2/g), which facilitates the adsorption of organic compounds, heavy metals, and various pollutants (Bansal and Goyal, 2005; Marsh and Rodríguez-Reinoso, 2006). It is commonly utilized in various applications such as air filtration, water purification, chemical processing, energy storage, adsorption, catalysis, odor removal, and medical treatments (Ceyhan et al., 2013) and, recently used in energy storage equipments like supercapacitors and lithium-ion batteries, the food and beverage industry for decolorization procedures, and the pharmaceutical industry for detoxification treatments (Bansal & Goyal, 2005). Cellulose, hemicellulose, lignin, and lignocellulosic materials are sources for producing activated carbon (Özsin, 2011). Agricultural wastes such as wood, corn husk, rice husks, vetch seeds, olive pits, coconut shells, grape seeds, peanut shells, and lotus are widely used for activated carbon (Kazempour ve Bagheri-Mohagheghi, 2023). Sumac seeds are widely consumed in the medicine and beverage industries since they are not poisonous. It contains valuable chemicals such as linoleic acid, oleic acid, and polyphenols (anthocyanins, gallic acid, and hydrolyzable tannins). Seeds have valuable ecological properties since they spread easily and grow rapidly in limited sunlight environments. It can also grow easily in poor soil conditions (Ahmad et al., 2020). It comprises 2.6% protein, 1.8% ash, 9.6% moisture, 7.4% oil, 63.8% water–soluble, 14.6% fibre, and is known as a carbon source.

Activated carbon has been prepared using physical and chemical activation methods. The chemical activation is performed in a single stage at high temperatures, as it reaches higher yields and well-developed microporosity textures. In contrast, physical activation is performed at lower temperatures (Özsin, 2011). Chemical activation involves treating organic resources with various chemical reagents to enhance surface morphologies such as pore volume, pore diameter, and surface area (Ahmed and Theydan, 2012). Both these processes significantly affect the resulting activated carbon's surface morphology and adsorption capacity, thereby enhancing its potential for diverse industrial applications (Zhang et al. 2020). The vacuum pyrolysis method is less costly than conventional production methods (Dos Santos et al., 2019). It is a specialised thermal decomposition process that occurs under reduced pressure, enabling the efficient breakdown of organic materials into valuable and environmentally safe chemical compounds. This method is especially beneficial for processing heat-sensitive materials, as the reduced pressure lowers their boiling points and decomposition temperatures, minimising thermal degradation and preserving valuable chemical properties (Lua and Ting Yang, 2004). Thanks to vacuum pyrolysis, the pyrolysis gases formed in the pyrolysis medium are quickly transported out of the pyrolysis environment, thus preventing possible side reactions on the activated carbon’s surface and pores (Cao et al., 2001). This process significantly affects the surface area, pore structure, particle size and distribution of the activated carbon, enhancing its potential for industrial applications (Bansal and Goyal, 2005).

This study uses the vacuum pyrolysis method to prepare activated carbon from sumac seeds. Iodine number values were calculated for the prepared activated carbon using the SS:$ZnCl_2$ ratio and activation temperature at various ranges. Sumac seeds and activated carbon were characterised by iodine number, BET (Brunauer–Emmett–Teller), SEM (Scanning Electron Microscopy), and FTIR (Fourier Transform Infrared Spectroscopy) analyses.

2. MATERIAL AND METHOD

2.1. Materials

The sumac seeds (SS) were supplied from a market in Turkey's Mediterranean region. Plant-based impurities (branches and leaves) were removed from the sumac seeds to obtain a mass comprising only seeds. Then, the dust on the seeds was removed using distilled water and dried at 80 °C for 24 hours in the oven. The dried sumac seeds were mechanically ground using a grinding machine. The resulting crushed seeds were stored in sealed containers for producing activated carbon.

2.2. Active carbon preparation method

10 g of sumac seeds are mixed with 20 ml of $ZnCl_2$ solutions to obtain samples with an SS:$ZnCl_2$ ratio of 1:0.5, 1:1, 1:1.5, and 1:2, and then stirred. The mixture is kept to ensure the impregnation of reagent into the interior of the sumac seed at room temperature for 24 hours, and then is treated with pretreatment at 80°C for 2 hours. The sample is transferred to a stainless steel reactor, and its lid is tightly closed to prevent the entering air into the reactor. It is placed into an oven operated at high temperature. The reactor lid is equipped with a stainless steel pipe to evacuate the air inside the reactor. The pipe is connected to a vacuum pump placed outside the oven. During activation, a vacuum is applied to decrease the oxygen level in the reactor. The sample in the reactor is pyrolysed at 600°C for 45 min. and then the reactor is kept to cool until room temperature. The obtained activated carbon is washed with a 0.5 M HCl solution to remove impurities from the pores. The washing process is continued using hot deionised water until the pH of the filtrate is up to >5. Finally, the washed activated carbons are dried at 80°C for 24 h and stored in sealed containers for characterisation. Various production conditions for the activated carbon production from sumac seed are shown in Table 1.

Table 1. Various production conditions performed for the activated carbon

Run	SS:$ZnCl_2$	Impregnation time (h)	Pretreatment temperature (°C)	Pretreatment time (h)	Activation temperature (°C)	Activation time (min.)	Iodine number (mg/g)
1	1:0.5	24	80	2	600	45	304.8
2	**1:1**				**600**		**1103.2**
3	1:1.5				600		1092.2
4	1:2				600		1054.1
5	1:1				400		479.8
6	1:1				500		962.1
7	1:1				700		1018.6

2.3. Characterisation methods

Iodine number:

Activated carbon is characterized based on the amount of the iodine number, as it can adsorb iodine, a low-molecular-weight compound (Ceyhan et al., 2013). 0.2 g of active carbon is weighed and mixed with 40 ml of 0.1 N iodine solution for 5 min. and then filtered. The filtrate is titrated with 0.05 N $Na_2S_2O_3.5H_2O$ solution. The iodine number is calculated using the following equation based on the amount of sodium thiosulfate consumed after the titration method (Pradhan, 2011).

$$Iodine\ number = \frac{(B - A) * 127 * N * 40}{m * B}$$

A: $Na_2S_2O_3.5H_2O$ consumed in the titration after the iodine adsorption on the activated carbon, ml.
B: $Na_2S_2O_3.5H_2O$ consumed in titration for 0.1 N iodine solution, ml.
m: the amount of used active carbon (g)
N: the concentration of iodine solution (N)

BET analysis:

Surface properties and surface area of activated carbon were examined at 77 K with N_2 adsorption based on the BET method on a Micromeritics TriStar II Plus surface analyser.

SEM analysis:

The surface morphologies of activated carbon and sumac seeds were characterised using a SEM instrument (FEI QUANTA FEG 250) with a 30 kV accelerating voltage. Samples were dried at 105 °C under vacuum for 12 h before SEM analysis.

FTIR analysis:

FTIR analysis was carried out to determine the functional groups in the sumac seeds and activated carbon prepared from sumac seeds. FTIR spectra were recorded between 4000 and 400 cm^{-1} wavenumber using a JASCO FT/IR-4700 spectrophotometer.

3. RESULTS

3.1. Iodine number tests

The iodine number test is a widely used method for predicting the surface area of activated carbons. An increase in the iodine number indicates a higher surface area, highly micro- and mesoporous structures (Ceyhan et al., 2013). The SS:$ZnCl_2$ ratio is one variable that affects the surface morphologies of activated carbon prepared by chemical activation. The SS-to-$ZnCl_2$ ratio was varied from 1:0.5 to 1:2 to determine the various iodine numbers. At the same time, other production parameters such as the pretreatment time, the pretreatment temperature, activation time, and activation temperature were kept constant. The iodine number values of activated carbons obtained at various SS:$ZnCl_2$ ratios are shown in Fig. 1a. As seen in Fig. 1a, the iodine numbers rise with increasing the SS-to-$ZnCl_2$ ratio from 1:0.5 to 1:2, and reduced with rising the SS-to-$ZnCl_2$ ratio from 1:1 to 1:2. The highest iodine number was calculated to be 1103.2 mg/g for the 1:1 ratio. The rise in iodine number values results from the enhanced pores of activated carbon. Activation temperature is also one of the most crucial parameters that profoundly affect the surface morphology of the activated carbon. The iodine number values of activated carbons obtained at various activation temperatures between 400 and 700°C and the SS-to-$ZnCl_2$ ratio of 1:1 are indicated in Fig. 1b. The iodine number values increased with rising temperature in a range of 400–600°C and reduced with rising temperature from 600 to 700°C; thus, the optimum activation temperature was determined to be 600°C.

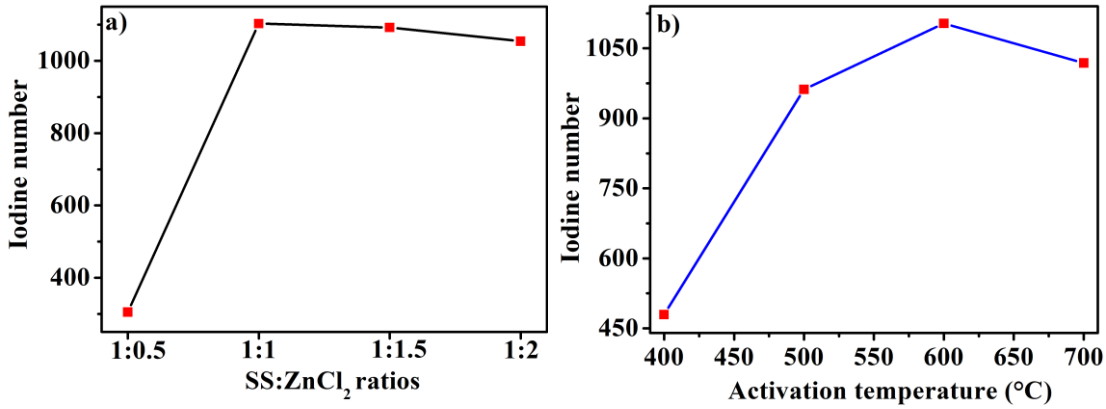

Figure 1. Iodine number values of activated carbons prepared a) at various SS:$ZnCl_2$ ratios and b) activation temperatures.

3.2. BET analysis

Nitrogen adsorption is generally used to ascertain the physical properties of the adsorbents (Ceyhan et al., 2013). The nitrogen adsorption isotherm on the activated carbon produced at 600°C is illustrated in Fig. 2, and its BET surface area was determined to be 1374.55 m^2/g. According to IUPAC, the activated carbon obtained from sumac seed exhibited an adsorption isotherm of type I (Zhang et al., 2016). The maximum micropore volume, T-method external surface area, BJH pore volume, and micropore surface area for the sample produced at 600°C were 0.81 cm^3/g, 1202.61 m^2/g, 0.53 cm^3/g, and 1509.03 m^2/g, indicating that the pores of activated carbon with the highest BET surface area are in the mesopore range. The activated carbon's pores are commonly classified as micropores (diameter < 2 nm), mesopores (2–50 nm), and macropores (>50 nm) (Ceyhan et al., 2013). The average pore diameter of activated carbon produced at 600°C is 2.35 nm, indicating this sample is mesoporous.

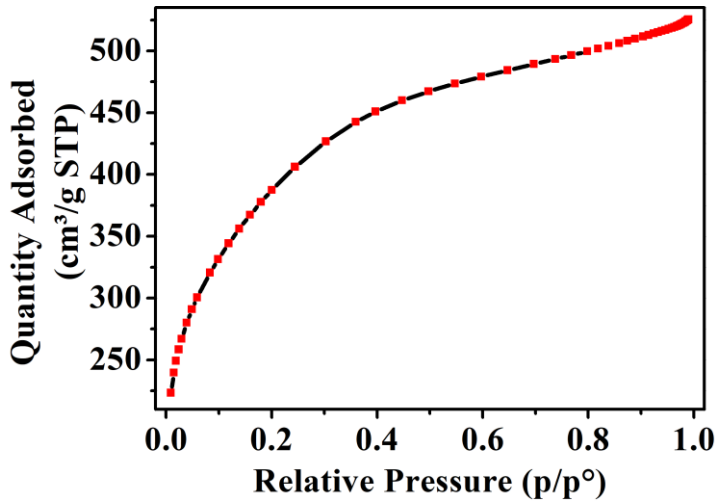

Figure 2. Adsorption isotherm curve of the activated carbon produced at 600°C.

3.3. Surface characterisation by SEM

SEM photographs of sumac seeds and samples produced at 600°C and 700°C are illustrated in Figure 3. Figure 3a indicates that sumac seeds have a flat surface of micron particles. The surface properties of sumac seeds were completely changed by performing different activation temperatures (Fig. 3b and 3c). As the activation temperature increases, a rough texture with a heterogeneous surface consisting of individual particles is formed. These new surfaces were quite dense, with cracks of different depths and lengths, which shows that irregular, rough, and cracked structures increase the activated carbon's surface area. According to SEM images, it can be said that the newly formed surface is due to the displacement of $ZnCl_2$ and H_2O from the structure during carbonisation (Ceyhan et al., 2013).

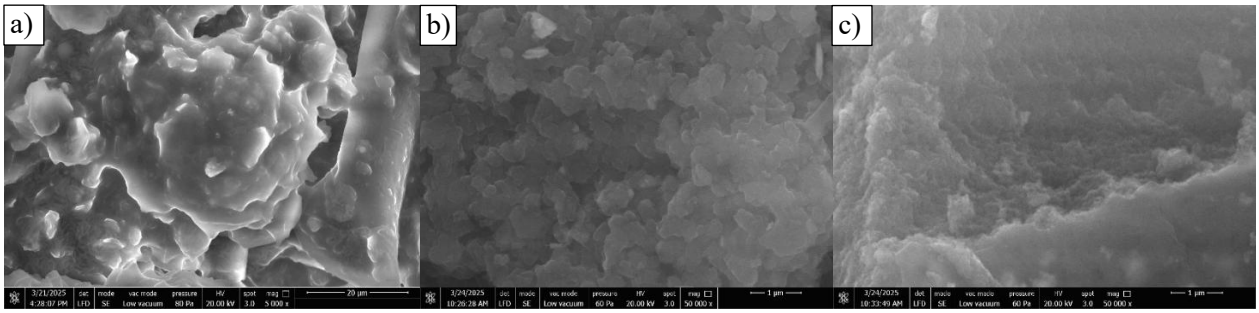

Figure 3. SEM images of a) sumac seed and activated carbons prepared at b) 600°C and c) 700°C activation temperature.

3.4. Function groups in sumac seed and activated carbon

Figure 4 shows the FTIR spectra of sumac seeds and activated carbon obtained from seeds at 700 °C activation temperature. The broad peak at 3300 cm^{-1} can be associated with the -OH stretching vibration mode of phenol, alcohol, and carboxylic acid in the structure of sumac seeds, while the asymmetric and symmetric C–H vibrations at 2950–2820 cm^{-1} indicate the presence of aliphatic structures in the seed structure. Similarly, the peaks between 1750-1600 cm^{-1} are the C=C and C=O vibrations in the aromatic structure, and the peaks between 1480-1360 cm^{-1} are assigned as the result of C–H bonds (Altıntıg et al., 2015; Yalçın, 2016). The peaks at 1250–950 cm^{-1} (especially at 1157.08 cm^{-1}) are the result of νC–O stretching vibrations originating from ester, hydroxyl, and ether functional groups in the structure of the raw material (Alshuiael et al., 2020; Yalçın, 2016). The peaks between 900-600 cm^{-1} (719.32 cm-1) show the presence of C–H out-of-plane bending in benzene and its derivatives (Guo and Lua, 2000) (Fig. 4a). Fig. 4b indicates that volatile compounds such as NO_X, SO_X, and H_2O in the seed structure are removed from the framework by the pyrolysis of sumac seeds at high temperatures. On the other hand, peaks at 1700-4000 cm^{-1} in the structure of the produced activated carbon are not present, which were associated with the decomposition of some functional groups in the structure of seeds due to pyrolysis. A small peak at 1064.51 cm^{-1} shows that an amount of aromatic ether is present in the structure of activated carbon, which formation of aromatic ether was associated with the presence of ether in the structure of sumac seeds (Barroso-Bogeat et al., 2014).

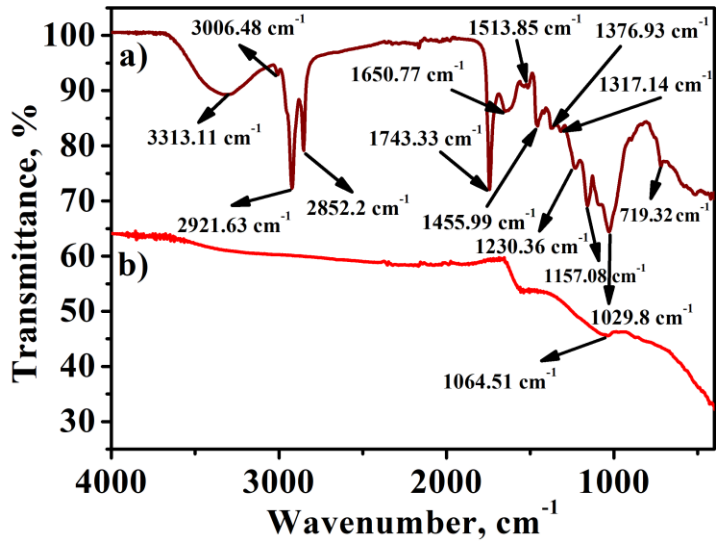

Figure 4. FTIR curves of a) sumac seed and activated carbon prepared at b) 600°C activation temperature.

4. DISCUSSION AND CONCLUSIONS

The vacuum pyrolysis technique was successfully applied for the activated carbon preparation from sumac seeds. Samples with various surface properties were characterized with iodine number, BET, SEM, and FTIR analysis. The pretreatment time, the pretreatment temperature, and the activation time were kept constant for all experimental studies. The highest iodine number, the BET surface area, and average pore diameter of activated carbon prepared at the SS-to-$ZnCl_2$ ratio of 1:1 and activation temperature of 600°C were determined to be 1103.2 mg/g, 1374.55 m^2/g, and 2.35 nm, respectively, indicating that this sample is mesoporous. SEM analysis shows that sumac seeds have a flat surface with micron-sized particles. The surface properties of sumac seeds were completely changed by performing high activation temperatures. The prepared activated carbons have a rough texture with a heterogeneous surface of individual particles, indicating irregular and rough structures with cracks of different depths and lengths. FTIR analysis indicates that sumac seeds contain alcohol, ester, hydroxyl, phenol, carboxylic acid, and ether functional groups in the aromatic/aliphatic structure. The pyrolysis of sumac seeds at high temperatures degrades these functional groups from the seed structure, enhancing the surface morphologies of activated carbon.

Acknowledgements
The authors gratefully acknowledge the Scientific and Technological Research Institution of Türkiye (TÜBİTAK) for the financial support of the 2209-A Project (Project No: 1919B012323539) throughout the research.

Author Contributions
Conceptualisation: Ç.S., A.S.H., Y.A.; Investigation: Ç.S., A.S.H., Y.A.; Material and Methodology: Ç.S., A.S.H., Y.A.; Supervision: Y.A.; Visualisation: Ç.S., Y.A.; Writing-Original Draft: Ç.S., Y.A.; Writing-review & Editing: Ç.S., Y.A.; Other: All authors have read and agreed to the published version of the manuscript.

Conflict of Interest
The authors have no conflicts of interest to declare.

Funding
The authors declared that this study was funded by the Scientific and Technological Research Institution of Türkiye (TÜBİTAK).

REFERENCES

Ahmad, M. S., Liu, H., Alhumade, H., Tahir, M. H., Çakman, G., Yıldız, A., ... & Shen, B. (2020). A modified DAEM: To study the bioenergy potential of invasive Staghorn Sumac through pyrolysis, ANN, TGA, kinetic modelling, FTIR and GC–MS analysis. Energy Conversion and Management, 221, 113173. https://doi.org/10.1016/j.enconman.2020.113173.

Alshuiael, S. M., Al-Ghouti, M. A. (2020). Multivariate analysis for FTIR in understanding treatment of used cooking oil using activated carbon prepared from olive stone. Plos one, 15(5), e0232997. https://doi.org/10.1371/journal.pone.0232997.

Altıntıg, E., Acar, I., Altundag, H., Ozyıldırım, O. (2015). Production of activated carbon from rice husk to support Zn2+ ions. Fresenius Environmental Bulletin, 24(4), 1499-1506.

Bansal, R.C., Goyal, M. (2005). Activated carbon adsorption. CRC press, Boca Raton.

Barroso-Bogeat, A., Alexandre-Franco, M., Fernández-González, C., Gómez-Serrano, V. (2014). FT-IR analysis of pyrone and chromene structures in activated carbon. Energy & fuels, 28(6), 4096-4103. https://doi.org/10.1021/ef5004733.

Marsh, H., Reinoso, F.R. (2006). Activated carbon. Elsevier.

Cao, N., Darmstadt, H., Roy, C. (2001). Activated carbon produced from charcoal obtained by vacuum pyrolysis of softwood bark residues. Energy & fuels, 15(5), 1263-1269. https://doi.org/10.1021/ef0100698.

Ceyhan, A. A., Şahin, Ö., Saka, C., Yalçın, A. (2013). A novel thermal process for activated carbon production from the vetch biomass with air at low temperature by two-stage procedure. Journal of analytical and applied pyrolysis, 104, 170-175. https://doi.org/10.1016/j.jaap.2013.08.007.

Dos Santos, K. J. L., de Souza dos Santos, G. E., de Sá, Í. M. G. L., de Carvalho, S. H. V., Soletti, J. I., Meili, L., ... & Dotto, G. L. (2019). Syagrus oleracea–activated carbon prepared by vacuum pyrolysis for methylene blue adsorption. Environmental Science and Pollution Research, 26, 16470-16481. https://doi.org/10.1007/s11356-019-05083-4.

Guo, J., Lua, A. (2000). Effect of heating temperature on the properties of chars and activated carbons prepared from oil palm stones. Journal of Thermal Analysis and Calorimetry, 60(2), 417-425. https://doi.org/10.1023/a:1010137308378.

Kazempour, A., Bagheri-Mohagheghi, M. M. (2023). Activated Carbon/Zeolite Hybrid Nanocomposite for Drinking Water Treatment Applications: Structural, Optical, and Surface Adsorption Properties. Water, Air, & Soil Pollution, 234(11), 669. https://doi.org/10.1007/s11270-023-06676-z.

Lua, A.C., Yang, T. (2004). Effects of vacuum pyrolysis conditions on the characteristics of activated carbons derived from pistachio-nut shells. Journal of colloid and interface science. 276(2), 364-372. https://doi.org/10.1016/j.jcis.2004.03.071.

Özsin, G., (2011). Production and characterization of activated carbon from pistachio-nut shell, Master's Degree, Graduate School of Natural and Applied Sciences, Middle East Technical University, Ankara.

Yalçın, A., (2016). Adi fiğ'den elde edilen aktif karbonun sulu çözeltilerdeki adsorpsiyon özelliklerinin incelenmesi, Selçuk Üniversitesi, Fen Bilimleri Enstitüsü, Yüksek Lisans Tezi, Konya.

Zhang, Y., Shao, D., Yan, J., Jia, X., Li, Y., Yu, P., Zhang, T. (2016). The pore size distribution and its relationship with shale gas capacity in organic-rich mudstone of Wufeng-Longmaxi Formations, Sichuan Basin, China. Journal of Natural Gas Geoscience, 1(3), 213-220. https://doi.org/10.1016/j.jnggs.2016.08.002.

Determination of Cytotoxic and Apoptotic Activity of Omeprazole on HS578T Cell Line

CEMAL KOZANSOY[1], FUNDA KESKİN[1], KÜBRA KOCABIYIK[1*], SEVKI ARSLAN[1]

Abstract: Triple-negative breast cancer (TNBC) represents one of the most challenging breast cancer subtypes due to the absence of estrogen receptor (ER), progesterone receptor (PR), and HER2 expression. This molecular profile is associated with poor prognosis, aggressive tumor behavior, and limited treatment options. The HS578T cell line, derived from human breast tissue, is a well-established in vitro model for TNBC due to its invasive nature and resistance to standard therapies. This study explores the cytotoxic and pro-apoptotic effects of omeprazole, a commonly used proton pump inhibitor (PPI), on the HS578T cell line. Originally designed to treat acid-related gastrointestinal disorders, omeprazole has recently gained interest in oncology research for its ability to alter the acidic tumor microenvironment and potentially sensitize cancer cells to treatment. Cell viability was evaluated using the MTT assay after 24-hour exposure to omeprazole at concentrations calculated as 473.62 µM, while a slightly lower EC_{50} of 422.81 µM was observed in non-cancerous Hek293 cells. Apoptosis analysis using Annexin V-FITC/PI staining and flow cytometry revealed that omeprazole induced higher apoptotic rates (20.99%) compared to the control (8.24%) and the positive control paclitaxel (9.52%). Furthermore, necrotic cell populations were elevated in both omeprazole and paclitaxel-treated groups. These results support the potential anticancer activity of omeprazole in TNBC cells and suggest its utility as a candidate for drug repurposing strategies. Further studies are warranted to explore its mechanism of action and in vivo efficacy in combination with other therapeutic agents.

Keywords: Cytotoxicity, apoptosis, Omeprazole, HS578T cell line

[1]**Address:** Pamukkale University, Faculty of Science, Denizli/Turkiye

***Corresponding author**: kkocabiyik@pau.edu.tr

1. INTRODUCTION

Breast cancer remains the most prevalent malignancy among women worldwide and continues to be a major contributor to morbidity and mortality. According to the 2020 GLOBOCAN report, approximately 2.3 million new cases of breast cancer are diagnosed annually, representing 11.7% of all cancer incidences globally (Sung et al., 2021). Among its various molecular subtypes, triple-negative breast cancer (TNBC)-defined by the lack of estrogen receptor (ER), progesterone receptor (PR), and HER2 expression-exhibits the poorest prognosis. TNBC is characterized by aggressive progression, an elevated risk of metastasis, and limited therapeutic options (Bianchini et al., 2016).

The HS578T cell line, commonly employed in laboratory research to model the biological features of TNBC, is distinguished by its invasive phenotype and its potential to develop chemoresistance (Hackett et al., 1977). This cell line serves as a critical platform for the evaluation of novel anticancer agents and for the elucidation of underlying molecular mechanisms. Recently, the strategy of drug repurposing, which explores new therapeutic applications for existing pharmacological agents, has gained prominence, offering advantages such as reduced development timelines and lower costs (Pushpakom et al., 2019).

In this context, proton pump inhibitors (PPIs), originally developed for the management of gastric acid-related disorders, have emerged as promising candidates for oncological repurposing. Omeprazole, a widely used PPI, functions by inhibiting the H^+/K^+-ATPase enzyme in gastric parietal cells, thereby reducing acid secretion (Forgacs & Loganayagam, 2008). Furthermore, omeprazole has demonstrated efficacy in promoting mucosal healing in conditions such as peptic ulcer disease (Minalyan et al., 2017; Numico et al., 2017)

Emerging evidence suggests that omeprazole's effects extend beyond the gastrointestinal tract, notably influencing the tumor microenvironment (De Milito & Fais, 2005). Owing to the metabolic shift known as the Warburg effect, cancer cells produce excessive lactic acid, leading to the development of an acidic microenvironment surrounding tumors (Luciani et al., 2004). This acidic milieu can impair the cellular uptake of chemotherapeutic agents, thereby diminishing treatment efficacy. PPIs such as omeprazole have been shown to neutralize extracellular acidity, potentially enhancing drug uptake and triggering apoptotic pathways (Spugnini et al., 2011).

The HS578T cell line derived from human breast cancer is frequently used in cancer research due to its triple-negative status, characterized by the absence of estrogen receptors, progesterone receptors, and HER2 expression. This phenotype makes HS578T a valuable model for studying aggressive breast cancers resistant to traditional hormone therapies (Paz et al., 2020). Omeprazole, a proton pump inhibitor (PPI), is used to treat gastroesophageal disorders by reducing stomach acid secretion. It has drawn attention in oncology due to its potential to alter the pH of the tumor microenvironment and affect cancer cell viability(Hou et al., 2018). Recently, the effects of omeprazole on cancer cells have begun to be investigated, including its ability to modulate drug resistance and induce cytotoxic effects in specific cell lines such as HS578T. This study aims to address the gap in anticancer research by conducting cytotoxicity and apoptosis experiments on the HS578T cell line using omeprazole, as reported in the literature.

2. MATERIAL AND METHOD

In this study, the experimental approaches were organized into distinct sections, each outlining the specific techniques implemented to assess the cytotoxic, apoptotic properties of omeprazole on the investigated cell lines.

2.1. Cell culture

Cell viability percentages were determined using the MTT (3-(4,5-dimethylthiazol-2-yl)-2,5-diphenyltetrazolium bromide) assay (MTT Cell Proliferation Assay Kit, BioVision). Epithelial cells (HS578T) isolated from breast tissue and human embryonic kidney (Hek293) cells were cultured in Dulbecco's Modified Eagle Medium (DMEM) supplemented with 100 U/mL penicillin, 10% fetal bovine serum (FBS), and 1% streptomycin-penicillin mixture at 37°C in a humidified atmosphere containing 5% CO_2 (Konus et al., 2022). When the cells reached a density of 80-90% in the plates, they were used for experiments after passage.

2.2. Cytotoxic activity by using MTT test

Cells were seeded at a density of 2×10^4 into a 96-well plate and incubated for 24 hours. The culture medium was replaced, and the cells were treated with omeprazole at increasing concentrations of 20, 30, 50, 100, 200, 300, and 500 µM. These compounds were dissolved in dimethyl sulfoxide (DMSO). After a 24-hour exposure period, the culture medium was carefully removed, and 110 µL of culture medium containing 10 µL of MTT (5 mg/mL) was added, followed by incubation at 37°C for an additional 2 hours. To dissolve the formazan product, 50 µL of DMSO (Sigma) was used, and the absorbance value of the resulting solution was measured at 590 nm using an Epoch spectrophotometer (BioTek, USA). Each experimental condition was repeated three times. Viability was compared to the DMSO control and expressed as a percentage of viability (Çam et al., 2024).

2.3. Evaluation of apoptotic activity

Apoptosis was assessed using the Annexin V-FITC Apoptosis Assay Kit (Elabscience, Texas, USA) and analyzed with a fluorescent cell counter. Following 24 hours of culture, cells were stained with Annexin V-FITC and propidium iodide (PI), and the EC_{50} concentration of the compounds was evaluated for their ability to induce apoptosis in cancer cells. Briefly, cells were resuspended in 100 µL of 1× Annexin V binding buffer and incubated with 2.5 µL of Annexin V-FITC and 1 µL of PI for 20 minutes at room temperature in the dark. Finally, the percentages of live, apoptotic, and necrotic cells were determined using flow cytometry (Secme et al., 2023).

2.4. Statistical analysis

Each experiment conducted within the scope of this study was repeated three times. All data are expressed as means, and standard deviation values are highlighted in the figures. When dose groups were compared with the control group, a P value less than 0.05 ($P<0.005$) was considered statistically significant and denoted with an asterisk (*). Statistical analysis was performed using GraphPad Prism 9.0 software.

3. RESULTS

3.1. Cytotoxicity of omeprazole on HS578T cell line

The 24-hour cytotoxic activity of omeprazole was investigated using the MTT assay on the HS578T cancer cell line and the Hek293 healthy cell line. In the study, omeprazole was evaluated at concentrations of 20, 30, 50, 100, 200, 300, and 500 µM. The study demonstrated that omeprazole exhibited effects at the concentrations evaluated. The half-maximal lethal dose (EC_{50}) of omeprazole determined by the MTT assay was 473.62 µM. When tested on the Hek293 cell line used as the control group, omeprazole exhibited a slightly higher toxic effect with an EC_{50} dose of 422.81 µM.

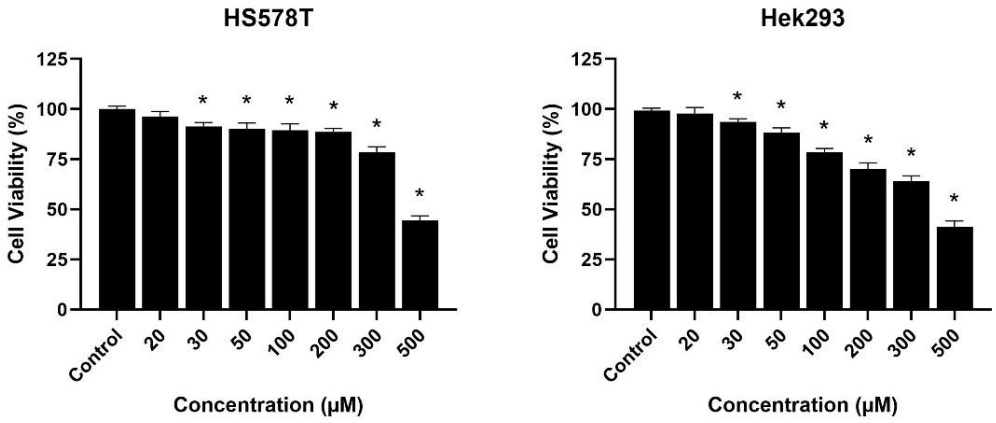

Figure 1: The effects of different doses of omeprazole on the HS578T cell line over 24 hours were determined using a cell viability test. *P < 0.05 indicates a statistically significant difference compared to the control group.

3.2. Apoptosis via omeprazole in HS578T cells

To determine apoptosis activity, the half-lethal dose of the omeprazole molecule was selected and the cells were treated with it for 24 hours in the HS578T cell line. The control group was treated with the same amount of DMSO, and the substance was compared with DMSO (control) and positive control paclitaxel (PTX). After 24 hours, the culture medium was removed, and the cells were harvested using trypsin-EDTA and centrifuged at 2000 rpm for 5 minutes. The supernatant was then removed, and the cell pellet was washed with PBS and centrifuged again. The percentages of live, dead, and apoptotic cells were analyzed using flow cytometry as described in the methods section.

The results obtained showed that omeprazole had an effect on the HS578T cell line. When compared with the control and positive control, the results obtained were 8.24% for the control, 9.52% for PTX, and 20.99% for omeprazole. In addition, more necrotic activity was detected in PTX and omeprazole than in the control.

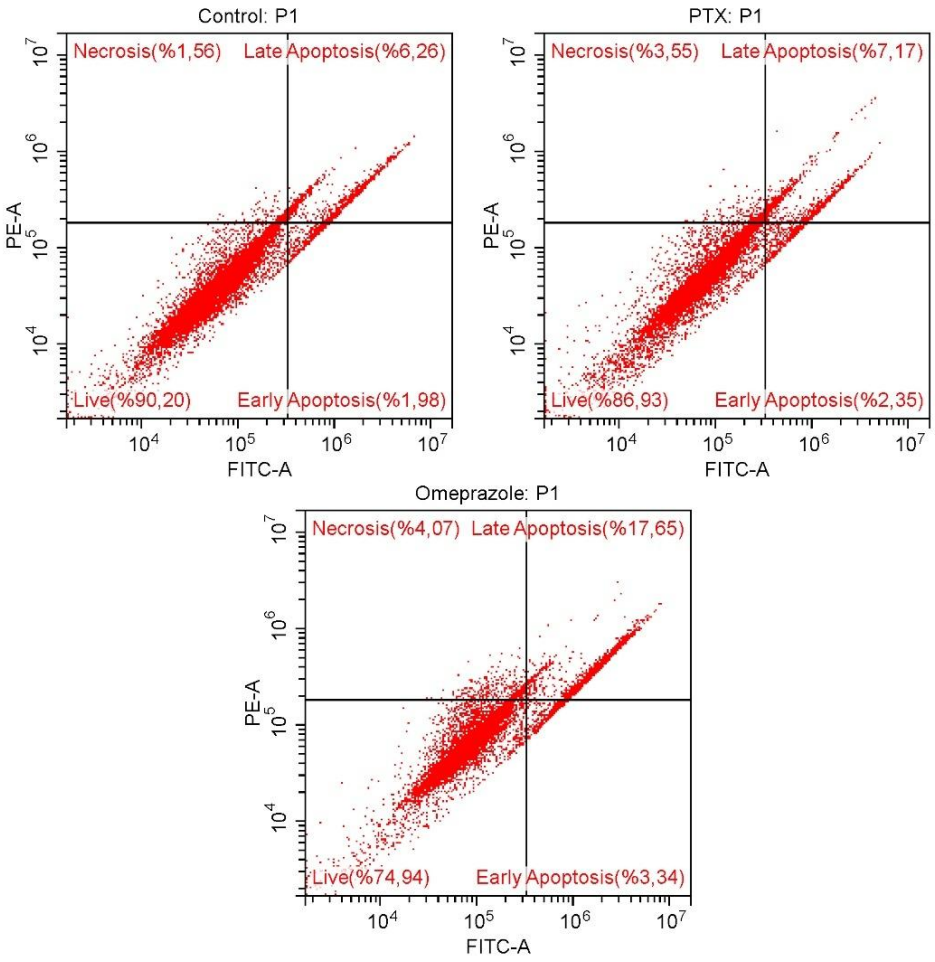

Figure 2: Using the Annexin V-FITC/PI staining method, flow cytometry was employed to determine the results of omeprazole's apoptotic effects on the HS578T cell line after 24 hours of treatment. A positive control of 11.4 µM PTX was used. Significant difference from the negative control (*P<0.05).

4. DISCUSSION

Triple-negative breast cancer (TNBC) represents one of the most challenging subtypes of breast malignancies due to its aggressive behavior, high metastatic potential, and lack of targeted hormonal therapies (Bianchini et al., 2016). The absence of estrogen receptor (ER), progesterone receptor (PR), and HER2 expression limits treatment options to conventional chemotherapy, which often results in drug resistance and tumor recurrence (Jin et al., 2014a). Therefore, identifying novel therapeutic strategies or repurposing existing drugs with anticancer potential remains a critical objective in oncology research.

In this study, the cytotoxic and apoptotic effects of omeprazole on the HS578T triple-negative breast cancer cell line were investigated. The results indicated that omeprazole was capable of reducing cell viability at high concentrations and promoting apoptosis. According to the MTT assay, the half-maximal effective concentration (EC_{50}) of omeprazole in HS578T cells was determined to be 473.62 µM. This suggests that omeprazole can exhibit cytotoxic properties under in vitro conditions.

To assess apoptosis, cells were treated with the EC_{50} concentration of omeprazole for 24 hours. Annexin V-FITC/PI staining showed a marked increase in apoptotic cell populations in the omeprazole group (20.99%) compared to the control group (8.24%) and the positive control paclitaxel group (9.52%). In addition, a higher rate of necrotic cells was observed in the omeprazole-treated samples, indicating that cell death may occur through both apoptotic and necrotic pathways.

These findings suggest that omeprazole has the potential to induce programmed cell death in aggressive breast cancer cells and may alter cellular homeostasis in a dose-dependent manner. Given the aggressive and therapy-resistant nature of triple-negative breast cancer, identifying compounds that can trigger cell death in such models is of critical importance.

However, the necessity of relatively high concentrations to achieve these effects implies certain limitations in terms of clinical applicability.

Omeprazole has garnered increasing attention as a potential therapeutic adjunct in oncology, particularly in the treatment of triple-negative breast cancer (TNBC). Several studies have highlighted its promising role beyond gastric acid suppression, indicating its ability to interfere with key cancer-related pathways.

For instance, a pivotal study conducted on the MDA-MB-231 TNBC cell line demonstrated that omeprazole significantly inhibited both invasion and metastatic potential. The researchers identified that this inhibitory effect was mediated by downregulation of CXCR4, a chemokine receptor strongly associated with cancer metastasis. This suppression occurred via activation of the aryl hydrocarbon receptor (AHR) signaling pathway, which in turn downregulated genes involved in metastasis. As a result, omeprazole effectively prevented the dissemination of cancer cells to distant organs such as the lungs, pointing to its anti-metastatic potential (Jin et al., 2014b).

In another notable investigation, omeprazole was found to promote the degradation of Snail, a transcription factor that plays a key role in initiating epithelial-mesenchymal transition (EMT)—a process linked to cancer cell invasiveness and metastasis. By facilitating Snail degradation, omeprazole inhibited EMT, restricted cancer cell cycle progression, and ultimately suppressed tumor growth. These findings suggest that omeprazole may serve as a promising modulator of tumor cell plasticity and progression (Li et al., 2022).

Furthermore, Ihraiz et al. (Ihraiz et al., 2020) reported that omeprazole exhibited notable cytotoxic and anti-migratory effects in several breast cancer cell lines, including MCF-7, T47D, and MDA-MB-231. Importantly, the study demonstrated that omeprazole not only induced apoptosis but also enhanced the efficacy of conventional chemotherapeutic agents when used in combination. This synergistic effect resulted in significantly reduced cell proliferation and increased drug sensitivity, reinforcing the potential utility of omeprazole in combination cancer therapies.

While our findings suggest that omeprazole may have potential as a supportive treatment for TNBC, several limitations should be noted. The concentrations needed to see effects in vitro were relatively high, which may not be easily achievable in vivo without side effects. Moreover, the study focused on only one cell line and did not assess the drug's performance in other models or in combination with standard treatments. Still, the data support further exploration of omeprazole's role in modulating the tumor environment and promoting cancer cell death. To better understand its potential in clinical settings, additional in vivo studies and well-designed trials will be essential.

5. CONCLUSIONS

In conclusion, this study highlights the potential of omeprazole, a commonly used proton pump inhibitor, as a repurposed agent with anticancer activity against triple-negative breast cancer cells. The results obtained from cytotoxicity and apoptosis assays demonstrated that omeprazole exhibits a dose-dependent inhibitory effect on cell viability and significantly induces apoptosis in the HS578T cell line. These findings support existing literature indicating that omeprazole can interfere with tumor cell survival by modulating the tumor microenvironment and intracellular signaling pathways. Given its established safety profile and low cost, omeprazole presents a promising candidate for combination therapies aimed at enhancing the efficacy of current treatment regimens for aggressive breast cancers. However, further preclinical studies and in vivo evaluations are essential to elucidate the molecular mechanisms underlying its anticancer effects and to validate its clinical applicability.

Acknowledgements
We would like to express our sincere gratitude to Amine Hafis Abdelsalam and the entire Molecular Biochemistry Laboratory team for their valuable support and contributions throughout this study.

Ethics Committee Approval
N/A

Peer-review
Externally peer-reviewed.

Author Contributions
Conceptualization: C.K.; Investigation: C.K., F.K..; Material and Methodology: K.K, S.A.; Supervision: S.A.; Visualization: C.K, K.K.; Writing-Original Draft: C.K., F.K, K.K; Writing-review & Editing: K.K, S.A.; Other: All authors have read and agreed to the published version of manuscript.

Conflict of Interest
The authors have no conflicts of interest to declare.

Funding
The authors declared that this study has received no financial support.

REFERENCES / KAYNAKLAR

Bianchini, G., Balko, J. M., Mayer, I. A., Sanders, M. E., & Gianni, L. (2016). Triple-negative breast cancer: challenges and opportunities of a heterogeneous disease. *Nature Reviews Clinical Oncology*, *13*(11), 674–690. https://doi.org/10.1038/nrclinonc.2016.66

Çam, D., Çakır, C., Karaman, A. H., Abdelsalam, A. H., Sıcak, Y., Akata, I., Arslan, S., & Öztürk, M. (2024). Characterization of the Cytotoxic Compounds of *Lactarius salmonicolor* R. Heim and Leclair by Gas Chromatography-Mass Spectrometry and Chemometrics. *Analytical Letters*, 1–19. https://doi.org/10.1080/00032719.2024.2372670

De Milito, A., & Fais, S. (2005). Proton pump inhibitors may reduce tumour resistance. *Expert Opinion on Pharmacotherapy*, *6*(7), 1049–1054. https://doi.org/10.1517/14656566.6.7.1049

Forgacs, I., & Loganayagam, A. (2008). Overprescribing proton pump inhibitors. *BMJ*, *336*(7634), 2–3. https://doi.org/10.1136/bmj.39406.449456.BE

Hackett, A. J., Smith, H. S., Springer, E. L., Owens, R. B., Nelson-Rees, W. A., Riggs, J. L., & Gardner, M. B. (1977). Two Syngeneic Cell Lines from Human Breast Tissue: The Aneuploid Mammary Epithelial (Hs578T) and the Diploid Myoepithelial (Hs578Bst) Cell Lines 2. *JNCI: Journal of the National Cancer Institute*, *58*(6), 1795–1806. https://doi.org/10.1093/jnci/58.6.1795

Hou, Y., Hu, Q., Huang, J., & Xiong, H. (2018). Omeprazole Inhibits Cell Proliferation and Induces G0/G1 Cell Cycle Arrest through Up-regulating miR-203a-3p Expression in Barrett's Esophagus Cells. *Frontiers in Pharmacology*, *8*. https://doi.org/10.3389/fphar.2017.00968

Ihraiz, W. G., Ahram, M., & Bardaweel, S. K. (2020). Proton pump inhibitors enhance chemosensitivity, promote apoptosis, and suppress migration of breast cancer cells. *Acta Pharmaceutica*, *70*(2), 179–190. https://doi.org/10.2478/acph-2020-0020

Jin, U.-H., Lee, S.-O., Pfent, C., & Safe, S. (2014a). The aryl hydrocarbon receptor ligand omeprazole inhibits breast cancer cell invasion and metastasis. *BMC Cancer*, *14*(1), 498. https://doi.org/10.1186/1471-2407-14-498

Jin, U.-H., Lee, S.-O., Pfent, C., & Safe, S. (2014b). The aryl hydrocarbon receptor ligand omeprazole inhibits breast cancer cell invasion and metastasis. *BMC Cancer*, *14*(1), 498. https://doi.org/10.1186/1471-2407-14-498

Konus, M., Çetin, D., Kızılkan, N. D., Yılmaz, C., Fidan, C., Algso, M., Kavak, E., Kivrak, A., Kurt-Kızıldoğan, A., Otur, Ç., Mutlu, D., Abdelsalam, A. H., & Arslan, S. (2022). Synthesis and biological activity of new indole based derivatives as potent anticancer, antioxidant and antimicrobial agents. *Journal of Molecular Structure*, *1263*, 133168. https://doi.org/10.1016/j.molstruc.2022.133168

Li, Y., Ren, B., Li, H., Lu, T., Fu, R., & Wu, Z. (2022). Omeprazole suppresses aggressive cancer growth and metastasis in mice through promoting Snail degradation. *Acta Pharmacologica Sinica*, *43*(7), 1816–1828. https://doi.org/10.1038/s41401-021-00787-1

Luciani, F., Spada, M., De Milito, A., Molinari, A., Rivoltini, L., Montinaro, A., Marra, M., Lugini, L., Logozzi, M., Lozupone, F., Federici, C., Iessi, E., Parmiani, G., Arancia, G., Belardelli, F., & Fais, S. (2004). Effect of Proton Pump Inhibitor Pretreatment on Resistance of Solid Tumors to Cytotoxic Drugs. *JNCI Journal of the National Cancer Institute*, *96*(22), 1702–1713. https://doi.org/10.1093/jnci/djh305

Minalyan, A., Benhammou, J. N., Artashesyan, A., Lewis, M., & Pisegna, J. R. (2017). Autoimmune atrophic gastritis: current perspectives. *Clinical and Experimental Gastroenterology*, *Volume 10*, 19–27. https://doi.org/10.2147/CEG.S109123

Numico, G., Fusco, V., Franco, P., & Roila, F. (2017). Proton Pump Inhibitors in cancer patients: How useful they are? A review of the most common indications for their use. *Critical Reviews in Oncology/Hematology*, *111*, 144–151. https://doi.org/10.1016/j.critrevonc.2017.01.014

Paz, M. F. C. J., de Alencar, M. V. O. B., de Lima, R. M. P., Sobral, A. L. P., do Nascimento, G. T. M., dos Reis, C. A., Coêlho, M. do P. S. de S., do Nascimento, M. L. L. B., Gomes Júnior, A. L., Machado, K. da C., de Menezes, A.-A. P. M., de Lima, R. M. T., de Oliveira Filho, J. W. G., Dias, A. C. S., dos Reis, A. C., da Mata, A. M. O. F., Machado, S. A., Sousa, C. D. de C., da Silva, F. C. C., … Melo Cavalcante, A. A. de C. (2020). Pharmacological Effects and Toxicogenetic Impacts of Omeprazole: Genomic Instability and Cancer. *Oxidative Medicine and Cellular Longevity*, *2020*, 1–21. https://doi.org/10.1155/2020/3457890

Pushpakom, S., Iorio, F., Eyers, P. A., Escott, K. J., Hopper, S., Wells, A., Doig, A., Guilliams, T., Latimer, J., McNamee, C., Norris, A., Sanseau, P., Cavalla, D., & Pirmohamed, M. (2019). Drug repurposing: progress, challenges and recommendations. *Nature Reviews Drug Discovery*, *18*(1), 41–58. https://doi.org/10.1038/nrd.2018.168

Secme, M., Mutlu, D., Elmas, L., & Arslan, S. (2023). Assessing effects of caffeic acid on cytotoxicity, apoptosis, invasion, GST enzyme activity, oxidant, antioxidant status and micro-RNA expressions in HCT116 colorectal cancer cells. *South African Journal of Botany*, *157*, 19–26. https://doi.org/10.1016/j.sajb.2023.03.046

Spugnini, E. P., Baldi, A., Buglioni, S., Carocci, F., Milesi de Bazzichini, G., Betti, G., Pantaleo, I., Menicagli, F., Citro, G., & Fais, S. (2011). Lansoprazole as a rescue agent in chemoresistant tumors: a phase I/II study in companion animals with spontaneously occurring tumors. *Journal of Translational Medicine*, *9*(1), 221. https://doi.org/10.1186/1479-5876-9-221

Sung, H., Ferlay, J., Siegel, R. L., Laversanne, M., Soerjomataram, I., Jemal, A., & Bray, F. (2021). Global Cancer Statistics 2020: GLOBOCAN Estimates of Incidence and Mortality Worldwide for 36 Cancers in 185 Countries. *CA: A Cancer Journal for Clinicians*, *71*(3), 209–249. https://doi.org/10.3322/caac.21660

Spermidine-Induced Cytotoxicity, Apoptosis, and Inhibition of Cell Migration in HTB-114 Cells

Kübra KOCABIYIK[1]*, Büşra Meryem TAHTA[1], Sevki ARSLAN[1]

Abstract: Cancer represents a multifactorial disease characterized by uncontrolled cell division and the ability to metastasize, often resulting in poor clinical outcomes. Conventional therapeutic approaches such as chemotherapy, radiotherapy, and surgical intervention remain insufficient in many cases due to their limited targeting precision, high toxicity, and the emergence of resistance mechanisms. These limitations emphasize the need for novel therapeutic strategies, particularly those capable of inhibiting tumor proliferation and metastasis with fewer side effects. Spermidine, a naturally occurring polyamine, plays a crucial role in maintaining cellular homeostasis by interacting with nucleic acids and proteins through electrostatic interactions. It participates in essential biological processes, including autophagy, apoptosis, oxidative stress regulation, and gene expression. Elevated levels of polyamines such as spermidine are often found in rapidly dividing cells and have been associated with tumor progression and poor prognosis. The biosynthesis of spermidine is frequently upregulated in cancer due to increased activity of enzymes like ornithine decarboxylase, which is transcriptionally regulated by oncogenic stimuli. This study aimed to investigate the cytotoxic, apoptotic, and anti-migratory effects of spermidine on the HTB-114 uterine leiomyosarcoma cell line. Cytotoxicity was assessed using the MTT assay, revealing EC_{50} values of 40.57 μM for HTB-114 and 11.85 μM for HUVEC cells. Apoptotic activity was measured via Annexin V/PI staining and flow cytometry. Spermidine induced apoptosis in 9.82% of HTB-114 cells, compared to 4.36% in the negative control and 19.15% in the paclitaxel-treated group. A wound-healing assay was conducted to evaluate migration, demonstrating that spermidine significantly delayed wound closure, with 72.5% of the wound area remaining at 48 hours compared to 29.33% in the control. Overall, our findings suggest that spermidine exerts moderate cytotoxic and apoptotic effects while inhibiting cell migration in uterine leiomyosarcoma cells. These results support further investigation into spermidine's potential as a therapeutic agent in the treatment of aggressive uterine cancers.

Keywords: Spermidine, Cytotoxicity, Apoptosis, Colony formation assay, HTB-114

[1]Address: Pamukkale University, Faculty of Science, Denizli/Turkiye

***Corresponding author**: kkocabiyik@pau.edu.tr

1. INTRODUCTION

Cancer represents a heterogeneous pathology characterized by uncontrolled cellular proliferation and the frequent potential for dissemination to secondary sites, known as metastasis. This complex condition arises from a cascade of multiple molecular events, including oncogene activation and the loss of function of tumor suppressor genes. Conventional cancer treatment modalities, such as radiotherapy, surgery, and chemotherapy, can exhibit limited efficacy in certain clinical scenarios. The underlying factors contributing to the inadequacy of these treatments include the imprecise targeting of tumors, suboptimal penetration of therapeutic agents into the tumor microenvironment, the prominence of adverse effects associated with pharmacological agents, the development of drug resistance mechanisms, and the presence of metastatic spread (Otur et al., 2023).

Spermidine, a polyamine member, is a trivalent cationic molecule widely distributed within eukaryotic cells. The positively charged spermidine molecule readily interacts with negatively charged polyanions, such as nucleic acids, proteins, and ATP, via electrostatic attraction, thereby assuming significant roles in cellular physiology. Because of this interaction, spermidine, a polyamine, participates in the maintenance of DNA integrity. Its other functions encompass the modulation of fundamental processes including transcription and translation regulation, autophagy, apoptosis, oxidative stress, and intercellular communication (Müller et al., 2001).

Polyamines, initially identified in seminal fluid, are present in varying concentrations across all cell types, with the highest level observed in tissues exhibiting rapid cellular turnover. In eukaryotes, polyamine synthesis commences with ornithine, a product derived from the urea cycle [5]. The elevated activity of enzymes involved in polyamine biosynthesis, particularly ornithine decarboxylase (ODC), is also observed in tumors. ODC, a key rate-limiting enzyme in the polyamine synthesis pathway, is frequently overexpressed and transcriptionally regulated by tumor-promoting agents in various cancers (Fan et al., 2020).

Given that elevated polyamine levels are often correlated with poor prognosis and exhibit a decrease following tumor eradication and a subsequent increase upon recurrence, the impact of polyamines on the metastasis and invasion of cancer

cells, along with the underlying mechanisms mediating these effects, has become a significant focus of extensive research (Kalač & Krausová, 2005).

Uterine leiomyosarcoma is a rare but aggressive form of cancer that arises from the smooth muscle tissue of the uterus and is characterized by poor prognosis and limited treatment options (Pistilli et al., 2015). Conventional therapies such as surgery, chemotherapy, and radiotherapy have shown limited efficacy, highlighting the urgent need for new therapeutic approaches. Spermidine, a naturally occurring polyamine, has attracted increasing attention due to its roles in cellular processes such as proliferation, apoptosis, and autophagy (Fan et al., 2020). Recent studies have suggested that spermidine may exhibit anticancer properties by modulating cell viability, inducing programmed cell death, and affecting cell motility. However, the effects of spermidine on uterine leiomyosarcoma cells have not been well characterized. Therefore, this study aims to investigate the cytotoxic, apoptotic, and migratory effects of spermidine on HTB-114 uterine leiomyosarcoma cells through MTT assay, Annexin V/PI staining, and scratch-wound healing assay, respectively.

2. MATERIAL AND METHOD

The experimental procedures employed in this study have been systematically presented under specific subheadings, each detailing the methodology used to evaluate the cytotoxic, apoptotic, and migratory effects of spermidine on the selected cell lines.

2.1. Cell culture

In this study, HTB-114 (Uterine leiomyosarcoma) and HUVEC (Umbilical vein endothelial cells) cell lines were used. The cells were incubated with DMEM and MEM medium supplemented with 10% fetal bovine serum and 1% penicillin-streptomycin at 37°C with 95% humidity in a CO2 incubator. Cells were subcultured when they reached the 90% confluence. A thoma chamber and trypan blue dye were used for cell counting (Arslan et al., 2020).

2.2. Evaluation of cytotoxicity using the MTT assay

To evaluate the cytotoxicity of spermidine on HTB-114 and HUVEC cell lines, 2×10^3 cells were seeded into 96-well plates. Spermidine was dissolved and diluted in DMSO to obtain final concentrations ranging from 125 µM to 7.8 µM. DMSO was also used as a control. The cells were treated with different concentrations of spermidine for 48 hours in a CO_2 incubator. After incubation, the medium was removed and replaced with 100 µL of fresh medium and 10 µL of MTT solution. The cells were then incubated for 2–3 hours at 37°C. The resulting formazan crystals were dissolved in 50 µL of DMSO and incubated for an additional 30 minutes at 37°C. Absorbance was measured at 540 nm using a microplate reader. EC_{50} values were calculated and used for further analyses (Konus et al., 2022).

2.3. Apoptotic activity in HTB-114 cell line

To determine the apoptotic activity of spermidine on the HTB-114 cell line, 20×10^3 cells were seeded into a 6-well plate. The EC_{50} concentration of spermidine was applied to the cells for 48 hours. Paclitaxel was used as a positive control, and DMSO served as a negative control. After treatment, the cells were collected using trypsin and transferred into centrifuge tubes. The supernatant was removed, and the cells were washed twice with PBS. Cells were then incubated with Annexin V/PI staining solution for 20 minutes. The percentages of apoptotic and necrotic cells were analyzed using flow cytometry (Sahin et al., 2024).

2.4. Cell migration analysis by scratch assay

Cell migration was assessed using the wound-scratch assay in HTB-114 cells. To evaluate cell migration, 30×10^3 cells were seeded into a 6-well plate and incubated until they reached approximately 90% confluency. After incubation, a straight-line scratch was made across the cell monolayer using a sterile 200 µL pipette tip. Detached cells and debris were gently removed by washing the wells twice with PBS. Fresh medium containing the EC_{50} concentration of spermidine was then added to each well. The cells were exposed to spermidine for 48 hours. Cell migration was monitored at 0, 24, and 48 hours by taking photographs, and the wound closure area was quantified using ImageJ software (Mutlu et al., 2022).

2.5. Statistical analysis

All experimental procedures were performed in triplicate to ensure reproducibility and reliability of the results. Data obtained from cytotoxicity, apoptosis, and wound healing assays were expressed as mean ± standard deviation (SD). Statistical analysis was carried out using GraphPad Prism version 9. Appropriate statistical tests were applied depending on the nature of the data and the comparison groups. Dose-response curves were generated to calculate EC_{50} values for spermidine. For all analyses, a p-value of less than 0.05 was considered statistically significant.

3. RESULTS

3.1. Cytotoxicity of spermidine on cell lines

The cytotoxic activity of spermidine on HTB-114 and HUVEC cell lines was evaluated using the MTT assay. For this purpose, cells were seeded into 96-well plates and treated with five different concentrations of spermidine (ranging from 7.8 to 125 µM). Following a 24-hour incubation period, viable cells converted MTT into formazan crystals, which were subsequently dissolved in DMSO. The absorbance of each well was measured at 540 nm. Based on the absorbance values, dose-response curves were generated (Figure 1), and EC50 values were calculated using GraphPad software. The EC50 value of spermidine was determined to be 40.57 µM for the HTB-114 cell line and 11.85 µM for the HUVEC cell line.

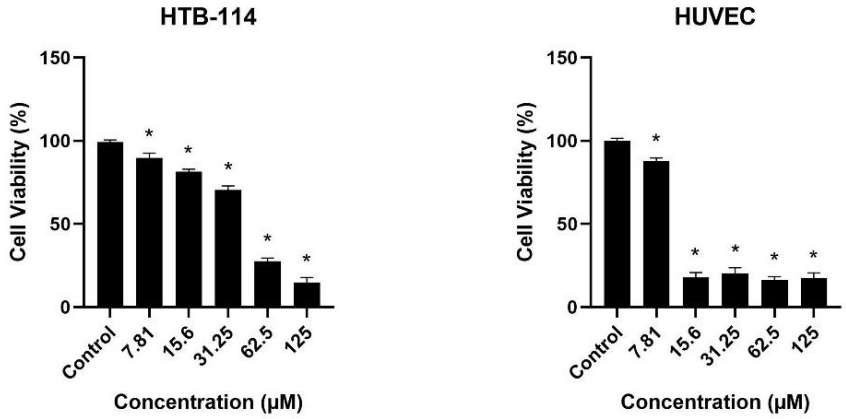

Figure 3. Cytotoxic activity of spermidine on HTB-114 and HUVEC cell lines. *=P<0.05

3.2. Determination of apoptosis

Spermidine-induced apoptosis in HTB-114 cells was determined using flow cytometry. For this purpose, cells were seeded into 6-well plates and treated with the EC_{50} dose of spermidine. DMSO was used as a negative control, while paclitaxel was used as a positive control to evaluate apoptosis. After incubation, cells were stained with Annexin V/PI and incubated in the dark. The percentages of apoptotic, necrotic, and viable cells were evaluated and are presented in Figure 2. The results indicated that spermidine exhibited an apoptotic effect compared to the negative control. As shown in the dot plot images, the percentage of apoptotic cells was 4.36% in the control group, 19.15% in the positive control group, and 9.82% in the spermidine-treated group.

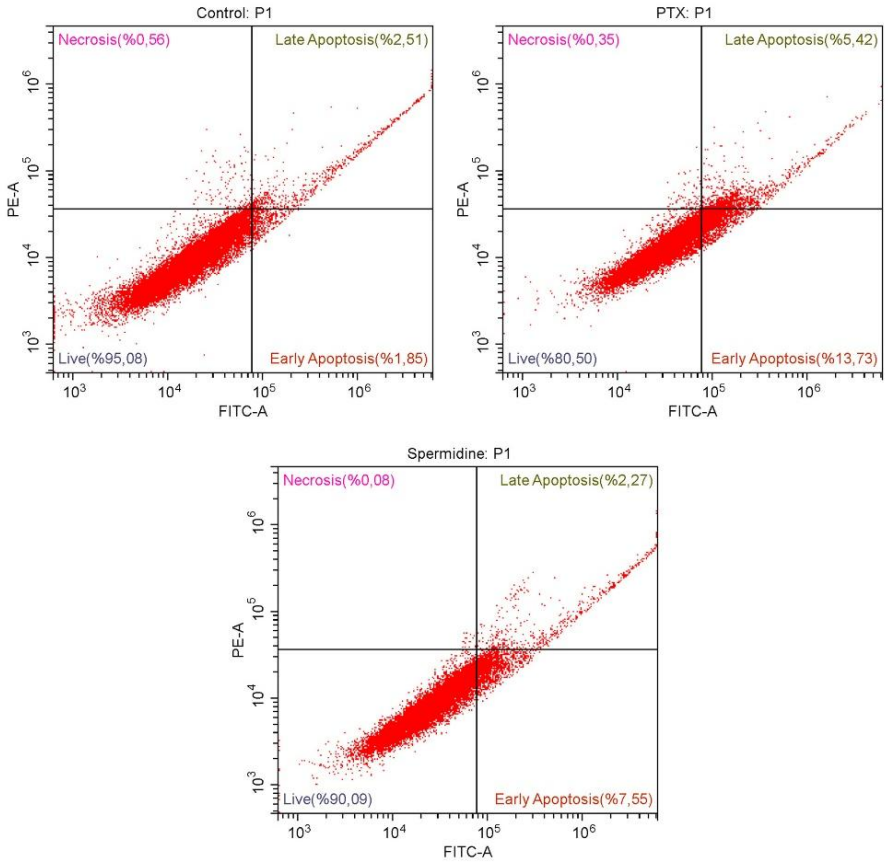

Figure 4. Flow cytometry figures showing the apoptotic activity of spermidine in the HTB-114 cell line. Paclitaxel (PTX) was used as a positive control.

3.3. Cell Migration Analysis

To investigate the effect of spermidine on cell migration in the HTB-114 cell line, a scratch assay was performed. Cells were seeded into 6-well plates, and once they reached approximately 90% confluency, a straight scratch was made across the monolayer using a sterile pipette tip to create a wound area. The cells were then treated with the EC_{50} concentration of spermidine. Images were captured at 0, 24, and 48 hours to monitor wound closure, and the migration rate was calculated based on the relative reduction of the wound area. The wound area at 0 hours was set as 100%. After 24 hours, the wound area was measured as 88.98% in the control group and 91.53% in the spermidine-treated cells. At 48 hours, the remaining wound area was 29.33% in the control, while it was 72.5% in the spermidine group (Figure 3). These findings suggest that spermidine, at its EC50 dose, delays cell migration in HTB-114 cells.

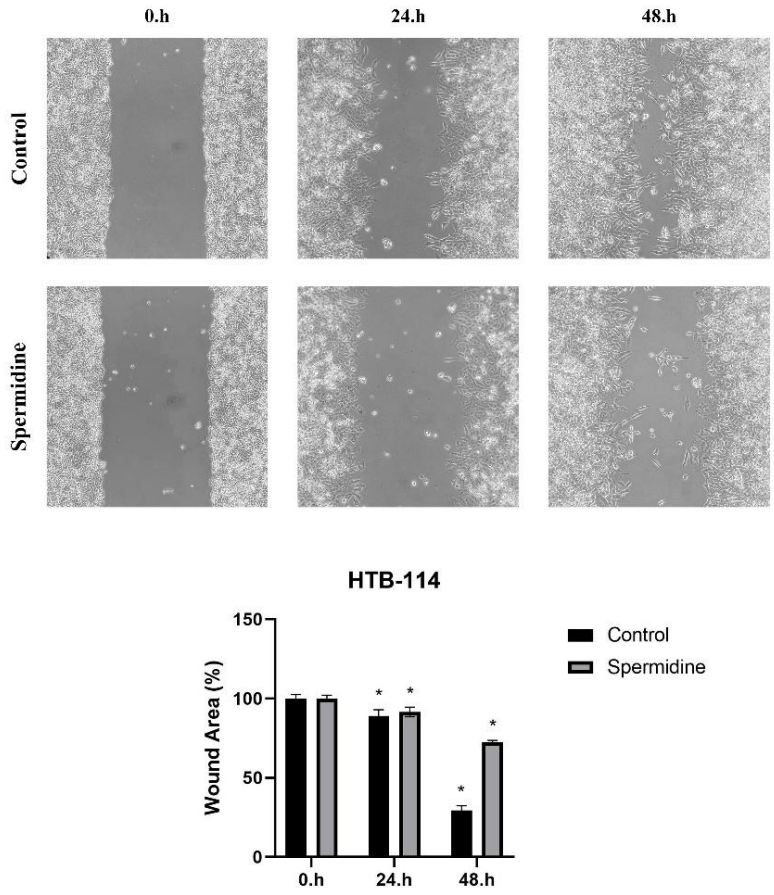

Figure 5. Representative images from the scratch wound healing assay of HTB-114 cell lines at 0, 24 and 48 hours are shown. The relative wound area (%) of migrated cells was calculated using densitometric measurements with ImageJ. *P < 0.05 compared to the control group.

4. DISCUSSION

This study explored the cytotoxic, apoptotic, and anti-migratory effects of spermidine on HTB-114 uterine leiomyosarcoma and HUVEC cell lines. The findings provide preliminary evidence that spermidine exhibits selective biological activity, particularly in cancer cells, while also offering insights into its potential mechanism of action.

MTT assay results demonstrated that spermidine reduces cell viability in a dose-dependent manner in both HTB-114 and HUVEC cell lines. However, the observed EC_{50} value was significantly lower in HUVEC cells (11.85 µM) compared to HTB-114 cells (40.57 µM), suggesting that non-cancerous endothelial cells may be more sensitive to spermidine at certain concentrations. Similar dose-dependent cytotoxic effects have been reported in previous studies, where spermidine exhibited antiproliferative activity in several cancer models, including breast and colon cancer cells, by modulating autophagy and apoptosis pathways (Eisenberg et al., 2009; Madeo et al., 2018).

Flow cytometry analysis further confirmed that spermidine induces apoptosis in HTB-114 cells. Although the apoptotic rate (9.82%) was lower than that of the positive control (paclitaxel, 19.15%), it was still significantly elevated compared to the negative control group. This finding supports the hypothesis that spermidine can activate programmed cell death in malignant cells. The mechanism of spermidine-induced apoptosis has been linked to mitochondrial dysfunction and oxidative stress, which triggers caspase activation and DNA fragmentation (Morselli et al., 2011). It is noteworthy that in this study, spermidine did not cause a strong necrotic effect, indicating its potential to selectively promote apoptosis over necrosis, a desirable property in anticancer agents.

In addition to its cytotoxic and apoptotic effects, spermidine was also found to suppress cell migration in HTB-114 cells. The wound healing assay revealed that the closure of the scratch area was significantly delayed in spermidine-treated cells compared to the control, particularly at the 48-hour mark. While the control group showed substantial wound closure (29.33% of the original wound area remaining), the spermidine group exhibited a markedly higher remaining wound area (72.5%). These results suggest that spermidine impairs the migratory capacity of HTB-114 cells, potentially reducing metastatic risk. Previous studies have proposed that spermidine interferes with cytoskeletal remodeling and cellular adhesion-key processes in cancer cell migration (Pietrocola et al., 2015). This is particularly relevant for uterine leiomyosarcoma, which is known for its aggressive nature and high metastatic potential.

Overall, the findings of this study highlight the multifaceted effects of spermidine on cancer-related processes. While its lower EC_{50} in HUVEC cells raises concerns regarding selectivity, the pro-apoptotic and anti-migratory activities observed in HTB-114 cells suggest its potential as a candidate for further preclinical investigation. Future studies should aim to elucidate the molecular pathways involved in spermidine's actions and assess its effects in vivo, with a particular focus on its impact on normal tissues and long-term safety profile.

5. CONCLUSION

This study demonstrates that spermidine exhibits moderate cytotoxic effects on both HTB-114 and HUVEC cell lines, with greater sensitivity observed in non-cancerous HUVEC cells. Flow cytometry results revealed that spermidine induces apoptosis in HTB-114 cells, although to a lesser extent than paclitaxel. Furthermore, the scratch assay results showed that spermidine delays cell migration, suggesting a potential anti-metastatic property. Taken together, these findings highlight the promising yet cell-specific biological effects of spermidine and support further research to elucidate its underlying molecular mechanisms and possible therapeutic applications in cancer treatment.

Acknowledgements
We would like to express our sincere gratitude to Amine Hafis Abdelsalam and the entire Molecular Biochemistry Laboratory team for their valuable support and contributions throughout this study.

Ethics Committee Approval
N/A

Peer-review
Externally peer-reviewed.

Author Contributions
Conceptualization: K.K..; Investigation: K.K., B.M.T.; Material and Methodology: S.A., K.K; Supervision: S.A.; Visualization: K.K, B.M.T.; Writing-Original Draft: K.K, B.M.T.; Writing-review & Editing: K.K, B.M.T., S.A. Other: All authors have read and agreed to the published version of manuscript.

Conflict of Interest
The authors have no conflicts of interest to declare.

Funding
The authors declared that this study has received no financial support.

REFERENCES

Arslan, Ş., Kocabıyık, K., Mutlu, D., & Semiz, G. (2020). Assessment of Cytotoxic and Apoptotic Effects of Salvia syriaca L. in Colorectal Adenocarcinoma Cell Line (Caco-2). *Iranian Journal of Pharmaceutical Research*, *20*(3), 235–242.

Eisenberg, T., Knauer, H., Schauer, A., Büttner, S., Ruckenstuhl, C., Carmona-Gutierrez, D., Ring, J., Schroeder, S., Magnes, C., Antonacci, L., Fussi, H., Deszcz, L., Hartl, R., Schraml, E., Criollo, A., Megalou, E., Weiskopf, D., Laun, P., Heeren, G., … Madeo, F. (2009). Induction of autophagy by spermidine promotes longevity. *Nature Cell Biology*, *11*(11), 1305–1314. https://doi.org/10.1038/ncb1975

Fan, J., Feng, Z., & Chen, N. (2020). Spermidine as a target for cancer therapy. *Pharmacological Research*, *159*, 104943. https://doi.org/10.1016/j.phrs.2020.104943

Kalač, P., & Krausová, P. (2005). A review of dietary polyamines: Formation, implications for growth and health and occurrence in foods. *Food Chemistry*, *90*(1–2), 219–230. https://doi.org/10.1016/j.foodchem.2004.03.044

Konus, M., Çetin, D., Kızılkan, N. D., Yılmaz, C., Fidan, C., Algso, M., Kavak, E., Kivrak, A., Kurt-Kızıldoğan, A., Otur, Ç., Mutlu, D., Abdelsalam, A. H., & Arslan, S. (2022). Synthesis and biological activity of new indole based derivatives as potent anticancer, antioxidant and antimicrobial agents. *Journal of Molecular Structure*, *1263*, 133168. https://doi.org/10.1016/j.molstruc.2022.133168

Madeo, F., Eisenberg, T., Pietrocola, F., & Kroemer, G. (2018). Spermidine in health and disease. *Science*, *359*(6374). https://doi.org/10.1126/science.aan2788

Morselli, E., Mariño, G., Bennetzen, M. V., Eisenberg, T., Megalou, E., Schroeder, S., Cabrera, S., Bénit, P., Rustin, P., Criollo, A., Kepp, O., Galluzzi, L., Shen, S., Malik, S. A., Maiuri, M. C., Horio, Y., López-Otín, C., Andersen, J. S.,

Tavernarakis, N., … Kroemer, G. (2011). Spermidine and resveratrol induce autophagy by distinct pathways converging on the acetylproteome. *Journal of Cell Biology*, *192*(4), 615–629. https://doi.org/10.1083/jcb.201008167

Mutlu, D., Cakir, C., Ozturk, M., & Arslan, S. (2022). Anticancer and apoptotic effects of a polysaccharide extract isolated from Lactarius chrysorrheus Fr. in HepG2 and PANC-1 cell lines. *Archives of Biological Sciences*, *74*(4), 315–324. https://doi.org/10.2298/ABS220803030M

Müller, S., Coombs, G. H., & Walter, R. D. (2001). Targeting polyamines of parasitic protozoa in chemotherapy. *Trends in Parasitology*, *17*(5), 242–249. https://doi.org/10.1016/S1471-4922(01)01908-0

Otur, Ç., Okay, S., & Kurt-Kızıldoğan, A. (2023). Whole genome analysis of Flavobacterium aziz-sancarii sp. nov., isolated from Ardley Island (Antarctica), revealed a rich resistome and bioremediation potential. *Chemosphere*, *313*, 137511. https://doi.org/10.1016/j.chemosphere.2022.137511

Pietrocola, F., Lachkar, S., Enot, D. P., Niso-Santano, M., Bravo-San Pedro, J. M., Sica, V., Izzo, V., Maiuri, M. C., Madeo, F., Mariño, G., & Kroemer, G. (2015). Spermidine induces autophagy by inhibiting the acetyltransferase EP300. *Cell Death & Differentiation*, *22*(3), 509–516. https://doi.org/10.1038/cdd.2014.215

Pistilli, A., Rende, M., Crispoltoni, L., Montagnoli, C., & Stabile, A. M. (2015). LY294002 induces *in vitro* apoptosis and overexpression of p75NTR in human uterine leiomyosarcoma HTB 114 cells. *Growth Factors*, *33*(5–6), 376–383. https://doi.org/10.3109/08977194.2015.1118096

Sahin, C., Mutlu, D., Erdem, A., Kilincarslan, R., & Arslan, S. (2024). New cyclometalated iridium(III) complexes bearing substituted 2-(1H-benzimidazol-2-yl)quinoline: Synthesis, characterization, electrochemical and anticancer studies. *Bioorganic Chemistry*, *151*, 107706. https://doi.org/10.1016/j.bioorg.2024.107706


iconst